



Fernando Bastos Fernandes

**Integro-Differential Solutions for Formation
Mechanical Damage Control During Oil Flow
in Permeability-Pressure-Sensitive Reservoirs**

Tese de Doutorado

Thesis presented to the Programa de Pós-graduação em Engenharia Mecânica of PUC-Rio in partial fulfillment of the requirements for the degree of Doutor em Engenharia Mecânica.

Advisor : Prof. Arthur Martins Barbosa Braga

Co-advisor: Prof. Antônio Cláudio Soares

Rio de Janeiro
November 2021



Fernando Bastos Fernandes

**Integro-Differential Solutions for Formation
Mechanical Damage Control During Oil Flow
in Permeability-Pressure-Sensitive Reservoirs**

Thesis presented to the Programa de Pós-graduação em Engenharia Mecânica of PUC-Rio in partial fulfillment of the requirements for the degree of Doutor em Engenharia Mecânica.
Approved by the Examination Committee.

Prof. Arthur Martins Barbosa Braga

Advisor

Departamento de Engenharia Mecânica – PUC-Rio

Prof. Antônio Cláudio Soares

Co-advisor

Departamento de Engenharia Química e de Petróleo – UFF

Prof. Antônio Luiz Serra de Souza

Departamento de Engenharia Civil – PUC-Rio

Prof. Ivan Fabio Mota de Menezes

Departamento de Engenharia Mecânica – PUC-Rio

Prof. Raquel Quadros Velloso

Departamento de Engenharia Civil – PUC-Rio

Prof. Alfredo Moisés Vallejos Carrasco

Departamento de Engenharia Química e de Petróleo – UFF

Prof. Marcos Antônio Rosolen

Departamento de Engenharia de Petróleo – Unicamp

Rio de Janeiro, November 17th, 2021

All rights reserved.

Fernando Bastos Fernandes

Undergraduated and graduated in petroleum engineering from Federal University of Rio de Janeiro (UFRJ) with a master's in mechanical engineering with an area of concentration in thermosciences by Pontifical Catholic University of Rio de Janeiro. **Fernandes** was a young apprentice of Pride International and worked as a field specialist at Halliburton. Nowadays, Fernandes works in the well engineering department at Petrobras. He is an SPE paper contest jury member, session chair, and technical reviewer from Offshore Technology Conference (OTC Houston and OTC Brazil), scientific reviewer, and technical program leader for American Rock Mechanics Association (ARMA) and Brazillian Petroleum and Biofuels Institute (IBP). Moreover, he is a scientific reviewer from the Journal of Petroleum Science and Engineering from Elsevier®.

Bibliographic data

Fernandes, Fernando Bastos

Integro-Differential Solutions for Formation Mechanical Damage Control During Oil Flow in Permeability-Pressure-Sensitive Reservoirs / Fernando Bastos Fernandes; advisor: Arthur Martins Barbosa Braga; co-advisor: Antônio Cláudio Soares. – Rio de Janeiro: PUC-Rio, Departamento de Engenharia Mecânica, 2021.

v., 301 f: il. color. ; 30 cm

Tese de Doutorado - Pontifical Catholic University of Rio de Janeiro, Departamento de Engenharia Mecânica.

Inclui bibliografia

1. Mechanical Engineering – Teses.
 2. Engenharia de Petróleo;. 3. Funções de Green;. 4. Escoamento em Meios Porosos;. 5. Soluções por Método da Perturbação;. 6. Equação da Difusividade Hidráulica Não-Linear;. 7. Variação de Permeabilidade com a Pressão de Poros..
- I. Pontifical Catholic University of Rio de Janeiro. Departamento de Engenharia Mecânica. II. Título.

To my timeless dad Antônio Carlos Fernandes (*In Memoriam*), to my honey wife Danielle Salles Sampaio, to our dear daughter Meg, to my mom Rosa Maria Bastos Fernandes and my sister Fernanda Bastos Fernandes, for their love, support and encouragement.

Acknowledgments

I thank God for always blessing my life and giving me strength when I needed it most.

To my dad Antonio Carlos Fernandes (*In Memoriam*), for being my best friend, loving me, and helping to plan my life through his wise advice. Thank you for everything, dad I miss you so much.

To my honey wife, Danielle Salles Sampaio, for being, in addition to wife, my companion and best friend, from the moment of my father's passing, until today. To our daughters Meg (*In Memoriam*) and Julieta and our son Grigri (my little polar bear) for blessing our lives, for all her love and companionship, during the construction of this work and in the most critical moments of my life. I love you all.

To my dear nephew Leonardo Henrique Alves (*In Memoriam*) because this angel blessed our lives and taught us so much. Rest in peace, little angel.

To my mom Rosa Maria Bastos Fernandes, my aunt Teresa Fernandes, and my sister Fernanda Bastos Fernandes, for all the love, affection, and wisdom in my bad times.

To my dear friends from Gracie Barra Jiu-Jitsu Botafogo. In special to our master Laércio, his assistant Maurício on Thursdays and Fridays excellent classes, and, finally to our multi-champion Kristian. Thanks for your classes, brilliant teachings, and patience.

In special, to Doctor Cláudio Crispi and his team, for helping us in the bad moments we have in 2019.

To our dear Eugênia Sampaio and Cristiano Pontes, for all their affection and advice.

To my dear friends Almir Souza, Anderson Alves, Gabriel Albanex, Marina Ribeiro, Paulo Sérgio Jr., Rafael Dias, Ralph Canhete, Rita Aragão and Yago Soares for all the motivation for conclusion of the course.

To professors Abelardo Barreto Jr., Antônio Cláudio Soares, Arthur Braga, Antônio Luiz, Dan Marchesin and Raquel Velloso, for the support during this work.

In special to professor Ivan Menezes for accepting me into the Graduate program and for all the advice given during my moments of doubt.

To the Pontifical Catholic University of Rio de Janeiro (PUC-Rio), for the grant through a scholarship for this course.

To Petrobras, for providing papers for the construction of this work.

This study was financed in part by the Coordenação de Aperfeiçoamento de Pessoal de Nível Superior - Brasil (CAPES) - Finance Code 001

Abstract

Fernandes, Fernando Bastos; Braga, Arthur Martins Barbosa (Advisor); Soares, Antônio Cláudio (Co-advisor). **Integro-Differential Solutions for Formation Mechanical Damage Control During Oil Flow in Permeability-Pressure-Sensitive Reservoirs**. Rio de Janeiro, 2021. 301p. Tese de Doutorado – Department of Engenharia Mecânica, Pontifical Catholic University of Rio de Janeiro.

The Nonlinear Hydraulic Diffusivity Equation (NHDE) models the single-phase flow of fluids in porous media, considering the variation in the properties of the rock and the fluid present inside its pores. Usually, the dimensionless linear solution for the flow of oil is performed using the Laplace and Fourier transforms or Boltzmann transformation and provides the unsteady-state pressure profile in Cartesian coordinates given by complementary error function $\text{erfc}(x_D, y_D, t_D)$ and in cylindrical coordinates described by the exponential integral function $\text{Ei}(r_D, t_D)$. This work develops a new integro-differential solution to predict the formation mechanical damage caused by the permeability loss during the well-reservoir life-cycle for several oil flow problems. The appropriate Green's function (GF) to solve NHDE for each well-reservoir setting approached in this thesis is used. The general solution is implemented in the Matlab[®], and the model calibration is carried out by comparing the solution obtained in this work to the porous media finite difference oil flow simulator named IMEX[®]. The solution of the NHDE is computed by the sum of the linear solution (constant permeability) and the first-order term of the asymptotic expansion, composed of the nonlinear effect of the permeability loss. Geomechanical effects are incorporated in the proposed model and the role of Biot's coefficient and overburden stress were evaluated. The instantaneous permeability loss effect is clearly noticed in the log-log and semi-log plots.

Keywords

Petroleum Engineering; Green's Functions; Flow in Porous Media; Perturbative Solutions; Nonlinear Hydraulic Diffusivity Equation; Permeability Pressure-Sensitive.

Resumo

Fernandes, Fernando Bastos; Braga, Arthur Martins Barbosa (Orientador); Soares, Antônio Cláudio (Coorientador). **Soluções Íntegro-Diferenciais para Controle de Dano Mecânico à Formação durante Escoamento de Óleo em Reservatórios com Permeabilidade Dependente da Pressão de Poros**. Rio de Janeiro, 2021. 301p. Tese de Doutorado – Departamento de Engenharia Mecânica da Pontifícia Universidade Católica do Rio de Janeiro.

A Equação da Difusividade Hidráulica Não-Linear (EDHN) modela o escoamento monofásico de fluidos em meios porosos levando em conta a variação das propriedades da rocha e do fluido presente no interior de seus poros. Normalmente, a solução adimensional da linha-fonte $p_D(r_D, t_D)$ para escoamento de líquidos é encontrada por meio do uso da transformada de Laplace ou transformação de Boltzmann, o qual, o perfil transiente de pressões em coordenadas cartesianas é descrito pela função erro complementar $\text{erfc}(x_D, y_D, t_D)$ e, em coordenadas cilíndricas pela função integral exponencial $\text{Ei}(r_D, t_D)$.

Este trabalho propõe a solução analítica pelo método de expansão assintótica de primeira ordem em séries, para solução de alguns problemas de escoamento de petróleo em meios porosos com permeabilidade dependente da pressão de poros e termo fonte. A solução geral será implementada no software Matlab® e a calibração do modelo matemático será realizada comparando-se a solução obtida neste trabalho com a solução calculada por meio de um simulador de fluxo óleo em meios porosos denominado IMEX®, amplamente usado na indústria de petróleo e em pesquisas científicas e que usa o método de diferenças finitas. A solução geral da equação diferencial é dada pela soma da solução para escoamento de líquidos com permeabilidade constante e o termo de primeira ordem da expansão assintótica, composto pela não linearidade devido à variação de permeabilidade. Os efeitos da variação instantânea de permeabilidade em função da pressão de poros e tensões efetivas de Biot são claramente demonstrados nos gráficos log-log e semi-log apresentados.

Palavras-chave

Engenharia de Petróleo; Funções de Green; Escoamento em Meios Porosos; Soluções por Método da Perturbação; Equação da Difusividade Hidráulica Não-Linear; Variação de Permeabilidade com a Pressão de Poros.

Summary

1	Introduction	25
1.1	Motivation	26
1.2	Green's Function Method	27
1.3	State of the Art	30
1.4	Scientific Methodology	35
1.5	Thesis Organization	36
2	Literature Review	37
2.1	Formation Mechanical Damage Literature	37
2.2	Analytical Solutions for Nonlinear Flow through Porous Media Literature	41
2.3	Nonlinear Oil Flow in Hydraulically Fractured Wells Literature	43
2.4	Pressure Transient Analysis and Well-Testing Literature	46
2.5	A New Analytical Model to Mechanical Formation Damage Management During Oil Flow in Pressure-Sensitive Reservoirs	52
3	Problem Statement	54
3.1	Theoretical Definitions	57
3.2	Integro-Differential Solution for Mechanical Formation Damage Control	57
3.3	Computational Methodology	59
3.4	Experimental Methodology and Field Data	61
4	Theoretical Formulation	75
4.1	Continuity Equation for Oil Flow in Pressure-Sensitive Reservoirs	76
4.2	Nonlinear Hydraulic Diffusivity Equation in terms of Pressure	77
4.3	Nonlinear Hydraulic Diffusivity Equation for Permeability Pressure-Sensitive Reservoirs	81
4.4	Dimensionless Variables	83
4.5	Asymptotic Series Expansion Method	86
5	Integro-Differential Solutions for Constant Oil Flow Rate	94
5.1	Oil Flow in a Vertical Well Fully Penetrating an Infinite Reservoir	94
5.2	Oil Flow in a Vertical Well Near an Infinite Sealing Fault	127
5.3	Oil Flow in a Well with an Infinite Extension Hydraulic Fracture	170
5.4	Oil Flow in a Well with Finite Extension Hydraulic Fracture	194
6	Integro-Differential Solutions for Variable Oil Flow Rate	215
6.1	Permeability Loss/Restoration Management During Well-Reservoir Oil Loading/Unloading Cycles	215
6.2	Permeability-Hysteresis Identification During Oil Loading-Unloading Well-Reservoir Cycles	244
7	Integro-Differential Solution for Permeability Loss Management with Geomechanical Coupling	254
7.1	Theoretical Definitions	255
7.2	Model Calibration, Results and Discussions	260

8	Conclusions and Future Works	269
8.1	Model Advantages	270
8.2	Model Limitations	270
8.3	Model Extension	271
9	References	272
A	Transcendental Functions	285
B	Laplace Transforms and Inverses	287
C	Verification of Duhamel's Principle (Time's Superposition)	289
D	Integro-Differential Solution Verification	295
E	Dimensionless Wellbore Line-Source Solution Derivation	300

List of figures

Figure 1.1	Sketch of a reservoir rock element. (a): Undamaged rock grains (no production). (b): Crushed rock grains caused by the well-reservoir production (damaged reservoir).	25
Figure 1.2	Dimensionless GF as a function of the dimensionless radial component, for several dimensionless time variation.	28
Figure 1.3	Computational methodology used to predict the mechanical formation damage in pressure-sensitive oil reservoirs with source term.	36
Figure 3.1	Log-log plot of the dimensionless permeability loss as a function of the linear solution over the well-reservoir life-cycle.	54
Figure 3.2	Sketch of oil production from the reservoir layers A and B separately (no interlayer cross-flow). (a) Oil production from layer A, and the layer B shut by standing valve (SS). (b) Oil production from layer B, and the layer A shut by standing valve (SS).	55
Figure 3.3	Log-log plot of the hydraulic diffusivity deviator factor as a function of the line-source solution.	59
Figure 3.4	Log-log plot of the permeability pseudo-pressure as a function of the pore pressure.	60
Figure 3.5	Permeability curve for the linear fitting.	64
Figure 3.6	Permeability curve for the exponential fitting.	65
Figure 3.7	Permeability curve for the parabolic fitting.	65
Figure 3.8	Permeability curve for the hyperbolic fitting.	66
Figure 3.9	Dimensionless permeability as a function of the dimensionless oil source for several dimensionless pressure variation values (Case study A).	68
Figure 3.10	Dimensionless permeability as a function of the dimensionless oil source for several dimensionless pressure variation values (Case study B).	69
Figure 3.11	Dimensionless permeability with respect to the dimensionless pressure variation for several dimensionless oil flow rates (Case study A)	70
Figure 3.12	Dimensionless permeability with respect to the dimensionless pressure variation for several dimensionless oil flow rates (Case study B).	70
Figure 3.13	Dimensionless pressure variation as a function of the dimensionless oil source for several dimensionless permeability (Case study A).	71
Figure 3.14	Dimensionless pressure variation as a function of the dimensionless oil source for several dimensionless permeability (Case study B).	71
Figure 3.15	Diffusivity deviator factor as a function of the dimensionless inverse oil source for several dimensionless pressure variation (Case study A).	72
Figure 3.16	Diffusivity deviator factor as a function of the dimensionless inverse oil source for several dimensionless pressure variation (Case study B).	73
Figure 3.18	Hydraulic diffusivity deviator factor as a function of the dimensionless pressure variation for several inverse oil sources (Case study B).	74
Figure 3.17	Hydraulic diffusivity deviator factor as a function of the dimensionless pressure variation for several inverse oil sources (Case study A).	74
Figure 4.1	Infinitesimal reservoir rock element.	76

Figure 5.1	Sketch of a vertical well in an infinite reservoir.	94
Figure 5.2	Semi-log plot of the dimensionless pseudo-pressure derivative for several fitting functions for case study A.	117
Figure 5.3	Semi-log plot of the dimensionless pseudo-pressure derivative for several fitting functions for case study B.	118
Figure 5.4	Semi-log plot of the dimensionless first-order term for several fitting functions for case study A.	119
Figure 5.5	Semi-log plot of the dimensionless first-order term for several fitting functions for case study B.	119
Figure 5.6	Semi-log plot of the dimensionless general solution for several fitting functions for case study A.	120
Figure 5.7	Semi-log plot of the dimensionless general solution for several fitting functions for case study B.	120
Figure 5.8	Log-log plot of the dimensionless first-order nonlinear term calibrated by IMEX [®] .	121
Figure 5.9	Log-log plot of the dimensionless linear solution (constant permeability) with respect to IMEX [®] .	122
Figure 5.10	Log-log plot of the dimensionless general solution and the derivative calibrated by IMEX [®] .	122
Figure 5.11	Log-log plot of the role of the zeroth-order source term in the dimensionless pseudo-pressure solution.	123
Figure 5.12	Log-log plot of the effect of the hydraulic diffusivity deviation factor in the nonlinear first-order term.	124
Figure 5.13	Semi-log plot of the comparison between the dimensionless general solution with respect to the linear solution.	124
Figure 5.14	Semi-log plot of the amplification of the permeability loss with respect to the linear solution.	125
Figure 5.15	Log-log plot of the dimensionless first-order term for several dimensionless oil sources.	125
Figure 5.16	Log-log plot of the dimensionless general solution derivative for several dimensionless oil sources.	126
Figure 5.17	Semi-log plot of the hydraulic diffusivity deviator factor effect in the dimensionless general solution.	126
Figure 5.18	Semi-log plot of the amplification of hydraulic diffusivity deviator factor effect in the dimensionless general solution.	127
Figure 5.19	Side view of a vertical well near a sealing fault sketch.	128
Figure 5.20	Diagnostic plot of the comparison between IARF and sealing fault curves of the dimensionless pseudo-pressure and its derivative for the case studies A and B.	147
Figure 5.21	Diagnostic plot of the calibration of the constant permeability solution with respect to IMEX [®] .	148
Figure 5.22	Log-log plot of the first-order term calibrated by IMEX [®] . This plot shows that, the nonlinearity that results in permeability loss is more severe during the early-times.	149
Figure 5.23	Semi-log plot of the dimensionless general solution for several fitting functions for the case study A.	150
Figure 5.24	Semi-log plot of the dimensionless general solution for several fitting functions for the case study B.	150

Figure 5.25	Log-log plot of the dimensionless general solution derivative for several fitting functions for the case study A.	151
Figure 5.26	Log-log plot of the dimensionless general solution derivative for several fitting functions for the case study B.	152
Figure 5.27	Log-log plot of the dimensionless first-order term for several fitting functions for the case study A.	153
Figure 5.28	Log-log plot of the dimensionless first-order term for several fitting functions for the case study B.	153
Figure 5.29	Log-log plot of the IARF and sealing fault curves of the dimensionless pseudo-pressure derivative for several sources for the case study A.	154
Figure 5.30	Log-log plot of the IARF and sealing fault curves of the dimensionless pseudo-pressure derivative for several sources for the case study B.	154
Figure 5.31	Log-log plot of the comparison between IARF and sealing fault curves of the dimensionless general solution for several oil sources for the case study B.	155
Figure 5.32	Log-log plot of the IARF and sealing fault curves of the dimensionless general solution for several oil sources for the case study B.	156
Figure 5.33	Semi-log plot of the IARF and sealing fault curves of the dimensionless general solution for several oil sources for the case study A.	156
Figure 5.34	Semi-log plot of the IARF and sealing fault curves of the dimensionless general solution for several oil sources for the case study B.	157
Figure 5.35	Log-log plot of the IARF and sealing fault curves of the dimensionless first-order term for several oil sources for the case study A.	158
Figure 5.36	Log-log plot of the IARF and sealing fault curves of the dimensionless first-order term for several oil sources for the case study B.	158
Figure 5.37	Diagnostic plot of the dimensionless pseudo-pressure derivative for several dimensionless well-sealing fault distances for the case study A.	159
Figure 5.38	Diagnostic plot of the dimensionless pseudo-pressure derivative for several dimensionless well-sealing fault distances for the case study B.	159
Figure 5.39	Diagnostic plot of the dimensionless pseudo-pressure for several dimensionless well-sealing fault distances for the case study A.	160
Figure 5.40	Diagnostic plot of the dimensionless pseudo-pressure for several dimensionless well-sealing fault distances for the case study B.	161
Figure 5.41	Semi-log plot of the effect of the hydraulic diffusivity deviation factor in the dimensionless pseudo-pressure for the case study A.	162
Figure 5.42	Semi-log plot of the effect of the hydraulic diffusivity deviation factor in the dimensionless pseudo-pressure for the case study B.	162
Figure 5.43	Log-log plot of the role of the deviation factor in the dimensionless derivative for case study A.	163
Figure 5.44	Log-log plot of the role of the deviation factor in the dimensionless derivative for case study B.	163
Figure 5.45	Semi-log plot of the effect several first-order source terms on pseudo-pressure solution for case study A.	164

Figure 5.46	Semi-log plot of the effect several first-order source terms on pseudo-pressure solution for case study B.	164
Figure 5.47	Semi-log plot of the effect of the first-order oil source on the corrective term for case study A.	166
Figure 5.48	Semi-log plot of the effect of the first-order oil source on the corrective term for case study B.	166
Figure 5.49	Log-log plot of the influence of the first-order source term in the derivative for case study A.	167
Figure 5.50	Log-log plot of the influence of the first-order source in the derivative for case study B.	167
Figure 5.51	Log-log plot of the amplification of the influence of the first-order source in the derivative for case study A.	168
Figure 5.52	Log-log plot of the amplification of the influence of the first-order source in the derivative for case study B.	168
Figure 5.53	Diagnostic plot of the permeability change for the case studies A and B.	169
Figure 5.54	Detail of an infinite extension hydraulic fracture.	170
Figure 5.55	Dimensionless effective permeability as a function of the pore pressure ratio for the case studies A and B.	182
Figure 5.56	Log-log plot of the effective permeability pseudo-pressure for case studies A and B.	183
Figure 5.57	Log-log plot of the effective deviation factor for case studies A and B.	184
Figure 5.58	Diagnostic plot of the dimensionless linear solution (constant permeability) in comparison to IMEX [®] .	184
Figure 5.59	Diagnostic plot of the dimensionless first-order pseudo-pressure against IMEX [®] for the case studies A and B.	185
Figure 5.60	Diagnostic plot of the dimensionless pseudo-pressure against IMEX [®] for the case studies A and B.	185
Figure 5.61	Diagnostic plot of the dimensionless pseudo-pressure derivative against IMEX [®] for the case studies A and B.	186
Figure 5.62	Dimensionless effective permeability as a function of the pore pressure ratio for several proppant package arrangements for the case studies A and B.	187
Figure 5.63	Effective permeability pseudo-pressure as a function of the pore pressure for several proppant package arrangements for the case studies A and B.	187
Figure 5.64	Effective hydraulic diffusivity deviator factor as a function of the pore pressure for several proppant package arrangements for the case studies A and B.	188
Figure 5.65	Semi-log plot of the pseudo-pressure derivative for several proppant package arrangements for the case studies A and B.	189
Figure 5.66	Semi-log plot of the amplification of the pseudo-pressure derivative for several proppant package arrangements for the case studies A and B.	189
Figure 5.67	Log-log plot of the first-order term for several proppant package arrangements for the case studies A and B.	190

Figure 5.68	Semi-log plot of the dimensionless pseudo-pressure for several proppant package arrangements for the case studies A and B.	190
Figure 5.69	Log-log plot of the dimensionless first-order term for several sorting index values for the case studies A and B.	191
Figure 5.70	Semi-log plot of the dimensionless pseudo-pressure derivative for several sorting index values for the case studies A and B.	192
Figure 5.71	Semi-log plot of the dimensionless pseudo-pressure for several sorting index values for the case studies A and B.	192
Figure 5.72	Log-log plot of the dimensionless first-order term for several cementation exponent values for the case studies A and B.	193
Figure 5.73	Semi-log plot of the dimensionless pseudo-pressure derivative for several cementation exponent values for the case studies A and B.	193
Figure 5.74	Semi-log plot of the dimensionless pseudo-pressure for several cementation exponent values for the case studies A and B.	194
Figure 5.75	Scheme of a finite extension hydraulic fracture.	194
Figure 5.76	Log-log plot of the calibration of the dimensionless linear solution using IMEX [®] .	202
Figure 5.77	Log-log plot of the calibration of the dimensionless general solution for the case studies A and B using IMEX [®] .	202
Figure 5.78	Log-log plot of the calibration of the dimensionless pseudo-pressure derivative for the case studies A and B using IMEX [®] .	203
Figure 5.79	Log-log plot of the calibration of the dimensionless first-order corrective term for the case studies A and B using IMEX [®] .	203
Figure 5.80	Log-log plot of the effect from the zeroth-order oil source in the pseudo-pressure derivative.	205
Figure 5.81	Log-log plot of the comparison between the pseudo-pressure for the finite and infinite hydraulic fractures.	205
Figure 5.82	Log-log plot of the comparison between the pseudo-pressure derivative for the finite and infinite hydraulic fractures.	206
Figure 5.83	Log-log plot of the comparison between the first-order term for the finite and infinite hydraulic fractures.	206
Figure 5.84	Semi-log plot of the effect of the proppant porosity arrangements in the dimensionless first-order term.	207
Figure 5.85	Semi-log plot of the effect of the proppant porosity arrangements in the dimensionless pseudo-pressure derivative.	207
Figure 5.86	Semi-log plot of the amplification of the effect of the proppant porosity arrangements in the dimensionless pseudo-pressure derivative.	208
Figure 5.87	Semi-log plot of the effect of the proppant porosity arrangements in the dimensionless pseudo-pressure.	208
Figure 5.88	Semi-log plot of the amplification of the effect of the proppant porosity arrangements in the dimensionless pseudo-pressure.	209
Figure 5.89	Semi-log plot of the dimensionless pseudo-pressure for several dimensionless sources.	209
Figure 5.90	Semi-log plot of the dimensionless pseudo-pressure derivative for several dimensionless sources.	210
Figure 5.91	Semi-log plot of the dimensionless first-order term for several sorting index values.	210

Figure 5.92	Semi-log plot of the dimensionless pseudo-pressure for several sorting index values.	211
Figure 5.93	Semi-log plot of the dimensionless pseudo-pressure derivative for several sorting index values.	211
Figure 5.94	Semi-log plot of the dimensionless first-order term for several cementation exponents.	212
Figure 5.95	Semi-log plot of the dimensionless pseudo-pressure derivative for several cementation exponents.	212
Figure 5.96	Semi-log plot of the the dimensionless pseudo-pressure for several cementation exponents.	213
Figure 5.97	Semi-log plot of the effective permeability loss effect.	214
Figure 6.1	Pressure transient response during oil loading/unloading cycles.	215
Figure 6.2	Log-log plot of the calibration of the dimensionless linear solution against IMEX [®] .	225
Figure 6.3	Log-log plot of the calibration of the dimensionless pseudo-pressure first-order term against IMEX [®] for the drawdown period.	226
Figure 6.4	Log-log plot of the calibration of the dimensionless pseudo-pressure first-order term against IMEX [®] for the build-up period.	227
Figure 6.5	Log-log plot of the calibration of dimensionless pseudo-pressure first-order term against IMEX [®] for build-up period.	228
Figure 6.6	Log-log plot of the dimensionless pseudo-pressure first-order term for several hydraulic diffusivity deviator factors for build-up period.	228
Figure 6.7	Log-log plot of the dimensionless pseudo-pressure first-order term for several hydraulic dimensionless production's time for build-up period.	229
Figure 6.8	Semi-log plot of the calibration of the dimensionless pseudo-pressure first-order term against IMEX [®] .	230
Figure 6.9	Semi-log plot of the dimensionless pseudo-pressure first-order term for several dimensionless oil sources.	230
Figure 6.10	Semi-log plot of the dimensionless pseudo-pressure first-order term for several hydraulic diffusivity deviator factors.	231
Figure 6.11	Semi-log plot of the dimensionless pseudo-pressure first-order term for several dimensionless production's time.	232
Figure 6.12	<i>Horner plot</i> of the calibration of the dimensionless linear solution and pseudo-pressure change against IMEX [®] .	232
Figure 6.13	<i>Horner plot</i> of the dimensionless linear solution and pseudo-pressure change for several dimensionless oil sources against IMEX [®] .	233
Figure 6.14	<i>Horner plot</i> of the calibration of the dimensionless linear solution and pseudo-pressure change for several hydraulic diffusivity deviator factors.	234
Figure 6.15	<i>Horner plot</i> of the dimensionless linear solution and pseudo-pressure change for several dimensionless production's time.	235
Figure 6.16	Log-log plot of the calibration of the pseudo-pressure change and its derivative against IMEX [®] .	236
Figure 6.17	Log-log plot of the pseudo-pressure change and its derivative for several dimensionless oil sources.	236
Figure 6.18	Log-log plot of the pseudo-pressure change and its derivative for several hydraulic deviator factors.	237

Figure 6.19	Log-log plot of the pseudo-pressure change and its derivative for several dimensionless production's time.	238
Figure 6.20	Log-log plot of the dimensionless pseudo-pressure for several hydraulic diffusivity deviator factors for drawdown and build-up periods.	238
Figure 6.21	Semi-log plot of the dimensionless pseudo-pressure for several hydraulic diffusivity deviator factors for drawdown and build-up periods.	239
Figure 6.22	Semi-log plot of the dimensionless pseudo-pressure for several hydraulic diffusivity deviator factors for drawdown period.	240
Figure 6.23	Semi-log plot of the amplification of the dimensionless pseudo-pressure for several hydraulic diffusivity deviator factors for drawdown period.	240
Figure 6.24	Semi-log plot of the amplification of the dimensionless pseudo-pressure for several hydraulic diffusivity deviator factors for build-up period.	241
Figure 6.25	Semi-log plot of pseudo-pressure as a function of the time for several oil flow rates for the case study A.	242
Figure 6.26	Semi-log plot of pseudo-pressure as a function of the time for several oil flow rates for the case study B.	242
Figure 6.27	Semi-log plot of pseudo-pressure variation as a function of the time for several oil flow rates for the case study B.	243
Figure 6.28	Semi-log plot of pseudo-pressure variation as a function of the time for several oil flow rates for the case study B.	244
Figure 6.29	Log-log plot of the permeability-hysteresis response for the case study A.	245
Figure 6.30	Log-log plot of the permeability-hysteresis response for the case study B.	245
Figure 6.31	Log-log plot of the hysteresis variation with respect to different dimensionless production's times for the case studies A and B.	247
Figure 6.32	Log-log plot of the hydraulic diffusivity deviator factor variation with respect to different dimensionless production's times for the case studies A and B.	247
Figure 6.33	Log-log plot of the permeability-hysteresis response in the first-order term for $t_{pD} = 10^3$.	248
Figure 6.34	Log-log plot of the permeability-hysteresis response in the first-order term for $t_{pD} = 10^4$.	249
Figure 6.35	Semi-log plot of the permeability-hysteresis response in the first-order term for $t_{pD} = 10^3$.	249
Figure 6.36	Semi-log plot of the permeability-hysteresis response in the first-order term for $t_{pD} = 10^4$.	250
Figure 6.37	Log-log plot of the effect from the hydraulic diffusivity deviator factor on the first-order term with permeability-hysteresis.	251
Figure 6.38	Semi-log plot of pseudo-pressure variation as a function of the time for several oil flow rates for the case study B.	251
Figure 6.39	Semi-log plot of dimensionless pseudo-pressure change with hysteresis for the case studies A and B.	252
Figure 6.40	Semi-log plot of the amplification of the dimensionless pseudo-pressure change with hysteresis for the case studies A and B.	252

Figure 7.1	Log-log plot of the dimensionless permeability as a function of the dimensionless Biot's effective stress.	254
Figure 7.2	Log-log plot of Biot's effective stress-sensitive deviation factor versus dimensionless effective stress.	261
Figure 7.3	Log-log plot of the effective stress-sensitive pseudo-pressure ratio versus the pore pressure ratio.	262
Figure 7.4	Log-log plot of the constant permeability solution calibrated by IMEX®.	263
Figure 7.5	Log-log plot of Biot's effective stress-sensitive first-order term calibrated by IMEX®. This plot shows that, the nonlinearity that results in permeability loss is more severe during the early-times.	263
Figure 7.6	Log-log plot of the first-order term for several overburden stress.	264
Figure 7.7	Log-log plot of influence of Biot's coefficient in the permeability loss raise.	265
Figure 7.8	Log-log plot of influence of dimensionless first-order source in the permeability loss lowering (first-order term).	266
Figure 7.9	Log-log plot of influence of effective stress-sensitive deviator factor in the permeability loss lowering over the dimensionless elapsed time.	266
Figure 7.10	Log-log plot of the comparison between the model developed in this work with Biot's effective stress-sensitive effect and the solution presented by Fernandes et al. (2021a) . For this simulation, Biot's coefficient was fixed at the value $\alpha = 0.9$ (consolidated sandstones).	267
Figure 7.11	Semi-log plot of the comparison between constant permeability and Biot's effective stress-sensitive solution.	267

List of tables

Table 3.1	Wellbore-Rock-Fluid Field Data	62
Table 3.2	Proposed functions for permeability pressure decay.	64
Table 7.1	Dimensionless parameters used in the model presented in this paper (Lee, Rollins & Spivey, 2003)	257
Table B.1	Laplace Transform Properties	288

Nomenclature

∇ = Nabla operator

$\nabla(\dots)$ = Gradient operator

$\nabla \bullet (\dots)$ = Divergent operator

$\nabla^2(\dots)$ = Laplacian operator

$\mathbf{Ei}(\dots)$ = Exponential integral function

$\mathbf{erfc}(\dots)$ = Complementary error function

$\mathbf{I}_0(\dots)$ = First kind and zeroth-order modified Bessel function

$\mathbf{K}_0(\dots)$ = Second kind and zeroth-order modified Bessel function

$\delta(\dots)$ = Dirac delta function

$\mathcal{L}\{p_D(r_D, t_D)\}$ = Laplace transform operator

$\bar{p}_D(r_D, \mathcal{U})$ Dimensionless linear solution in the Laplace domain

\mathcal{U} = Laplace variable

L_c = Characteristic length

L = Well-sealing fault distance

L_D = Dimensionless well-sealing fault distance

r_D = Dimensionless radial component

t_D = Dimensionless time

(r_D, θ_D, z_D) = Dimensionless cylindrical coordinates;

(x_D, y_D, z_D) = Dimensionless Cartesian coordinates

$\partial/\partial r_D$ = Dimensionless partial differential operator in cylindrical coordinates

$\partial^2/\partial r_D^2 + 1/r_D(\partial/\partial r_D)$ = Dimensionless partial Laplacian operator in cylindrical coordinates

$\partial/\partial x_D$ = Dimensionless partial Laplacian operator in the x-direction of the Cartesian coordinates

$\partial/\partial y_D$ = Dimensionless partial Laplacian operator in the y-direction of the Cartesian coordinates

$\partial^2/\partial x_D^2$ = Dimensionless partial Laplacian operator in the x-direction of the Cartesian coordinates

$\partial^2/\partial y_D^2$ = Dimensionless partial Laplacian operator in the y-direction of the Cartesian coordinates

$\partial/\partial t_D$ = Dimensionless partial differential rate operator

r_w = Wellbore radius

r = Radial component

θ = Angular component

θ_0 = Initial angular component

z = Axial component

t = Time

\mathbf{r} = Displacement vector

\mathbf{u} = Darcian velocity field

V_p = Porous volume

ϵ = Perturbation parameter

p_i = Initial pressure

p_b = Reference pressure

$\Delta\hat{p}$ = Dimensionless pressure variation

$m(p)$ = Pseudo-pressure function

$\Delta m(p)$ = Pseudo-pressure variation function

$m(p_i)$ = Pseudo-pressure function in initial pressure

$\Delta m(p_i)$ = Pseudo-pressure variation function in initial pressure

ϕ = Porosity

ϕ_{eff} = Effective porosity

ϕ_p = Proppant package arrangement porosity

k_f = Hydraulic fracture permeability

$k_{eff}(p)$ = Effective permeability function

$k_{eff}(p_i)$ = Effective permeability function in the initial pressure

$k_{effD}(p)$ = Dimensionless effective permeability function

C = Sorting index

m = Cementation exponent

$\mathcal{D}(p)$ = Dimensionless inverse hydraulic diffusivity function

$\mathcal{D}_{eff}(p)$ = Dimensionless inverse effective hydraulic diffusivity function

\mathcal{D} = Dominant grain size

x_f = Hydraulic fracture length

h_f = Hydraulic fracture thick

$\eta(p_i)$ = Initial diffusivity

c_r = Rock compressibility

c_o = Oil compressibility

$\rho(p)$ = Oil density

μ = Oil dynamic viscosity

c_t = Total compressibility

$k(p)$ = Permeability function

$k(p_i)$ = Permeability in initial pressure

$\eta(p)$ = Hydraulic diffusivity function

$\eta_D(p)$ = Dimensionless diffusivity function

$k_D(p)$ = Dimensionless permeability function

$\xi(p)$ = Hydraulic diffusivity deviator factor

$\xi_{eff}(p)$ = Effective hydraulic diffusivity deviator factor

$f_D(r_D, \theta_D, t_D, k_D)$ = Dimensionless source term in cylindrical coordinates

$m_D(r_D, \theta_D, t_D, k_D)$ = Dimensionless pseudo-pressure in cylindrical coordinates

$m_D^{(0)}(r_D, \theta_D, t_D, k_D)$ = Dimensionless zero order term of pseudo-pressure in dimensionless cylindrical coordinates

$m_D^{(1)}(r_D, \theta_D, t_D, k_D)$ = Dimensionless first order term of pseudo-pressure in cylindrical coordinates

$m_D^{(k)}(r_D, \theta_D, t_D, k_D)$ = Dimensionless k^{th} order term of pseudo-pressure in cylindrical coordinates

$G_D(r_D, r'_D, \theta_D, \theta'_D, z_D, z'_D, t_D, t'_D)$ = Dimensionless Green's function in cylindrical coordinates

$f_D(x_D, y_D, z_D, t_D, k_D)$ = Dimensionless source term in dimensionless Cartesian coordinates

$m_D(x_D, y_D, z_D, t_D, k_D)$ = Dimensionless pseudo-pressure in dimensionless Cartesian coordinates

$m_D^{(0)}(x_D, y_D, z_D, t_D, k_D)$ = Dimensionless zero order term of pseudo-pressure in dimensionless Cartesian coordinates

$m_D^{(1)}(x_D, y_D, z_D, t_D, k_D)$ = Dimensionless first order term of pseudo-pressure in dimensionless Cartesian coordinates

$m_D^{(k)}(x_D, y_D, z_D, t_D, k_D)$ = Dimensionless k^{th} order term of pseudo-pressure in dimensionless Cartesian coordinates

$G_D(x_D, x'_D, y_D, y'_D, z_D, z'_D, t_D, t'_D)$ = Dimensionless Green's function in Cartesian coordinates

$S_D(r_D, \theta_D, t_D, k_D)$ = Dimensionless general oil source in cylindrical coordinates

$S_D^{(0)}(r_D, \theta_D, t_D, k_D)$ = Dimensionless zeroth order term of the general oil source in cylindrical coordinates

$S_D^{(1)}(r_D, \theta_D, t_D, k_D)$ = Dimensionless first order term of the general oil source in cylindrical coordinates

$S_D^{(k)}(r_D, \theta_D, t_D, k_D)$ = Dimensionless k^{th} order term of the general oil source in cylindrical coordinates

$S_D(x_D, y_D, z_D, t_D, k_D)$ = Dimensionless general oil source in Cartesian coordinates

$S_D^{(0)}(x_D, y_D, z_D, t_D, k_D)$ = Dimensionless zeroth order term of the general oil source in Cartesian coordinates

$S_D^{(1)}(x_D, y_D, z_D, t_D, k_D)$ = Dimensionless first order term of the general oil source in Cartesian coordinates

$S_D^{(k)}(x_D, y_D, z_D, t_D, k_D)$ = Dimensionless k^{th} order term of the general oil source in Cartesian coordinates

$m_{wD}(t_D, k_D)$ = Dimensionless pseudo-pressure in wellbore

$p_D(r_D, t_D)$ = Dimensionless linear solution

h = Reservoir net pay

q = Oil flow rate

$\tilde{q}(r, t)$ = Oil flow rate per volume unit

$\bar{q}(r, t)$ = Oil flow rate per area unit

α = Biot's coefficient

E = Young's modulus

$(\varepsilon_r, \varepsilon_\theta, \varepsilon_z)$ = Strain vector in cylindrical coordinates

ν = Poisson's ratio

σ_{ov} = Overburden stress

$\sigma_h(p_i)$ = initial horizontal stress

σ'_v = Vertical Biot's effective stress

σ'_h = Horizontal Biot's effective stress

σ_h = Horizontal stress

$\sigma'_v(p_i)$ = Initial vertical Biot's effective stress

"Scientist does not study nature because it is useful to do so. He studies it because he takes pleasure in it, and he takes pleasure in it because it is beautiful. If nature were not beautiful, it would not be worth knowing, and life would not be worth living."

Henri Poincaré, .

1 Introduction

Analytical solutions for the Nonlinear Hydraulic Diffusivity Equation (NHDE) have been studied for many years by geoscientists, well-testing, and reservoir engineers. The high acquisition costs involved in numerical oil flow simulators turn the analytical models attractive for simulating several flow in porous media problems. Perturbative solutions have been widely proposed to solve transport phenomena in porous media, electromagnetism, and seismic wave propagation problems, (Pedrosa Jr.; Nayfeh; Virieux, Flores-Luna & Gibert, 1986, 1991, 1994).

The Hydraulic Diffusivity Equation (HDE) is derived from the coupling between Darcy's law (Darcy, 1856), continuity equation and porous media constitutive equations for the rock and fluid properties, (Bear, 1972) and (Ahmed, 2010). Often in the petroleum engineering and dynamics of fluids in porous media literature, the Linear Hydraulic Diffusivity Equation (LHDE) is solved through Laplace and Fourier transform, (Everdingen & Hurst, 1949b) or Boltzmann transformation, (Peres, Serra & Reynolds, 1989). The oil flow rate decline during the reservoir production caused by the permeability changes have been noticed in several reservoir rocks in the world, (Soares; Soares, Freitas & Velloso; Soares & Ferreira, 2000, 2001, 2002). Figure 1.1 presents two conditions of the rock grains under Biot's effective stress.

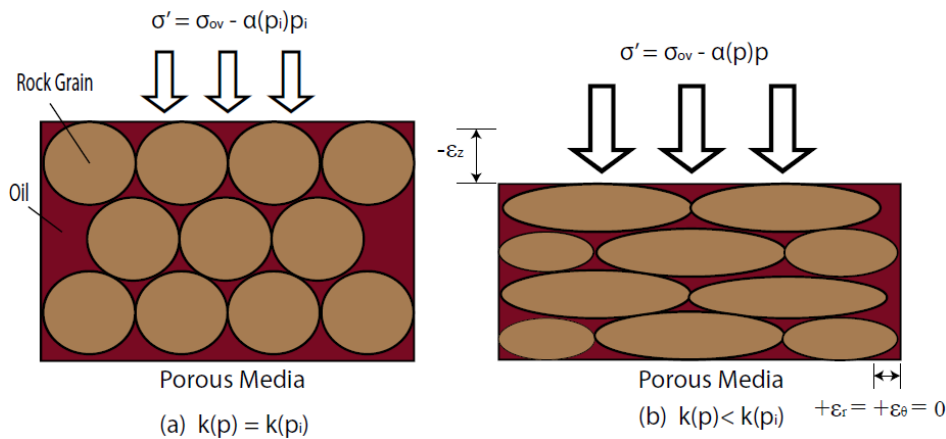


Figure 1.1: Sketch of a reservoir rock element. (a): Undamaged rock grains (no production). (b): Crushed rock grains caused by the well-reservoir production (damaged reservoir).

The sketch from the right side of the Figure 1.1 illustrates the rock grains under the initial effective stress, which depends on the initial pressure p_i , [MPa]. It also shows the strain $-\epsilon_z$ and $+\epsilon_\theta = +\epsilon_r = 0$ caused by the

effective stress over several years of well-reservoir production and, consequently, permeability change, where σ' is the Biot's effective stress vector, [MPa]; σ_{ov} is the total overburden stress vector, [MPa]; $(\varepsilon_r, \varepsilon_\theta, \varepsilon_z)$ is the volumetric strain vector, [dimensionless] in the cylindrical directions (r, θ, z) with respect to the Canonical basis $\{(1, 0, 0); (0, 1, 0); (0, 0, 1)\}$ of the Euclidean space $\in \mathbb{R}^3$, p is the pore pressure, [MPa] and α is the Biot's coefficient, [dimensionless]. The negative sign means the strain caused by compression stress, and the positive one means the strain caused by tension stress. The strain condition of the uni-axial test is similar to the one frequently encountered in actual problems, (Geertsma; Lambe & Whitman; Smits, Waal & Kooten, 1966, 1979, 1988). In many cases of the petroleum engineering literature, the oil flow in porous media is modeled by Darcy's law (Darcy, 1856).

Several attempts to linearize the NHDE were made until the introduction of the pseudo-pressure function in 1966 (Al-Hussainy, Ramey Jr. & Crawford, 1966). The Boltzmann transformation was applied by Peres, Serra & Reynolds (1989) to derive a closed-form analytical solution for the NHDE in terms of the pseudo-pressure function. They showed that the general dimensionless wellbore solution was given by: $m_D(r_D = 1, t_D) \approx p_D(r_D = 1, t_D) + m_D^{(1)}(r_D = 1, t_D)$, where $p_D(r_D = 1, t_D)$ is the line-source solution for constant permeability (linear solution) and $m_D^{(1)}(r_D = 1, t_D)$ is a corrective term caused by the nonlinearities of the diffusivity function $\eta(p)$ of the model.

1.1

Motivation

Minimizing the formation mechanical damage caused by the variation in the reservoir permeability over the productive life of an oil field constitutes a topic of significant importance for the petroleum industry. This phenomenon can impact significantly the technical and economic viability of production development projects caused by the impairment in the oil production curve. If the reservoir permeability decline occurs significantly early, providing a large decrease in oil production, in many cases, the wells in these fields may be temporarily or permanently abandoned.

This work develops a new analytical model to predict the instantaneous permeability response during the well-reservoir life-cycle. The proposed model is based on a perturbative-integro-differential solution using Green's Functions (GF) for the appropriate well-reservoir setting and boundary conditions considered. The solution provides the permeability response information to support the reservoir oil's production's performance management.

1.2

Green's Function Method

In the partial differential equations theory, the Green's function method is a powerful mathematical tool used to solve equations in three dimensions and unsteady conditions with source term, Carslaw & Jaeger (1959), Gringarten & Ramey Jr. (1974), Gringarten et al. (1979), Gringarten, Ramey Jr. & Raghavan (1975), Gringarten (1984), Duffy (2001), Gringarten (2008). This method is broadly used in transport phenomena literature and petroleum engineering. The oil source term is modeled through a Dirac delta function that represents an instantaneous-point oil pulse.

The Green's function (GF) for each well-reservoir setting and boundary conditions is associated with the equation:

$$\begin{aligned} \nabla^2 G_D^{(k)}(x_D, x'_D, y_D, y'_D, z_D, z'_D, t_D, t'_D) - \frac{\partial G_D^{(k)}(x_D, x'_D, y_D, y'_D, z_D, z'_D, t_D, t'_D)}{\partial t_D} = \\ = -\delta(x_D - x'_D)\delta(y_D - y'_D)\delta(z_D - z'_D)\delta(t_D - t'_D) \quad (1-1) \end{aligned}$$

The term on the right-hand side of the Eq. 1-5 is the oil point-source defined by the Dirac's delta function $\delta(x_D - x'_D)\delta(y_D - y'_D)\delta(z_D - z'_D)\delta(t_D - t'_D)$. The negative sign in the source term, expressed by the Dirac delta function, means that the oil is withdrawn from the reservoir. The parameters x'_D, y'_D, z'_D and t'_D in the argument of the GF, represent the dimensionless Cartesian position and time where and when the instantaneous oil pulse is applied, whereas x_D, y_D, z_D and t_D represent the Cartesian position and the time where and when the pulse is observed.

The associated initial condition is:

$$G_D^{(k)}(x_D, x'_D, y_D, y'_D, z_D, z'_D, t_D = 0, t'_D) = 0 \quad (1-2)$$

and the homogeneous external boundary condition becomes:

$$\lim_{(x_D, y_D, z_D) \rightarrow \infty} G_D^{(k)}(x_D, x'_D, y_D, y'_D, z_D, z'_D, t_D, t'_D) = 0 \quad (1-3)$$

Recently, new GF's-based analytical models have been developed to solve the NHDE for isothermal flow through porous media and have shown high accuracy when compared to the numerical flow simulators, Barreto Jr., Peres & Pires (2010), Barreto Jr., Peres & Pires (2012), Barreto Jr., Pires & Peres (2012), Sousa, Barreto Jr. & Peres (2016a), Fernandes et al. (2021a). Figure 1.2 presents the GF behavior as function of the dimensionless radius r_D

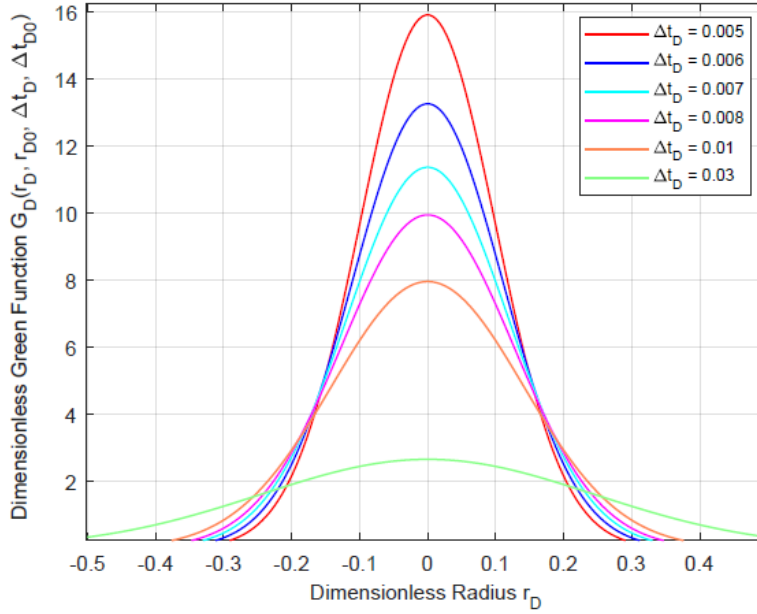


Figure 1.2: Dimensionless GF as a function of the dimensionless radial component, for several dimensionless time variation.

for several dimensionless time variation Δt_D . The pulse is applied in the dimensionless initial time variation $\Delta t_{D0} = t_D - t_{D0}$ and, in the dimensionless initial point r_{D0} . The GF behaves as an instantaneous point-source, where it reaches its maximum value in the point and the time of application of the pulse, and quickly it decays as a function of the dimensionless distance and of dimensionless time, (Fernandes, 2021a), (Fernandes, 2021b) and (Fernandes et al., 2021a). Moreover, the GF's profile shape becomes more flattened and tends to spread more uniformly over all the porous media domain, (Carslaw & Jaeger; Beck et al.; Ozisiki; Duffy; Cole, Beck & Haji-Sheikh, 1959, 1992, 1993, 2001, 2011). When obtained for a given domain \mathbb{D} , the GF yields the solution for any initial and boundary condition employing integration over the domain's boundary. In applying the GF's theory to unsteady flow in porous media, the source functions involved in the model are obtained through the integration of GF over the source volume, (Gringarten & Ramey Jr.; Gringarten & J.; Gringarten & Ramey Jr.; Gringarten, Ramey Jr. & Raghavan; Gringarten et al.; Gringarten; Schroeter & Gringarten, 1973, 1974, 1974, 1975, 1979, 1984, 2007).

This doctoral thesis presents a coupled perturbative-integro-differential-GF model to evaluate the instantaneous permeability decline as a function of pore pressure over the life-cycle of several petroleum well-reservoir settings. The settings simulated in this work are infinite-acting-radial-flow (IARF), a well near a sealing fault, and hydraulic fractured wells. For variable oil flow rate cases, this work evaluates the mechanical formation damage during the

drawdown period and the permeability restoration when the well is shut to perform the build-up test. The developed solution shows that the dimensionless oil source plays a key role in the permeability loss and the hysteresis control.

The single-phase oil flow in a homogeneous isotropic porous media with a flow source is modeled through the NHDE below:

$$\nabla \bullet \left[k(p) \nabla p \right] - \phi \mu c_t \frac{\partial p}{\partial t} = -\tilde{q}(\mathbf{r}, t) \mu \quad (1-4)$$

where p represents the pressure field inside the reservoir pores MPa; $k(p)$ is the permeability pressure dependent, [mD]; ϕ is the porosity, [dimensionless]; μ is the dynamic viscosity, [Pa sec]; t is the time, [sec]; c_t the total compressibility, [1/MPa] and $\tilde{q}(\mathbf{r}, t)$ is the oil flow rate per volume, [sec⁻¹] as a function of time and the appropriate coordinates for each well-reservoir setting. The permeability pseudo-pressure $m(p)$ developed by [Fernandes \(2022\)](#) is:

$$m(p) = \int_{p_b}^p k(p') dp' \quad (1-5)$$

where p' is the dummy integration variable, $k(p')$ is the permeability pressure-dependent function and p_b is a reference pressure. All these parameters are considered in the same unit system mentioned previously. Combining this transformation with the perturbation technique, the NHDE becomes similar to the slightly compressible flow partial differential equation with the pseudo-pressure $m(p)$ as the dependent variable instead of the pressure p . Thus:

$$\nabla^2 \left[m(p) \right] - \frac{1}{\eta \left[m(p) \right]} \frac{\partial m(p)}{\partial t} = -\tilde{q}(\mathbf{r}, t) \mu \quad (1-6)$$

Using pseudo-pressure definition (Eq. 1-5), the nonlinear hydraulic diffusivity equation can be written as follows:

$$\nabla^2 \left[\int_{p_b}^p k(p') dp' \right] - \frac{1}{\eta \left[\int_{p_b}^p k(p') dp' \right]} \frac{\partial}{\partial t} \left[\int_{p_b}^p k(p') dp' \right] = -\tilde{q}(\mathbf{r}, t) \mu \quad (1-7)$$

The model is solved for the aforementioned well-reservoir settings, using the appropriate GF for each case, from [Carslaw & Jaeger \(1959\)](#), [Beck et al. \(1992\)](#), [Ozisiki \(1993\)](#), [Duffy \(2001\)](#), [Cole, Beck & Haji-Sheikh \(2011\)](#).

Reservoir rocks, *e.g.* sandstones, carbonates, and limestones, are a type of rock constituted by permo-porous properties capable of storing gas, oil, and

water inside their pores. In terms of permo-porous characteristics, some source rocks *e.g.* tight shales can have permeabilities as low as 10^{-10} Darcy, while permeabilities in sandstones generally range from 0.1 to 1 Darcy, (Bjørlykke, 1994). The field data used in this work were withdrawn from two sandstone layers of the same infinite reservoir located in Brazil. The rock samples were addressed to the laboratory for experimental tests to get the pressure and permeability data. These data were used as input to the nonlinear term of the analytical model to evaluate the permeability drops over the well-reservoir life-cycle. Oftentimes, geoscientists and reservoir engineers do not consider the effect of *in situ* stresses on production, considering that permeability is constant during the whole productive well-reservoir life-cycle. However, this assumption is incorrect for limestones and unconsolidated sandstones, (Soares, Ferreira & Vargas Jr., 2002).

Compaction with porosity reduction can improve production by squeezing oil from rock into the wellbore. However, compaction can also impair permeability and reduce production. Understanding the interplay of these effects is essential for optimizing well placement, predicting production rates, and for reservoir management. The collective effects of compaction phenomena on oil production and reservoir behavior can be understood using mathematical experiments using synthetic, laboratory, and field data. Mathematical modelling can do reliable prediction of oil production, (Soares, 2000), (Soares, Freitas & Velloso, 2001), (Soares, Ferreira & Vargas Jr., 2002), (Soares & Ferreira, 2002).

1.3 State of the Art

Recently, new GF's based analytical models have been proposed to solve the NHDE for Darcian flow in porous media and have shown high convergence when compared to numerical oil and real gas flow simulators used in the petroleum industry. Geoscientists and reservoir engineers have broadly discussed the formation mechanical damage that occurred in permeability-pressure-sensitive reservoirs to optimize reservoir performance. This section deals with the state of the art of GF models for flow in porous media and reservoir geomechanics based on permeability decay as a function of pore pressure, addressing the most recent works on these subjects.

Tabatabaie, Pooladi-Darvish & Mattar (2015) presented a work about the drawdown effects in a multi-fractured pressure-sensitive porous media. The proposed model considered an exponential permeability decline as a function of the drawdown and the permeability modulus for a linear unsteady-state flow. Nonetheless, the model developed neglected source effects.

Tabatabaie et al. (2016) developed some analytical models to solve the NHDE in pressure-sensitive hydraulically fractured formations using the unsteady linear flow solution. The models were applied for the constant-pressure and variable flow rate and variable-pressure and constant-flow rate cases.

Sousa, Barreto Jr. & Peres (2016a) proposed a solution for the NHDE through GF's for the flow of real gases in porous media with constant permeability applied to formation tests, considering storage and skin effects. For the proposed model, the product viscosity-compressibility was considered dependent on pseudo-pressure. The reservoir was modeled as homogeneous, isotropic, and with infinite radial extension, and the well was considered vertical and represented by a line-source. The proposed model was also calibrated employing a commercial numerical simulator of well testing and the single and double integrals were made through a multidimensional numerical simulator package.

Sousa, Barreto Jr. & Peres (2016b) published a work that proposed an analytical model using pseudo-pressure function and GF's to study a finite-wellbore-radius solution for gas wells. In their work, they extended the theory in order to consider a finite-wellbore-radius (FWR) boundary condition for a vertical well with a Darcian constant gas flow rate. The product dynamic viscosity-total compressibility was rigorously modeled in the model, considering the nonlinearities in both variables. The model did not consider changes in permeability or skin and storage effects. Their work performed model calibration by a finite-difference gas reservoir simulator and agreed. They concluded that pseudo-pressure solutions using FWR boundary conditions do not match at early times. However, they agree to long flow times, representing the line-source wellbore solutions for slightly compressible fluids.

King, Wang & Datta-Gupta (2016) studied the unsteady pressure behavior during well testing and developed a model to compute pressure front in porous media defined as the maximum pressure driven by a source term and expressed by an Eikonal equation that is an asymptotic high-frequency solution for the partial differential equation of diffusivity for heterogeneous reservoirs. The solution to the Eikonal equation was developed using a class of solutions known as Fast Marching Method (FMM) for a Diffusive Time of Flight (DTOF) that models pressure front in the reservoir.

Almisned, Al-Quraishi & Al-Awad (2017) researched the effect of tri-axial stress on the absolute permeability of homogeneous and heterogeneous rocks. The absolute permeabilities of homogeneous and heterogeneous laminated rock samples were measured under hydrostatic and different laboratory-

simulated triaxial *in situ* stress loadings. Experiments were conducted using homogeneous, standard Berea and heterogeneous laminated sandstone cores (with lamination parallel to the flow direction). The effect of *in situ* stress variation on absolute permeability was investigated. This study presented a similar trend of permeability drop as axial load increases due to inferred matrix compaction. It has been concluded that absolute permeability changes due to lamination opening and closure due to loading magnitude and orientation. It is also concluded that the permeability of the formation is affected by heterogeneity depending on the direction of lamination, the state of the stresses applied, and the loading type.

Lonardelli et al. (2017) proposed a new geomechanical model for a case study about formation mechanical damage that integrates data from different supports and scales to obtain a reliable model. In their study, data *e.g.* well logs, injectivity tests, Leak-off Tests (LOT), and production history, as well as experimental rock mechanic tests, were considered.

Wang, Li & King (2017) presented a perturbative series expansion technique to solve the NHDE to compute the transient pressure of Multi-Fractured-Horizontal wells (MFH) and bounded reservoirs, considering the influence of stress sensitivity on reservoir formation and hydraulic fractures. This study was performed considering constant and variable flow rates and provided a direct relationship between the production data and the reservoir drainage volume. The model was calibrated using the Laplace transform method and a numerical flow simulator.

Wang & Xiangyi (2017) studied the application of the asymptotic expansion semi-analytical model to compute the solution of the three-dimensional (3-D) NHDE for many cases of heterogeneous porous media seeking to calibrate comparing with classical methods found in the literature. This study led numerous applications, *e.g.* fast numerical simulations, reservoir characterization, and inverse methods based on sensitivity analysis from production data. In this study, the authors extended the model to cases with wide variations in permeability and porosity of the reservoir, to fractured wells, for transient analysis of pressure behavior with storage and skin and unconventional reservoirs. The model it not only provides for direct calculation of various well-testing, rate transient, and well performance concepts *e.g.* depth of investigation, well-testing derivative, flow regimes, and well productivity, but the model can predict transient pressure and flux contour maps distribution.

Escobar, Bonilla & Hernández (2018) proposed a model based on the unique features of the pressure derivative plot to compute the distance for a discontinuity in anisotropic porous media from well-test interpretation.

The model considered a single-phase, slightly compressible oil flow, constant dynamic viscosity, and homogeneous reservoir. The solution was tested with two simulated examples and one field case example, and the results presented close convergence.

Ren & Guo (2018) developed a new analytical method based on Duhamel's principle to predict transient flow rate with variable permeability as a function of the rock stress state. The proposed analytical method was validated by comparing analytical flow-rate solutions for vertical wells with numerical flow-rate solutions. The production rates of a multi-stage fractured horizontal (MSFH) well with and without the effect of stress-sensitive permeability were obtained. A field case of an MSFH well was used to test the applicability of the proposed analytical method. It was found that the stress-sensitive effect negatively affected production rates of the MSFH well for the whole flow period, increasing with increasing drawdown pressure and permeability modulus. The proposed method is appropriate for various well types and reservoir scenarios.

Zhu et al. (2018) presented a 4D flow-geomechanical model of coalbed in Shouyang coal bed methane reservoir to investigate the permeability stress-sensitivity and stress evolution during depletion. However, the proposed solution required the use of a numerical method. A stress-dependent permeability model was proposed, and the nonlinear finite element analysis method was employed and highly developed as geomechanical simulator.

Wu et al. (2019) presented a paper where the dynamic threshold pressure gradient and permeability modulus were respectively utilized to characterize the low-velocity non-Darcy flow and permeability stress sensitivity. The dimensionless pressure and pressure derivative curve identified six flow regimes in this work. They were fracture-linear flow regime, early-transition flow regime, radial-flow regime, cross-flow regime, advanced-transition flow regime, and boundary-controlling flow regime, respectively. The work showed that the reservoir-stress-sensitivity and dynamic threshold pressure gradient greatly affected the dimensionless pressure and pressure derivative curves.

Jiang, Liu & Yang (2019a) developed a semi-analytical model for predicting the transient pressure behavior in a fractured horizontal well located in a naturally fractured reservoir. The model considered the permeability pressure-sensitive and non-Darcy flow effects. The results showed that the non-Darcy flow influenced the early-time bi-linear and linear flow regimes. It was also noticed that the stress-sensitivity effect played a significant role in the flow regimes beyond the compound-linear flow one.

Jiang, Liu & Yang (2019b) established a semi-analytical solution to quantify the combined effects of non-Darcy flow and stress sensitivity on the transient pressure behavior for a fractured horizontal well in a naturally fractured reservoir. The Barree-Conway model was used to investigate the non-Darcy flow behavior in the hydraulic fractures (HFs), while the permeability modulus was inputted into mathematical models to consider the stress-sensitivity effect. Therewith, the resulting nonlinearity of the mathematical models was weakened by using Pedrosa's transform formulation. It is found that non-Darcy flow mainly affects the early-stage bi-linear and linear flow regimes, leading to an increase in pressure drop and pressure derivative.

Ceia et al. (2019) presented a work about the relationship between porosity, permeability, and pore compressibility using experimental data analysis to provide empirical models that relate those properties. The results indicated that power-law models are appropriate for explaining such inter-dependence and bounced that pore compressibility as the key factor in describing the behavior of porosity and permeability of the rocks under external pressure.

Alfataierge et al. (2018), Miskimins (2019), Miskimins & Alotaibi (2019), Weijermars et al. (2020) conducted several studies about hydraulic fracturing design optimization and proppant transport in pressure-sensitive reservoirs. Some analytical and numerical models were developed, and, in some cases, the non-Darcyan flow was also modeled. Nonetheless, the solutions presented did not address either source/sink effects or geomechanical response coupled to permeability change.

Civan (2020) researched the effective-stress coefficients of porous media under shocks and loading/unloading conditions to evaluate the reservoir rock hysteresis. His work presented a correlation of Biot's coefficient controlling the bulk volumetric strain. Some experimental field data were used to couple physical properties in the proposed model, and simulate hysteresis and shocks response.

Zhang & Yang (2021) derived a semi-analytical technique to research the stress-sensitive effect on the transient pressure responses of a multiple-fractured horizontal well in an unconventional reservoir with an arbitrary shape. The authors used the boundary element method to simulate the flow behavior by incorporating the permeability modulus to consider the stress-sensitive effect to describe the flow behavior within the hydraulic fractures. The stress-sensitive effects of hydraulic fractures could be examined, and the corresponding pressure responses and pressure derivative curves were obtained.

Xu et al. (2021) formulated a model to approach the pressure transient analysis of the multi-stage fractured horizontal wells (MFHWs) with stress-sensitive effects. Laplace transform, pressure drop superposition, and Gaussian elimination were used to obtain the wellbore pressure solution for MFHWs. Comparison results reached high convergence by model validation. Based on pseudo-pressure derivative curve characteristics, eight flow regimes could be noticed: well storage, skin affection, bi-linear flow, early-linear flow, early-radial flow, middle-linear flow, inter-porosity flow, and later-radial flow regime.

Fernandes et al. (2021a), Fernandes et al. (2021b), Fernandes (2021a), Fernandes (2021b), Fernandes (2022), Fernandes (2021a), Fernandes (2021b), Fernandes et al. (2022a), Fernandes et al. (2022b) published various studies regarding evaluation of the permeability drop and its restoration as a function of the pressure for nonlinear oil flow. The solution for the NHDE developed was based on a coupled integro-differential-GF-model. For these works, a numerical porous media oil flow simulator was used for model calibration, and the results presented close accuracy. Nevertheless, the research of some effects of the deviation factor on permeability response were missing.

1.4

Scientific Methodology

A new analytical modeling of permeability loss during oil flow in permeability-pressure-sensitive reservoirs with source term is derived in this doctoral thesis. The proposed solution is based on the extension of the real gas flow in porous media theory, developed by Barreto Jr., Peres & Pires (2010). An extensive review of the scientific literature was conducted, and it was concluded that the model proposed by the aforementioned authors could be applied to model the permeability response during the oil's production curve to avoid uncontrolled-permeability loss and improve the well-reservoir performance.

A mathematical modeling was made to derive the new oil flow model with pressure-sensitive permeability with source term, and a new hydraulic diffusivity deviator factor $\xi(p)$ is presented. This factor provides the key information on the formation mechanical damage caused by the pressure-dependent permeability change.

The integro-differential solutions addressed in this work also identifies the permeability hysteresis phenomenon and the role of the production and shut-in time in the nonlinear term in the hysteretic response. The dimensionless instantaneous point-source is represented by a Dirac's delta function, the NHDE is expanded by a first-order asymptotic series, and a small perturbation parameter ϵ is introduced to handle the nonlinearity of the equation. The

pore pressure and permeability field data to input in the deviator factor were obtained from experimental works of Soares (2000), Soares, Freitas & Velloso (2001), Soares, Ferreira & Vargas Jr. (2002), Soares & Ferreira (2002). Their study used a uni-axial test to carry out the experiments of permeability change as a function of the pressure.

A flowchart is presented in Fig. 1.3 to represent the step-by-step of procedure to run the code developed in this work. This flowchart shows that the workflow to predict permeability response over the well-reservoir oil production curve is simple and, thereby, constitutes an attractive tool for field purposes.

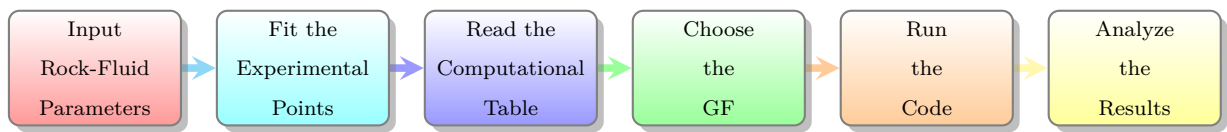


Figure 1.3: Computational methodology used to predict the mechanical formation damage in pressure-sensitive oil reservoirs with source term.

1.5

Thesis Organization

1. Chapter One: It consists of introducing the subject, where the relevance of scientific study in the context of petroleum engineering and state of the art is approached.
2. Chapter Two: It deals with the literature review, where the main published works are mentioned, as well as the methods used and the results obtained from the relevant works.
3. Chapter Three: Deals with the problem statement and the presentation of an overview of the subject.
4. Chapter Four: It approaches the general mathematical formulation, as well as the boundary conditions.
5. Chapter Five: Presents the integro-differential solutions for the problems with constant oil flow rate.
6. Chapter Six: Presents the integro-differential solutions for the problems with variable oil flow rates and also models the hysteresis phenomenon.
7. Chapter Seven: This chapter approaches the conclusions and future works.
8. Chapter Eight: It is composed of the references used in this thesis.

2

Literature Review

The unsteady-state reservoir geomechanical behavior of rock layers that constitute a petroleum system has been studied since the 40's by geoscientists and petroleum engineers to understand how the properties of rocks change depending on *in situ* state of stress (Terzaghi, 1943). Several researches related to the stress-sensitive permeability loss were also performed, mostly experimentally, caused by high costs and the absence of high-performance numerical software and rock-flow simulators (Kikani & Pedrosa Jr., 1991).

This chapter deals with main published studies on mechanical formation damage due to the change of permeability with *in situ* state of stress and pore pressure, as well as the coupling of this problem with the studies on solving nonlinear partial differential equation diffusivity for flow in porous media with pore pressure-dependent permeability, thus constituting the main problem to be solved in this work.

2.1

Formation Mechanical Damage Literature

Biot (1941) and Biot (1956) studied the pressure decay in wells during oil and gas production, and they noticed that it results in an increase of overburden effective stress in the porous matrix. Hence, this phenomenon may lead to permeability loss due to pore collapse.

Terzaghi (1943) showed experimentally that permeability is a function of effective rock stress. These dependencies should be considered in calculations for well and reservoir behavior predictions. The compressibility of sandstone grains is very small, and it cannot explain permeability and porosity decrease during the production period in real fields.

Everdingen & Hurst (1949a) presented an analytical solution based on Laplace transform for an unsteady hydraulic diffusivity equation with constant diffusivity. This solution indicated that once the pressure solution in the Laplace domain under constant-rate-production condition has been known, the flow-rate solution under constant-pressure-production conditions could be obtained.

Geertsma (1957) researched the effect of the pressure decline on the volumetric changes in a homogeneous and isotropic porous media, and the model was independent of the shape of the pores. The main conclusions obtained from this theory were that only three elastic constants and three viscous con-

stants are required for describing pore and rock bulk volume variations if the porosity is explicitly introduced into the treatment. In addition, reasonable approximations were introduced for various types of reservoir rock, *e.g.*, sandstones, limestones, and shales, which led to further simplifications of the basic equations.

Mc Latchie, Hemstock & Young (1958) investigated the effects of the reservoir compressibility on the permeability decline in limestones and sandstone samples. The rock's effective compressibility was measured by subjecting the core material to an overburden load and reducing the pore pressure. The results showed relatively high effective compressibilities for limestones and sandstones.

Gray & Fatt (1963) researched the effects of mechanical stress on reservoir rock parameters. They showed that the permeability anisotropy of several sandstones was a function of the overburden stress. Their study also showed that the permeability reduction of cylindrical samples of two sandstones, when subjected to mechanical stress, was a function of the ratio of radial to axial stress.

Wilhelmi & Somerton (1967) made measures of permeability variation in three types of sandstones (Berea, Boise, and Bandera) caused by the increase in deviating stress, in the triaxial cells, for different confining pressures. They showed that, in samples subjected to deviating stresses of 80% of the breaking stress, permeability reduction was greater in magnitude than the change in porosity. Reductions in permeability were in the order of 10 to 20% for the Berea and Bandera sandstones and were in the 65% range for the Boise sandstone. The same occurred for hydrostatic loading, with greater changes in permeability than in porosity. It is perceived, in their work, that the permeability variation depends on the stress path of the test.

Risnes *et al.* (1982) computed an analytical solution to the wellbore stress using a formulation theory of poroelasticity and plasticity. In their work, they showed that a plasticized zone would be developed in a sufficiently weak formation under certain stress conditions. This zone would increase in extension as the pressure of pores in the wellbore decreased (increasing the effective stress in the rock), with a limit higher in the flow over which the formation will reach a state of total collapse. They believed that the plasticized zone could represent a possible source of production of sand, which in turn is undesirable for petroleum engineering.

Holt (1990) presented a work that has its reference in many works on the dependence of the permeability to the state of stress. Tests were carried out with different stress paths and verified the dependence of the

permeability to the state of stress for high porosity sandstones and the North Sea permeabilities.

Teufel et al. (1993) performed a wide of permeability studies for a naturally fractured chalk reservoir in the North Sea and demonstrated the strong influence of horizontal stress anisotropy on fracture conductivity and reservoir permeability. In this study, they used the stress path concept. For them, hydrostatic loadings are not representative of reservoirs that follow non-hydrostatic stress paths. The stress paths were represented by the relationship permeability between Biot's effective horizontal and vertical stresses.

Celis et al. (1994) used the permeability modulus definition to solve the NHDE analytically for an unsteady and pseudo-steady state oil flow in a naturally fractured-stress-sensitive porous media.

Zhu & Wong (1996) presented a work in which they studied the permeability behavior in Berea sandstones when subjected to swelling, that is, a state of stress such that it causes an increase in porous volume due to the appearance of micro-cracks in the rock. The dilation was expected to cause an increase in permeability.

Sa & Soares (1997) published a work about the rock parameters determination to evaluate the wellbore stability problems in Marlim and Albacora fields, both located in Campos Basin in Brazil. These fields produce from unconsolidated sandstones. Based on a reservoir study performed with a numerical simulator, horizontal wells drilled in such formations are suggested to be more practical and cost-effective than vertical wells. This study developed two different procedures to prepare core samples from that unconsolidated sandstone.

Keaney, Meredith & Murrell (1998) carried out tests on heavily cemented sandstones with very low permeability, using the transient pulse measurement technique of permeability in hydrostatic and non-hydrostatic tests. Tests have shown that permeability depends on a complex interaction between the history of hydrostatic stresses and not hydrostatic.

Yale & Crawford (1998) presented a work on pore collapse showing that the permeability depended on the stress path. Were performed tests on limestone rocks, where they used a formulation named the *critical state model* to obtain the plasticity of the material. Their work concluded that the permeability variation was strongly related to the relative contribution of compaction and micro-fractures it produced.

Davies & Davies (1999) carried out works relating the permeability as dependent on the state of stress for unconsolidated and high sandstone porosities and consolidated reservoirs. Bouteuca, Sarda & Vincke (2000)

presented a constitutive equation for sandstone permeability changes over the well-reservoir life cycle. This research proposed a differential equation based on the permeability decline as a function of the vertical and horizontal stress difference. The results were similar to the presented in the literature, and they noticed that, for small permeability evolution, the exponential decline based on the permeability modulus definition was appropriate.

Soares (2000), Soares, Freitas & Velloso (2001) and Soares & Ferreira (2002) carried out a series of experimental tests, in which they studied the behavior stress-strain, with flow and velocity measurements of elastic compressive and shear wave propagation, to evaluate the effects on the permeability and the occurrence of pore collapse for ductile behavior reservoirs.

Jones et al. (2001) presented some studies of the petrophysical properties of the sandstone rocks to obtain the correlations for the permeability prediction. The experimental studies measured compressional wave velocity, porosity, permeability, and electrical resistivity. The measurements presented a high degree of stress sensitivity for some sandstone cores. The work provided a classification from the less sensitive to the more sensitive rock samples.

Soares, Ferreira & Vargas Jr. (2002) presented an experimental work about the mechanical damage through triaxial tests that were carried out in different stress paths, with measurements of P and S-wave acoustic velocity and permeability, to evaluate the effect of the permeability decline as a function of the pore pressure. The authors developed an analytical model using a permeability function as input in the nonlinear hydraulic diffusivity equation in this study. This methodology allowed near-wellbore evaluation and permeability investigations using a stress-path concept. Usually, reservoir engineers do not consider the effect of *in situ* stresses on production, considering that permeability is constant during reservoir oil production. Nevertheless, this assumption is not valid for limestone and unconsolidated sandstone *e.g.* deepwater reservoirs in the Campos Basin.

Gonzalez, A. & Cinco-Ley (2006) developed a mathematical model to study the behavior of a well with variable finite-conductivity and skin fracture for a vertical fracture in an infinite reservoir. The solution was valid for slightly compressible fluid and real gases applying the pseudo-pressure definition. A field test was analyzed to detect the changes in the properties. The authors concluded that the model was a useful tool for analyzing real cases when the fracture properties were affected during the well's productive life.

Bedrikovetsky et al. (2009), Reid et al. (2009), Nunes et al. (2009), Correa et al. (2013), Souza, Farias & Carvalho (2013), Souza & Falcão (2015), Souza (2016) combined analytical solutions and experimental studies to deal with

the formation damage minimization in oil and gas reservoirs to improve the well-reservoir performance. The results showed high accuracy in respect to the experimental measurements.

Yao, Zeng & Liu (2013) derived a semi-analytical model for the transient pressure analysis in hydraulically fractured Wells With stress-sensitive conductivities. The hydraulic fractures were discretized into several slab source segments. The results showed that, as the fracture conductivity decreases, the pressure and corresponding pressure derivative curves rise quickly, and when the conductivity declines to the minimum value, the increasing pressure drop slows down.

Zhang et al. (2014) developed a model to predict the pressure behavior of vertically fractured wells with stress-sensitive conductivity. They presented a new function to model the fracture permeability changes concerning the pore pressure. It was concluded that the stress sensitivity behavior of a producing fractured well could not be determined from a single build-up test.

2.2

Analytical Solutions for Nonlinear Flow through Porous Media Literature

Theis (1940) used the Kelvin (1882) line-source solution to wellbore study of the unsteady Darcian flow in an infinite radial porous media near aquifers with constant flow rate.

Al-Hussainy, Ramey Jr. & Crawford (1966) studied real gas flow in porous media and realized that the pseudo-pressure solution and liquid solution approximately match during early times and for low gas-flow rates during unsteady flow. However, for a long time, they deviate from each other.

Gringarten & Ramey Jr. (1973) presented work about using GF's and Newman's product methods to solve unsteady flow in petroleum reservoirs. Their model assumed small pressure gradients, constant permeability, porosity, and fluid dynamic viscosity. The model developed was based on point-source as part of the more general theory of GFs to solve difficult flow problems. In this model, the strength of point-source is the oil flow rate instantaneously withdrawn from the reservoir rock at a point as a function of time and the source location.

Brace (1977) developed some experimental models of permeability porosity-dependent based on pore shape, hydraulic radius, and formation factor for some types of sandstones, ceramics, and granites. He also used the input data from well resistivity logging to predict permeability for these types of rocks. In his research, he noticed that permeability could also change as a function of stress.

Samaniego, Brigham & Miller (1977) performed research about the influence of pressure-dependent fluid properties and stress-sensitive rock properties on pressure transient analysis for a single-phase flow in porous media. The model was based on a pseudo-pressure function evaluated in the wellbore (unity dimensionless radial distance). The study considered a wide value of flow rates, boundary conditions, and geometries. They noticed that for all practical production rates and most boundary conditions, the pseudo-pressure solutions, in terms of dimensionless pseudo-pressure, were essentially the same as the conventional line-source solution that has been documented for slightly compressible liquid flow.

Pedrosa Jr. (1986) used a new variable related to the pressure to decrease the nonlinearity of the seepage model with the stress-sensitive effect and proposed a pressure solution with a first-order approximation based on the perturbation technique. Nevertheless, source effects were not simulated in his study.

Peres, Serra & Reynolds (1989) derived a closed-form analytical solution through Boltzmann transformation that satisfied pseudo-pressure NHDE for a line-source well in an infinite and homogeneous gas well. They realized that two or three iterations were enough to reach the convergence. Their study wrote the dimensionless general pseudo-pressure solution as a slightly compressible fluids solution plus a correction with the nonlinearities caused by dynamic viscosity-total compressibility product variation.

Kikani & Pedrosa Jr. (1991) developed an analytical model based on the perturbation technique and the permeability modulus to derive the pressure solution with third-order approximation considering the stress-sensitive effect in a field study. The solution considered the effects of storage, skin, and boundary. The results showed that the third-order expansion was of the same order of magnitude as the second-order term. Hence, it was included in the solution of the NHDE.

Wu & Pruess (2000) presented an integral model for studying unsteady-state fluid flow through a porous media with pressure-dependent permeability. Approximate analytical solutions have been obtained for one-dimensional linear and radial flow by an integral-solution technique, in which the density of the fluid, and the porosity and permeability of the formation, are treated as arbitrary functions of pressure.

Barreto Jr., Peres & Pires (2010) studied real gas flow in porous media near a sealing fault represented by a linear no-flow boundary across the reservoir, using GF's. This study showed that, for early times, i.e., before the fault presence affects the well behavior, a *semi-log plot* of wellbore pressure

versus dimensionless time showed a straight line whose slope m is inversely proportional to formation permeability.

Barreto Jr., Pires & Peres (2012) proposed a pseudo-pressure to research the real gas flow in a fractured porous media using GF, and they concluded that the general solution was expressed by the sum of the slightly compressible flow solution plus a corrective first-order term of the series expansion. The results showed high convergence in comparison to the numerical gas flow simulator.

2.3

Nonlinear Oil Flow in Hydraulically Fractured Wells Literature

Clark (1949) researched the hydraulic fracturing procedure to improve the oil flow in petroleum reservoirs, and he concluded that the reservoir stimulation using the hydraulic fracturing technique had less associated costs than the acidizing one.

Howard & Fast (1957) used the classic Carter's equation for the area of a hydraulic fracture as a function of uniform average width, fluid injection rate at the wellbore, the fluid loss rate into the formation, and elapsed time. They noticed that the explicit form of the solution of Carter's equation would depend on the functional representation of the fluid loss.

Warpinski et al. (1981), Warpinski et al. (1981), Warpinski et al. (1982), Warpinski, Schmidt & Northrop (1982), Warpinski, Branagan & Wilmer (1985) carried out a series of field experiments to research the *in situ* stresses and geological discontinuities that influence the growth of the hydraulic fracture.

Nolte & Smith (1981) presented a work about the pressure interpretation to identify periods of confined-height extension, uncontrolled height growth, and critical pressure during hydraulic fracture manufacturing. However, source term and permeability loss management were not researched in this work.

Cinco-Ley & Samaniego (1977), Cinco-Ley & Samaniego (1981), Cinco-Ley (1981), Cinco-Ley & Samaniego (1982) developed a new technique for analyzing hydraulically fractured wells with a finite-conductivity fracture. The approach used the pressure and pressure derivative methods for cases with no fracture skin and no wellbore storage and cases with fracture skin and wellbore storage during the bi-linear-flow period. New type curves were presented and applied to some field cases. The proposed model concluded that using the pressure derivative with pressure-behavior type curves reduces the uniqueness problem in type-curve matching and gives greater confidence in the results.

Nolte (1988) published a work about the fluid flow within the hydraulic fractures, approaching the key considerations to provide an efficient hydraulic fracturing treatment. This work considered the effects of slip flow, the proppant

role in the fluid's dynamic viscosity, fracture width variations on the velocity profile, and the pressure gradient, among others.

[Ozkan & Raghavan \(1991\)](#) derived various analytical solutions for hydraulically fractured oil and gas wells with source term. In their approach, they used Laplace transform and the source/sink term was modeled through Green's functions (GF's) for fractured well-reservoir setting. Nevertheless, they did not couple geomechanics effects to the flow model.

[Rodríguez, Cinco-Ley & Samaniego \(1992\)](#) formulated a graphical technique to evaluate the asymmetry of hydraulically fractured wells. This technique is based on a new analytical solution for the pressure behavior of a finite-conductivity, asymmetrically fractured well during the pseudo-linear flow period, and the known bi-linear flow solution. A semi-analytical solution for transient flow toward finite-conductivity, asymmetrically fractured wells producing at a constant rate is also presented. This solution was used with the analytical solution to analyze the pseudo-linear flow pressure behavior. An expression relating dimensionless fracture conductivity and asymmetry factor was developed by combining the pseudo-linear and bi-linear flow solutions. Nevertheless, the proposed solution required a numerical method to solve the NHDE and they did not approach permeability change effects.

[Warpinski et al. \(1993\)](#) analyzed a cored hydraulic fracture in a gas well in two different intervals to investigate the abnormal fracturing pressuring occurrences, fracture height growth, and proppant transport. However, this study did not evaluate permeability change and source effects.

[Raghavan, C. & Agarwal \(1997\)](#) presented a mathematical model to evaluate the characteristic responses of a multiply-fractured horizontal well. A systematic discussion of pressure behaviors and new interpretations and conclusions were provided. The consequences of perforating selective sections after fracturing were also examined, and the pressure behaviors were used to analyze the responses of a field test. The test was conducted on a medium-radius horizontal well completed in a dolomite/anhydrite formation with a 1900 feet of horizontal section. Four distinct intervals were perforated and individually stimulated. Despite the results presented being accurate, geomechanical-flow coupling was not approached, and permeability was considered constant.

[Chin, Raghavan & Thomas \(2000\)](#), [Raghavan & Chin \(2004\)](#) derived a fully coupled geomechanics and fluid-flow model to analyze pressure-transient problems in stress-sensitive reservoirs with nonlinear elastic and plastic constitutive behavior. This study presented several practical applications illustrating various aspects of well behavior of stress-sensitive reservoirs. Nonetheless, the proposed model did not address the source/sink term and required using a

numerical method, which may raise computational costs.

Daneshy (2004), Daneshy et al. (2004) presented the concept of off-balance growth to deal with the hydraulic fractures deviation from the classical bi-wings shape. This research could verify that the fracture propagates according to the least resistance local path, not the global path. This work also showed that this *in situ* stress state may lead to the fracture branch, shear fractures, and growth pattern dominated by the tip conditions of the hydraulic fracture. Finally, it was noticed that these effects could significantly influence the fluid flow and proppant transport within the fracture, as well as the reservoir production.

Daneshy (2007) researched the impact of the fluid pressure inside the hydraulic fracture and noticed that the hydraulic fracture conductivity is extremely nonuniform, having high values near the wellbore and becoming low in the middle sections and in the fracture tip. This study also verified that the fluid pressure and fracture width drop significantly along the fracture length.

Adachi et al. (2007) proposed an analytical model for the fluid flow inside the hydraulic fractures based on the lubrication Reynolds theory, and this formulation is used in many works to calibrate new numerical and analytical models.

Ozkan et al. (2009) proposed a discussion of fractured horizontal well performance in conventional and unconventional reservoirs, and it provided interpretations of the objective of fracturing horizontal wells in both formations. A tri-linear-flow model showed that the drainage volume of multiply-fractured-horizontal-wells was limited to the inner reservoir between the fractures even for relatively large matrix permeabilities. In any case, the formulation proposed did not approach stress-sensitive responses, as well as the role of the source/sink term in the final solution of the NHDE.

Kuchuk & Biryukov (2013), Kuchuk, Morton & Biryukov (2015), Kuchuk, Morton & Biryukov (2016) investigated the rate and pressure-transient behavior of multistage fractured horizontal wells in conventional and unconventional homogeneous and naturally fractured reservoirs, the latter of which can contain any spatial distribution of finite or infinite-conductivity fractures of arbitrary length and orientation. The number and type of fractures (hydraulic or natural) intersecting the wellbore and self-intersecting were unlimited. They showed that many factors dominate the rate transient behavior of horizontal wells intersected by multiple hydraulic fractures in naturally fractured reservoirs, *e.g.* fracture conductivity, length, and distribution, as well as whether or not fractures intersect the wellbore. Nonetheless, the model derived in this work did

not consider permeability change, source/sink term, and geomechanical effects.

2.4

Pressure Transient Analysis and Well-Testing Literature

Muskat (1937) studied the relationship between the bottom hole pressure, fluid level, and permeability prediction. This work proposed a quantitative and qualitative analysis based on a partial differential equation relating pressure and fluid level rate. The differential equation solution was plotted in a *semi-log plot* to predict the permeability of the reservoir.

Horner (1951) presented a study of the pressure build-up testing and showed that the pressure in the build-up period was a linear function of the logarithm of the shut-in time. In the *semi-log plot*, known as Horner plot, he showed that the straight line slope was inversely proportional to the rock permeability.

Cunningham & Nelson (1967) derived a new method for estimating *in-place* hydrocarbons from pressure build-up tests. This method was applied to actual well-test data. A derivative application of the method was described for calculating the stabilization time of gas wells with well-defined production-pressure decline curves from which reliable estimates of gas *in place* could be made.

Ramey & Cobb William (1970) presented a general pressure build-up theory for a well in a closed drainage area. The model was based on constant permeability, porosity, rock and fluid properties, uniform reservoir thickness, and small pressure gradients.

Agarwal, Al-Hussainy & Ramey Jr. (1970) proposed an analytical model to investigate the storage and skin effects in the transient oil flow in a well during the short-time well-testing analysis. In this work, they realized that the steady-state skin effect concept was not valid for a short time. They also concluded that the time required to reach the straight line is normally not affected significantly by a finite skin effect. The method allowed normalizing the field data in order to use the existing drawdown-type curves.

Ramey Jr. (1970) presented a study of the early-times flow and build-up periods to characterize the wellbore storage, skin effects, and fractured reservoir zones. The research was based on the interpretation of the testing through field examples. In this work, he noticed that the storage effect provided a difference in the oil flow rate at standard conditions from the sand face. He also realized that the storage could occur by the fluid compression in a completely filled wellbore or through a movement of a gas-liquid interface.

Gringarten & Ramey Jr. (1974) studied the well-testing applied to

the unsteady-state pressure distributions created by a well with an infinite-conductivity vertical fracture. This study presented an analytical GF model that considered the vertical fracture penetrating a horizontal, homogeneous, and isotropic reservoir. They also considered that the production pressure was uniform over the fracture. The external boundary condition established that the pressure was kept constant and equal to the initial pressure as the distance from the well became infinitely large.

Gringarten, Ramey Jr. & Raghavan (1975) compared the applicability of type-curve and conventional *semi-log* methods. This study approached two boundary conditions: firstly, the fracture plane is of infinite conductivity. This implies that there is no pressure drop along the fracture plane at any instant in time. The second approach, known as the uniform-flux solution, gives the appearance of a high, but not infinite, conductivity fracture. Therefore, the pressure along the fracture plane changed. The application of these solutions to field data indicated that the uniform flux solution usually provides a more realistic pressure behavior of wells intersecting natural fractures.

Cobb & Smith (1975) developed two methods of pressure build-up analysis for bounded reservoirs. The pressure build-up data for various well locations within various rectangular drainage shapes were generated, and the results were plotted according to both methods investigated. The resulting curves were studied for diagnostic features and rules. Basically, the test required that a producing well be shut in and that the associated change in bottom-hole pressure is measured as a function of shut-in time.

Gringarten et al. (1979) published a comparative study between the different skin and wellbore storage type-curves for transient analysis during the early-times. The work investigated the relationship between classic and new interpretation methods for pressure response. It has been shown that the classic methods constitute a small set of the techniques available for interpretation, and therefore provide only limited results compared to what can be obtained with all the different methods specific to the various flow regimes identified on the test data.

Agarwal (1980) proposed a new method to eliminate the production's time influence when the drawdown type curves were used to predict the build-up behavior during well-testing operations. The presented method could be applied to fractured and non-fractured wells and evaluate the skin and storage effects. The method was based on comparing the magnitude of the production time and the shut-in time.

Blacker (1982) presented the results of the perforating program for the first forty wells in the Kuparuk River Field in Alaska. Several different types of

perforating guns were used to perforate the wells at varying shot densities. The pressure transient tests were conducted on each well to measure skin damage and flow efficiency. A method of analysis was presented that allowed non-Darcy flow skin factors to be calculated when gas saturation was also causing a skin effect. It was noticed that, during the early times of development of the field, the wells had unusually high formation damage as determined from pressure build-up tests.

Cinco-Ley & Samaniego (1982) proposed new methods for interpreting pressure transient tests for wells in naturally fractured reservoirs. This work demonstrates that the behavior of a naturally fractured reservoir could be correlated by using three dimensionless parameters. Some information was provided on estimating fracture area per unit matrix volume or matrix parameters from the transition period *trans-log* straight line. It was also shown that matrix geometry might be identified when pressure data are smooth.

Gringarten (1984) researched the reservoirs' double-porosity behavior, *e.g.* naturally fissured reservoirs and multilayered reservoirs with high permeability contrast between layers. The first part of the work presented the available solutions to the hydraulic diffusivity equation. The second part discussed the methods for solving the inverse problem, *i.e.* identifying a double-porosity behavior and evaluating all corresponding well and reservoir parameters.

Aguilera (1987a) presented approximate solutions of radial flow for pressure-build-up analysis in naturally fractured reservoirs with tectonic pressure build-up analysis in naturally fractured reservoirs with tectonic, regional, and contractional fractures. The solutions were satisfactory for most cases of practical interest. The author concluded that a conventional pressure plot on Cartesian coordinates should result in two parallel straight lines with a transition period that depends on the shape of the matrix blocks.

Aguilera (1987b) researched a well-testing in naturally fractured reservoirs, and the methods used in this work allowed to compute important parameters *e.g.* investigation radius, storage capacity coefficient, skin, fracture porosity, and transmissivity, among others.

Ayan & Lee (1988) developed a two-dimensional, three-phase variable bubble point reservoir simulator to simulate pressure build-up tests involving multiple phases. The model runs indicated that non-uniform saturation distributions throughout the drainage area could cause erroneous interpretations when single liquid phase techniques were used during the analysis.

Rahim & Lee (1989) presented an iterative technique for interpreting early-time pressure-build-up data for hydraulically fractured wells. The technique used a modified square-root-of-time analysis with permeability and

fracture-length correction curves from the flow equations for finite-conductivity fractures. The method was applied to low-permeability reservoirs.

Blasingame & Lee (1989) presented a new method of estimating a constant-rate analog for a variable-rate flow followed by a build-up test. The time and rate were analog to the generation of a conventional Homer plot for the build-up test. The approximation solution was derived rigorously from the Horner and variable-rate superposition equations. The method has been verified for several variable-rate schemes with a finite-difference numerical simulator.

Bourdet, Ayoub & Pirard (1989) developed an interpretation method based on the analysis of the time rate of change of pressure, together with the actual pressure response. A differentiation algorithm was proposed, and several field examples were provided to illustrate how the method simplifies the analysis process. This algorithm's development made the well-test interpretation easier and more accurate.

Peres, Onur & Reynolds (1989) presented a new method for determining formation flow capacity and skin factor from slug test. The new procedure was based on an exact deconvolution equation that converts the measured slug test pressure data into an equivalent pressure response that would be obtained if the well were produced at a constant surface flow rate. The new technique did not require knowledge of the sand face flow rate and did not depend on the flow regime within the reservoir.

Jones & Seetharam (1990) developed a new technique named as Maximum Rate Horner (MRH) method to analyze the data from pressure build-up tests with significant after flow. It could also be used when the build-up period was preceded by sequentially declining variable rates. This method plotted the pressure against a modified Horner time, defined using the effective flowing and build-up times.

Johnston & Lee (1991) proposed applying the deconvolution method to analyze wellbore storage distorted pressure build-up test data from low-productivity gas wells. As gas wells generally require long times to reach the correct *semi-log* straight line, the deconvolution method removed the effects of wellbore storage and allowed for the process removes the effects of wellbore storage and allows for the use *semi-log* analysis. The method has shown that the time required for build-up tests could be reduced by more than an order of magnitude with no loss in accuracy in results.

Robinson et al. (1991) approached the pressure transient testing and stimulation treatment programs for four development/exploratory programs presented for four development/exploratory wells located in the River Basin.

While pressure build-up tests conducted during initial completion yielded relatively high permeabilities and severe skin for all but the initial well, core analyses yielded much lower permeabilities and suggested low susceptibility to permeabilities and damage susceptibility. The core data were discounted, and the build-up test data were relied upon to design small hydraulic fracture treatments to overcome suspected near-wellbore damage. As a result of the treatments, significant productivity increases occurred, which verified the build-up interpretation.

Ramey Jr. (1992) approached the main advances in the practical well-testing analysis using type curves and derivative methods. In his work, it was demonstrated that the use of both methods provided reasonable results when compared to field data.

Liao & Lee (1993) presented an equivalent drawdown time for hydraulically fractured wells. This new equivalent time was derived from a general elliptical flow model. This new variable was helpful in the post-fracture pressure build-up test analysis for wells with finite-conductivity fractures, including wellbore storage and fracture-face skin.

Ambastha & Ramey Jr. (1993) published a work about the drawdown and build-up pressure derivative type-curves for a well producing at a constant rate from the center of a finite, circular reservoir. Early-times response (wellbore storage and skin effects) and late-times response (outer boundary effects) were approached. The outer boundary may be closed or at constant pressure. Design relations were developed for the time to the beginning and the end of infinite-acting radial flow. Producing time effects on build-up response were also discussed.

Agarwal et al. (1999) developed new production decline curves for analyzing well production data from radial and vertically fractured oil and gas wells. These curves have been developed by combining decline-curve and type-curve analysis concepts to result in a practical tool that we feel can more easily estimate the gas (or oil) in place and estimate parameters *e.g.* reservoir permeability, skin effect, fracture length, conductivity. The accuracy of this new method has been verified with numerical simulations, and the methods have been used to perform analyses using production data from several different kinds of gas wells. Field and simulated examples are included to demonstrate the applicability and versatility of this technology.

Brown, Sawyer & Frantz (2004) presented an algorithm for computing the pressure response for a well with constant wellbore storage and non-Darcy skin factor across the completion. The algorithm has been used to generate type curves for drawdown and build-up tests. The effective skin factor was graphed

as a function of flow rate, allowing the Darcy and non-Darcy components to be determined from a straight-line fit through the data.

Schroeter & Gringarten (2004) developed a new time-domain method for the deconvolution of well-testing data. The resulting separable nonlinear TLS problem was solved using the Variable Projection algorithm, and comprehensive error analysis was presented. The work also included tests with a simulated example and an application to large field examples.

Ehlig-Economides & Wells (2005) proposed a method to predict the average pressure in horizontal wells located in bounded reservoirs during a build-up test. The method used a general solution for the horizontal well arbitrarily located in a rectangular drainage area, the pressure curves were provided for the difference between the average pressure and the extrapolated pressure from the linear flow trend in the pressure build-up data. Knowing the production time before the build-up, the well position, and drainage volume shape, and the extrapolated pressure from the linear flow trend determined from the pressure build-up data, the new horizontal well correction plots allowed the estimation of average reservoir pressure. Correction plots have been determined for various horizontal well positions and reservoir shape combinations.

Ehlig-Economides, Nduonyi & Abiazie (2006) presented work about the design considerations for horizontal and vertical permeability determination from a conventional pressure build-up test. A standard limited entry model for the pressure transient behavior was used to determine the timing for the transient interpretation's start and end of key flow regimes. Equations that can be used to design a test for vertical permeability determination were also used to indicate ranges of the reservoir, fluid, and well properties that result in a successful test.

Schroeter & Gringarten (2007) investigated the superposition principle applied to non-linear problems. However, the author simplifies the problem by considering beforehand the diffusivity term η as a constant.

Gringarten (2008) published a review of the evolution of well-testing analysis techniques from the straight line plots until the deconvolution theory. This work concluded that the reliability of the transient data interpretation was significantly increased with the deconvolution theory.

Onur et al. (2008) investigated the deconvolution methods presented in the literature. It was verified that the presented works offered new solution methods to the long-standing deconvolution problem and made deconvolution a viable tool for well-test and production-data analysis. However, no study presented an independent assessment of all these methods, revealing and

discussing specific features associated with the use of each method in a unified manner. In this work, three synthetic cases and one field case were studied.

Onur, Ayan & Kuchuk (2009) researched the use of pressure-pressure (p-p) deconvolution to interpret conventional multi-well interference and interval pressure transient tests. It is shown that the recent deconvolution algorithms developed for pressure-rate (p-r) deconvolution could also be used for performing p-p deconvolution by simply replacing the rate data in p-r deconvolution algorithms with the pressure change data recorded at the source/sink location or at one of the observation locations.

Onur et al. (2011) presented a new spherical-flow cubic-analysis procedure for estimating horizontal and vertical permeabilities from pressure-transient data acquired at an observation probe of a dual-packer-probe wireline formation tester. It is shown that the procedure provided unique estimates of horizontal and vertical permeabilities from observation-probe pressure data obtained along both vertical and horizontal wellbores.

Deng et al. (2015) presented a general method for analyzing pressure build-up data from a well located in a multi-well reservoir. This work analyzed the effect of multi-well interference on the pressure build-up curve. The method was obtained with the superposition principle and is general in dealing with any combination of producing, injecting, or shutting in conditions of testing well and adjoining wells.

2.5

A New Analytical Model to Mechanical Formation Damage Management During Oil Flow in Pressure-Sensitive Reservoirs

Even though various authors have researched the nonlinear flow through porous media, there are many lacks in the mathematical modeling of the oil flow with source terms in pressure-sensitive reservoirs with variable permeability in the reservoir literature.

This doctoral thesis extends the theoretical formulation for real gas flow through porous media developed by Barreto Jr., Peres & Pires (2010), Barreto Jr., Pires & Peres (2012), Sousa, Barreto Jr. & Peres (2016a), Sousa, Barreto Jr. & Peres (2016b) and derives a new integro-differential solution for the oil flow through permeability pressure-sensitive reservoirs with oil source term.

The works from Soares (2000), Soares, Freitas & Velloso (2001), Soares, Ferreira & Vargas Jr. (2002), Soares & Ferreira (2002) mention that permeability pressure-sensitive effect is caused by the fact that, as the well begins its production, the pores of the reservoir rock tend to collapse, causing formation mechanical damage and reducing its permeability. This phenomenon

occurs because, when removing the mass of fluid from inside the pores, the viscous damping caused by pore pressure is lowered. Thereby, the overburden stress acting on rock layers increases the compaction of the reservoir rock. As a result of the pore pressure decay during well-reservoir production's life-cycle, the overburden Biot's effective stress in the rock matrix increases. The effect of the permeability loss during the reservoir life-cycle is investigated for several well-reservoir settings to provide adequate formation mechanical damage control and prevent the impairments caused by severe uncontrolled permeability decline.

A new hydraulic diffusivity deviator factor representing the permeability loss phenomenon is derived and coupled to the NHDE using the well-known perturbative technique. A permeability-based pseudo-pressure function is proposed to represent the permeability loss, and the general solution is developed in terms of this function in the dimensionless form.

3 Problem Statement

Mechanical formation damage control plays a fundamental role in the appropriate well-reservoir performance management since uncontrolled reservoir compaction may lead to severe oil production losses, resulting in economic impairments (Soares, Freitas & Velloso, 2001). This thesis develops a new model to predict the mechanical damage caused by the permeability loss during the oil's production period and its full and partial restoration when the well is shut. The field data from two sandstone reservoir layers named case study A and case study B, which constitute two layers of the same sandstone reservoir, are researched, and some fitting functions are proposed.

As mentioned in chapter 1, the general solution for estimating permeability loss as a function of the production time is expressed by the sum of the constant permeability solution $p_D(r_D = 1, t_D)$ and the nonlinear term $m_D^{(1)}(r_D = 1, t_D)$, that considers pressure drop, and pressure-sensitive permeability response. The dimensionless permeability loss curve as a function of the dimensionless linear solution during production time is illustrated in Figure 3.1.

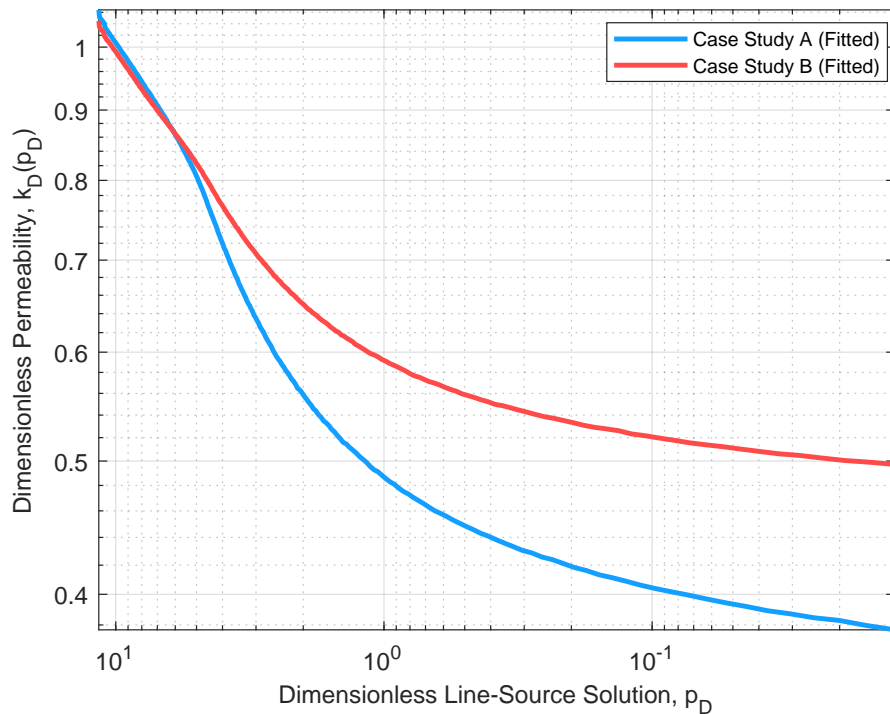


Figure 3.1: Log-log plot of the dimensionless permeability loss as a function of the linear solution over the well-reservoir life-cycle.

Since the dimensionless pressure drop assumes negative values, this curve

presents its absolute values $|p_D|$, and it was built through the field data from both case studies. Figure 3.2 presents a sketch of a vertical well of radius r_w that fully penetrates two sandstones layers with thickness h_a and h_b of the same reservoir. The rock layers a and b have permeability at initial pressure values of $k_a=340$ md and $k_b=170$ md, respectively. The figures illustrate the oil flow in two periods separately. Before the start of the production, the Standing Valve (SV) placed inside the production tubing is shut (no production rate). To start the well production, the packers P1 and P2 are placed into the annular space between the production tubing and the wellbore.

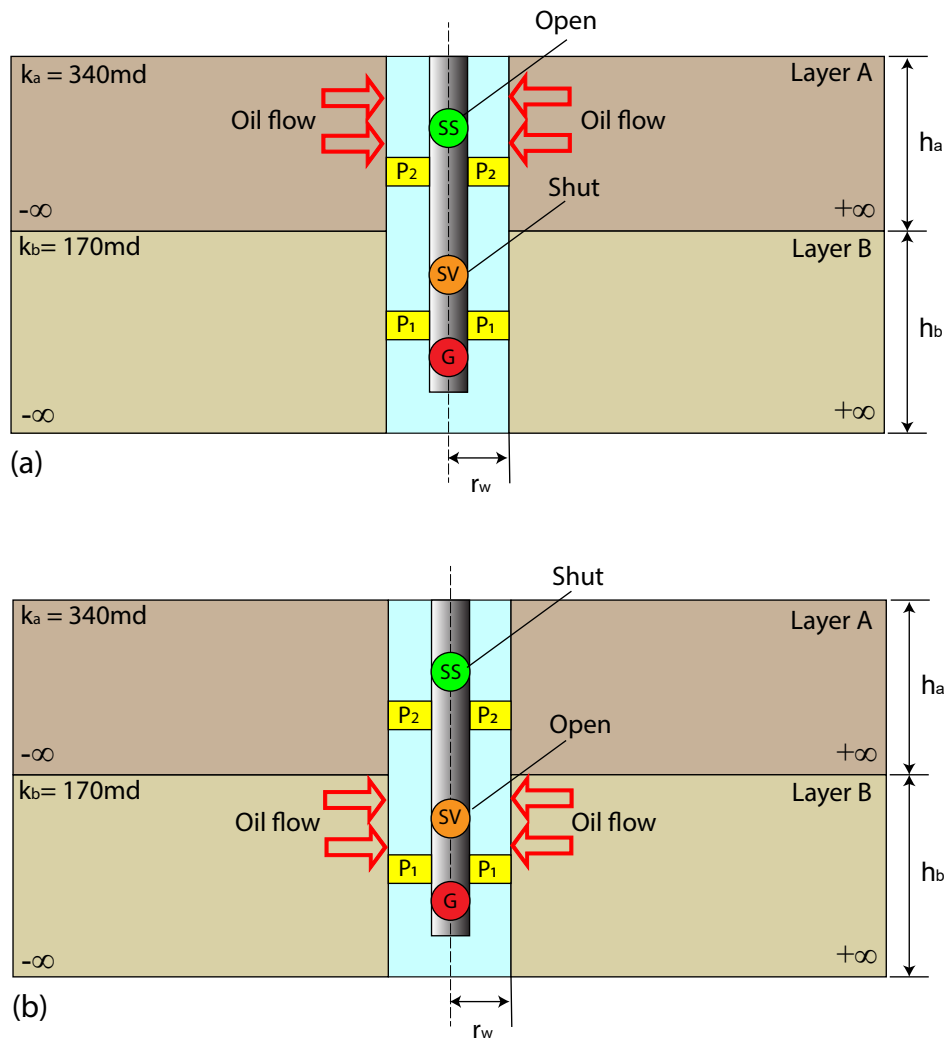


Figure 3.2: Sketch of oil production from the reservoir layers A and B separately (no interlayer cross-flow). (a) Oil production from layer A, and the layer B shut by standing valve (SS). (b) Oil production from layer B, and the layer A shut by standing valve (SS).

As the model developed in this work approaches each reservoir layer separately (no interlayer cross-flow), a Sliding Sleeve (SS) must be placed inside the production tubing to provide selectivity between the reservoir layers.

Initially, the well is filled by the completion fluid, and before the packer inflation, there is no oil flow from the formation towards the wellbore (no production). The completion fluid no longer damps the well when the packer is inflated. Hence, a Stand Valve (SV) must be placed inside the production tubing to keep the well shut (no production rate).

The pressure gauge (G) records the drawdown flow in real-time over the well-reservoir life-cycle (Fernandes, 2021b). As the well produces, the pressure inside of the pores in the formation decreases due to the removal of the mass of fluid contained within it. As a result, the term responsible for damping the overburden stresses applied in the formation loses intensity, and it provides a decline in the reservoir's permeability caused by the collapse of the pores. The grains that constitute the reservoir rock are accommodated in such a way that their permeability favors the flow of oil from the pore space towards the wellbore, (Fernandes et al., 2021b). This arrangement is due to the Biot's damping caused by the oil inside the pores of the rock, (Biot, 1956). The changes in permeability affect the flow mechanisms of reservoir fluids and the production performance of the well, (Ren & Guo, 2018). Therefore, it is critical to geoscientists and petroleum engineers to understand the influence of pore pressure in permeability decay on the unsteady pressure and flow rate in reservoirs. This geomechanical phenomenon of permeability loss caused by compaction in a petroleum reservoir is known in the petroleum literature as formation mechanical damage, and its control is extremely important to avoid early-permeability loss over the well-reservoir life-cycle.

A new integro-differential solution for dimensionless pseudo-pressure behavior for oil flow towards wells in a deformable porous media is derived, and the problem for the unsteady-state depletion processes is formulated. The solution is expressed by an analytical formula based on asymptotic series first-order expansion computed by software Matlab[®] and the general solution is composed by $m_D(r_D = 1, t_D, k_D) \approx p_D(r_D = 1, t_D) + m_D^{(1)}(r_D = 1, t_D, k_D)$, where $p_D(r_D = 1, t_D)$ is the classical linear solution for constant permeability and the term $m_D^{(1)}(r_D = 1, t_D, k_D)$ is responsible by the nonlinear effect caused by pressure-sensitive permeability. Hence, the time-dependent permeability loss addressed in this thesis is caused by the time-dependent pressure drop in the first term and the permeability change due to pore pressure in the corrective first-order term.

3.1

Theoretical Definitions

In a dimensionless Euclidean space, let $\mathbf{r}_D = (x_D, y_D, z_D) \in \mathbb{R}^3$, $t_D \in \mathbb{R}$ and let yet, the NHDE with source term expressed by:

$$\nabla^2 m_D - \frac{1}{\eta_D(p)} \frac{\partial m_D}{\partial t_D} = -f_D(x_D, y_D, z_D, t_D) \quad (3-1)$$

where $\eta_D(p)$ is the dimensionless hydraulic diffusivity function, m_D is the dimensionless permeability pseudo-pressure, t_D is the dimensionless time and $f_D(x_D, y_D, z_D, t_D)$ is the dimensionless oil source/sink term. The new analytical model proposed in this thesis to solve the NHDE is based on asymptotic series expansion technique through the perturbation method, expressed through the infinite series (Kale & Mattar, 1980):

$$m_D = m_D^{(0)} + \sum_{k=1}^{\infty} \varepsilon^{(k)} m_D^{(k)} \quad (3-2)$$

This technique is widely used in reservoir engineering and formation evaluation literature to deal with the nonlinearity of partial differential equations with source/sink terms. It considers that the unsteady-state term of the NHDE can be coupled to a perturbation term parameter ε because this term changes low regarding pressure drop. Using a first-order approximation (Peres, Serra & Reynolds, 1989):

$$m_D \approx m_D^{(0)} + m_D^{(1)} \quad (3-3)$$

Thereby, this thesis will show that the unsteady-state permeability change is expressed by the sum of the effects of the pressure drop and zeroth-order source (zeroth-order term) as well as the pressure-dependent permeability loss $k(p)$ and the first-order source present in the deviation factor coupled to the first-order term.

3.2

Integro-Differential Solution for Mechanical Formation Damage Control

Applying the asymptotic expansion technique, the zeroth-order term of the NHDE is:

$$m_D^{(0)} = - \int_{-\infty}^{+\infty} \int_{-\infty}^{+\infty} \int_{-\infty}^{+\infty} \int_0^{t_D} f_D(x'_D, y'_D, z'_D, t'_D, k_D) \times \\ \times G_D(x_D, x'_D, y_D, y'_D, z_D, z'_D, t_D, t'_D) dt'_D dx'_D dy'_D dz'_D \quad (3-4)$$

The first-order term is:

$$m_D^{(1)} = - \int_{-\infty}^{+\infty} \int_{-\infty}^{+\infty} \int_{-\infty}^{+\infty} \int_0^{t_D} G_D(x_D, x'_D, y_D, y'_D, z_D, z'_D, t_D, t'_D) \times \\ \times \xi^{(0)} \frac{\partial m_D^{(0)}}{\partial t'_D} dt'_D dx'_D dy'_D dz'_D \quad (3-5)$$

and the k^{th} -Order term is:

$$m_D^{(k)} = - \int_{-\infty}^{+\infty} \int_{-\infty}^{+\infty} \int_{-\infty}^{+\infty} \int_0^{t_D} G_D(x_D, x'_D, y_D, y'_D, z_D, z'_D, t_D, t'_D) \times \\ \times \xi^{(k-1)} \frac{\partial m_D^{(k-1)}}{\partial t'_D} dt'_D dx'_D dy'_D dz'_D \quad (3-6)$$

The dimensionless k^{th} -order source term $\hat{\mathcal{S}}_{oD}^{(k)}$ is:

$$\hat{\mathcal{S}}_{oD}^{(k)} = \xi^{(k)}(m_D) \frac{\partial m_D^{(j)}}{\partial t_D} \quad (3-7)$$

Where ξ^{th} -order source/sink term is:

$$\xi^{(k)}(m_D) = \sum_{j=0}^{k-1} \xi \left[m_D^{(j)} \right] \quad (3-8)$$

Then:

$$\hat{\mathcal{S}}_{oD}^{(k)} = \sum_{j=0}^{k-1} \xi \left[m_D^{(j)} \right] \frac{\partial m_D^{(j)}}{\partial t_D} \quad (3-9)$$

where ξ is the hydraulic diffusivity deviator factor related to the permeability-pressure sensitive response over the well-reservoir life-cycle. Hence, it can be concluded that, the hydraulic diffusivity deviation factor depends on the order of the dimensionless general solution of the previous iteration. The dimensionless general solution in terms of the general oil source is:

$$m_D^{(k)} = - \int_{-\infty}^{+\infty} \int_{-\infty}^{+\infty} \int_{-\infty}^{+\infty} \int_0^{t_D} S^{(k)}(x'_D, y'_D, z'_D, t'_D, k_D) \times \\ \times G_D(x_D, x'_D, y_D, y'_D, z_D, z'_D, t_D, t'_D) dt'_D dx'_D dy'_D dz'_D \quad (3-10)$$

Replacing Eq. 3-9 into Eq. 3-10:

$$m_D^{(k)} = - \int_{-\infty}^{+\infty} \int_{-\infty}^{+\infty} \int_{-\infty}^{+\infty} \int_0^{t_D} \sum_{j=0}^{k-1} \xi \left[m_D^{(j)} \right] \frac{\partial m_D^{(j)}}{\partial t_D} \times \\ \times G_D(x_D, x'_D, y_D, y'_D, z_D, z'_D, t_D, t'_D) dt'_D dx'_D dy'_D dz'_D \quad (3-11)$$

The dimensionless pseudo-pressure initial condition is:

$$m_D(x_D, y_D, z_D, t_D = 0) = 0 \quad (3-12)$$

The external boundary condition is:

$$\lim_{(x_D, y_D, z_D) \rightarrow +\infty} m_D(x_D, y_D, z_D, t_D) = 0 \quad (3-13)$$

The inner boundary condition is coupled to the proposed model through the dimensionless permeability pseudo-pressure definition that will be presented in the next sections.

3.3 Computational Methodology

The analytical model derived in this thesis is solved through a computational code developed in Matlab®. The general solution comprises the linear solution (constant permeability) plus a first-order corrective term that requires solving a multiple implicit integral. To evaluate the nonlinearities caused by the permeability change as a function of the pressure values, a hydraulic diffusivity deviator factor $\xi(p_D)$, as shown in Figure 3.3 was derived.

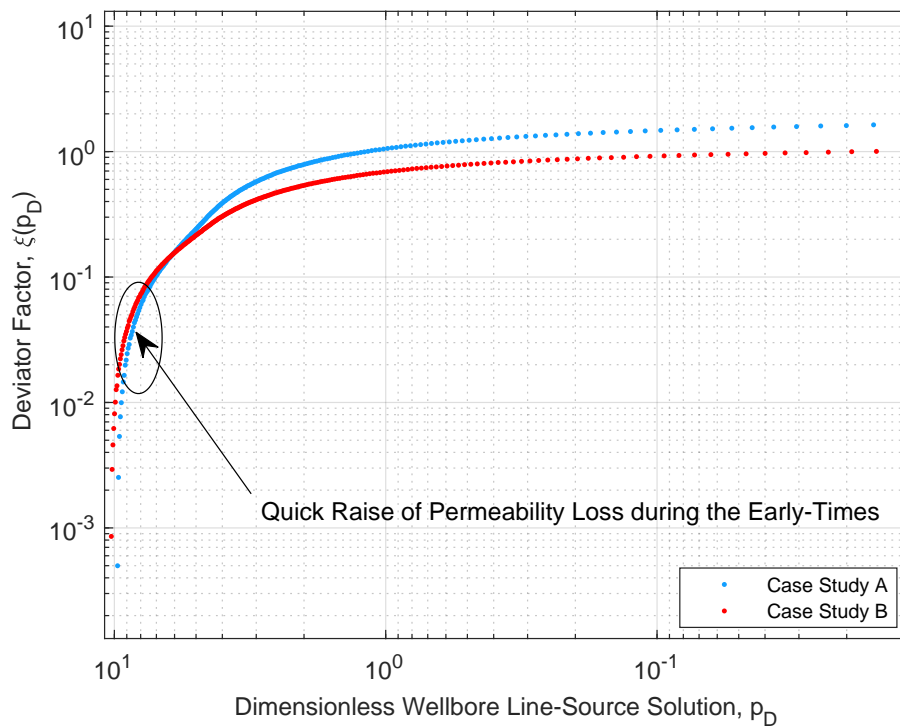


Figure 3.3: Log-log plot of the hydraulic diffusivity deviator factor as a function of the line-source solution.

This parameter represents the total deviation of the nonlinear solution with respect to the linear one (constant reservoir permeability case). Since this factor is given by $\xi(p) = 1/k_D(p) - 1$ and the dimensionless permeability is $k_D(p) = k(p)/k(p_i)$, for constant permeability response, the dimensionless permeability value tends to unity and the general solution, becomes the linear one. After the diffusivity deviator factor derivation, the NHDE is reformulated, considering it to model the unsteady-state permeability change effect. The code developed for both case studies was compared to IMEX[®] to calibrate the model. The calibration methodology was performed based on replacing the set of values of $(p, k(p))$ from the experimental data for the case studies as input information to the oil flow simulator. The pressure output data from the simulator was transformed to the pseudo-pressure $m(p)$ through Figure 3.4.

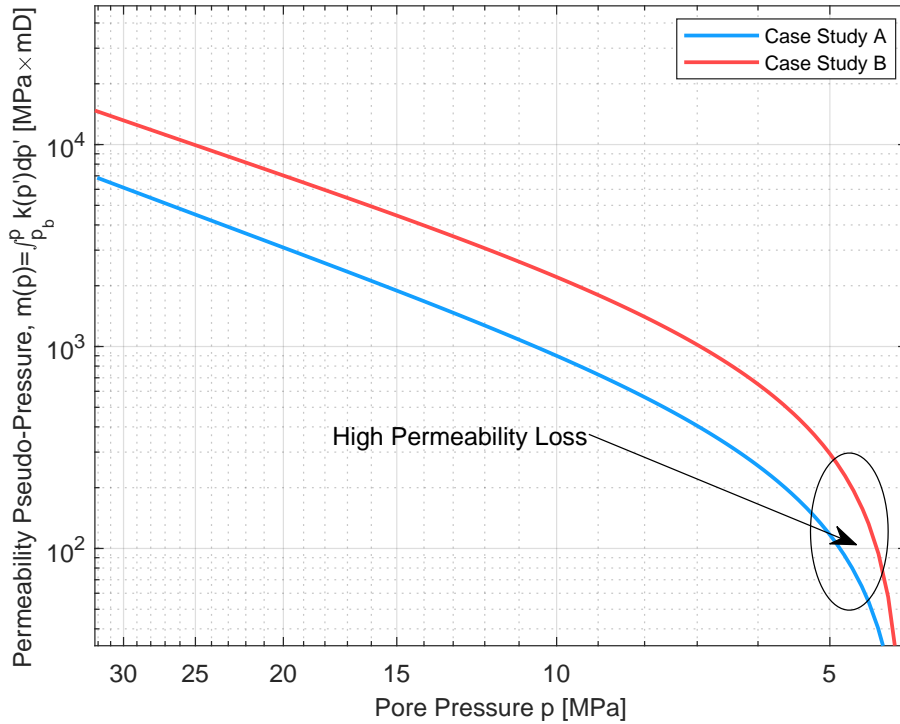


Figure 3.4: Log-log plot of the permeability pseudo-pressure as a function of the pore pressure.

It can be noticed that the pseudo-pressure vanishes for low values of the pore pressure. As the function $m(p)$ represents the permeability loss, it means that, for low values of the pore pressure, the permeability tends to zero. The linear solution, expressed by the exponential integral function $-(1/2)\mathbf{Ei}(-1/4t_D)$ is computed through the command $ei(t_D)$ in the Matlab scientific library. The multiple integral to compute the first-order term $m_D^{(1)}(r_D = 1, t_D)$ is composed of the linear solution derivative $m_D^{\prime(0)}(r_D = 1, t_D) = p_D'(r_D = 1, t_D)$, the hydraulic diffusivity deviator factor $\xi(p_D)$ and the dimensionless GF

$G_D(x_D, x'_D, y_D, y'_D, z_D, z'_D, t_D, t'_D)$ for the appropriate well-reservoir setting and boundary conditions. This integral is solved through the command *int3*, and the linear solution derivative is easily computed through Leibniz's rule applied to the *ei*($r_D = 1, t_D$) command. To run the model, the pore pressure, as well as the permeability values input for the Case studies A and B, were imported from the field data measured experimentally in work performed by Soares (2000), Soares, Freitas & Velloso (2001), Soares & Ferreira (2002) to evaluate the permeability pressure-sensitive response in the dimensionless corrective first-order term $m_D^{(1)}$. The proposed pseudo-pressure provides information on the permeability changes as a function of the pressure. It is possible to notice that, as the pressure decreases, the pseudo-pressure tends to zero. This behavior is caused by the permeability dependence in the proposed pseudo-pressure function (Fernandes, 2021b).

After the transformation, $p \mapsto m(p)$, the pseudo-pressure data are inserted into the code to verify the qualitative and quantitative behavior of the solutions. The dimensionless linear solution term was computed analytically for 40 dimensionless time values. Extensive sensitive runs of time and space steps were performed in the model in order to find an accurate convergence to IMEX[®]. The Matlab[®] code was developed to read the computational table of experimental data and to use four types of correlations fitting functions to enter in the diffusivity deviator factor in the proposed model. After these parameters were inputted in IMEX[®], the next step was to build a table with the permeabilities and pressures values through a proper rock-fluid table computational command. Sensitive runs were performed to find the best grid size. After the data input, the simulator ran and presented the pressure output values to input in the proposed pseudo-pressure in the Matlab[®] computational code. A 2-D cylindrical grid was built to represent a vertical well in IMEX[®], and the sensitive runs have shown that a grid with 250 cells in the r-direction is enough to obtain accurate results. To model the sealing fault well-reservoir setting, a Cartesian grid with 260 cells in the x-y directions was used. The sealing fault was represented as a zone with low transmissibility in IMEX[®].

3.4 Experimental Methodology and Field Data

The developments of deepwater fields, which the majority of reservoirs have been constituted of unconsolidated sandstones, brought some technical and scientific challenges with respect to the effect of reservoir compaction on oil production, (Soares, 2000), (Soares, Freitas & Velloso, 2001) and (Soares & Ferreira, 2002).

Recent works have been noticed the influence of the stress path in the permeability loss in several reservoirs, (Soares, 2000). Pressure and permeability data for carrying out this thesis were used based on the works from (Soares; Soares, Freitas & Velloso; Soares & Ferreira, 2000, 2001, 2002). The rock samples used in this work constitute two layers of the same reservoir rock and the proposed model deals with each rock layer separately (no interlayer cross-flow). Uni-axial tests were performed to measure the rock strain ε and to evaluate the permeability decline as a function of pore pressure to input in the hydraulic diffusivity deviator factor in the computational code. The tests considered the rock samples under a constant overburden stress (Table 3.1).

Rock/Fluid/Well Parameter	Case Study A	Case Study B
Young's Modulus (E)	10.1 GPa	10.2 GPa
Poisson's Ratio (ν)	0.26	0.25
Initial Pressure (p_i)	32.58 MPa	31 MPa
Overburden Stress (σ_{ov})	53.43 MPa	54.25 MPa
Initial Horiz. Stress ($\sigma_h(p_i)$)	21.72 MPa	20.90 MPa
Initial Vert. Effec. Stress ($\sigma'_v(p_i)$)	20.85 MPa	23.25 MPa
Initial Horiz. Effec. Stress ($\sigma'_h(p_i)$)	88.71 MPa	83.61 MPa
Biot's coefficient (α)	1	1
Porosity (ϕ)	26.46%	27.39%
Initial Permeability ($k(p_i)$)	$1.68 \times 10^{-13} \text{ m}^2$	$3.36 \times 10^{-13} \text{ m}^2$
Bulk Density (ρ_b)	$2.2 \times 10^3 \text{ kg/m}^3$	$2.2 \times 10^3 \text{ kg/m}^3$
Fluid Dynamic Viscosity (μ)	$1.79 \times 10^3 \text{ Pa sec}$	$1.79 \times 10^3 \text{ Pa sec}$
Fluid Density (ρ)	$1.066 \times 10^3 \text{ kg/m}^3$	$1.066 \times 10^3 \text{ kg/m}^3$
Total Compressibility (c_t)	$2.51 \times 10^{-4} \text{ 1/MPa}$	$2.51 \times 10^{-4} \text{ 1/MPa}$
Wellbore Radius (r_w)	0.1 m	0.1 m
Reservoir Net pay (h)	40 m	40 m

Table 3.1: Wellbore-Rock-Fluid Field Data

The pressure values were computed from Biot (1941), Biot (1956) equation of poroelasticity:

$$\vec{\sigma}' = \vec{\sigma} - \alpha \vec{p} \quad (3-14)$$

Combining the generalized Hooke's law and Biot's equation, in the matrix form, the Eq. 3-14 becomes:

$$\begin{pmatrix} \sigma'_r \\ \sigma'_\theta \\ \sigma'_z \end{pmatrix} = \frac{E}{(1+\nu)(1-2\nu)} \begin{pmatrix} (1-\nu) & \nu & \nu \\ \nu & (1-\nu) & \nu \\ \nu & \nu & (1-\nu) \end{pmatrix} \begin{pmatrix} \varepsilon_r \\ \varepsilon_\theta \\ \varepsilon_z \end{pmatrix} - \alpha \begin{pmatrix} p \\ p \\ p \end{pmatrix} \quad (3-15)$$

The variables in Eqs. 3-14 and 3-15 were defined in the chapter 1 of this work. The pore pressure and permeability data were obtained from a uni-axial strain test. The test consisted of applying an axial load while the strains in the horizontal directions were prevented. Thus, as suggested by (Geertsma, 1966), the axial strain is exactly equal to the volumetric strain. The test was performed in two sandstone samples with cylindrical geometry that were taken from the depths of 3,094 m and 3,139 m in an offshore field located in Brazil. The choice of this field occurred because it presented a severe decrease in oil rate production and its oil recovery was lower than that predicted by the reservoir engineering simulations. To simulate the fluid inside the reservoir rock pores, inert oil was used to avoid fluid/rock interaction.

3.4.1 Elastic Parameters

In the experiment conducted in this work, the primary wave (p-wave) and shear wave (s-wave) velocities were measured to monitor the rearrangement of the rock structure through velocities variation. After the measurements of these wave's velocities, it was possible to compute Young's modulus using the Eq. 3-16 (Akbar et al., 2019):

$$E = \rho_b v_s^2 \left[\frac{(3v_p^2 - 4v_s^2)}{v_p^2 - v_s^2} \right] \quad (3-16)$$

and Poisson's ratio, as follows:

$$\nu = \frac{1}{2} \left[\frac{(v_p/v_s)^2 - 2}{(v_p/v_s)^2 - 1} \right] \quad (3-17)$$

Where ρ_b is the bulk density, [kg/m^3]; v_p and v_s are the p-wave and s-wave velocity, respectively, [m/sec]. The uni-axial strain and effective stress were also measured under constant overburden in the experiment. Combining these measurements to Young's modulus and Poisson's ratio, obtained from the p and s waves and, using Biot's coefficient $\alpha = 1$, the pore pressure field was computed through the Eq. 3-15. Finally, after the pore pressure values were computed, the permeability curve was computed through Darcy's law, and a computational table of pressure and permeability values were generated and used in the Matlab® code.

3.4.2 Rock-Fluid Data

The experimental pressure and permeability data obtained from the two samples of sandstone layers were used as input to the computational code running the proposed model. The rock and fluid properties and wellbore geometry to run the model are listed in Table 3.1.

3.4.3 Permeability-Pressure Sensitive Functions

The model presented in this work requires a permeability decay function to fit the experimental $(p, k(p))$ points and compute the ξ -factor. To fit these points, the author researched four types of functions (Table 3.2). These functions have been implemented in the computational code, and the results are presented in the Figures 3.5 to 3.8. The constants values A , B , and C are computed through the pressure data obtained experimentally.

Model Decay	Pressure-Sensitive Function $k(p)$
Linear	$k(p) = Ap + B$
Exponential	$k(p) = Ae^{Bp}$
Parabolic	$k(p) = Ap^2 + Bp + C$
Hyperbolic	$k(p) = A/p$

Table 3.2: Proposed functions for permeability pressure decay.

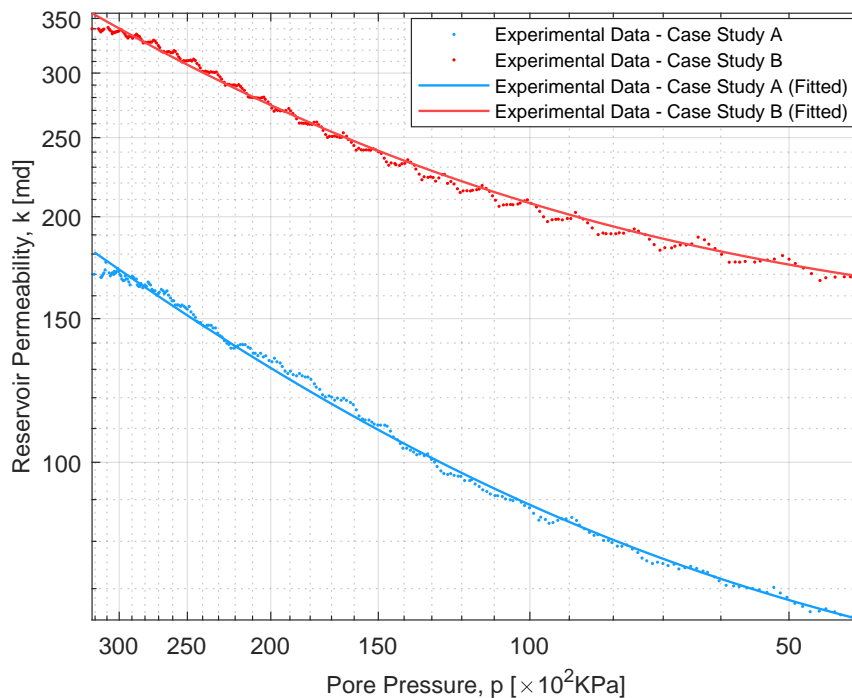


Figure 3.5: Permeability curve for the linear fitting.

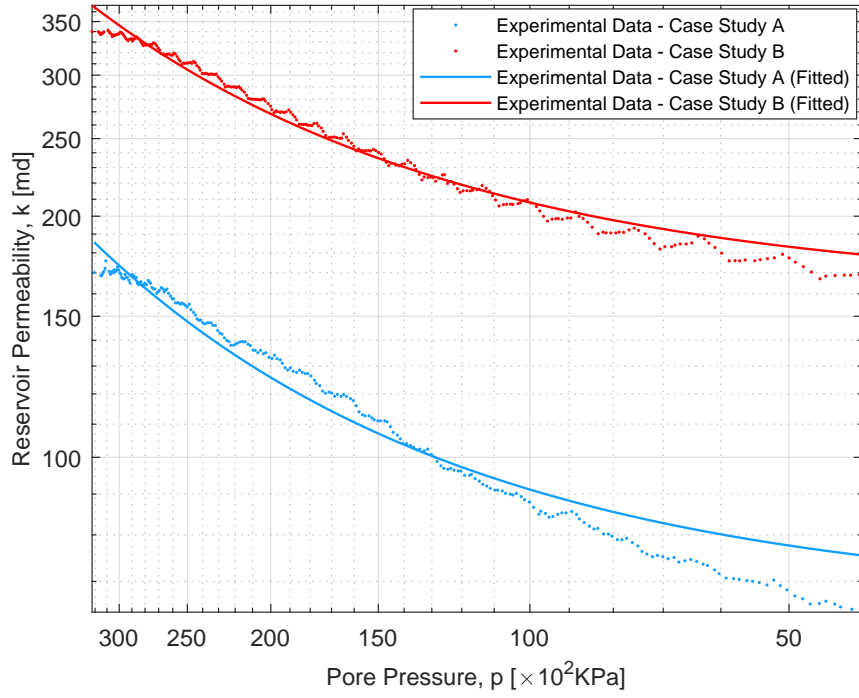


Figure 3.6: Permeability curve for the exponential fitting.

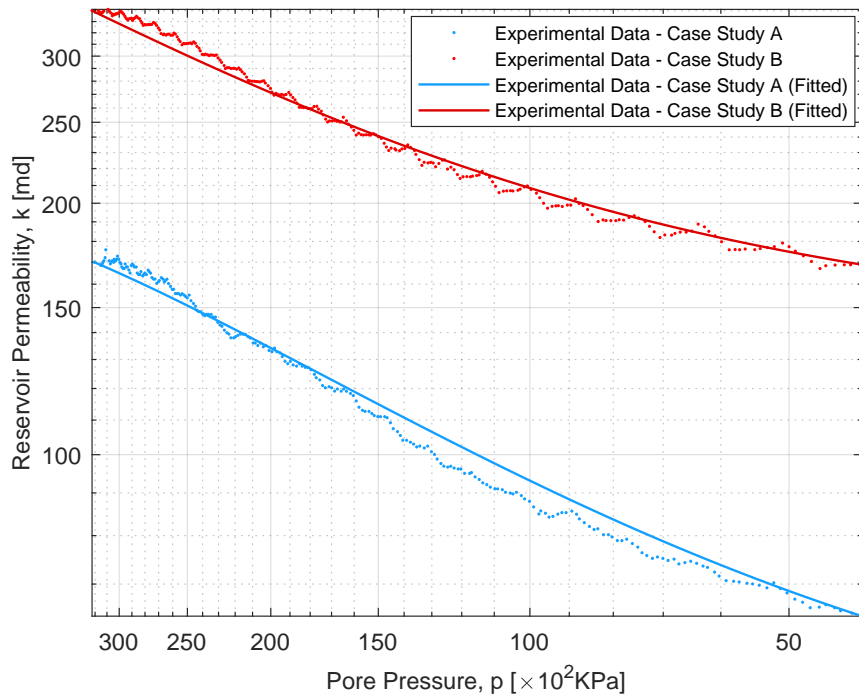


Figure 3.7: Permeability curve for the parabolic fitting.

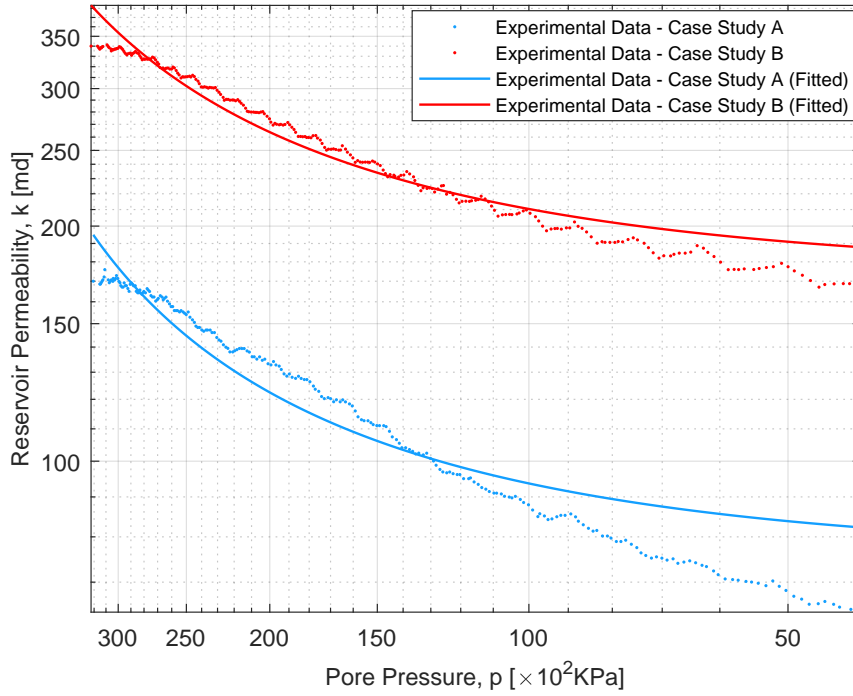


Figure 3.8: Permeability curve for the hyperbolic fitting.

Based on the results presented in the fitting plots, the author chose to use the linear fitting function because this function provided the most accurate fitting of the experimental points. It is simpler to implement in the code, saving computational costs.

3.4.4 Sensitivity Analysis

This subsection deals with a sensitivity analysis of the rock-fluid parameters to evaluate the influence of each variable in the permeability decline to support the well-reservoir management. As the analytical general solution $m_D(r_D = 1, t_D)$ is expressed by the linear solution $p_D(r_D = 1, t_D)$ plus a first-order corrective term $m_D^{(1)}(r_D = 1, t_D)$, it is appropriate to research the effect of each rock and fluid parameter in the nonlinear term. The analysis was performed through the pressure and permeability data obtained experimentally, as well as through some synthetic dimensionless oil source values.

According to the Darcy's law, (Darcy, 1856)

$$\frac{q\mu}{2\pi k(p)h} = r \frac{\partial p}{\partial r} \quad (3-18)$$

Thus, we can notice that, as the right-hand side, the variables group of the left-hand side of the Eq. 3-18 also has pressure unity, *i.e.*, [MPa]. So, we can define the dimensionless oil flow source f_D as:

$$f_D = \frac{2\pi hk(p)(p_i - p)}{q\mu} \quad (3-19)$$

Multiplying both sides of the Eq. 3-19 by the inverse permeability at initial pressure $1/k(p_i)$:

$$\frac{1}{k(p_i)} \times f_D = \frac{1}{k(p_i)} \times \frac{2\pi hk(p)(p_i - p)}{q\mu} \quad (3-20)$$

As:

$$\frac{k(p)}{k(p_i)} = k_D(p) \quad (3-21)$$

Thus, the dimensionless oil source becomes:

$$f_D = \frac{2\pi hk(p_i)k_D(p)(p_i - p)}{q\mu} \quad (3-22)$$

Defining the dimensionless pressure variation $\Delta\hat{p}$ as:

$$\Delta\hat{p} = \frac{(p_i - p)}{(p_i - p_b)} \quad (3-23)$$

Replacing the dimensionless pressure variation definition in Eq. 3-22, the dimensionless oil source can be expressed as follows:

$$f_D = \frac{2\pi hk(p_i)(p_i - p_b)k_D(p)\Delta\hat{p}}{q\mu} \quad (3-24)$$

To compute the hydraulic diffusivity deviator factor $\xi(p)$, initially we have to write the Eq. 3-24 as a function of the dimensionless inverse permeability $1/k_D(p)$:

$$\frac{1}{k_D(p)} = \frac{2\pi hk(p_i)(p_i - p_b)\Delta\hat{p}}{q\mu f_D} \quad (3-25)$$

Adding (-1) unity in both sides of the Eq. 3-25:

$$\frac{1}{k_D(p)} - 1 = \frac{2\pi hk(p_i)(p_i - p_b)\Delta\hat{p}}{q\mu f_D} - 1 \quad (3-26)$$

By the hydraulic diffusivity deviator factor definition:

$$\xi(p) = \frac{1}{k_D(p)} - 1 \quad (3-27)$$

Finally, replacing the Eq. 3-27 in the Eq. 3-26, we have the hydraulic diffusivity deviator factor $\xi(p)$ as a function of the well-fluid-reservoir parameters:

$$\xi(p) = \frac{2\pi h k(p_i)(p_i - p_b)\Delta\hat{p}}{q\mu f_D} - 1 \quad (3-28)$$

Figs. 3.9 and 3.10 show the behavior of the dimensionless permeability function $k_D(p)$ with respect to the dimensionless oil source f_D for several dimensionless pressures variation $\Delta\hat{p}$ for the case studies A and B, respectively. Analyzing a fixed dimensionless oil source value, it can be noticed that the dimensionless permeability decline is directly related to the dimensionless pressure variation growth. We can also realize that, for small increase values of the oil flow source ($1/2 < f_D < 2$), a significant dimensionless permeability drop occurs. It provides the increase of the nonlinearity caused permeability pressure-sensitive behavior in the first-order term $m_D^{(1)}(r_D = 1, t_D)$. So, the dimensionless oil flow source plays a key role in the permeability decline.

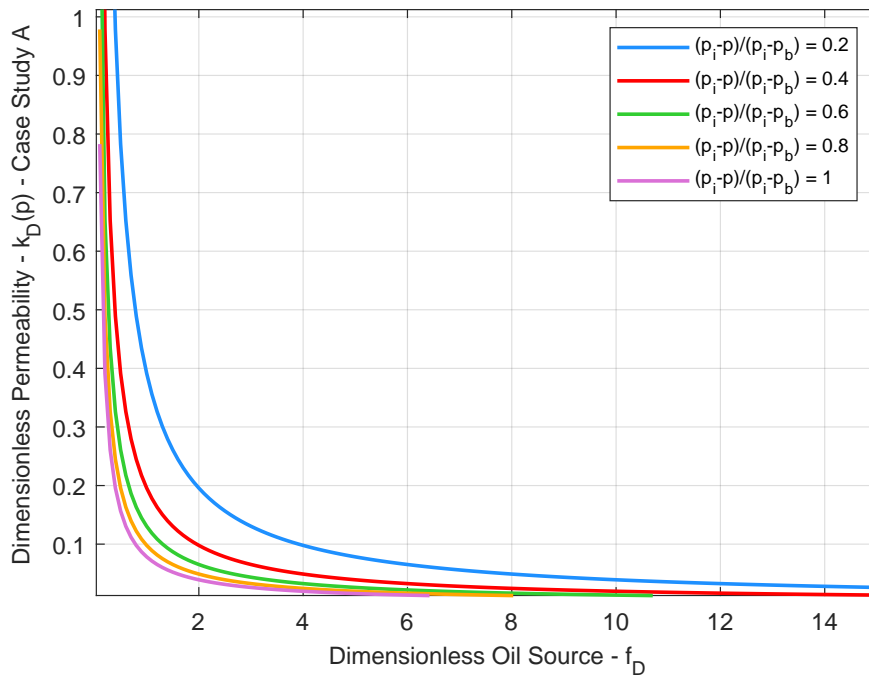


Figure 3.9: Dimensionless permeability as a function of the dimensionless oil source for several dimensionless pressure variation values (Case study A).

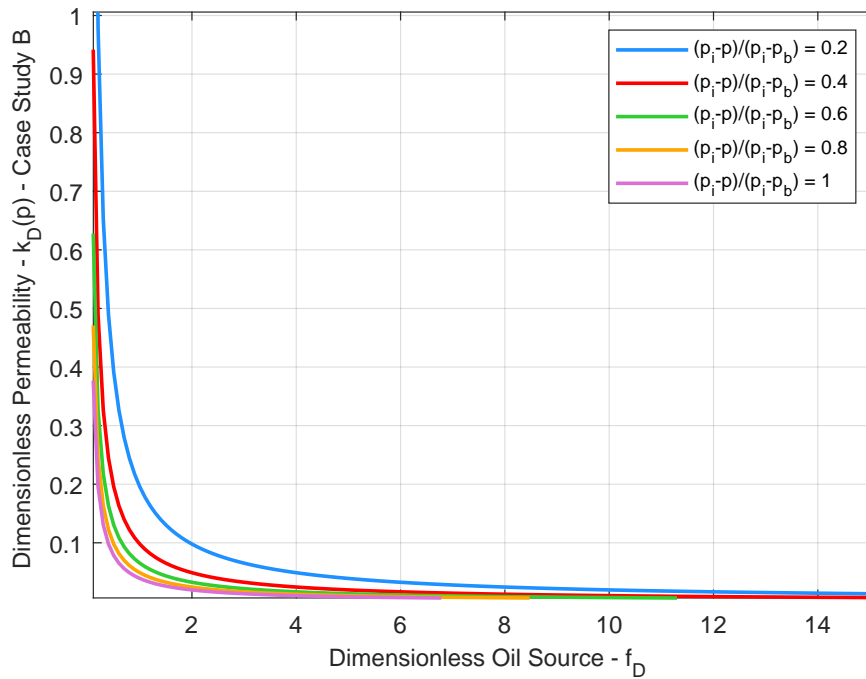


Figure 3.10: Dimensionless permeability as a function of the dimensionless oil source for several dimensionless pressure variation values (Case study B).

The proposed model may assist the geosciences and reservoir engineering team choose the oil flow rate that minimizes the permeability drop for a given dimensionless pressure variation curve. Figs. 3.11 and 3.12 show the dimensionless permeability function with respect to the dimensionless pressure variation for several dimensionless oil flow rates for case studies A and B, respectively. It can be seen that, for a fixed dimensionless pressure variation value, the dimensionless permeability declines as the dimensionless oil flow rate increases. According to the plots, we notice that this effect is more severe for small dimensionless pressure variation values ($\Delta\hat{p} < 0.1$). It also increases the nonlinearity caused by permeability pressure-sensitive behavior in the first-order term. Based on the results above, it can be concluded that the dimensionless pressure variation is an important hydraulic parameter to predict the reservoir permeability decline over the well-reservoir life-cycle. The solution proposed in this work allows, in a simple manner, to compute the permeability value for a given dimensionless oil flow source curve as a function of the dimensionless pressure variation.

Figs. 3.13 and 3.14 show the dimensionless pressure variation concerning the dimensionless oil flow source for several dimensionless permeability functions for case studies A and B, respectively.

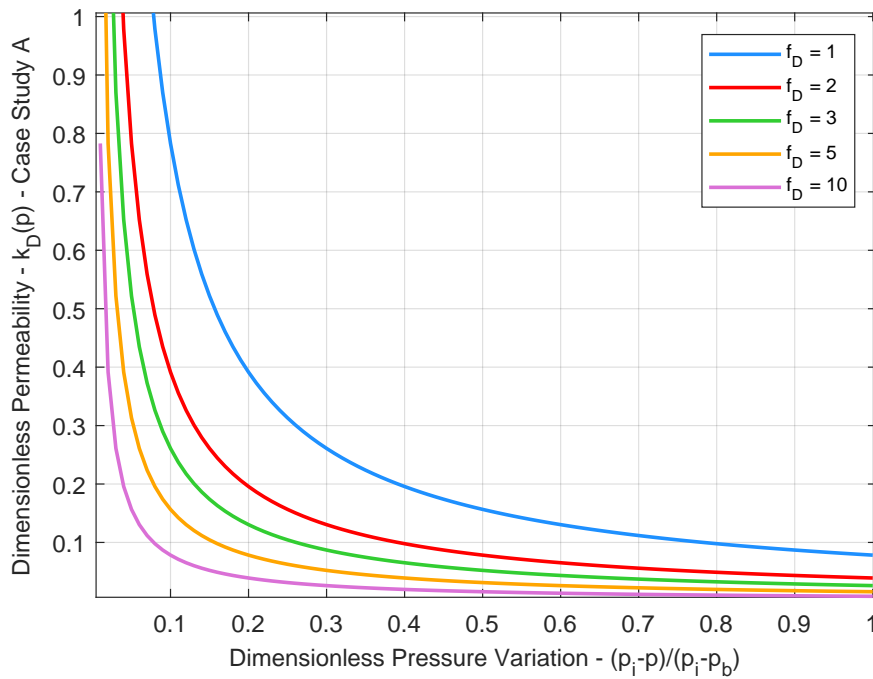


Figure 3.11: Dimensionless permeability with respect to the dimensionless pressure variation for several dimensionless oil flow rates (Case study A)

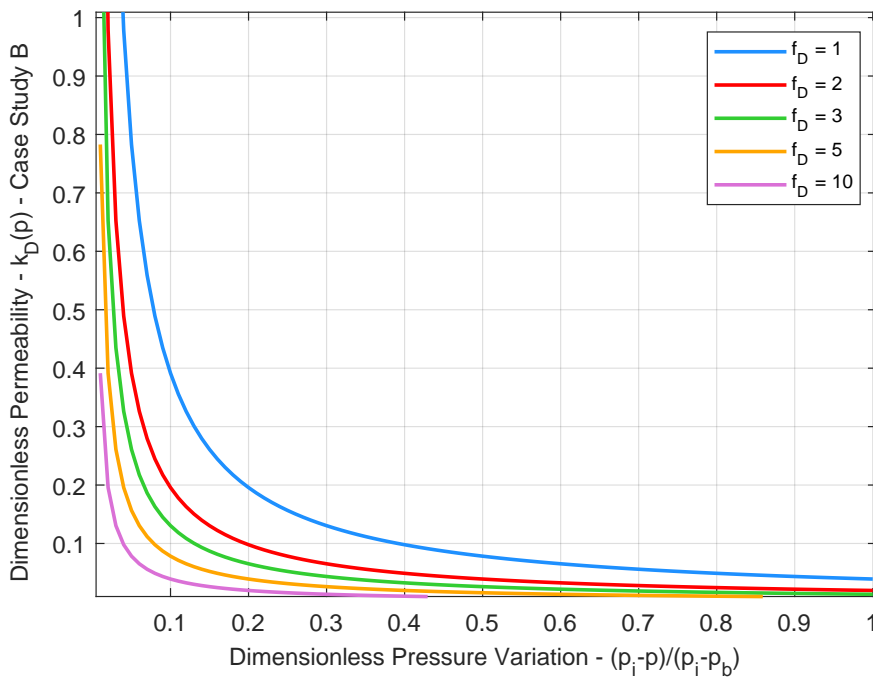


Figure 3.12: Dimensionless permeability with respect to the dimensionless pressure variation for several dimensionless oil flow rates (Case study B).

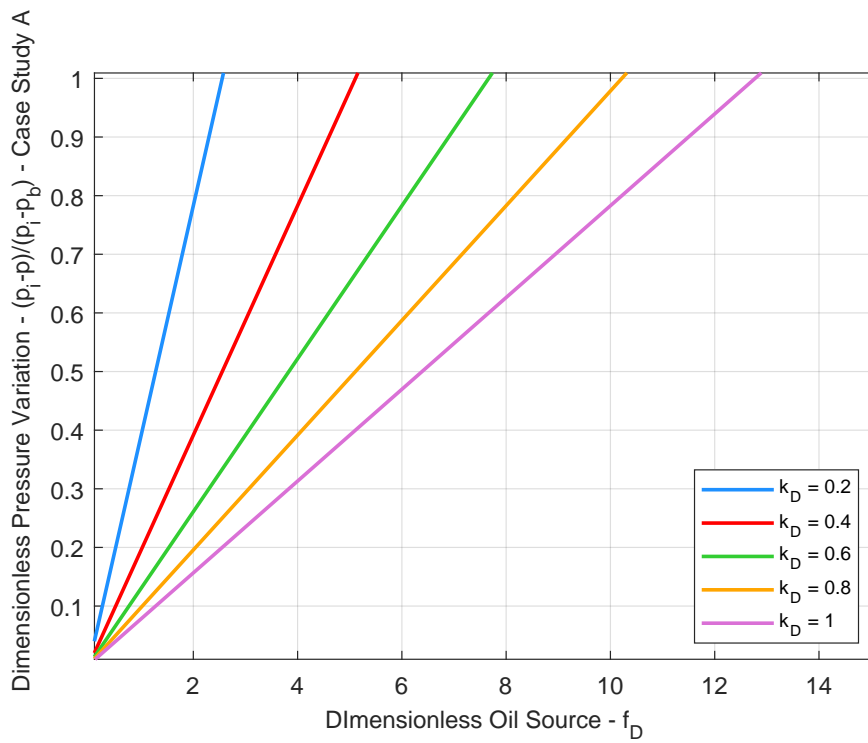


Figure 3.13: Dimensionless pressure variation as a function of the dimensionless oil source for several dimensionless permeability (Case study A).

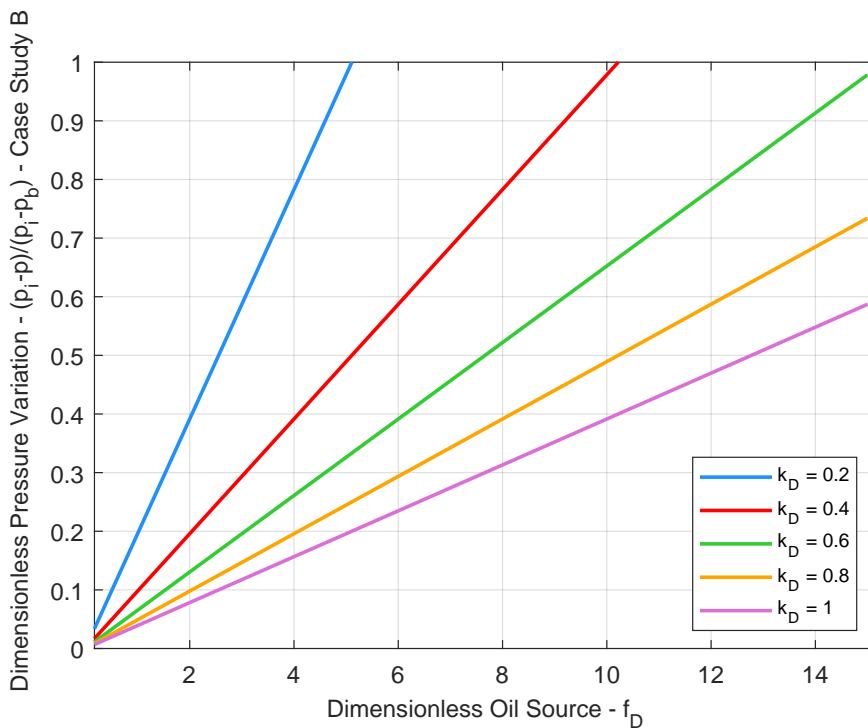


Figure 3.14: Dimensionless pressure variation as a function of the dimensionless oil source for several dimensionless permeability (Case study B).

As expected, the results show that the dimensionless pressure variation increases linearly with respect to the dimensionless oil source, *i.e.*, the increase of the oil flow rate results in the pressure decline and, consequently, the permeability loss. In a complementary way, for a fixed dimensionless oil flow source value, the dimensionless pressure variation rises (pressure drops) as the dimensionless permeability values decrease. Figs. 3.15 and 3.16 show the response of the hydraulic deviator factor ξ as a function of the dimensionless inverse oil flow source $1/f_D$ for several dimensionless pressure variations for the case studies A and B, respectively. It can be seen that the hydraulic diffusivity deviator factor declines as the dimensionless inverse oil source increases. Through Eq. 3-28, we notice that, as the dimensionless oil source increases, the group $2\pi hk(p_i)(p_i - p_b)\Delta\hat{p}/q\mu f_D$ vanishes. Consequently, the deviator factor tends to the unity (maximum value). The maximum value of this factor means that the permeability loss reaches its maximum value, *i.e.*, the permeability tends to zero. On the other hand, if the group $2\pi hk(p_i)(p_i - p_b)\Delta\hat{p}/q\mu f_D$ tends to the unity, *i.e.*, $2\pi hk(p_i)(p_i - p_b)\Delta\hat{p} \approx q\mu f_D$, the deviator factor tends to zero. Thus an equilibrium between the rock and fluid parameters is reached. The dimensionless general solution $m_D(r_D = 1, t_D)$ tends to the linear solution $p_D(r_D = 1, t_D)$.

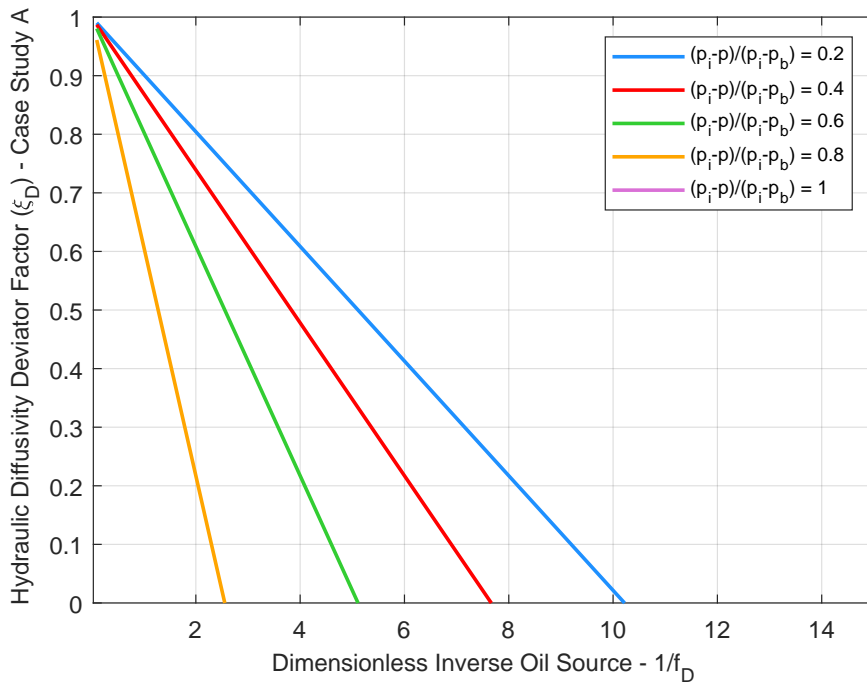


Figure 3.15: Diffusivity deviator factor as a function of the dimensionless inverse oil source for several dimensionless pressure variation (Case study A).

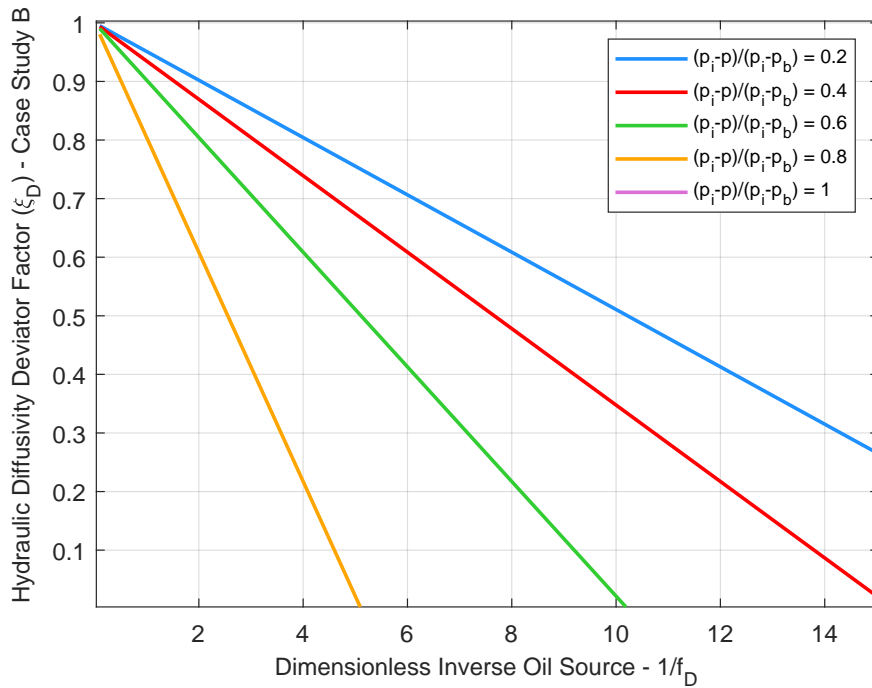


Figure 3.16: Diffusivity deviator factor as a function of the dimensionless inverse oil source for several dimensionless pressure variation (Case study B).

Mathematically, we can write:

$$\lim_{f_D \rightarrow +\infty} \xi = 1 \quad (3-29)$$

and

$$\lim_{2\pi h k(p_i)(p_i - p_b) \Delta \hat{p} \rightarrow q \mu f_D} \xi = 0 \quad (3-30)$$

It can also be noticed that the hydraulic deviator factor declines as the dimensionless pressure variation increases for a fixed dimensionless inverse oil flow source value. It reduces the nonlinearity caused by permeability pressure-sensitive behavior in the first-order term. In a complementary way, Figs. 3.17 and 3.18 show the behavior of the hydraulic deviator factor ξ as a function of the dimensionless pressure variation $\Delta \hat{p}$ for several dimensionless inverse oil sources $1/f_D$ for both case studies. Through the proposed model, it is possible to compute the hydraulic diffusivity deviator factor values for a given dimensionless oil source curve (or its inverse) as a function of the dimensionless pressure variation.

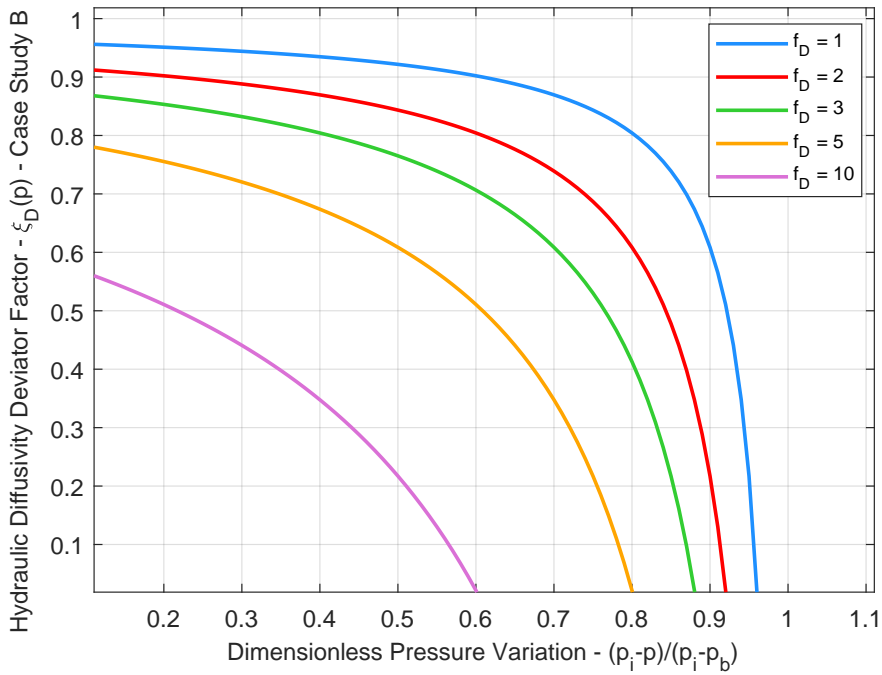


Figure 3.18: Hydraulic diffusivity deviator factor as a function of the dimensionless pressure variation for several inverse oil sources (Case study B).

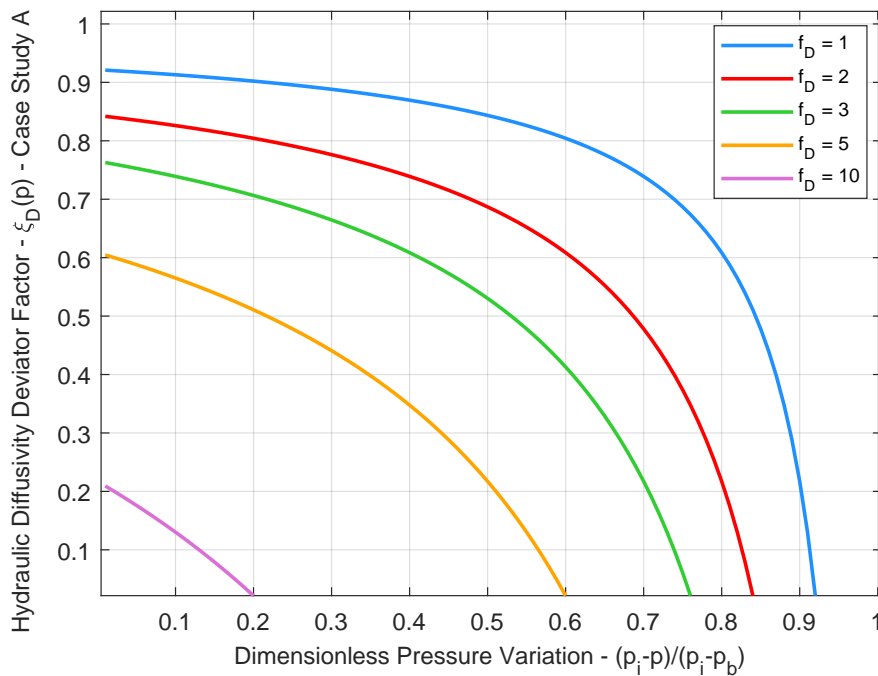


Figure 3.17: Hydraulic diffusivity deviator factor as a function of the dimensionless pressure variation for several inverse oil sources (Case study A).

4

Theoretical Formulation

The isothermal single-phase and compressible oil flow through porous media with diffusivity as a function of the pressure is modeled by NHDE. Several analytical solutions are sought in the reservoir engineering and formation evaluation literature to deal with the NHDE considering source term. The main advantages of analytical models compared to numerical ones are saving computational costs and providing reliable results with high accuracy. In this chapter, a general model formulation for Darcian oil flow in a deformable porous medium with permeability pressure-sensitive is derived through the NHDE. A new general solution and an approximate solution based on asymptotic series expansion coupled with Green's functions (GF's) will also be presented. The solution will be derived from the continuity equation for an incompressible fluid with source term in Cartesian coordinates.

For modeling of oil flow problem in porous media, the following premises are assumed:

- 1 Pressure-sensitive permeability
- 2 Low pressure gradient
- 3 Newtonian fluid inside the porous media
- 4 Well fully penetrates reservoir rock
- 5 Deformable, homogeneous, linear elastic and isotropic reservoir
- 6 Isothermal, single-phase, and compressible flow in the porous media
- 7 The fluid present inside the pores of the reservoir rock does not react chemically with the rock matrix
- 8 Skin and storage effects are not considered
- 9 The well is located at the origin of the system of coordinates $(0, 0, 0)$
- 10 No fluid flow across the top and bottom of the formation

4.1

Continuity Equation for Oil Flow in Pressure-Sensitive Reservoirs

The oil flow in a pressure-sensitive permeability reservoir is modeled by a coupled process between the fluid movement and the rock deformation. This process is in general described by the flow potential gradient and the permeability of the formation according to Darcy's law, (Darcy, 1856). When fluid flow occurs in porous media, *e.g.* a petroleum reservoir, the flow potential will change in space and time, as well as, the fluid pressure, (Bear; Ahmed, 1972, 2010).

Let the two-dimensional (2-D) representation of an infinitesimal reservoir rock volume element (Figure 4.1) below and $\mathbf{u}(x, y, z, t) = (u(x, y, z, t), v(x, y, z, t), w(x, y, z, t))$ the velocity field vector, $\mathbf{u} \in \mathbb{R}^3$ and $t \in \mathbb{R}$.

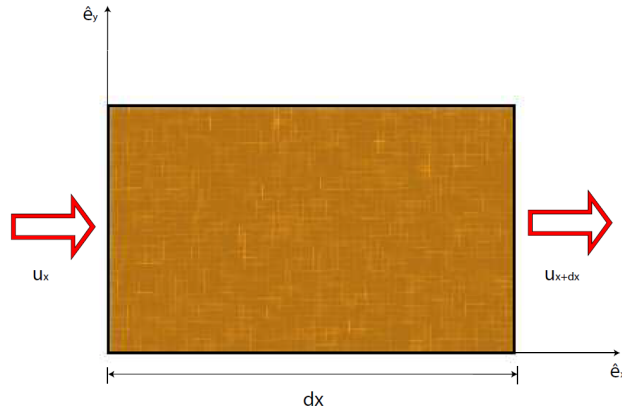


Figure 4.1: Infinitesimal reservoir rock element.

The fluid mass rate that cross the porous media volume V_p is:

$$\begin{aligned} \frac{\partial}{\partial t}(\rho V_p) = & (\rho u dy dz)_x - (\rho u dy dz)_{x+dx} + (\rho v dx dz)_y - (\rho v dx dz)_{y+dy} + (\rho w dx dy)_z + \\ & - (\rho w dx dy)_{z+dz} + \frac{\rho \tilde{q}(x, y, z, t)}{2\pi} \quad (4-1) \end{aligned}$$

We can rewrite the Eq. 4-1 as follows:

$$\begin{aligned} \frac{\partial}{\partial t}(\rho V_p) = & \left[\frac{(\rho u)_x - (\rho u)_{x+dx}}{dx} \right] dx dy dz + \left[\frac{(\rho v)_y - (\rho v)_{y+dy}}{dy} \right] dx dy dz + \\ & + \left[\frac{(\rho w)_z - (\rho w)_{z+dz}}{dz} \right] dx dy dz + \frac{\rho \tilde{q}(x, y, z, t)}{2\pi} dx dy dz \quad (4-2) \end{aligned}$$

The porous volume is given by:

$$V_p = \phi dx dy dz \quad (4-3)$$

where ρ is fluid density, [kg/m^3]; $\tilde{q}(x, y, z, t)$ is volumetric oil flow rate per volume, [$1/sec$] and ϕ is total porosity of rock, [dimensionless]. Replacing the Eq.4-3 in Eq.4-2:

$$\frac{\partial}{\partial t}(\rho\phi dx dy dz) = - \left[\frac{\partial(\rho u)}{\partial x} + \frac{\partial(\rho v)}{\partial y} + \frac{\partial(\rho w)}{\partial z} - \frac{\rho\tilde{q}(x, y, z, t)}{2\pi} \right] dx dy dz \quad (4-4)$$

Finally, the continuity equation that describes the mass conservation for flow in porous media with source is expressed, in the vector notation, by (Bear; Ahmed, 1972, 2010):

$$\frac{\partial}{\partial t}(\rho\phi) + \nabla \bullet (\rho\mathbf{u}) = \frac{\rho\tilde{q}(x, y, z, t)}{2\pi} \quad (4-5)$$

The positive sign of the source term in the right-hand side of Eq. 4-5 means that the oil flow occurs from the wellbore to the reservoir (fluid injection), which does not correspond to the modeling developed in the thesis. Hence a negative sign represents an oil sink instead of a source. The next section will show that the negative sign in the right-hand side of Eq. 4-5 arises spontaneously from the momentum transport equation (Darcy's law) and the constitutive equations for rock and fluid compressibilities.

4.2

Nonlinear Hydraulic Diffusivity Equation in terms of Pressure

Let the velocity field $\mathbf{u} = (u(\mathbf{r}, t), v(\mathbf{r}, t), w(\mathbf{r}, t))$. Where \mathbf{r} is the displacement vector such as $\mathbf{r} \in \mathbb{R}^3$. Let yet the fluid density, reservoir porosity and permeability, slightly pressure-sensitive. Thereby, the continuity equation for flow in porous media is expressed as follows (Bear; Ahmed, 1972, 2010):

$$\frac{\partial}{\partial t} \left[\rho(p)\phi(p) \right] + \nabla \bullet \left[\rho(p)\mathbf{u} \right] = \frac{\rho\tilde{q}(x, y, z, t)}{2\pi} \quad (4-6)$$

The analytical model developed in this thesis deals with constant oil flow rate in space and time. Hence $\tilde{q}(x, y, z, t) \mapsto \tilde{q}$. By Darcy's law, the velocity field for oil flow in pressure-sensitive permeability reservoir is expressed by:

$$\mathbf{u} = - \frac{k(p)}{\mu} \nabla p \quad (4-7)$$

where $k(p)$ is the pressure-sensitive permeability, [md] and μ is the fluid

dynamic viscosity, [Pa sec]. The negative sign in Eq. 4-7 means that the fluid is being withdrawn from the reservoir, *i.e.*, it represents an oil sink. Replacing Eq. 4-7 in the Eq. 4-6:

$$\frac{\partial}{\partial t} [\rho(p)\phi(p)] + \nabla \bullet \left[-\rho(p) \frac{k(p)}{\mu} \nabla p \right] = \frac{\rho \tilde{q}(x, y, z, t)}{2\pi} \quad (4-8)$$

Thus:

$$\frac{\partial}{\partial t} [\rho(p)\phi(p)] - \nabla \bullet \left[\rho(p) \frac{k(p)}{\mu} \nabla p \right] = \frac{\rho \tilde{q}(x, y, z, t)}{2\pi} \quad (4-9)$$

Using product's rule in the first term of Eq. 4-9:

$$\frac{\partial}{\partial t} [\rho(p)\phi(p)] = \phi(p) \frac{\partial \rho(p)}{\partial t} + \rho(p) \frac{\partial \phi(p)}{\partial t} \quad (4-10)$$

By the chain's rule, the density rate is:

$$\frac{\partial \rho(p)}{\partial t} = \frac{\partial \rho(p)}{\partial p} \frac{\partial p}{\partial t} \quad (4-11)$$

Applying the chain's rule again, the porosity rate is:

$$\frac{\partial \phi(p)}{\partial t} = \frac{\partial \phi(p)}{\partial p} \frac{\partial p}{\partial t} \quad (4-12)$$

Replacing the Eq. 4-11 and Eq. 4-12 in the Eq. 4-10:

$$\frac{\partial}{\partial t} [\rho(p)\phi(p)] = \phi(p) \frac{\partial \rho(p)}{\partial p} \frac{\partial p}{\partial t} + \rho(p) \frac{\partial \phi(p)}{\partial p} \frac{\partial p}{\partial t} \quad (4-13)$$

By the fluid compressibility definition $c_o(p)$:

$$c_o(p) = -\frac{1}{\rho(p)} \frac{\partial \rho(p)}{\partial p} \quad (4-14)$$

So as the rock compressibility $c_r(p)$:

$$c_r(p) = -\frac{1}{\phi(p)} \frac{\partial \phi(p)}{\partial p} \quad (4-15)$$

Thus, the density derivative with respect to the pressure can be rewritten as:

$$\frac{\partial \rho(p)}{\partial p} = -\rho(p) c_o(p) \quad (4-16)$$

And porosity derivative with respect to pressure, as:

$$\frac{\partial \phi(p)}{\partial p} = -\phi(p)c_r(p) \quad (4-17)$$

Combining the Eqs. 4-16, 4-17 and 4-13, the transient term of the 4-8 yields to:

$$\frac{\partial}{\partial t} [\rho(p)\phi(p)] = -\rho(p)\phi(p) [c_o(p) + c_r(p)] \frac{\partial p}{\partial t} \quad (4-18)$$

The total compressibility is defined by (Bear, 1972):

$$c_t(p) = c_o(p) + c_r(p) \quad (4-19)$$

Replacing the Eq. 4-19 in the Eq. 4-18, the unsteady-state term of the Eq. 4-8 can be expressed in terms of the total compressibility:

$$\frac{\partial}{\partial t} [\rho(p)\phi(p)] = -\rho(p)\phi(p)c_t(p) \frac{\partial p}{\partial t} \quad (4-20)$$

Replacing the Eq. 4-20 in the Eq. 4-1:

$$-\left\{ \nabla \bullet \left[\frac{\rho(p)k(p)\nabla p}{\mu} \right] + \rho(p)\phi(p)c_t(p) \frac{\partial p}{\partial t} \right\} = \frac{\rho(p)\tilde{q}}{2\pi} \quad (4-21)$$

Multiplying both sides of Eq. 4-21 by -1 :

$$\nabla \bullet \left[\frac{\rho(p)k(p)\nabla p}{\mu} \right] + \rho(p)\phi(p)c_t(p) \frac{\partial p}{\partial t} = -\frac{\rho(p)\tilde{q}}{2\pi} \quad (4-22)$$

Since the fluid dynamic viscosity μ is constant for this modeling, the Eq. 4-21 becomes:

$$\nabla \bullet \left[\rho(p)k(p)\nabla p \right] + \rho(p)\phi(p)\mu c_t(p) \frac{\partial p}{\partial t} = -\frac{\rho(p)\tilde{q}\mu}{2\pi} \quad (4-23)$$

Expanding the terms inside the brackets:

$$\begin{aligned} k(p)\nabla p \bullet \nabla \rho(p) + \rho(p)k(p)\nabla^2 p + \rho(p)\nabla p \bullet \nabla k(p) + \rho(p)\phi(p)\mu c_t(p) \frac{\partial p}{\partial t} = \\ -\frac{\rho(p)\tilde{q}\mu}{2\pi} \end{aligned} \quad (4-24)$$

Considering that, the fluid density does not change in space, $\nabla\rho(p) = 0$. Then, Eq. 4-24 yields to:

$$k(p)\nabla^2 p + \nabla p \bullet \nabla k(p) + \phi(p)\mu c_t(p) \frac{\partial p}{\partial t} = -\frac{\tilde{q}\mu}{2\pi} \quad (4-25)$$

Dividing both sides of the Eq. 4-25 by the pressure-sensitive permeability $k(p)$:

$$\nabla^2 p + \frac{\nabla k(p) \bullet \nabla p}{k(p)} - \frac{\phi(p)\mu c_t(p)}{k(p)} \frac{\partial p}{\partial t} = -\frac{\tilde{q}\mu}{2\pi k(p)} \quad (4-26)$$

The pressure-sensitive permeability gradient is:

$$\nabla k(p) = \frac{\partial k(p)}{\partial p} \nabla p \quad (4-27)$$

Replacing the Eq. 4-27 in the Eq. 4-26:

$$\nabla^2 p + \frac{1}{k(p)} \frac{\partial k(p)}{\partial p} \nabla p \bullet \nabla p - \frac{\phi(p)\mu c_t(p)}{k(p)} \frac{\partial p}{\partial t} = -\frac{\tilde{q}\mu}{2\pi k(p)} \quad (4-28)$$

As the scalar product $\nabla p \bullet \nabla p = (\nabla p)^2$. Thereby:

$$\nabla^2 p + \frac{1}{k(p)} \frac{\partial k(p)}{\partial p} (\nabla p)^2 - \frac{\phi(p)\mu c_t(p)}{k(p)} \frac{\partial p}{\partial t} = -\frac{\tilde{q}\mu}{2\pi k(p)} \quad (4-29)$$

Considering the low pressure gradient, the second term of the left-hand side of the Eq. 4-29 can be neglected. Therewith:

$$\nabla^2 p - \frac{\phi(p)\mu c_t(p)}{k(p)} \frac{\partial p}{\partial t} = -\frac{\tilde{q}\mu}{2\pi k(p)} \quad (4-30)$$

The group $\phi(p)\mu c_t(p)/k(p)$ is the pressure-sensitive-hydraulic diffusivity inverse $1/\eta(p)$. Thus, $\eta(p)$ is:

$$\eta(p) = \frac{k(p)}{\phi(p)\mu c_t(p)} \quad (4-31)$$

Finally, the NHDE with source in terms of pressure is expressed as follows:

$$\nabla^2 p - \frac{1}{\eta(p)} \frac{\partial p}{\partial t} = -\frac{\tilde{q}\mu}{2\pi k(p)} \quad (4-32)$$

The initial condition is:

$$p(\mathbf{r}, t = 0) = p_i \quad (4-33)$$

The external boundary condition is:

$$\lim_{|\mathbf{r}| \rightarrow \infty} p(\mathbf{r}, t) = p_i \quad (4-34)$$

And the inner boundary condition is:

$$\left[\mathbf{r} \cdot \nabla p \right]_{(r=r_w)} = -\frac{q\mu}{2\pi k(p_i)h} \quad (4-35)$$

Where p_i is the initial pressure, [MPa] and r_w is the wellbore radius, [m].

4.3

Nonlinear Hydraulic Diffusivity Equation for Permeability Pressure-Sensitive Reservoirs

As the theory presented in the previous section, the NHDE with oil source term is expressed by:

$$\nabla^2 p - \frac{\phi\mu c_t}{k(p)} \frac{\partial p}{\partial t} = -\frac{\tilde{q}\mu}{2\pi} \quad (4-36)$$

Let the permeability pseudo-pressure function defined as (Fernandes, 2022):

$$m(p) = \int_{p_b}^p k(p') dp' \quad (4-37)$$

where the pseudo-pressure $m(p)$ is expressed in [md MPa] and p_b is a reference pressure, [MPa].

By Leibniz's rule, the pseudo-pressure gradient is:

$$\nabla m(p) = \frac{\partial m(p)}{\partial p} \nabla p \quad (4-38)$$

And the pseudo-pressure derivative with respect to the pressure is:

$$\frac{\partial m(p)}{\partial p} = \frac{\partial}{\partial p} \int_{p_b}^p k(p') dp' \quad (4-39)$$

Applying Leibniz's rule again, it can be noticed that the pseudo-pressure derivative concerning the pressure yields the pressure-sensitive permeability function:

$$\frac{\partial m(p)}{\partial p} = k(p) \quad (4-40)$$

Replacing the Eq. 4-40 in the Eq. 4-38, the pseudo-pressure gradient becomes:

$$\nabla m(p) = k(p)\nabla p \quad (4-41)$$

According to the Eq. 4-41, the divergent of the gradient of the pseudo-pressure can be expressed by:

$$\nabla \bullet [\nabla m(p)] = \nabla \bullet [k(p)\nabla p] \quad (4-42)$$

As the divergent of the gradient is the Laplacian, thus:

$$\nabla^2 m(p) = \nabla \bullet [k(p)\nabla p] \quad (4-43)$$

The pseudo-pressure rate is:

$$\frac{\partial m(p)}{\partial t} = \frac{\partial m(p)}{\partial p} \frac{\partial p}{\partial t} \quad (4-44)$$

Replacing the Eq. 4-40 in the Eq. 4-44, the pseudo-pressure rate yields to:

$$\frac{\partial m(p)}{\partial t} = k(p) \frac{\partial p}{\partial t} \quad (4-45)$$

Replacing the Eq. 4-45 and the Eq. 4-43 into the NHDE:

$$\nabla^2 m(p) - \frac{\phi \mu c_t}{k(p)} \frac{\partial m(p)}{\partial t} = -\frac{\tilde{q}\mu}{2\pi} \quad (4-46)$$

In terms of pseudo-pressure definition, Eq. 4-46 is:

$$\nabla^2 \left[\int_{p_b}^p k(p') dp' \right] - \frac{\phi \mu c_t}{k(p)} \frac{\partial}{\partial t} \left[\int_{p_b}^p k(p') dp' \right] = -\frac{\tilde{q}\mu}{2\pi} \quad (4-47)$$

Finally, we have NHDE with an oil source regarding the permeability pseudo-pressure. The pressure-sensitive permeability function is coupled to the hydraulic diffusivity function. It means that the partial differential equation is still nonlinear. In this formulation, we can also notice that the NHDE has no dependence on permeability function in the oil source term.

Let the permeability pseudo-pressure variation defined as:

$$\Delta m(p) = m(p_i) - m(p), \quad m(p_i) \geq m(p) \quad (4-48)$$

According to the Eq. 4-37:

$$\Delta m(p) = \int_{p_b}^{p_i} k(p') dp' - \int_{p_b}^p k(p') dp' \quad (4-49)$$

Using the calculus fundamental theorem, the integral above yields to:

$$\Delta m(p) = \int_p^{p_i} k(p') dp' \quad (4-50)$$

So, the NHDE can be represented in terms of the permeability pseudo-pressure variation $\Delta m(p)$:

$$\nabla^2 \Delta m(p) - \frac{1}{\eta(p)} \frac{\partial \Delta m(p)}{\partial t} = -\frac{\tilde{q}\mu}{2\pi} \quad (4-51)$$

The NHDE in terms of Eq. 4-50 is:

$$\nabla^2 \left[\int_p^{p_i} k(p') dp' \right] - \frac{1}{\eta(p)} \frac{\partial}{\partial t} \left[\int_p^{p_i} k(p') dp' \right] = -\frac{\tilde{q}\mu}{2\pi} \quad (4-52)$$

The next section will develop the dimensionless form of the Eq. 4-52.

4.4 Dimensionless Variables

For the dimensionless formulation of the pressure-sensitive permeability response model, it is necessary to define the relationship between the rock and fluid properties, as well as, the space and time variables. Thus, the dimensionless variables discussed in the proposed solution in this thesis are:

4.4.1 Dimensionless Laplacian

The dimensionless Laplacian is:

$$\nabla_D^2 = l_c^2 \nabla^2 \quad (4-53)$$

where l_c is a characteristic length, [m].

4.4.2 Dimensionless Permeability

The dimensionless permeability is:

$$k_D(p) = \frac{k(p)}{k(p_i)} \quad (4-54)$$

where $k(p_i)$ is pressure-sensitive permeability on the initial pressure, [md].

4.4.3

Dimensionless Time

The dimensionless time is expressed by:

$$t_D = \frac{k(p_i)t}{\phi\mu c_t l_c^2} \quad (4-55)$$

4.4.4

Dimensionless Radial Distance

The dimensionless radial distance is expressed by:

$$r_D = \frac{r}{r_w} \quad (4-56)$$

4.4.5

Dimensionless Hydraulic Diffusivity

The dimensionless hydraulic diffusivity is:

$$\eta_D(p) = \frac{k(p)}{k(p_i)} \quad (4-57)$$

4.4.6

Dimensionless Hydraulic Diffusivity Deviation Factor

The hydraulic diffusivity deviation factor is expressed by:

$$\xi(p) = \frac{k(p_i)}{k(p)} - 1 \quad (4-58)$$

Thus:

$$\xi(p) = \frac{1}{k_D(p)} - 1 \quad (4-59)$$

4.4.7

Dimensionless permeability pseudo-pressure

Based on the dimensionless variables aforementioned, dimensionless pseudo-pressure can be expressed through the inner boundary condition as follows:

$$m_D = \frac{2\pi h}{q\mu} \int_p^{p_i} k(p') dp', \quad m(p_i) \geq m(p) \quad (4-60)$$

where h is the reservoir net pay, [m]. Let NHDE in terms of pseudo-pressure variation:

$$\nabla^2 \Delta m(p) - \frac{1}{\eta(p)} \frac{\partial \Delta m(p)}{\partial t} = -\frac{\tilde{q}\mu}{2\pi} \quad (4-61)$$

Let the hydraulic diffusivity function in the initial condition:

$$\eta(p_i) = \frac{k(p_i)}{\phi\mu c_t} \quad (4-62)$$

As the dimensionless pseudo-pressure is:

$$m_D = \frac{2\pi h \Delta m(p)}{q\mu}, \quad \Delta m(p) \geq 0 \quad (4-63)$$

and, the pseudo-pressure variation is:

$$\Delta m(p) = m(p_i) - m(p), \quad m(p_i) \geq m(p) \quad (4-64)$$

The dimensionless pseudo-pressure Laplacian can be expressed as follows:

$$\nabla_D^2 m_D = \frac{2\pi l_c^2 h}{q\mu} \nabla^2 \Delta m(p) \quad (4-65)$$

Rewriting the Eq. 4-65:

$$\nabla^2 \Delta m(p) = \frac{q\mu}{2\pi l_c^2 h} \nabla_D^2 m_D \quad (4-66)$$

The dimensionless pseudo-pressure variation rate is:

$$\frac{\partial m_D}{\partial t} = \frac{2\pi h}{q\mu} \frac{\partial \Delta m(p)}{\partial t} \quad (4-67)$$

Rewriting the Eq. 4-67:

$$\frac{\partial \Delta m(p)}{\partial t} = \frac{q\mu}{2\pi h} \frac{\partial m_D}{\partial t} \quad (4-68)$$

Since:

$$t_D = \frac{k(p_i)t}{\phi\mu c_t l_c^2} \quad (4-69)$$

Then:

$$\frac{1}{t} = \frac{k(p_i)}{\phi\mu c_t l_c^2 t_D} \quad (4-70)$$

Thus, the time differential partial operator is:

$$\frac{\partial}{\partial t} = \frac{k(p_i)}{\phi\mu c_t l_c^2} \frac{\partial}{\partial t_D} \quad (4-71)$$

Replacing the Eqs. 4-66, 4-68 and 4-71 in the Eq. 4-61, the NHDE yields to:

$$\frac{q}{2\pi l_c^2 h} \left[\nabla_D^2 m_D - \frac{\phi\mu c_t k(p_i)}{\phi\mu c_t k(p)} \frac{\partial m_D}{\partial t_D} \right] = -\frac{\tilde{q}}{2\pi} \quad (4-72)$$

Since $\tilde{q} = q/l_c^2 h$, hence, Eq. 4-72 can be expressed as follows:

$$\nabla_D^2 m_D - \frac{1}{k_D(p)} \frac{\partial m_D}{\partial t_D} = -1 \quad (4-73)$$

Thereby, Eq. 4-73 is the final form of the dimensionless NHDE that models the permeability response during oil flow in pressure-sensitive reservoirs. The dimensionless pseudo-pressure initial condition is:

$$m_D(\mathbf{r}_D, t_D = 0) = 0 \quad (4-74)$$

And the external boundary condition is:

$$\lim_{|\mathbf{r}_D| \rightarrow +\infty} m_D(\mathbf{r}_D, t_D) = 0 \quad (4-75)$$

4.5 Asymptotic Series Expansion Method

In the asymptotic series expansion method, the solution of the pressure-sensitive permeability NHDE is expressed by the series (Kale & Mattar; Pedrosa Jr.; Kikani & Pedrosa Jr., 1980, 1986, 1991):

$$m_D(\mathbf{r}_D, t_D) = m_D^{(0)}(\mathbf{r}_D, t_D) + \epsilon m_D^{(1)}(\mathbf{r}_D, t_D) + \epsilon^2 m_D^{(2)}(\mathbf{r}_D, t_D) + \dots + \epsilon^k m_D^{(k)}(\mathbf{r}_D, t_D) \quad (4-76)$$

where ϵ is the perturbation parameter and $m_D^{(k)}(\mathbf{r}_D, t_D)$ are the coefficients of the series to be determined. In this method, the partial differential diffusivity equation is perturbed by the introduction of variable ϵ by multiplying the hydraulic diffusivity deviator factor $\xi(p)$ that is responsible for the nonlinearity of the equation.

The perturbed equation is expressed as follows:

$$\nabla_D^2 m_D - [1 + \epsilon\xi(p)] \frac{\partial m_D}{\partial t_D} = -f_D(x_D, y_D, z_D, t_D) \quad (4-77)$$

When $\epsilon = 0$, the partial differential diffusivity equation becomes linear, representing the constant permeability solution. Replacing the Eq. 4-76 in the Eq. 4-77 and after grouping terms of the same power in ϵ , the NHDE yields to:

$$\begin{aligned} & \epsilon^0 \left[\nabla_D^2 m_D - \frac{\partial m_D^{(0)}}{\partial t_D} + f_D(x_D, y_D, z_D, t_D) \right] + \epsilon^1 \left[\nabla_D^2 m_D - \frac{\partial m_D^{(0)}}{\partial t_D} - \xi^{(0)}(p) \frac{\partial m_D^{(0)}}{\partial t_D} \right] + \\ & + \epsilon^2 \left[\nabla_D^2 m_D - \frac{\partial m_D^{(1)}}{\partial t_D} - \xi^{(1)}(p) \frac{\partial m_D^{(1)}}{\partial t_D} \right] + \dots + \epsilon^k \left[\nabla_D^2 m_D - \frac{\partial m_D^{(k)}}{\partial t_D} - \xi^{(k-1)}(p) \frac{\partial m_D^{(k-1)}}{\partial t_D} \right] \\ & = 0 \quad (4-78) \end{aligned}$$

Using the definition of the hydraulic diffusivity deviation factor into Eq. 4-78 (Fernandes, 2022):

$$\begin{aligned} & \epsilon^0 \left[\nabla_D^2 m_D - \frac{\partial m_D^{(0)}}{\partial t_D} + f_D(x_D, y_D, z_D, t_D) \right] + \\ & + \epsilon^1 \left\{ \nabla_D^2 m_D - \frac{\partial m_D^{(0)}}{\partial t_D} - \left[\frac{1}{k_D(m_D^{(0)})} - 1 \right] \frac{\partial m_D^{(0)}}{\partial t_D} \right\} + \\ & + \epsilon^2 \left\{ \nabla_D^2 m_D - \frac{\partial m_D^{(1)}}{\partial t_D} - \left[\frac{1}{k_D(m_D^{(1)})} - 1 \right] \frac{\partial m_D^{(1)}}{\partial t_D} \right\} + \dots \\ & \dots + \epsilon^k \left\{ \nabla_D^2 m_D - \frac{\partial m_D^{(k)}}{\partial t_D} - \left[\frac{1}{k_D(m_D^{(k-1)})} - 1 \right] \frac{\partial m_D^{(k-1)}}{\partial t_D} \right\} \\ & = 0 \quad (4-79) \end{aligned}$$

Using a first-order approximation (Barreto Jr., Peres & Pires, 2010):

$$\begin{aligned} & \epsilon^0 \left[\nabla_D^2 m_D - \frac{\partial m_D^{(0)}}{\partial t_D} + f_D(x_D, y_D, z_D, t_D) \right] + \\ & + \epsilon^1 \left\{ \nabla_D^2 m_D - \frac{\partial m_D^{(0)}}{\partial t_D} - \left[\frac{1}{k_D(m_D^{(0)})} - 1 \right] \frac{\partial m_D^{(0)}}{\partial t_D} \right\} = 0 \quad (4-80) \end{aligned}$$

Expanding the terms inside the brackets from Eq. 4-80:

$$\begin{aligned} & \nabla_D^2 m_D + \epsilon \nabla_D^2 m_D + f_D - \frac{\partial m_D^{(0)}}{\partial t_D} - \epsilon \frac{\partial m_D^{(0)}}{\partial t_D} - \epsilon \left[\frac{1}{k_D(m_D^{(k-1)})} - 1 \right] \frac{\partial m_D^{(0)}}{\partial t_D} = 0 \\ & \quad (4-81) \end{aligned}$$

Regrouping some terms of Eq. 4-81:

$$(\epsilon + 1)\nabla_D^2 m_D + f_D - (\epsilon + 1)\frac{\partial m_D^{(0)}}{\partial t_D} - \epsilon \left[\frac{1}{k_D(m_D^{(k-1)})} - 1 \right] \frac{\partial m_D^{(0)}}{\partial t_D} = 0 \quad (4-82)$$

Regrouping again:

$$(\epsilon + 1) \left[\nabla_D^2 m_D - \frac{\partial m_D^{(0)}}{\partial t_D} \right] + f_D - \epsilon \left[\frac{1}{k_D(m_D^{(k-1)})} - 1 \right] \frac{\partial m_D^{(0)}}{\partial t_D} = 0 \quad (4-83)$$

Moving the source and nonlinear term to the right-hand side of the Eq. 4-83, we have the final form of the perturbed NHDE:

$$(\epsilon + 1) \left[\nabla_D^2 m_D - \frac{\partial m_D^{(0)}}{\partial t_D} \right] = -f_D + \epsilon \left[\frac{1}{k_D(m_D^{(k-1)})} - 1 \right] \frac{\partial m_D^{(0)}}{\partial t_D} \quad (4-84)$$

The right-hand side of Eq. 4-84 represents a general nonlinear source term, $\hat{\hat{\mathcal{S}}}_{oD}$. Applying the Eq. 4-76 in the initial and boundary conditions:

$$\sum_{k=0}^{\infty} \epsilon^k m_D^{(k)}(x_D, y_D, z_D, t_D = 0) = 0 \quad (4-85)$$

$$\lim_{(x_D, y_D, z_D) \rightarrow \infty} \sum_{k=0}^{\infty} \epsilon^k m_D^{(k)}(x_D, y_D, z_D, t_D) = 0 \quad (4-86)$$

Expanding the Eq. 4-86 in terms of epsilon powers:

$$\begin{aligned} & \epsilon^0 m_D^{(0)}(x_D, y_D, z_D, t_D = 0) + \epsilon^1 m_D^{(1)}(x_D, y_D, z_D, t_D = 0) + \\ & + \epsilon^2 m_D^{(2)}(x_D, y_D, z_D, t_D = 0) + \dots + \epsilon^k m_D^{(k)}(x_D, y_D, z_D, t_D = 0) = 0 \end{aligned} \quad (4-87)$$

Expanding again:

$$\begin{aligned} & \lim_{(x_D, y_D, z_D) \rightarrow \infty} \epsilon^0 m_D^{(0)}(x_D, y_D, z_D, t_D) + \lim_{x_D, y_D, z_D \rightarrow \infty} \epsilon^1 m_D^{(1)}(x_D, y_D, z_D, t_D, k_D) + \\ & + \lim_{(x_D, y_D, z_D) \rightarrow \infty} \epsilon^2 m_D^{(2)}(x_D, y_D, z_D, t_D, k_D) + \dots + \lim_{(x_D, y_D, z_D) \rightarrow \infty} \epsilon^k m_D^{(k)}(x_D, y_D, z_D, t_D, k_D) = 0 \end{aligned} \quad (4-88)$$

Expanding the dimensionless general oil source term $\hat{\hat{\mathcal{S}}}_{oD}^{(k)}$:

$$\begin{aligned} \hat{\hat{\mathcal{S}}}_{oD}^{(k)}(x_D, y_D, z_D, t_D) &= \hat{\hat{\mathcal{S}}}_{oD}^{(0)}(x_D, y_D, z_D, t_D) + \hat{\hat{\mathcal{S}}}_{oD}^{(1)}(x_D, y_D, z_D, t_D) + \\ &+ \hat{\hat{\mathcal{S}}}_{oD}^{(2)}(x_D, y_D, z_D, t_D) + \dots + \hat{\hat{\mathcal{S}}}_{oD}^{(k)}(x_D, y_D, z_D, t_D) \end{aligned} \quad (4-89)$$

Zeroth-Order

$$\hat{\hat{\mathcal{S}}}_{oD}^{(0)}(x_D, y_D, z_D, t_D) = f_D(x_D, y_D, z_D, t_D) \quad (4-90)$$

First-order

$$\hat{\hat{\mathcal{S}}}_{oD}^{(1)}(x_D, y_D, z_D, t_D) = \xi^{(0)} \frac{\partial m_D^{(0)}}{\partial t_D} \quad (4-91)$$

Second-Order

$$\hat{\hat{\mathcal{S}}}_{oD}^{(2)}(x_D, y_D, z_D, t_D) = \xi^{(1)} \frac{\partial m_D^{(1)}}{\partial t_D} \quad (4-92)$$

$k^{(th)}$ Order

$$\hat{\hat{\mathcal{S}}}_{oD}^{(k)}(x_D, y_D, z_D, t_D) = \xi^{(k-1)} \frac{\partial m_D^{(k-1)}}{\partial t_D} \quad (4-93)$$

For $k = 1, 2, \dots$. This implies that to find the solution of the $k^{(th)}$ term, it is necessary to solve the problem $k-1$ before. So the system of equations must be solved sequentially, starting from the zero order problem. Since the deviation factor ξ is a function of m_D , in solving the problem of order k , it is only possible to compute the ξ factor with the pseudo-pressure values calculated up to the previous order. Thus, the ξ factor can be expressed by:

$$\xi^{(k-1)} = \xi \left[\sum_{j=0}^{(k-1)} m_D^{(j)} \right] \quad (4-94)$$

For $k = 1, 2, \dots$

The dimensionless total oil source becomes:

$$\begin{aligned} \hat{\hat{\mathcal{S}}}_{oD}^{(k)}(x_D, y_D, z_D, t_D) &= f_D(x_D, y_D, z_D, t_D) + \xi^{(0)} \frac{\partial m_D^{(0)}}{\partial t_D} + \xi^{(1)} \frac{\partial m_D^{(1)}}{\partial t_D} + \\ &+ \xi^{(k-1)} \frac{\partial m_D^{(k-1)}}{\partial t_D} + \dots \end{aligned} \quad (4-95)$$

The dimensionless total oil source as a function of the pressure-sensitive

permeability is:

$$\begin{aligned} \hat{\hat{S}}_{oD}^{(k)}(x_D, y_D, z_D, t_D) = & f_D(x_D, y_D, z_D, t_D) + \left[\frac{1}{k_D(m_D^{(0)})} - 1 \right] \frac{\partial m_D^{(0)}}{\partial t_D} + \\ & + \left[\frac{1}{k_D(m_D^{(1)})} - 1 \right] \frac{\partial m_D^{(1)}}{\partial t_D} + \left[\frac{1}{k_D(m_D^{(k-1)})} - 1 \right] \frac{\partial m_D^{(k-1)}}{\partial t_D} + \dots \end{aligned} \quad (4-96)$$

This thesis develops the analytical solution for the dimensionless NHDE through a first-order series expansion. Hence, the general oil source must be truncated at the first-order. Thus, the total oil source becomes:

$$\hat{\hat{S}}_{oD}^{(k)}(x_D, y_D, z_D, t_D) \approx f_D(x_D, y_D, z_D, t_D) + \xi^{(0)} \frac{\partial m_D^{(0)}}{\partial t_D} \quad (4-97)$$

The first-order total oil source as a function of the pressure-sensitive permeability is:

$$\hat{\hat{S}}_{oD}^{(k)}(x_D, y_D, z_D, t_D) \approx f_D(x_D, y_D, z_D, t_D) + \left[\frac{1}{k_D(m_D^{(0)})} - 1 \right] \frac{\partial m_D^{(0)}}{\partial t_D} \quad (4-98)$$

The dimensionless $k^{(th)}$ order solution of the NHDE using GF is associated with the equation:

$$\begin{aligned} \nabla^2 G_D^{(k)}(x_D, x'_D, y_D, y'_D, z_D, z'_D, t_D, t'_D) - \frac{\partial G_D^{(k)}(x_D, x'_D, y_D, y'_D, z_D, z'_D, t_D, t'_D)}{\partial t_D} = \\ = -\delta(x_D - x'_D)\delta(y_D - y'_D)\delta(z_D - z'_D)\delta(t_D - t'_D) \end{aligned} \quad (4-99)$$

The parameters x'_D, y'_D, z'_D and t'_D represent the position and time where and when the instantaneous oil pulse is applied, whereas x_D, y_D, z_D and t_D represent the position and the time where and when the pulse is observed. The term on the right-hand side of the Eq. 4-99 is the oil point-source represented by the Dirac's delta function $\delta(x_D - x'_D)\delta(y_D - y'_D)\delta(z_D - z'_D)\delta(t_D - t'_D)$.

The associated initial condition is:

$$G_D^{(k)}(x_D, x'_D, y_D, y'_D, z_D, z'_D, t_D = 0, t'_D) = 0 \quad (4-100)$$

and, the homogeneous external boundary condition becomes:

$$\lim_{(x_D, y_D, z_D) \rightarrow \infty} G_D^{(k)}(x_D, x'_D, y_D, y'_D, z_D, z'_D, t_D, t'_D) = 0 \quad (4-101)$$

The solution of the k order differential equation is expressed by:

$$m_D^{(k)}(x_D, y_D, z_D, t_D) = - \int_{-\infty}^{+\infty} \int_{-\infty}^{+\infty} \int_{-\infty}^{+\infty} \int_0^{t_D} \hat{\hat{S}}_{oD}^{(k)}(x'_D, y'_D, z'_D, t'_D, k_D) \times \\ \times G_D^{(k)}(x_D, x'_D, y_D, y'_D, z_D, z'_D, t_D, t'_D) dt'_D dx'_D dy'_D dz'_D \quad (4-102)$$

The problem approached by the Eqs. 4-99, 4-100 and 4-101 is exactly the same for all k , thereby, the GF's are the same. Thus:

$$G_D^{(k)}(x_D, x'_D, y_D, y'_D, z_D, z'_D, t_D, t'_D) = G_D(x_D, x'_D, y_D, y'_D, z_D, z'_D, t_D, t'_D) \quad (4-103)$$

Replacing the definition of the dimensionless general oil source $\hat{\hat{S}}_{oD}^{(k)}(x_D, y_D, z_D, t_D)$ and from the $G_D^{(k)}(x_D, x'_D, y_D, y'_D, z_D, z'_D, t_D, t'_D)$ in the Eq. 4-102, the general solution can be expanded as follows:

Zeroth-Order

$$m_D^{(0)}(x_D, y_D, z_D, t_D) = - \int_{-\infty}^{+\infty} \int_{-\infty}^{+\infty} \int_{-\infty}^{+\infty} \int_0^{t_D} f_D(x'_D, y'_D, z'_D, t'_D, k_D) \times \\ \times G_D(x_D, x'_D, y_D, y'_D, z_D, z'_D, t_D, t'_D) dt'_D dx'_D dy'_D dz'_D \quad (4-104)$$

First-order

$$m_D^{(1)}(x_D, y_D, z_D, t_D) = - \int_{-\infty}^{+\infty} \int_{-\infty}^{+\infty} \int_{-\infty}^{+\infty} \int_0^{t_D} \xi^{(0)} \frac{\partial m_D^{(0)}}{\partial t'_D} \times \\ \times G_D(x_D, x'_D, y_D, y'_D, z_D, z'_D, t_D, t'_D) dt'_D dx'_D dy'_D dz'_D \quad (4-105)$$

Second-Order

$$m_D^{(2)}(x_D, y_D, z_D, t_D) = - \int_{-\infty}^{+\infty} \int_{-\infty}^{+\infty} \int_{-\infty}^{+\infty} \int_0^{t_D} \xi^{(1)} \frac{\partial m_D^{(1)}}{\partial t'_D} \times \\ \times G_D(x_D, x'_D, y_D, y'_D, z_D, z'_D, t_D, t'_D) dt'_D dx'_D dy'_D dz'_D \quad (4-106)$$

k^{th} Order

$$m_D^{(k)}(x_D, y_D, z_D, t_D) = - \int_{-\infty}^{+\infty} \int_{-\infty}^{+\infty} \int_{-\infty}^{+\infty} \int_0^{t_D} \xi^{(k-1)} \frac{\partial m_D^{(k-1)}}{\partial t'_D} \times \\ \times G_D(x_D, x'_D, y_D, y'_D, z_D, z'_D, t_D, t'_D) dt'_D dx'_D dy'_D dz'_D \quad (4-107)$$

Replacing the hydraulic diffusivity deviator factor definition in the Eqs. 4-104 to 4-107, the general solution yields to:

Zeroth-Order

$$\begin{aligned}
m_D^{(0)}(x_D, y_D, z_D, t_D) = & \\
& - \int_{-\infty}^{+\infty} \int_{-\infty}^{+\infty} \int_{-\infty}^{+\infty} \int_0^{t_D} f_D(x'_D, y'_D, z'_D, t'_D, k_D) \times \\
& \times G_D(x_D, x'_D, y_D, y'_D, z_D, z'_D, t_D, t'_D) dt'_D dx'_D dy'_D dz'_D \quad (4-108)
\end{aligned}$$

First-order

$$\begin{aligned}
m_D^{(1)}(x_D, y_D, z_D, t_D) = & \\
& - \int_{-\infty}^{+\infty} \int_{-\infty}^{+\infty} \int_{-\infty}^{+\infty} \int_0^{t_D} \left[\frac{1}{k_D(m_D^{(0)})} - 1 \right] \frac{\partial m_D^{(0)}}{\partial t'_D} \times \\
& \times G_D(x_D, x'_D, y_D, y'_D, z_D, z'_D, t_D, t'_D) dt'_D dx'_D dy'_D dz'_D \quad (4-109)
\end{aligned}$$

Second-Order

$$\begin{aligned}
m_D^{(2)}(x_D, y_D, z_D, t_D) = & \\
& - \int_{-\infty}^{+\infty} \int_{-\infty}^{+\infty} \int_{-\infty}^{+\infty} \int_0^{t_D} \left[\frac{1}{k_D(m_D^{(1)})} - 1 \right] \frac{\partial m_D^{(1)}}{\partial t'_D} \times \\
& \times G_D(x_D, x'_D, y_D, y'_D, z_D, z'_D, t_D, t'_D) dt'_D dx'_D dy'_D dz'_D \quad (4-110)
\end{aligned}$$

 k^{th} Order

$$\begin{aligned}
m_D^{(k)}(x_D, y_D, z_D, t_D) = & \\
& - \int_{-\infty}^{+\infty} \int_{-\infty}^{+\infty} \int_{-\infty}^{+\infty} \int_0^{t_D} \left[\frac{1}{k_D(m_D^{(k-1)})} - 1 \right] \frac{\partial m_D^{(k-1)}}{\partial t'_D} \times \\
& \times G_D(x_D, x'_D, y_D, y'_D, z_D, z'_D, t_D, t'_D) dt'_D dx'_D dy'_D dz'_D \quad (4-111)
\end{aligned}$$

Using the asymptotic expansion method (Kale & Mattar, 1980) and replacing the k terms of the series (4-108 to 4-111) in the Eq. 4-76 and considering the perturbation parameter $\epsilon \rightarrow 1$ in the Eq. 4-78, the dimensionless integro-differential solution is expressed by:

$$\begin{aligned}
m_D^{(k)}(x_D, y_D, z_D, t_D) = & \\
& - \int_{-\infty}^{+\infty} \int_{-\infty}^{+\infty} \int_{-\infty}^{+\infty} \int_0^{t_D} \left\{ f_D(x'_D, y'_D, z'_D, t'_D, k_D) + \sum_{j=1}^k \left[\xi^{(j-1)} \frac{\partial m_D^{(j-1)}}{\partial t'_D} \right] \right\} \times \\
& \times G_D(x_D, x'_D, y_D, y'_D, z_D, z'_D, t_D, t'_D) dt'_D dx'_D dy'_D dz'_D \quad (4-112)
\end{aligned}$$

Using a first-order approximation ([Barreto Jr., Peres & Pires, 2010](#)):

$$\begin{aligned}
 m_D(x_D, y_D, z_D, t_D) \approx & - \int_{-\infty}^{+\infty} \int_{-\infty}^{+\infty} \int_{-\infty}^{+\infty} \int_0^{t_D} f_D(x'_D, y'_D, z'_D, t'_D, k_D) \times \\
 & \times G_D(x_D, x'_D, y_D, y'_D, z_D, z'_D, t_D, t'_D) dt'_D dx'_D dy'_D dz'_D - \\
 & + \int_{-\infty}^{+\infty} \int_{-\infty}^{+\infty} \int_{-\infty}^{+\infty} \int_0^{t_D} \xi[m_D^{(0)}] \frac{\partial m_D^{(0)}}{\partial t'_D} \times \\
 & \times G_D(x_D, x'_D, y_D, y'_D, z_D, z'_D, t_D, t'_D) dt'_D dx'_D dy'_D dz'_D \quad (4-113)
 \end{aligned}$$

Finally, using the hydraulic diffusivity deviation factor definition ([Fernandes, 2022](#)) into Eq. 4-113, the dimensionless first-order integro-differential solution for the unsteady-state mechanical formation damage control caused by the permeability loss is expressed as:

$$\begin{aligned}
 m_D(x_D, y_D, z_D, t_D) \approx & - \int_{-\infty}^{+\infty} \int_{-\infty}^{+\infty} \int_{-\infty}^{+\infty} \int_0^{t_D} f_D(x'_D, y'_D, z'_D, t'_D, k_D) \times \\
 & \times G_D(x_D, x'_D, y_D, y'_D, z_D, z'_D, t_D, t'_D) dt'_D dx'_D dy'_D dz'_D - \\
 & + \int_{-\infty}^{+\infty} \int_{-\infty}^{+\infty} \int_{-\infty}^{+\infty} \int_0^{t_D} \left[\frac{1}{k_D(m_D^{(0)})} - 1 \right] \frac{\partial m_D^{(0)}}{\partial t'_D} \times \\
 & \times G_D(x_D, x'_D, y_D, y'_D, z_D, z'_D, t_D, t'_D) dt'_D dx'_D dy'_D dz'_D \quad (4-114)
 \end{aligned}$$

5

Integro-Differential Solutions for Constant Oil Flow Rate

This chapter presents the integro-differential solutions coupled to asymptotic expansion technique to solve the NHDE for several well-reservoir settings during the drawdown period. For this approach, the oil flow rate is considered as constant over the reservoir life-cycle. The general solution is derived through the GF technique, as well as, an integro-differential approach. The dimensionless oil source term $f_D(x_D, y_D, z_D, t_D)$ for each setting is derived, using the change scale and sampling properties of the instantaneous point-source Dirac delta function $\delta(x_D - x'_D)\delta(y_D - y'_D)\delta(z_D - z'_D)\delta(t_D - t'_D)$ and, the inner boundary condition.

5.1

Oil Flow in a Vertical Well Fully Penetrating an Infinite Reservoir

This section deals with the analytical solution for the Infinite-Acting-Radial-Flow (IARF) well-reservoir setting. The developed model is based on an integro-differential formulation combined to a first-order asymptotic series expansion and the appropriate GF for the aforementioned setting. In this problem, a constant radial oil flow in a cylindrical porous medium of infinite radial dimension and thickness h_a and h_b will be studied separately (Figure 5.1). The unsteady radial flow NHDE pore pressure-dependent permeability is solved by proposed model in terms of the dimensionless pseudo-pressure $m_{wD}(t_D)$, such that $r_w \ll r$. The GF related to this geometry is obtained from (Carslaw & Jaeger, 1959).

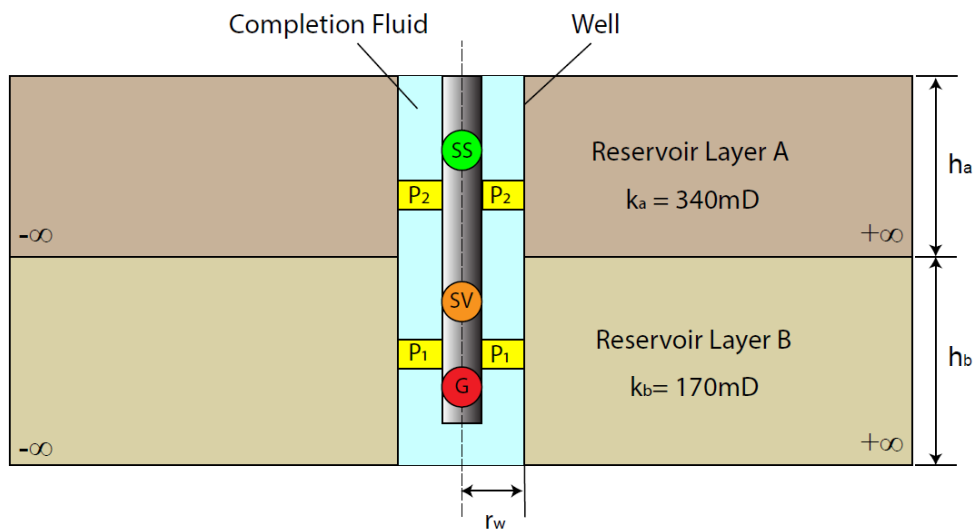


Figure 5.1: Sketch of a vertical well in an infinite reservoir.

5.1.1

Model Assumptions

For modeling of oil flow problem in porous media by means of the asymptotic series expansion of the solution of the pressure diffusivity equation in terms of pseudo-pressure, the following premises are assumed:

1. Constant oil flow rate in the well
2. Pressure-sensitive permeability
3. Darcian oil flow in porous media
4. Well fully penetrates reservoir rock
5. Deformable, homogeneous, linear elastic and isotropic reservoir
6. The well is located at the origin of cylindrical system of coordinates (0,0)
7. Isothermal, single-phase and compressible flow in the reservoir
8. The fluid present inside the pores of the reservoir rock does not react chemically with the rock matrix
9. One dimensional and unsteady flow
10. Small pressure gradient
11. Skin and storage effects not considered
12. Permeability hysteresis of porous media is negligible
13. No fluid flow across the top and bottom of the formation
14. Infinite extent reservoir in r-direction
15. Reservoir with uniform net pay

5.1.2

Nonlinear Hydraulic Diffusivity Equation Derivation

The analytical model developed in this work for unsteady radial oil flow in a pressure-sensitive reservoir is expressed by the NHDE in cylindrical coordinates:

$$\frac{1}{r} \frac{\partial}{\partial r} \left[rk(p) \frac{\partial p}{\partial r} \right] - \phi \mu c_t \frac{\partial p}{\partial t} = -\frac{\tilde{q}(r, t) \mu}{2\pi} \quad (5-1)$$

Applying the product's rule in the Eq. 5-1:

$$\frac{1}{r} \left\{ k(p) \frac{\partial p}{\partial r} + r \frac{\partial p}{\partial r} \left[\frac{dk(p)}{dp} \frac{\partial p}{\partial r} \right] + rk(p) \frac{\partial^2 p}{\partial r^2} \right\} - \phi \mu c_t \frac{\partial p}{\partial t} = -\frac{\tilde{q}(r, t) \mu}{2\pi} \quad (5-2)$$

The Eq. 5-2 can be rewritten as follows:

$$\frac{1}{r} \left[k(p) \frac{\partial p}{\partial r} + r \frac{dk(p)}{dp} \left(\frac{\partial p}{\partial r} \right)^2 + rk(p) \frac{\partial^2 p}{\partial r^2} \right] - \phi \mu c_t \frac{\partial p}{\partial t} = -\frac{\tilde{q}(r, t) \mu}{2\pi} \quad (5-3)$$

Considering the small pressure gradient assumption, the Eq. 5-3 becomes:

$$\frac{1}{r} \left[k(p) \frac{\partial p}{\partial r} + rk(p) \frac{\partial^2 p}{\partial r^2} \right] - \phi \mu c_t \frac{\partial p}{\partial t} = -\frac{\tilde{q}(r, t) \mu}{2\pi} \quad (5-4)$$

Rewriting the Eq. 5-4 with the pressure-sensitive permeability outside from the Laplacian:

$$k(p) \left(\frac{\partial^2 p}{\partial r^2} + \frac{1}{r} \frac{\partial p}{\partial r} \right) - \phi \mu c_t \frac{\partial p}{\partial t} = -\frac{\tilde{q}(r, t) \mu}{2\pi} \quad (5-5)$$

After the rearrangement of the Laplacian, the Eq. 5-5 yields to:

$$k(p) \left[\frac{1}{r} \frac{\partial}{\partial r} \left(r \frac{\partial p}{\partial r} \right) \right] - \phi \mu c_t \frac{\partial p}{\partial t} = -\frac{\tilde{q}(r, t) \mu}{2\pi} \quad (5-6)$$

Dividing both sides of the Eq. 5-6 by the permeability function $k(p)$:

$$\frac{1}{r} \frac{\partial}{\partial r} \left(r \frac{\partial p}{\partial r} \right) - \frac{\phi \mu c_t}{k(p)} \frac{\partial p}{\partial t} = -\frac{\tilde{q}(r, t) \mu}{2\pi k(p)} \quad (5-7)$$

As approached in the chapter 4, the permeability pseudo-pressure $m(p)$ is defined as (Fernandes, 2022):

$$m(p) = \int_{p_b}^p k(p') dp' \quad (5-8)$$

The pseudo-pressure's gradient is:

$$\frac{\partial m(p)}{\partial r} = \frac{dm(p)}{dp} \frac{\partial p}{\partial r} \quad (5-9)$$

The pseudo-pressure derivative with respect to the pressure is:

$$\frac{dm(p)}{dp} = \frac{d}{dp} \int_{p_b}^p k(p') dp' \quad (5-10)$$

That results in:

$$\frac{dm(p)}{dp} = k(p) \quad (5-11)$$

Replacing the Eq.5-11 into Eq.5-9, the pseudo-pressure gradient yields to:

$$\frac{\partial m(p)}{\partial r} = k(p) \frac{\partial p}{\partial r} \quad (5-12)$$

The pseudo-pressure's instantaneous rate is:

$$\frac{\partial m(p)}{\partial t} = \frac{dm(p)}{dp} \frac{\partial p}{\partial t} \quad (5-13)$$

Replacing the Eq.5-11 into Eq.5-13, the pseudo-pressure rate becomes:

$$\frac{\partial m(p)}{\partial t} = k(p) \frac{\partial p}{\partial t} \quad (5-14)$$

Replacing the Eq.5-12 into Eq.5-14, in the Eq. 5-6, the NHDE is expressed by:

$$\frac{1}{r} \frac{\partial}{\partial r} \left[\frac{1}{k(p)} r \frac{\partial m(p)}{\partial r} \right] - \frac{\phi \mu c_t}{k(p)^2} \frac{\partial m(p)}{\partial t} = - \frac{\tilde{q}(r, t) \mu}{2\pi k(p)} \quad (5-15)$$

Applying the quotient and chain's rule in the Eq. 5-15:

$$\begin{aligned} \frac{1}{r} \left\{ \frac{1}{k(p)} \frac{\partial m(p)}{\partial r} - \frac{r}{k(p)^2} \frac{dk(p)}{dp} \left[\frac{\partial m(p)}{\partial r} \right]^2 + \frac{r}{k(p)} \frac{\partial^2 m(p)}{\partial r^2} \right\} - \frac{\phi \mu c_t}{k(p)^2} \frac{\partial m(p)}{\partial t} = \\ = - \frac{\tilde{q}(r, t) \mu}{2\pi k(p)} \quad (5-16) \end{aligned}$$

For small pseudo-pressure gradient, the Eq. 5-16 becomes:

$$\frac{1}{r} \left[\frac{1}{k(p)} \frac{\partial m(p)}{\partial r} + \frac{r}{k(p)} \frac{\partial^2 m(p)}{\partial r^2} \right] - \frac{\phi \mu c_t}{k(p)^2} \frac{\partial m(p)}{\partial t} = - \frac{\tilde{q}(r, t) \mu}{2\pi k(p)} \quad (5-17)$$

Rewriting the Eq. 5-17:

$$\frac{1}{k(p)} \left\{ \frac{1}{r} \left[r \frac{\partial^2 m(p)}{\partial r^2} + \frac{\partial m(p)}{\partial r} \right] \right\} - \frac{\phi \mu c_t}{k(p)^2} \frac{\partial m(p)}{\partial t} = - \frac{\tilde{q}(r, t) \mu}{2\pi k(p)} \quad (5-18)$$

Multiplying both sides of the Eq. 5-18 by the permeability function $k(p)$:

$$\frac{1}{r} \frac{\partial}{\partial r} \left[r \frac{\partial m(p)}{\partial r} \right] - \frac{\phi \mu c_t}{k(p)} \frac{\partial m(p)}{\partial t} = - \frac{\tilde{q}(r, t) \mu}{2\pi} \quad (5-19)$$

According to the pseudo-pressure variation definition:

$$\Delta m(p) = \int_{p_b}^{p_i} k(p') dp' - \int_{p_b}^p k(p') dp' \quad (5-20)$$

That yields to:

$$\Delta m(p) = \int_p^{p_i} k(p') dp' \quad (5-21)$$

Thereby, the pseudo-pressure variation gradient can be expressed by:

$$\frac{\partial \Delta m(p)}{\partial r} = - \frac{\partial m(p)}{\partial r} \quad (5-22)$$

and the pseudo-pressure instantaneous rate, as follows:

$$\frac{\partial \Delta m(p)}{\partial t} = - \frac{\partial m(p)}{\partial t} \quad (5-23)$$

Replacing the Eqs. 5-22 and 5-23 in the Eq. 5-19, the final form for the NHDE in terms of permeability pseudo-pressure variation is:

$$\frac{1}{r} \frac{\partial}{\partial r} \left[r \frac{\partial \Delta m(p)}{\partial r} \right] - \frac{\phi \mu c_t}{k(p)} \frac{\partial \Delta m(p)}{\partial t} = - \frac{\tilde{q}(r, t) \mu}{2\pi} \quad (5-24)$$

The initial condition is:

$$\Delta m(p)(r, t = 0) = 0 \quad (5-25)$$

The external boundary condition is:

$$\lim_{r \rightarrow \infty} \Delta m(p)(r, t) = 0 \quad (5-26)$$

The inner boundary condition in terms of pressure is expressed by:

$$q = -\frac{2\pi k(p)h}{\mu} \left(r \frac{\partial p}{\partial r} \right)_{r=r_w} \quad (5-27)$$

Let the pressure variation defined as:

$$\Delta p(r, t) = p(r = r_w, 0) - p(r, t) \quad (5-28)$$

The wellbore pressure value in the initial time $t = 0$ is $p(r = r_w, t = 0) = p_i$.

Thus:

$$\Delta p(r, t) = p_i - p(r, t) \quad (5-29)$$

The pressure variation gradient is:

$$\frac{\partial \Delta p}{\partial r} = -\frac{\partial p}{\partial r} \quad (5-30)$$

Replacing the Eq. 5-30 in the Eq. 5-12, the pressure variation gradient can be expressed in terms of the pseudo-pressure variation:

$$\frac{\partial \Delta p}{\partial r} = \frac{1}{k(p)} \frac{\partial \Delta m(p)}{\partial r} \quad (5-31)$$

Thus, the inner boundary condition becomes:

$$q = -\frac{2\pi k(p)h}{\mu} \left[r \frac{1}{k(p)} \frac{\partial \Delta m(p)}{\partial r} \right]_{r=r_w} \quad (5-32)$$

The final form of the inner boundary condition is expressed as:

$$q = -\frac{2\pi h}{\mu} \left[r \frac{\partial \Delta m(p)}{\partial r} \right]_{r=r_w} \quad (5-33)$$

Despite the pressure-sensitive permeability function $k(p)$ does not appear explicitly in the inner boundary condition (Eq. 5-33), this function is coupled in the model through the pseudo-pressure variation definition (Eq. 5-20).

5.1.3

Dimensionless Pseudo-Pressure Model Derivation

Based on the dimensionless variables defined previously in the chapter 4, the pseudo-pressure variation gradient is:

$$\frac{\partial \Delta m(p)}{\partial r} = \frac{\partial \Delta m(p)}{\partial r_D} \frac{dr_D}{dr} \quad (5-34)$$

The dimensionless radial component derivative with respect to the radial component is:

$$\frac{dr_D}{dr} = \frac{d}{dr} \left(\frac{r}{r_w} \right) \quad (5-35)$$

That results in:

$$\frac{dr_D}{dr} = \frac{1}{r_w} \quad (5-36)$$

Thus, the pseudo-pressure variation gradient yields to:

$$\frac{\partial \Delta m(p)}{\partial r} = \frac{1}{r_w} \frac{\partial \Delta m(p)}{\partial r_D} \quad (5-37)$$

The initial condition in terms of the dimensionless radial component is:

$$\Delta m(p)(r_D, t = 0) = 0 \quad (5-38)$$

And the external boundary condition is:

$$\lim_{r_D \rightarrow \infty} \Delta m(p)(r_D, t) = 0 \quad (5-39)$$

The dimensionless initial condition yields to:

$$\Delta m(p)(r_D, t_D = 0) = 0 \quad (5-40)$$

The dimensionless external boundary condition becomes:

$$\lim_{r_D \rightarrow \infty} \Delta m(p)(r_D, t_D, k_D) = 0 \quad (5-41)$$

The pseudo-pressure variation instantaneous rate is:

$$\frac{\partial \Delta m(p)}{\partial t} = \frac{\partial \Delta m(p)}{\partial t_D} \frac{dt_D}{dt} \quad (5-42)$$

The dimensionless time derivative with respect to the time is:

$$\frac{dt_D}{dt} = \frac{d}{dt} \left[\frac{k(p_i)t}{\phi \mu c_t r_w^2} \right] \quad (5-43)$$

Replacing the Eq. 5-43 in the Eq. 5-42, the pseudo-pressure variation rate becomes:

$$\frac{\partial \Delta m(p)}{\partial t} = \frac{k(p_i)}{\phi \mu c_t r_w^2} \frac{\partial \Delta m(p)}{\partial t_D} \quad (5-44)$$

The partial differential operator is:

$$\frac{1}{r} \frac{\partial}{\partial r} = \frac{1}{r_D r_w} \frac{\partial}{\partial (r_D r_w)} \quad (5-45)$$

That results in:

$$\frac{1}{r} \frac{\partial}{\partial r} = \frac{1}{r_w^2 r_D} \frac{\partial}{\partial r_D} \quad (5-46)$$

Replacing the Eqs. 5-37, 5-44 and 5-46 in the Eq. 5-23:

$$\frac{1}{r_w^2} \frac{1}{r_D} \frac{\partial}{\partial r_D} \left[\frac{r_w}{r_w} r_D \frac{\partial \Delta m(p)}{r_D} \right] - \frac{\phi \mu c_t k(p_i)}{\phi \mu c_t r_w^2 k(p)} \frac{\partial \Delta m(p)}{\partial t_D} = -\frac{\tilde{q}(r, t) \mu}{2\pi} \quad (5-47)$$

Thus, the NHDE in terms of pseudo-pressure variation for the dimensionless space-time variables yields to:

$$\frac{1}{r_D} \frac{\partial}{\partial r_D} \left[r_D \frac{\partial \Delta m(p)}{\partial r_D} \right] - \frac{1}{k_D(p)} \frac{\partial \Delta m(p)}{\partial t_D} = -\frac{\tilde{q}(r, t) \mu r_w^2}{2\pi} \quad (5-48)$$

The dimensionless pseudo-pressure $m_D(r_D, t_D, k_D)$ was defined in the chapter 4 as follows:

$$m_D(r_D, t_D, k_D) = \frac{2\pi h \Delta m(p)}{q\mu} \quad (5-49)$$

The dimensionless pseudo-pressure gradient is:

$$\frac{\partial m_D}{\partial r_D} = \frac{2\pi h}{q\mu} \frac{\partial \Delta m(p)}{\partial r_D} \quad (5-50)$$

The dimensionless pseudo-pressure rate is:

$$\frac{\partial m_D}{\partial t_D} = \frac{2\pi h}{q\mu} \frac{\partial \Delta m(p)}{\partial t_D} \quad (5-51)$$

Combining the Eqs. 5-48, 5-50 and 5-51, the NHDE becomes:

$$\frac{1}{r_D} \frac{\partial}{\partial r_D} \left[\frac{q\mu}{2\pi h} r_D \frac{\partial m_D}{\partial r_D} \right] - \frac{q\mu}{2\pi h k_D(p)} \frac{\partial m_D}{\partial t_D} = -\frac{\tilde{q}(r, t) \mu r_w^2}{2\pi} \quad (5-52)$$

Rewriting the Eq. 5-53:

$$\frac{q\mu}{2\pi h} \left[\frac{1}{r_D} \frac{\partial}{\partial r_D} \left(r_D \frac{\partial m_D}{\partial r_D} \right) \right] - \frac{q\mu}{2\pi h k_D(p)} \frac{\partial m_D}{\partial t_D} = -\frac{\tilde{q}(r, t)\mu r_w^2}{2\pi} \quad (5-53)$$

Thus:

$$\frac{1}{r_D} \frac{\partial}{\partial r_D} \left(r_D \frac{\partial m_D}{\partial r_D} \right) - \frac{1}{k_D(p)} \frac{\partial m_D}{\partial t_D} = -\frac{2\pi r_w^2 h \tilde{q}(r, t)}{2\pi q} \quad (5-54)$$

The ratio $\tilde{q}(r, t)/q$ has $[m^{-3}]$ unit. Thus, the right-hand side of the Eq. 5-54 is a dimensionless unity oil source term $f_D(r_D, t_D, k_D) = 1$. The negative sign means that, the fluid is being withdrawn from the reservoir. Finally, the dimensionless form of the NHDE in terms of pseudo-pressure is expressed by:

$$\frac{1}{r_D} \frac{\partial}{\partial r_D} \left(r_D \frac{\partial m_D}{\partial r_D} \right) - \frac{1}{k_D(p)} \frac{\partial m_D}{\partial t_D} = -f_D(r_D, t_D, k_D) \quad (5-55)$$

The dimensionless initial condition is:

$$m_D(r_D, t_D = 0, k_D) = 0 \quad (5-56)$$

The external boundary condition is:

$$\lim_{r_D \rightarrow \infty} m_D(r_D, t_D, k_D) = 0 \quad (5-57)$$

And the inner boundary condition is:

$$\left(r_D \frac{\partial m_D}{\partial r_D} \right)_{r_D=1} = -1 \quad (5-58)$$

In order to introduce the hydraulic diffusivity deviator factor approach in the developed model, the dimensionless inverse pressure-sensitive permeability diffusivity function $1/k_D(p)$ is transformed in a new function denominated inverse hydraulic diffusivity function $\mathcal{D}(p)$.

Thereby:

$$\mathcal{D}(p) = \frac{1}{k_D(p)} \quad (5-59)$$

The relationship between the inverse hydraulic diffusivity function $\mathcal{D}(p)$ and the hydraulic diffusivity deviator factor $\xi(p)$ is:

$$\mathcal{D}(p) = \xi(p) + 1 \quad (5-60)$$

Thus, the dimensionless NHDE in terms of pseudo-pressure with constant source term is:

$$\frac{1}{r_D} \frac{\partial}{\partial r_D} \left(r_D \frac{\partial m_D}{\partial r_D} \right) - \mathcal{D}(p) \frac{\partial m_D}{\partial t_D} = -f_D(r_D, t_D, k_D) \quad (5-61)$$

Replacing the Eq. 5-60 in the Eq. 5-61, we have the dimensionless form of the NHDE as a function of the hydraulic diffusivity deviation factor:

$$\frac{1}{r_D} \frac{\partial}{\partial r_D} \left(r_D \frac{\partial m_D}{\partial r_D} \right) - [\xi(p) + 1] \frac{\partial m_D}{\partial t_D} = -f_D(r_D, t_D, k_D) \quad (5-62)$$

5.1.4

Asymptotic Series Expansion Method for an Infinite Reservoir

As mentioned in the chapter 4, the dimensionless general solution for the NHDE in terms of pseudo-pressure can be expressed by a k^{th} order asymptotic series expansion (Kale & Mattar, 1980), (Pedrosa Jr., 1986) and (Kikani & Pedrosa Jr., 1991):

$$m_D = \sum_{k=0}^{+\infty} \epsilon^k m_D^{(k)} \quad (5-63)$$

Where ϵ is perturbation parameter. Thus, dimensionless NHDE becomes:

$$\frac{1}{r_D} \frac{\partial}{\partial r_D} \left(r_D \frac{\partial m_D}{\partial r_D} \right) - (1 + \epsilon \xi) \frac{\partial m_D}{\partial t_D} = -f_D(r_D, t_D, k_D) \quad (5-64)$$

The k^{th} -order hydraulic diffusivity deviation factor is defined as:

$$\xi^{(k)} = \xi \left[m_D^{(k-1)} \right] \frac{\partial m_D^{(k-1)}}{\partial t_D} \quad (5-65)$$

Then $\xi(p)$ becomes $\xi(m_D)$. The zeroth-order deviation factor $\xi^{(0)}$ is expressed by:

$$\xi^{(0)} = \hat{\mathcal{S}}_{oD}^{(0)}(r_D, t_D) \quad (5-66)$$

Where $\hat{\mathcal{S}}_{oD}^{(0)}(r_D, t_D)$ is the zeroth-order oil source term. The perturbed dimensionless NHDE for a vertical oil well in a pressure-sensitive reservoir is expressed in cylindrical coordinates as follows:

$$\begin{aligned}
& \epsilon^0 \left[\frac{1}{r_D} \frac{\partial}{\partial r_D} \left(r_D \frac{\partial m_D}{\partial r_D} \right) - \frac{\partial m_D^{(0)}}{\partial t_D} + \hat{\mathcal{S}}_{oD}^{(0)}(r_D, t_D) \right] + \\
& \quad + \epsilon^1 \left[\frac{1}{r_D} \frac{\partial}{\partial r_D} \left(r_D \frac{\partial m_D}{\partial r_D} \right) - \frac{\partial m_D^{(0)}}{\partial t_D} - \xi^{(0)} \frac{\partial m_D^{(0)}}{\partial t_D} \right] + \\
& \quad + \epsilon^2 \left[\frac{1}{r_D} \frac{\partial}{\partial r_D} \left(r_D \frac{\partial m_D}{\partial r_D} \right) - \frac{\partial m_D^{(1)}}{\partial t_D} - \xi^{(1)} \frac{\partial m_D^{(1)}}{\partial t_D} \right] + \dots \\
& \quad + \epsilon^k \left[\frac{1}{r_D} \frac{\partial}{\partial r_D} \left(r_D \frac{\partial m_D}{\partial r_D} \right) - \frac{\partial m_D^{(k-1)}}{\partial t_D} - \xi^{(k-1)} \frac{\partial m_D^{(k-1)}}{\partial t_D} \right] = 0 \quad (5-67)
\end{aligned}$$

Combining Eqs. 5-65 and 5-66, the expanded NHDE can be given by:

$$\begin{aligned}
& \epsilon^0 \left[\frac{1}{r_D} \frac{\partial}{\partial r_D} \left(r_D \frac{\partial m_D}{\partial r_D} \right) - \frac{\partial m_D^{(0)}}{\partial t_D} + \hat{\mathcal{S}}_{oD}^{(0)}(r_D, t_D) \right] + \\
& \quad + \epsilon^1 \left\{ \frac{1}{r_D} \frac{\partial}{\partial r_D} \left[r_D \frac{\partial m_D}{\partial r_D} \right] - \frac{\partial m_D^{(0)}}{\partial t_D} - \left[\frac{1}{k_D(m_D^{(0)})} - 1 \right] \frac{\partial m_D^{(0)}}{\partial t_D} \right\} + \\
& \quad + \epsilon^2 \left\{ \frac{1}{r_D} \frac{\partial}{\partial r_D} \left(r_D \frac{\partial m_D}{\partial r_D} \right) - \frac{\partial m_D^{(1)}}{\partial t_D} - \left[\frac{1}{k_D(m_D^{(1)})} - 1 \right] \frac{\partial m_D^{(1)}}{\partial t_D} \right\} + \dots \\
& \quad + \epsilon^k \left\{ \frac{1}{r_D} \frac{\partial}{\partial r_D} \left(r_D \frac{\partial m_D}{\partial r_D} \right) - \frac{\partial m_D^{(k-1)}}{\partial t_D} - \left[\frac{1}{k_D(m_D^{(k-1)})} - 1 \right] \frac{\partial m_D^{(k-1)}}{\partial t_D} \right\} = 0 \quad (5-68)
\end{aligned}$$

Using a first-order series expansion:

$$\begin{aligned}
& \epsilon^0 \left[\frac{1}{r_D} \frac{\partial}{\partial r_D} \left(r_D \frac{\partial m_D}{\partial r_D} \right) - \frac{\partial m_D^{(0)}}{\partial t_D} + \hat{\mathcal{S}}_{oD}^{(0)}(r_D, t_D) \right] + \\
& \quad + \epsilon^1 \left\{ \frac{1}{r_D} \frac{\partial}{\partial r_D} \left[r_D \frac{\partial m_D}{\partial r_D} \right] - \frac{\partial m_D^{(0)}}{\partial t_D} - \left[\frac{1}{k_D(m_D^{(0)})} - 1 \right] \frac{\partial m_D^{(0)}}{\partial t_D} \right\} = 0 \quad (5-69)
\end{aligned}$$

Regrouping the terms of Eq. 5-69

$$(\epsilon+1) \left[\frac{1}{r_D} \frac{\partial}{\partial r_D} \left(r_D \frac{\partial m_D}{\partial r_D} \right) \right] - (\epsilon+1) \left\{ \left[\frac{1}{k_D(m_D^{(0)})} + 1 \right] \frac{\partial m_D^{(0)}}{\partial t_D} \right\} + \hat{\mathcal{S}}_{oD}^{(0)}(r_D, t_D) = 0 \quad (5-70)$$

Rewriting Eq. 5-70:

$$(\epsilon + 1) \left\{ \frac{1}{r_D} \frac{\partial}{\partial r_D} \left(r_D \frac{\partial m_D}{\partial r_D} \right) - \left[\frac{1}{k_D(m_D^{(0)})} + 1 \right] \frac{\partial m_D^{(0)}}{\partial t_D} \right\} + \hat{\mathcal{S}}_{oD}^{(0)}(r_D, t_D) = 0 \quad (5-71)$$

As ϵ is a perturbation parameter, Eq. 5-71 can be expressed as follows:

$$\begin{aligned} \lim_{\epsilon \rightarrow 0} \left\{ (\epsilon + 1) \left\{ \frac{1}{r_D} \frac{\partial}{\partial r_D} \left(r_D \frac{\partial m_D}{\partial r_D} \right) - \left[\frac{1}{k_D(m_D^{(0)})} + 1 \right] \frac{\partial m_D^{(0)}}{\partial t_D} \right\} + \hat{\mathcal{S}}_{oD}^{(0)}(r_D, t_D) \right\} = \\ = \left\{ \frac{1}{r_D} \frac{\partial}{\partial r_D} \left(r_D \frac{\partial m_D}{\partial r_D} \right) - \left[\frac{1}{k_D(m_D^{(0)})} + 1 \right] \frac{\partial m_D^{(0)}}{\partial t_D} \right\} + \hat{\mathcal{S}}_{oD}^{(0)}(r_D, t_D) \end{aligned} \quad (5-72)$$

Finally, the expanded NHDE that models the slightly compressible oil flow in permeability pressure-sensitive reservoirs is expressed as:

$$\frac{1}{r_D} \frac{\partial}{\partial r_D} \left(r_D \frac{\partial m_D}{\partial r_D} \right) - \left[\frac{1}{k_D(m_D^{(0)})} + 1 \right] \frac{\partial m_D^{(0)}}{\partial t_D} + \hat{\mathcal{S}}_{oD}^{(0)}(r_D, t_D) = 0 \quad (5-73)$$

Applying Eq.5-175 in the initial condition (IC) in terms of epsilon powers

$$\begin{aligned} \epsilon^0 m_D^{(0)}(r_D, t_D = 0) + \epsilon^1 m_D^{(1)}(r_D, t_D = 0) + \epsilon^2 m_D^{(2)}(r_D, t_D = 0) + \dots \\ + \epsilon^k m_D^{(k)}(r_D, t_D = 0) = 0 \end{aligned} \quad (5-74)$$

And, in the external boundary condition (EBC)

$$\begin{aligned} \lim_{r_D \rightarrow \infty} \epsilon^0 m_D^{(0)}(r_D, t_D) + \lim_{r_D \rightarrow \infty} \epsilon^1 m_D^{(1)}(r_D, t_D) + \lim_{r_D \rightarrow \infty} \epsilon^2 m_D^{(2)}(r_D, t_D) + \dots \\ + \lim_{r_D \rightarrow \infty} \epsilon^k m_D^{(k)}(r_D, t_D) = 0 \end{aligned} \quad (5-75)$$

The higher order terms ($k > 1$) can be solved by the GF technique, (Gringarten & Ramey Jr., 1973), (Gringarten & J., 1974), (Gringarten & Ramey Jr., 1974), (Gringarten, Ramey Jr. & Raghavan, 1975), (Gringarten et al., 1979), (Gringarten, 1984), (Gringarten, 2008) and (Sousa, Barreto Jr. & Peres, 2016a):

$$\begin{aligned} \frac{1}{r_D} \frac{\partial}{\partial r_D} \left[r_D \frac{\partial G_D(r_D, r'_D, t_D, t'_D)}{\partial r_D} \right] - \frac{\partial G_D(r_D, r'_D, t_D, t'_D)}{\partial t_D} = -\frac{1}{2\pi r_D} \times \\ \times \delta(r_D - r'_D) \times \delta(t_D - t'_D) \end{aligned} \quad (5-76)$$

The initial condition for the associated problem is:

$$G_D(r_D, r'_D, t_D, t'_D = 0) = 0 \quad (5-77)$$

And the external boundary condition is:

$$\lim_{r_D \rightarrow \infty} G_D(r_D, r'_D, t_D, t'_D) = 0 \quad (5-78)$$

It is appropriate to mention that, the inner boundary condition is coupled to the model through the relationship between the dimensionless pseudo-pressure m_D and the pseudo-pressure variation $\Delta m(p)$. To continue the derivation of the proposed model, it is necessary to establish the solution of the Eq. 5-64, as well as, for the initial and boundary conditions (Eq. ?? and ??) that satisfies the associated problem (Eq. 5-76 and 5-78). Because the differential operator in the left-hand side of the Eq. 5-64 and Eq. 5-76 is not self-adjoint, to compute the general solution $m_D(r_D, t_D, k_D)$ it is necessary to resort to the adjoint GF $G_D^*(r_D, r'_D, t_D, t'_D)$ which satisfies the following adjoint problem:

$$\frac{1}{r_D} \frac{\partial}{\partial r_D} \left[r_D \frac{\partial G_D^*(r_D, r'_D, t_D, t'_D)}{\partial r_D} \right] + \frac{\partial G_D^*(r_D, r'_D, t_D, t'_D)}{\partial t_D} = -\frac{1}{2\pi r_D} \times \\ \times \delta(r_D - r'_D) \times \delta(t_D - t'_D) \quad (5-79)$$

With the adjoint initial condition:

$$G_D^*(r_D, r'_D, t_D, t'_D = 0) = 0 \quad (5-80)$$

and external boundary condition:

$$\lim_{r_D \rightarrow \infty} G_D^*(r_D, r'_D, t_D, t'_D) = 0 \quad (5-81)$$

The parameters r'_D , t'_D , r_D and t_D in the argument of the GF are the same spatial and instantaneous variables aforementioned in the chapter 1. The Eq. 5-80 is the causality clause for the adjoint problem. Thereby it is not necessary to solve the adjoint problem, because the adjoint GF is related to the regular one by the reciprocity principle (Carslaw & Jaeger, 1959), (Beck et al., 1992), (Ozisiki, 1993), (Duffy, 2001) and (Cole, Beck & Haji-Sheikh, 2011):

$$G_D^*(r_D, r'_D, t_D, t'_D) = G_D(r_D, r'_D, t_D, t'_D) \quad (5-82)$$

Replacing the identity given in the Eq. 5-82 in the Eqs. 5-79 to 5-81, the adjoint problem yields to:

$$\frac{1}{r_D} \frac{\partial}{\partial r_D} \left[r_D \frac{\partial G_D(r_D, r'_D, t_D, t'_D)}{\partial r_D} \right] + \frac{\partial G_D(r_D, r'_D, t_D, t'_D)}{\partial t_D} = -\frac{1}{2\pi r_D} \times \delta(r_D - r'_D) \times \delta(t_D - t'_D) \quad (5-83)$$

With the initial condition:

$$G_D(r_D, r'_D, t_D, t'_D = 0) = 0 \quad (5-84)$$

and external boundary condition:

$$\lim_{r_D \rightarrow \infty} G_D(r_D, r'_D, t_D, t'_D) = 0 \quad (5-85)$$

Multiplying the Eq. 5-64 by $2\pi r_D G_D(r_D, r'_D, t_D, t'_D)$ and the Eq. 5-79 by $2\pi r_D m_D(r_D, t_D, k_D)$, it is possible to represent the general solution $m_D(r_D, t_D, k_D)$ in terms of the GF.

$$2\pi r_D G_D(r_D, r'_D, t_D, t'_D) \left\{ \frac{1}{r_D} \frac{\partial}{\partial r_D} \left(r_D \frac{\partial m_D}{\partial r_D} \right) - [1 + \epsilon \xi(p)] \frac{\partial m_D}{\partial t_D} \right\} = -2\pi r_D \times G_D(r_D, r'_D, t_D, t'_D) f_D(r_D, t_D, k_D) \quad (5-86)$$

and

$$2\pi r_D m_D(r_D, t_D, k_D) \left\{ \frac{1}{r_D} \frac{\partial}{\partial r_D} \left[r_D \frac{\partial G_D(r_D, r'_D, t_D, t'_D)}{\partial r_D} \right] + \frac{\partial G_D(r_D, r'_D, t_D, t'_D)}{\partial t_D} \right\} = -2\pi r_D m_D(r_D, t_D, k_D) \frac{1}{2\pi r_D} \delta(r_D - r'_D) \times \delta(t_D - t'_D) \quad (5-87)$$

The Eq. 5-86 and 5-87 must be subtracted, therewith:

$$2\pi r_D G_D(r_D, r'_D, t_D, t'_D) \left\{ \frac{1}{r_D} \frac{\partial}{\partial r_D} \left[r_D \frac{\partial m_D(r_D, t_D, k_D)}{\partial r_D} \right] - [1 + \epsilon \xi(p)] \right\} - 2\pi r_D \times m_D(r_D, t_D, k_D) \left\{ \frac{1}{r_D} \frac{\partial}{\partial r_D} \left[r_D \frac{\partial G_D(r_D, r'_D, t_D, t'_D)}{\partial r_D} \right] + \frac{\partial G_D(r_D, r'_D, t_D, t'_D)}{\partial t_D} \right\} = m_D(r_D, t_D, k_D) \delta(r_D - r'_D) \times \delta(t_D - t'_D) - 2\pi r_D G_D(r_D, r'_D, t_D, t'_D) f_D(r_D, t_D, k_D) \quad (5-88)$$

Expanding the terms of the Eq. 5-88:

$$\begin{aligned}
& 2\pi G_D(r_D, r'_D, t_D, t'_D) \times \frac{\partial}{\partial r_D} \left[r_D \frac{\partial m_D(r_D, t_D, k_D)}{\partial r_D} \right] - 2\pi r_D G_D(r_D, r'_D, t_D, t'_D) \\
& \times \left[1 + \epsilon \xi(p) \right] \frac{\partial m_D(r_D, t_D, k_D)}{\partial t_D} - 2\pi m_D(r_D, t_D, k_D) \times \frac{\partial}{\partial r_D} \left[r_D \frac{\partial G_D(r_D, r'_D, t_D, t'_D)}{\partial r_D} \right] - \\
& + 2\pi r_D m_D(r_D, t_D, k_D) \times \frac{\partial G_D(r_D, r'_D, t_D, t'_D)}{\partial t_D} = m_D(r_D, t_D, k_D) \times \\
& \times \delta(r_D - r'_D) \times \delta(t_D - t'_D) - 2\pi r_D G_D(r_D, r'_D, t_D, t'_D) f_D(r_D, t_D, k_D) \quad (5-89)
\end{aligned}$$

Let:

$$\lim_{\epsilon \rightarrow 1} \left[1 + \epsilon \xi(p) \right] = 1 + \xi(p) \quad (5-90)$$

The Eq. 5-89 becomes:

$$\begin{aligned}
& 2\pi G_D(r_D, r'_D, t_D, t'_D) \times \frac{\partial}{\partial r_D} \left[r_D \frac{\partial m_D(r_D, t_D, k_D)}{\partial r_D} \right] - 2\pi r_D G_D(r_D, r'_D, t_D, t'_D) \\
& \times \left[1 + \xi(p) \right] \frac{\partial m_D(r_D, t_D, k_D)}{\partial t_D} - 2\pi m_D(r_D, t_D, k_D) \times \frac{\partial}{\partial r_D} \left[r_D \frac{\partial G_D(r_D, r'_D, t_D, t'_D)}{\partial r_D} \right] - \\
& + 2\pi r_D m_D(r_D, t_D, k_D) \frac{\partial G_D(r_D, r'_D, t_D, t'_D)}{\partial t_D} = m_D(r_D, t_D, k_D) \times \\
& \times \delta(r_D - r'_D) \times \delta(t_D - t'_D) - 2\pi r_D G_D(r_D, r'_D, t_D, t'_D) f_D(r_D, t_D, k_D) \quad (5-91)
\end{aligned}$$

Expanding the nonlinear term of the Eq. 5-91:

$$\begin{aligned}
& 2\pi G_D(r_D, r'_D, t_D, t'_D) \times \frac{\partial}{\partial r_D} \left[r_D \frac{\partial m_D(r_D, t_D, k_D)}{\partial r_D} \right] - 2\pi r_D \times G_D(r_D, r'_D, t_D, t'_D) \times \\
& \times \frac{\partial m_D(r_D, t_D, k_D)}{\partial t_D} - 2\pi r_D \xi(p) \times G_D(r_D, r'_D, t_D, t'_D) \frac{\partial m_D(r_D, t_D, k_D)}{\partial t_D} - \\
& + 2\pi m_D(r_D, t_D, k_D) \frac{\partial}{\partial r_D} \left[r_D \frac{\partial G_D(r_D, r'_D, t_D, t'_D)}{\partial r_D} \right] - 2\pi r_D m_D(r_D, t_D, k_D) \times \\
& \times \frac{\partial G_D(r_D, r'_D, t_D, t'_D)}{\partial t_D} = m_D(r_D, t_D, k_D) \times \delta(r_D - r'_D) \times \delta(t_D - t'_D) - \\
& + 2\pi r_D G_D(r_D, r'_D, t_D, t'_D) f_D(r_D, t_D, k_D) \quad (5-92)
\end{aligned}$$

Integrating the Eq. 5-92

$$\begin{aligned}
& 2\pi \times \left\{ \int_0^\infty \int_0^{t_D} G_D(r_D, r'_D, t_D, t'_D) \times \frac{\partial}{\partial r'_D} \left[r'_D \frac{\partial m_D(r'_D, t'_D, k_D)}{\partial r'_D} \right] dt'_D dr'_D - \right. \\
& \quad + \int_0^\infty \int_0^{t_D} r'_D G_D(r_D, r'_D, t_D, t'_D) \frac{\partial m_D(r'_D, t'_D, k_D)}{\partial t'_D} dt'_D dr'_D - \\
& \quad + \int_0^\infty \int_0^{t_D} \xi(p) r'_D G_D(r_D, r'_D, t_D, t'_D) \frac{\partial m_D(r'_D, t'_D, k_D)}{\partial t'_D} dt'_D dr'_D - \\
& \quad + \int_0^\infty \int_0^{t_D} m_D(r'_D, t'_D, k_D) \frac{\partial}{\partial r'_D} \left[r'_D \frac{\partial G_D(r_D, r'_D, t_D, t'_D)}{\partial r'_D} \right] dt'_D dr'_D - \\
& \quad \left. + \int_0^\infty \int_0^{t_D} r'_D m_D(r'_D, t'_D, k_D) \times \frac{\partial G_D(r_D, r'_D, t_D, t'_D)}{\partial t_D} dt'_D dr'_D \right\} = \\
& = \int_0^\infty \int_0^{t_D} m_D(r'_D, t'_D, k_D) \delta(r_D - r'_D) \times \delta(t_D - t'_D) dt'_D dr'_D - \\
& \quad + 2\pi \times \int_0^\infty \int_0^{t_D} r'_D G_D(r_D, r'_D, t_D, t'_D) f_D(r'_D, t'_D, k_D) dt'_D dr'_D \quad (5-93)
\end{aligned}$$

One can simplify some terms in the Eq. 5-93 as follows. After performing the spatial integration of the first and fourth terms of the left-hand side of the Eq. 5-93 by parts, we have:

$$\begin{aligned}
& 2\pi \times \int_0^\infty \left\{ G_D(r_D, r'_D, t_D, t'_D) \times \frac{\partial}{\partial r'_D} \left[r'_D \frac{\partial m_D(r'_D, t'_D, k_D)}{\partial r'_D} \right] - m_D(r'_D, t'_D, k_D) \times \right. \\
& \quad \left. \times \frac{\partial}{\partial r'_D} \left[r'_D \frac{\partial G_D(r_D, r'_D, t_D, t'_D)}{\partial r'_D} \right] \right\} dr'_D = 2\pi \times \left[G_D(r_D, r'_D, t_D, t'_D) \times \right. \\
& \quad \left. \times \frac{\partial m_D(r'_D, t'_D, k_D)}{\partial r'_D} - m_D(r'_D, t'_D, k_D) \frac{\partial G_D(r_D, r'_D, t_D, t'_D)}{\partial r'_D} \right]_{r'_D=0}^{r'_D \rightarrow \infty} \quad (5-94)
\end{aligned}$$

The functions in the integrand of the second and fifth integrals in the left-hand side of Eq. 5-93 represent the time derivative of the product of two functions. Thereby:

$$\begin{aligned}
& 2\pi \times \int_0^{t_D} \left\{ r'_D \times \left[G_D(r_D, r'_D, t_D, t'_D) \times \frac{\partial m_D(r'_D, t'_D, k_D)}{\partial t'_D} + m_D(r'_D, t'_D, k_D) \right. \right. \\
& \quad \left. \left. \times \frac{\partial G_D(r_D, r'_D, t_D, t'_D)}{\partial t'_D} \right] \right\} dt'_D = 2\pi r'_D \times \int_0^{t_D} \frac{\partial}{\partial t'_D} \left[G_D(r_D, r'_D, t_D, t'_D) \times m_D(r'_D, t'_D, k_D) \right] dt'_D \\
& \hspace{20em} (5-95)
\end{aligned}$$

Using the Leibniz rule from the integral of derivatives:

$$2\pi r'_D \times \int_0^{t_D} \frac{\partial}{\partial t'_D} \left[G_D(r_D, r'_D, t_D, t'_D) \times m_D(r'_D, t'_D, k_D) \right] dt'_D = 2\pi r'_D \times \left[G_D(r_D, r'_D, t_D, t'_D) \times m_D(r'_D, t'_D, k_D) \right]_{t'_D=0}^{t'_D=t_D} \quad (5-96)$$

Thus, the Eq. 5-96 yields to:

$$2\pi r'_D \times \left[G_D(r_D, r'_D, t_D, t'_D) \times m_D(r'_D, t'_D, k_D) \right]_{t'_D=0}^{t'_D=t_D} = 2\pi r'_D G_D(r_D, r'_D, t_D, 0) \times m_D(r'_D, t'_D = 0) \quad (5-97)$$

By the use of the homogeneous initial condition, the Eq. 5-97 becomes:

$$G_D(r_D, r'_D, t_D, 0) \times m_D(r'_D, t'_D = 0, k_D) = 0 \quad (5-98)$$

Finally, the sampling property of the Dirac Delta function can be applied on the term $\int_0^\infty \int_0^{t_D} m_D(r'_D, t'_D, k_D) \delta(r'_D - r_{D0}) \times \delta(t'_D - t_{D0}) dt'_D dr'_D$. Thereby:

$$\int_0^\infty \int_0^{t_D} m_D(r'_D, t'_D, k_D) \delta(r'_D - r_{D0}) \times \delta(t'_D - t_{D0}) dt'_D dr'_D = m_D(r_D, t_D, k_D) \quad (5-99)$$

The total oil source is expressed by the sum of zero and first-order source terms:

$$\hat{\hat{\mathcal{S}}}_{oD}^{(k)}(r_D, t_D, k_D) = \hat{\hat{\mathcal{S}}}_{oD}^{(0)}(r_D, t_D, k_D) + \hat{\hat{\mathcal{S}}}_{oD}^{(1)}(r_D, t_D, k_D) + \hat{\hat{\mathcal{S}}}_{oD}^{(2)}(r_D, t_D, k_D) + \dots \quad (5-100)$$

Using the first-order series expansion, the total oil source yields to:

$$\hat{\hat{\mathcal{S}}}_{oD}(r_D, t_D, k_D) \approx \hat{\hat{\mathcal{S}}}_{oD}^{(0)}(r_D, t_D, k_D) + \hat{\hat{\mathcal{S}}}_{oD}^{(1)}(r_D, t_D, k_D) \quad (5-101)$$

The zeroth-order oil source term is:

$$\hat{\hat{\mathcal{S}}}_{oD}^{(0)}(r_D, t_D, k_D) = f_D(r_D, t_D, k_D) \quad (5-102)$$

and the first-order is:

$$\hat{\hat{\mathcal{S}}}_{oD}^{(1)}(r_D, t_D, k_D) = \xi(m_D) \frac{\partial m_D(r_D, t_D, k_D)}{\partial t_D} \quad (5-103)$$

Therewith:

$$\hat{\hat{S}}_{oD}(r_D, t_D, k_D) \approx f_D(r_D, t_D, k_D) + \xi(m_D) \frac{\partial m_D(r_D, t_D, k_D)}{\partial t_D} \quad (5-104)$$

Combining the Eqs. 5-94, 5-97, 5-98 and 5-104 to the use of the initial and boundary conditions from both $m_D(r_D, t_D, k_D)$ and $G_D(r_D, r'_D, t_D, t'_D)$ problems in the Eq. 5-93, the general solution of the NHDE for the radial oil flow through an infinite reservoir can be expressed as follows:

$$m_D(r_D, t_D, k_D) = \int_0^\infty \int_0^{t_D} \left\{ f_D(r'_D, t'_D, k_D) + \xi(m_D) \frac{\partial m_D}{\partial t'_D} \right\} \times \\ \times G_D(r'_D, r_{D0}, t'_D, t_{D0}) dt'_D dr'_D \quad (5-105)$$

The model is applied to the oil flow at wellbore, *i.e.*, $r_D = 1$ and in the dimensionless position and time $r_{D0} = 0$ and $t_{D0} = 0$, respectively. Thereby:

$$G_D(r_D, r_{D0}, t_D, t_{D0}) = G_D(1, 0, t_D, 0) \quad (5-106)$$

Expanding the terms inside the brackets:

$$m_D(r_D, t_D, k_D) = \int_0^\infty \int_0^{t_D} f_D(r'_D, t'_D, k_D) \times G_D(r'_D, r_{D0}, t'_D, t_{D0}) dt'_D dr'_D + \\ + \int_0^\infty \int_0^{t_D} \xi(m_D) \frac{\partial m_D}{\partial t'_D} \times G_D(r'_D, r_{D0}, t'_D, t_{D0}) dt'_D dr'_D \quad (5-107)$$

According to the definition of the hydraulic diffusivity deviator factor, the Eq. 5-107 becomes:

$$m_D(r_D, t_D, k_D) = \int_0^\infty \int_0^{t_D} f_D(r'_D, t'_D, k_D) \times G_D(r'_D, r_{D0}, t'_D, t_{D0}) dt'_D dr'_D + \\ + \int_0^\infty \int_0^{t_D} \left[\frac{1}{k_D(m_D)} - 1 \right] \frac{\partial m_D}{\partial t'_D} \times G_D(r'_D, r_{D0}, t'_D, t_{D0}) dt'_D dr'_D \quad (5-108)$$

5.1.5 Dimensionless Oil Source Term

Let the oil flow rate in the reservoir and standard conditions expressed by $q(r, t)$ and q_{sc} , respectively. Let us define the cylindrical oil flow rate intensity as $\hat{q} = q(r, t) \times \delta(r - r_0)$. Where r_0 is the initial point of application of the oil pulse. This flow rate represents the a cylindrical source acting in the position r and in the time t .

The dimensionless oil source is expressed by (Fernandes, 2022):

$$f_D(r_D, t_D) = -2\pi r_w \frac{q(r, t)}{q_{sc}} \delta(r - r_0) \quad (5-109)$$

Then, the dimensionless oil source yields to:

$$f_D(r_D, t_D) = -2\pi r_w q_D(r_D, t_D) r_w \frac{\delta(r - r_0)}{r_w} \quad (5-110)$$

Where $q_D(r_D, t_D) = q(r, t)/q_{sc}$ is the dimensionless oil flow rate. By the space scaling property of the Dirac delta function:

$$\delta(\lambda r) = \frac{\delta(r)}{|\lambda|}, \quad \lambda \in \mathbb{R} \quad (5-111)$$

Since $r = r_w \times r_D$ and $|r_w| = r_w$, thus: $\delta(r - r_0) = \delta(r_w r_D - r_w r_{D0})$. So, the space scaling property becomes:

$$\delta(r_w r_D) = \frac{\delta(r_D)}{r_w} \quad (5-112)$$

Then, the dimensionless oil source can be expressed as follows:

$$f_D(r_D, t_D) = -2\pi r_w q_D(r_D, t_D) \delta(r_w r_D - r_w r_{D0}) \quad (5-113)$$

Rewriting the Eq. 5-113:

$$f_D(r_D, t_D) = -2\pi r_w q_D(r_D, t_D) \frac{\delta(r_D - r_{D0})}{r_w} \quad (5-114)$$

Finally, the dimensionless source in the wellbore ($r_D = 1$) is expressed by:

$$f_D(r_D, t_D) = -2\pi q_D(r_D = 1, t_D) \delta(r_D - r_{D0}) \quad (5-115)$$

5.1.6 Dimensionless General Solution

Replacing the Eq. 5-115 in the Eq. 5-107 and changing the dimensionless oil flow rate notation ($q_D(r_D = 1, t_D) \mapsto q_D(t_D)$):

$$m_D(r_D, t_D, k_D) = -2\pi \int_0^\infty \int_0^{t_D} q_D(t'_D) \delta(r'_D - r_{D0}) G_D(r'_D, r_{D0}, t'_D, t_{D0}) dt'_D dr'_D + \\ + \int_0^\infty \int_0^{t_D} \xi(m_D) \frac{\partial m_D}{\partial t'_D} G_D(r'_D, r_{D0}, t'_D, t_{D0}) dt'_D dr'_D \quad (5-116)$$

Applying the hydraulic diffusivity deviator factor definition:

$$m_D(r_D, t_D, k_D) = -2\pi \int_0^\infty \int_0^{t_D} q_D(t'_D) \delta(r'_D - r_{D0}) G_D(r'_D, r_{D0}, t'_D, t_{D0}) dt'_D dr'_D + \\ + \int_0^\infty \int_0^{t_D} \left[\frac{1}{k_D(m_D)} - 1 \right] \frac{\partial m_D}{\partial t'_D} G_D(r'_D, r_{D0}, t'_D, t_{D0}) dt'_D dr'_D \quad (5-117)$$

As $q = q_{sc}$, thus, the dimensionless oil flow rate becomes to the unity:

$$m_D(r_D, t_D, k_D) = -2\pi \int_0^\infty \int_0^{t_D} \delta(r'_D - r_{D0}) G_D(r'_D, r_{D0}, t'_D, t_{D0}) dt'_D dr'_D + \\ + \int_0^\infty \int_0^{t_D} \left[\frac{1}{k_D(m_D)} - 1 \right] \frac{\partial m_D}{\partial t'_D} G_D(r'_D, r_{D0}, t'_D, t_{D0}) dt'_D dr'_D \quad (5-118)$$

Again, by the Dirac delta sampling property:

$$\int_0^\infty \int_0^{t_D} \delta(r'_D - r_{D0}) G_D(r'_D, r_{D0}, t'_D, t_{D0}) dt'_D dr'_D = \int_0^{t_D} G_D(r_D, r_{D0}, t_D, t'_D) dt'_D \quad (5-119)$$

Thereby, the Eq.5-118 can be rewritten as follows:

$$m_D(r_D, t_D, k_D) = -2\pi \int_0^{t_D} G_D(r_D, r_{D0}, t_D, t'_D) dt'_D + \int_0^\infty \int_0^{t_D} \left[\frac{1}{k_D(m_D)} - 1 \right] \times \\ \times \frac{\partial m_D}{\partial t'_D} G_D(r'_D, r_{D0}, t'_D, t_{D0}) dt'_D dr'_D \quad (5-120)$$

The second term has $(k - 1)$ order, so $m_D(r_D, t_D, k_D) \mapsto p_D(r_D, t_D, k_D)$ in the argument of the deviator factor:

$$m_D(r_D, t_D, k_D) = -2\pi \int_0^{t_D} G_D(r_D, r_{D0}, t_D, t'_D) dt'_D + \int_0^\infty \int_0^{t_D} \left[\frac{1}{k_D(p_D)} - 1 \right] \times \\ \times \frac{\partial p_D}{\partial t'_D} G_D(r'_D, r_{D0}, t'_D, t_{D0}) dt'_D dr'_D \quad (5-121)$$

The zeroth-order term is:

$$m_D^{(0)}(r_D, t_D, k_D) = -2\pi \int_0^{t_D} G_D(r_D, r_{D0}, t_D, t'_D) dt'_D \quad (5-122)$$

The GF for transient radial flow in porous media with source term located at position r_{D0} is defined by:

$$G_D(r_D, r_{D0}, t_D, t_{D0}) = \frac{e^{\left[-\frac{r_D^2 - r_{D0}^2}{4(t_D - t_{D0})}\right]}}{4\pi(t_D - t_{D0})} \times \mathbf{I}_0 \left[\frac{r_D r_{D0}}{4(t_D - t_{D0})} \right] \quad (5-123)$$

Replacing Eq.5-123 in the Eq. 5-122:

$$m_D^{(0)}(r_D, t_D, k_D) = -2\pi \int_0^{t_D} \frac{e^{\left[-\frac{r_D^2 - r_{D0}^2}{4(t_D - t_{D0})}\right]}}{4\pi(t_D - t_{D0})} \times \mathbf{I}_0 \left[\frac{r'_D r_{D0}}{4(t'_D - t_{D0})} \right] dt'_D \quad (5-124)$$

where \mathbf{I}_0 is the modified Bessel function of zero order and first kind. The dimensionless oil source is located at $r_{D0} = 0$ and, according to [Abramowitz & Stegun \(1972\)](#): $\mathbf{I}_0(0) = 1$, so:

$$m_D^{(0)}(r_D, t_D, k_D) = -\frac{1}{2} \int_0^{t_D} \frac{e^{\left[-\frac{r_D^2 - r_{D0}^2}{4(t_D - t_{D0})}\right]}}{(t_D - t_{D0})} dt'_D \quad (5-125)$$

The developed model is computed at the wellbore ($r_D = 1$), thus, changing the notation $m_D^{(0)}(r_D, t_D, k_D)$ by $m_{wD}^{(0)}(t_D)$ to denote the wellbore solution, it can be shown that zero order term of the series expansion, is the line-source solution (constant permeability) for flow in porous media $p_D(r_D, t_D, k_D)$:

$$m_{wD}^{(0)}(t_D) = p_{wD}(t_D) \quad (5-126)$$

Thus, the linear solution (constant permeability) is:

$$p_{wD}(t_D) = -\frac{1}{2} \mathbf{Ei} \left(-\frac{1}{4t_D} \right) \quad (5-127)$$

Where $\mathbf{Ei}(-1/4t_D) = \mathbf{Ei} \left[-\frac{\phi \mu c_t r_w^2}{4k(p_i)t} \right]$ is the transcendental exponential integral function, expressed by ([Abramowitz & Stegun, 1972](#)):

$$\mathbf{Ei} \left[-\frac{\phi \mu c_t r_w^2}{4k(p_i)t} \right] = -\int_{-\frac{\phi \mu c_t r_w^2}{4k(p_i)t}}^{+\infty} \frac{e^{-u}}{u} du \quad (5-128)$$

Thus, the dimensionless general solution can be represented by a linear solution plus the infinite sum of the nonlinear terms as follows:

$$m_{wD}(t_D) = -\frac{1}{2}\mathbf{Ei}\left(-\frac{1}{4t_D}\right) + \sum_{k=1}^{\infty} \epsilon^{(k)} m_{wD}^{(k)}(t_D) \quad (5-129)$$

Thereby, the dimensionless general solution is composed by a linear solution for constant permeability plus an infinite sum of the corrective terms that takes into account the nonlinearities caused by the permeability decline over the well-reservoir life-cycle. Using the first-order asymptotic series expansion, the Eq. 5-129 becomes:

$$m_{wD}(t_D) = -\frac{1}{2}\mathbf{Ei}\left(-\frac{1}{4t_D}\right) + m_{wD}^{(1)}(t_D) \quad (5-130)$$

According to the Eq. 5-121, the nonlinear first-order term is:

$$m_{wD}^{(1)}(t_D) = \int_0^{\infty} \int_0^{t_D} \left[\frac{1}{k_D(p_{wD})} - 1 \right] \frac{\partial p_{wD}}{\partial t'_D} \frac{e^{\left[-\frac{r_D^2 - r_{D0}^2}{4(t_D - t_{D0})}\right]}}{4\pi(t_D - t_{D0})} dt'_D dr'_D \quad (5-131)$$

Combining the first-order asymptotic series expansion to the developed integro-differential solution, the dimensionless general solution $m_{wD}(t_D)$ is expressed as follows:

$$\begin{aligned} m_{wD}(t_D) &= \\ &= -\frac{1}{2}\mathbf{Ei}\left(-\frac{1}{4t_D}\right) + \frac{1}{4\pi} \int_0^{\infty} \int_0^{t_D} \left[\frac{1}{k_D(p_{wD})} - 1 \right] \frac{\partial p_{wD}}{\partial t'_D} \frac{e^{\left[-\frac{r_D^2 - r_{D0}^2}{4(t_D - t_{D0})}\right]}}{(t_D - t_{D0})} dt'_D dr'_D \end{aligned} \quad (5-132)$$

Using the linear pressure-sensitive permeability function presented in the chapter 3, the Eq. 7-35 yields to:

$$\begin{aligned} m_{wD}(t_D) &= -\frac{1}{2}\mathbf{Ei}\left(-\frac{1}{4t_D}\right) + \frac{1}{4\pi} \int_0^{\infty} \int_0^{t_D} \left[\frac{1}{-\frac{A}{2}\mathbf{Ei}\left(-\frac{1}{4t_D}\right) + B} - 1 \right] \frac{\partial p_{wD}}{\partial t'_D} \times \\ &\quad \times \frac{e^{\left[-\frac{r_D^2 - r_{D0}^2}{4(t_D - t_{D0})}\right]}}{(t_D - t_{D0})} dt'_D dr'_D \end{aligned} \quad (5-133)$$

The Eq. 7-36 models the nonlinear radial oil flow in porous media with variable permeability, and the hydraulic diffusivity deviator factor has a key role in this nonlinearity because the pore pressure and permeability field data are inserted in this factor to predict future permeability loss over the well-reservoir production's life.

5.1.7

Model Calibration, Results, and Discussions

For the developed analytical model runs, it was used a computational table of pressure p and permeability $k(p)$ values obtained from the geomechanical elastic parameters and experimental test. As aforementioned, the experiment was performed through a uni-axial cell, two cylindrical sandstone samples (representing case studies A and B of this work), and fluid to simulate the oil inside the reservoir rock pores.

The experimental data of pressure and permeability changes for the reservoir samples were fitted and inserted in the permeability-based pseudo-pressure function $m(p)$. The NHDE was solved through the command *int2* from Matlab[®] to compute the implicit term inside the integrand. To check the accuracy of the proposed solution, the results obtained from the model were compared with a numerical porous media oil flow simulator. This numerical simulator, named IMEX[®], is well-known in the petroleum industry. It is widely used in reservoir engineering and formation evaluation works to calibrate new models because of its high reliability. Sensitive runs were performed in IMEX[®] to determine the best time and space step choice to achieve the mesh accuracy necessary to calibrate the model. A wide range of tests for the Matlab[®] code was also checked to find the optimum time and radial space steps. Thereby, the space and time steps used were 10^{-2} m and 10^{-4} seconds. As the GF provides a quick pseudo-pressure decay, it was noticed that the radial domain size was of the order of 100. As almost all the functions involved in the analytical solution are available in the Matlab[®] library, the time to run the computational code was quite low (25 seconds using the linear fitting in the ξ -factor, against 1 minute and 18 seconds of the numerical simulator for the value of 100 space steps). For the other proposed fitting functions, the run time was less than 2 minutes. Thus, the computational costs saving of the developed analytical model constitutes a great advantage, in comparison to the numerical oil flow simulator.

Figures 5.2 and 5.3 present the Semi-log plot of the dimensionless first-order corrective term $m_{wD}^{(1)}(t_D)$ for the case studies A and B using the proposed fitting functions. These plots show that, all the proposed functions presented satisfactory accuracy for this term in comparison to IMEX[®]. These functions were developed through the coefficients calculations by choosing some $(p, k(p))$ points of the experimental data. An interesting fact is, that, despite the hyperbolic and exponential decay functions do not provide close fit to this set of experimental data, the Figures 5.2 and 5.3 show that, it did not influence in the first-order corrective term.

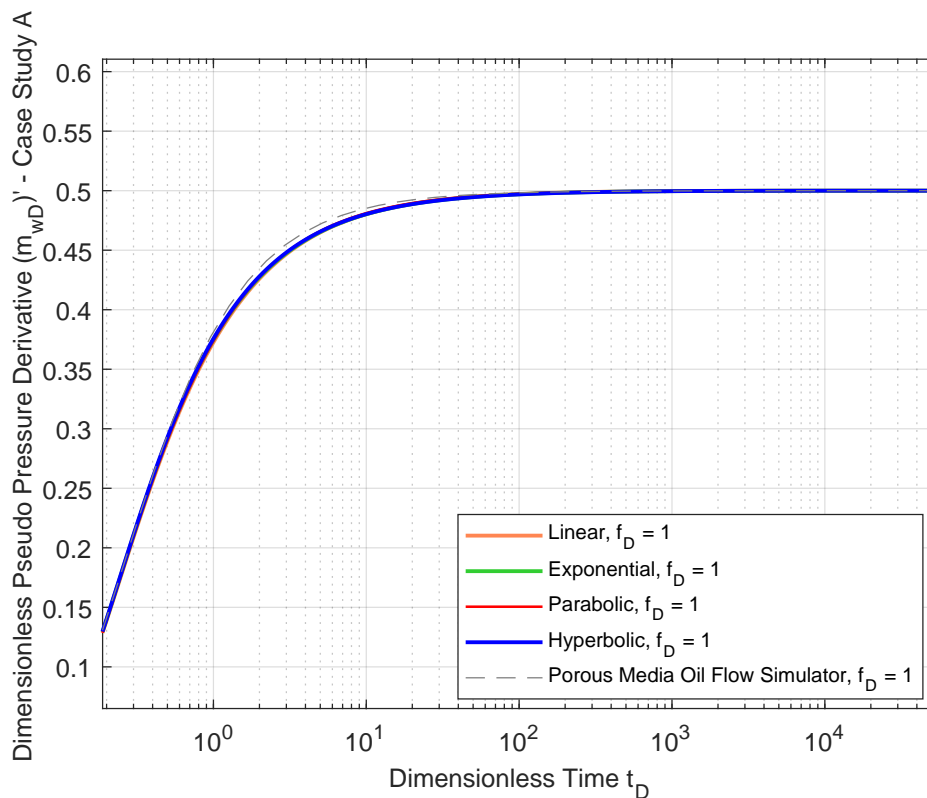


Figure 5.2: Semi-log plot of the dimensionless pseudo-pressure derivative for several fitting functions for case study A.

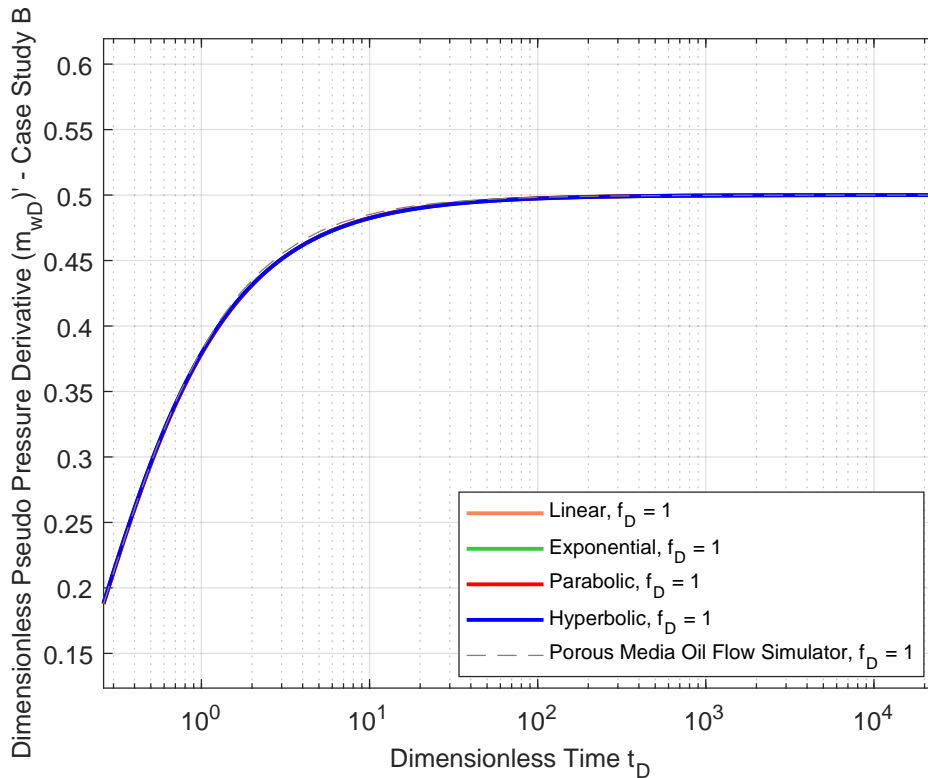


Figure 5.3: Semi-log plot of the dimensionless pseudo-pressure derivative for several fitting functions for case study B.

Figure 5.4 and 5.5 present the Semi-log plot of the dimensionless first-order corrective term $m_{wD}^{(1)}(t_D)$ for the case studies A and B using the proposed fitting functions. The plots show that, the linear function presented satisfactory accuracy for this term in comparison to IMEX[®]. For $t_D > 10^2$, the linear function presented close accuracy with respect to the simulator curve for the case study A. For the case study B, the linear function did not provide close accuracy, however, for both case studies, this function was the best among the fitting functions approached in this work. Figure 5.6 and 5.7 present the Semi-log plot of the several pressure-sensitive permeability functions used in the dimensionless pseudo-pressure for the case studies A and B, respectively. The results show that the type of fitting does not have significant effect in the general solution. The IMEX[®] curve was also plotted and the results are accurate.

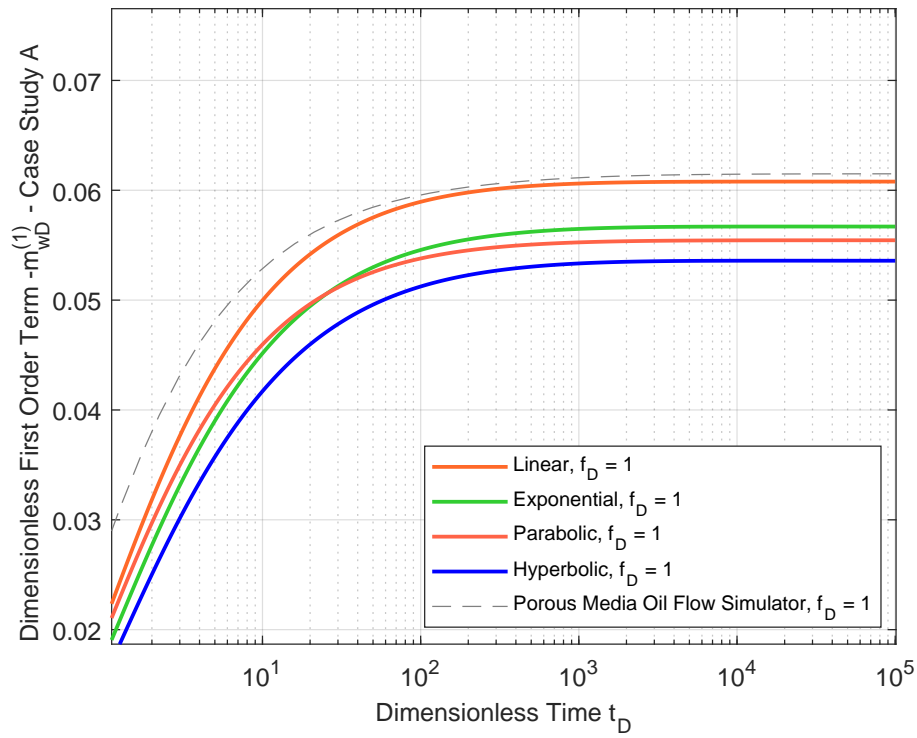


Figure 5.4: Semi-log plot of the dimensionless first-order term for several fitting functions for case study A.

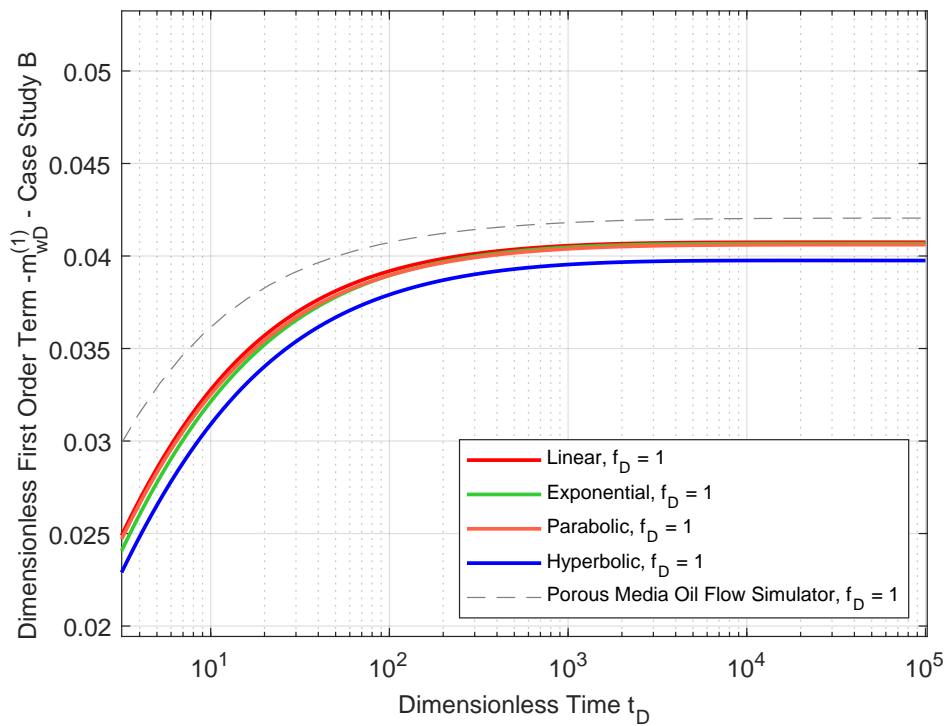


Figure 5.5: Semi-log plot of the dimensionless first-order term for several fitting functions for case study B.

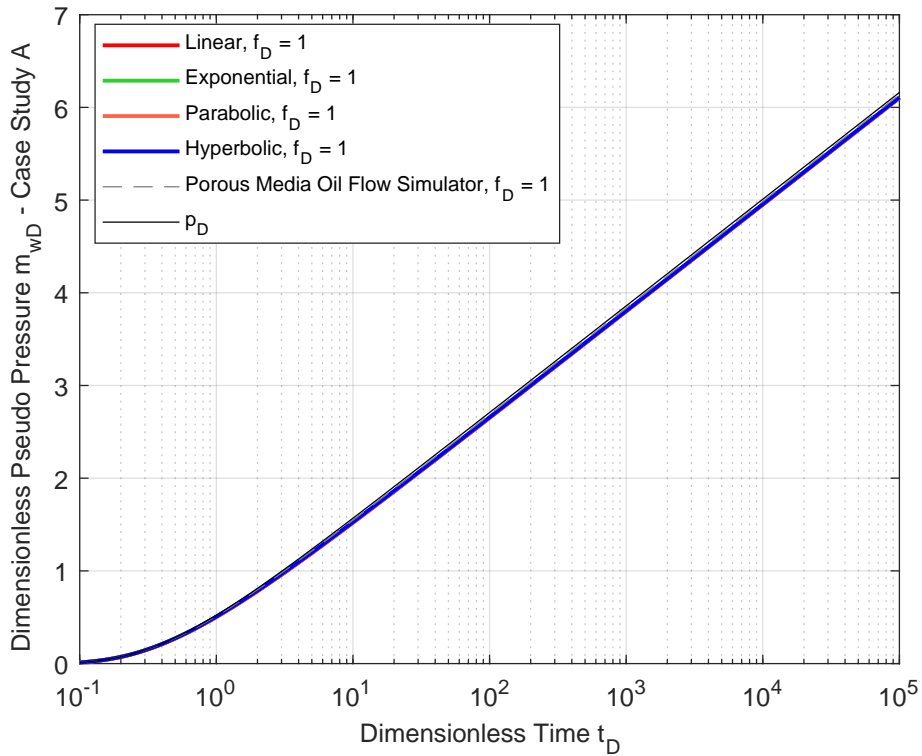


Figure 5.6: Semi-log plot of the dimensionless general solution for several fitting functions for case study A.

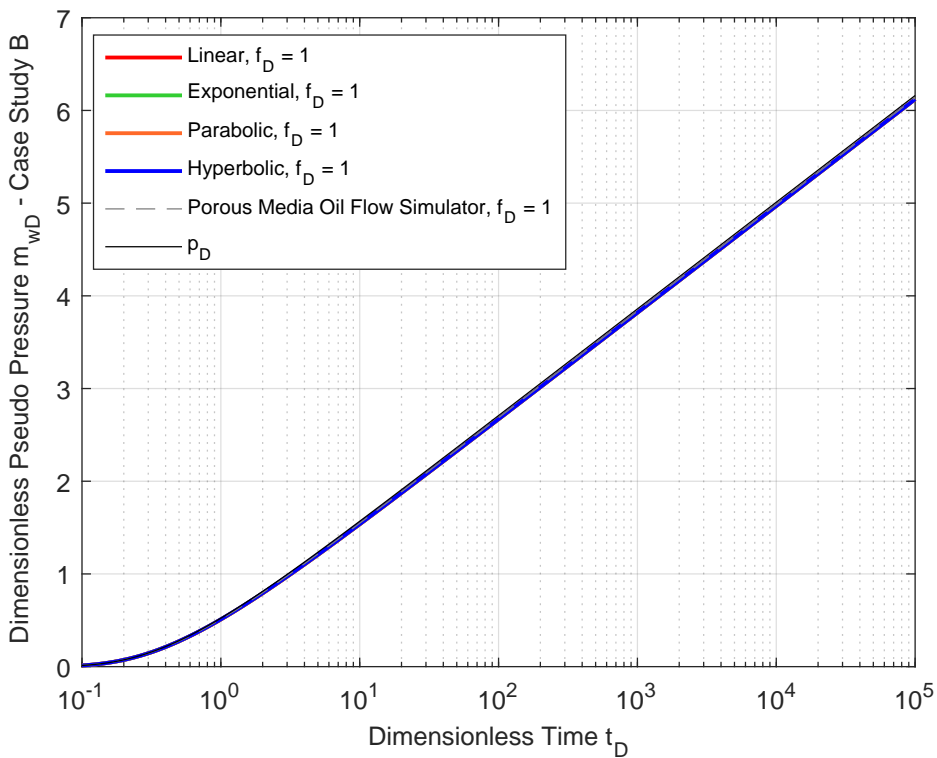


Figure 5.7: Semi-log plot of the dimensionless general solution for several fitting functions for case study B.

Figure 7.4 presents the calibration of the nonlinear first-order term, and it shows close agreement for the late dimensionless times when compared to IMEX[®]. The set of pore pressure and permeability values was implemented in Matlab[®] and compared to IMEX[®] using a computational table named CROCKTAB. This table reads the pore pressure and permeability field data to represent the physical phenomenon of the permeability loss. For this approach, the linear permeability-pressure sensitive function provided close accuracy with respect to IMEX[®].

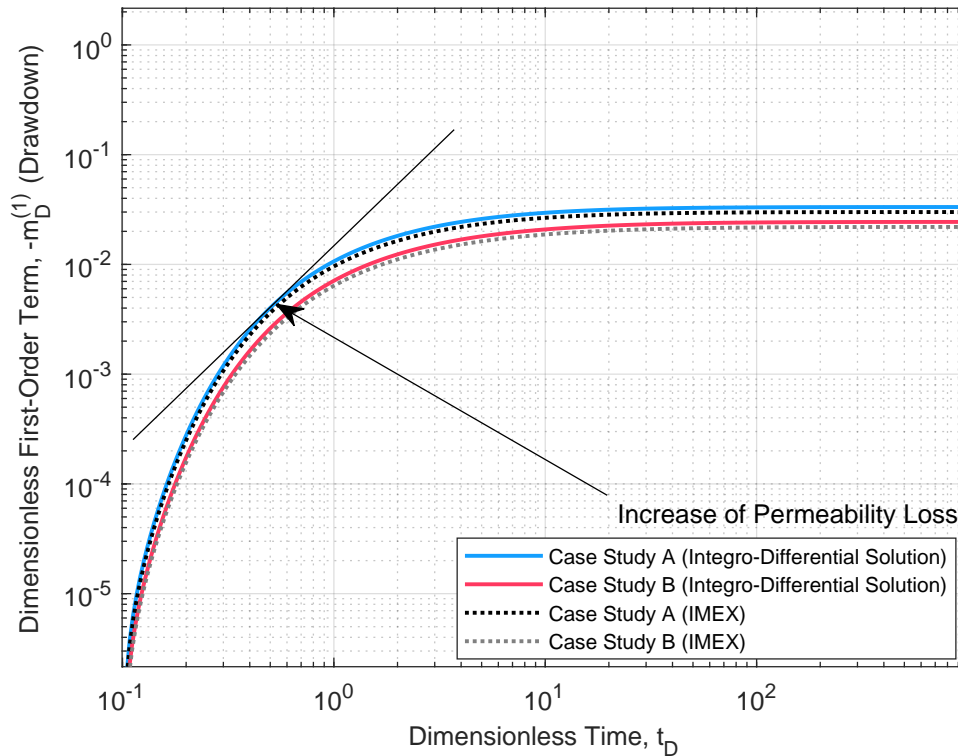


Figure 5.8: Log-log plot of the dimensionless first-order nonlinear term calibrated by IMEX[®].

Figure 5.9 presents the calibration of the dimensionless linear solution. The results were compared to IMEX[®] and they presented high accuracy. The dimensionless general solution's calibration and the derivative are presented in Figure 5.10. We realize that the results are accurate compared to IMEX[®] (black and gray dotted lines), and the IARF regime can also be identified as a 1/2 slope in the derivative. The effect of the oil source term in the dimensionless pseudo-pressure (total unsteady-state permeability loss) is presented in Figure 5.11. For this plot, it was plotted the absolute value of the dimensionless oil source f_D and, it can be noticed the displacement in the general solution curve in the vertical axis. This plot shows that the dimensionless pseudo-pressure rises as a function of the source. This response is caused by the oil source coupled with the linear term (Eq. 7-36).

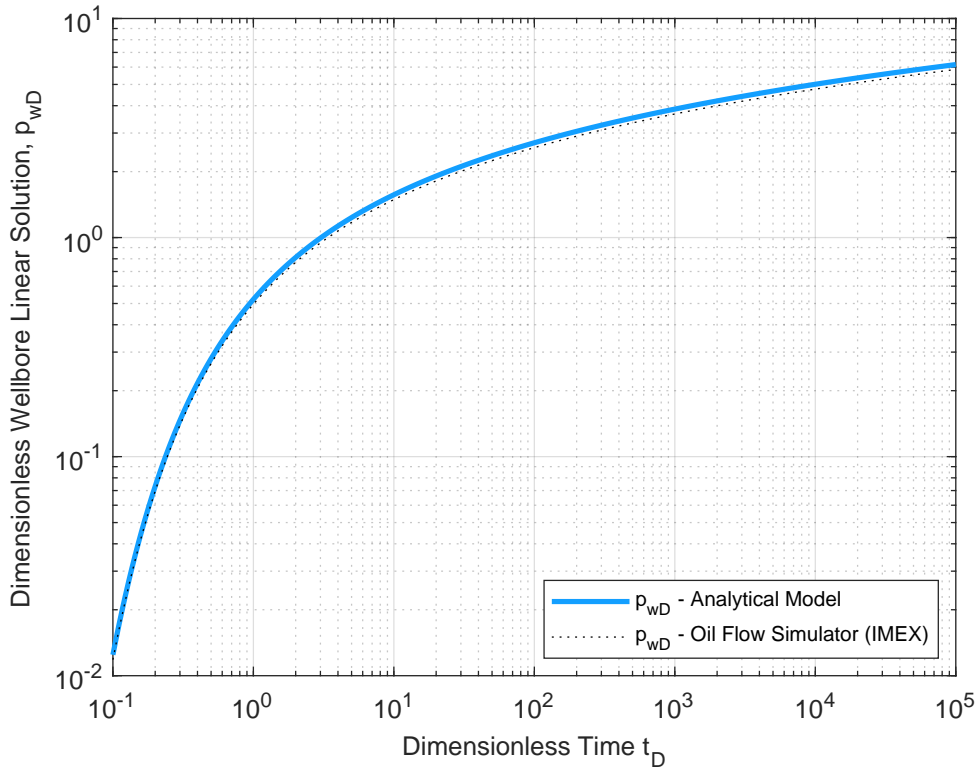


Figure 5.9: Log-log plot of the dimensionless linear solution (constant permeability) with respect to IMEX[®].

PUC-Rio - Certificação Digital N° 1912769/CA

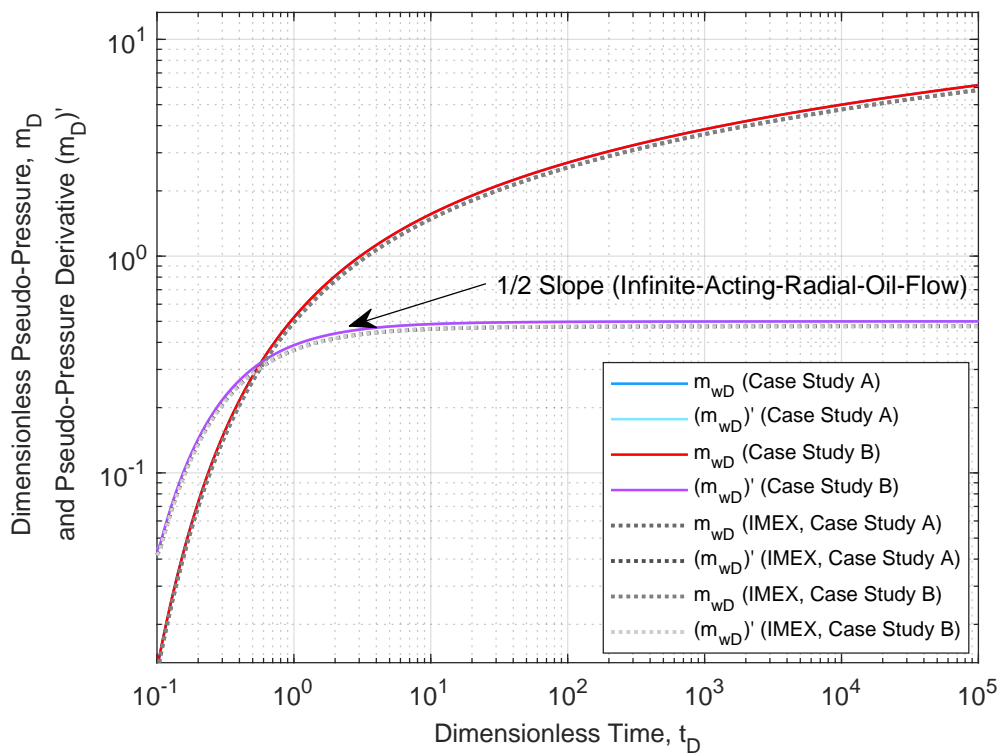


Figure 5.10: Log-log plot of the dimensionless general solution and the derivative calibrated by IMEX[®].

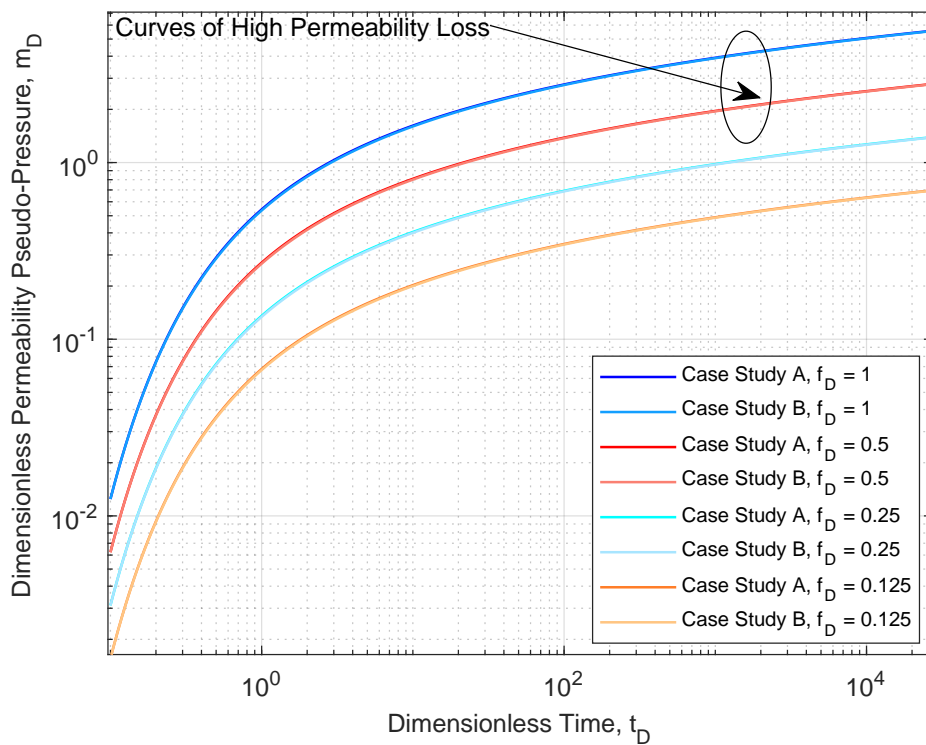


Figure 5.11: Log-log plot of the role of the zeroth-order source term in the dimensionless pseudo-pressure solution.

Figure 7.6 shows the role of the hydraulic diffusivity deviation factor in the dimensionless pseudo-pressure solution. This parameter has the role of the first-order source term $\hat{\mathcal{S}}_{oD}^{(1)}(r_D, t_D, k_D) = \xi[m_D^{(0)}] \frac{\partial m_D^{(0)}}{\partial t_D}$ and it drives the effect of the pressure-dependent permeability. It is possible to realize that this factor increases the nonlinear term. As this factor represents the deviation of the permeability values from the initial one, as the permeability change increases, this factor also tends to increase. Therefore, monitoring this factor is essential for appropriate well-reservoir performance management. The effect of the permeability loss during the oil's production for the case studies A and B can be noticed in the Figures 5.13 and 5.14. The deviation with respect to the linear solution is caused by the first-order nonlinear term of the general solution and it models the permeability decline over the well-reservoir life-cycle. The deviation begins low and it becomes larger over the time. Figure 5.15 presents the log-log plot of the effect of the dimensionless oil source in the dimensionless first-order term. We notice that the source plays a key role in the nonlinearity response of the first-order term, as well as, in the pseudo-pressure general solution. Therewith, the appropriate choice of this parameter is essential to improve the well-reservoir performance. The same effect can be noticed in the pseudo-pressure derivative (Figure 5.16).

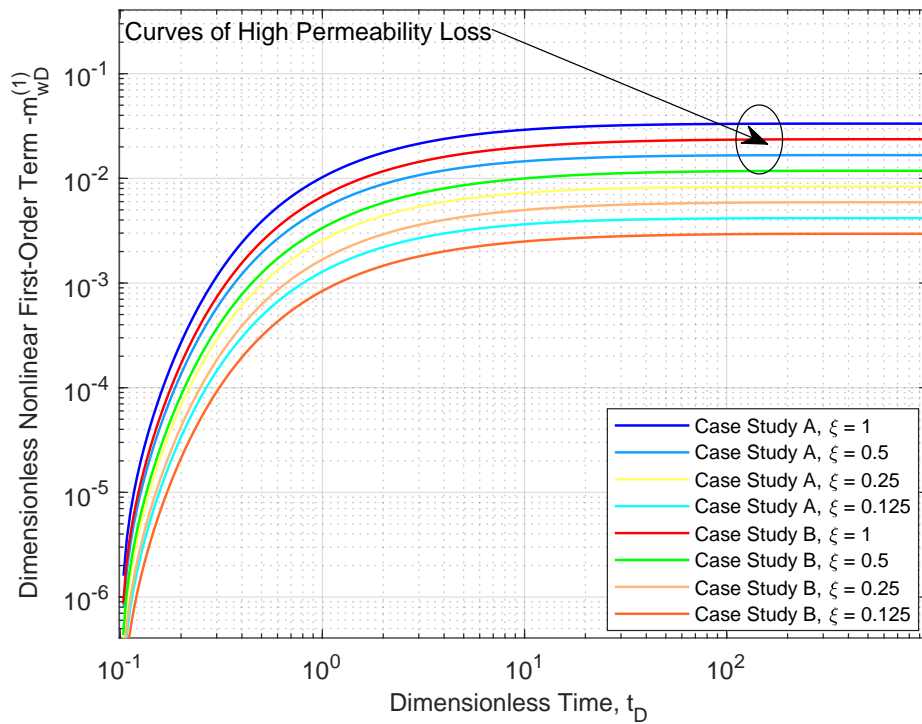


Figure 5.12: Log-log plot of the effect of the hydraulic diffusivity deviation factor in the nonlinear first-order term.

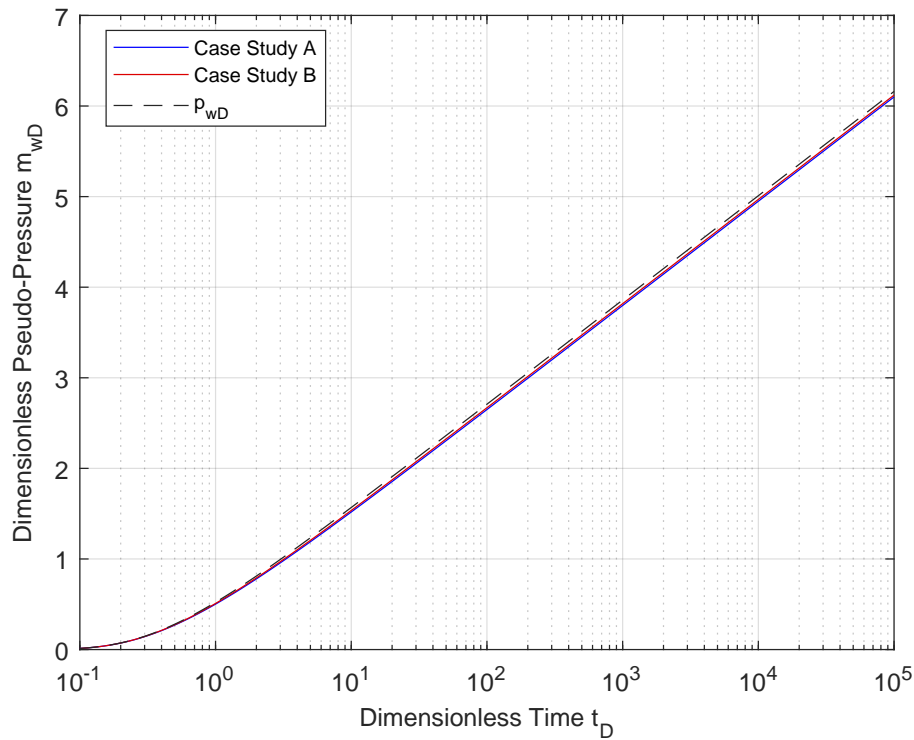


Figure 5.13: Semi-log plot of the comparison between the dimensionless general solution with respect to the linear solution.

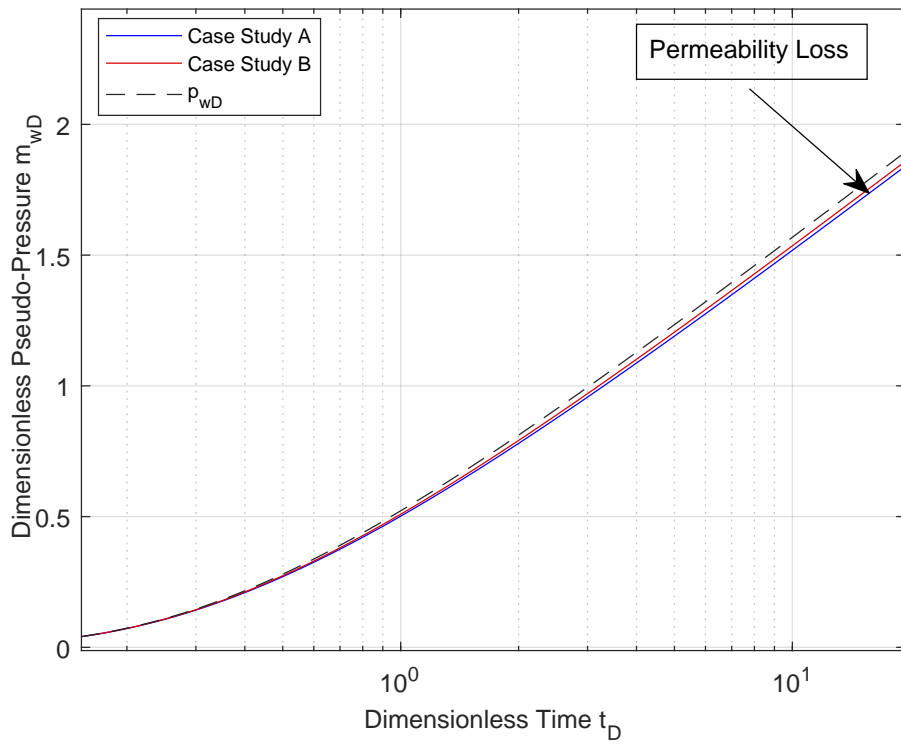


Figure 5.14: Semi-log plot of the amplification of the permeability loss with respect to the linear solution.

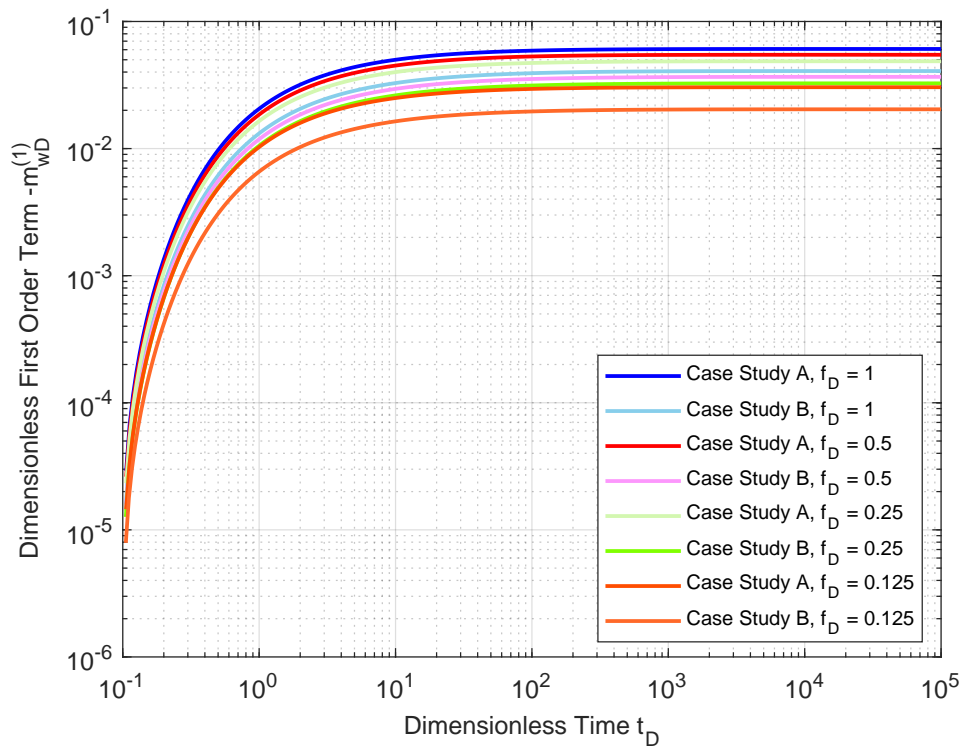


Figure 5.15: Log-log plot of the dimensionless first-order term for several dimensionless oil sources.

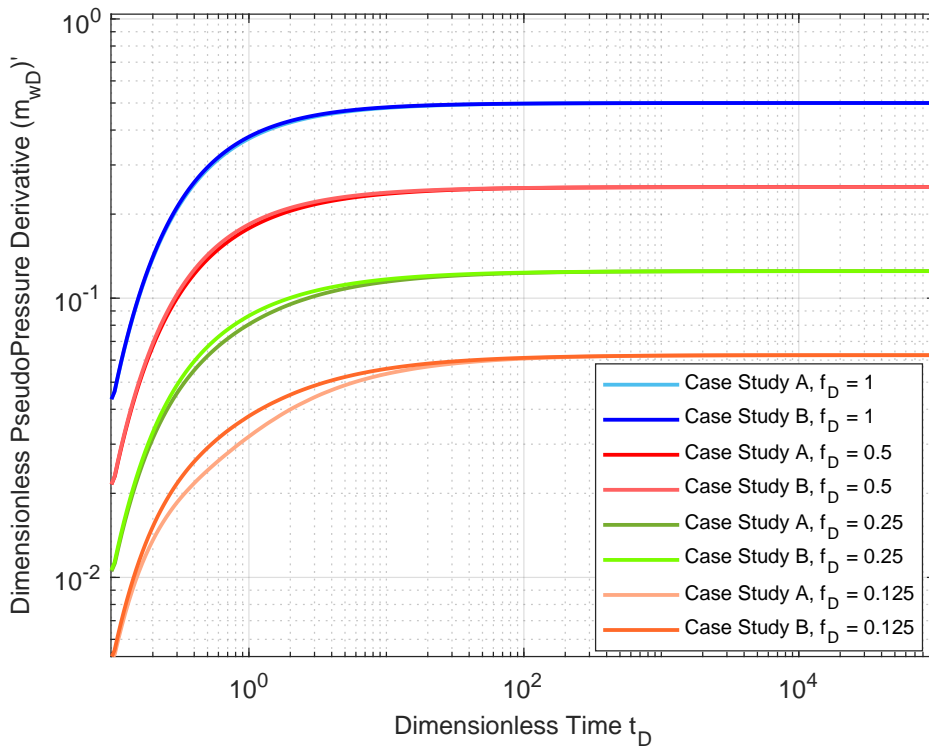


Figure 5.16: Log-log plot of the dimensionless general solution derivative for several dimensionless oil sources.

PUC-Rio - Certificação Digital N° 1912769/CA

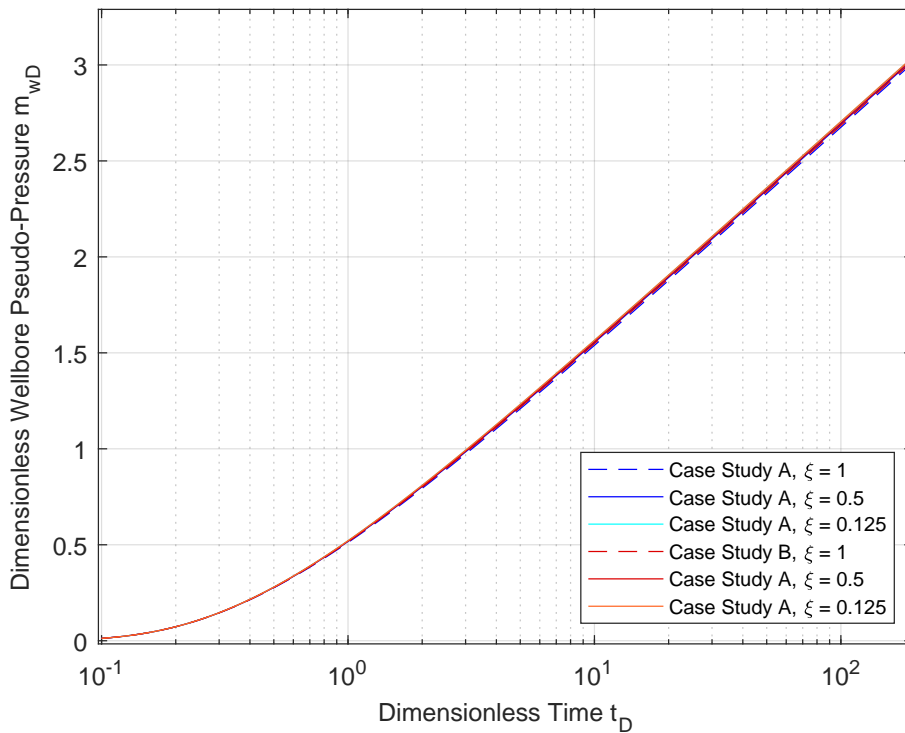


Figure 5.17: Semi-log plot of the hydraulic diffusivity deviator factor effect in the dimensionless general solution.

The hydraulic diffusivity deviator factor response can be shown in the Figures 5.17 and 5.18. As this factor is related to the permeability loss, when it increases, the permeability decays and the well-reservoir performance is jeopardized. The amplification presented in the Figure 5.18 shows clearly that, when this factor raises, the pseudo-pressure becomes lower, as well as, the permeability.

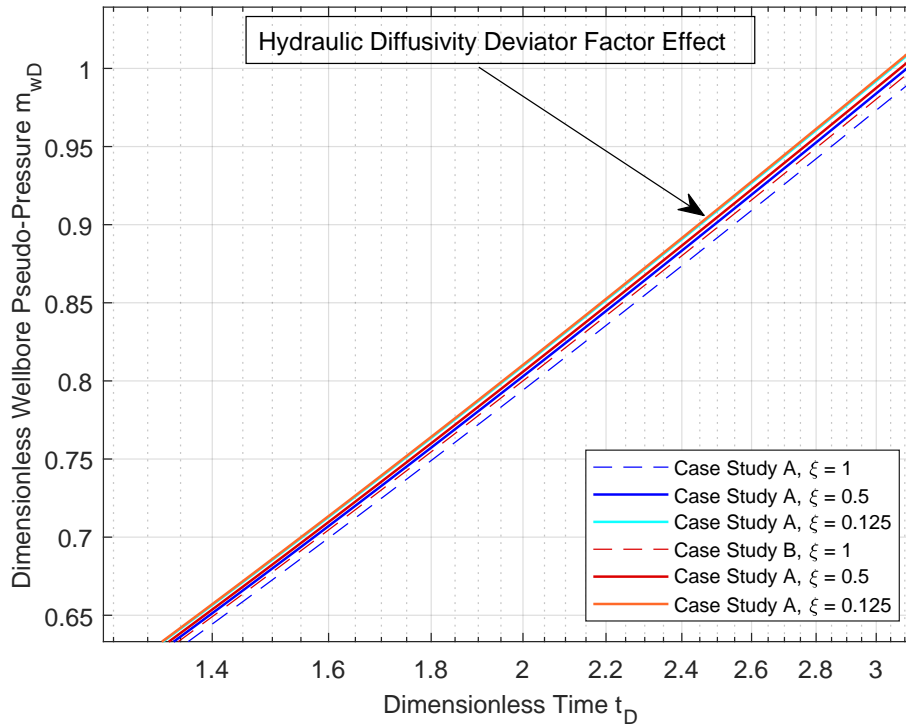


Figure 5.18: Semi-log plot of the amplification of hydraulic diffusivity deviator factor effect in the dimensionless general solution.

5.2

Oil Flow in a Vertical Well Near an Infinite Sealing Fault

Sealing faults may significantly impact the fluid flow patterns within a petroleum reservoir, (Kuchuk & Kabir, 1988). Thereby, the knowledge of fault zones is essential for the economic viability analysis of exploration projects to prevent early depletion during the well-reservoir performance management, (Knipe, Jones & Fisher, 1998). The mathematical modeling of the permeability pressure-dependent effect through the nonlinear hydraulic diffusivity equation (NHDE) with source term is still challenging in the petroleum industry. Therefore, accurate analytical models for the nonlinear source term have been extensively researched to save computational resources and calibrate new reservoir models. Image data and pressure transient analysis constitute useful, practical tools to identify sealed zones, (Bengtson, 1981). In this section, the

NHDE is solved through a GF's-based model of oil flow in a wellbore near a sealing fault (Figure 5.19). A sealing fault can be understood as a zone with no permeability that makes a barrier stopping the oil flow from the reservoir. Let the porous media semi-infinite in y direction and the sealing fault dimensionless distance defined as L_D . The presence of this fault creates a combined oil flow in porous media. Near the wellbore and far from the fault, the oil flow has a radial behavior, and as the flow gets far from the wellbore and closer to the fault, it tends to a combined flow, named pseudo-radial flow. The selectivity between the reservoir layers is provided by a sliding sleeve (SS), and a standing valve (SV) assembled in the testing column.

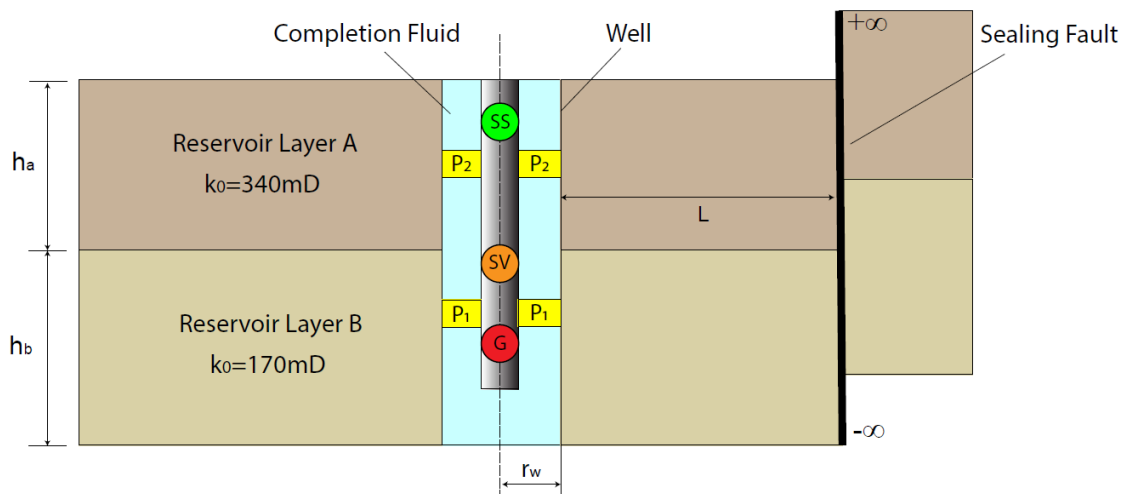


Figure 5.19: Side view of a vertical well near a sealing fault sketch.

5.2.1 Model Assumptions

For modeling of oil flow problem in porous media by means of the asymptotic series expansion of the solution of the pressure diffusivity equation in terms of pseudo-pressure, the following premises are assumed:

1. Constant flow rate in the well
2. Pressure-sensitive permeability
3. Darcian flow in porous media
4. Well fully penetrates reservoir rock
5. Deformable, homogeneous, linear elastic and isotropic reservoir
6. The well is located at the origin of cylindrical system of coordinates (0,0)
7. Isothermal, single-phase and compressible flow in the reservoir
8. The fluid present inside the pores of the reservoir rock does not react chemically with the rock matrix

9. Two dimensional (2-D) and unsteady oil flow
10. Small pressure gradient
11. Skin and storage effects not considered
12. Permeability hysteresis of porous media is negligible
13. No fluid flow across the top and bottom of the formation
14. Infinite extent reservoir in x-direction
15. Reservoir with uniform net pay

5.2.2

Model Derivation

Let the sealing fault model in Cartesian coordinates $\mathbf{r}_D = (x_D, y_D) \in \mathbb{R}^2$ and $t_D \in \mathbb{R}$. For this model, dimensionless variables are: $x_D = x/r_w$, $y_D = y/r_w$ and $L_D = L/r_w$. Where (x, y) are the Cartesian coordinates, [m] and L is the well-sealing fault distance, [m]. The dimensionless time and pseudo-pressure remain the same as the infinite radial problem in chapter 5. The NHDE in terms of pressure in Cartesian coordinates is:

$$\frac{\partial^2 p}{\partial x^2} + \frac{\partial^2 p}{\partial y^2} - \frac{1}{\eta(p)} \frac{\partial p}{\partial t} = -f(x, y, t) \quad (5-134)$$

Let the pseudo-pressure function (Fernandes, 2022):

$$m(p) = \int_{p_b}^p k(p') dp' \quad (5-135)$$

The Cartesian x-y components of the pseudo-pressure gradients are:

For the x-component:

$$\frac{\partial m(p)}{\partial x} = \frac{dm(p)}{dp} \frac{\partial p}{\partial x} \quad (5-136)$$

For the y-component:

$$\frac{\partial m(p)}{\partial y} = \frac{dm(p)}{dp} \frac{\partial p}{\partial y} \quad (5-137)$$

As presented in the previous chapters, the pseudo-pressure derivative with respect to the pressure is expressed by:

$$\frac{dm(p)}{dp} = k(p) \quad (5-138)$$

Replacing the Eq. 5-138 in the Eqs. 5-136 and 5-137, the pseudo-pressure gradients for become:

For the x-component:

$$\frac{\partial m(p)}{\partial x} = k(p) \frac{\partial p}{\partial x} \quad (5-139)$$

For the y-component:

$$\frac{\partial m(p)}{\partial y} = k(p) \frac{\partial p}{\partial y} \quad (5-140)$$

Applying the product's rule, the x-y Cartesian components of pseudo-pressure Laplacian are:

For the x-component:

$$\frac{\partial^2 m(p)}{\partial x^2} = \frac{dk(p)}{dp} \frac{\partial p}{\partial x} \frac{\partial p}{\partial x} + k(p) \frac{\partial^2 p}{\partial x^2} \quad (5-141)$$

Rewriting the Eq. 5-141:

$$\frac{\partial^2 m(p)}{\partial x^2} = \frac{dk(p)}{dp} \left(\frac{\partial p}{\partial x} \right)^2 + k(p) \frac{\partial^2 p}{\partial x^2} \quad (5-142)$$

For the y-component:

$$\frac{\partial^2 m(p)}{\partial y^2} = \frac{dk(p)}{dp} \frac{\partial p}{\partial y} \frac{\partial p}{\partial y} + k(p) \frac{\partial^2 p}{\partial y^2} \quad (5-143)$$

Rewriting the Eq. 5-143:

$$\frac{\partial^2 m(p)}{\partial y^2} = \frac{dk(p)}{dp} \left(\frac{\partial p}{\partial y} \right)^2 + k(p) \frac{\partial^2 p}{\partial y^2} \quad (5-144)$$

For small pressure gradients, the Eq. 5-142 yields to:

$$\frac{\partial^2 m(p)}{\partial x^2} = k(p) \frac{\partial^2 p}{\partial x^2} \quad (5-145)$$

and the Eq. 5-144 becomes:

$$\frac{\partial^2 m(p)}{\partial y^2} = k(p) \frac{\partial^2 p}{\partial y^2} \quad (5-146)$$

Rewriting the Eqs. 5-145 and 5-146:

For the x-component:

$$\frac{\partial^2 p}{\partial x^2} = \frac{1}{k(p)} \frac{\partial^2 m(p)}{\partial x^2} \quad (5-147)$$

For the y-component:

$$\frac{\partial^2 p}{\partial y^2} = \frac{1}{k(p)} \frac{\partial^2 m(p)}{\partial y^2} \quad (5-148)$$

The pseudo-pressure rate is:

$$\frac{\partial m(p)}{\partial t} = \frac{dm(p)}{dp} \frac{\partial p}{\partial t} \quad (5-149)$$

Replacing the Eq. 5-138 in the Eq. 5-149:

$$\frac{\partial m(p)}{\partial t} = k(p) \frac{\partial p}{\partial t} \quad (5-150)$$

Rewriting the Eq. 5-150 in terms of the pressure instantaneous rate:

$$\frac{\partial p}{\partial t} = \frac{1}{k(p)} \frac{\partial m(p)}{\partial t} \quad (5-151)$$

Replacing the Eqs. 5-147, 5-148 and 5-151 in the Eq. 5-134, the NHDE yields to:

$$\frac{1}{k(p)} \frac{\partial^2 m(p)}{\partial x^2} + \frac{1}{k(p)} \frac{\partial^2 m(p)}{\partial y^2} - \frac{1}{k(p)\eta(p)} \frac{\partial m(p)}{\partial t} = -f(x, y, t) \quad (5-152)$$

Multiplying both sides of the Eq. 5-152 by the pressure-sensitive permeability function $k(p)$:

$$\frac{\partial^2 m(p)}{\partial x^2} + \frac{\partial^2 m(p)}{\partial y^2} - \frac{1}{\eta(p)} \frac{\partial m(p)}{\partial t} = -k(p)f(x, y, t) \quad (5-153)$$

Let pseudo-pressure variation:

$$\Delta m(p) = \int_{p_b}^{p_i} k(p') dp' - \int_p^p k(p') dp' \quad (5-154)$$

That results in:

$$\Delta m(p) = \int_p^{p_i} k(p') dp' \quad (5-155)$$

The NHDE in terms of pseudo-pressure variation is:

$$\frac{\partial^2 \Delta m(p)}{\partial x^2} + \frac{\partial^2 \Delta m(p)}{\partial y^2} - \frac{1}{\eta(p)} \frac{\partial \Delta m(p)}{\partial t} = -k(p)f(x, y, t) \quad (5-156)$$

The initial condition is:

$$\Delta m(p)(x, y, t = 0) = 0 \quad (5-157)$$

The external boundary conditions are:

For the x-component:

$$\lim_{x \rightarrow \infty} \Delta m(p)(x, t) = 0 \quad (5-158)$$

For the y-component:

$$\lim_{y \rightarrow \infty} \Delta m(p)(y, t) = 0 \quad (5-159)$$

5.2.3

Dimensionless Model

Let the dimensionless pseudo-pressure:

$$m_D(x, y, t) = \frac{2\pi h}{q\mu} \Delta m(p) \quad (5-160)$$

The partial differential operators are:

For x-component:

$$\frac{\partial}{\partial x} = \frac{\partial}{\partial (l_c x_D)} = \frac{1}{l_c} \frac{\partial}{\partial x_D} \quad (5-161)$$

For y-component:

$$\frac{\partial}{\partial y} = \frac{\partial}{\partial (l_c y_D)} = \frac{1}{l_c} \frac{\partial}{\partial y_D} \quad (5-162)$$

The second-order partial differential operators for x-y Cartesian coordinates are:

For x-component:

$$\frac{\partial^2}{\partial x^2} = \frac{\partial^2}{\partial (l_c^2 x_D^2)} = \frac{1}{l_c^2} \frac{\partial^2}{\partial x_D^2} \quad (5-163)$$

For y-component:

$$\frac{\partial^2}{\partial y^2} = \frac{\partial^2}{\partial (l_c^2 y_D^2)} = \frac{1}{l_c^2} \frac{\partial^2}{\partial y_D^2} \quad (5-164)$$

The instantaneous rate operator is:

$$\frac{\partial}{\partial t} = \frac{k(p_i)}{\phi \mu c_t l_c^2} \frac{\partial}{\partial t_D} \quad (5-165)$$

Replacing the Eqs. 5-160, 5-163, 5-164 and 5-165 in the Eq. 5-156, the NHDE becomes:

$$\frac{q\mu}{2\pi h l_c^2} \frac{\partial^2 m_D}{\partial x_D^2} + \frac{q\mu}{2\pi h l_c^2} \frac{\partial^2 m_D}{\partial y_D^2} - \frac{q\mu}{2\pi h l_c^2} \frac{\phi \mu c_t k(p_i)}{\phi \mu c_t k(p)} \frac{\partial m_D}{\partial t_D} = -k(p) f(x, y, t) \quad (5-166)$$

$$\frac{\partial^2 m_D}{\partial x_D^2} + \frac{\partial^2 m_D}{\partial y_D^2} - \frac{1}{k_D(p)} \frac{\partial m_D}{\partial t_D} = -\frac{2\pi k(p) l_c^2}{q\mu} f(x, y, t) \quad (5-167)$$

Since the dimensionless oil source term is:

$$\frac{2\pi k(p) l_c^2}{q\mu} f(x, y, t) = f_D(x_D, y_D, t_D) \quad (5-168)$$

Thus, final form of dimensionless pseudo-pressure NHDE is:

$$\frac{\partial^2 m_D}{\partial x_D^2} + \frac{\partial^2 m_D}{\partial y_D^2} - \frac{1}{k_D(m_D)} \frac{\partial m_D}{\partial t_D} = f_D(x_D, y_D, t_D) \quad (5-169)$$

The initial condition is:

$$m_D(x_D, y_D, t_D = 0, k_D) = 0 \quad (5-170)$$

External boundary conditions are:

For x-component:

$$\lim_{x_D \rightarrow +\infty} m_D(x_D, y_D, t_D, k_D) = 0 \quad (5-171)$$

For y-component:

$$\lim_{y_D \rightarrow +\infty} m_D(x_D, y_D, t_D, k_D) = 0 \quad (5-172)$$

The dimensionless source term is:

$$f_D(x_D, y_D, t_D) = -2\pi l_c^2 \delta(x - L) \delta(y - 0) \quad (5-173)$$

In terms of the dimensionless spatial variables:

$$f_D(x_D, y_D, t_D) = -2\pi\delta(x_D - L_D)\delta(y_D) \quad (5-174)$$

5.2.4

Asymptotic Series Expansion Method for a Well Near a Sealing Fault

The dimensionless general solution for the NHDE in terms of pseudo-pressure can be expressed by a k^{th} order asymptotic series expansion:

$$m_D = \sum_{k=0}^{+\infty} \epsilon^k m_D^{(k)} \quad (5-175)$$

Let us define a relationship between the inverse dimensionless permeability function $1/k_D(p)$ and a diffusivity deviation factor $\xi(p)$ as:

$$\xi(p) = \frac{1}{k_D(p)} - 1 \quad (5-176)$$

Thus:

$$\frac{1}{k_D(p)} = \xi(p) + 1 \quad (5-177)$$

Thereby, we can rewrite Eq. 5-169 as follows:

$$\frac{\partial^2 m_D}{\partial x_D^2} + \frac{\partial^2 m_D}{\partial y_D^2} - \left[\xi(p) + 1 \right] \frac{\partial m_D}{\partial t_D} = -\hat{\mathcal{S}}_{oD}^{(k)}(x_D, y_D, t_D) \quad (5-178)$$

The dimensionless k^{th} -order source term $\hat{\mathcal{S}}_{oD}^{(k)}$ is:

$$\hat{\mathcal{S}}_{oD}^{(k)} = \xi^{(k-1)}(m_D) \frac{\partial m_D^{(j)}}{\partial t_D} \quad (5-179)$$

The k^{th} -order deviation factor $\xi^{(k)}$ is:

$$\xi^{(k)} = \sum_{j=0}^{k-1} \xi \left[m_D^{(j)} \right] \frac{\partial m_D^{(j)}}{\partial t_D} \quad (5-180)$$

That results in:

$$\hat{\mathcal{S}}_{oD}^{(k)} = f_D(x_D, y_D, t_D) + \xi^{(0)} \frac{\partial m_D^{(0)}}{\partial t_D} + \xi^{(1)} \frac{\partial m_D^{(1)}}{\partial t_D} + \xi^{(k-1)} \frac{\partial m_D^{(k-1)}}{\partial t_D} + \dots \quad (5-181)$$

Let us use the perturbation technique proposed by Kale & Mattar (1980), Pedrosa Jr. (1986), Kikani & Pedrosa Jr. (1991) to expand the NHDE combining Eqs. 5-175, 5-179, 5-180 and 5-181 to Eq. 5-178:

$$\begin{aligned} & \epsilon^0 \left[\frac{\partial^2 m_D}{\partial x_D^2} + \frac{\partial^2 m_D}{\partial y_D^2} - \frac{\partial m_D^{(0)}}{\partial t_D} + f_D(x_D, y_D, t_D) \right] + \\ & \quad + \epsilon^1 \left[\frac{\partial^2 m_D}{\partial x_D^2} + \frac{\partial^2 m_D}{\partial y_D^2} - \frac{\partial m_D^{(0)}}{\partial t_D} - \xi^{(0)} \frac{\partial m_D^{(0)}}{\partial t_D} \right] + \\ & \quad + \epsilon^2 \left[\frac{\partial^2 m_D}{\partial x_D^2} + \frac{\partial^2 m_D}{\partial y_D^2} - \frac{\partial m_D^{(1)}}{\partial t_D} - \xi^{(1)} \frac{\partial m_D^{(1)}}{\partial t_D} \right] + \dots \\ & \quad + \epsilon^k \left[\frac{\partial^2 m_D}{\partial x_D^2} + \frac{\partial^2 m_D}{\partial y_D^2} - \frac{\partial m_D^{(k-1)}}{\partial t_D} - \xi^{(k-1)} \frac{\partial m_D^{(k-1)}}{\partial t_D} \right] = 0 \quad (5-182) \end{aligned}$$

Where $f_D(x_D, y_D, t_D)$ represents the dimensionless zeroth-order source term. Applying the definition of the diffusivity deviation factor, Eq. 5-182 yields to:

$$\begin{aligned} & \epsilon^0 \left[\frac{\partial^2 m_D}{\partial x_D^2} + \frac{\partial^2 m_D}{\partial y_D^2} - \frac{\partial m_D^{(0)}}{\partial t_D} + f_D(x_D, y_D, t_D) \right] + \\ & \quad + \epsilon^1 \left\{ \frac{\partial^2 m_D}{\partial x_D^2} + \frac{\partial^2 m_D}{\partial y_D^2} - \frac{\partial m_D^{(0)}}{\partial t_D} - \left[\frac{1}{k_D [m_D^{(0)}]} + 1 \right] \frac{\partial m_D^{(0)}}{\partial t_D} \right\} + \\ & \quad + \epsilon^2 \left\{ \frac{\partial^2 m_D}{\partial x_D^2} + \frac{\partial^2 m_D}{\partial y_D^2} - \frac{\partial m_D^{(1)}}{\partial t_D} - \left[\frac{1}{k_D [m_D^{(1)}]} + 1 \right] \frac{\partial m_D^{(1)}}{\partial t_D} \right\} + \dots \\ & \quad + \epsilon^k \left\{ \frac{\partial^2 m_D}{\partial x_D^2} + \frac{\partial^2 m_D}{\partial y_D^2} - \frac{\partial m_D^{(k-1)}}{\partial t_D} - \left[\frac{1}{k_D [m_D^{(k-1)}]} + 1 \right] \frac{\partial m_D^{(k-1)}}{\partial t_D} \right\} = 0 \quad (5-183) \end{aligned}$$

Using a first-order expansion:

$$\begin{aligned} & \epsilon^0 \left[\frac{\partial^2 m_D}{\partial x_D^2} + \frac{\partial^2 m_D}{\partial y_D^2} - \frac{\partial m_D^{(0)}}{\partial t_D} + f_D(x_D, y_D, t_D) \right] + \\ & \quad + \epsilon^1 \left\{ \frac{\partial^2 m_D}{\partial x_D^2} + \frac{\partial^2 m_D}{\partial y_D^2} - \frac{\partial m_D^{(0)}}{\partial t_D} - \left[\frac{1}{k_D [m_D^{(0)}]} + 1 \right] \frac{\partial m_D^{(0)}}{\partial t_D} \right\} = 0 \quad (5-184) \end{aligned}$$

Regrouping the terms of Eq. 5-184:

$$(\epsilon + 1) \left(\frac{\partial^2 m_D}{\partial x_D^2} + \frac{\partial^2 m_D}{\partial y_D^2} \right) - (\epsilon + 1) \left\{ \left[\frac{1}{k_D [m_D^{(0)}]} + 1 \right] \frac{\partial m_D^{(0)}}{\partial t_D} \right\} + f_D(x_D, y_D, t_D) = 0 \quad (5-185)$$

Rewriting Eq. 5-185

$$(\epsilon + 1) \left\{ \frac{\partial^2 m_D}{\partial x_D^2} + \frac{\partial^2 m_D}{\partial y_D^2} - \left[\frac{1}{k_D [m_D^{(0)}]} + 1 \right] \frac{\partial m_D^{(0)}}{\partial t_D} \right\} = -f_D(x_D, y_D, t_D) \quad (5-186)$$

Applying Eq. 5-175 in the IC:

$$m_D = \sum_{k=0}^{\infty} \epsilon^k m_D^{(k)}(x_D, y_D, t_D = 0) = 0 \quad (5-187)$$

Expanding Eq. 5-187 in terms of epsilon powers for the x-direction:

$$\begin{aligned} \epsilon^0 m_D^{(0)}(x_D, t_D = 0) + \epsilon^1 m_D^{(1)}(x_D, t_D = 0) + \epsilon^2 m_D^{(2)}(x_D, t_D = 0) + \dots \\ + \epsilon^k m_D^{(k)}(x_D, t_D = 0) = 0 \end{aligned} \quad (5-188)$$

For the y-direction:

$$\begin{aligned} \epsilon^0 m_D^{(0)}(y_D, t_D = 0) + \epsilon^1 m_D^{(1)}(y_D, t_D = 0) + \epsilon^2 m_D^{(2)}(y_D, t_D = 0) + \dots \\ + \epsilon^k m_D^{(k)}(y_D, t_D = 0) = 0 \end{aligned} \quad (5-189)$$

The perturbed EBC is:

$$\lim_{|x_D, y_D, z_D| \rightarrow \infty} \sum_{k=0}^{\infty} \epsilon^k m_D^{(k)}(x_D, y_D, t_D) = 0 \quad (5-190)$$

Expanding Eq. 5-190 in terms of epsilon powers for the x-direction:

$$\begin{aligned} \lim_{x_D \rightarrow \infty} \epsilon^0 m_D^{(0)}(x_D, t_D) + \lim_{x_D \rightarrow \infty} \epsilon^1 m_D^{(1)}(x_D, t_D) + \lim_{x_D \rightarrow \infty} \epsilon^2 m_D^{(2)}(x_D, t_D) + \dots \\ + \lim_{x_D \rightarrow \infty} \epsilon^k m_D^{(k)}(x_D, t_D) = 0 \end{aligned} \quad (5-191)$$

and, for the y-direction:

$$\begin{aligned} \lim_{y_D \rightarrow \infty} \epsilon^0 m_D^{(0)}(y_D, t_D) + \lim_{y_D \rightarrow \infty} \epsilon^1 m_D^{(1)}(y_D, t_D) + \lim_{y_D \rightarrow \infty} \epsilon^2 m_D^{(2)}(y_D, t_D) + \dots \\ + \lim_{y_D \rightarrow \infty} \epsilon^k m_D^{(k)}(y_D, t_D) = 0 \end{aligned} \quad (5-192)$$

Using the GF technique for the higher order terms ($k > 1$) of the proposed solution, (Barreto Jr., Peres & Pires, 2010):

$$\frac{\partial^2 G_D(x_D, x'_D, y_D, y'_D, t_D, t'_D)}{\partial x_D^2} + \frac{\partial^2 G_D(x_D, x'_D, y_D, y'_D, t_D, t'_D)}{\partial y_D^2} + \frac{\partial G_D(x_D, x'_D, y_D, y'_D, t_D, t'_D)}{\partial t_D} = -2\pi\delta(x_D - L_D)\delta(y_D)\delta(t_D - t'_D) \quad (5-193)$$

The initial condition for the associated problem is:

$$G_D(x_D, x'_D, y_D, y'_D, t_D, t'_D = 0) = 0 \quad (5-194)$$

and the external boundary condition is:

$$\lim_{|x_D, y_D| \rightarrow \infty} G_D(x_D, x'_D, y_D, y'_D, t_D, t'_D) = 0 \quad (5-195)$$

Where the parameters x'_D, y'_D and t'_D represent the x-y position and time where and when the instantaneous oil pulse is applied, whereas x_D, y_D and t_D represent the x-y position and the time where and when the pulse is observed. As performed in the previous chapter, it is necessary to establish the solution of the Eq. 5-193, as well as, for the initial and boundary conditions that satisfies the associated problem. Because the differential operator on the left-hand side of the Eqs. 5-178 and 5-193 is not self-adjoint, to compute the general solution $m_D(x_D, y_D, t_D, k_D)$ it is necessary to resort to the adjoint GF $G_D^*(x_D, x'_D, y_D, y'_D, t_D, t'_D)$ which satisfies the following adjoint problem:

$$\frac{\partial^2 G_D^*(x_D, x'_D, y_D, y'_D, t_D, t'_D)}{\partial x_D^2} + \frac{\partial^2 G_D^*(x_D, x'_D, y_D, y'_D, t_D, t'_D)}{\partial y_D^2} + \frac{\partial G_D^*(x_D, x'_D, y_D, y'_D, t_D, t'_D)}{\partial t_D} = -2\pi\delta(x_D - L_D)\delta(y_D)\delta(t_D - t'_D) \quad (5-196)$$

With the adjoint initial condition:

$$G_D^*(x_D, x'_D, y_D, y'_D, t_D, t'_D = 0) = 0 \quad (5-197)$$

and external boundary condition:

$$\lim_{|x_D, y_D| \rightarrow \infty} G_D^*(x_D, x'_D, y_D, y'_D, t_D, t'_D) = 0 \quad (5-198)$$

The parameters x'_D, y'_D, t'_D and x_D, y_D, t_D are the same spatial and instantaneous variables aforementioned. The Eq. is the causality clause for the adjoint

problem. Thereby it is not necessary to solve the adjoint problem, because the adjoint GF is related to the regular one by the reciprocity principle (Carslaw & Jaeger, 1959):

$$G_D^*(x_D, x'_D, y_D, y'_D, t_D, t'_D) = G_D(x_D, x'_D, y_D, y'_D, t_D, t'_D) \quad (5-199)$$

Replacing the identity expressed by the Eq. 5-199 in the Eqs. 5-196 to 5.2.4, the adjoint problem yields to:

$$\begin{aligned} & \frac{\partial^2 G_D(x_D, x'_D, y_D, y'_D, t_D, t'_D)}{\partial x_D^2} + \frac{\partial^2 G_D(x_D, x'_D, y_D, y'_D, t_D, t'_D)}{\partial y_D^2} + \\ & + \frac{\partial G_D(x_D, x'_D, y_D, y'_D, t_D, t'_D)}{\partial t_D} = -2\pi\delta(x_D - L_D)\delta(y_D)\delta(t_D - t'_D) \end{aligned} \quad (5-200)$$

With the initial condition:

$$G_D(x_D, x'_D, y_D, y'_D, t_D, t'_D = 0) = 0 \quad (5-201)$$

and external boundary condition:

$$\lim_{|x_D, y_D| \rightarrow \infty} G_D(x_D, x'_D, y_D, y'_D, t_D, t'_D) = 0 \quad (5-202)$$

Multiplying the Eq. 5-178 by $1/2\pi \times G_D(x_D, x'_D, y_D, y'_D, t_D, t'_D)$ and the Eq. 5-200 by $1/2\pi m_D(x_D, y_D, t_D, k_D)$, it is possible to represent the general solution $m_D(x_D, y_D, t_D, k_D)$ in terms of the GF:

$$\begin{aligned} & \frac{1}{2\pi} G_D(x_D, x'_D, y_D, y'_D, t_D, t'_D) \left[\frac{\partial^2 m_D(x_D, y_D, t_D, k_D)}{\partial x_D^2} + \frac{\partial^2 m_D(x_D, y_D, t_D, k_D)}{\partial y_D^2} \right. \\ & \left. + (1+\epsilon\xi) \times \frac{\partial m_D(x_D, y_D, t_D, k_D)}{\partial t_D} \right] = -\frac{1}{2\pi} G_D(x_D, x'_D, y_D, y'_D, t_D, t'_D) f_D(x_D, y_D, t_D) \end{aligned} \quad (5-203)$$

and

$$\begin{aligned} & \frac{1}{2\pi} m_D(x_D, y_D, t_D, k_D) \left[\frac{\partial^2 G_D(x_D, x'_D, y_D, y'_D, t_D, t'_D)}{\partial x_D^2} + \frac{\partial^2 G_D(x_D, x'_D, y_D, y'_D, t_D, t'_D)}{\partial y_D^2} \right. \\ & \left. + \frac{\partial G_D(x_D, x'_D, y_D, y'_D, t_D, t'_D)}{\partial t_D} \right] = -\frac{1}{2\pi} m_D(x_D, y_D, t_D) 2\pi\delta(x_D - L_D)\delta(y_D)\delta(t_D - t'_D) \end{aligned} \quad (5-204)$$

The Eq. 5-203 and Eq. 5-204 must be subtracted, therewith:

$$\begin{aligned} & \frac{1}{2\pi} G_D(x_D, x'_D, y_D, y'_D, t_D, t'_D) \left[\frac{\partial^2 m_D(x_D, y_D, t_D)}{\partial x_D^2} + \frac{\partial^2 m_D(x_D, y_D, t_D)}{\partial y_D^2} - (1 + \epsilon\xi) \times \right. \\ & \left. \times \frac{\partial m_D(x_D, y_D, t_D)}{\partial t_D} \right] - \frac{1}{2\pi} \times m_D(x_D, y_D, t_D) \left[\frac{\partial^2 G_D(x_D, x'_D, y_D, y'_D, t_D, t'_D)}{\partial x_D^2} + \right. \\ & \left. + \frac{\partial^2 G_D(x_D, x'_D, y_D, y'_D, t_D, t'_D)}{\partial y_D^2} + \frac{\partial G_D(x_D, x'_D, y_D, y'_D, t_D, t'_D)}{\partial t_D} \right] = m_D(x_D, y_D, t_D) \times \\ & \times \delta(x_D - L_D) \delta(y_D) \delta(t_D - t'_D) - \frac{1}{2\pi} G_D(x_D, x'_D, y_D, y'_D, t_D, t'_D) f_D(x_D, y_D, t_D) \end{aligned} \quad (5-205)$$

Expanding the terms of the Eq. 5-205:

$$\begin{aligned} & \frac{1}{2\pi} G_D(x_D, x'_D, y_D, y'_D, t_D, t'_D) \left[\frac{\partial^2 m_D(x_D, y_D, t_D)}{\partial x_D^2} + \frac{\partial^2 m_D(x_D, y_D, t_D)}{\partial y_D^2} \right] - \frac{1}{2\pi} \times \\ & \times G_D(x_D, x'_D, y_D, y'_D, t_D, t'_D) (1 + \epsilon\xi) \frac{\partial m_D(x_D, y_D, t_D)}{\partial t_D} - \frac{1}{2\pi} m_D(x_D, y_D, t_D) \times \\ & \times \left[\frac{\partial^2 G_D(x_D, x'_D, y_D, y'_D, t_D, t'_D)}{\partial x_D^2} + \frac{\partial^2 G_D(x_D, x'_D, y_D, y'_D, t_D, t'_D)}{\partial y_D^2} \right] - \frac{1}{2\pi} \times \\ & \times m_D(x_D, y_D, t_D) \frac{\partial G_D(x_D, x'_D, y_D, y'_D, t_D, t'_D)}{\partial t_D} = m_D(x_D, y_D, t_D) \delta(x_D - L_D) \times \\ & \times \delta(y_D) \delta(t_D - t'_D) - \frac{1}{2\pi} G_D(x_D, x'_D, y_D, y'_D, t_D, t'_D) f_D(x_D, y_D, t_D) \end{aligned} \quad (5-206)$$

Let:

$$\lim_{\epsilon \rightarrow 1} \left[1 + \epsilon\xi(p) \right] = 1 + \xi(p) \quad (5-207)$$

The Eq. 5-206 becomes:

$$\begin{aligned} & \frac{1}{2\pi} G_D(x_D, x'_D, y_D, y'_D, t_D, t'_D) \left[\frac{\partial^2 m_D(x_D, y_D, t_D)}{\partial x_D^2} + \frac{\partial^2 m_D(x_D, y_D, t_D)}{\partial y_D^2} \right] - \frac{1}{2\pi} \times \\ & \times G_D(x_D, x'_D, y_D, y'_D, t_D, t'_D) (1 + \xi) \frac{\partial m_D(x_D, y_D, t_D)}{\partial t_D} - \frac{1}{2\pi} m_D(x_D, y_D, t_D) \times \\ & \times \left[\frac{\partial^2 G_D(x_D, x'_D, y_D, y'_D, t_D, t'_D)}{\partial x_D^2} + \frac{\partial^2 G_D(x_D, x'_D, y_D, y'_D, t_D, t'_D)}{\partial y_D^2} \right] - \frac{1}{2\pi} \times \\ & \times m_D(x_D, y_D, t_D) \frac{\partial G_D(x_D, x'_D, y_D, y'_D, t_D, t'_D)}{\partial t_D} = m_D(x_D, y_D, t_D) \delta(x_D - L_D) \times \\ & \times \delta(y_D) \delta(t_D - t'_D) - \frac{1}{2\pi} G_D(x_D, x'_D, y_D, y'_D, t_D, t'_D) f_D(x_D, y_D, t_D) \end{aligned} \quad (5-208)$$

Expanding the nonlinear term of the Eq. 5-208:

$$\begin{aligned}
& \frac{1}{2\pi} G_D(x_D, x'_D, y_D, y'_D, t_D, t'_D) \left[\frac{\partial^2 m_D(x_D, y_D, t_D)}{\partial x_D^2} + \frac{\partial^2 m_D(x_D, y_D, t_D)}{\partial y_D^2} \right] - \frac{1}{2\pi} \times \\
& \times G_D(x_D, x'_D, y_D, y'_D, t_D, t'_D) \frac{\partial m_D(x_D, y_D, t_D)}{\partial t_D} - \frac{1}{2\pi} \xi(p) G_D(x_D, x'_D, y_D, y'_D, t_D, t'_D) \times \\
& \times \frac{\partial m_D(x_D, y_D, t_D)}{\partial t_D} - \frac{1}{2\pi} m_D(x_D, y_D, t_D) \left[\frac{\partial^2 G_D(x_D, x'_D, y_D, y'_D, t_D, t'_D)}{\partial x_D^2} + \right. \\
& \left. + \frac{\partial^2 G_D(x_D, x'_D, y_D, y'_D, t_D, t'_D)}{\partial y_D^2} \right] - \frac{1}{2\pi} m_D(x_D, y_D, t_D) \frac{\partial G_D(x_D, x'_D, y_D, y'_D, t_D, t'_D)}{\partial t_D} = \\
& = m_D(x_D, y_D, t_D) \delta(x_D - L_D) \delta(y_D) \delta(t_D - t'_D) - \frac{1}{2\pi} \times \\
& \times G_D(x_D, x'_D, y_D, y'_D, t_D, t'_D) f_D(x_D, y_D, t_D) \quad (5-209)
\end{aligned}$$

Integrating the Eq. 5-209:

$$\begin{aligned}
& \frac{1}{2\pi} \int_{-\infty}^{+\infty} \int_0^{+\infty} \int_0^{t_D} \left\{ G_D(x'_D, x_{D0}, y'_D, y_{D0}, t'_D, t_{D0}) \left[\frac{\partial^2 m_D(x'_D, y'_D, t'_D)}{\partial x_D'^2} + \right. \right. \\
& \left. \left. + \frac{\partial^2 m_D(x'_D, y'_D, t'_D)}{\partial y_D'^2} \right] - G_D(x'_D, x_{D0}, y'_D, y_{D0}, t'_D, t_{D0}) \frac{\partial m_D(x'_D, y'_D, t'_D)}{\partial t'_D} - \right. \\
& \left. + \xi(p) G_D(x'_D, x_{D0}, y'_D, y_{D0}, t'_D, t_{D0}) \frac{\partial m_D(x'_D, y'_D, t'_D)}{\partial t'_D} - m_D(x'_D, y'_D, t'_D) \times \right. \\
& \left. \times \left[\frac{\partial^2 G_D(x'_D, x_{D0}, y'_D, y_{D0}, t'_D, t_{D0})}{\partial x_D'^2} + \frac{\partial^2 G_D(x'_D, x_{D0}, y'_D, y_{D0}, t'_D, t_{D0})}{\partial y_D'^2} \right] - \right. \\
& \left. \left. + m_D(x'_D, y'_D, t'_D) \frac{\partial G_D(x'_D, x_{D0}, y'_D, y_{D0}, t'_D, t_{D0})}{\partial t'_D} \right\} dt'_D dx'_D dy'_D = \\
& = \int_{-\infty}^{+\infty} \int_0^{+\infty} \int_0^{t_D} \left[m_D(x'_D, y'_D, t'_D) \delta(x'_D - L_D) \delta(y'_D) \delta(t'_D - t_{D0}) - \right. \\
& \left. + \frac{1}{2\pi} G_D(x'_D, x_{D0}, y'_D, y_{D0}, t'_D, t_{D0}) f_D(x'_D, y'_D, t'_D) \right] dt'_D dx'_D dy'_D \quad (5-210)
\end{aligned}$$

After performing the spatial integration of the first and fourth terms of the left-hand side of the Eq. 5-210 by parts:

$$\begin{aligned}
& \frac{1}{2\pi} \int_{-\infty}^{+\infty} \int_0^{+\infty} \left\{ G_D(x'_D, x_{D0}, y'_D, y_{D0}, t'_D, t_{D0}) \left[\frac{\partial^2 m_D(x'_D, y'_D, t'_D)}{\partial x_D'^2} + \right. \right. \\
& \left. \left. + \frac{\partial^2 m_D(x'_D, y'_D, t'_D)}{\partial y_D'^2} \right] - m_D(x'_D, y'_D, t'_D) \left[\frac{\partial^2 G_D(x'_D, x_{D0}, y'_D, y_{D0}, t'_D, t_{D0})}{\partial x_D'^2} + \right. \right. \\
& \left. \left. + \frac{\partial^2 G_D(x'_D, x_{D0}, y'_D, y_{D0}, t'_D, t_{D0})}{\partial y_D'^2} \right] \right\} dx'_D dy'_D = \frac{1}{2\pi} \left\{ \left\{ G_D(x'_D, x_{D0}, y'_D, y_{D0}, t'_D, t_{D0}) \times \right. \right. \\
& \quad \times \left[\frac{\partial m_D(x'_D, y'_D, t'_D)}{\partial x'_D} + \frac{\partial m_D(x'_D, y'_D, t'_D)}{\partial y'_D} \right] - m_D(x'_D, y'_D, t'_D) \times \\
& \quad \times \left. \left. \left[\frac{\partial G_D(x'_D, x_{D0}, y'_D, y_{D0}, t'_D, t_{D0})}{\partial x'_D} + \frac{\partial G_D(x'_D, x_{D0}, y'_D, y_{D0}, t'_D, t_{D0})}{\partial y'_D} \right] \right\}_{x'_D=0}^{x'_D \rightarrow +\infty} \right\}_{y'_D=-\infty}^{y'_D \rightarrow +\infty} \quad (5-211)
\end{aligned}$$

The second and fifth terms on the left-hand side of the Eq. 5-210 represent the time derivative of the product of two functions. Thereby:

$$\begin{aligned}
& \frac{1}{2\pi} \int_0^{t_D} \left[G_D(x'_D, x_{D0}, y'_D, y_{D0}, t'_D, t_{D0}) \frac{\partial m_D(x'_D, y'_D, t'_D)}{\partial t'_D} + m_D(x'_D, y'_D, t'_D) \times \right. \\
& \quad \left. \times \frac{\partial G_D(x'_D, x_{D0}, y'_D, y_{D0}, t'_D, t_{D0})}{\partial t'_D} \right] dt'_D = \\
& = \frac{1}{2\pi} \int_0^{t_D} \frac{\partial}{\partial t'_D} \left[G_D(x'_D, x_{D0}, y'_D, y_{D0}, t'_D, t_{D0}) m_D(x'_D, y'_D, t'_D) \right] dt'_D \quad (5-212)
\end{aligned}$$

Using the Leibniz rule from the integral of derivatives:

$$\begin{aligned}
& \int_0^{t_D} \frac{\partial}{\partial t'_D} \left[G_D(x'_D, x_{D0}, y'_D, y_{D0}, t'_D, t_{D0}) m_D(x'_D, y'_D, t'_D) \right] dt'_D = \\
& = \left[G_D(x'_D, x_{D0}, y'_D, y_{D0}, t'_D, t_{D0}) m_D(x'_D, y'_D, t'_D) \right]_{t'_D=0}^{t'_D=t_D} \quad (5-213)
\end{aligned}$$

Thus, the Eq. 5-213 yields to:

$$\begin{aligned}
& \left[G_D(x'_D, x_{D0}, y'_D, y_{D0}, t'_D, t_{D0}) m_D(x'_D, y'_D, t'_D) \right]_{t'_D=0}^{t'_D=t_D} = \\
& = G_D(x'_D, x_{D0}, y'_D, y_{D0}, t'_D = 0, t_{D0}) m_D(x'_D, y'_D, t'_D = 0) \quad (5-214)
\end{aligned}$$

After the use of the homogeneous IC, the Eq. 5-214 becomes:

$$G_D(x'_D, x_{D0}, y'_D, y_{D0}, t'_D = 0, t_{D0})m_D(x'_D, y'_D, t'_D = 0) = 0 \quad (5-215)$$

Finally, by the sampling property of the Dirac Delta function:

$$\begin{aligned} \int_{-\infty}^{+\infty} \int_0^{+\infty} \int_0^{t_D} m_D(x'_D, y'_D, t'_D) \delta(x'_D - L_D) \delta(y'_D) \delta(t'_D - t_{D0}) dt'_D dx'_D dy'_D = \\ = m_D(x_D, y_D, t_D) \end{aligned} \quad (5-216)$$

5.2.5

Dimensionless Oil Source for a Well near a Sealing Fault

The oil source term proposed in this paper is expressed through an instantaneous point-source and it has a key role in the permeability loss over the well-reservoir life-cycle once it also takes in account the hydraulic diffusivity deviator factor in its formula. The total oil source is expressed by the infinite series below:

$$\tilde{S}_D(x_D, y_D, t_D) = \tilde{S}_D^{(0)}(x_D, y_D, t_D) + \tilde{S}_D^{(1)}(x_D, y_D, t_D) + \tilde{S}_D^{(2)}(x_D, y_D, t_D) + \dots \quad (5-217)$$

Where $\tilde{S}_D(x_D, y_D, t_D) = 2\pi \hat{\hat{S}}_{oD}(x_D, y_D, t_D)$

In this approach, the series expansion is truncated on the first-order term.

Thereby:

$$\tilde{S}_D(x_D, y_D, t_D) \approx \tilde{S}_D^{(0)}(x_D, y_D, t_D) + \tilde{S}_D^{(1)}(x_D, y_D, t_D) \quad (5-218)$$

The zeroth-order source term is:

$$\tilde{S}_D^{(0)}(x_D, y_D, t_D) = 2\pi f_D(x_D, y_D, t_D) \quad (5-219)$$

And the first-order is:

$$\tilde{S}_D^{(1)}(x_D, y_D, t_D) = 2\pi \xi(m_D) \frac{\partial m_D(x_D, y_D, t_D)}{\partial t_D} \quad (5-220)$$

Replacing the Eqs.5-219 and 5-220 in the Eq. 5-218, the dimensionless general oil source term can be expressed by:

$$\hat{\hat{S}}_{oD}(x_D, y_D, t_D) \approx 2\pi f_D(x_D, y_D, t_D) + 2\pi \xi(m_D) \frac{\partial m_D(x_D, y_D, t_D)}{\partial t_D} \quad (5-221)$$

Combining the Eqs. 5-211, 5-214, 5-216 and 5-218 to the use of the initial and boundary conditions from both $m_D(x_D, y_D, t_D)$ and $G_D(x_D, x'_D, y_D, y'_D, t_D, t'_D)$ problems in the Eq. 39, the general solution of the NHDE for the oil flow through a fully penetrating vertical well near a sealing fault can be expressed as follows:

$$m_D(x_D, y_D, t_D) \approx 2\pi \int_{-\infty}^{+\infty} \int_0^{+\infty} \int_0^{t_D} \left[f_D(x'_D, y'_D, t'_D) + \xi(m_D) \frac{\partial m_D(x'_D, y'_D, t'_D)}{\partial t'_D} \right] \times \\ \times G_D(x'_D, x_{D0}, y'_D, y_{D0}, t'_D, t_{D0}) dt'_D dx'_D dy'_D \quad (5-222)$$

Expanding the terms inside the brackets:

$$m_D(x_D, y_D, t_D) = 2\pi \int_{-\infty}^{+\infty} \int_0^{+\infty} \int_0^{t_D} f_D(x'_D, y'_D, t'_D) \times \\ \times G_D(x'_D, x_{D0}, y'_D, y_{D0}, t'_D, t_{D0}) dt'_D dx'_D dy'_D + 2\pi \int_0^{\infty} \int_0^{t_D} \xi(m_D) \times \\ \times \frac{\partial m_D(x'_D, y'_D, t'_D)}{\partial t'_D} G_D(x'_D, x_{D0}, y'_D, y_{D0}, t'_D, t_{D0}) dt'_D dx'_D dy'_D \quad (5-223)$$

Let the oil flow rate in the reservoir and standard conditions expressed by $q(x, y, t)$ and q_{sc} , respectively. The dimensionless source term is:

$$f_D(x_D, y_D, t_D) = -2\pi r_w^2 \frac{q(x, y, t)}{q_{sc}} \delta(x - L) \delta(y - 0) \delta(t - 0) \quad (5-224)$$

Where $q_D(x_D, y_D, t_D) = q(x, y, t)/q_{sc}$ is the dimensionless oil flow rate. The meaning of the negative sign in the source term is because the oil is produced from the reservoir. In terms of the dimensionless oil flow rate, the Eq. 5-224 becomes:

$$f_D(x_D, y_D, t_D) = -2\pi r_w^2 q_D(x_D, y_D, t_D) \delta(x - L) \delta(y - 0) \delta(t - 0) \quad (5-225)$$

By the space scaling property of the Dirac delta function:

$$\delta(\lambda x) = \frac{\delta(x)}{|\lambda|}, \quad \lambda \in \mathbb{R} \quad (5-226)$$

Since $x = x_D \times r_w$, $L = L_D \times r_w$, $y = y_D \times r_w$ and $|r_w| = r_w$, thus: $\delta(x - L) = \delta(x_D r_w - L_D r_w)$ and $\delta(y) = \delta(y_D r_w)$.

$$\delta(x_D r_w - L_D r_w) = \frac{\delta(x_D - L_D)}{r_w} \quad (5-227)$$

and

$$\delta(y_D r_w) = \frac{\delta(y_D)}{r_w} \quad (5-228)$$

As the oil flow rate in the reservoir and standard conditions are the same: $q(x, y, t) = q_{sc}$, it implies that the dimensionless oil flow rate $q_D(x_D, y_D, t_D) = 1$, thus, combining the Eqs. 5-225, 5-227 and 5-228, the dimensionless oil source can be expressed as follows:

$$f_D(x_D, y_D, t_D) = -2\pi\delta(x_D - L_D)\delta(y_D) \quad (5-229)$$

The dimensionless general solution of the pseudo-pressure NHDE is expressed by:

$$m_D(x_D, y_D, t_D) \approx p_D(x_D, y_D, t_D) + m_D^{(1)}(x_D, y_D, t_D) \quad (5-230)$$

Where the corrective first-order term $m_D^{(1)}(x_D, y_D, t_D)$ is:

$$m_D^{(1)}(x_D, y_D, t_D) = - \int_{-\infty}^{+\infty} \int_0^{+\infty} \int_0^{t_D} \xi(m_D) \frac{\partial m_D(x'_D, y'_D, t'_D)}{\partial t'_D} \times \\ \times G_D(x'_D, x_{D0}, y'_D, y_{D0}, t'_D, t_{D0}) dt'_D dx'_D dy'_D \quad (5-231)$$

Thus, the dimensionless pseudo-pressure general solution becomes:

$$m_D(x_D, y_D, t_D) \approx p_D(x_D, y_D, t_D) - \int_{-\infty}^{+\infty} \int_0^{+\infty} \int_0^{t_D} \xi(m_D) \times \\ \times \frac{\partial m_D(x'_D, y'_D, t'_D)}{\partial t'_D} G_D(x_D, x'_D, y_D, y'_D, t_D, t'_D) dt'_D dx'_D dy'_D \quad (5-232)$$

The dimensionless GF associated to the sealing fault problem is (Carslaw & Jaeger, 1959), (Beck et al., 1992), (Ozisiki, 1993), (Duffy, 2001) and (Cole, Beck & Haji-Sheikh, 2011):

$$G_D(x_D, x_{D0}, y_D, y_{D0}, t_D, t_{D0}) = \\ = \frac{e \left[-\frac{(x_D - x_{D0})^2 + (y_D - y_{D0})^2}{4(t_D - t_{D0})} \right]}{4\pi(t_D - t_{D0})} + \frac{e \left[-\frac{(x_D - x_{D0} - 2L_D)^2 + (y_D - y_{D0})^2}{4(t_D - t_{D0})} \right]}{4\pi(t_D - t_{D0})} \quad (5-233)$$

Replacing Eq. 5-233 in Eq. 5-232:

$$\begin{aligned}
 m_D(x_D, y_D, t_D) &= \\
 &= p_D(x_D, y_D, t_D) - \int_{-\infty}^{+\infty} \int_0^{+\infty} \int_0^{t_D} \left[\xi(m_D) \frac{\partial m_D(x'_D, y'_D, t'_D)}{\partial t'_D} \right] \times \\
 &\times \left\{ \frac{e \left[-\frac{(x'_D - x_{D0})^2 + (y'_D - y_{D0})^2}{4(t'_D - t_{D0})} \right] + e \left[-\frac{(x'_D - x_{D0} - 2L_D)^2 + (y'_D - y_{D0})^2}{4(t'_D - t_{D0})} \right]}{4\pi(t'_D - t_{D0})} \right\} dt'_D dx'_D dy'_D
 \end{aligned} \tag{5-234}$$

According to the image method the dimensionless linear solution $p_D(x_D, y_D, t_D)$ is (Carslaw & Jaeger, 1959), (Beck et al., 1992), (Ozisiki, 1993), (Duffy, 2001) and (Cole, Beck & Haji-Sheikh, 2011):

$$p_D(x_D, y_D, t_D) = -\frac{1}{2} \mathbf{Ei} \left(-\frac{x_D^2 + y_D^2}{4t_D} \right) - \frac{1}{2} \mathbf{Ei} \left[-\frac{(x_D - 2L_D)^2 + y_D^2}{4t_D} \right] \tag{5-235}$$

Thus, the dimensionless general solution becomes:

$$\begin{aligned}
 m_D(x_D, y_D, t_D) &= -\frac{1}{2} \mathbf{Ei} \left(-\frac{x_D^2 + y_D^2}{4t_D} \right) - \frac{1}{2} \mathbf{Ei} \left[-\frac{(x_D - 2L_D)^2 + y_D^2}{4t_D} \right] - \\
 &\quad + \int_{-\infty}^{+\infty} \int_0^{+\infty} \int_0^{t_D} \left[\xi(m_D) \frac{\partial m_D(x'_D, y'_D, t'_D)}{\partial t'_D} \right] \times \\
 &\quad \times \left\{ \frac{e \left[-\frac{(x'_D - x_{D0})^2 + (y'_D - y_{D0})^2}{4(t'_D - t_{D0})} \right] + e \left[-\frac{(x'_D - x_{D0} - 2L_D)^2 + (y'_D - y_{D0})^2}{4(t'_D - t_{D0})} \right]}{4\pi(t'_D - t_{D0})} \right\} dt'_D dx'_D dy'_D
 \end{aligned} \tag{5-236}$$

As the diffusivity deviator factor $\xi(m_D)$ is:

$$\xi(m_D) = \frac{1}{k_D [m_D(x_D, y_D, t_D)]} - 1 \tag{5-237}$$

Replacing the Eq.5-237 in the Eq. 5-236:

$$\begin{aligned}
 m_D(x_D, y_D, t_D) = & -\frac{1}{2}\mathbf{Ei}\left(-\frac{x_D^2 + y_D^2}{4t_D}\right) - \frac{1}{2}\mathbf{Ei}\left[-\frac{(x_D - 2L_D)^2 + y_D^2}{4t_D}\right] - \\
 & + \int_{-\infty}^{+\infty} \int_0^{+\infty} \int_0^{t_D} \left\{ \left[\frac{1}{k_D(m_D(x'_D, y'_D, t'_D))} - 1 \right] \frac{\partial m_D(x'_D, y'_D, t'_D)}{\partial t'_D} \times \right. \\
 & \left. \times \left\{ \frac{e\left[-\frac{(x'_D - x_{D0})^2 + (y'_D - y_{D0})^2}{4(t'_D - t_{D0})}\right]}{4\pi(t'_D - t_{D0})} + e\left[-\frac{(x'_D - x_{D0} - 2L_D)^2 + (y'_D - y_{D0})^2}{4(t'_D - t_{D0})}\right]}{4\pi(t'_D - t_{D0})} \right\} \right\} \quad (5-238)
 \end{aligned}$$

Since this work makes the asymptotic expansion truncation in the first-order term $m_D^{(1)}(x_D, y_D, t_D)$, the pseudo-pressure in the hydraulic diffusivity deviator factor argument and the pseudo-pressure derivative multiplying it and the GF in the integral must have order zero, *i.e.*, $m_D(x_D, y_D, t_D) = p_D(x_D, y_D, t_D)$. Thus:

$$\begin{aligned}
 m_D(x_D, y_D, t_D) = & -\frac{1}{2}\mathbf{Ei}\left(-\frac{x_D^2 + y_D^2}{4t_D}\right) - \frac{1}{2}\mathbf{Ei}\left[-\frac{(x_D - 2L_D)^2 + y_D^2}{4t_D}\right] - \\
 & + \int_{-\infty}^{+\infty} \int_0^{+\infty} \int_0^{t_D} \left\{ \left[\frac{1}{k_D(p_D(x'_D, y'_D, t'_D))} - 1 \right] \frac{\partial p_D(x'_D, y'_D, t'_D)}{\partial t'_D} \times \right. \\
 & \left. \times \left\{ \frac{e\left[-\frac{(x'_D - x_{D0})^2 + (y'_D - y_{D0})^2}{4(t'_D - t_{D0})}\right]}{4\pi(t'_D - t_{D0})} + e\left[-\frac{(x'_D - x_{D0} - 2L_D)^2 + (y'_D - y_{D0})^2}{4(t'_D - t_{D0})}\right]}{4\pi(t'_D - t_{D0})} \right\} \right\} \quad (5-239)
 \end{aligned}$$

Using the linear pressure-sensitive permeability function, the Eq. 5-239 is expressed by:

$$\begin{aligned}
 m_D(x_D, y_D, t_D) = & -\frac{1}{2}\mathbf{Ei}\left(-\frac{x_D^2 + y_D^2}{4t_D}\right) - \frac{1}{2}\mathbf{Ei}\left[-\frac{(x_D - 2L_D)^2 + y_D^2}{4t_D}\right] - \\
 & + \int_{-\infty}^{+\infty} \int_0^{+\infty} \int_0^{t_D} \left\{ \left[\frac{1}{-\frac{A}{2}\mathbf{Ei}\left(-\frac{x_D^2 + y_D^2}{4t'_D}\right) - \frac{A}{2}\mathbf{Ei}\left[-\frac{(x_D - 2L_D)^2 + y_D^2}{4t'_D}\right] + B} - 1 \right] \times \right. \\
 & \left. \times \left\{ \frac{e\left[-\frac{(x'_D - x_{D0})^2 + (y'_D - y_{D0})^2}{4(t'_D - t_{D0})}\right]}{4\pi(t'_D - t_{D0})} + e\left[-\frac{(x'_D - x_{D0} - 2L_D)^2 + (y'_D - y_{D0})^2}{4(t'_D - t_{D0})}\right]}{4\pi(t'_D - t_{D0})} \right\} \times \right. \\
 & \left. \times \frac{\partial p_D(x'_D, y'_D, t'_D)}{\partial t'_D} \right\} dt'_D dx'_D dy'_D \quad (5-240)
 \end{aligned}$$

5.2.6 Model Calibration and Results

For the analytical solution of the NHDE runs, it was used the same computational table of pressure p and permeability $k(p)$ values obtained from synthetic field data presented previously by Soares (2000), Soares, Freitas & Velloso (2001), Soares, Ferreira & Vargas Jr. (2002), Soares & Ferreira (2002). As mentioned previously, the experiment was performed through a cylindrical uni-axial cell, two cylindrical sandstones layers sample (representing the case studies A and B of this work), a fluid to represent the oil inside of the reservoir rock pores and a pressure gauge to record the pressure values during the experiment. The experimental data of pressure and permeability changes for two reservoir layers were fitted and inserted in the permeability-based pseudo-pressure function $m(p)$. The NHDE was solved through the command `int3` from Matlab[®] to compute the implicit term inside the integrand. Figure 5.20 presents the diagnostic plot of the dimensionless pseudo-pressure and its derivative for IARF and well-sealing fault setting for both case studies.

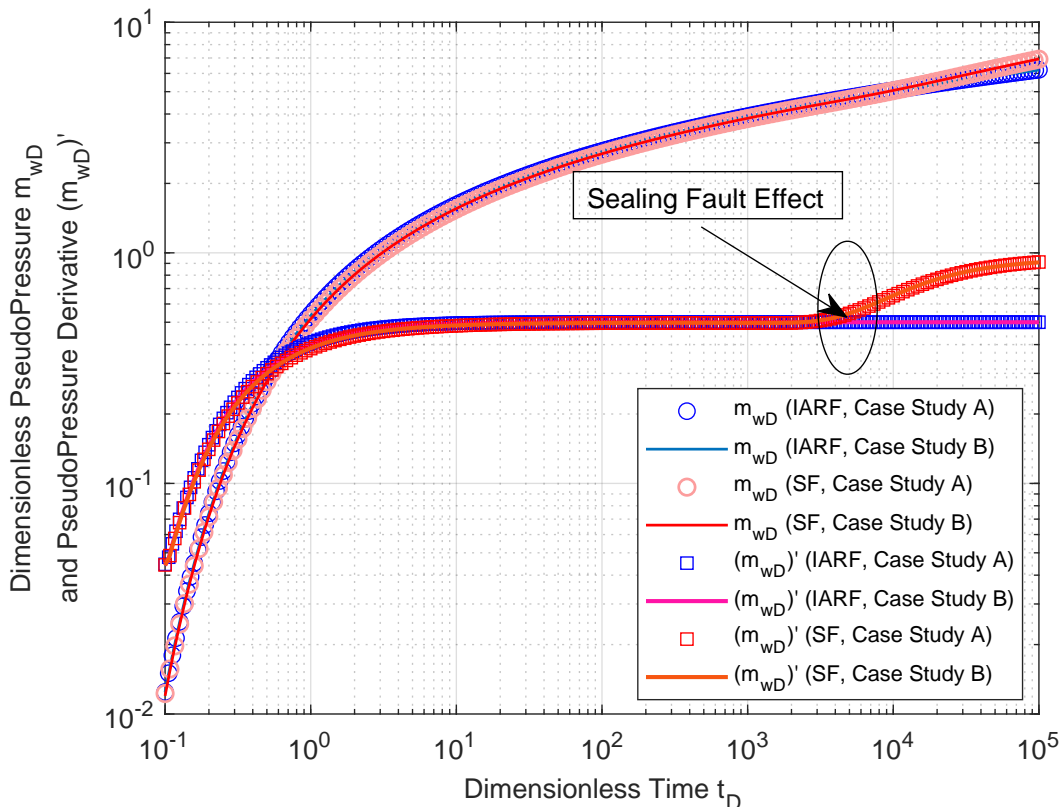


Figure 5.20: Diagnostic plot of the comparison between IARF and sealing fault curves of the dimensionless pseudo-pressure and its derivative for the case studies A and B.

To run the model, the dimensionless distances L_D from the well to the sealing fault used were 300, 500, 800 and 1000. In order to represent a sealed layer in IMEX[®], it was built a Cartesian grid with a block characterized as a zone of low transmissibility placed in a boundary of the computational cell. The sealing fault effect can be noticed as a doubled-slope value in the dimensionless pseudo-pressure derivative curve in the Figure 5.20.

Figure 5.21 presents the calibration of the constant permeability solution with respect to IMEX[®]. The results show high accuracy. This linear solution was computed analytically in Matlab[®] using the command $ei(t_D)$ and the time-steps were implemented as a geometric progression.

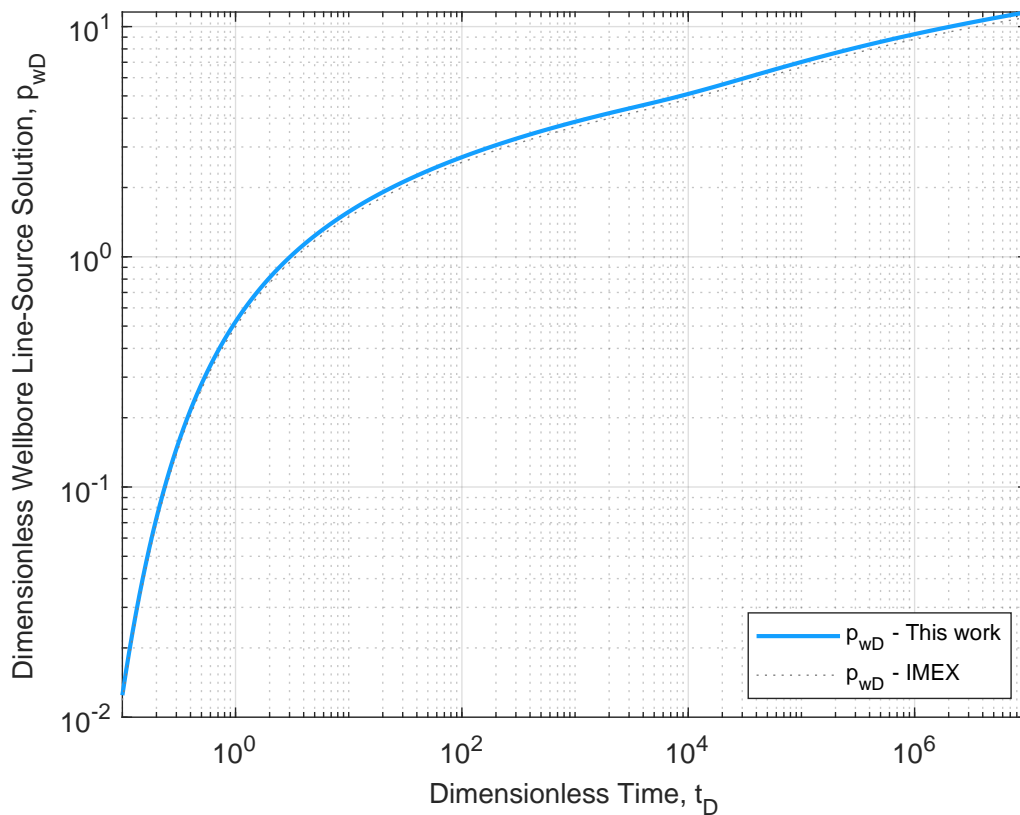


Figure 5.21: Diagnostic plot of the calibration of the constant permeability solution with respect to IMEX[®].

Figure 5.22 shows the log-log plot of the calibration of the dimensionless first-order term $m_D^{(1)}(t_D)$ and it has shown an excellent convergence, when compared to IMEX[®], even in the early-times. Hence, as presented in previous works of Peres, Serra & Reynolds (1989), Barreto Jr., Peres & Pires (2010), Fernandes (2022) it is possible to conclude that the first-order asymptotic series expansion represents, accurately, the nonlinearity caused by the permeability change as a function of pressure in the analytical model presented in this paper.

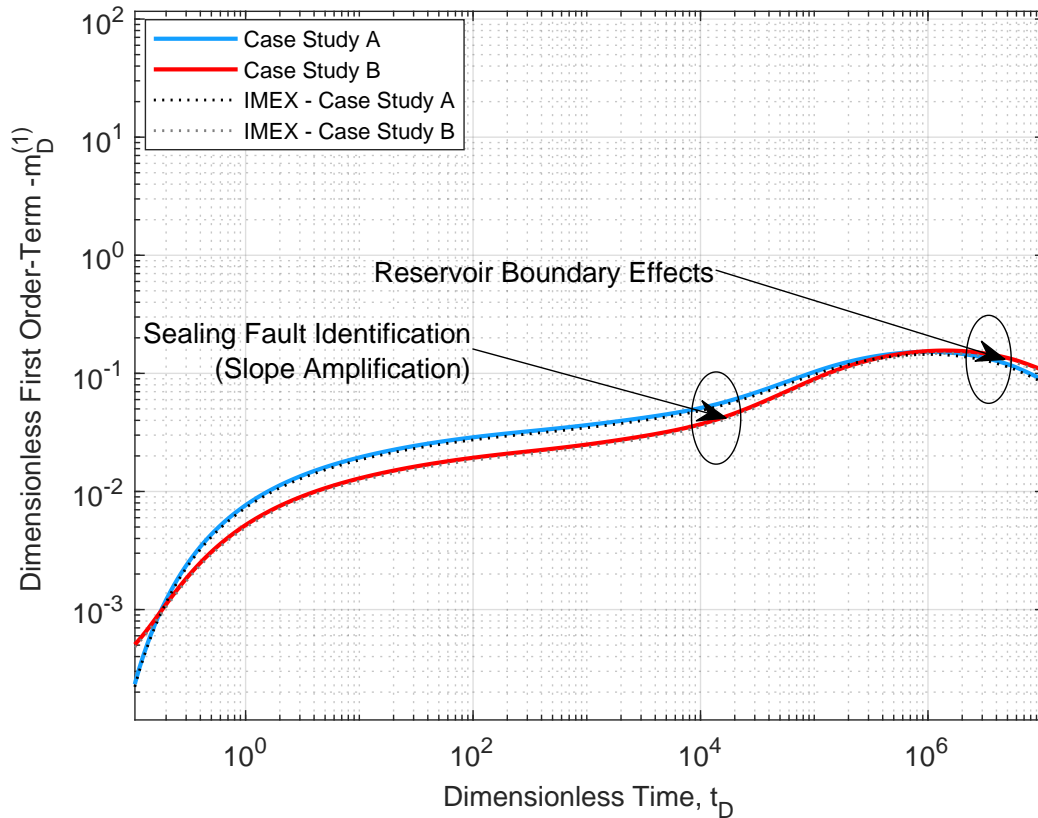


Figure 5.22: Log-log plot of the first-order term calibrated by IMEX[®]. This plot shows that, the nonlinearity that results in permeability loss is more severe during the early-times.

This plot also reveals the high accuracy of the model developed with respect to IMEX[®] (black and gray dashed lines). The dimensionless linear solution was computed analytically through the command $ei(t_D)$ from Matlab[®]. The model was calibrated through the $(p, k(p))$ values from the computational table implemented in the oil flow simulator, and the output pressure values were transformed into pseudo-pressures. Subsequently, the values were inserted into the code to run the model.

Figure 5.23 and Figure 5.24 present the Semi-log plot of the dimensionless pseudo-pressure for the four types of the pressure-sensitive permeability functions proposed in this work for the case studies A and B. The IMEX[®] curve is also plotted and it can be realized that, there is no significant difference among the curves compared to IMEX[®]. The sealing fault presence can be noticed with high accuracy in both plots for all the proposed functions.

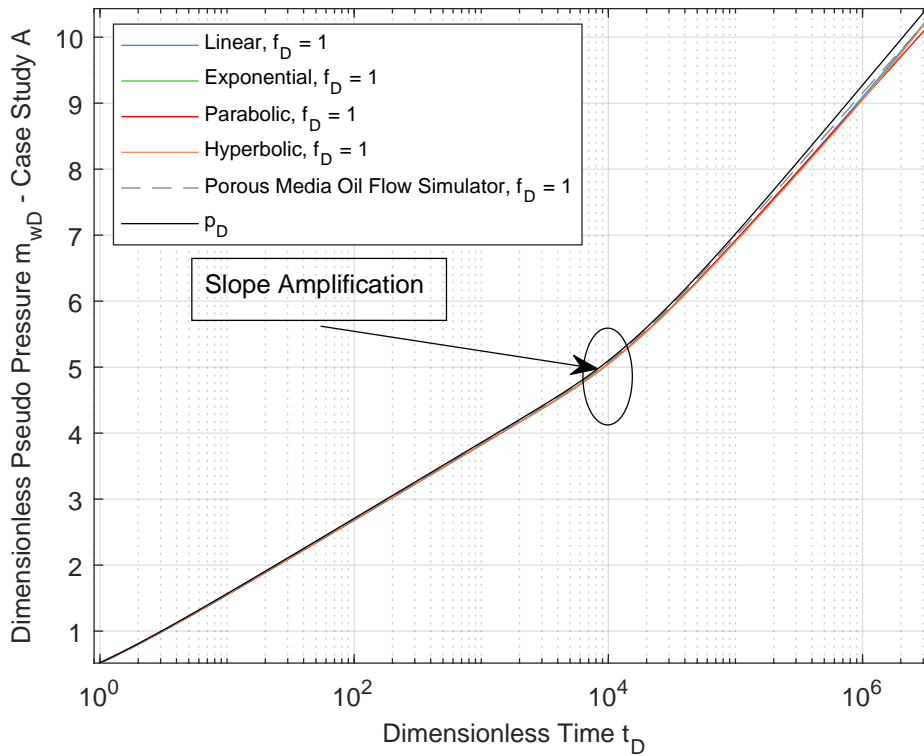


Figure 5.23: Semi-log plot of the dimensionless general solution for several fitting functions for the case study A.

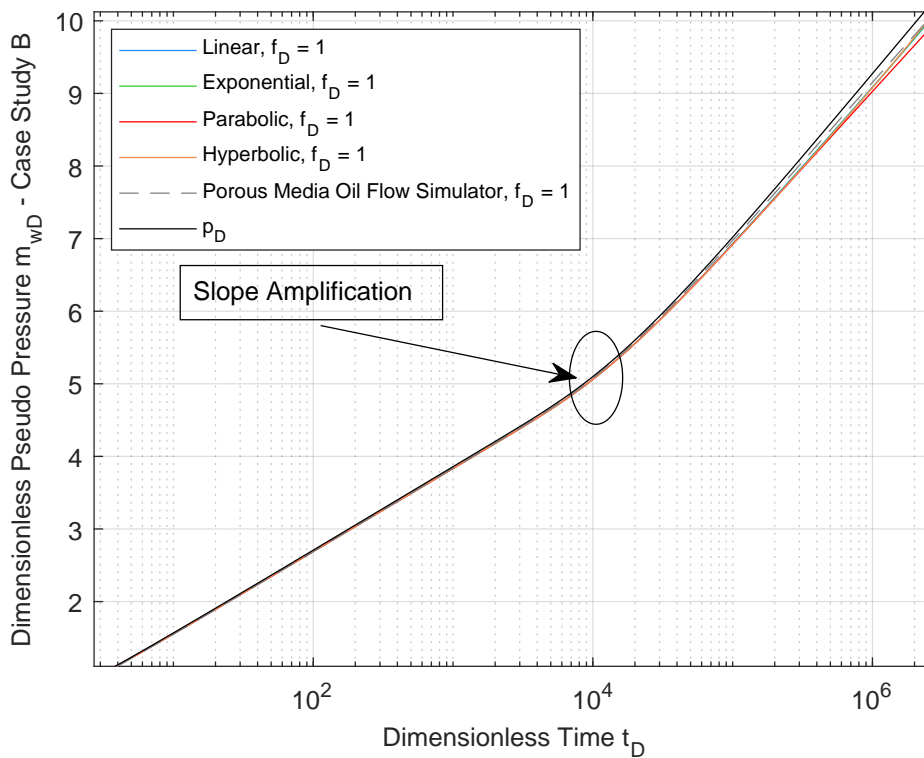


Figure 5.24: Semi-log plot of the dimensionless general solution for several fitting functions for the case study B.

Figure 5.25 and Figure 5.26 show the Log-log plot of the dimensionless pseudo-pressure derivative for the same pressure-sensitive permeability functions aforementioned for the case studies A and B. For this plot, it was used the dimensionless well-sealing fault distance $L_D = 300$. This derivative was also computed through the Bourdet algorithm (Bourdet, Ayoub & Pirard; Bourdet, 1989, 2002). The plots also present high accuracy in comparison to IMEX[®] and, as noticed in the Figure 5.23 and Figure 5.24, the fitting functions did not presented significant discrepancies with respect to the IMEX[®] results.

Figure 5.27 and Figure 5.28 present the Log-log plot of the dimensionless first-order corrective term $m_{wD}^{(1)}(t_D)$. The plot shows that, the linear, exponential and parabolic fitting functions presented satisfactory accuracy for this term for the experimental points.

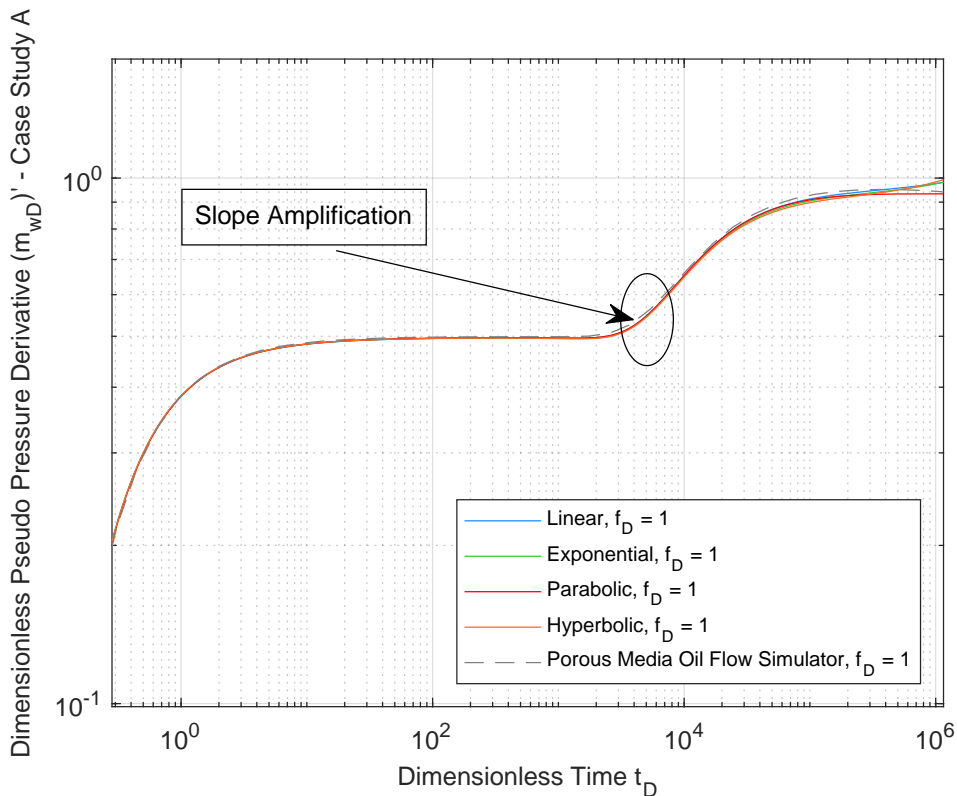


Figure 5.25: Log-log plot of the dimensionless general solution derivative for several fitting functions for the case study A.

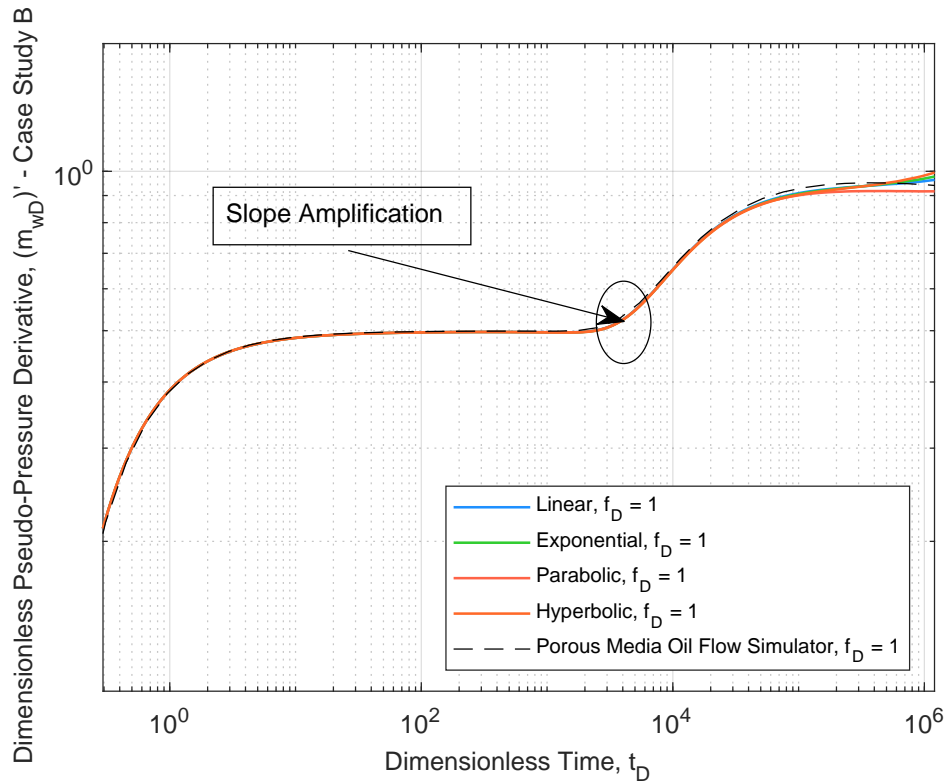


Figure 5.26: Log-log plot of the dimensionless general solution derivative for several fitting functions for the case study B.

The sealing fault presence is noticed for the dimensionless time $10^3 < t_D < 10^4$ in the Log-log plot. These plots also show that, for the *case study A*, the proposed pressure-sensitive permeability fitting functions provide close convergence in the interval $10^2 < t_D < 10^6$. For the *case study B*, a close fitting occurs in the interval $10^0 < t_D < 10^3$.

Figure 5.29 and Figure 5.30 show the Log-log plot of the dimensionless pseudo-pressure derivative for the IARF and well-sealing fault setting for several dimensionless oil flow rates in both case studies. The effect of the oil sources is described as a displacement in the $m'_{wD}(t_D)$ axis. We also can notice the superposition of the two well-reservoir setting curves until the pressure response reaches the sealing fault. It occurs for dimensionless time $10^3 < t_D < 10^4$ and from this time, the double slope is developed.

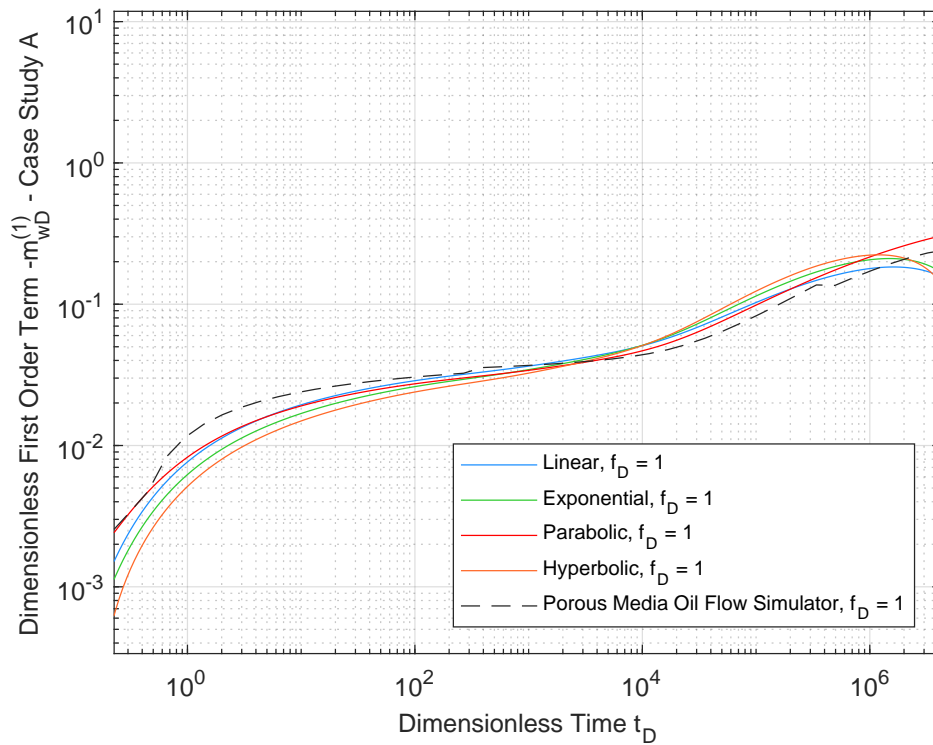


Figure 5.27: Log-log plot of the dimensionless first-order term for several fitting functions for the case study A.

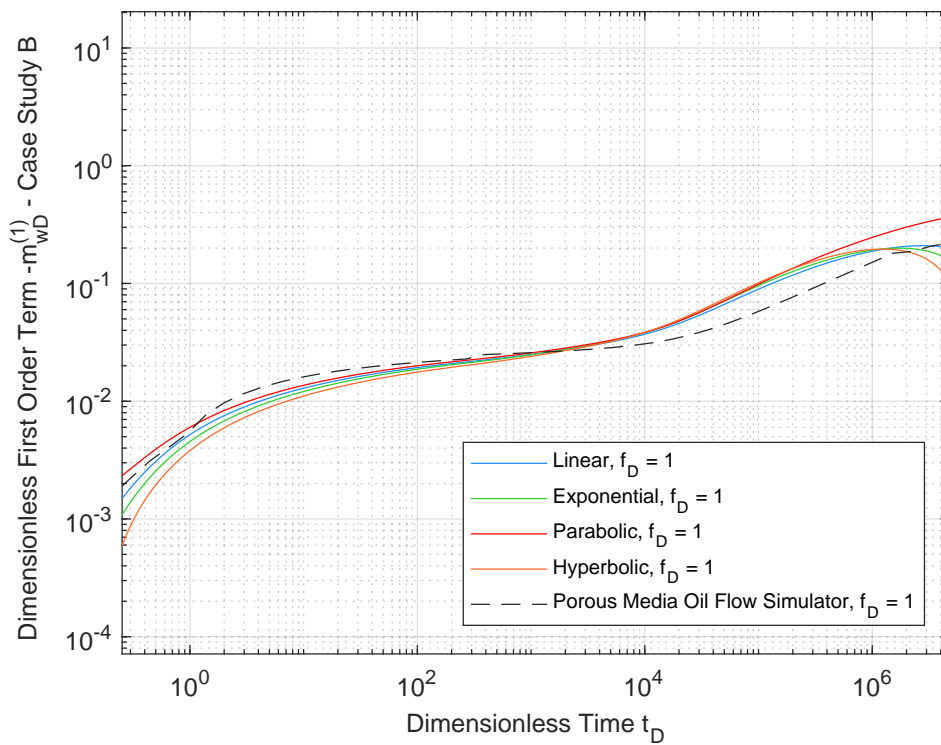


Figure 5.28: Log-log plot of the dimensionless first-order term for several fitting functions for the case study B.

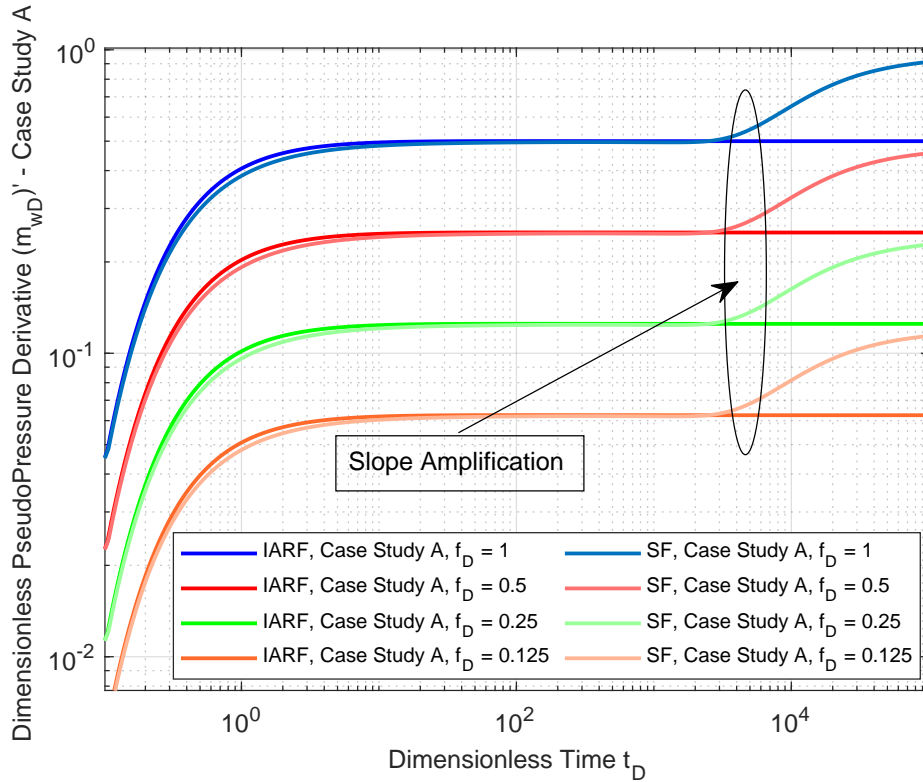


Figure 5.29: Log-log plot of the IARF and sealing fault curves of the dimensionless pseudo-pressure derivative for several sources for the case study A.

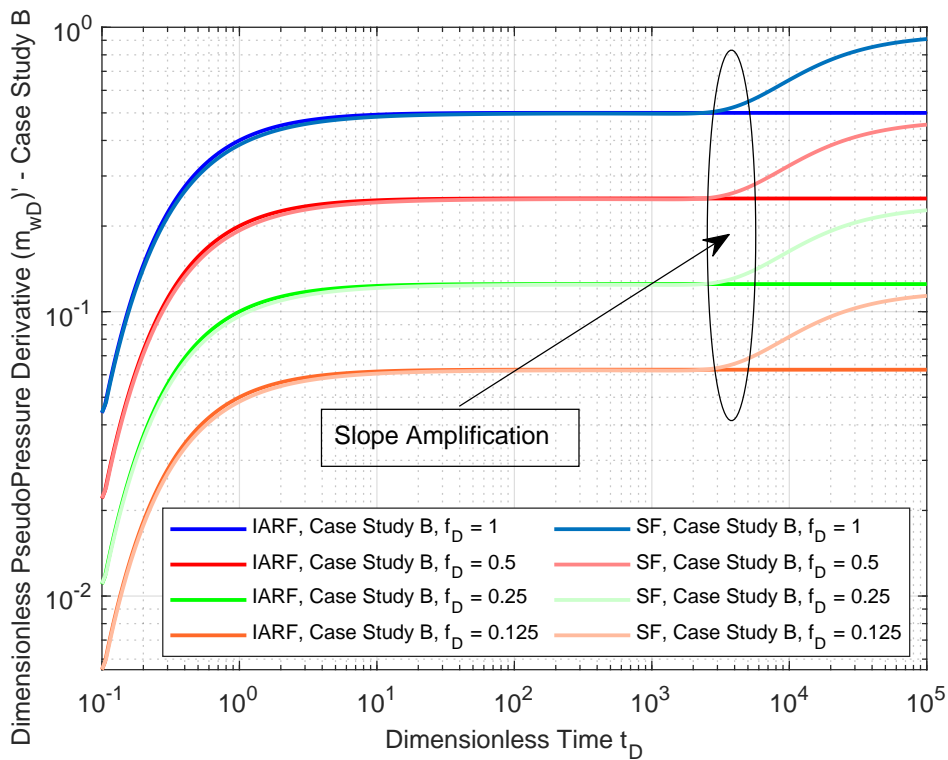


Figure 5.30: Log-log plot of the IARF and sealing fault curves of the dimensionless pseudo-pressure derivative for several sources for the case study B.

Figure 5.31 and Figure 5.32 present the Log-log plot of the dimensionless pseudo-pressure for the IARF and well-sealing fault settings for several dimensionless oil sources for the case studies A and B, respectively. The results show that dimensionless oil flow rate has a key role in pseudo-pressure behavior curves and consequently, in the permeability decline as well. The dimensionless pseudo-pressure increases as the oil source also increases.

The sealing fault presence is noticed as a smooth slope increase for the dimensionless time values $10^3 < t_D < 10^4$. This effect is more notable in the Semi-log plot, broadly used in formation evaluation practices for flow regimes identification. Therefore, Figure 5.33 and Figure 5.34 present these plots.

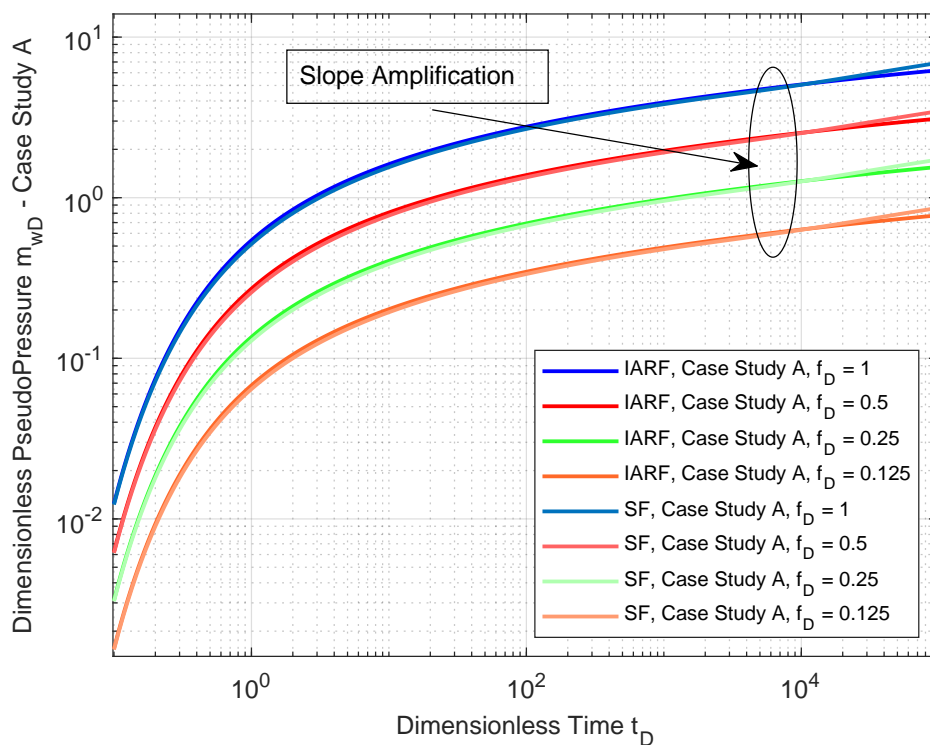


Figure 5.31: Log-log plot of the comparison between IARF and sealing fault curves of the dimensionless general solution for several oil sources for the case study B.

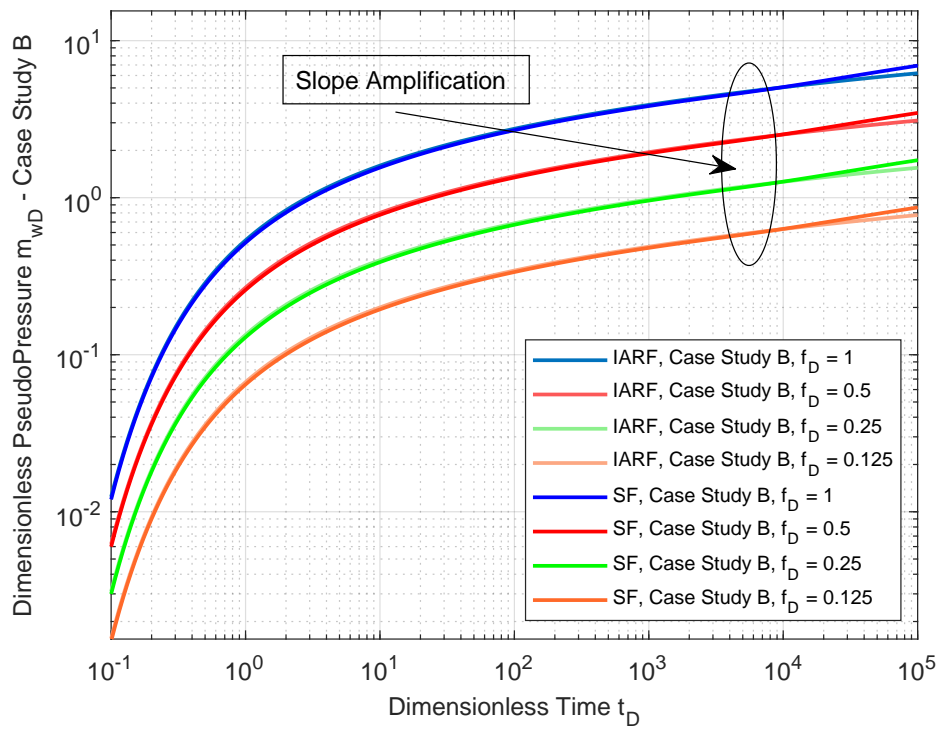


Figure 5.32: Log-log plot of the IARF and sealing fault curves of the dimensionless general solution for several oil sources for the case study B.

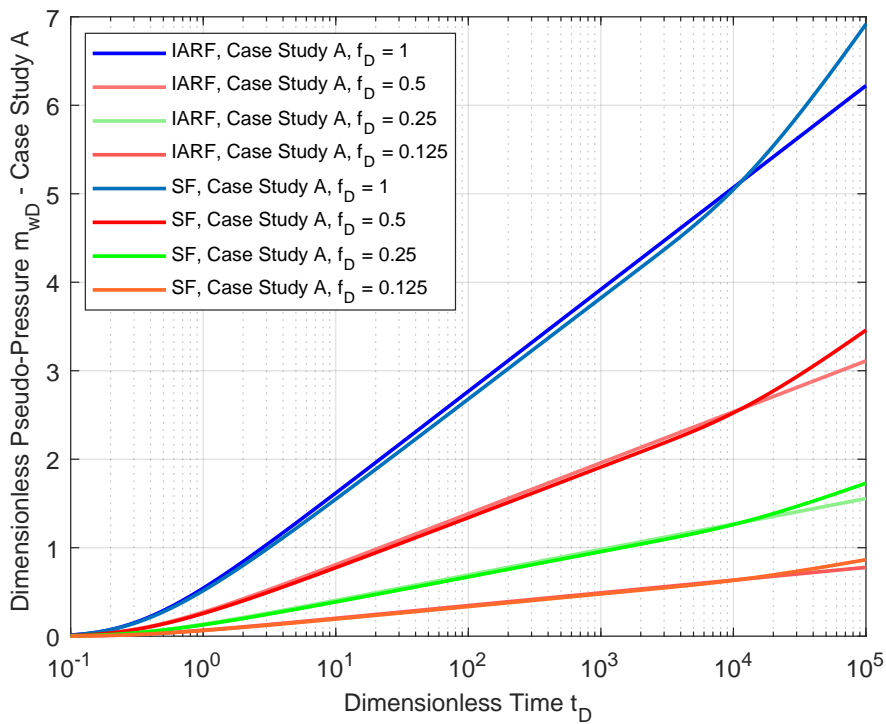


Figure 5.33: Semi-log plot of the IARF and sealing fault curves of the dimensionless general solution for several oil sources for the case study A.

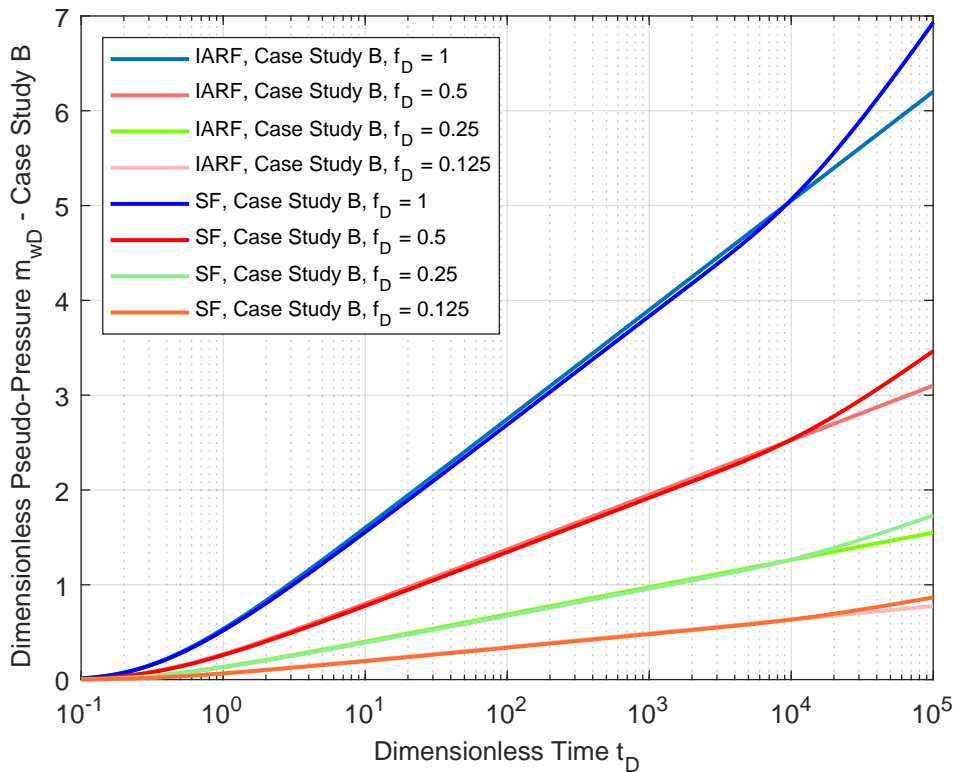


Figure 5.34: Semi-log plot of the IARF and sealing fault curves of the dimensionless general solution for several oil sources for the case study B.

Figure 5.35 and Figure 5.36 present the Log-log plot of the corrective term $m_{wD}^{(1)}(t_D)$ for comparison of the IARF and sealing fault models for *case studies A and B* with different dimensionless oil sources. It is possible to notice that, the different dimensionless source provide a vertical displacement in the first-order term. As the dimensionless oil source increases, the $m_{wD}^{(1)}(t_D)$ term also increases and it rises the nonlinearity effect in the NHDE. This increasing of the nonlinearity results in quicker permeability decline and it jeopardizes the well-reservoir life-cycle. Therefore, the hydraulic diffusivity deviator factor monitoring is fundamental for the well-reservoir performance management. This factor can be monitored by choosing the appropriate oil flow rate and through the often pressure gauge readings to avoid uncontrolled severe pressure changes throughout the oil's production's curve.

Figure 5.37 and Figure 5.38 show the Log-log plot of the dimensionless pseudo-pressure derivative as a function of dimensionless time t_D for several dimensionless well-sealing fault distances L_D for both case studies. The effect of the well-sealing fault distance is clearly shown as a displacement in the slope amplification with respect to the dimensionless time axis. We notice that, for large well-sealing fault distances (black line), the sealing fault presence becomes weak and the curve does not match to IMEX[®].

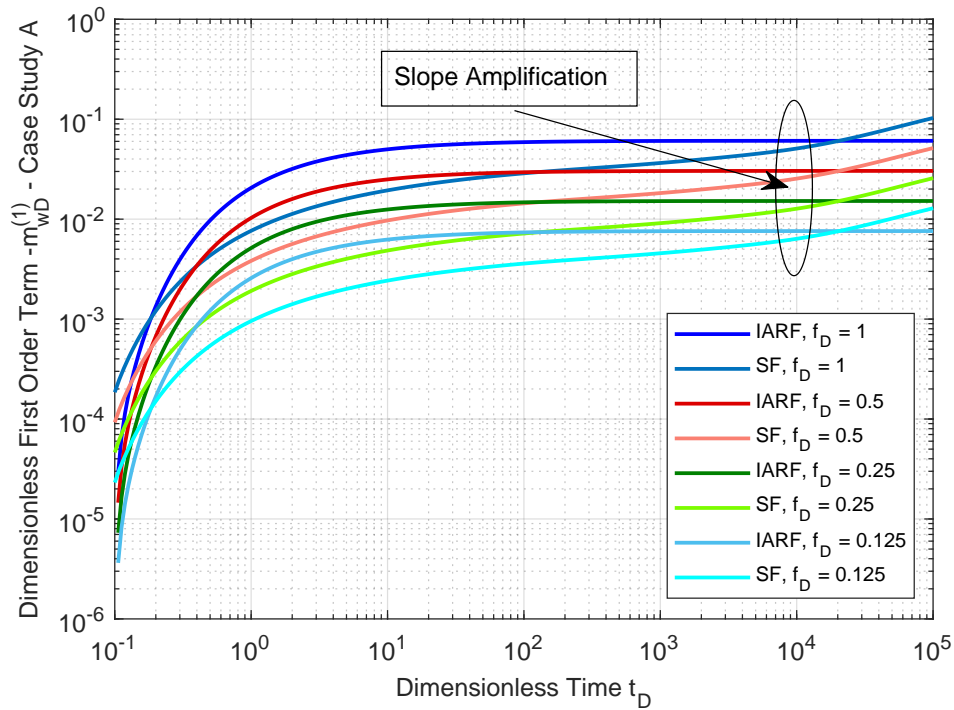


Figure 5.35: Log-log plot of the IARF and sealing fault curves of the dimensionless first-order term for several oil sources for the case study A.

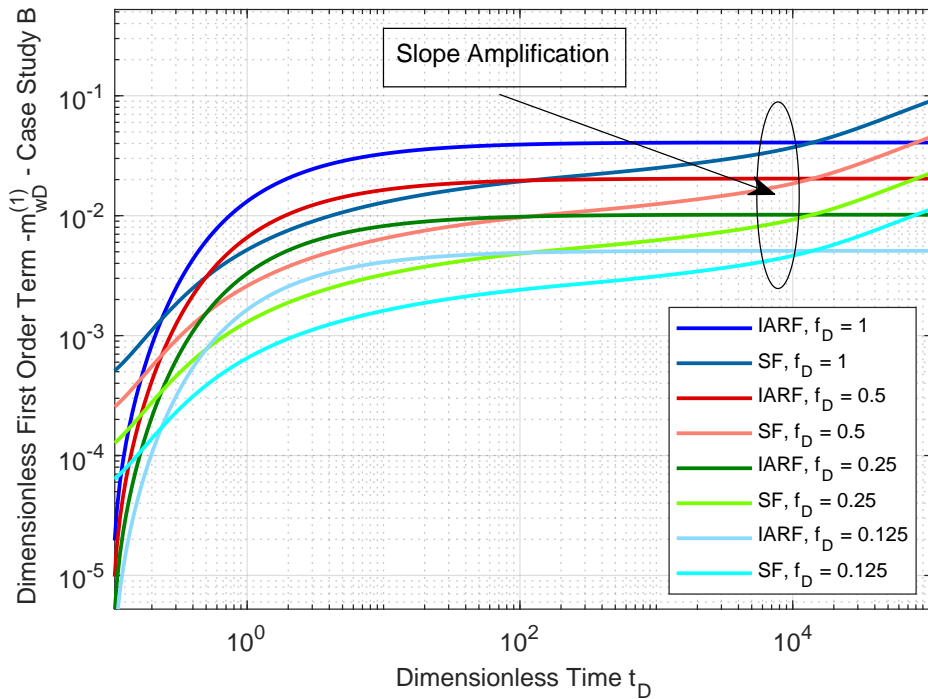


Figure 5.36: Log-log plot of the IARF and sealing fault curves of the dimensionless first-order term for several oil sources for the case study B.

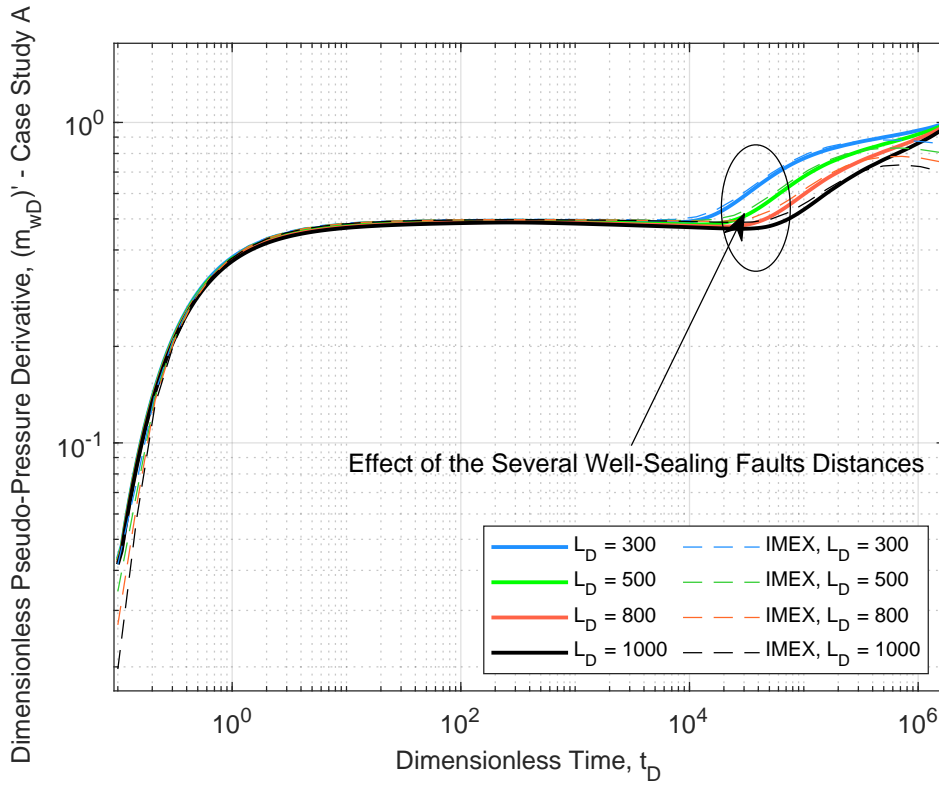


Figure 5.37: Diagnostic plot of the dimensionless pseudo-pressure derivative for several dimensionless well-sealing fault distances for the case study A.

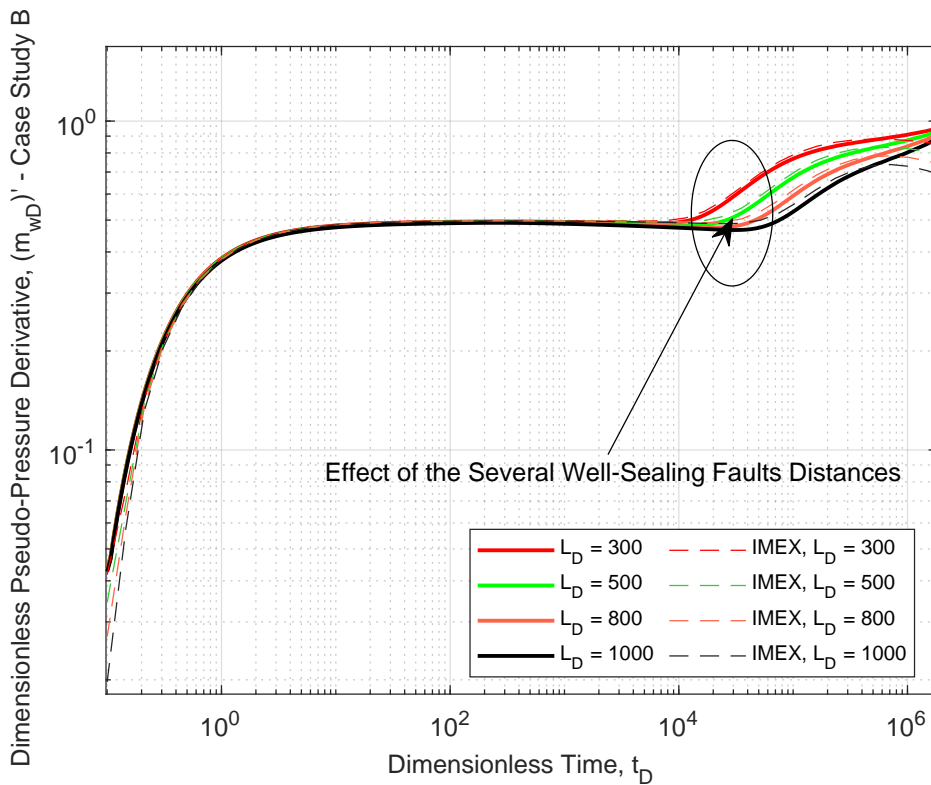


Figure 5.38: Diagnostic plot of the dimensionless pseudo-pressure derivative for several dimensionless well-sealing fault distances for the case study B.

Figure 5.39 and Figure 5.40 present the diagnostic plots of the effects from the several well-sealing fault dimensionless distances in the dimensionless pseudo-pressure for both case studies. The results presented high convergence with respect to IMEX[®].

The deviations and the displacements are notable in this Semi-log plot. Thereby, the model developed in this work provides a simple graphical interpretation that allows to predict the well-sealing fault distances through some pressure and permeability responses along the time. These plots also show the linear solution behavior for several dimensionless sealing fault distances. Therewith, even though for constant permeability scenarios, this model is capable to represent the response to well-sealing fault distances identification, as well as, boundary effects and reservoir characterization. The analytical solution for the NHDE developed in this paper is composed of a linear term that models the pressure drop during oil production and a first-order nonlinear term coupled to a hydraulic diffusivity deviation factor $\xi(p)$ that represents the permeability change caused by pressure reduction and its deviation with respect the permeability on the initial condition. The role of this parameter in case studies A and B is presented in Figures 5.41 and 5.42.

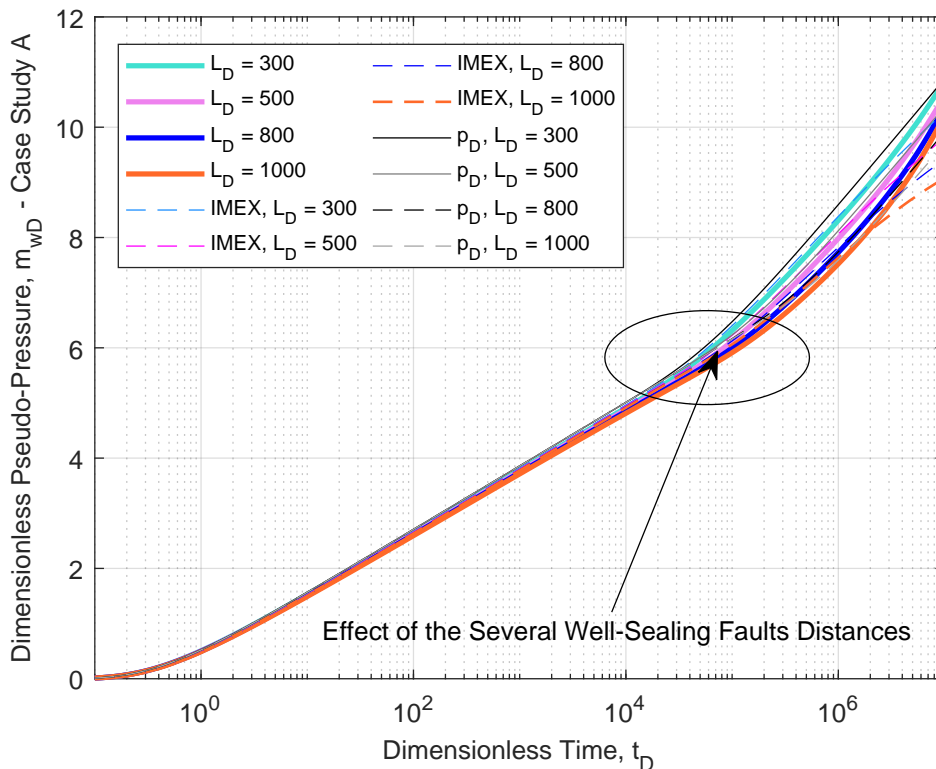


Figure 5.39: Diagnostic plot of the dimensionless pseudo-pressure for several dimensionless well-sealing fault distances for the case study A.

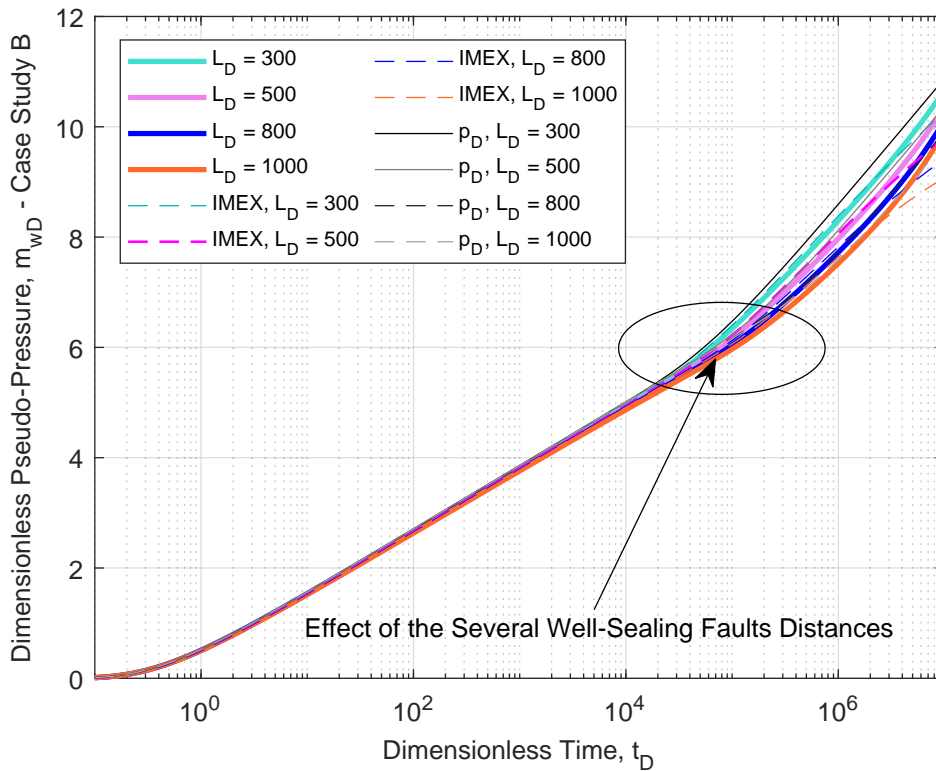


Figure 5.40: Diagnostic plot of the dimensionless pseudo-pressure for several dimensionless well-sealing fault distances for the case study B.

These plots were built using the absolute values for permeability change because log-log plots do not deal with negative ones. The results presented show that for low values of this factor ($\xi(p) = 0.1$ and 0.25), the total permeability change, m_{wD} is also low. Whereas, for $\xi(p) = 0.5$ and 0.75 , the difference in permeability increases (high deviation of the curves). Finally, the sealing fault identification (slope amplification) is also shown in these plots. The sealing fault detection and the role of the deviation factor in the dimensionless derivative for both case studies addressed in this paper are shown in the log-log plots of the Figures. 5.43 and 5.44. These plots reveal that the increase in the values of the deviation factor results in an abrupt drop of the derivative (green, blue and orange curves). It means that the permeability loss is more severe in these curves. Hence, adequate control of the oil flow rate that influences pressure drop is essential to prevent the rise of this deviation factor and accentuated permeability change.

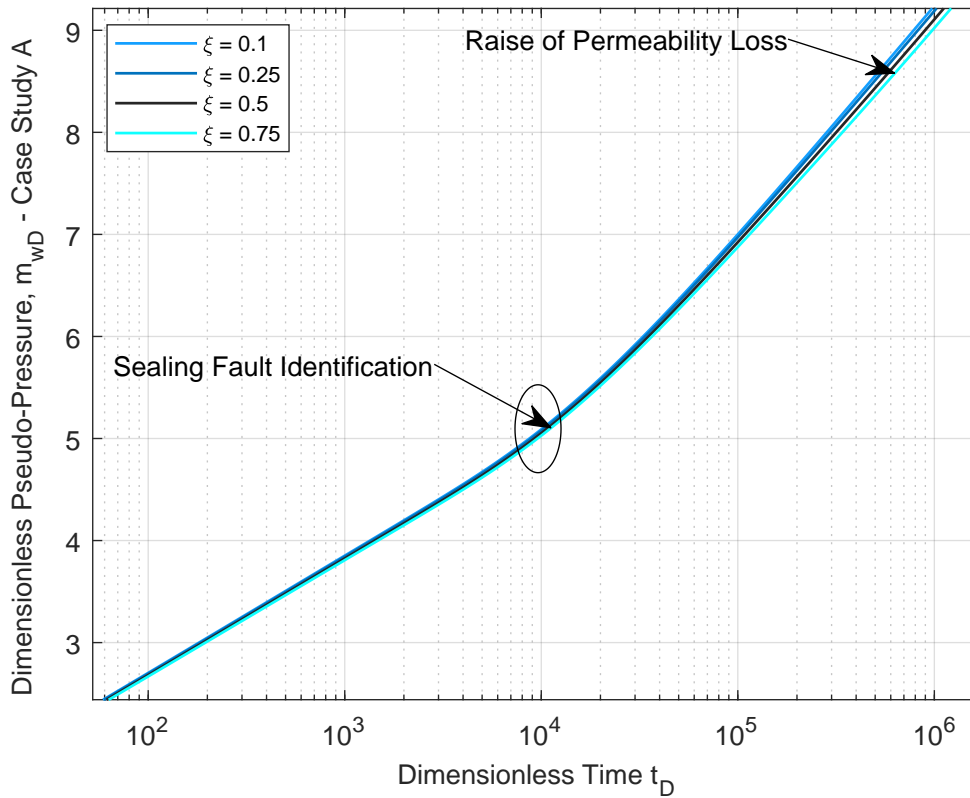


Figure 5.41: Semi-log plot of the effect of the hydraulic diffusivity deviation factor in the dimensionless pseudo-pressure for the case study A.

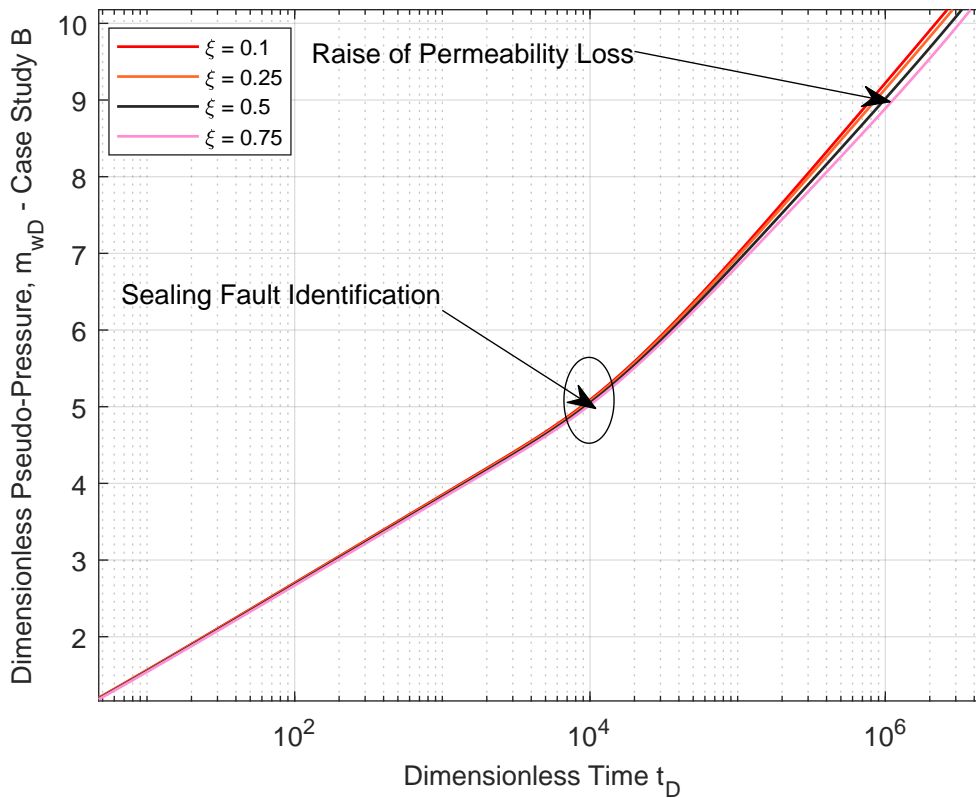


Figure 5.42: Semi-log plot of the effect of the hydraulic diffusivity deviation factor in the dimensionless pseudo-pressure for the case study B.

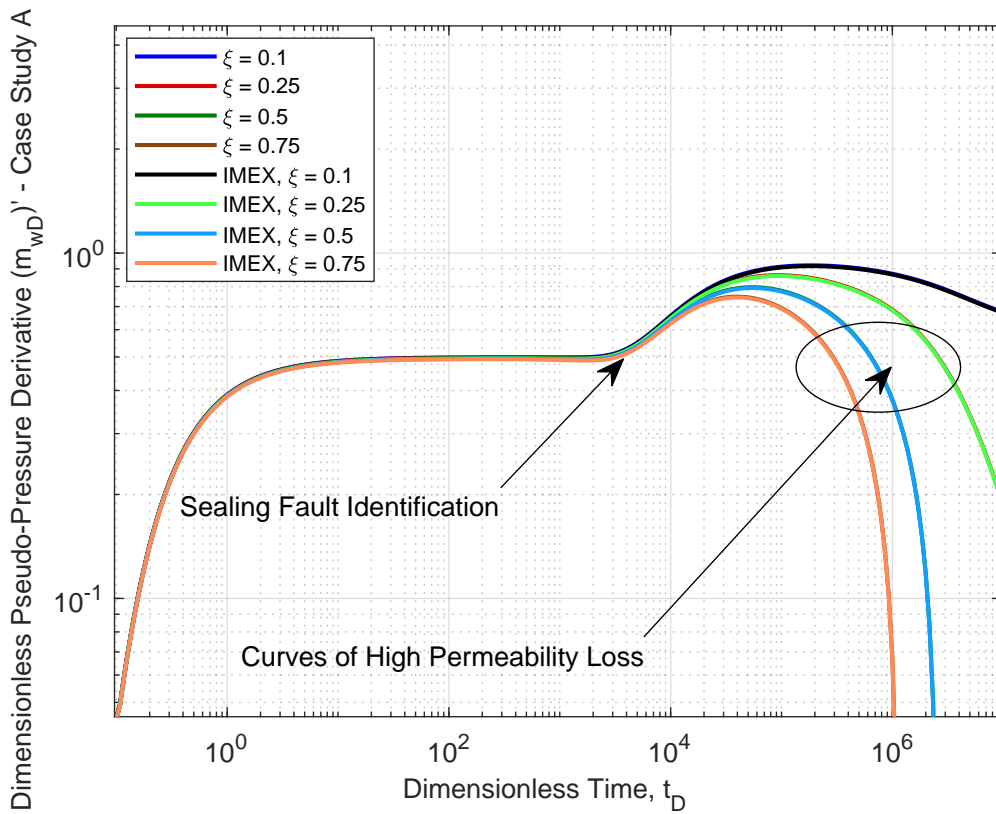


Figure 5.43: Log-log plot of the role of the deviation factor in the dimensionless derivative for case study A.

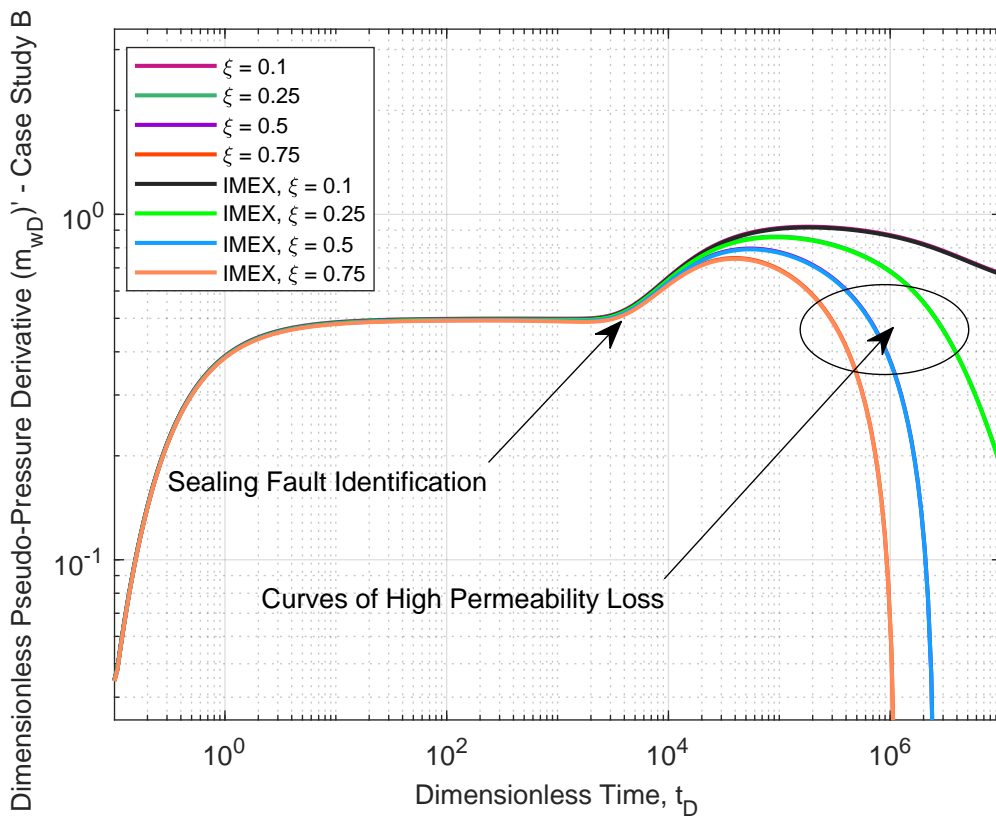


Figure 5.44: Log-log plot of the role of the deviation factor in the dimensionless derivative for case study B.

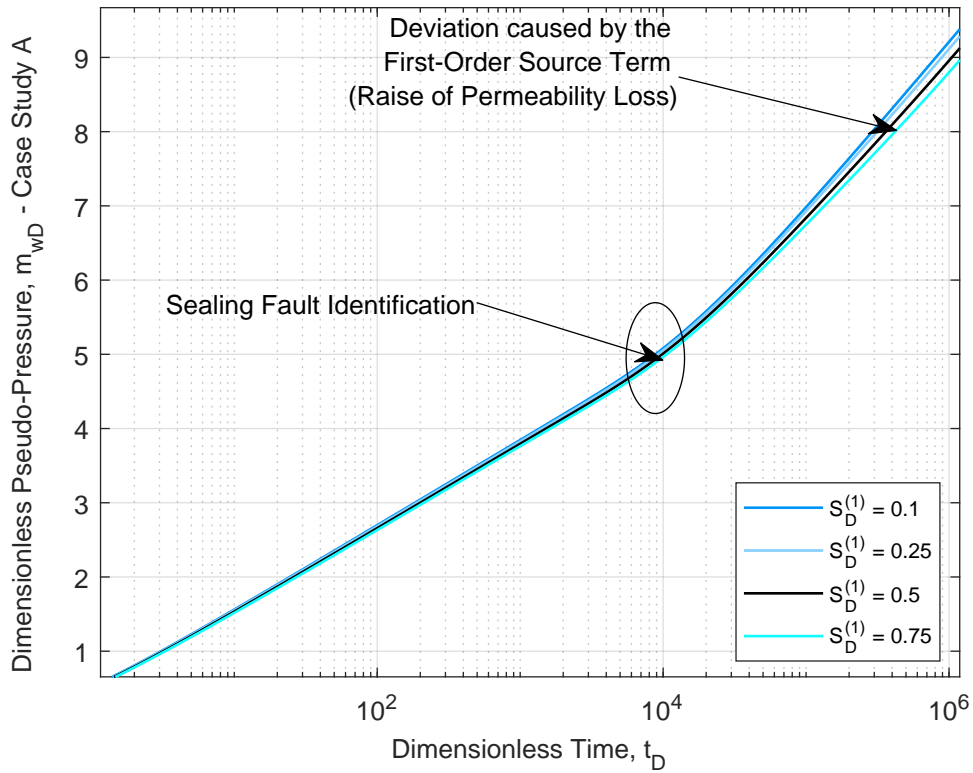


Figure 5.45: Semi-log plot of the effect several first-order source terms on pseudo-pressure solution for case study A.

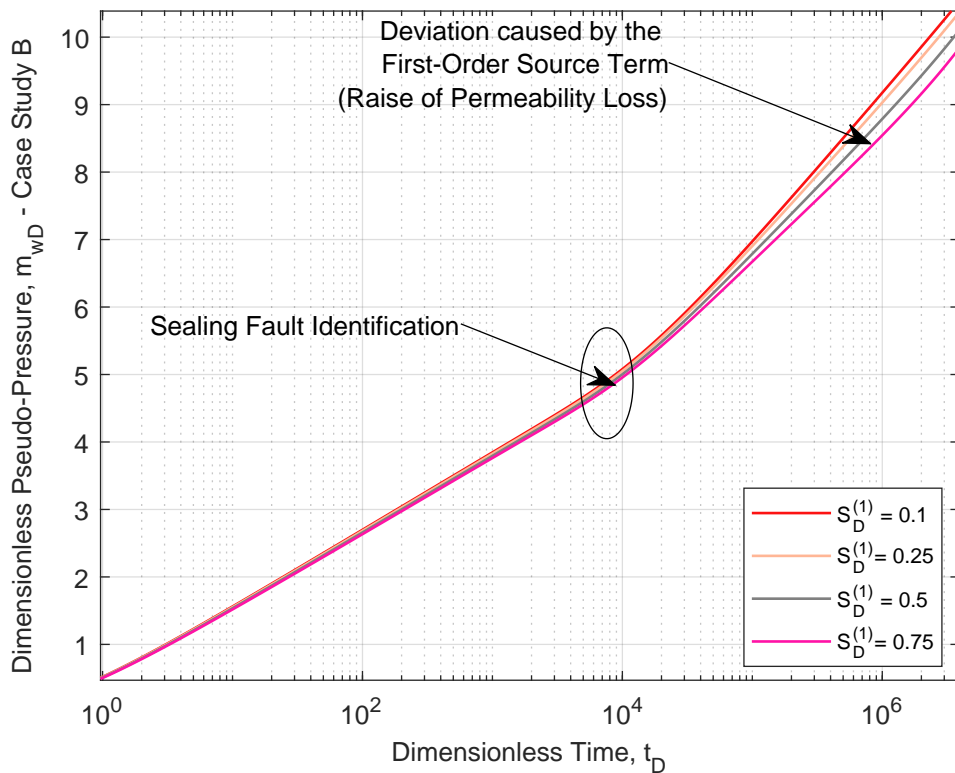


Figure 5.46: Semi-log plot of the effect several first-order source terms on pseudo-pressure solution for case study B.

The influence of the first-order source term in the dimensionless pseudo-pressure solution is presented in Figures 5.45 and 5.46 (case studies A and B, respectively). We can realize that the increase in the values of the source term (oil flow rate) results in lowering the dimensionless pseudo-pressure solution. It means that the oil flow rate increase favors permeability reduction. Then, the adequate management of this parameter is essential to prevent uncontrolled permeability loss. A sealing fault detection is also noticed in these plots for dimensionless time $t_D \approx 10^4$. According to the asymptotic series expansion technique addressed by (Fernandes, 2022), the first-order source term is a function of the deviation factor and the pseudo-pressure derivative. Hence, Figures 5.45 and 5.46 allow us to identify the response of these parameters in the general solution proposed in this thesis.

The effect of the source term also can be seen in the case studies A and B of the nonlinear corrective first-order term (Figures 5.47 and 5.48). The blue and orange curves represent the first-order term for high values of the oil source ($S_D^{(1)} = 0.125$ and $S_D^{(1)} = 0.1$, respectively). These curves show that as higher the oil source, the higher the nonlinear term. Consequently, it results in an increase in permeability loss over production. Low values of the oil source are illustrated in the green and pink curves ($S_D^{(1)} = 0.025$ and $S_D^{(1)} = 0.01$, respectively). We notice that the corrective nonlinear term is low for low values of the source, so permeability loss is lower for these curves. The diagnostic plots presented in Figures 5.49 and 5.50 show the response of the first-order source term on pseudo-pressure derivative. We realize that the results are accurate compared with IMEX[®]. As shown in the dimensionless general solution and first-order corrective term, the increase of the source results in decrease of the derivative, *i.e.*, it favors permeability loss. Another fact notable in these plots is the sealing fault identification. Hence, the use of the derivative plot allows to predict the permeability loss and identify flow regimes, which can be used to formation evaluation and reservoir management purposes. The effect of the source term in the derivative response are clearer in Figures 5.51 and 5.52, because these plots were amplified. For case study A, we notice that the displacement among the derivative type curves is low compared to case study B. This fact shows us that the initial permeability drives the response of the future permeability values. For this simulation, the time steps were of the order of 0.001 and the space steps of 0.01. The code ran quickly, and the implementation was simple because the GF and line-source solution that composes the corrective term are easily implemented in Matlab[®]. These issues make the proposed solution competitive against numerical oil flow simulators and save computational costs and applicable for field practical purposes.

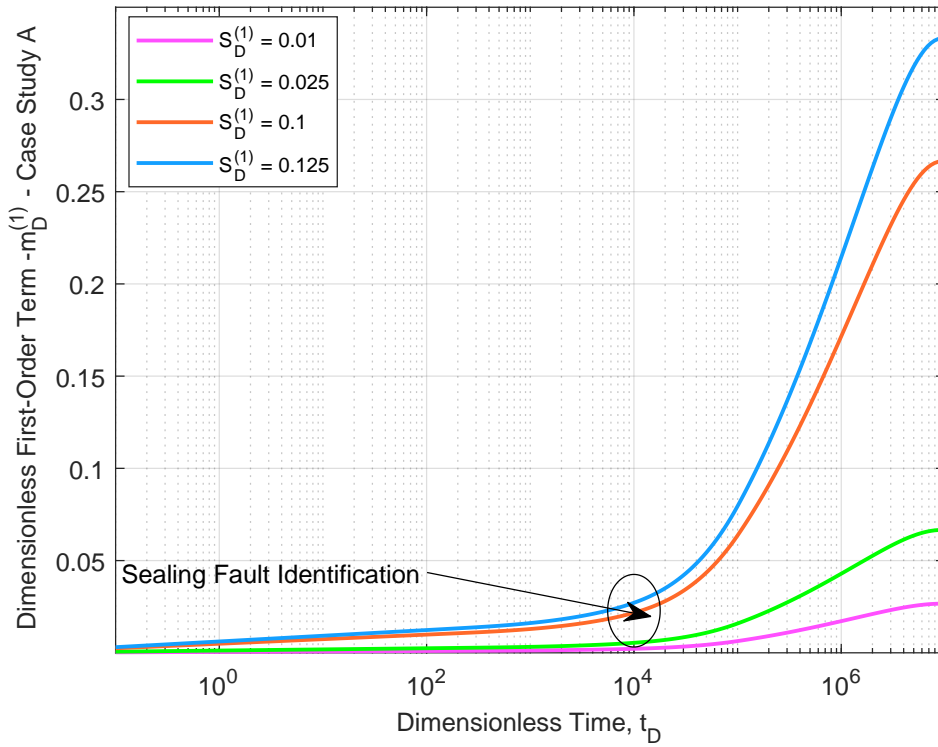


Figure 5.47: Semi-log plot of the effect of the first-order oil source on the corrective term for case study A.

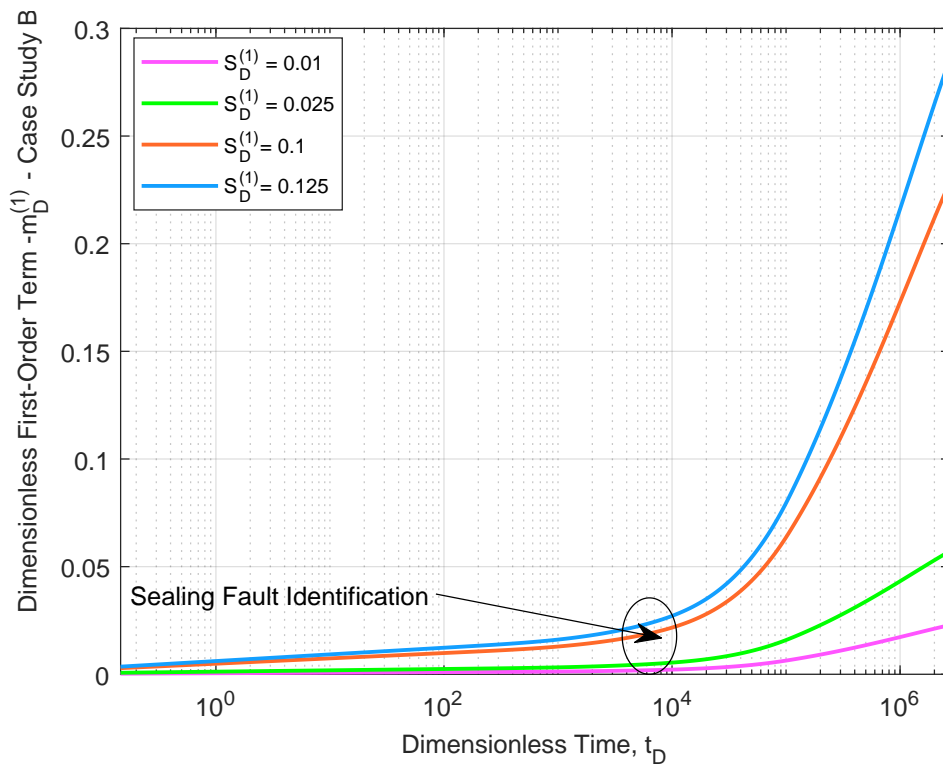


Figure 5.48: Semi-log plot of the effect of the first-order oil source on the corrective term for case study B.

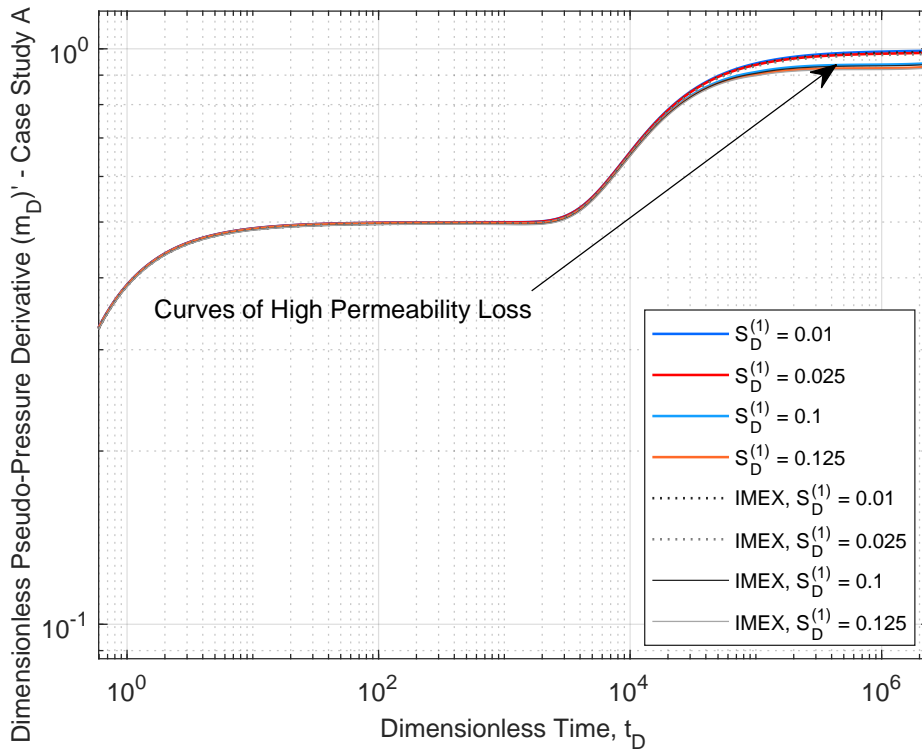


Figure 5.49: Log-log plot of the influence of the first-order source term in the derivative for case study A.

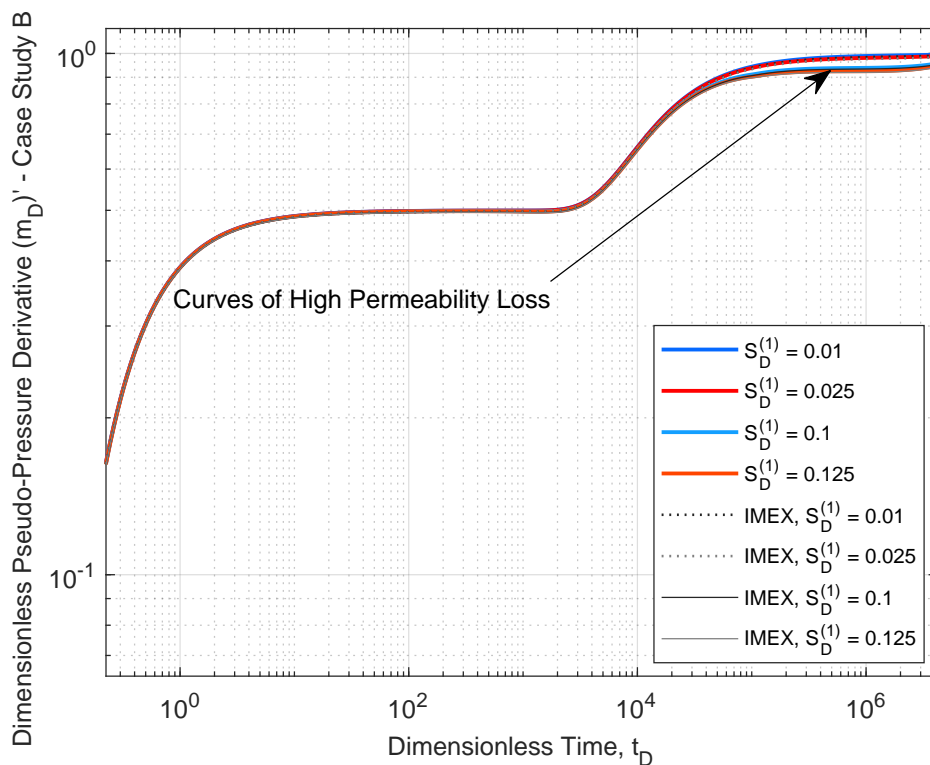


Figure 5.50: Log-log plot of the influence of the first-order source in the derivative for case study B.

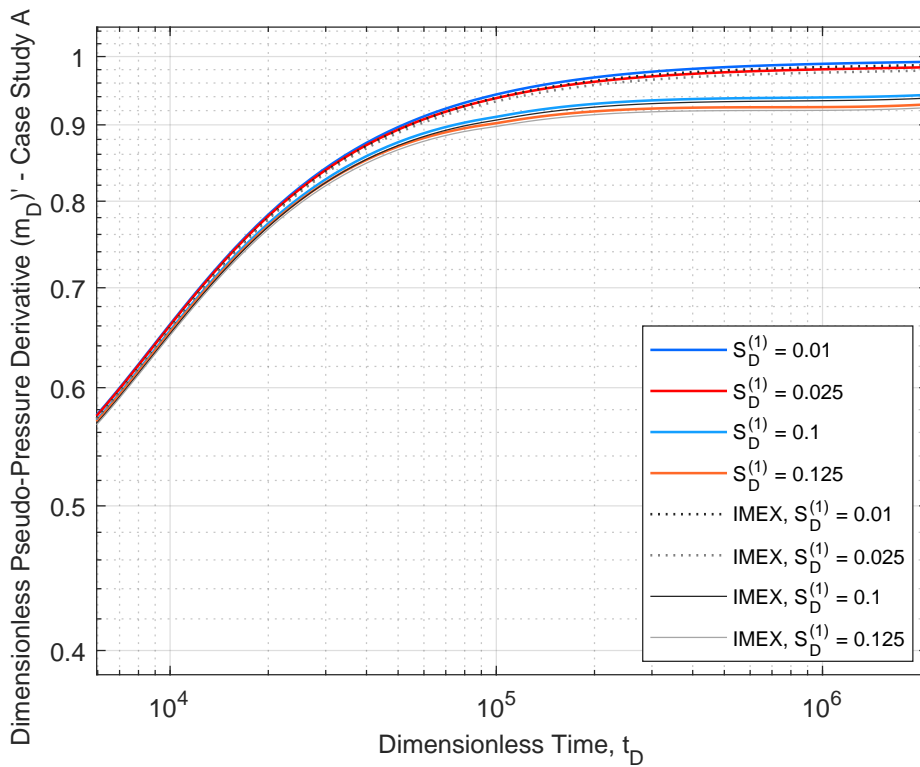


Figure 5.51: Log-log plot of the amplification of the influence of the first-order source in the derivative for case study A.

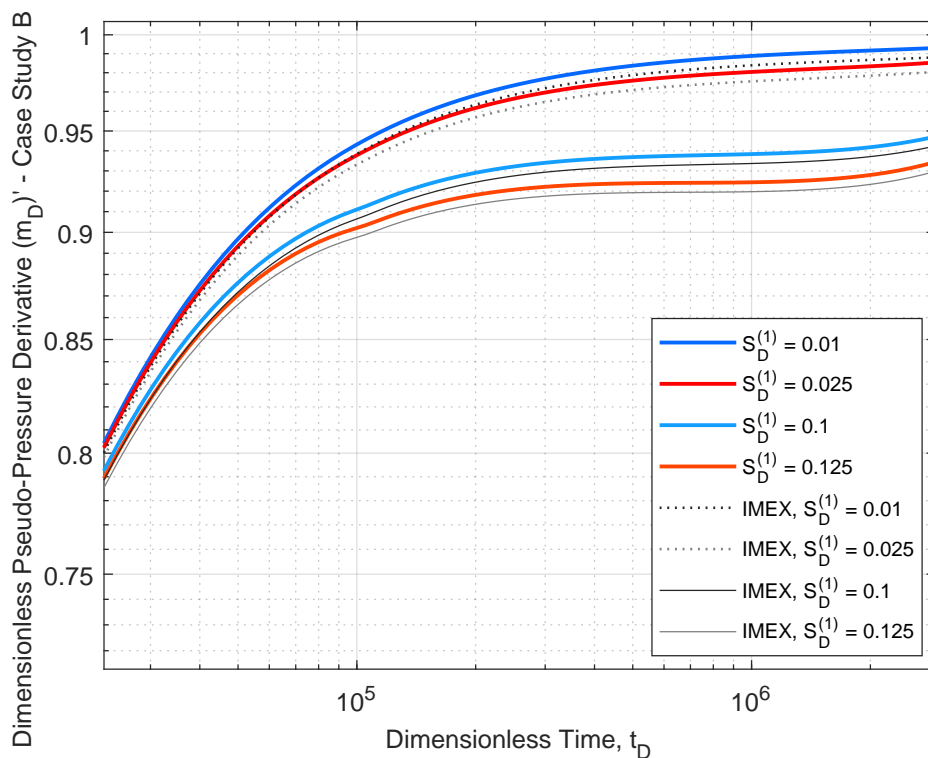


Figure 5.52: Log-log plot of the amplification of the influence of the first-order source in the derivative for case study B.

Finally, the permeability change over the well-reservoir life-cycle can be visualized in the Semi-log plot from the Figure 5.53. The deviation from the linear solution (constant permeability) is shown clearly. We also notice that, the phenomenon of the permeability loss starts smoothly and it becomes higher over the production's life of the oilfield.

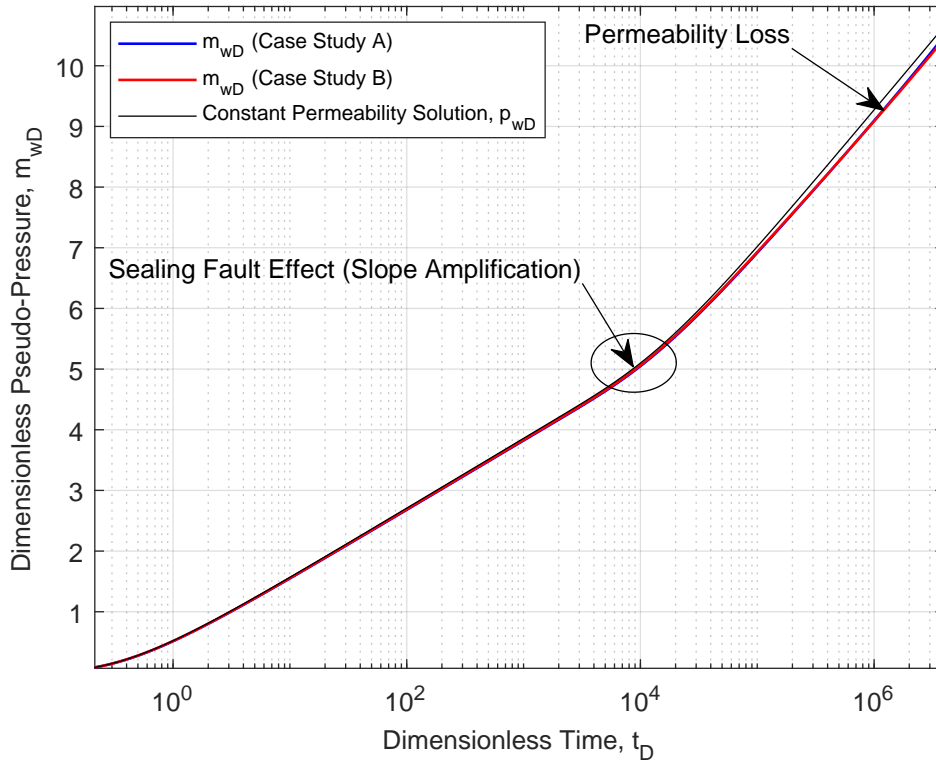


Figure 5.53: Diagnostic plot of the permeability change for the case studies A and B.

5.3

Oil Flow in a Well with an Infinite Extension Hydraulic Fracture

Large oil volumes can be found in low permeability reservoirs in the world. The reservoir stimulation techniques *e.g.* acidizing, acid and hydraulic fracturing are used to make the production's curve economically attractive. These techniques are also used to improve the oil production's curve when the reservoir permeability drops and the minimum viable oil flow rate is reached. Hydraulically fractured petroleum reservoirs may increase significantly the oil production's curve and make many projects more attractive economically. Since its threshold, hydraulic fracturing technology has been used by petroleum industry to solve a variety of problems and providing the understanding for many of difficult issues, (Economides & Noltes, 2000). Hydraulic fracturing is a well stimulation technique widely used in the world to enhance, accelerate or sometimes restore production by reducing the oil flow-path resistance from the porous media to the well, (Miskimins, 2019).

In this section, the oil flow through an infinite hydraulic fracture in x -direction (Figure 5.54) is modeled using the proposed coupled-integro-differential-GF solution. The fact of the fracture is infinite in the x -direction and it goes through the whole reservoir net pay implies that the oil flow occurs only in the y -direction. Thus the partial differential equation is derived only with respect to the Cartesian y -direction and to the time t .

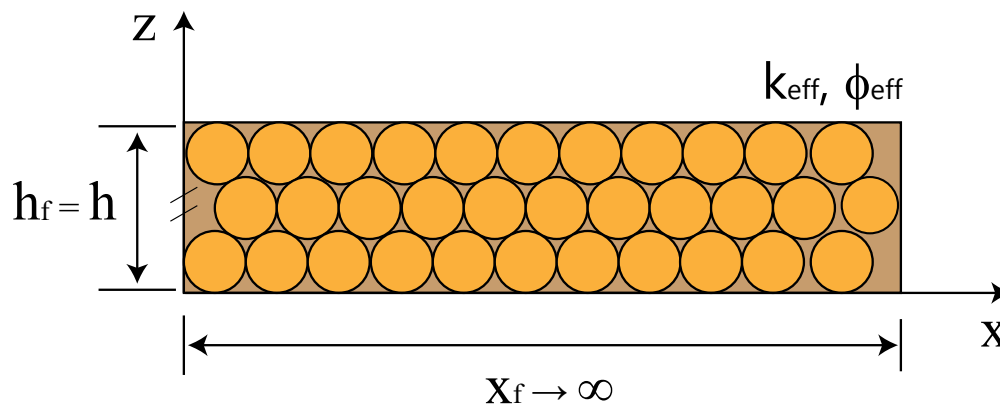


Figure 5.54: Detail of an infinite extension hydraulic fracture.

5.3.1

Model Assumptions

For modeling of oil flow problem in porous media by means of the asymptotic series expansion of the solution of the pressure diffusivity equation in terms of pseudo-pressure, the following premises are assumed:

1. Constant oil flow rate in the well
2. Pressure-sensitive effective permeability
3. Non-Darcian effects not considered
4. Hydraulic fracture roughness neglected
5. Well fully penetrates reservoir rock
6. Deformable, homogeneous, linear elastic and isotropic reservoir
7. The well is located at the origin of the Cartesian system of coordinates
8. Isothermal, single-phase and compressible flow in the porous medium
9. The fluid present inside the pores of the reservoir rock does not react chemically with the rock matrix
10. One dimensional and unsteady flow
11. Small pressure gradient
12. The hydraulic fracture is propped and undeformable
13. Skin and storage effects not considered
14. Permeability hysteresis of porous media is negligible
15. No fluid flow across the top and bottom of the formation
16. Infinite extent reservoir in the x-direction
17. Reservoir with uniform net pay

5.3.2

Model Derivation

Let the oil flow through an infinite hydraulic fracture model in a permeability pore pressure dependent porous media in the dimensionless Cartesian coordinates $\mathbf{r}_D = (0, y_D, 0) \in \mathbb{R}$ and $t_D \in \mathbb{R}$.

The pressure NHDE in Cartesian coordinates is:

$$\frac{\partial^2 p}{\partial y^2} - \frac{1}{\eta_{eff}(p)} \frac{\partial p}{\partial t} = -g(y, t) \quad (5-241)$$

Where $g(y, t)$ is a source function and $\eta_{eff}(p)$ is the effective hydraulic diffusivity function, expressed by:

$$\eta_{eff}(p) = \frac{k_{eff}(p)}{\phi_p \mu C_t} \quad (5-242)$$

Where ϕ_p is the porosity of the proppant package, *i.e.*, the porosity for the proppant arrangement inside the fracture [dimensionless]; $k_{eff}(p)$ is the effective permeability function, that takes into account both: the matrix $k_m(p)$ and fracture permeability k_f [md]. This function is expressed as follows (Cho, Apaydin & Ozkan, 2013):

$$k_{eff}(p) = k_m(p) + \phi_p k_f \quad (5-243)$$

5.3.3

Theoretical Model for the Propped Fracture

According to Teng, Li & Yu (2020), for the condition that, the hydraulic fracture remains undamaged as the reservoir permeability drops, results in $k_f = k_p$, where k_p is the proppant package permeability. Thereby, using the model developed by van Baaren (1979) for sandstones, the fracture permeability can be expressed by:

$$k_f = 10D^2 C^{-3.64} \phi_p^{3.64+m} \quad (5-244)$$

Where D is the dominant grain size, [μm]; C is the sorting index, [dimensionless] and m is the cementation exponent, [dimensionless].

Replacing the Eq. 5-244 in the Eq. 5-315:

$$k_{eff}(p) = k_m(p) + 10D^2 C^{-3.64} \phi_p^{4.64+m} \quad (5-245)$$

Let the pseudo-pressure function:

$$m(p) = \int_{p_b}^p k_{eff}(p') dp' \quad (5-246)$$

The Cartesian y component of pseudo-pressure gradient is:

$$\frac{\partial m(p)}{\partial y} = \frac{dm(p)}{dp} \frac{\partial p}{\partial y} \quad (5-247)$$

The pseudo-pressure Laplacian is:

$$\frac{\partial^2 m(p)}{\partial y^2} = \frac{\partial}{\partial y} \left[\frac{dm(p)}{dp} \frac{\partial p}{\partial y} \right] \quad (5-248)$$

By the product's rule:

$$\frac{\partial^2 m(p)}{\partial y^2} = \frac{\partial}{\partial y} \left[\frac{dm(p)}{dp} \right] \frac{\partial p}{\partial y} + \frac{dm(p)}{dp} \frac{\partial^2 p}{\partial y^2} \quad (5-249)$$

The pseudo-pressure derivative with respect to the pore pressure is:

$$\frac{dm(p)}{dp} = \frac{d}{dp} \left[\int_{p_b}^p k_{eff}(p') dp' \right] \quad (5-250)$$

Replacing the Eq. 5-250 into the Eq. 5-249:

$$\frac{\partial^2 m(p)}{\partial y^2} = \frac{\partial}{\partial y} \left\{ \frac{d}{dp} \left[\int_{p_b}^p k_{eff}(p') dp' \right] \right\} \frac{\partial p}{\partial y} + \frac{dm(p)}{dp} \frac{\partial^2 p}{\partial y^2} \quad (5-251)$$

Applying the Leibniz's rule:

$$\frac{dm(p)}{dp} = \frac{d(p)}{dp} k_{eff}(p) - \frac{d(p_b)}{dp} k_{eff}(p) \quad (5-252)$$

As:

$$\frac{d(p)}{dp} = 1 \quad (5-253)$$

and

$$\frac{d(p_b)}{dp} = 0 \quad (5-254)$$

Thus, the Eq. 5-252 becomes:

$$\frac{dm(p)}{dp} = k_{eff}(p) \quad (5-255)$$

Replacing the Eq. 5-255 into the Eq. 5-251:

$$\frac{\partial^2 m(p)}{\partial y^2} = \frac{\partial k_{eff}(p)}{\partial y} \frac{\partial p}{\partial y} + k_{eff}(p) \frac{\partial^2 p}{\partial y^2} \quad (5-256)$$

By the chain's rule:

$$\frac{\partial k_{eff}(p)}{\partial y} = \frac{dk_{eff}(p)}{dp} \frac{\partial p}{\partial y} \quad (5-257)$$

Replacing the Eq. 5-257 into the Eq. 5-256:

$$\frac{\partial^2 m(p)}{\partial y^2} = \left[\frac{dk_{eff}(p)}{dp} \frac{\partial p}{\partial y} \right] \frac{\partial p}{\partial y} + k_{eff}(p) \frac{\partial^2 p}{\partial y^2} \quad (5-258)$$

The Eq. 5-258 becomes:

$$\frac{\partial^2 m(p)}{\partial y^2} = \frac{dk_{eff}(p)}{dp} \left(\frac{\partial p}{\partial y} \right)^2 + k_{eff}(p) \frac{\partial^2 p}{\partial y^2} \quad (5-259)$$

For small pressure gradient:

$$\left(\frac{\partial p}{\partial y} \right)^2 \ll 1 \quad (5-260)$$

Thus, this term can be neglected. The Eq. 5-259 becomes:

$$\frac{\partial^2 m(p)}{\partial y^2} = k_{eff}(p) \frac{\partial^2 p}{\partial y^2} \quad (5-261)$$

Rewriting in terms of the pressure Laplacian:

$$\frac{\partial^2 p}{\partial y^2} = \frac{1}{k_{eff}(p)} \frac{\partial^2 m(p)}{\partial y^2} \quad (5-262)$$

The pseudo-pressure rate is:

$$\frac{\partial m(p)}{\partial t} = \frac{dm(p)}{dp} \frac{\partial p}{\partial t} \quad (5-263)$$

Replacing the Eq. 5-255 in the Eq. 5-263:

$$\frac{\partial m(p)}{\partial t} = k_{eff}(p) \frac{\partial p}{\partial t} \quad (5-264)$$

Thus, the pressure rate is:

$$\frac{\partial p}{\partial t} = \frac{1}{k_{eff}(p)} \frac{\partial m(p)}{\partial t} \quad (5-265)$$

The initial condition is:

$$p(y, t = 0) = p_i \quad (5-266)$$

And the external boundary condition is:

$$\lim_{y \rightarrow \infty} p(y, t) = p_i \quad (5-267)$$

Replacing the Eq. 5-262 and Eq. 5-265 in the Eq. 7-1:

$$\frac{1}{k_{eff}(p)} \frac{\partial^2 m(p)}{\partial y^2} - \frac{1}{\eta_{eff}(p)} \frac{1}{k_{eff}(p)} \frac{\partial m(p)}{\partial t} = g(y, t) \quad (5-268)$$

The effective diffusivity function $\eta_{eff}(p)$ is:

$$\eta_{eff}(p) = \frac{k_{eff}(p)}{\phi_p \mu c_t} \quad (5-269)$$

Thus, the Eq. 5-268 can be expressed as a function of the effective permeability as follows:

$$\frac{1}{k_{eff}(p)} \frac{\partial^2 m(p)}{\partial y^2} - \frac{\phi_p \mu c_t}{k_{eff}(p)} \frac{1}{k_{eff}(p)} \frac{\partial m(p)}{\partial t} = g(y, t) \quad (5-270)$$

Rewriting the Eq. 5-270:

$$\frac{1}{k_{eff}(p)} \frac{\partial^2 m(p)}{\partial y^2} - \frac{\phi_p \mu c_t}{[k_{eff}(p)]^2} \frac{\partial m(p)}{\partial t} = g(y, t) \quad (5-271)$$

Multiplying both sides of the Eq. 5-271 by the effective permeability function $k_{eff}(p)$, the NHDE in terms of the pseudo-pressure yields to:

$$\frac{\partial^2 m(p)}{\partial y^2} - \frac{\phi_p \mu c_t}{k_{eff}(p)} \frac{\partial m(p)}{\partial t} = k_{eff}(p) g(y, t) \quad (5-272)$$

Let the pseudo-pressure variation:

$$\Delta m(p) = \int_{p_b}^{p_i} k_{eff}(p') dp' - \int_{p_b}^p k_{eff}(p') dp' \quad (5-273)$$

Thus:

$$\Delta m(p) = \int_p^{p_i} k_{eff}(p') dp' \quad (5-274)$$

Rewriting:

$$\Delta m(p) = k_{eff}(p_i) - k_{eff}(p) = m(p_i) - m(p) \quad (5-275)$$

The pseudo-pressure variation gradient is:

$$\frac{\partial \Delta m(p)}{\partial y} = -\frac{\partial m(p)}{\partial y} \quad (5-276)$$

The pseudo-pressure variation Laplacian is:

$$\frac{\partial^2 \Delta m(p)}{\partial y^2} = -\frac{\partial^2 m(p)}{\partial y^2} \quad (5-277)$$

The pseudo-pressure variation rate is:

$$\frac{\partial \Delta m(p)}{\partial t} = -\frac{\partial m(p)}{\partial t} \quad (5-278)$$

Replacing the Eq. 5-277 and Eq. 5-278 in the Eq. 5-272:

$$-\frac{\partial^2 \Delta m(p)}{\partial y^2} + \frac{\phi_p \mu c_t}{k_{eff}(p)} \frac{\partial \Delta m(p)}{\partial t} = k_{eff}(p) g(y, t) \quad (5-279)$$

Multiplying both sides of the Eq. 5-279 by (-1):

$$\frac{\partial^2 \Delta m(p)}{\partial y^2} - \frac{\phi_p \mu c_t}{k_{eff}(p)} \frac{\partial \Delta m(p)}{\partial t} = -k_{eff}(p) g(y, t) \quad (5-280)$$

Finally, the NHDE in terms of pseudo-pressure variation is:

$$\frac{\partial^2 \Delta m(p)}{\partial y^2} - \frac{1}{k_{eff}(p)} \frac{\partial \Delta m(p)}{\partial t} = -k_{eff}(p) g(y, t) \quad (5-281)$$

5.3.4

Dimensionless Model

For this model, the dimensionless variables are:

$$y_D = \frac{y}{l_c}, \quad t_D = \frac{k(p_i)t}{\phi_p \mu c_t l_c^2}, \quad k_{effD} = \frac{k_{eff}(p)}{k_{eff}(p_i)} \quad (5-282)$$

Where t is the time, [sec]; ϕ_p is the porosity of the proppant package, [dimensionless]; μ is the dynamic viscosity, [Pa×sec]; c_t is the total compressibility, [1/MPa]; y is the Cartesian distance to the hydraulic fracture, [m]; l_c is the characteristic length for an infinite hydraulic fracture is: $l_c = x_f$ and x_f is the half fracture length, [m] and $k_{eff}(p_i) = k_m(p_i) + \phi_p k_f$, [md]. A conversion factor $\beta = 9.869 \times 10^{-16}$ is used to convert the permeability from [m²] to [md].

The dimensionless pseudo-pressure is:

$$m_D(y, t) = \frac{x_f}{q\mu} \Delta m(p) \quad (5-283)$$

The partial differential operator for y in Cartesian coordinates is:

$$\frac{\partial}{\partial y} = \frac{\partial}{\partial(l_c y_D)} = \frac{1}{l_c} \frac{\partial}{\partial y_D} \quad (5-284)$$

The second-order partial differential operator for y in Cartesian coordinates is:

$$\frac{\partial^2}{\partial y^2} = \frac{\partial^2}{\partial(l_c^2 y_D^2)} = \frac{1}{l_c^2} \frac{\partial^2}{\partial y_D^2} \quad (5-285)$$

rate operator is:

$$\frac{\partial}{\partial t} = \frac{k(p_i)}{\phi_p \mu c_t l_c^2} \frac{\partial}{\partial t_D} \quad (5-286)$$

Replacing the Eq. 5-284, 5-286 and 5-287 into the Eq. 5-281:

$$\frac{q\mu}{x_f l_c^2} \frac{\partial^2 m_D}{\partial y_D^2} - \frac{q\mu}{x_f l_c^2} \frac{\phi_p \mu c_t k_{eff}(p_i)}{\phi_p \mu c_t k_{eff}(p)} \frac{\partial m_D}{\partial t_D} = -k_{eff}(p) g(y, t) \quad (5-287)$$

As the characteristic length $l_c = x_f$, the Eq. 5-287 becomes:

$$\frac{\partial^2 m_D}{\partial y_D^2} - \frac{k_{eff}(p_i)}{k_{eff}(p)} \frac{\partial m_D}{\partial t_D} = -\frac{x_f^3 k_{eff}(p)}{q\mu} g(y, t) \quad (5-288)$$

The right-hand side of the 5-288 is the dimensionless oil source term $g_D(y_D, t_D)$:

$$\frac{k_{eff}(p)x_f^3}{q\mu}g(y,t) = g_D(y_D,t_D) \quad (5-289)$$

Finally, the dimensionless NHDE in terms of pseudo-pressure for the oil flow in an infinite hydraulic fracture is:

$$\frac{\partial^2 m_D}{\partial y_D^2} - \frac{1}{k_{effD}(m_D)} \frac{\partial m_D}{\partial t_D} = -g_D(y_D,t_D) \quad (5-290)$$

The dimensionless initial condition is:

$$m_D(y_D,t_D = 0) = 0 \quad (5-291)$$

And the external boundary condition is:

$$\lim_{y_D \rightarrow \infty} m_D(x_D,y_D,t_D) = 0 \quad (5-292)$$

5.3.5

Integro-Differential Solution for an Infinite Hydraulic Fracture

The dimensionless general solution of the NHDE for the infinite hydraulic fracture in a vertical well follows the same procedures presented in the previous chapters. Thereby:

$$\begin{aligned} m_D(y_D,t_D) &= \\ &= - \int_0^{w_f} \int_0^{t_D} \left[g_D(y'_D,t'_D) + \xi_{eff}(p) \frac{\partial m_D(y'_D,t'_D)}{\partial t'_D} \right] G_D(y_D,y'_D,t_D,t'_D) dt'_D dy'_D \end{aligned} \quad (5-293)$$

Where w_f is the hydraulic fracture width, [m]. Let the dimensionless oil source term expressed by:

$$g_D(y_D,t_D) = \frac{\bar{q}_{sc}(y,t)}{q_{ref}} w_f \quad (5-294)$$

Where $\bar{q}_{sc}(y,t)$ is the oil flow rate per length unit at standard conditions, [m^2/sec]. The relationship between $\bar{q}_{sc}(y,t)$ and $\tilde{q}(y,t)$ is expressed as follows:

$$\bar{q}_{sc}(y,t) = \tilde{q}(x,y,z,t) w_f h_f \quad (5-295)$$

Where h_f is the hydraulic fracture height, [m]. For a unique hydraulic fracture placed in the dimensionless Cartesian position $y_D = 0$ and with constant oil flow rate q_{sc} distributed along the fracture with fracture equivalent area A_f

expressed by $A_f = 2w_f h_f$, the oil flow rate per volume unit is:

$$\tilde{q}_{sc}(x, y, z, t) = -\frac{q_{sc}}{2w_f h_f} \delta(y - 0) \quad (5-296)$$

Replacing the Eq. 5-295 in the Eq. 5-296, the oil flow rate can be expressed as follows:

$$\bar{q}_{sc}(y, t) = -\frac{q_{sc}}{2} \delta(y - 0) \quad (5-297)$$

Replacing the Eq. 5-297 in the Eq. 5-294, the dimensionless oil source becomes:

$$g_D(y_D, t_D) = -\frac{\bar{q}_{sc}}{2q_{ref}} w_f \delta(y - 0) \quad (5-298)$$

By the space scaling property of the Dirac delta function, $w_f \delta(y - 0) = \delta(y_D - 0)$. Moreover, the reference oil flow rates and, in the standard condition are the same ($q_{sc} = q_{ref}$), therewith, $q_{sc}/q_{ref} = 1$. The Eq. 5-298 yields to:

$$g_D(y_D, t_D) = -\frac{1}{2} \delta(y_D - 0) \quad (5-299)$$

Replacing the Eq. 5-299 in the Eq. 5-293, the integro-differential solution can be expressed by:

$$\begin{aligned} m_D(y_D, t_D) &= \\ &= \int_0^{w_f} \int_0^{t_D} \left[\frac{1}{2} \delta(y'_D - 0) + \xi_{eff}(p) \frac{\partial m_D(y'_D, t'_D)}{\partial t'_D} \right] G_D(y_D, y'_D, t_D, t'_D) dt'_D dy'_D \end{aligned} \quad (5-300)$$

Splitting the double integral in two terms, the Eq. 5-300 can be written as follows:

$$\begin{aligned} m_D(y_D, t_D) &= \int_0^{w_f} \int_0^{t_D} \frac{1}{2} \delta(y'_D - 0) G_D(y_D, y'_D, t_D, t'_D) dt'_D dy'_D - \\ &+ \int_0^{w_f} \int_0^{t_D} \xi_{eff}(p) \frac{\partial m_D(y'_D, t'_D)}{\partial t'_D} G_D(y_D, y'_D, t_D, t'_D) dt'_D dy'_D \end{aligned} \quad (5-301)$$

According to the sampling property from the Dirac delta function, the first double integral of the Eq. 5-301 becomes a simple integral of the dimensionless GF:

$$m_D(y_D, t_D) = \frac{1}{2} \int_0^{t_D} G_D(y_D, y'_D, t_D, t'_D) dt'_D - \int_0^{w_f} \int_0^{t_D} \xi_{eff}(p) \frac{\partial m_D(y'_D, t'_D)}{\partial t'_D} \times \\ \times G_D(y_D, y'_D, t_D, t'_D) dt'_D dy'_D \quad (5-302)$$

The GF related to an infinite source-plan is expressed by (Carslaw & Jaeger, 1959), (Beck et al., 1992), (Ozisiki, 1993), (Duffy, 2001) and (Cole, Beck & Haji-Sheikh, 2011):

$$G_D(y_D, y_{D0}, t_D, t_{D0}) = \frac{e^{-\frac{(y_D - y_{D0})^2}{4(t_D - t_{D0})}}}{2\sqrt{\pi(t_D - t_{D0})}} \quad (5-303)$$

Computing the GF in the oil source-plan position $y_{D0} = 0$, the dimensionless GF becomes:

$$G_D(y_D, 0, t_D, t_{D0}) = \frac{e^{-\frac{y_D^2}{4(t_D - t_{D0})}}}{2\sqrt{\pi(t_D - t_{D0})}} \quad (5-304)$$

Replacing the Eq. 5-304 in the Eq. 5-302, the integro-differential solution yields to:

$$m_D(y_D, t_D) = \frac{1}{2} \int_0^{t_D} \frac{e^{-\frac{y_D^2}{4(t_D - t'_D)}}}{2\sqrt{\pi(t_D - t'_D)}} dt'_D - \int_0^{w_f} \int_0^{t_D} \xi_{eff}(p) \frac{\partial m_D(y'_D, t'_D)}{\partial t'_D} \times \\ \times G_D(y_D, y'_D, t_D, t'_D) dt'_D dy'_D \quad (5-305)$$

Let us define the effective hydraulic diffusivity deviator factor $\xi_{eff}(p)$ as:

$$\xi_{eff}(p) = \frac{1}{k_{effD}(p)} - 1 \quad (5-306)$$

Replacing the Eq. 5-306 in the Eq. 5-305, the integro-differential solution is written as a function of the dimensionless effective pressure-dependent permeability $k_{effD}(p)$:

$$m_D(y_D, t_D) = \frac{1}{2} \int_0^{t_D} \frac{e^{-\frac{y_D^2}{4(t_D - t'_D)}}}{2\sqrt{\pi(t_D - t'_D)}} dt'_D - \int_0^{w_f} \int_0^{t_D} \left[\frac{1}{k_{effD}(p)} - 1 \right] \frac{\partial m_D(y'_D, t'_D)}{\partial t'_D} \times \\ \times G_D(y_D, y'_D, t_D, t'_D) dt'_D dy'_D \quad (5-307)$$

The first integral of the Eq. 5-307 can be solved by parts integration technique. Thereby:

$$m_D(y_D, t_D) = \frac{\sqrt{t_D} e^{y_D^2/4t_D}}{2\sqrt{\pi}} - \frac{|y_D|}{4} \operatorname{erfc}\left(\frac{|y_D|}{2\sqrt{t_D}}\right) - \int_0^{w_f} \int_0^{t_D} \left[\frac{1}{k_{effD}(p)} - 1 \right] \times \\ \times \frac{\partial m_D(y'_D, t'_D)}{\partial t'_D} G_D(y_D, y'_D, t_D, t'_D) dt'_D dy'_D \quad (5-308)$$

Where $\operatorname{erfc}(y_D, t_D)$ is the complementary error function (**Appendix A**), ([Abramowitz & Stegun, 1972](#)). As approached previously, the dimensionless pseudo-pressure derivative corresponds to the linear solution $p_D(y_D, t_D)$ derivative. Thus:

$$m_D(y_D, t_D) = \frac{\sqrt{t_D} e^{y_D^2/4t_D}}{2\sqrt{\pi}} - \frac{|y_D|}{4} \operatorname{erfc}\left(\frac{|y_D|}{2\sqrt{t_D}}\right) - \int_0^{w_f} \int_0^{t_D} \left[\frac{1}{k_{effD}(p)} - 1 \right] \times \\ \times \frac{\partial p_D(y'_D, t'_D)}{\partial t'_D} G_D(y_D, y'_D, t_D, t'_D) dt'_D dy'_D \quad (5-309)$$

Hence, the first two terms of the Eq. 5-309 represent the linear solution $p_D(y_D, t_D)$:

$$p_D(y_D, t_D) = \frac{\sqrt{t_D} e^{y_D^2/4t_D}}{2\sqrt{\pi}} - \frac{|y_D|}{4} \operatorname{erfc}\left(\frac{|y_D|}{2\sqrt{t_D}}\right) \quad (5-310)$$

In the position $y_D = 0$ in the oil source-plan, the general solution becomes:

$$m_D(y_D, t_D) = \sqrt{\pi t_D} - \int_0^{w_f} \int_0^{t_D} \left[\frac{1}{k_{effD}(p_D)} - 1 \right] \frac{\partial p_D(y'_D, t'_D)}{\partial t'_D} \times \\ \times G_D(y_D, y'_D, t_D, t'_D) dt'_D dy'_D \quad (5-311)$$

Finally, the dimensionless general solution in terms of the pressure-sensitive linear function is:

$$m_D(y_D, t_D) = \sqrt{\pi t_D} - \int_0^{w_f} \int_0^{t_D} \left[\frac{1}{A\sqrt{\pi t'_D} + B} - 1 \right] \frac{\partial p_D(y'_D, t'_D)}{\partial t'_D} \times \\ \times G_D(y_D, y'_D, t_D, t'_D) dt'_D dy'_D \quad (5-312)$$

5.3.6 Model Calibration and Results

For the simulation of the permeability loss in an infinite hydraulic fracture in a vertical well, it was used the same computational table of pressure p and permeability $k(p)$ values obtained from synthetic field data aforementioned. The experimental data of pressure and permeability changes for two reservoir layers were fitted using the linear function proposed in this work and these were inserted in the effective permeability-based pseudo-pressure function $m(p)$. The NHDE was solved through the command *int2* from Matlab[®] to compute the implicit term inside the integrand. In order to represent an infinite hydraulic fracture in the numerical simulator, it was built a grid with a block characterized as a zone of high transmissibility placed in a boundary of the computational cell. Figure 5.55 presents the log-log plot of the dimensionless effective permeability as a function of the pore pressure ratio p/p_i . We notice that, as the pore pressure ratio declines, the permeability loss increases.

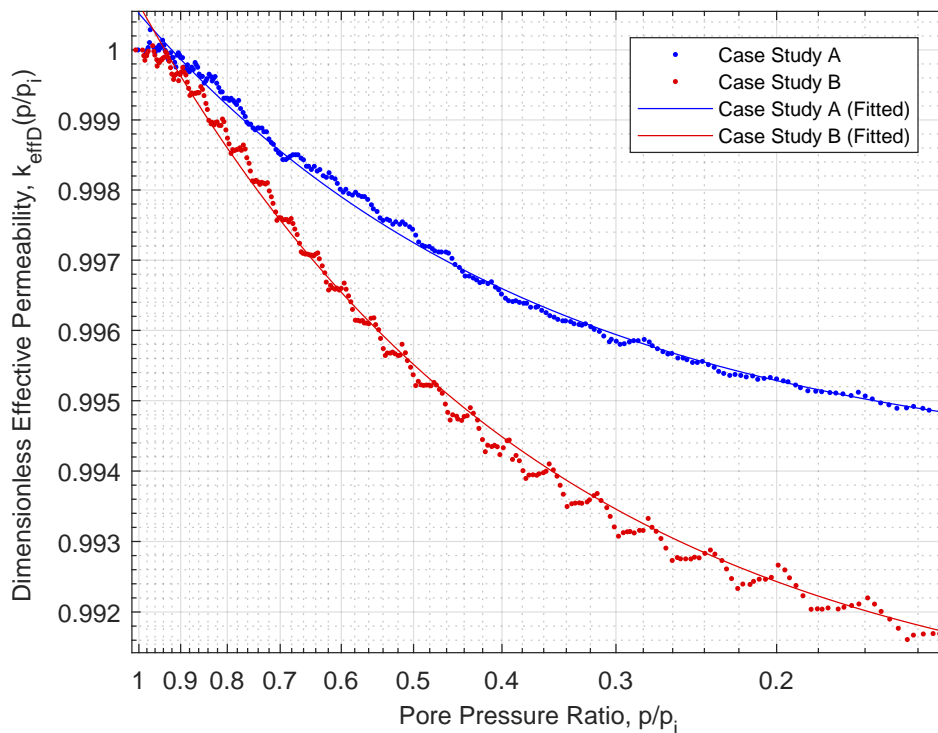


Figure 5.55: Dimensionless effective permeability as a function of the pore pressure ratio for the case studies A and B.

Figure 5.56 presents the log-log plot of the effective permeability pseudo-pressure, [MPa] as a function of the pressure, [MPa]. This plot shows that, the pseudo-pressure declines severely when the pressure reaches low values ($p \approx 50$ MPa). As the pseudo-pressure is related to the permeability loss, this pressure response influences significantly the permeability loss over the well-reservoir life-cycle. Figure 5.58 presents the diagnostic plot of the dimensionless linear solution against IMEX[®] and the results are accurate. The diagnostic plot can also be used to the monitoring of the effective deviation factor Figure 5.57. We notice that there is an abrupt increase in this factor and, consequently, in the permeability loss, in the interval $[260 \times 10^2 \text{ KPa} < p < 300 \times 10^2 \text{ KPa}]$. The response of this factor is extremely important to minimize this peak presented in this plot and avoid uncontrolled permeability decline during the well-reservoir's production. This plot can be used in field operations to monitor the pressure variation that prevents this abrupt deviation factor response.

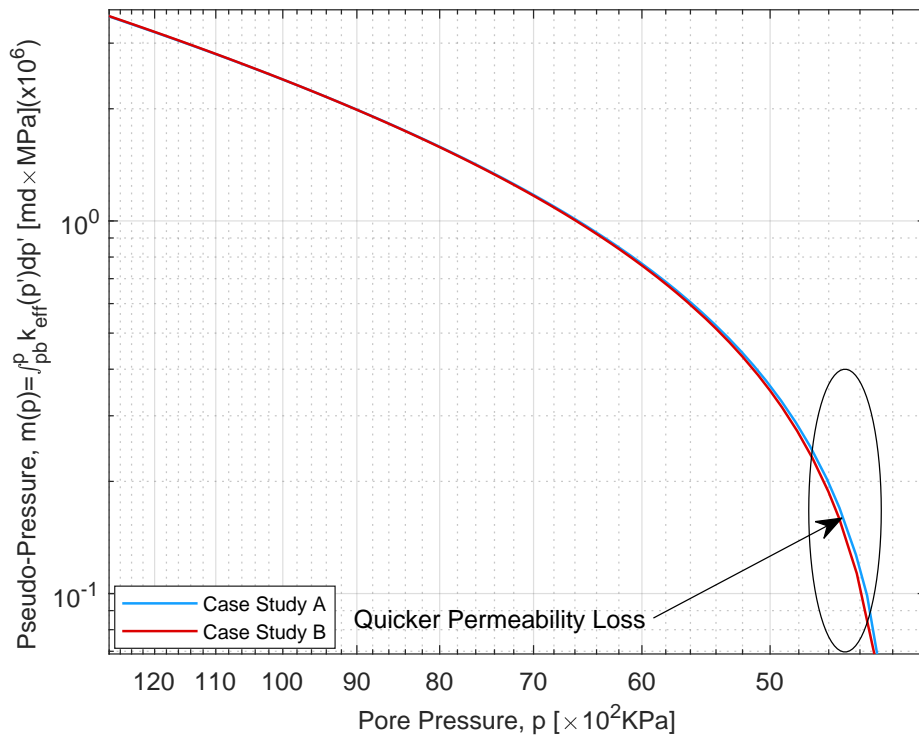


Figure 5.56: Log-log plot of the effective permeability pseudo-pressure for case studies A and B.

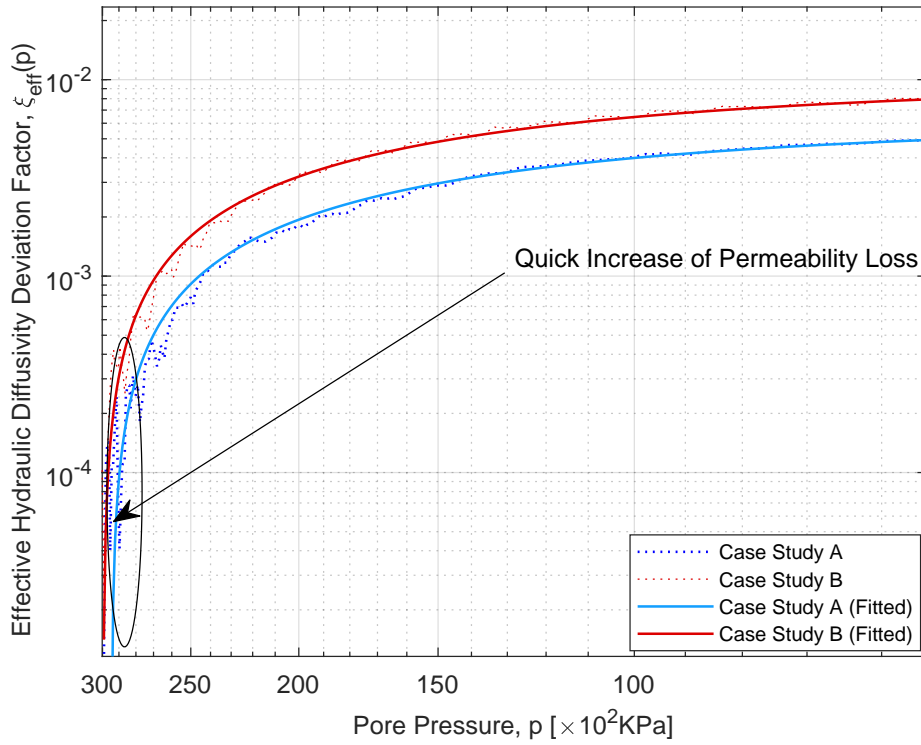


Figure 5.57: Log-log plot of the effective deviation factor for case studies A and B.

PUC-Rio - Certificação Digital N° 1912769/CA

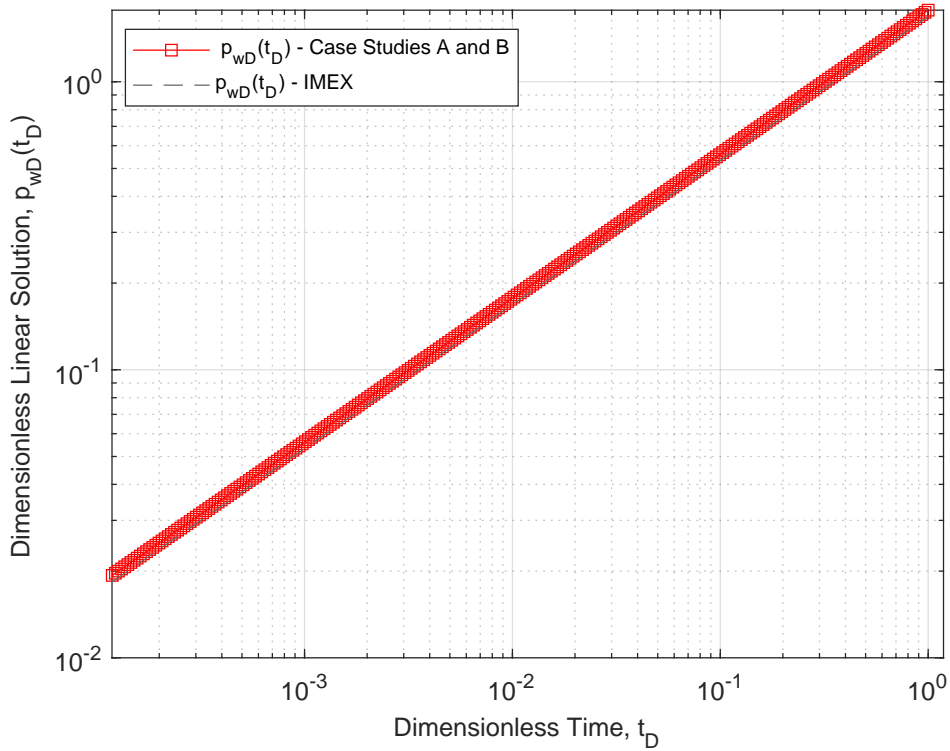


Figure 5.58: Diagnostic plot of the dimensionless linear solution (constant permeability) in comparison to IMEX®.

Figure 5.59 presents the diagnostic plot of the dimensionless first-order pseudo-pressure against IMEX[®] for the case studies A and B. The results are accurate. Figure 5.60 presents the diagnostic plot of the dimensionless pseudo-pressure against IMEX[®] and the results are also accurate for both case studies.

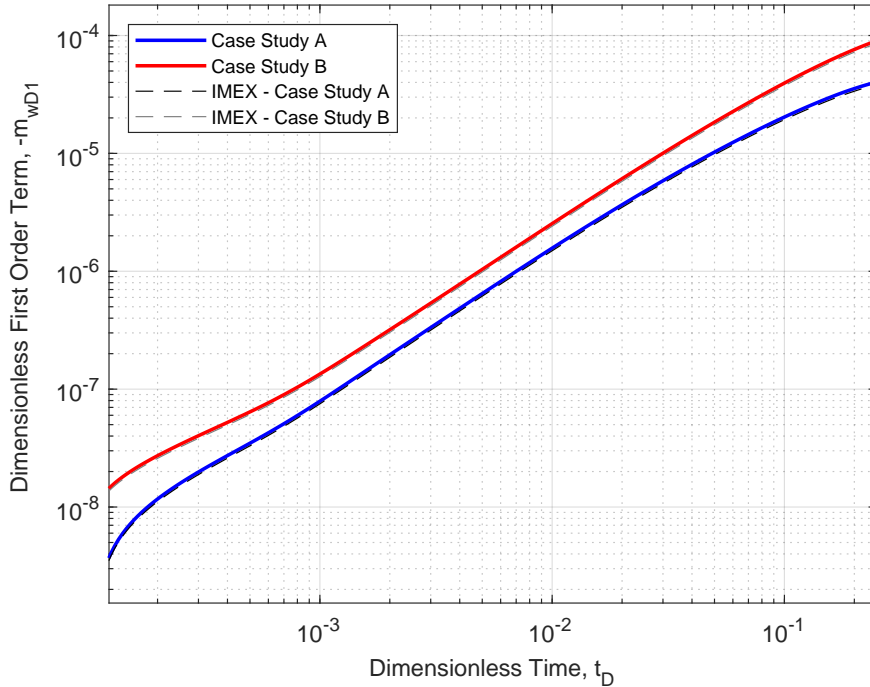


Figure 5.59: Diagnostic plot of the dimensionless first-order pseudo-pressure against IMEX[®] for the case studies A and B.

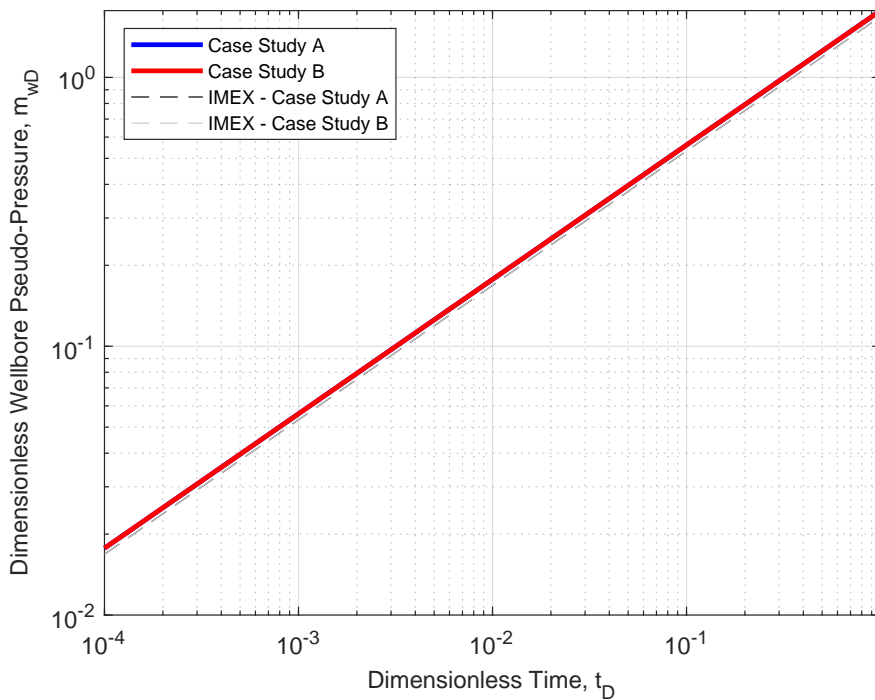


Figure 5.60: Diagnostic plot of the dimensionless pseudo-pressure against IMEX[®] for the case studies A and B.

Figure 5.61 presents the diagnostic plot of the dimensionless pseudo-pressure derivative against IMEX[®] for the case studies A and B. The Bourdet algorithm was used to compute this derivative. The results are accurate for both case studies. Figure 5.62 presents the role of the proppant package arrangement porosity ϕ_p in the dimensionless effective permeability as a function of the pressure ratio. As expected, the results show that, the higher the proppant package porosity value, the higher the dimensionless effective permeability. The arrangement cubic and orthorhombic present the larger porosity and, consequently, permeability values. The lower porosity values are rhombohedral and tetragonal settings. The rhombohedral value is close to the value used in the previous chapters of this work. Moreover, the rhombohedral and tetragonal arrangements decline severely, as the pressure ratio declines, whereas the cubic and orthorhombic decline slower as the pressure ratio drops. Figure 5.63 presents the log-log plot of the effective permeability pseudo-pressure as a function of the pore pressure for several proppant package arrangement porosities. We notice a severe drop for low values of pore pressure ($p \approx 50$ MPa).

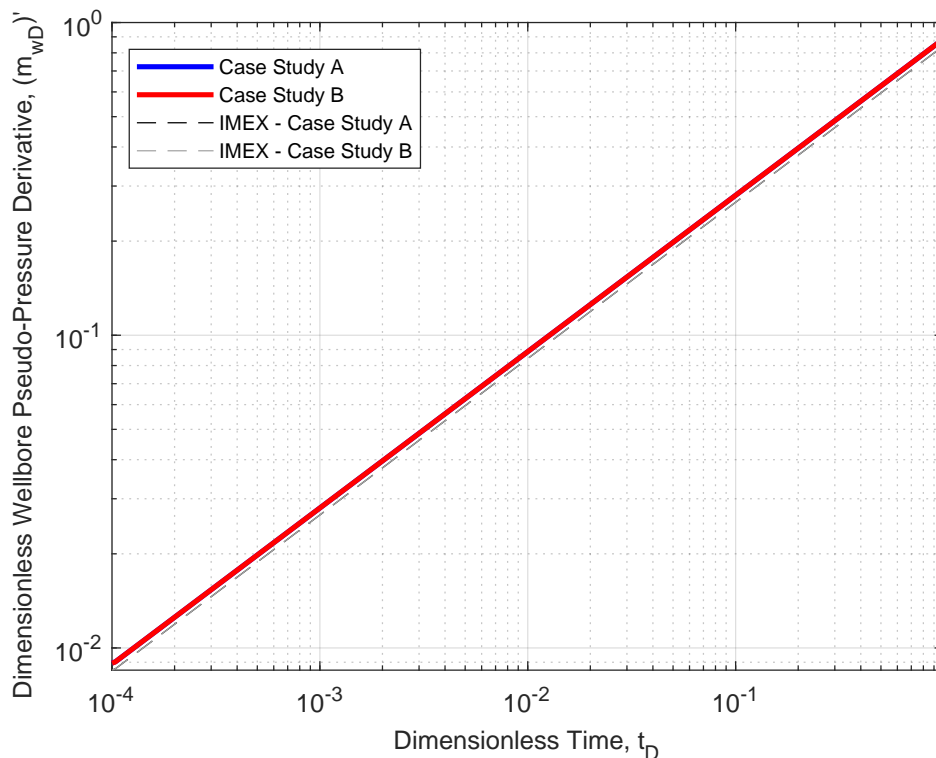


Figure 5.61: Diagnostic plot of the dimensionless pseudo-pressure derivative against IMEX[®] for the case studies A and B.

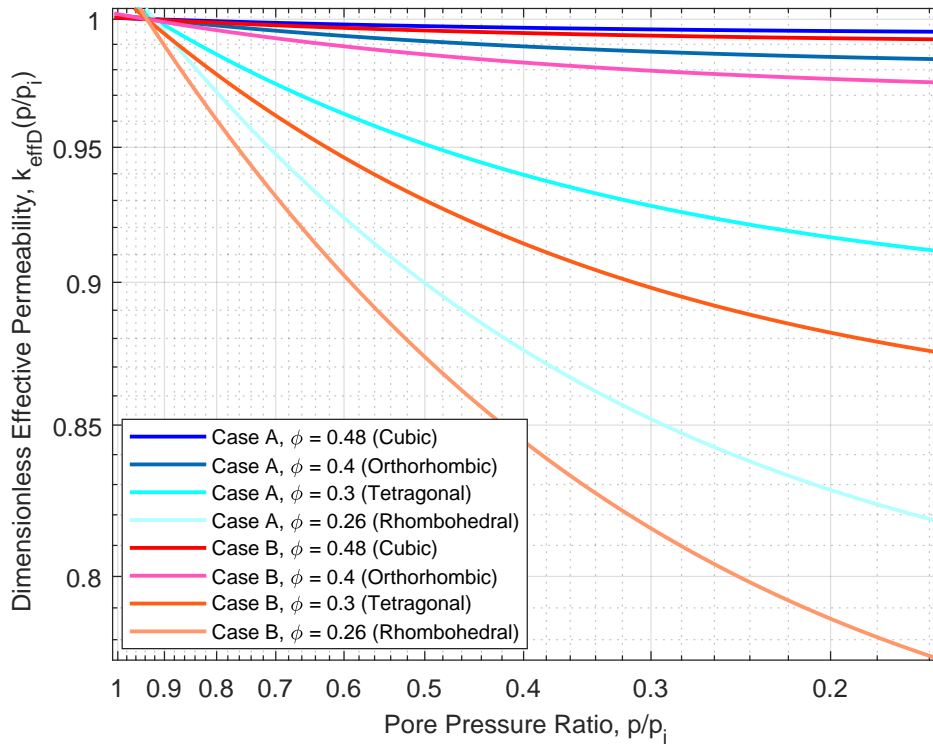


Figure 5.62: Dimensionless effective permeability as a function of the pore pressure ratio for several proppant package arrangements for the case studies A and B.

PUC-Rio - Certificação Digital N° 1912769/CA

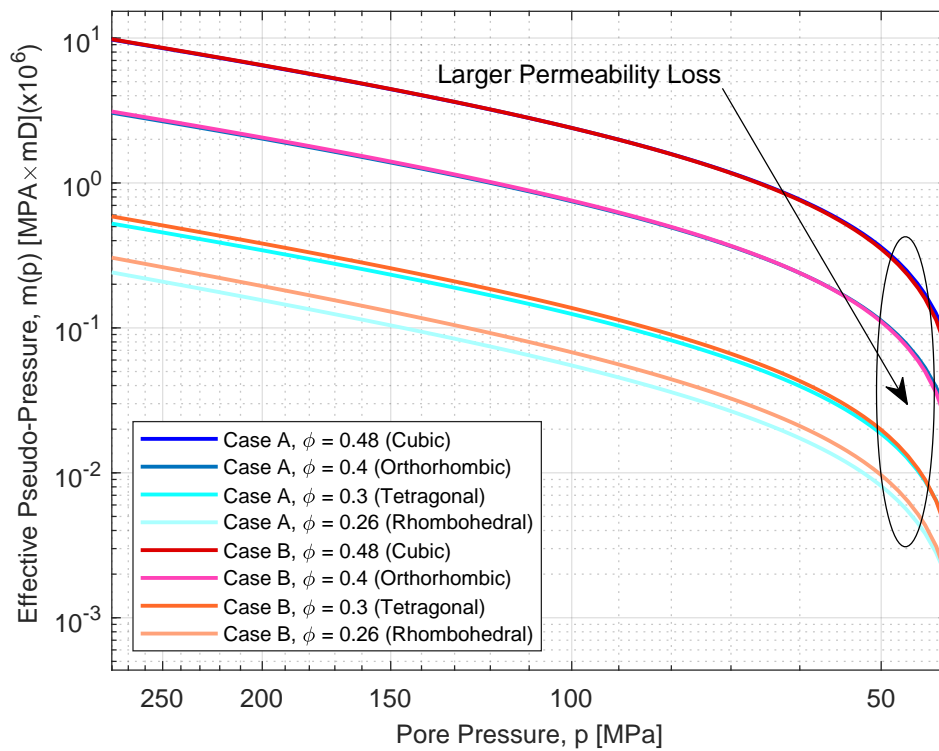


Figure 5.63: Effective permeability pseudo-pressure as a function of the pore pressure for several proppant package arrangements for the case studies A and B.

Figure 5.64 shows the effective hydraulic diffusivity deviator factor as a function of the pore pressure. The results show an abrupt increase of this factor for pore pressure $p \approx 300$ MPa. It occurs due the begin of the drawdown period. Figure 5.65 presents the effect of the proppant porosities package in the dimensionless pseudo-pressure derivative. We do not notice significant effect in this plot. The amplification of this plot is presented in the Figure 5.66 and we can realize that a smooth deviation occurs for larger dimensionless times. Figure 5.67 presents the log-log plot of the effect of the proppant porosities package in the dimensionless first-order term for several proppant package arrangements for the case studies A and B. The results show that, the cubic and the rhombohedral arrangements provide the lowest and highest nonlinear effect (permeability loss), respectively. Figure 5.68 presents the Semi-log plot of this same effect in the dimensionless pseudo-pressure and the results show that, there is no significant influence in the general solution.

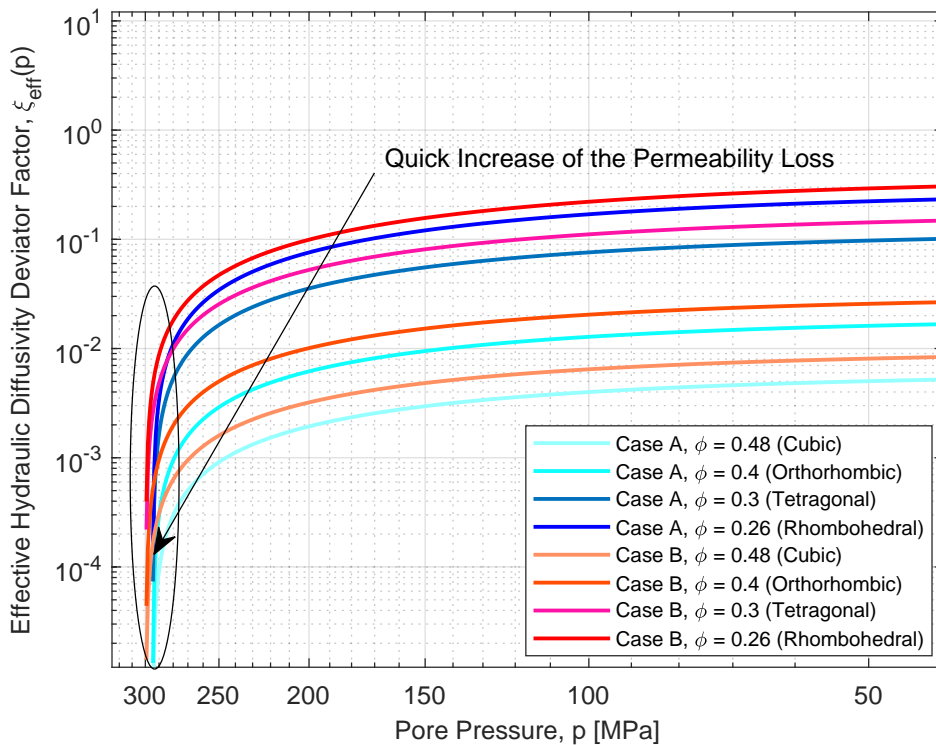


Figure 5.64: Effective hydraulic diffusivity deviator factor as a function of the pore pressure for several proppant package arrangements for the case studies A and B.

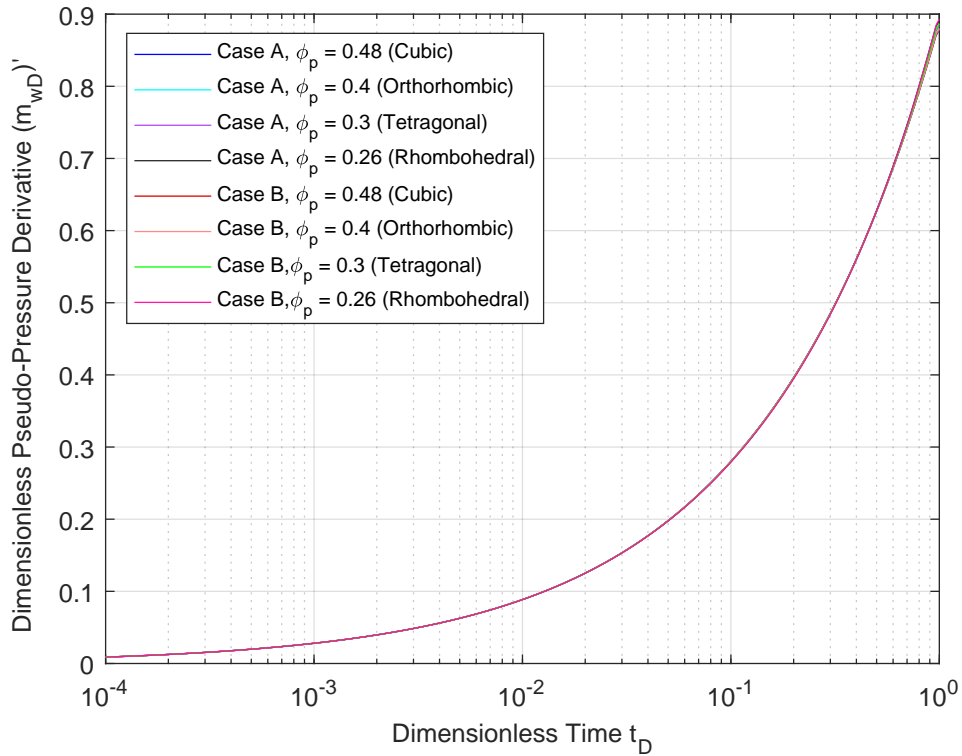


Figure 5.65: Semi-log plot of the pseudo-pressure derivative for several proppant package arrangements for the case studies A and B.

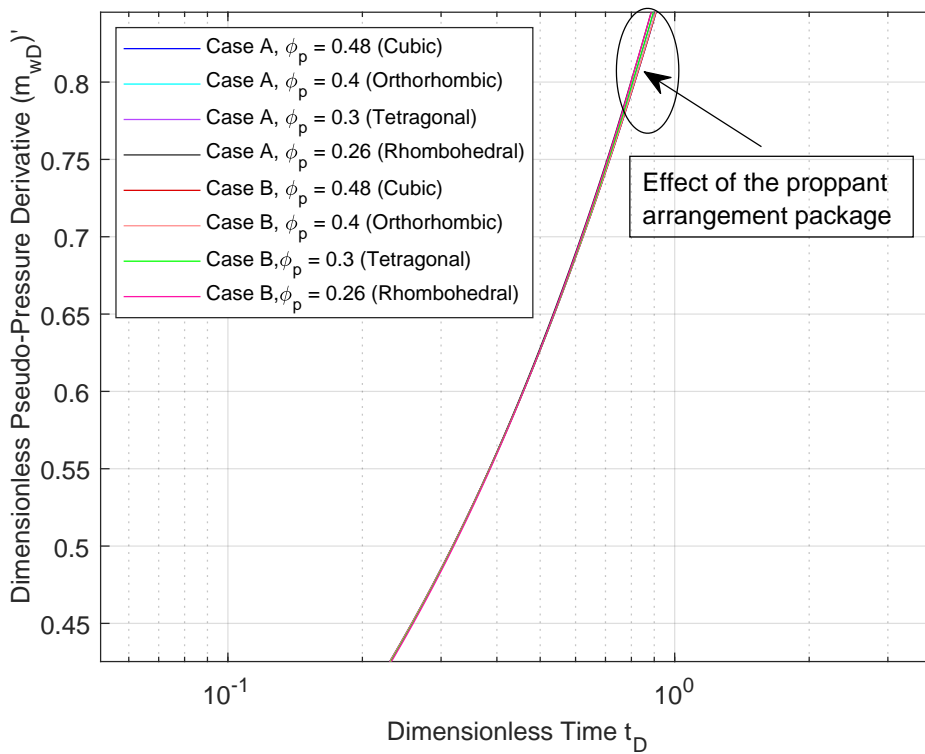


Figure 5.66: Semi-log plot of the amplification of the pseudo-pressure derivative for several proppant package arrangements for the case studies A and B.

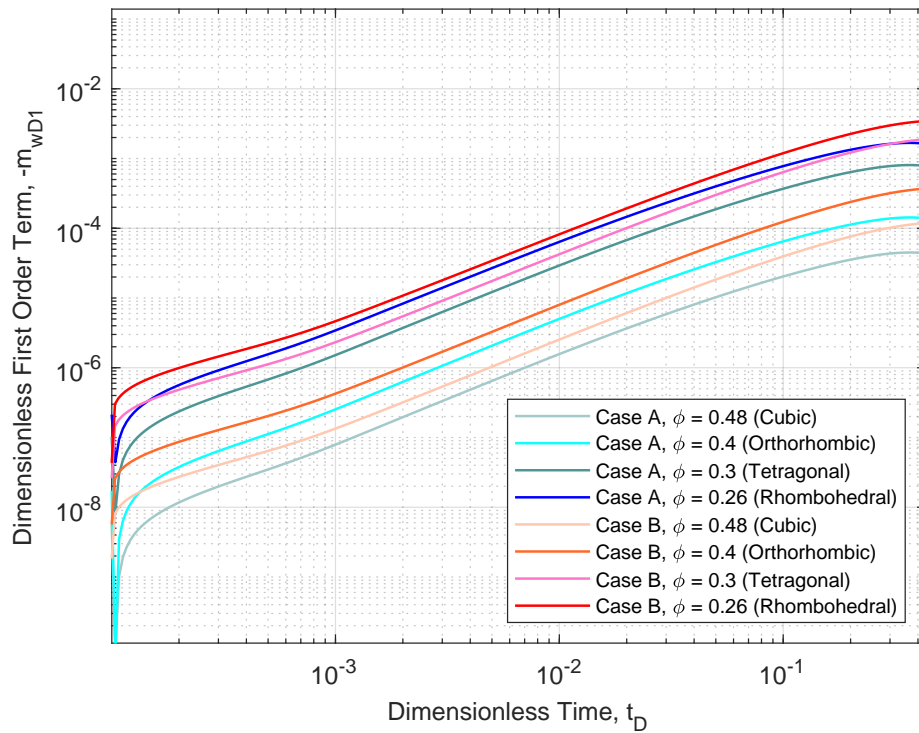


Figure 5.67: Log-log plot of the first-order term for several proppant package arrangements for the case studies A and B.

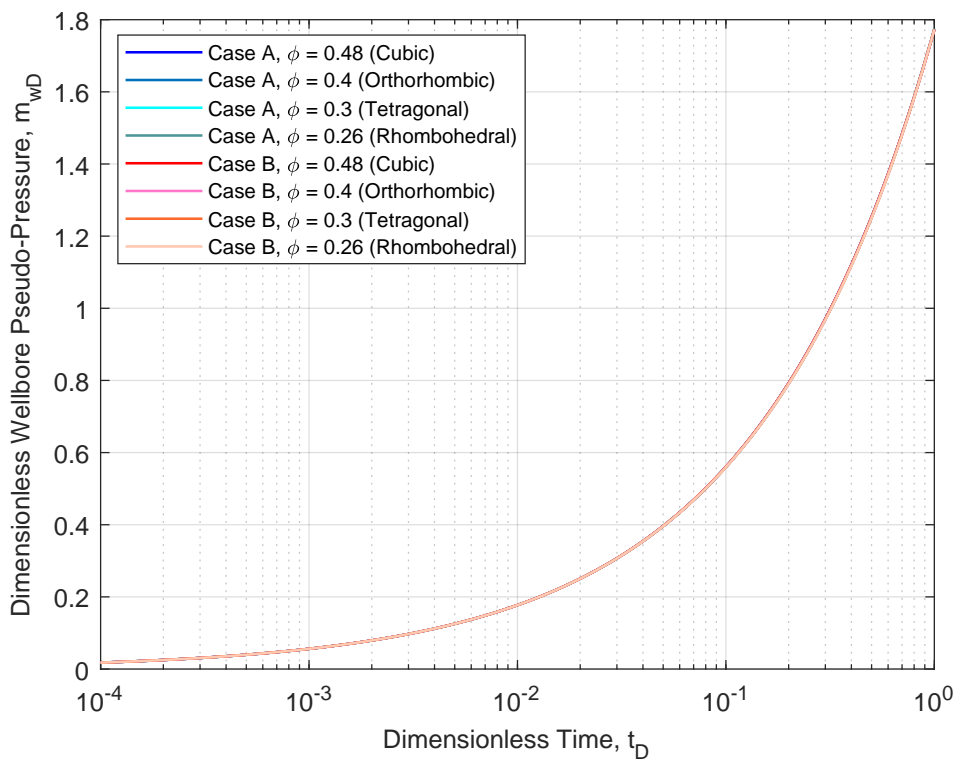


Figure 5.68: Semi-log plot of the dimensionless pseudo-pressure for several proppant package arrangements for the case studies A and B.

Figure 5.69 presents the log-log plot of the dimensionless first-order term for several sorting index values for the case studies A and B. The effect of this index is lower than the porosity package, however, the behavior of the curves are similar. For high values of this index, the nonlinearity is larger, resulting in more severe permeability loss. The effect of this index is not significant in the dimensionless pseudo-pressure and its derivative (Figures 5.70 and 5.71). Finally, the effect of the cementation exponent must be evaluated in the permeability loss response. This exponent provides an effect similar to the sorting index one for the dimensionless first-order term, pseudo-pressure and its derivative (Figures 5.72, 5.73 and 5.74).

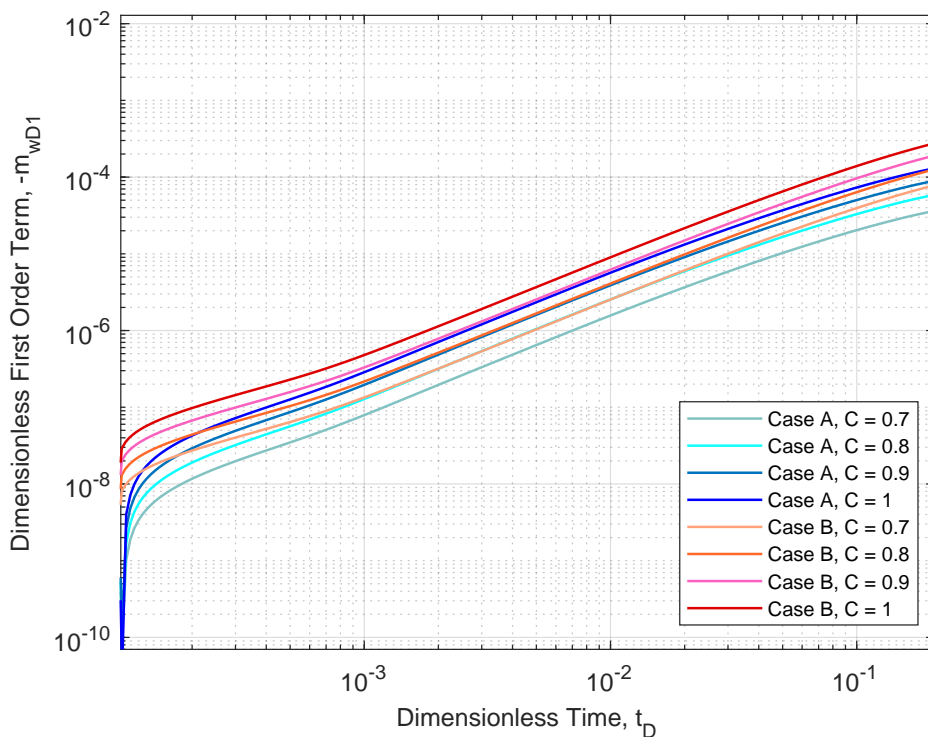


Figure 5.69: Log-log plot of the dimensionless first-order term for several sorting index values for the case studies A and B.

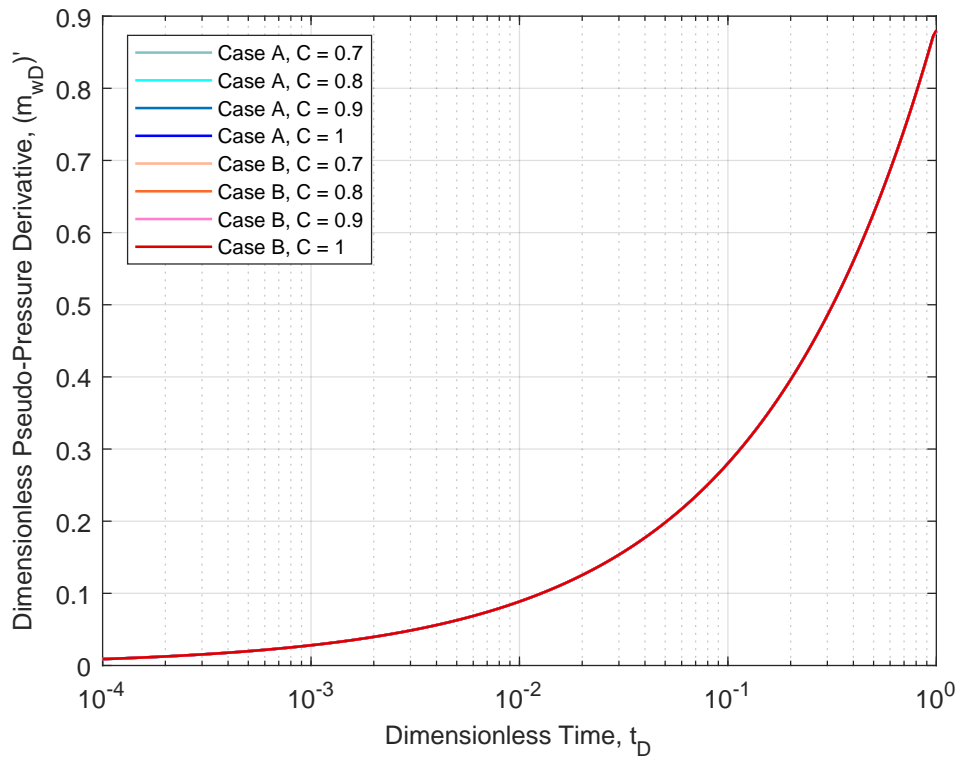


Figure 5.70: Semi-log plot of the dimensionless pseudo-pressure derivative for several sorting index values for the case studies A and B.

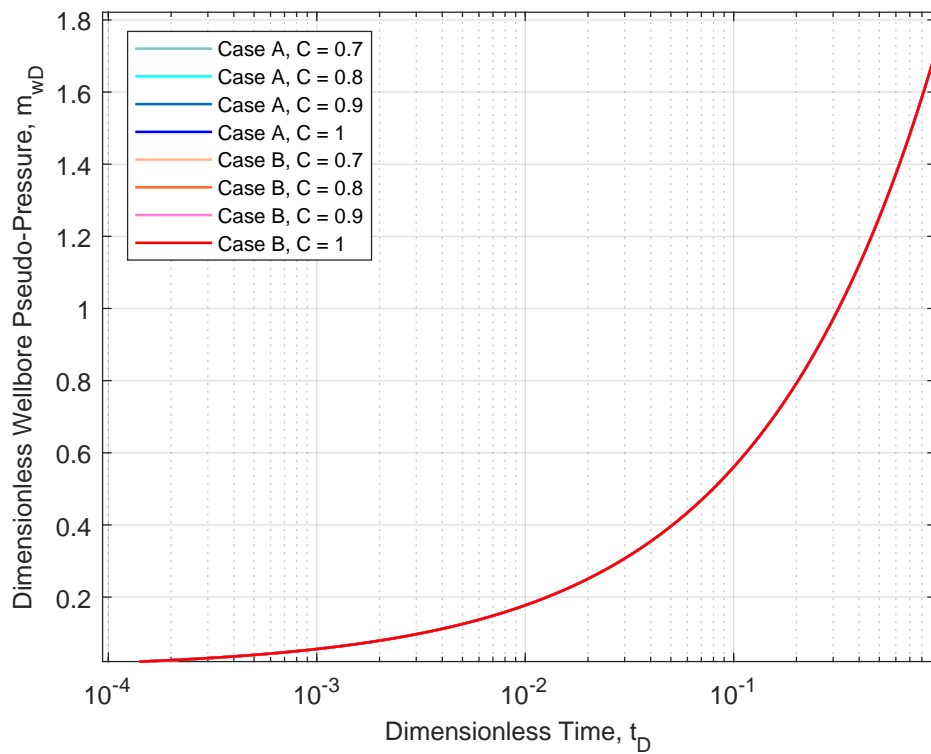


Figure 5.71: Semi-log plot of the dimensionless pseudo-pressure for several sorting index values for the case studies A and B.

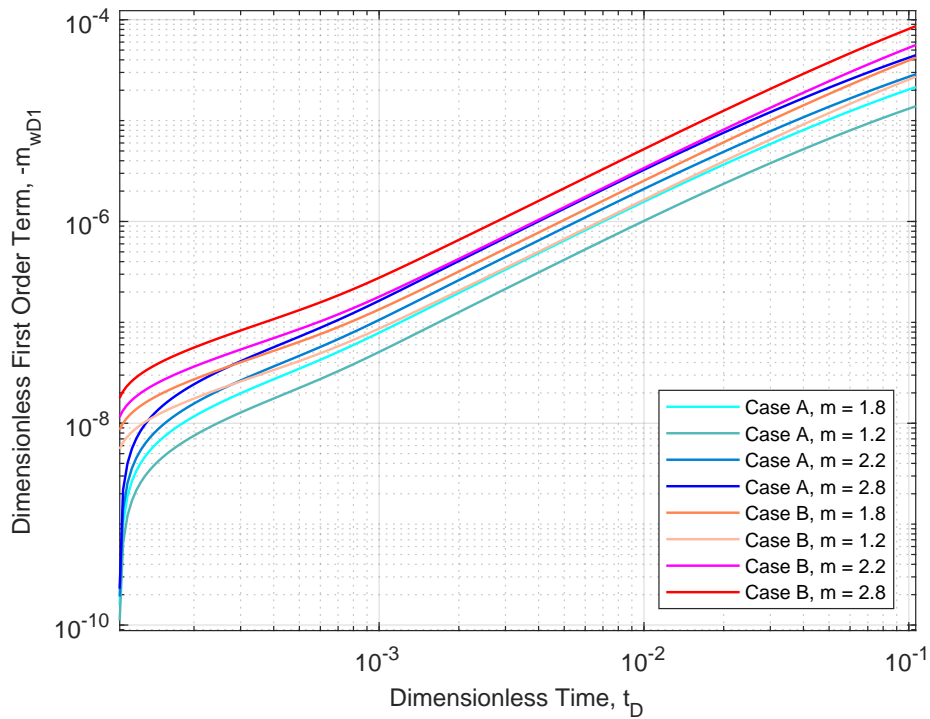


Figure 5.72: Log-log plot of the dimensionless first-order term for several cementation exponent values for the case studies A and B.

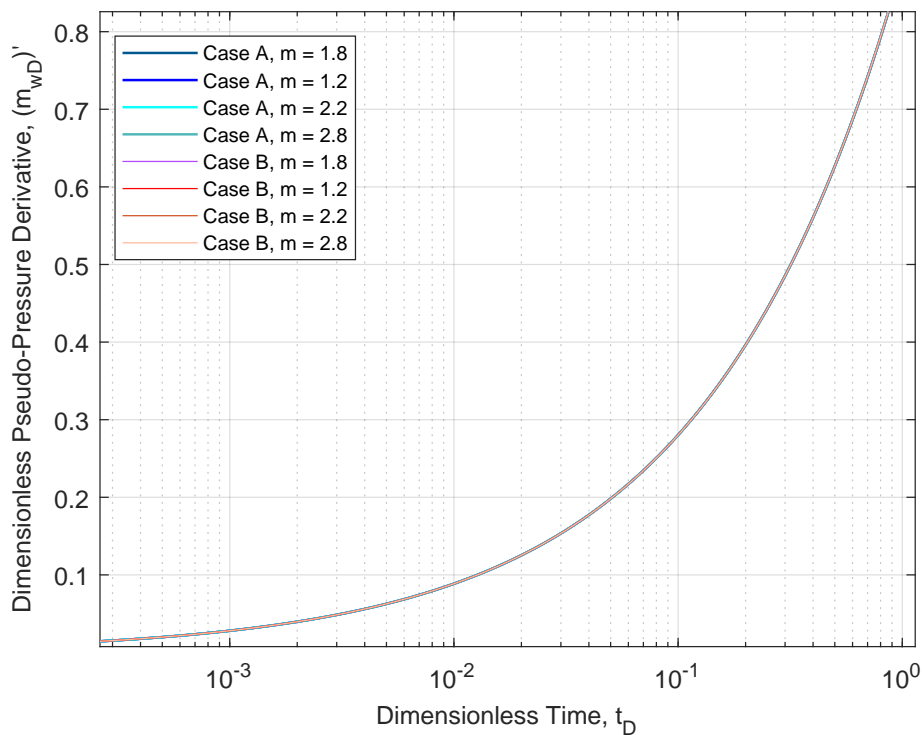


Figure 5.73: Semi-log plot of the dimensionless pseudo-pressure derivative for several cementation exponent values for the case studies A and B.

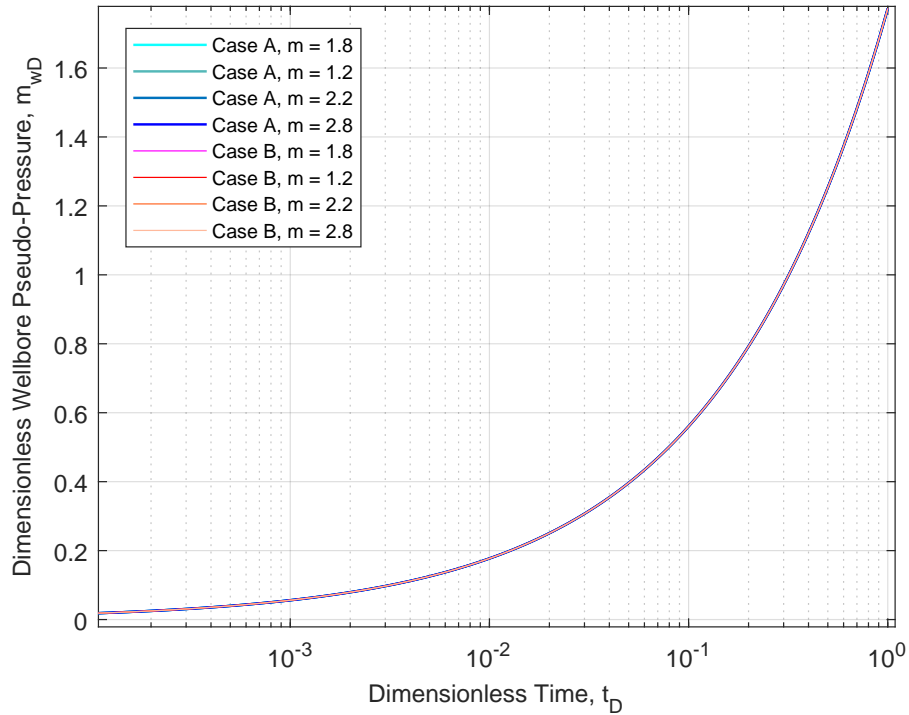


Figure 5.74: Semi-log plot of the dimensionless pseudo-pressure for several cementation exponent values for the case studies A and B.

5.4

Oil Flow in a Well with Finite Extension Hydraulic Fracture

In this section, the oil flow through a finite hydraulic fracture in x - y directions (Figure 5.75) is modeled using the proposed coupled-integro-differential-GF solution. For the condition of the hydraulic fracture with finite length, results in the oil flow occurs in both x - y directions (bi-linear flow).

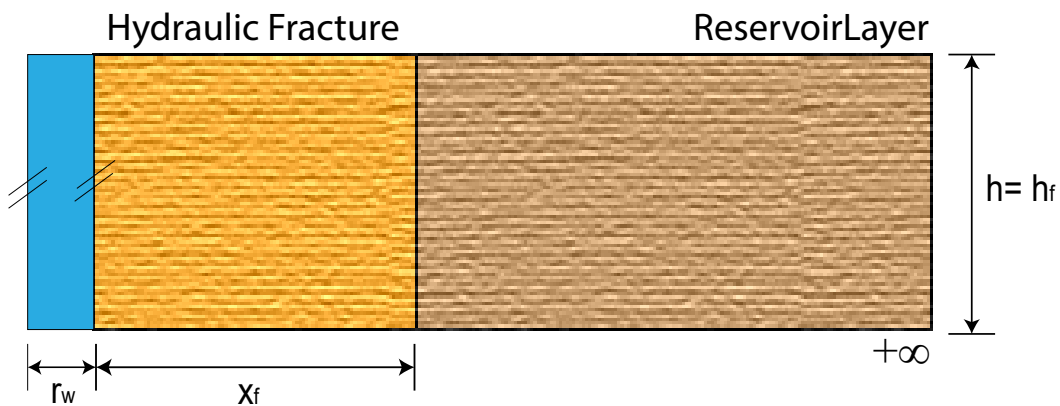


Figure 5.75: Scheme of a finite extension hydraulic fracture.

The flow regime for this well-reservoir setting is known in petroleum engineering as *elliptical flow*. Thus the partial differential equation is derived with respect to the Cartesian x-y directions and to the time t .

5.4.1

Model Assumptions

For modeling of oil flow problem in porous media by means of the asymptotic series expansion of the solution of the pressure diffusivity equation in terms of pseudo-pressure, the following premises are assumed:

1. Constant oil flow rate in the well
2. Pressure-sensitive effective permeability
3. Non-Darcian effects not considered
4. Hydraulic fracture roughness neglected
5. Well fully penetrates reservoir rock
6. Deformable, homogeneous, linear elastic and isotropic reservoir
7. The well is located at the origin of the Cartesian system of coordinates
8. Isothermal, single-phase and compressible flow in the porous medium
9. The fluid present inside the pores of the reservoir rock does not react chemically with the rock matrix
10. Two dimensional and unsteady flow
11. Hydraulic fracture with finite extension
12. Small pressure gradient
13. The hydraulic fracture is propped and undeformable
14. Skin and storage effects not considered
15. Permeability hysteresis of porous media is negligible
16. No fluid flow across the top and bottom of the formation
17. Infinite extent reservoir in x-y directions
18. Reservoir with uniform net pay

5.4.2 Model Derivation

Let the oil flow through a finite hydraulic fracture model in a pressure-sensitive permeability reservoir in the dimensionless Cartesian coordinates $\mathbf{r}_D = (x_D, y_D, 0) \in \mathbb{R}$ and $t_D \in \mathbb{R}$.

The pressure NHDE in Cartesian coordinates is:

$$\frac{\partial^2 p}{\partial x^2} + \frac{\partial^2 p}{\partial y^2} - \frac{1}{\eta_{eff}(p)} \frac{\partial p}{\partial t} = -f(x, y, t) \quad (5-313)$$

The same effective hydraulic diffusivity function $\eta_{eff}(p)$ is used for the finite hydraulic fracture and is expressed by:

$$\eta_{eff}(p) = \frac{k_{eff}(p)}{\phi_p \mu c_t} \quad (5-314)$$

Where the variables ϕ_p , [dimensionless]; $k_{eff}(p)$, [md]; $k_m(p)$, [md] and k_f , [md] are the same used in the section 5.3 The same effective permeability function is used and is expressed as follows (Cho, Apaydin & Ozkan, 2013):

$$k_{eff}(p) = k_m(p) + \phi_p k_f \quad (5-315)$$

The same dimensionless variables defined in the previous chapter are used for this model. The condition used by Teng, Li & Yu (2020) that, the hydraulic fracture remains undamaged as the reservoir permeability drops was used to model the oil flow in the finite hydraulic fracture.

5.4.3 Integro-Differential Solution for a Finite Hydraulic Fracture

The dimensionless general solution of the NHDE for the finite hydraulic fracture in a vertical well follows the same procedures presented in the previous sections for Cartesian coordinates. Thereby:

$$\begin{aligned} m_D(x_D, y_D, t_D) = & \\ = - \int_{-\infty}^{+\infty} \int_{-\infty}^{+\infty} \int_0^{t_D} & \left[f_D(x'_D, y'_D, t'_D) + \xi_{eff}(p) \frac{\partial m_D(x'_D, y'_D, t'_D)}{\partial t'_D} \right] \times \\ & \times G_D(x_D, x'_D, y_D, y'_D, t_D, t'_D) dt'_D dx'_D dy'_D \quad (5-316) \end{aligned}$$

Let the dimensionless oil source term for the two-dimensional (2-D) Cartesian geometry:

$$f_D(x_D, y_D, t_D) = \frac{2\pi \bar{q}_{sc}(x, y, t) l_c^2}{q_{ref}} \quad (5-317)$$

Where the characteristic length l_c remains as the half-wing fracture length x_f , [m]; $\bar{q}_{sc}(x, y, t)$ is the oil flow rate per fracture area unit at standard conditions, [m/sec]. For an unique hydraulic fracture with oil production uniformly distributed, located at $y_D = 0$ in the interval $-x_f < x < +x_f$, the dimensionless oil source is expressed as follows:

$$f_D(x_D, y_D, t_D) = -\frac{2\pi q_{sc}(t) x_f^2}{2x_f q_{ref}} \delta(y - 0) \quad (5-318)$$

As mentioned in the previous chapters, the reference oil flow rate and, in standard conditions are the same, thus the dimensionless oil source yields to:

$$f_D(x_D, y_D, t_D) = -\pi x_f \delta(y - 0) \quad (5-319)$$

Using the space scaling property of the Dirac delta function again, $x_f \delta(y - 0) = \delta(y_D - 0)$. Let us define the dimensionless x-position x_D as $x_D = x/x_f$. The dimensionless oil source is approached in the total fracture extension, *i.e.*, when $x = x_f$ ($x_D = \pm 1$). Thus, in the interval $-1 < x_D < 1$, the Eq. 5-298 yields to:

$$f_D(x_D, y_D, t_D) = -\pi \delta(y_D - 0) \quad (5-320)$$

Outside from the fracture's domain, *i.e.*, $x_D < -1$ and $x_D > 1$, the dimensionless oil source is zero. Replacing the Eq. 5-319 in the Eq. 5-316 and using the integration's limit in the interval $[-1 \leq x_D \leq 1]$:

$$m_D(x_D, y_D, t_D) = \int_{-\infty}^{+\infty} \int_{-1}^1 \int_0^{t_D} \left[\pi \delta(y_D - 0) - \xi_{eff}(p) \frac{\partial m_D(x'_D, y'_D, t'_D)}{\partial t'_D} \right] \times \\ \times G_D(x_D, x'_D, y_D, y'_D, t_D, t'_D) dt'_D dx'_D dy'_D \quad (5-321)$$

Expanding the Eq. 5-321, the integro-differential solution yields to:

$$m_D(x_D, y_D, t_D) = \\ = \int_{-\infty}^{+\infty} \int_{-1}^1 \int_0^{t_D} \pi \delta(y_D - 0) G_D(x_D, x'_D, y_D, y'_D, t_D, t'_D) dt'_D dx'_D dy'_D - \\ + \int_{-\infty}^{+\infty} \int_{-\infty}^{+\infty} \int_0^{t_D} \xi_{eff}(p) \frac{\partial m_D(x'_D, y'_D, t'_D)}{\partial t'_D} G_D(x_D, x'_D, y_D, y'_D, t_D, t'_D) dt'_D dx'_D dy'_D \quad (5-322)$$

The GF related to a finite source-plan with uniform oil flow rate is expressed by (Carslaw & Jaeger, 1959), (Beck et al., 1992), (Ozisiki, 1993), (Duffy, 2001) and (Cole, Beck & Haji-Sheikh, 2011):

$$G_D(x_D, x_{D0}, y_D, y_{D0}, t_D, t_{D0}) = \frac{e^{-\frac{(y_D - y_{D0})^2 + (x_D - x_{D0})^2}{4(t_D - t_{D0})}}}{4\sqrt{\pi(t_D - t_{D0})}} \quad (5-323)$$

Computing the GF in the oil source-plan position $y_{D0} = 0$, the dimensionless GF becomes:

$$G_D(x_D, x_{D0}, y_D, y_{D0}, t_D, t_{D0}) = \frac{e^{-\frac{y_D^2 + (x_D - x_{D0})^2}{4(t_D - t_{D0})}}}{4\pi(t_D - t_{D0})} \quad (5-324)$$

Replacing the Eq. 5-324 in the Eq. 5-322, the integro-differential solution yields to:

$$\begin{aligned} m_D(x_D, y_D, t_D) = & \int_{-\infty}^{+\infty} \int_{-1}^1 \int_0^{t_D} \pi \delta(y_D - 0) \frac{e^{-\frac{y_D^2 + (x_D - x'_D)^2}{4(t_D - t'_D)}}}{4\pi(t_D - t'_D)} dt'_D dx'_D dy'_D - \\ & + \int_{-\infty}^{+\infty} \int_{-\infty}^{+\infty} \int_0^{t_D} \xi_{eff}(p) \frac{\partial m_D(x'_D, y'_D, t'_D)}{\partial t'_D} \frac{e^{-\frac{y_D^2 + (x_D - x'_D)^2}{4(t_D - t'_D)}}}{4\pi(t_D - t'_D)} dt'_D dx'_D dy'_D \quad (5-325) \end{aligned}$$

Applying the sampling property of the Dirac delta function and the effective hydraulic diffusivity deviator factor (Eq. 5-307), the first triple integral of the Eq. 5-325 becomes:

$$\begin{aligned} m_D(x_D, y_D, t_D) = & \int_{-1}^1 \int_0^{t_D} \frac{e^{-\frac{y_D^2 + (x_D - x'_D)^2}{4(t_D - t'_D)}}}{4(t_D - t'_D)} dt'_D dx'_D - \int_{-\infty}^{+\infty} \int_{-\infty}^{+\infty} \int_0^{t_D} \left[\frac{1}{k_{effD}(m_D)} - 1 \right] \times \\ & \times \frac{\partial m_D(x'_D, y'_D, t'_D)}{\partial t'_D} \frac{e^{-\frac{y_D^2 + (x_D - x'_D)^2}{4(t_D - t'_D)}}}{4\pi(t_D - t'_D)} dt'_D dx'_D dy'_D \quad (5-326) \end{aligned}$$

As approached earlier, the derivative in the nonlinear term is related to the linear solution $p_D(x_D, y_D, t_D)$, thus:

$$\begin{aligned}
 m_D(x_D, y_D, t_D) &= \\
 &= \int_{-1}^1 \int_0^{t_D} \frac{e^{-\frac{y_D^2 + (x_D - x'_D)^2}{4(t_D - t'_D)}}}{4(t_D - t'_D)} dt'_D dx'_D - \int_{-\infty}^{+\infty} \int_{-\infty}^{+\infty} \int_0^{t_D} \left[\frac{1}{k_{effD}(p_D)} - 1 \right] \times \\
 &\quad \times \frac{\partial p_D(x'_D, y'_D, t'_D)}{\partial t'_D} \frac{e^{-\frac{y_D^2 + (x_D - x'_D)^2}{4(t_D - t'_D)}}}{4\pi(t_D - t'_D)} dt'_D dx'_D dy'_D \quad (5-327)
 \end{aligned}$$

The double integral on the right-hand side of the Eq. 5-327 can be expressed as:

$$\int_{-1}^1 \int_0^{t_D} \frac{e^{-\frac{y_D^2 + (x_D - x'_D)^2}{4(t_D - t'_D)}}}{4(t_D - t'_D)} dt'_D dx'_D = \int_{-1}^1 \left[\int_0^{t_D} \frac{e^{-\frac{y_D^2 + (x_D - x'_D)^2}{4(t_D - t'_D)}}}{4(t_D - t'_D)} dt'_D \right] dx'_D \quad (5-328)$$

According to [Abramowitz & Stegun \(1972\)](#):

$$\int_0^{t_D} \frac{e^{-\frac{y_D^2 + (x_D - x'_D)^2}{4(t_D - t'_D)}}}{4(t_D - t'_D)} dt'_D = \int_{\frac{y_D^2 + (x_D - x'_D)^2}{4(t_D - t'_D)}}^{+\infty} \frac{e^{-u}}{u} du \quad (5-329)$$

Thereby, the Eq. 5-328 can be expressed as:

$$\int_{-1}^1 \int_0^{t_D} \frac{e^{-\frac{y_D^2 + (x_D - x'_D)^2}{4(t_D - t'_D)}}}{4(t_D - t'_D)} dt'_D dx'_D = -\frac{1}{4} \int_{-1}^1 \mathbf{Ei} \left[-\frac{y_D^2 + (x_D - x'_D)^2}{4(t_D - t'_D)} \right] dx'_D \quad (5-330)$$

The Eq. 5-330 represents the linear solution $p_D(x_D, y_D, t_D)$ for the constant oil flow production through a finite hydraulic fracture. Therewith:

$$p_D(x_D, y_D, t_D) = -\frac{1}{4} \int_{-1}^1 \mathbf{Ei} \left[-\frac{y_D^2 + (x_D - x'_D)^2}{4(t_D - t'_D)} \right] dx'_D \quad (5-331)$$

Replacing the Eq. 5-331 in the Eq. 5-327, the solution becomes:

$$\begin{aligned}
 m_D(x_D, y_D, t_D) &= \\
 &= -\frac{1}{4} \int_{-1}^1 \mathbf{Ei} \left[-\frac{y_D^2 + (x_D - x'_D)^2}{4(t_D - t'_D)} \right] dx'_D - \int_{-\infty}^{+\infty} \int_{-\infty}^{+\infty} \int_0^{t_D} \left[\frac{1}{k_{effD}(p_D)} - 1 \right] \times \\
 &\quad \times \frac{\partial p_D(x'_D, y'_D, t'_D)}{\partial t'_D} \frac{e^{-\frac{y_D^2 + (x_D - x'_D)^2}{4(t_D - t'_D)}}}{4\pi(t_D - t'_D)} dt'_D dx'_D dy'_D \quad (5-332)
 \end{aligned}$$

The general solution evaluated in the wellbore ($x_D = 0$ and $y_D = 0$) is expressed as follows:

$$\begin{aligned}
 m_D(x_D, y_D, t_D) &= \\
 &= -\frac{1}{4} \int_{-1}^1 \mathbf{Ei} \left(-\frac{x_D'^2}{4t_D} \right) dx'_D - \int_{-\infty}^{+\infty} \int_{-\infty}^{+\infty} \int_0^{t_D} \left[\frac{1}{k_{effD}(p_D)} - 1 \right] \times \\
 &\quad \times \frac{\partial p_D(x'_D, y'_D, t'_D)}{\partial t'_D} \frac{e^{-\frac{y_D^2 + (x_D - x'_D)^2}{4(t_D - t'_D)}}}{4\pi(t_D - t'_D)} dt'_D dx'_D dy'_D \quad (5-333)
 \end{aligned}$$

Integrating by parts, the Eq. 5-330 yields to:

$$p_D(x_D, y_D, t_D) = \sqrt{\pi t_D} \mathbf{erf} \left(\frac{1}{2\sqrt{t_D}} \right) - \frac{1}{2} \mathbf{Ei} \left(-\frac{1}{4t_D} \right) \quad (5-334)$$

Replacing the Eq. 5-334 in the Eq. 5-333, the dimensionless general solution for the permeability loss evaluation in a finite hydraulic fracture is:

$$\begin{aligned}
 m_D(x_D, y_D, t_D) &= \\
 &= \sqrt{\pi t_D} \mathbf{erf} \left(\frac{1}{2\sqrt{t_D}} \right) - \frac{1}{2} \mathbf{Ei} \left(-\frac{1}{4t_D} \right) - \int_{-\infty}^{+\infty} \int_{-\infty}^{+\infty} \int_0^{t_D} \left[\frac{1}{k_{effD}(p_D)} - 1 \right] \times \\
 &\quad \times \frac{\partial p_D(x'_D, y'_D, t'_D)}{\partial t'_D} \frac{e^{-\frac{y_D^2 + (x_D - x'_D)^2}{4(t_D - t'_D)}}}{4\pi(t_D - t'_D)} dt'_D dx'_D dy'_D \quad (5-335)
 \end{aligned}$$

Finally, the integro-differential solution in terms of the pressure-sensitive linear function is:

$$\begin{aligned}
 m_D(x_D, y_D, t_D) = & \sqrt{\pi t_D} \operatorname{erf}\left(\frac{1}{2\sqrt{t_D}}\right) - \frac{1}{2} \mathbf{Ei}\left(-\frac{1}{4t_D}\right) - \\
 & + \int_{-\infty}^{+\infty} \int_{-\infty}^{+\infty} \int_0^{t_D} \left\{ \frac{1}{A \left[\sqrt{\pi t'_D} \operatorname{erf}\left(\frac{1}{2\sqrt{t'_D}}\right) - \frac{1}{2} \mathbf{Ei}\left(-\frac{1}{4t'_D}\right) \right] + B} - 1 \right\} \times \\
 & \times \frac{\partial p_D(x'_D, y'_D, t'_D)}{\partial t'_D} \frac{e^{-\frac{y_D^2 + (x_D - x'_D)^2}{4(t_D - t'_D)}}}{4\pi(t_D - t'_D)} dt'_D dx'_D dy'_D \quad (5-336)
 \end{aligned}$$

As expected, the Eq. 5-336 shows that, the oil flow in a finite hydraulic fracture is expressed by the sum of the linear flow (first term) plus a radial flow (second term), that results in an elliptical flow.

5.4.4

Model Calibration and Results

For the simulation of the permeability loss in a finite hydraulic fracture in a vertical well, it was used the same computational table of pressure p and permeability $k(p)$ values obtained from field data aforementioned. The experimental data were fitted also using the linear function proposed in this work and these were inserted in the effective permeability-based pseudo-pressure function $m(p)$. The NHDE was solved through the command *int3* from Matlab[®] to compute the implicit term inside the integrand. To represent a finite hydraulic fracture in IMEX[®], it was built a grid with a zone of high transmissibility placed in a boundary of the computational cell. Figure 5.76 presents the log-log plot of the calibration of the dimensionless linear solution for the case studies A and B using IMEX[®]. The results presented close fitting. In this plot, we also notice the beginning of the bi-linear flow in the hydraulic fracture, characterizing its finite length effect. Figures 5.77 and 5.78 present the log-log plot of the calibration of the dimensionless general solution and its derivative for the case studies A and B using IMEX[®]. The results also presented high convergence and the slope change caused by the hydraulic fracture finite length was also noticed. The calibration of the dimensionless first-order term is presented in the Figure 5.79. The effect of the dimensionless zeroth-order oil source f_D in the proposed solution is presented in Figure 5.80. The values of the source are negative because the oil is being withdrawn from the reservoir. As the Log-log plot requires only positive values, the source terms presented in this plot represent the absolute values. We clearly realize that, as the oil source

increases (in absolute values), the dimensionless pseudo-pressure decreases.

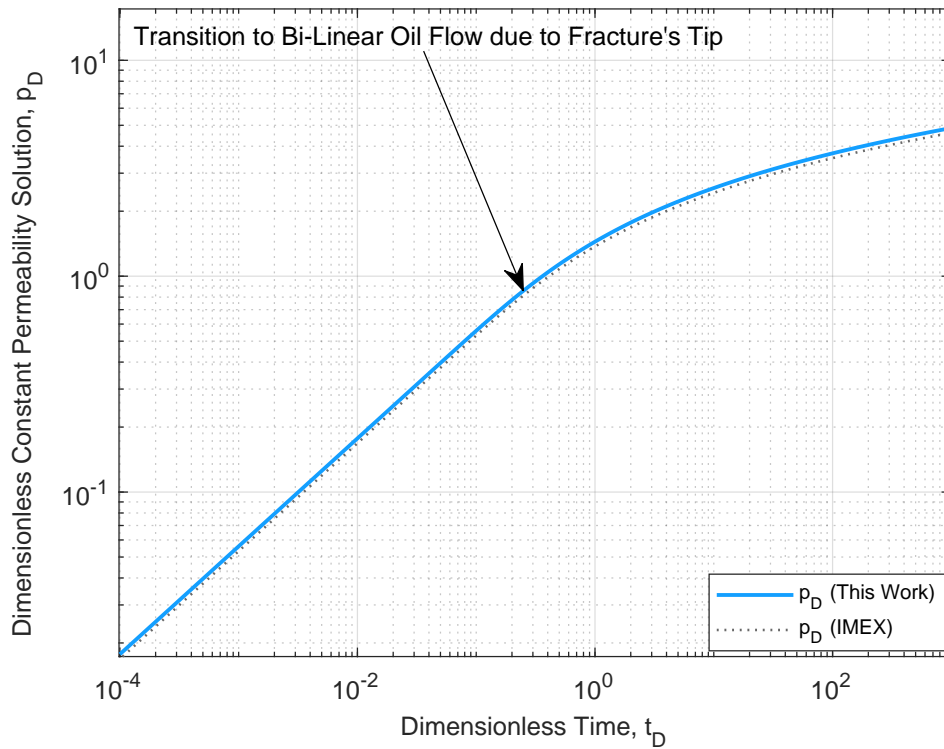


Figure 5.76: Log-log plot of the calibration of the dimensionless linear solution using IMEX®.

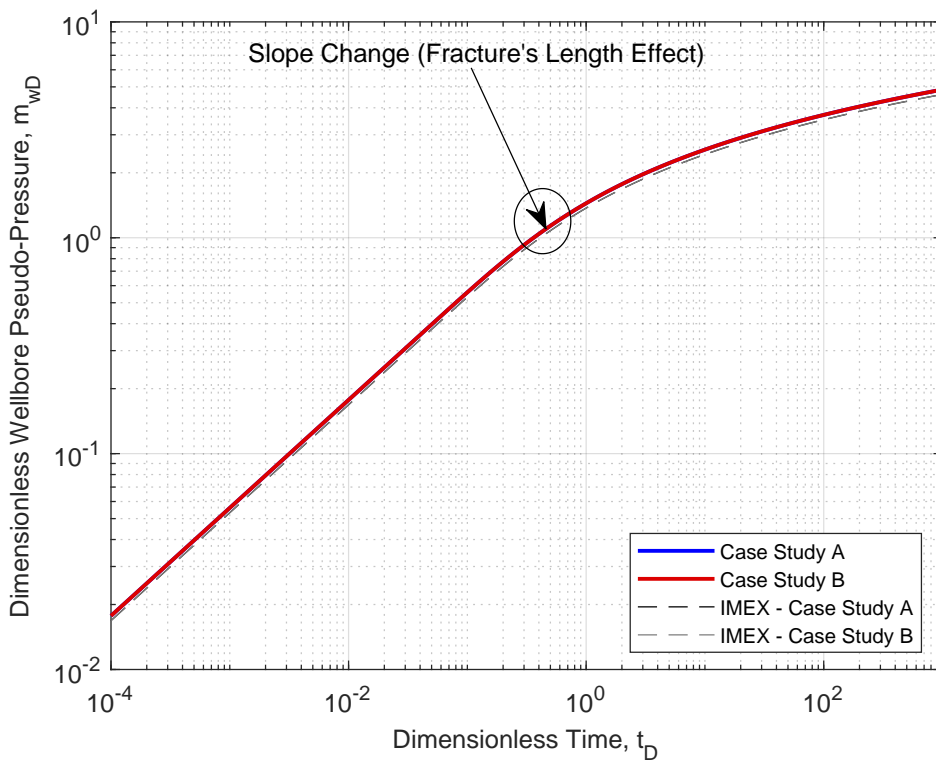


Figure 5.77: Log-log plot of the calibration of the dimensionless general solution for the case studies A and B using IMEX®.

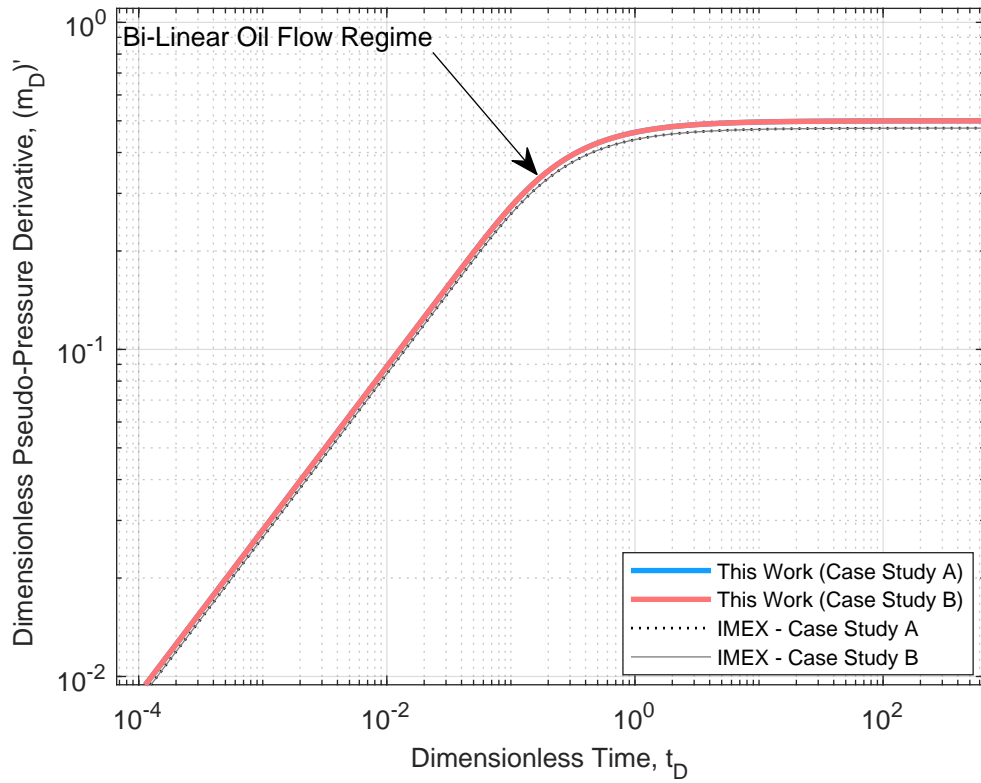


Figure 5.78: Log-log plot of the calibration of the dimensionless pseudo-pressure derivative for the case studies A and B using IMEX[®].

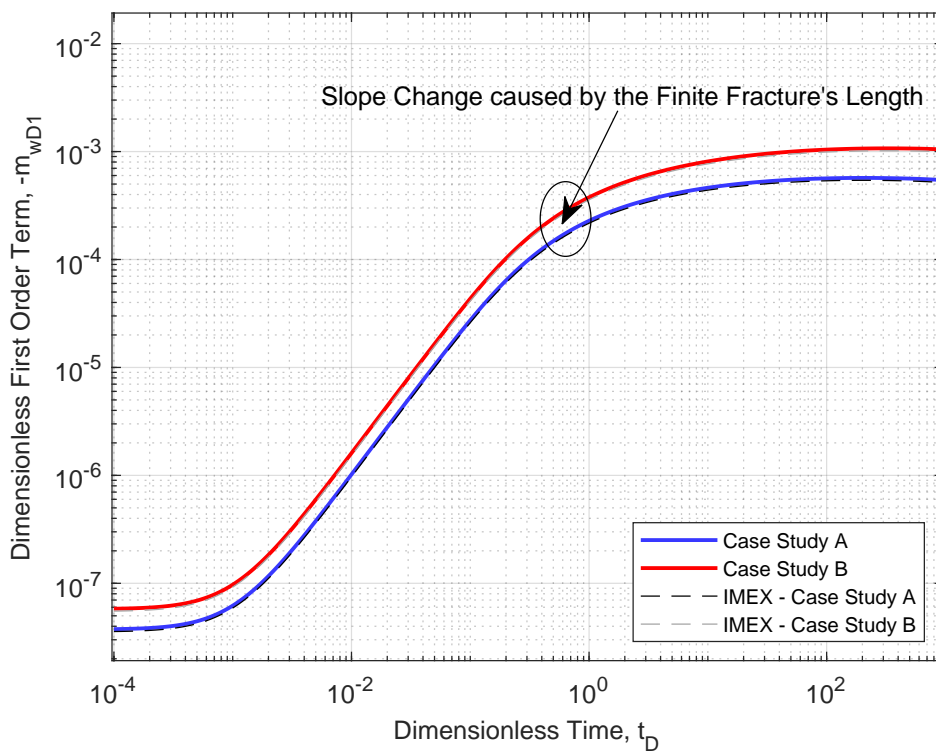


Figure 5.79: Log-log plot of the calibration of the dimensionless first-order corrective term for the case studies A and B using IMEX[®].

It means that, the nonlinear term raises, resulting in large permeability loss. As well as the oil source, the proppant package arrangements also influences in the permeability loss response during the oil production. The results are accurate and the bi-linear flow regime is also identified. The comparison between the flow regimes for the infinite and finite hydraulic fractures is presented in the Figures 5.81 and 5.82. Both log-log plots allow to identify the deviation caused by the hydraulic fracture length with respect to the infinite one. This plot is a useful tool to provide the support for the stimulation team to predict if the hydraulic fracturing operation was successfully performed, *i.e.*, if the fracture's extension reached in the field is the same as the planned. Figure 5.83 illustrates the comparison between the first-order term for the infinite and finite hydraulic fractures and the results also are capable to represent the difference between both flow regimes. The effect of the proppant porosity arrangement is presented in the Figures 5.84 to 5.88. In Figure 5.84, it can be noticed that the an increase of the effective permeability loss occurs caused by the fracture's edge effect. As shown previously, the rhombohedral arrangement presented the largest nonlinearity increase, because its low porosity value. This effect is also noticed in the Figure 5.85 and it is amplified in the Figure 5.86 for a better visualization. Although, this effect is not significant with respect to the general solution, as shown in the Figures 5.87 and 5.88. Figures 5.89 and 5.90 present the effect of the dimensionless oil source f_D in the general solution and its derivative. As presented in the previous chapters, this source plays a key role in the permeability response. Figure 5.91 presents the effect of the sorting index in the first-order term. A similar permeability loss response obtained with respect to the porosity arrangements previously is presented caused by the fracture's edge. Figures 5.92 and 5.93 show that, this index there is no significant influence in the pseudo-pressure and its derivative curves. Figures 5.94 to 5.96 present the cement exponent in the first-order term, pseudo-pressure and in its derivative. As we noticed previously, for the infinite hydraulic fracture, this parameter increases the nonlinearity in the corrective term caused by the edge effect, although it does not have significant response in the general solution and its derivative (Figures 5.95 and Figures 5.96).

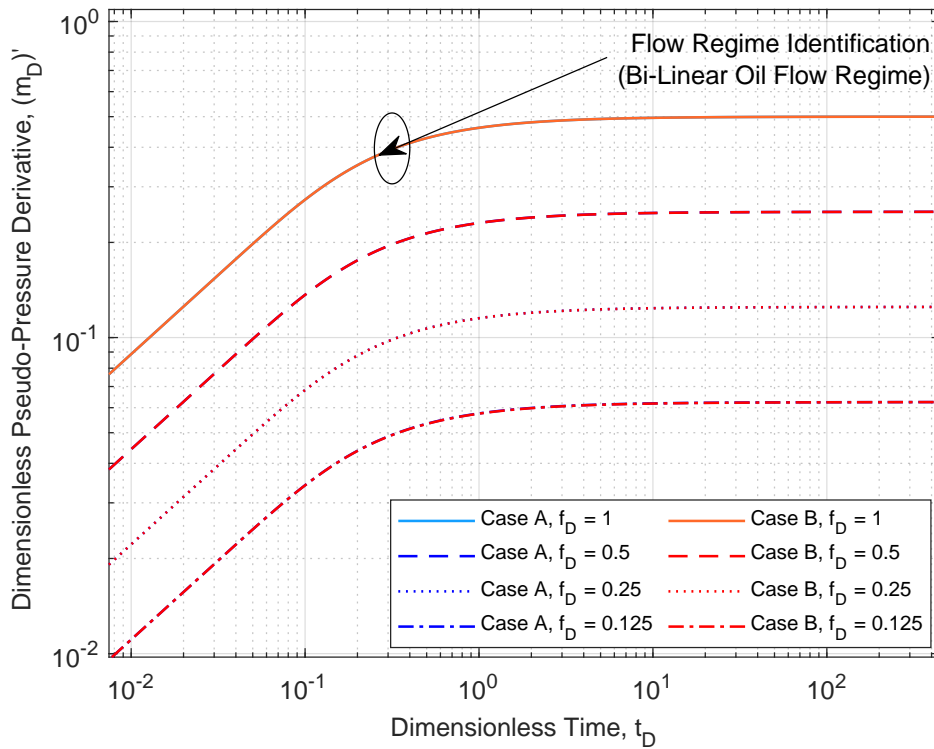


Figure 5.80: Log-log plot of the effect from the zeroth-order oil source in the pseudo-pressure derivative.

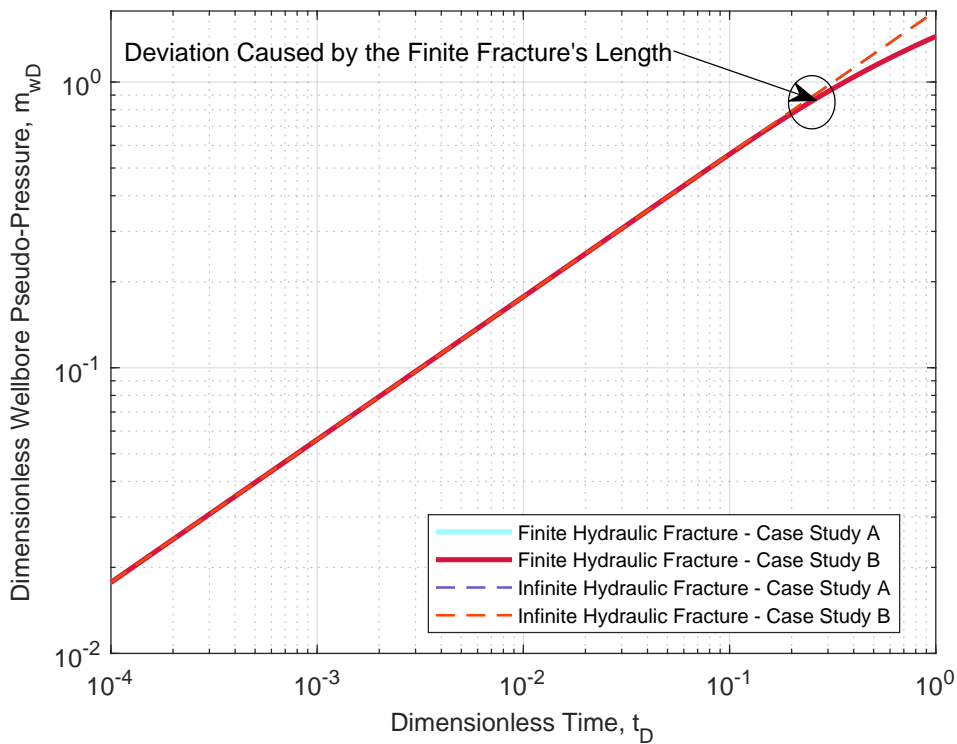


Figure 5.81: Log-log plot of the comparison between the pseudo-pressure for the finite and infinite hydraulic fractures.

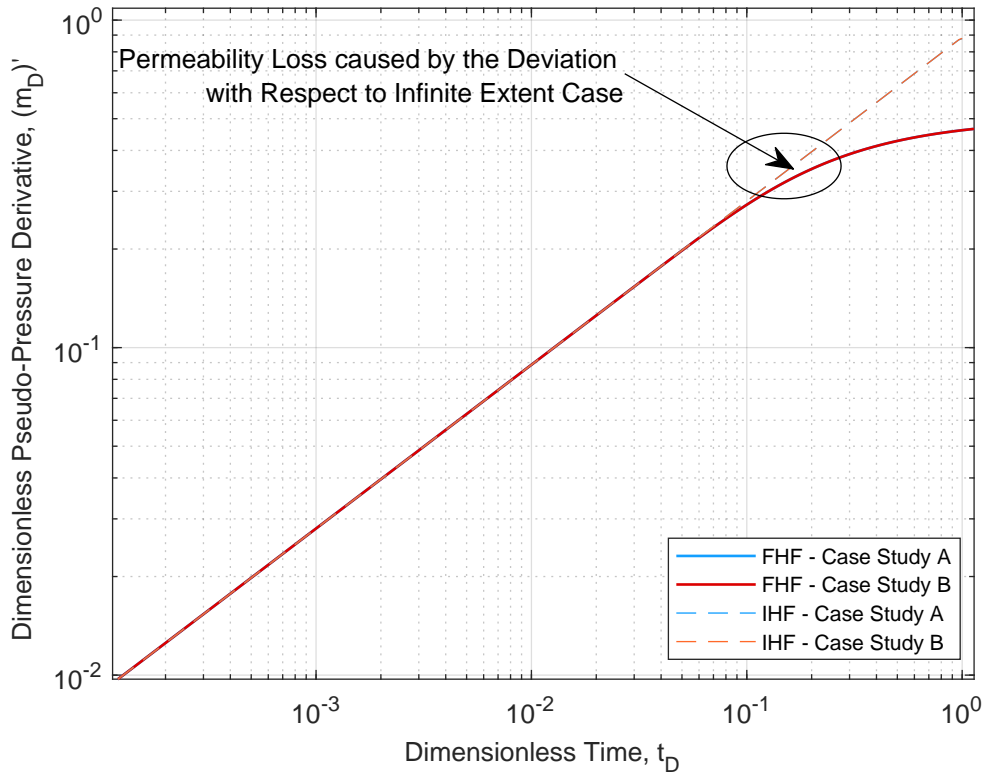


Figure 5.82: Log-log plot of the comparison between the pseudo-pressure derivative for the finite and infinite hydraulic fractures.

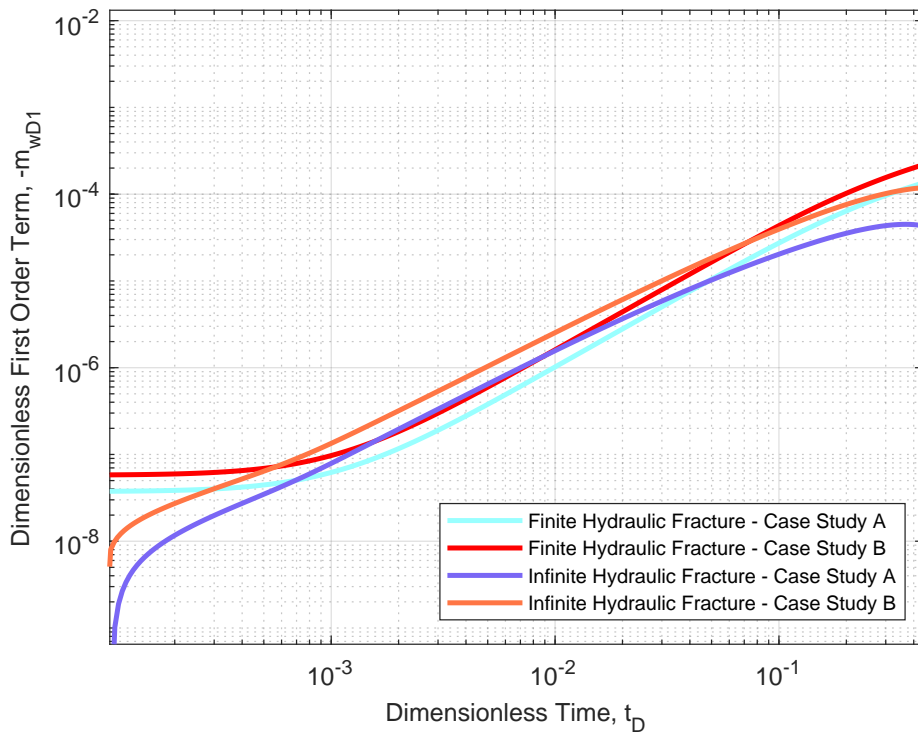


Figure 5.83: Log-log plot of the comparison between the first-order term for the finite and infinite hydraulic fractures.

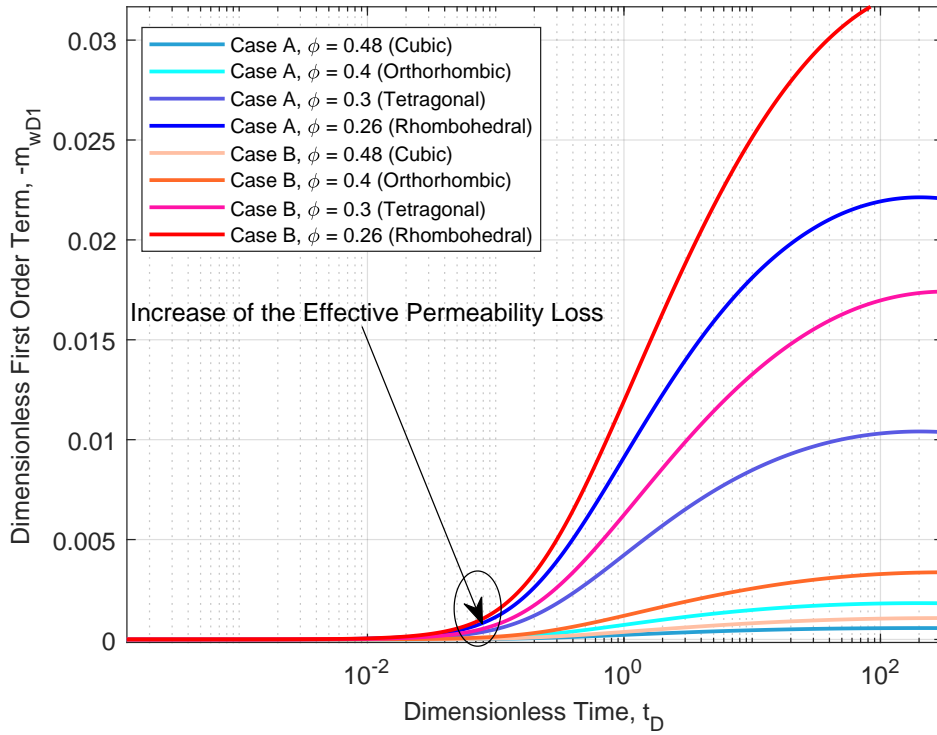


Figure 5.84: Semi-log plot of the effect of the proppant porosity arrangements in the dimensionless first-order term.

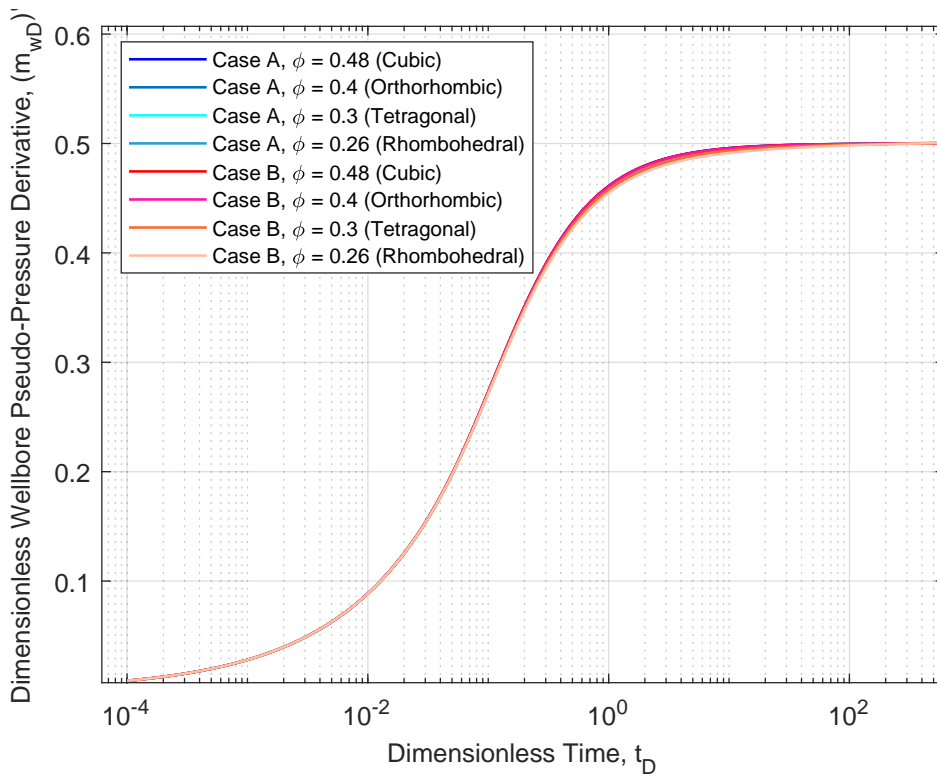


Figure 5.85: Semi-log plot of the effect of the proppant porosity arrangements in the dimensionless pseudo-pressure derivative.

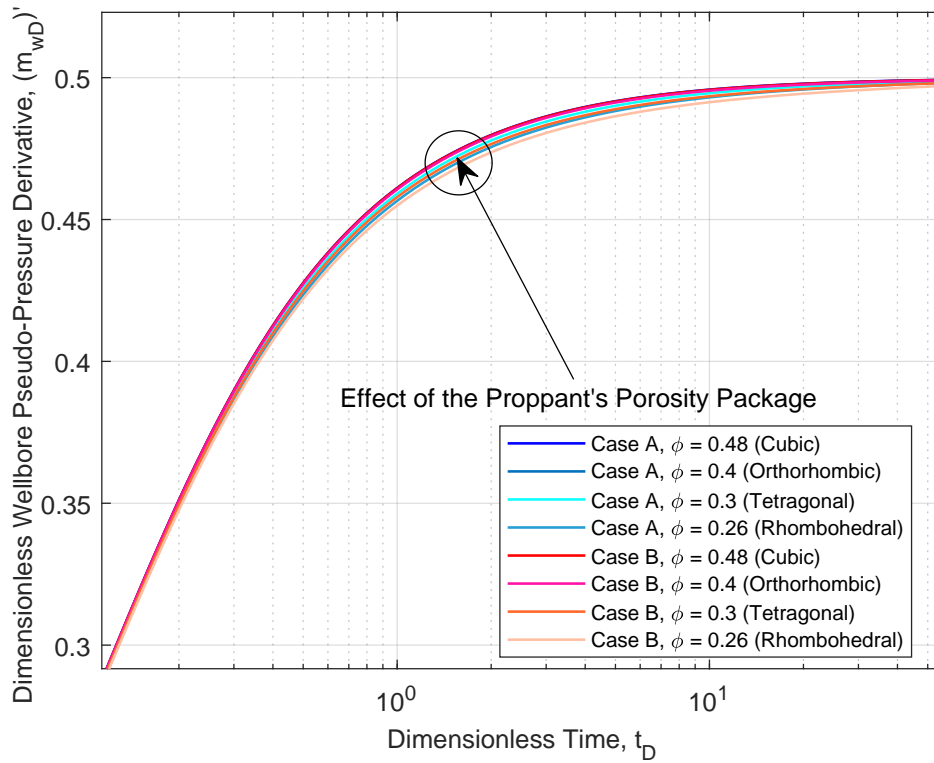


Figure 5.86: Semi-log plot of the amplification of the effect of the proppant porosity arrangements in the dimensionless pseudo-pressure derivative.

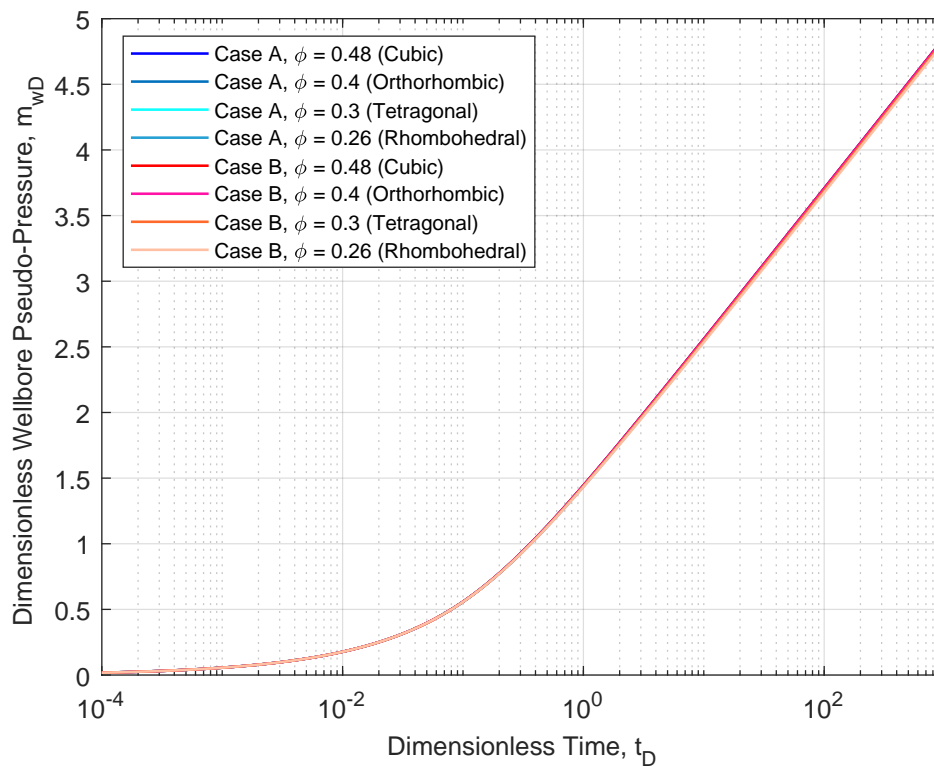


Figure 5.87: Semi-log plot of the effect of the proppant porosity arrangements in the dimensionless pseudo-pressure.

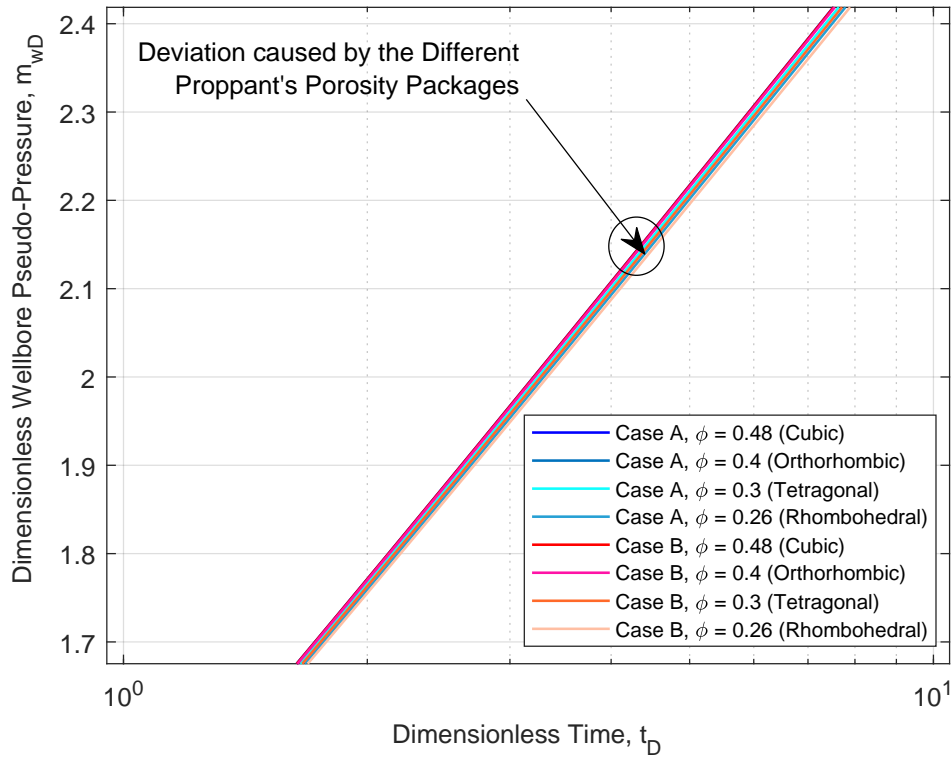


Figure 5.88: Semi-log plot of the amplification of the effect of the proppant porosity arrangements in the dimensionless pseudo-pressure.

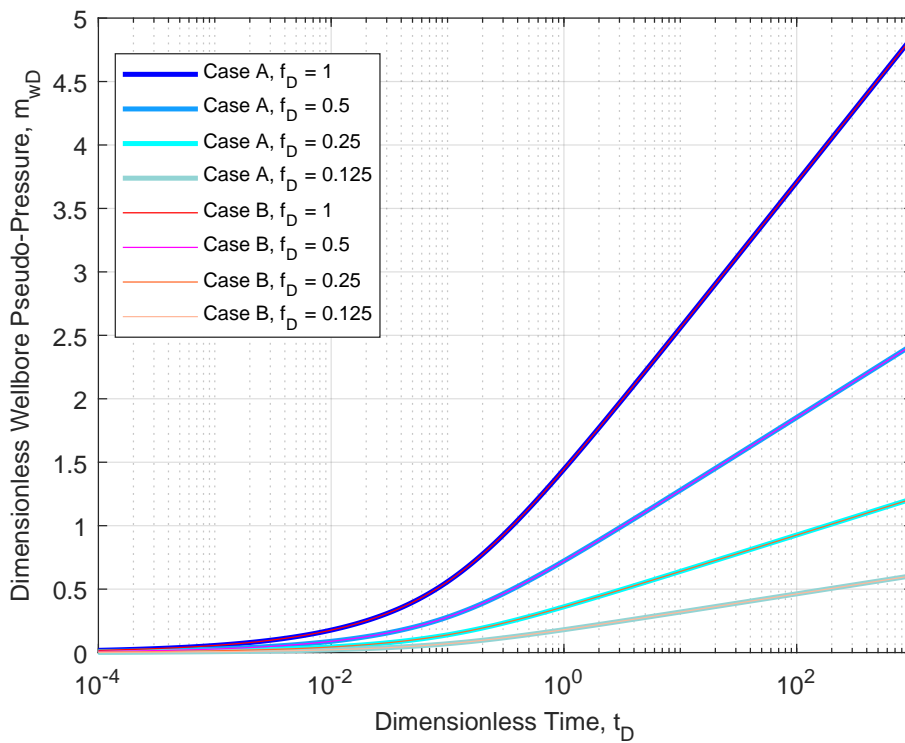


Figure 5.89: Semi-log plot of the dimensionless pseudo-pressure for several dimensionless sources.

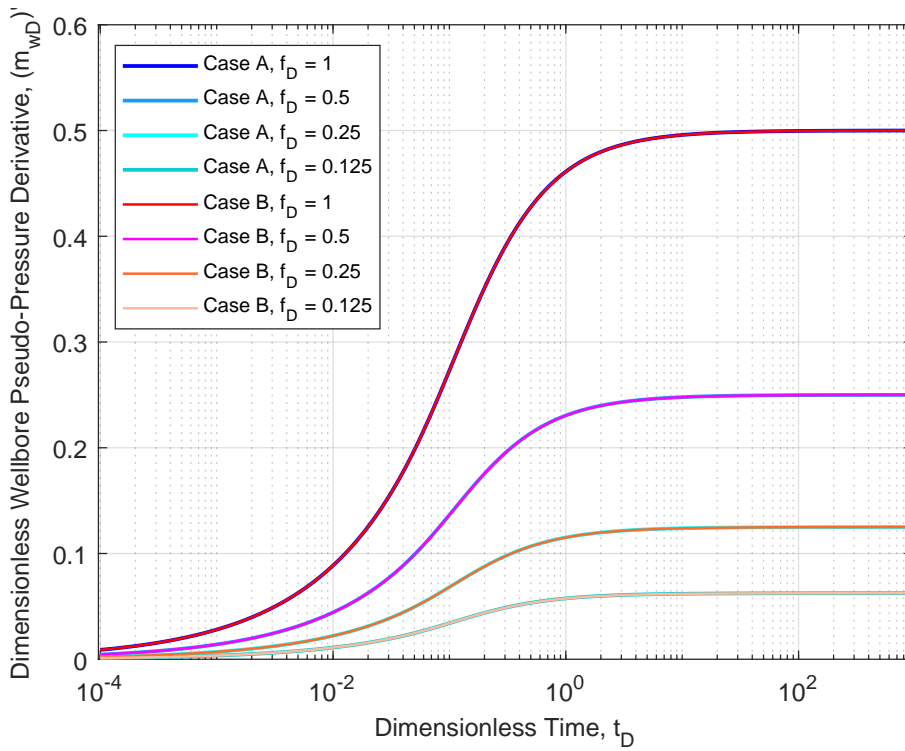


Figure 5.90: Semi-log plot of the dimensionless pseudo-pressure derivative for several dimensionless sources.

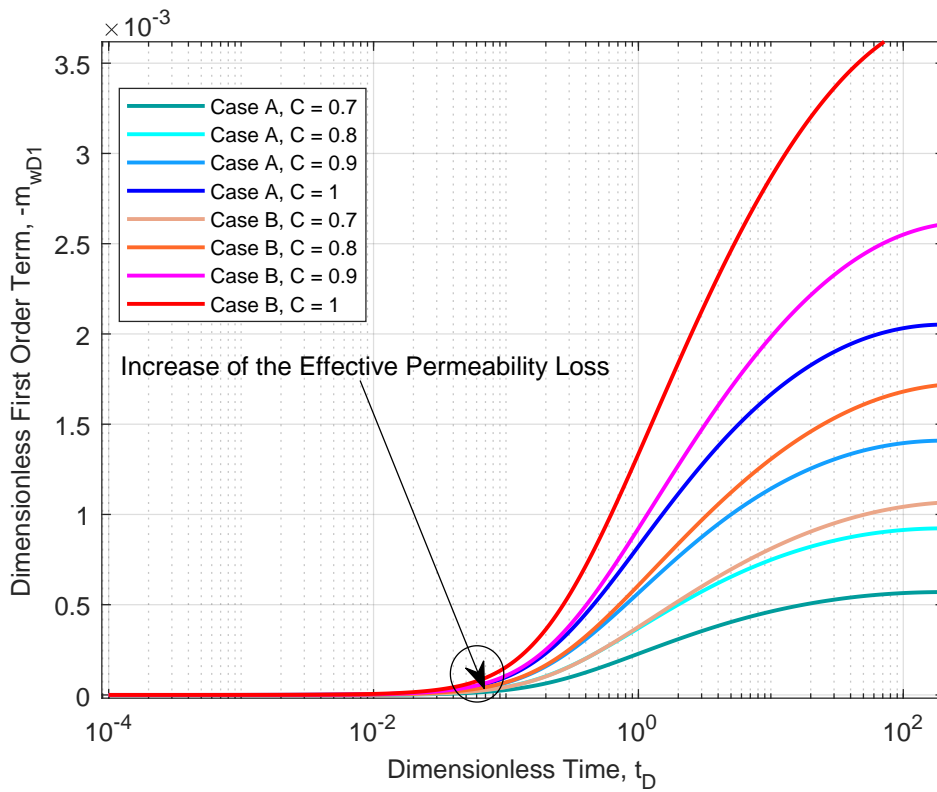


Figure 5.91: Semi-log plot of the dimensionless first-order term for several sorting index values.

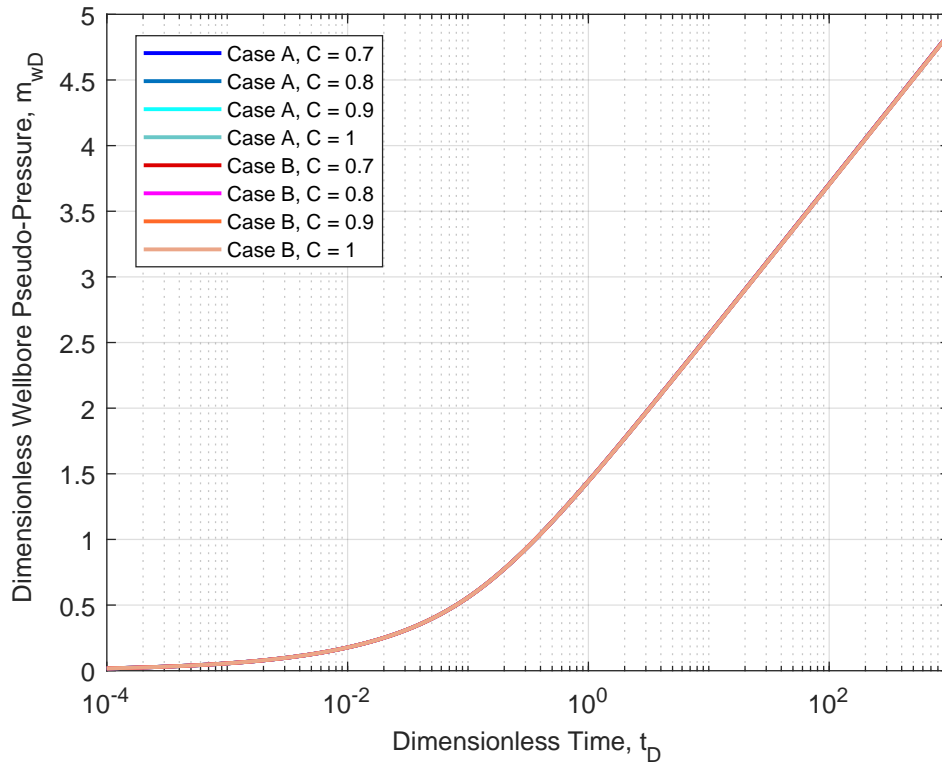


Figure 5.92: Semi-log plot of the dimensionless pseudo-pressure for several sorting index values.

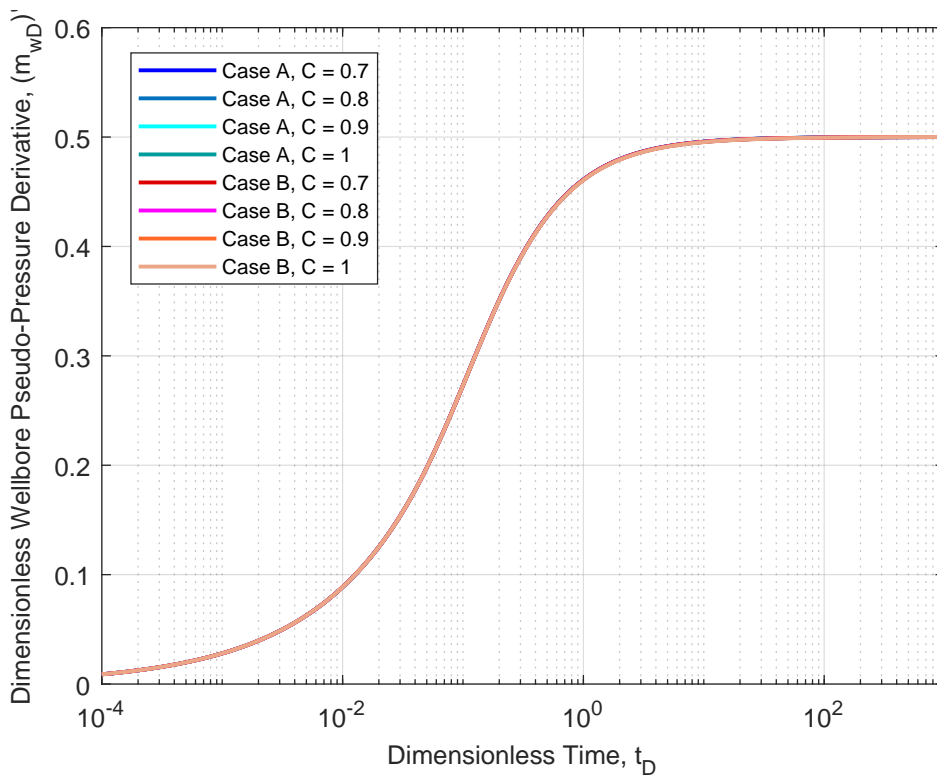


Figure 5.93: Semi-log plot of the dimensionless pseudo-pressure derivative for several sorting index values.

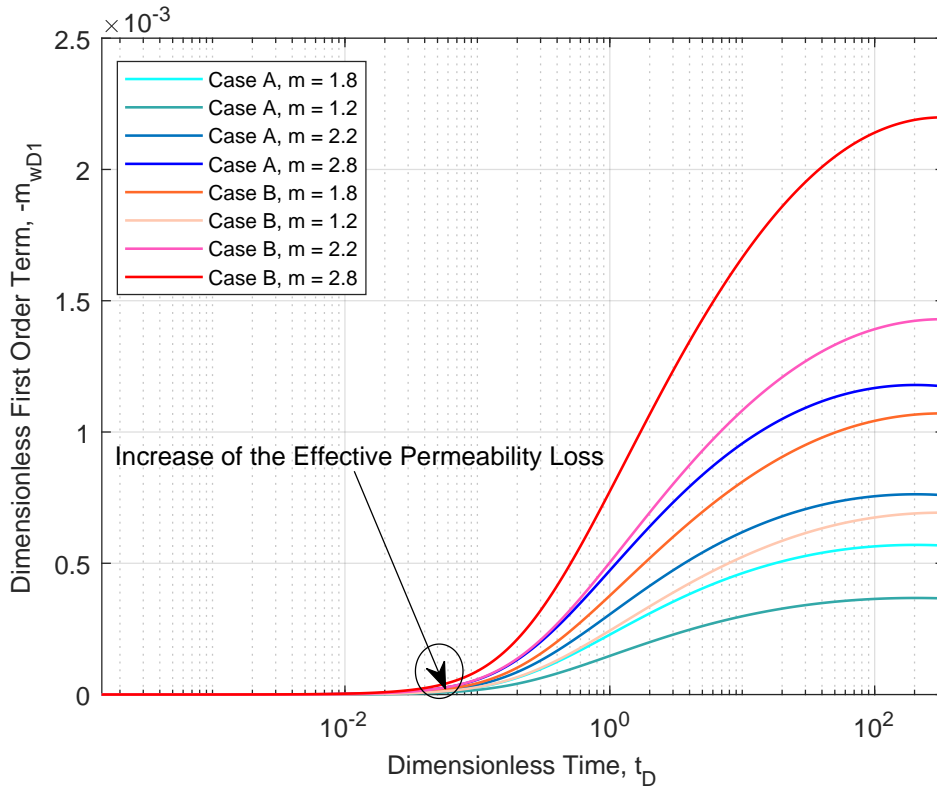


Figure 5.94: Semi-log plot of the dimensionless first-order term for several cementation exponents.

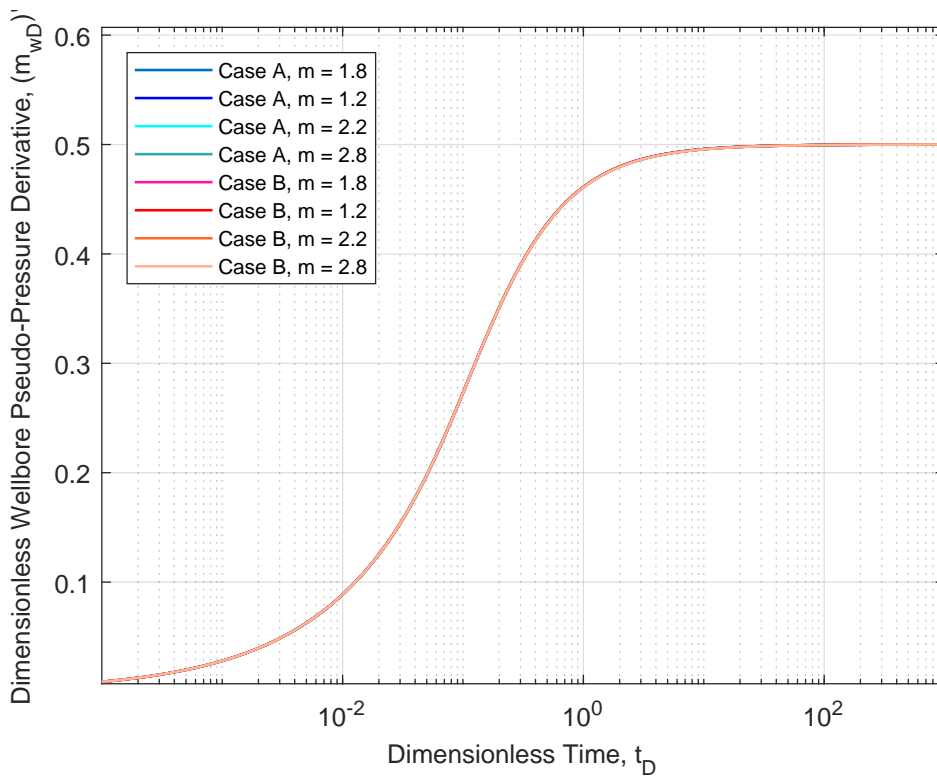


Figure 5.95: Semi-log plot of the dimensionless pseudo-pressure derivative for several cementation exponents.

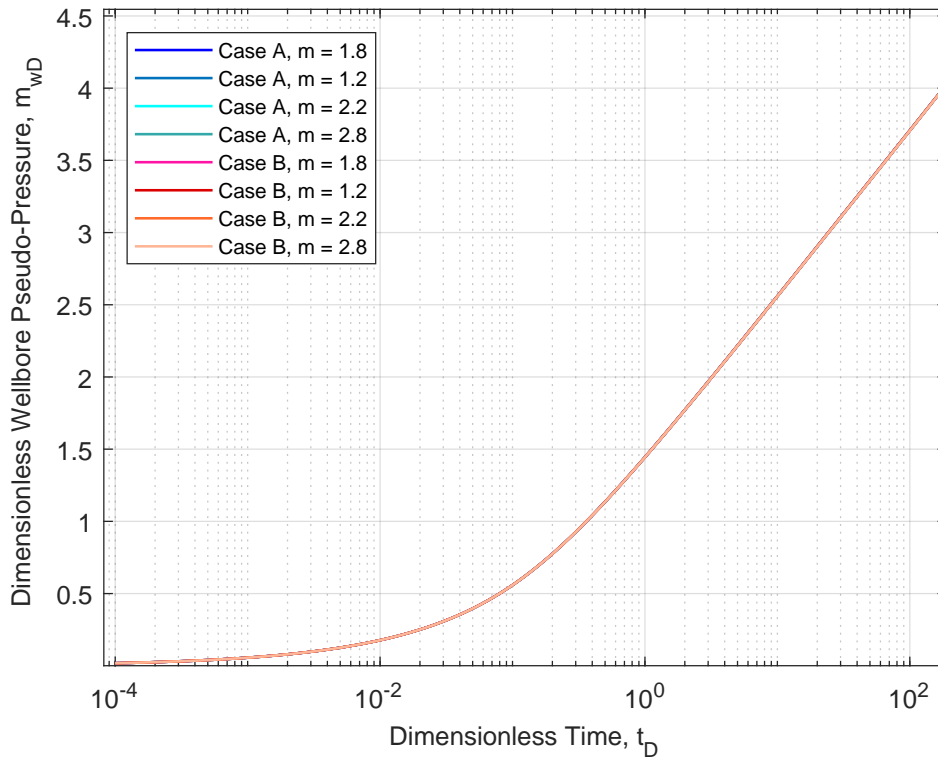


Figure 5.96: Semi-log plot of the the dimensionless pseudo-pressure for several cementation exponents.

Finally, Figure 5.97 presents the deviation caused by the effective permeability loss with respect to the constant permeability solution. It is notable that this deviation begins smoothly and it becomes larger over the well-reservoir life-cycle. The uncontrolled permeability loss may lead to reservoir impairments and the adequate choose of the oil flow rate, as well as, the pore pressure monitoring reduces the nonlinearity caused by the deviator factor and improves the well-reservoir performance. The hydraulic fracture length also plays a key role in the effective permeability loss. Therewith, the appropriate fracturing design must consider this parameter in order to avoid the production's loss caused by premature permeability decline.

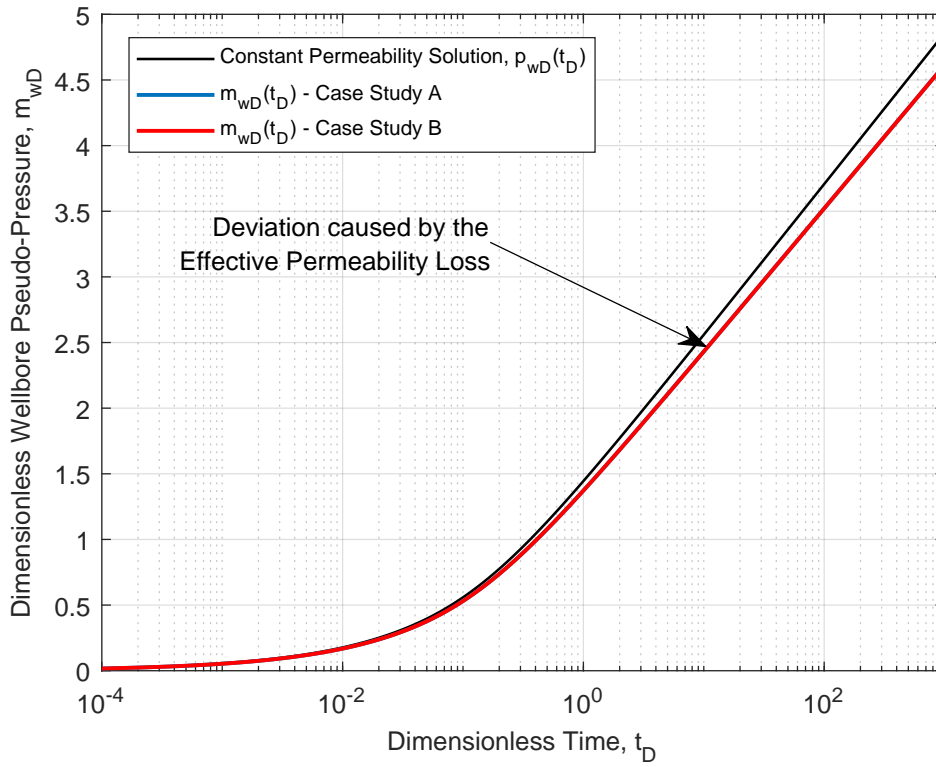


Figure 5.97: Semi-log plot of the effective permeability loss effect.

6

Integro-Differential Solutions for Variable Oil Flow Rate

This chapter addresses the effect of the permeability loss during the drawdown period and its restoration when the well is shut to the build-up test. Initially, the permeability restoration is simulated, neglecting the hysteresis effect during the drawdown/build-up cycle for the build-up test. Thereby, the permeability is fully restored when the well is shut. In the second case, the hysteretic behavior during one drawdown/build-up cycle is considered and modeled through a hysteresis factor that represents the fraction of permeability loss with respect to the previous drawdown period. This factor was determined synthetically, comparing the results from Matlab® to the IMEX®, to represent clearly the hysteresis phenomenon.

6.1

Permeability Loss/Restoration Management During Well-Reservoir Oil Loading/Unloading Cycles

Build-up test (Figure 6.1) is a useful technique broadly used in the petroleum industry to evaluate the coupling well-reservoir production's potential, predict the flow regimes, as well as, the reservoir extension.

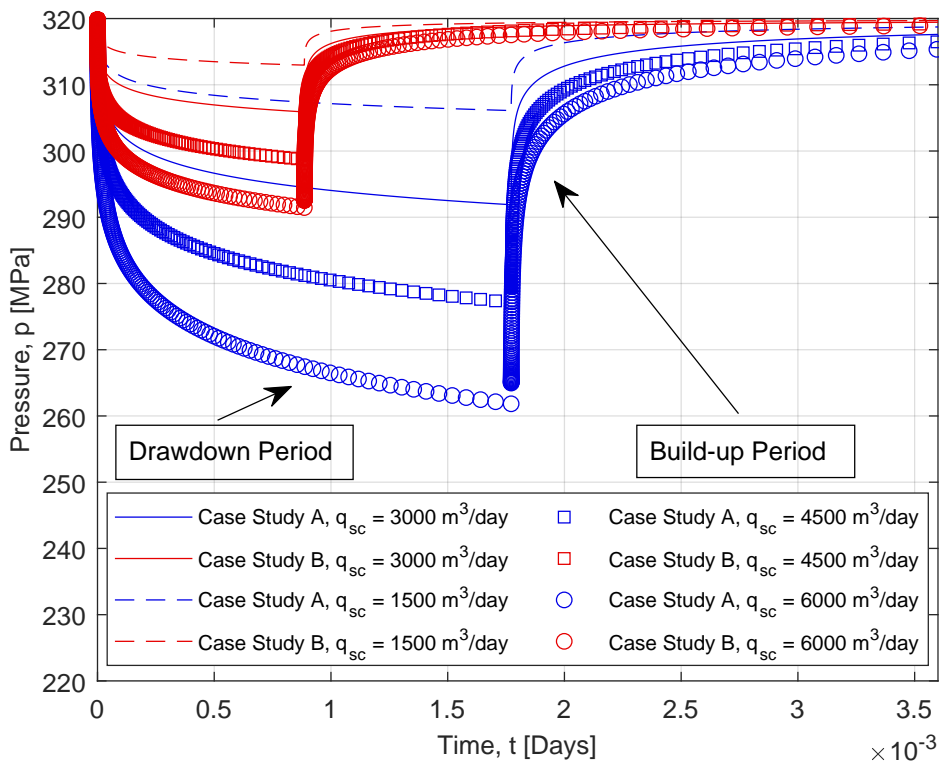


Figure 6.1: Pressure transient response during oil loading/unloading cycles.

For the permeability restoration simulation, it is considered that, the geomechanical phenomenon of the pore collapse did not occur in the reservoir. The proposed model couples the GF technique to the time superposition to derive the integro-differential solution for the oil flow in a pressure-sensitive reservoir. In reservoir engineering and formation evaluation works, new analytical methods are often sought to improve the interpretation accuracy and provide more reliable information to support the well-reservoir performance management (Agarwal; Agarwal et al.; Horner; Bourdet, Ayoub & Pirard; Bourdet, 1980, 1999, 1951, 1989, 2002).

The well-test technique is used to evaluate the coupling well-formation flow potential, to identify the flow regimes and visualization of boundary effects in order to predict the reservoir extension since the 30's. Several researches were conducted along of the years to improve the transient analysis interpretation methods and provide more reliable results (Gringarten, Ramey Jr. & Raghavan; Gringarten; Onur et al.; Onur, Ayan & Kuchuk; Onur et al., 1975, 2008, 2008, 2009, 2011). In this section, a dimensionless pseudo-pressure permeability-pore pressure dependent model is derived considering variable oil flow rate, in order to evaluate permeability decay with respect to dimensionless time.

6.1.1

Model Assumptions

For modeling of oil flow problem in porous media by means of the asymptotic series expansion of the solution of the pressure diffusivity equation in terms of pseudo-pressure, the following premises are assumed:

- 1 Variable step-rate in the well
- 2 Pressure-sensitive permeability
- 3 Darcian oil flow in porous media
- 4 Well fully penetrates reservoir rock
- 5 Deformable, homogeneous, linear elastic and isotropic reservoir
- 6 The well is located at the origin of cylindrical system of coordinates (0,0)
- 7 Isothermal, single-phase and compressible flow in the porous medium
- 8 The fluid present inside the pores of the reservoir rock does not react chemically with the rock matrix
- 9 Two dimensional (2-D) and unsteady flow
- 10 Small pressure gradient
- 11 Skin and storage effects not considered

- 12 Permeability-hysteresis of porous media is not considered
- 13 No fluid flow across the top and bottom of the formation
- 14 Infinite extent reservoir in the r-direction
- 15 Reservoir with uniform net pay

6.1.2

Model Derivation

As presented in the chapter 5, the integro-differential solution, coupled to a linear pressure-sensitive permeability function is expressed as follows:

$$m_{wD}(t_D) = -\frac{1}{2}\mathbf{Ei}\left(-\frac{1}{4t_D}\right) + \int_0^\infty \int_0^{t_D} \left[\frac{1}{-\frac{A}{2}\mathbf{Ei}\left(-\frac{1}{4t'_D}\right) + B} - 1 \right] \frac{\partial p_{wD}(t'_D)}{\partial t'_D} \times e^{\left[\frac{r_D^2 - r'^D^2}{4(t_D - t'_D)} \right]} \times \frac{dt'_D dr'_D}{4\pi(t_D - t'_D)} \quad (6-1)$$

Thereby, the Eq. 6-1 models the nonlinear radial oil flow in a pressure-sensitive permeability porous media for the drawdown period. The hydraulic diffusivity deviator factor has a key role in the nonlinearity present in the corrective term, because the pore pressure and permeability field data are coupled to this factor to predict future permeability loss over the well-reservoir production's life. After the derivation of the solution for the permeability response during the drawdown period, it is necessary to approach the build-up solution. Let us write the constant permeability solution $p_{wDC}(t_D)$ as a convolution integral using the Duhamel's principle. As the dimensionless variable oil flow rate is expressed as a step-function with values $q_D(t_D) = 1$ for the drawdown period and $q_D(t_D) = 0$ during the build-up, the Duhamel's principle satisfies the differential equation. Thereby:

$$p_{wDC}(t_D) = q_{wD}(t_D) * \frac{\partial p_{wDC}(t_D)}{\partial t_D} \quad (6-2)$$

Applying the convolution's definition:

$$q_{wD}(t_D) * \frac{\partial p_{wDC}(t_D)}{\partial t_D} = \int_0^{t_D} q_{wD}(t'_D) \frac{\partial p_{wDC}(t_D - t'_D)}{\partial t'_D} dt'_D \quad (6-3)$$

Combining the Eq. 6-2 and the Eq. 6-3:

$$p_{wDC}(t_D) = \int_0^{t_D} q_{wD}(t'_D) \frac{\partial p_{wDC}(t_D - t'_D)}{\partial t_D} dt'_D \quad (6-4)$$

Replacing the Eq. 6-4 in the Eq. 6-1, the general solution of NHDE can be written as:

$$m_{wD}(t_D) = \int_0^{t_D} q_{wD}(t'_D) \frac{\partial p_{wDC}(t_D - t'_D)}{\partial t'_D} dt'_D - \int_0^{t_D} \int_0^\infty \left[\frac{1}{k_D(m_{wD})} - 1 \right] \times \\ \times \frac{\partial m_{wD}}{\partial t'_D} G_D(r_D, r'_D, t_D, t'_D) dr'_D dt'_D \quad (6-5)$$

The oil flow rates for the drawdown and build-up periods are defined as:

$$q_{wD}(t_D) = \begin{cases} 1, & 0 < t_D < t_{pD} \\ 0, & t_D > t_{pD} \end{cases} \quad (6-6)$$

As mentioned previously, t_{pD} is the dimensionless production's time, *i.e.* the time when the well is shut to the build-up testing. Replacing the Eq. 6-6 in the Eq. 6-5:

$$m_{wD}(t_D) = \int_0^{t_{pD}} \frac{\partial p_{wDC}(t_D - t'_D)}{\partial t'_D} dt'_D - \int_0^{t_D} \int_0^\infty \left[\frac{1}{k_D(m_{wD})} - 1 \right] \frac{\partial m_{wD}}{\partial t'_D} \times \\ \times G_D(r_D, r'_D, t_D, t'_D) dr'_D dt'_D \quad (6-7)$$

The first integral of the Eq. 6-7 can be expressed as follows:

$$\int_0^{t_{pD}} \frac{\partial p_{wDC}(t_D - t'_D)}{\partial t'_D} dt'_D = \int_0^{t_D} \frac{\partial p_{wDC}(t_D - t'_D)}{\partial t'_D} dt'_D + \\ + \int_{t_D}^{t_{pD}} \frac{\partial p_{wDC}(t_D - t'_D)}{\partial t'_D} dt'_D \quad (6-8)$$

Applying the Leibniz's rule, the Eq. 6-8 becomes:

$$\int_0^{t_{pD}} \frac{\partial p_{wDC}(t_D - t'_D)}{\partial t'_D} dt'_D = \frac{\partial}{\partial t'_D} \int_0^{t_D} p_{wDC}(t_D - t'_D) dt'_D + \\ + \frac{\partial}{\partial t'_D} \int_{t_D}^{t_{pD}} p_{wDC}(t_D - t'_D) dt'_D \quad (6-9)$$

By the space and time superposition's principle, the dimensionless general solution can be expressed by:

$$m_{wD}(t_D) = p_{wDC}(t_D) - p_{wDC}(t_D - t_{pD}) - \int_0^{t_D} \int_0^\infty \left[\frac{1}{k_D(m_{wD})} - 1 \right] \frac{\partial m_{wD}}{\partial t'_D} \times \\ \times G_D(r_D, r'_D, t_D, t'_D) dr'_D dt'_D \quad (6-10)$$

The Eq. 6-10 is the coupled-drawdown-build-up period solution to simulate the well-reservoir loading/unloading cycles. In order to optimize computational resources, the time integral can be splitted in two terms. The sum of the constant permeability solution for the drawdown and build-up periods $p_{wDC}(t_D)$ and $p_{wDC}(t_D - t_{pD})$, respectively, yields to the dimensionless build-up solution:

$$p_{wDV}(t_D) = p_{wDC}(t_D) - p_{wDC}(t_D - t_{pD}) \quad (6-11)$$

Thereby, the Eq. 6-10 yields to:

$$\begin{aligned} m_{wD}(t_D) = p_{wDV}(t_D) - \int_0^\infty \int_0^{t_{pD}} \left\{ \frac{1}{k_D [p_{wDC}(t_D)]} - 1 \right\} \frac{\partial p_{wDC}(t'_D)}{\partial t'_D} \times \\ \times G_D(r_D, r'_D, t_D, t'_D) dt'_D dr'_D - \int_0^\infty \int_{t_{pD}}^{t_D} \left[\frac{1}{k_D (p_{wDV})} - 1 \right] \frac{\partial p_{wDV}(t'_D)}{\partial t'_D} \times \\ \times G_D(r_D, r'_D, t_D, t'_D) dt'_D dr'_D \end{aligned} \quad (6-12)$$

Let the dimensionless well shut-in time Δt_D defined as follows:

$$\Delta t_D = t_D - t_{pD} \quad (6-13)$$

According to (Bourdet, Ayoub & Pirard; Bourdet; Lee, Rollins & Spivey, 1989, 2002, 2003), the expressions for these periods are:

$$p_{wDV}(t_D) = -\frac{1}{2} \mathbf{Ei} \left(-\frac{1}{4t_D} \right) - \left\{ -\frac{1}{2} \mathbf{Ei} \left[-\frac{1}{4(t_D - t_{pD})} \right] \right\} \quad (6-14)$$

Rewriting the Eq. 6-14 in terms of the shut-in time:

$$p_{wDV}(t_D) = -\frac{1}{2} \mathbf{Ei} \left[-\frac{1}{4(t_{pD} + \Delta t_D)} \right] - \left[-\frac{1}{2} \mathbf{Ei} \left(-\frac{1}{4\Delta t_D} \right) \right] \quad (6-15)$$

Replacing the Eq. 6-15 in the Eq.6-10:

$$\begin{aligned}
 m_{wD}(t_D) &= \\
 &= -\frac{1}{2}\mathbf{Ei}\left[-\frac{1}{4(t_{pD} + \Delta t_D)}\right] - \left[-\frac{1}{2}\mathbf{Ei}\left(-\frac{1}{4\Delta t_D}\right)\right] - \\
 &+ \int_0^\infty \int_0^{t_{pD}} \left[\frac{1}{k_D(p_{wDC})} - 1\right] \frac{\partial p_{wDC}(t'_D)}{\partial t'_D} G_D(r_D, r'_D, t_D, t'_D) dt'_D dr'_D + \\
 &- \int_0^\infty \int_{t_{pD}}^{t_D} \left[\frac{1}{k_D(p_{wDV})} - 1\right] \frac{\partial p_{wDV}(t'_D)}{\partial t'_D} G_D(r_D, r'_D, t_D, t'_D) dt'_D dr'_D \quad (6-16)
 \end{aligned}$$

Rewriting the Eq. 6-16, we have:

$$\begin{aligned}
 m_{wD}(t_D) &= \\
 &= \frac{1}{2}\mathbf{Ei}\left(-\frac{1}{4\Delta t_D}\right) - \frac{1}{2}\mathbf{Ei}\left[-\frac{1}{4(t_{pD} + \Delta t_D)}\right] - \int_0^\infty \int_0^{t_{pD}} \left[\frac{1}{k_D(p_{wDC})} - 1\right] \times \\
 &\times \frac{\partial p_{wDC}(t'_D)}{\partial t'_D} G_D(r_D, r'_D, t_D, t'_D) dt'_D dr'_D - \int_0^\infty \int_{t_{pD}}^{t_D} \left[\frac{1}{k_D(p_{wDV})} - 1\right] \frac{\partial p_{wDV}(t'_D)}{\partial t'_D} \times \\
 &\times G_D(r_D, r'_D, t_D, t'_D) dt'_D dr'_D \quad (6-17)
 \end{aligned}$$

As the dimensionless GF associated to the problem is (Carslaw & Jaeger; Beck et al.; Ozisiki; Duffy; Cole, Beck & Haji-Sheikh, 1959, 1992, 1993, 2001, 2011):

$$G_D(r_D, r_{D0}, t_D, t_{D0}) = \frac{e^{-(r_D^2 + r_{D0}^2)/4(t_D - t_{D0})}}{4\pi(t_D - t_{D0})} \times \mathbf{I}_0\left[\frac{r_D r_{D0}}{2(t_D - t_{D0})}\right] \quad (6-18)$$

Replacing the Eq. 7-33 in the Eq. 6-17:

$$\begin{aligned}
 m_{wD}(t_D) &= \\
 &= \frac{1}{2}\mathbf{Ei}\left(-\frac{1}{4\Delta t_D}\right) - \frac{1}{2}\mathbf{Ei}\left[-\frac{1}{4(t_{pD} + \Delta t_D)}\right] - \int_0^\infty \int_0^{t_{pD}} \left[\frac{1}{k_D(p_{wDC})} - 1\right] \times \\
 &\times \frac{\partial p_{wDC}(t'_D)}{\partial t'_D} \frac{e^{-(r_D'^2 + r_{D0}^2)/4(t'_D - t_{D0})}}{4\pi(t'_D - t_{D0})} \times \mathbf{I}_0\left[\frac{r'_D r_{D0}}{2(t'_D - t_{D0})}\right] dt'_D dr'_D - \\
 &+ \int_0^\infty \int_{t_{pD}}^{t_D} \left[\frac{1}{k_D(p_{wDV})} - 1\right] \frac{\partial p_{wDV}(t'_D)}{\partial t'_D} \frac{e^{-(r_D'^2 + r_{D0}^2)/4(t'_D - t_{D0})}}{4\pi(t'_D - t_{D0})} \times \\
 &\times \mathbf{I}_0\left[\frac{r'_D r_{D0}}{2(t'_D - t_{D0})}\right] dt'_D dr'_D \quad (6-19)
 \end{aligned}$$

As mentioned previously, the modified first kind and zeroth-order Bessel

function $\mathbf{I}_0(0) = 1$. So, Eq.6-19 yields to:

$$\begin{aligned}
 m_{wD}(t_D) &= \\
 &= \frac{1}{2} \mathbf{Ei} \left(-\frac{1}{4\Delta t_D} \right) - \frac{1}{2} \mathbf{Ei} \left[-\frac{1}{4(t_{pD} + \Delta t_D)} \right] - \int_0^\infty \int_0^{t_{pD}} \left[\frac{1}{k_D(p_{wDC})} - 1 \right] \times \\
 &\quad \times \frac{\partial p_{wDC}(t'_D)}{\partial t'_D} \frac{e^{-(r_D'^2 + r_{D0}^2)/4(t'_D - t_{D0})}}{4\pi(t'_D - t_{D0})} dt'_D dr'_D - \int_0^\infty \int_{t_{pD}}^{t_D} \left[\frac{1}{k_D(p_{wDV})} - 1 \right] \times \\
 &\quad \times \frac{\partial p_{wDV}(t'_D)}{\partial t'_D} \frac{e^{-(r_D'^2 + r_{D0}^2)/4(t'_D - t_{D0})}}{4\pi(t'_D - t_{D0})} dt'_D dr'_D \quad (6-20)
 \end{aligned}$$

In the Eq.6-20, the first double integral represents the drawdown period and, therefore, its derivative is expressed by the linear solution derivative in the interval $[0, t_{pD}]$. The second integral is related to the build-up term and its derivative must be taken with respect to the time superposition interval $[t_{pD}, t_D]$, (Peres, Onur & Reynolds; Lee; Johnston & Lee; Lee, Rollins & Spivey; Barreto Jr., Peres & Pires, 1989, 1982, 1991, 2003, 2010). The same procedure is applied to the diffusivity deviator factor ξ . The build-up solution derivative is expressed by:

$$\frac{\partial p_{wDV}(t_D)}{\partial t_D} = \frac{\partial p_{wDC}(t_D)}{\partial t_D} - \frac{\partial p_{wDC}(t_D - t_{pD})}{\partial t_D} \quad (6-21)$$

For the drawdown period, we have:

$$\frac{\partial p_{wDC}(t_D)}{\partial t_D} = -\frac{1}{2} \frac{\partial}{\partial t_D} \left[\mathbf{Ei} \left(-\frac{1}{4t_D} \right) \right] \quad (6-22)$$

And for the build-up period:

$$\frac{\partial p_{wDV}(t_D)}{\partial t_D} = -\frac{1}{2} \frac{\partial}{\partial t_D} \left[\mathbf{Ei} \left(-\frac{1}{4t_D} \right) \right] + \frac{1}{2} \frac{\partial}{\partial t_D} \left\{ \mathbf{Ei} \left[-\frac{1}{4(t_D - t_{pD})} \right] \right\} \quad (6-23)$$

Replacing the Eqs.6-22 and 6-23 in the Eq.6-20:

$$\begin{aligned}
m_{wD}(t_D) = & \\
= & \frac{1}{2} \mathbf{Ei} \left(-\frac{1}{4\Delta t_D} \right) - \frac{1}{2} \mathbf{Ei} \left(-\frac{1}{4t_D} \right) - \int_0^\infty \int_0^{t_{pD}} \left[\frac{1}{k_D(p_{wDC})} - 1 \right] \times \\
& \times \left\{ \frac{\partial}{\partial t'_D} \left[\mathbf{Ei} \left(-\frac{1}{4t'_D} \right) \right] \right\} \frac{e^{-(r_D^2 + r_{D0}^2)/4(t'_D - t_{D0})}}{8\pi(t'_D - t_{D0})} dt'_D dr'_D + \\
& - \int_0^\infty \int_{t_{pD}}^{t_D} \left[\frac{1}{k_D(p_{wDV})} - 1 \right] \left\{ \left\{ \frac{\partial}{\partial t'_D} \left[\mathbf{Ei} \left(-\frac{1}{4t'_D} \right) \right] \right\} + \right. \\
& \left. - \frac{\partial}{\partial t'_D} \left\{ \mathbf{Ei} \left[-\frac{1}{4(t'_D - t_{pD})} \right] \right\} \right\} \frac{e^{-(r_D^2 + r_{D0}^2)/4(t'_D - t_{D0})}}{8\pi(t'_D - t_{D0})} dt'_D dr'_D \quad (6-24)
\end{aligned}$$

The hydraulic diffusivity deviator factor for the drawdown period is:

$$\xi \left[k_D(p_{wDC}) \right] = \frac{1}{k_D(p_{wDC})} - 1 \quad (6-25)$$

Because the linear pressure-sensitive permeability provided an accurate fitting, let us consider that the permeability decays linearly with respect to the pore pressure (Fernandes et al., 2021a):

$$k_D(p_{wDC}) = Ap_{wDC} + B, \quad A, B \in \mathbb{R} \quad (6-26)$$

As broadly discussed in this work, the linear solution for the drawdown period is expressed by:

$$p_{wDC}(t_D) = -\frac{1}{2} \mathbf{Ei} \left(-\frac{1}{4t_D} \right) \quad (6-27)$$

Replacing the Eq. 6-27 in the Eq. 6-26, the dimensionless permeability for the drawdown becomes:

$$k_D(p_{wDC}) = -\frac{A}{2} \mathbf{Ei} \left(-\frac{1}{4t_D} \right) + B \quad (6-28)$$

Replacing the Eq. 6-28 in the Eq. 6-25, the hydraulic diffusivity deviator factor for the drawdown yields to:

$$\xi(p_{wDC}) = 1 / \left\{ B - \frac{A}{2} \mathbf{Ei} \left(-\frac{1}{4t_D} \right) \right\} - 1 \quad (6-29)$$

The diffusivity deviator factor for the build-up period is:

$$\xi \left[k_D(p_{wDV}) \right] = \frac{1}{k_D(p_{wDV})} - 1 \quad (6-30)$$

Using the permeability function proposed by (Fernandes, 2022):

$$k_D(p_{wDV}) = Cp_{wDV} + D, \quad C, D \in \mathbb{R} \quad (6-31)$$

As the linear solution in terms of the shut-in time for the build-up period is expressed by:

$$p_{wDV} = \mathbf{Ei} \left[-\frac{1}{4(t_D - t_{pD})} \right] - \mathbf{Ei} \left(-\frac{1}{4t_D} \right) \quad (6-32)$$

After replacing the Eq. 6-32 in the Eq. 6-31, the dimensionless permeability becomes:

$$k_D(p_{wDV}) = \frac{C}{2} \left\{ \mathbf{Ei} \left[-\frac{1}{4(t_D - t_{pD})} \right] - \mathbf{Ei} \left(-\frac{1}{4t_D} \right) \right\} + D \quad (6-33)$$

Replacing the Eq. 6-33 in the Eq. 6-30, the hydraulic diffusivity deviator factor for the build-up period is expressed as follows:

$$\xi(p_{wDV}) = 1 / \left\{ \frac{C}{2} \left\{ \mathbf{Ei} \left[-\frac{1}{4(t_D - t_{pD})} \right] - \mathbf{Ei} \left(-\frac{1}{4t_D} \right) \right\} + D \right\} - 1 \quad (6-34)$$

The constants A, B, C, D in the hydraulic diffusivity deviator factors for the drawdown and build-up periods (6-29 and 6-34) are computed through the proposed pressure-sensitive permeability function for the experimental points $(p, k(p))$. Replacing the Eqs. 6-29 and 6-34 in the Eq. 6-24, the dimensionless general solution for the loading/unloading cycles is expressed by:

$$\begin{aligned}
m_{wD}(t_D) = & \frac{1}{2} \left\{ \mathbf{Ei} \left(-\frac{1}{4\Delta t_D} \right) - \mathbf{Ei} \left[-\frac{1}{4t_D} \right] \right\} - \\
& + \int_0^\infty \int_0^{t_{pD}} \left\{ \left[B - \frac{A}{2} \mathbf{Ei} \left(-\frac{1}{4t'_D} \right) \right]^{-1} - 1 \right\} \times \\
& \times \frac{\partial}{\partial t'_D} \left[\mathbf{Ei} \left(-\frac{1}{4t'_D} \right) \right] \frac{e^{-(r'_D{}^2 + r_{D0}^2)/4(t'_D - t_{D0})}}{8\pi(t'_D - t_{D0})} dt'_D dr'_D + \\
& + \int_0^\infty \int_{t_{pD}}^{t_D} \left\{ \left\{ \left\{ \frac{C}{2} \mathbf{Ei} \left[-\frac{1}{4(t'_D - t_{pD})} \right] + \mathbf{Ei} \left(-\frac{1}{4t'_D} \right) \right\} + D \right\}^{-1} - 1 \right\} \times \\
& \times \left\{ \frac{\partial}{\partial t'_D} \left\{ \mathbf{Ei} \left(-\frac{1}{4t'_D} \right) - \mathbf{Ei} \left[-\frac{1}{4(t'_D - t_{pD})} \right] \right\} \right\} \frac{e^{-(r'_D{}^2 + r_{D0}^2)/4(t'_D - t_{D0})}}{8\pi(t'_D - t_{D0})} dt'_D dr'_D
\end{aligned} \tag{6-35}$$

Using the time's superposition's principle and the logarithm approximation, the Eq. 6-35 can be expressed as follows:

$$\begin{aligned}
m_{wD}(t_D) = & \frac{1}{2} \ln \left(\frac{t_D}{t_D - t_{pD}} \right) - \int_0^\infty \int_0^{t_{pD}} \left\{ \left[B - \frac{A}{2} \mathbf{Ei} \left(-\frac{1}{4t'_D} \right) \right]^{-1} - 1 \right\} \times \\
& \times \frac{\partial}{\partial t'_D} \left\{ \mathbf{Ei} \left(-\frac{1}{4t'_D} \right) \right\} \frac{e^{-r'_D{}^2/4t'_D}}{8\pi t'_D} dt'_D dr'_D + \int_0^\infty \int_{t_{pD}}^{t_D} \left\{ \left[\frac{C}{2} \ln \left(\frac{t'_D}{t'_D - t_{pD}} \right) + \right. \right. \\
& \left. \left. + D \right]^{-1} - 1 \right\} \frac{\partial}{\partial t'_D} \left[\ln \left(\frac{t'_D}{t'_D - t_{pD}} \right) \right] \frac{e^{-r'_D{}^2/4t'_D}}{8\pi t'_D} dt'_D dr'_D
\end{aligned} \tag{6-36}$$

The constant permeability solution of the Eq. 6-36 ($p_{wDV}(t_D)$) can be expressed in terms of the *Horner time*, (Horner, 1951) as follows:

$$\begin{aligned}
m_{wD}(t_D) = & \frac{1}{2} \ln \left(\frac{t_{pD} + \Delta t_D}{\Delta t_D} \right) - \int_0^\infty \int_0^{t_{pD}} \left\{ \left[B - \frac{A}{2} \mathbf{Ei} \left(-\frac{1}{4t'_D} \right) \right]^{-1} - 1 \right\} \times \\
& \times \frac{\partial}{\partial t'_D} \left\{ \mathbf{Ei} \left(-\frac{1}{4t'_D} \right) \right\} \frac{e^{-r'_D{}^2/4t'_D}}{8\pi t'_D} dt'_D dr'_D + \int_0^\infty \int_{t_{pD}}^{t_D} \left\{ \left[\frac{C}{2} \ln \left(\frac{t'_D}{t'_D - t_{pD}} \right) + \right. \right. \\
& \left. \left. + D \right]^{-1} - 1 \right\} \frac{\partial}{\partial t'_D} \left[\ln \left(\frac{t'_D}{t'_D - t_{pD}} \right) \right] \frac{e^{-r'_D{}^2/4t'_D}}{8\pi t'_D} dt'_D dr'_D
\end{aligned} \tag{6-37}$$

Where the group $\frac{t_{pD} + \Delta t_D}{\Delta t_D}$ in the logarithm argument of the Eq. 6-37 is known in the reservoir engineering and formation evaluation literature as *Horner time*.

6.1.3 Model Calibration, Results and Discussions

The analytical model presented in this chapter is solved through a computational code developed in Matlab[®] that required the implementation of the constant permeability solution for the coupled-build-up and drawdown periods. Figure 6.2 presents the log-log plot of the linear solution with respect to the dimensionless time for the drawdown and build-up periods.

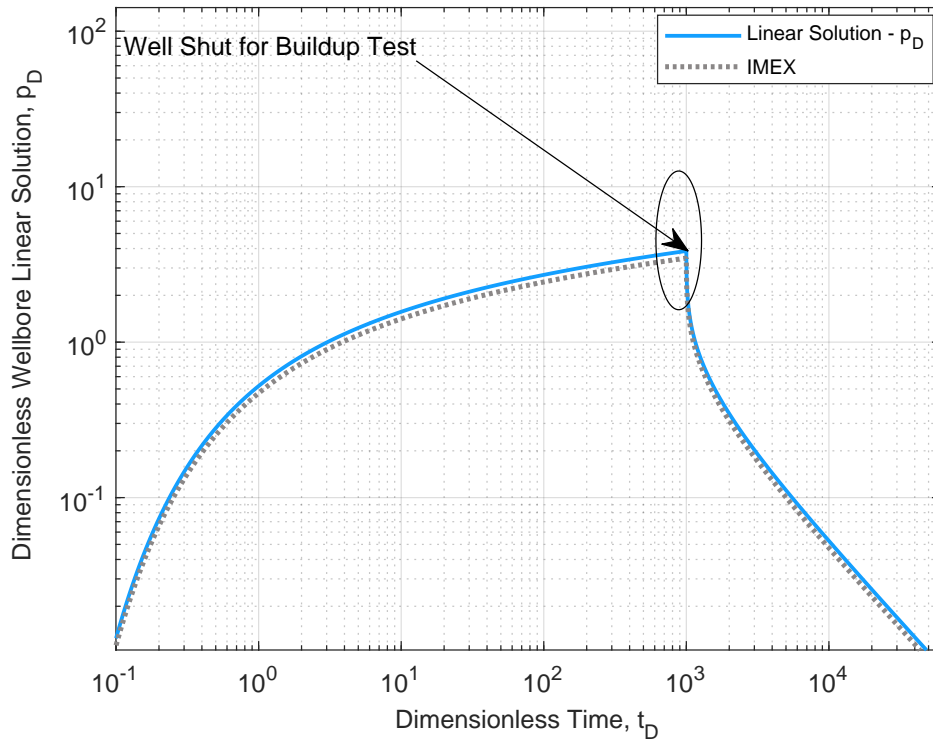


Figure 6.2: Log-log plot of the calibration of the dimensionless linear solution against IMEX[®].

Sensitive runs were performed in the simulator in order to find out the best time and space steps choice to achieve the mesh accuracy necessary to calibrate the model. Figure 6.3 shows the Log-log plot of the dimensionless first-order term $m_{wD}^{(1)}(t_D)$ and it has shown close convergence, when compared to IMEX[®], even in the early-times, therewith, it is possible to conclude that the first-order asymptotic series expansion represents, accurately, the nonlinearity caused by the permeability change in the analytical model presented in this paper. Thereby, an accurate prediction of the reservoir permeability can be predicted of a practical manner without the necessity of approaching the higher order terms of the series expansion.

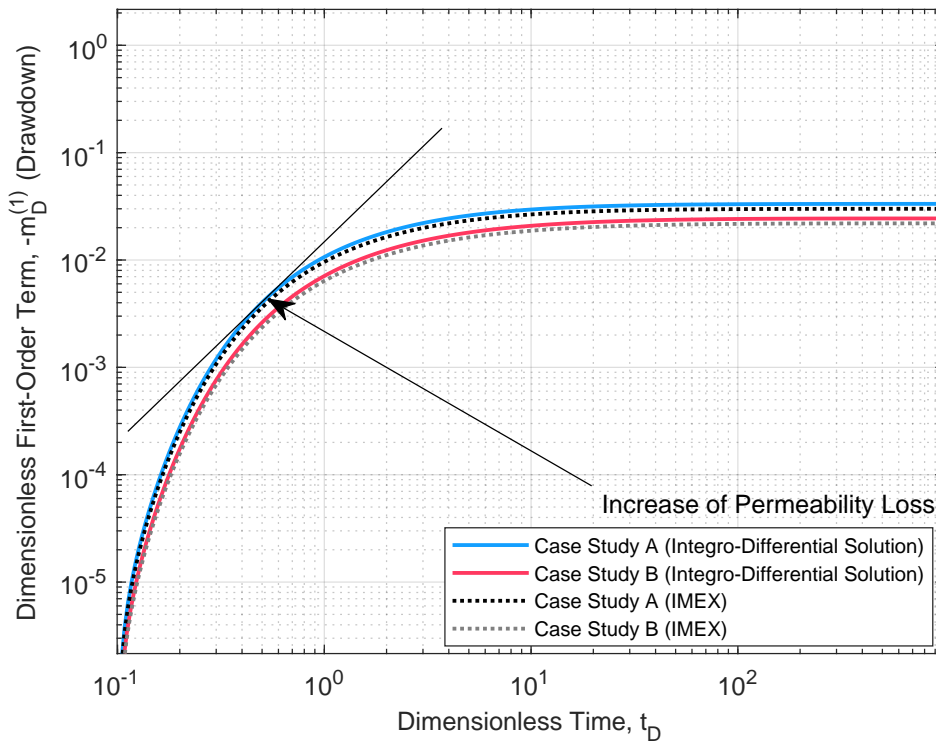


Figure 6.3: Log-log plot of the calibration of the dimensionless pseudo-pressure first-order term against IMEX[®] for the drawdown period.

A wide of tests for the Matlab[®] code was also checked to find the optimum time steps and radial space steps. The linear solution was computed through the command $ei(t_D)$ in the Matlab[®] scientific library. To solve the implicit double integral in the corrective term, it was used the trapezoid's rule and it presented close accuracy with time and space discretization of 10^{-3} and 10^{-2} , respectively. The calibration methodology was performed based on replace the set of values of $(p, k(p))$ from the experimental data for the case studies as an input information to IMEX[®]. The results showed high convergence when compared to IMEX[®] for both periods. It is notable that the dimensionless pressure curve presents a growth trend and it suddenly drops when the well is shut. This drop represents the beginning of the build-up period and the dimensionless build-up pressure $p_{wDV}(t_D = t_{pD})$ is recorded by the pressure gauge. The response of the dimensionless first-order term for the build-up period is presented in the Figure 6.4. This log-log plot shows that, as the dimensionless shut-in time increases, *i.e.*, the well remains shut for a long time, the corrective term dies. It means that, the nonlinearity and, consequently, the permeability loss also dies. It provides a permeability restoration caused by the reservoir grains rearrangement. Initially, the build-up $m_{wD}^{(1)}$ values remain in a plateau and it drops steadily toward zero as the dimensionless shut-in time Δt_D increases. From this plot, one can see that the build-up

pseudo-pressure derivative only approaches to a constant value asymptotically, because the corrective term never stabilizes, which is remarkably different from the drawdown case in which $m_w^{(1)}$ becomes constant for early-times and the Bourdet derivative reaches a constant value. Therefore, one can expect to get accurate flow capacity from the build-up plot only at long shut-in times Δt_D .

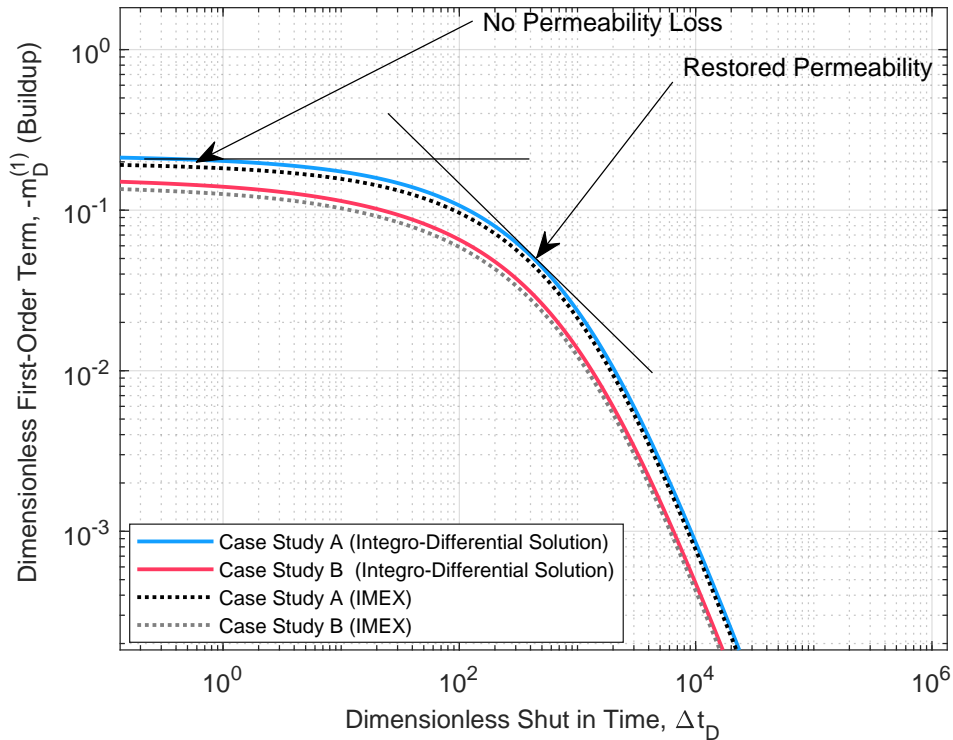


Figure 6.4: Log-log plot of the calibration of the dimensionless pseudo-pressure first-order term against IMEX[®] for the build-up period.

The Figures 6.5 and 6.6 show the role of the oil source and the hydraulic deviator factor in the first-order term for the build-up period. The increase of this term can be realized, as the oil sources also increase (Figure 6.5). For large values of the shut-in time, the dimensionless oil source effect becomes lower and the formation damage caused by the permeability loss is reduced.

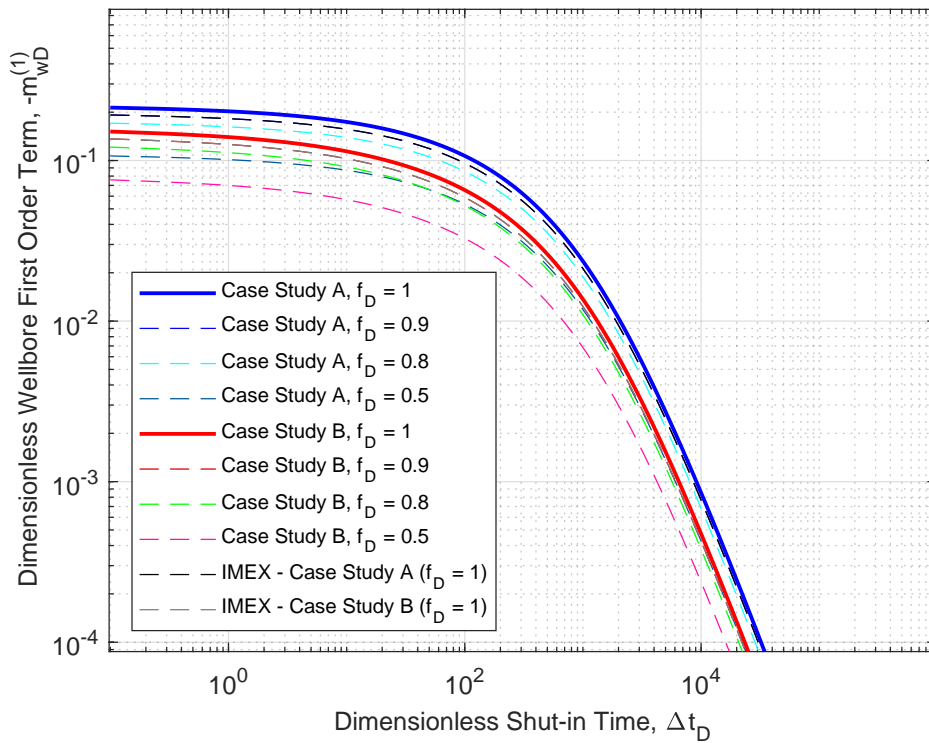


Figure 6.5: Log-log plot of the calibration of dimensionless pseudo-pressure first-order term against IMEX[®] for build-up period.

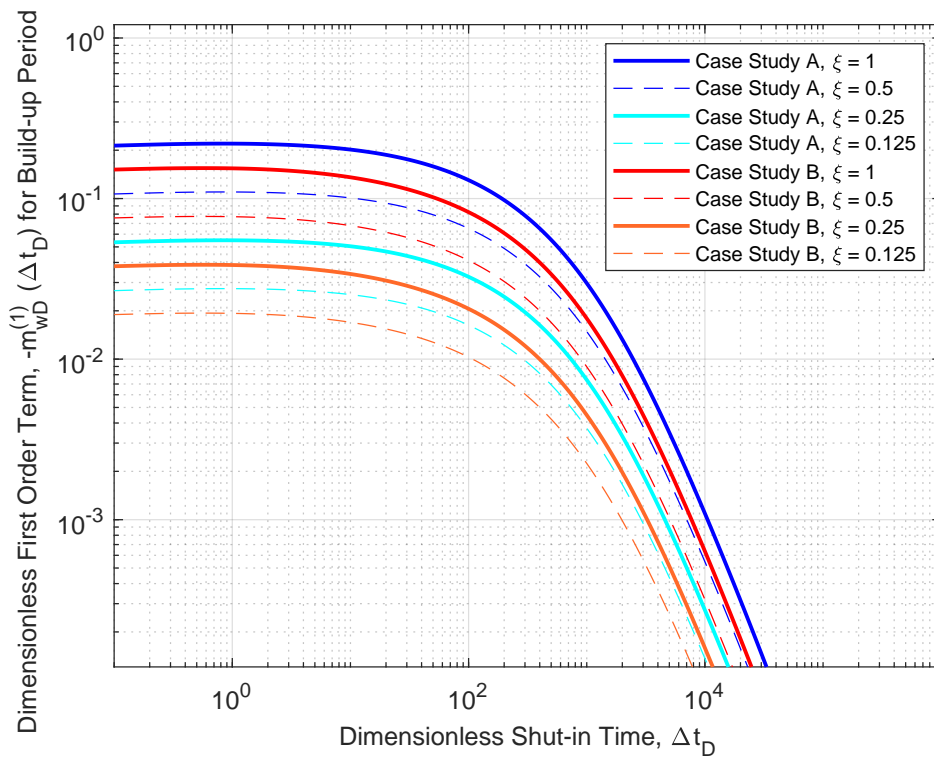


Figure 6.6: Log-log plot of the dimensionless pseudo-pressure first-order term for several hydraulic diffusivity deviator factors for build-up period.

This finding is important to support the well-reservoir performance-management, in order to avoid uncontrolled permeability loss. In Figure 6.6, we notice that, the influence of the deviator factor in the corrective term also results in the increase of the permeability loss. As presented in the Figure 6.5, this effect is reduced as the dimensionless shut-in time becomes larger. Figure 6.7 presents the log-log plot of the dimensionless first-order term for several dimensionless production's time during the shut-in period. We notice that, the corrective term increases for larger dimensionless production's time values. Thereby, it can be concluded that, for minimizing permeability loss, the formation evaluation team must start the build-up period at low times.

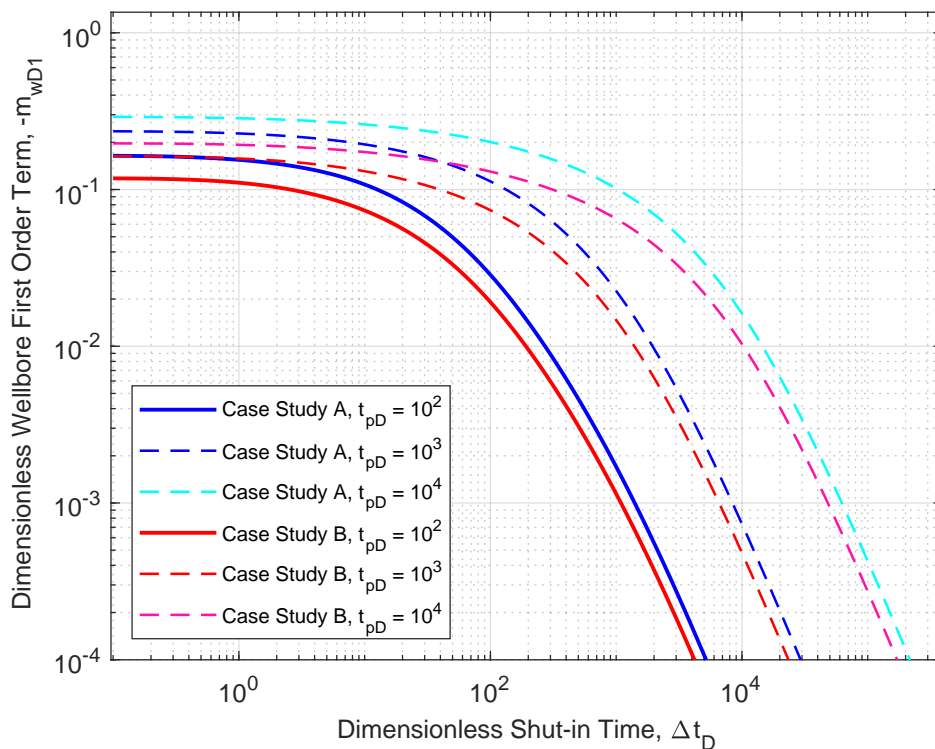


Figure 6.7: Log-log plot of the dimensionless pseudo-pressure first-order term for several hydraulic dimensionless production's time for build-up period.

Figure 6.8 shows the Semi-log plot of the first-order term with respect to the dimensionless time for the drawdown and build-up periods, whereas Figure 6.9 illustrates the Semi-log plot of the first-order term with respect to the dimensionless time for the drawdown and build-up periods for several dimensionless oil sources. The results presented in Figure 6.8 showed satisfactory convergence when compared to IMEX[®] for both periods. We can notice a peak in the corrective term instantaneously when the well is shut and it vanishes for large dimensionless time values. In Figure 6.9, the results also showed satisfactory convergence when compared to IMEX[®] for both periods and we can realize the influence of the dimensionless oil source in this term.

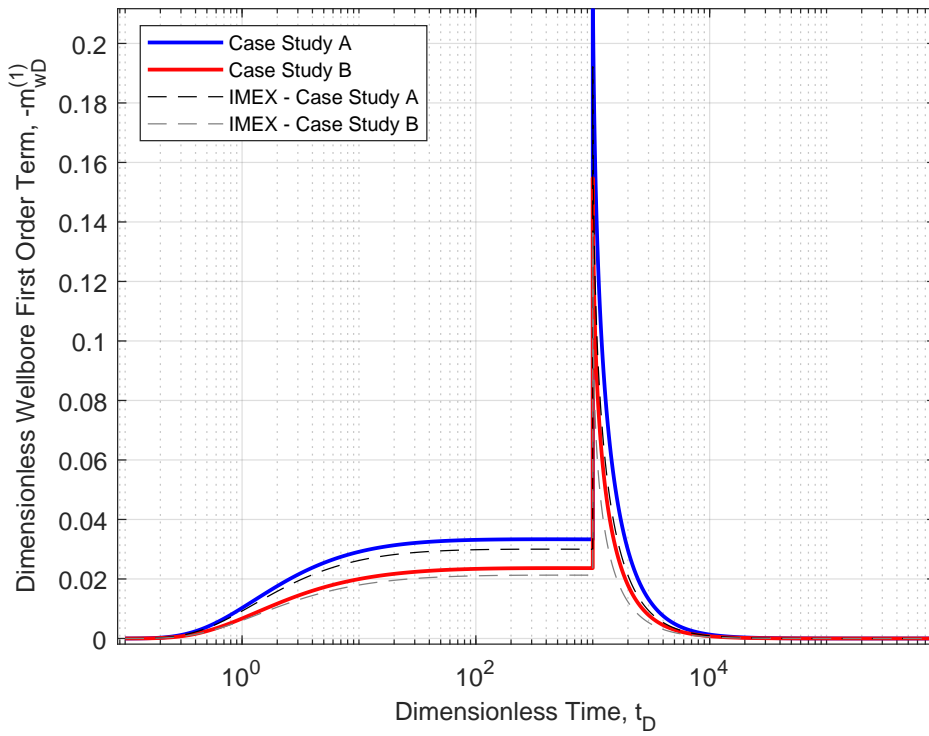


Figure 6.8: Semi-log plot of the calibration of the dimensionless pseudo-pressure first-order term against IMEX[®].

PUC-Rio - Certificação Digital N° 1912769/CA

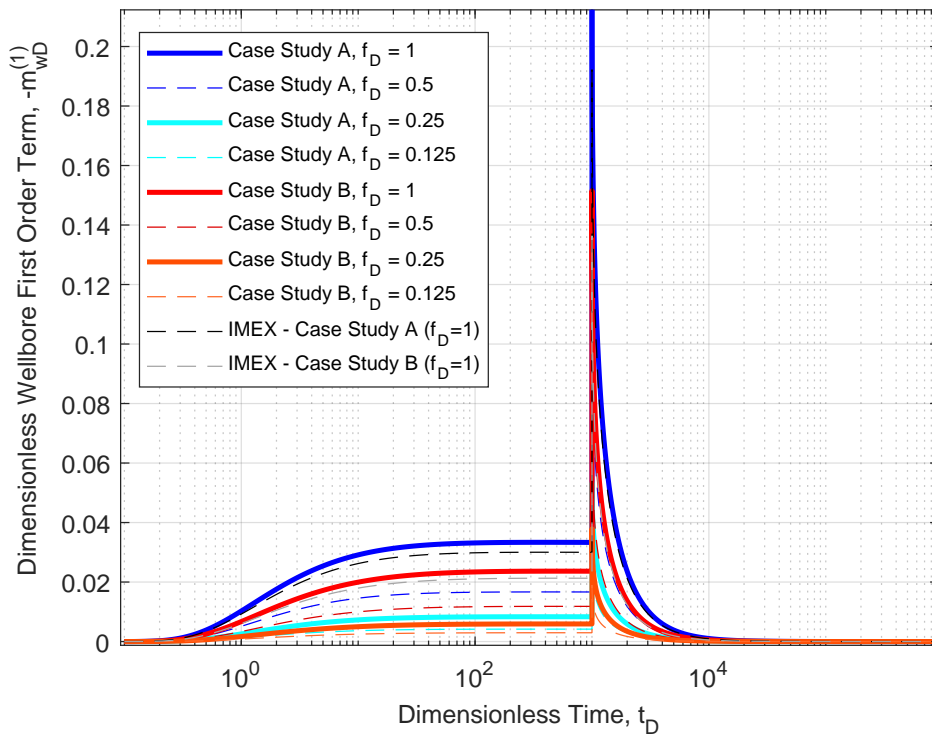


Figure 6.9: Semi-log plot of the dimensionless pseudo-pressure first-order term for several dimensionless oil sources.

The increase of the dimensionless oil sources also results in increase of the corrective term for both periods. Figure 6.10 shows the effect of the several hydraulic diffusivity deviator factor in the first-order term for the case studies A and B for the drawdown and build-up periods. It can be realized that, the increase of the deviator factor results in the increase of the permeability loss in the drawdown period. After the build-up period begins, we notice that, this factor tends to decrease, *i.e.*, the reservoir permeability tends to get restored.

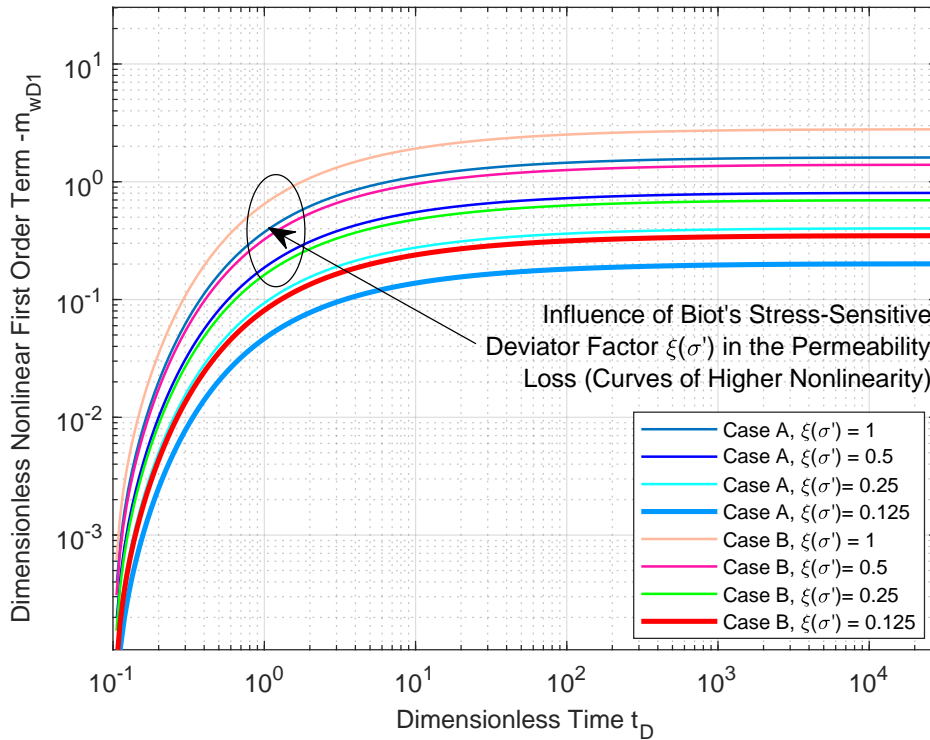


Figure 6.10: Semi-log plot of the dimensionless pseudo-pressure first-order term for several hydraulic diffusivity deviator factors.

Figure 6.11 presents the same plot with the effect of the several dimensionless production's time in the first-order term. It is notable that, for larger values of the dimensionless production's time, the pseudo-pressure first-order peak increases. It results in an increase of the nonlinearity and, consequently, in the permeability loss. Thereby, the model developed in this work is capable to support the formation evaluation team to avoid larger production's time during a well-test.

Figure 6.12 shows the effect of the nonlinearity caused by the permeability changes in the dimensionless Horner's plot for the dimensionless pseudo-pressure change and the comparison to IMEX[®] for both case studies.

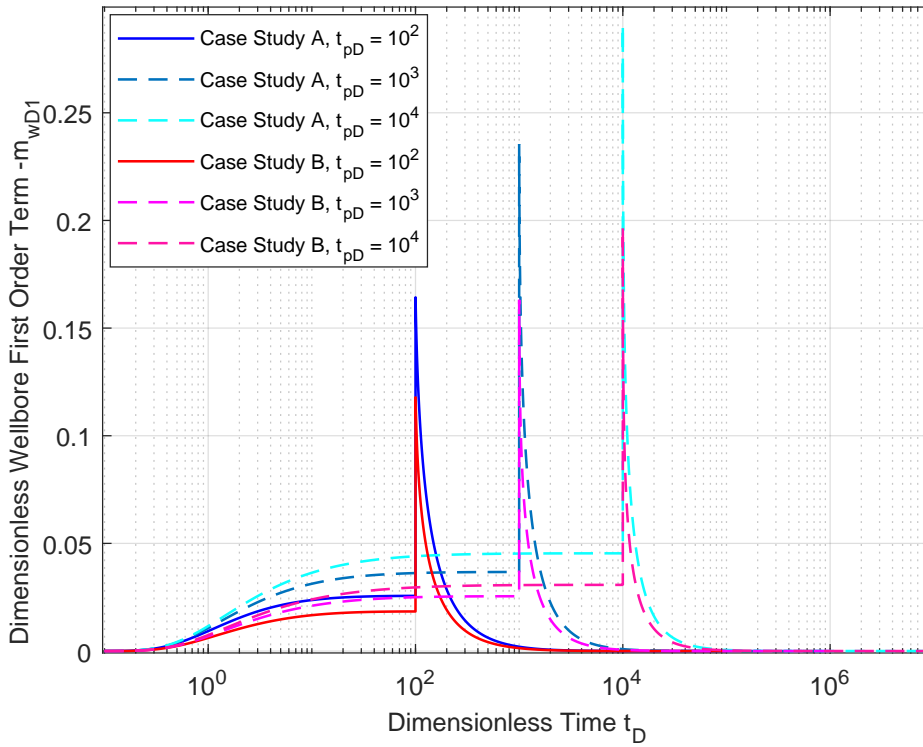


Figure 6.11: Semi-log plot of the dimensionless pseudo-pressure first-order term for several dimensionless production's time.

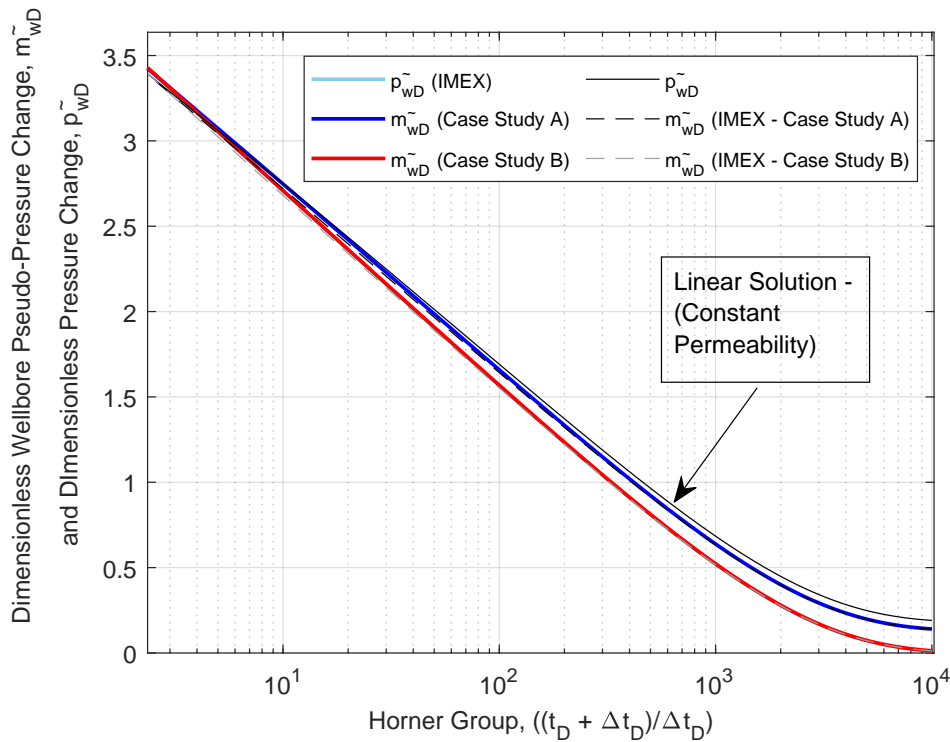


Figure 6.12: Horner plot of the calibration of the dimensionless linear solution and pseudo-pressure change against IMEX®.

The Horner's method (Horner, 1951) is a classical technique for build-up data analysis (Lee; Lee, Rollins & Spivey, 1982, 2003). In this method, the data points are plotted as a function of the dimensionless form of the Horner's time group $(t_{pD} + \Delta t_D)/\Delta t_D$. The dimensionless pseudo-pressure change is expressed by:

$$\tilde{m}_{wD} = m_{wD}(t_{pD}) - m_{wD}(t_{pD} + \Delta t_D) \quad (6-38)$$

The first term on the right side of the Eq. 6-38 is evaluated at $t_D = t_{pD}$, *i.e.*, at the end of the drawdown period, whereas the second term is the pseudo-pressure at the beginning of the build-up. The dimensionless linear solution change is expressed by:

$$\tilde{p}_{wDV}(\Delta t_D) = p_{wDV}(t_{pD}) - p_{wDV}(t_{pD} + \Delta t_D) \quad (6-39)$$

Where $p_{wDV}(t_{pD})$ and $p_{wDV}(t_{pD} + \Delta t_D)$ are the dimensionless constant permeability solution at the same periods aforementioned. The results were compared to IMEX[®] and presented close convergence. The nonlinearity can be seen as a smooth displacement between the linear solution's curve and the dimensionless pseudo-pressure change one. Figure 6.13 shows the same nonlinear effect in the dimensionless Horner plot for several oil flow rates.

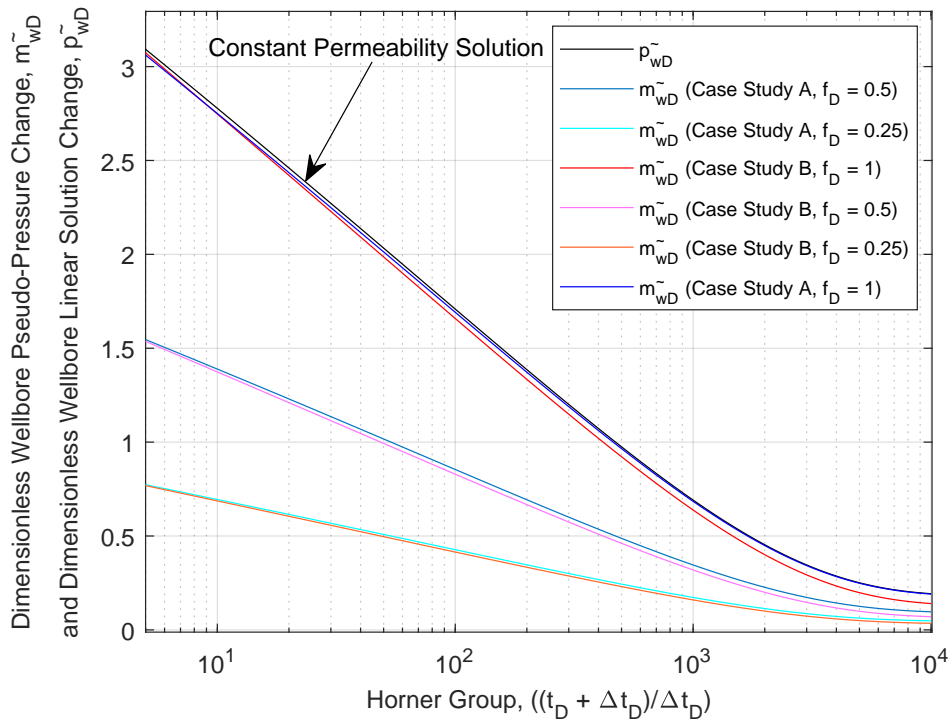


Figure 6.13: *Horner plot* of the dimensionless linear solution and pseudo-pressure change for several dimensionless oil sources against IMEX[®].

As expected, the oil flow rates variation provides the \tilde{m}_{wDV} slope change and displacements with respect to the other curves. Figure 6.14 shows the role of the deviator factor in the permeability changes in the dimensionless Horner's plot. We notice that, as this factor increases, the dimensionless pseudo-pressure change deviates from the constant permeability solution. It means that, the permeability loss increases.

The sensitivity analysis has shown that the pore pressure variation and the oil flow rate are key parameters to be considered in the well-reservoir production's curve plan. Therefore, the uncontrolled formation damage increase may be avoided by the appropriate control of the hydraulic deviator factor through the monitoring of these parameters aforementioned during the well-reservoir life-cycle.

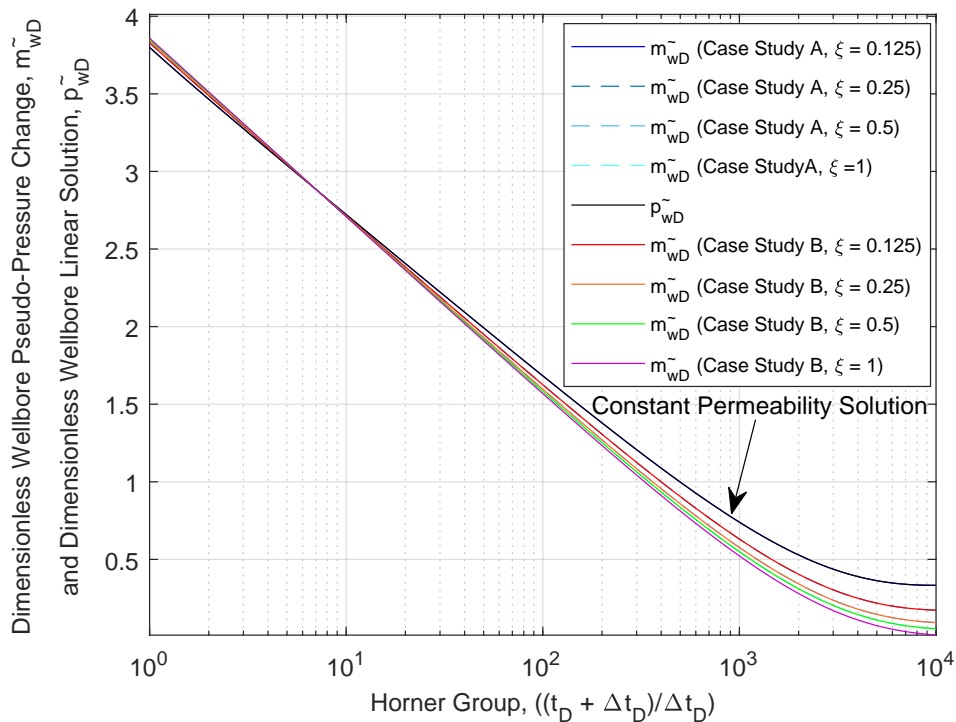


Figure 6.14: *Horner plot* of the calibration of the dimensionless linear solution and pseudo-pressure change for several hydraulic diffusivity deviator factors.

Figure 6.15 presents the dimensionless pseudo-pressure change for several dimensionless production's time in the Horner plot. We can realize a smooth increase of the deviation with respect to the linear solution, as the dimensionless production's time increases. It also results in an increase of the permeability loss. Therewith, the model presented in this work allows to plan the adequate build-up period, in order to avoid severe permeability loss and improve the well-reservoir performance management.

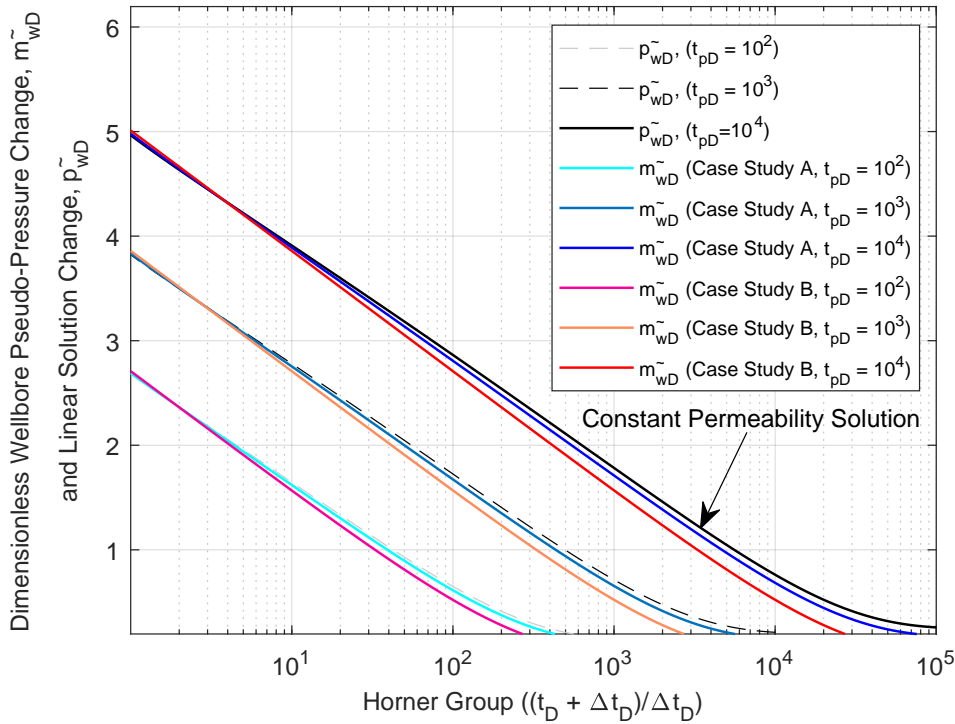


Figure 6.15: *Horner plot* of the dimensionless linear solution and pseudo-pressure change for several dimensionless production's time.

Figure 6.16 presents the log-log plot of the calibration of the dimensionless pseudo-pressure change \tilde{m}_{wD} and its derivative \tilde{m}'_{wD} as a function of the dimensionless shut-in time Δt_D observed during the build-up testing.

According to the Figure 6.16, the solution presented in this work presents high convergence for both case studies in comparison to IMEX[®].

The pseudo-pressure derivative \tilde{m}'_{wD} presents a growing behavior for dimensionless early times ($t_D \leq 10^0$), then it reaches a plateau in the interval $[10^0 < t_D < 10^2]$. From this value, the \tilde{m}'_{wD} curve begins to drop and, as expected, it tends asymptotically to zero with slope value of -1 .

Figure 6.17 presents the \tilde{m}_{wD} term and its derivative for several dimensionless oil flow sources in a Log-log plot. As shown in the drawdown plots, the oil flow rate also influences significantly these functions, causing variation in the nonlinearity of the first-order term and, consequently, in the reservoir permeability. It emphasizes the importance of the oil flow rate management during the well-reservoir life-cycle.

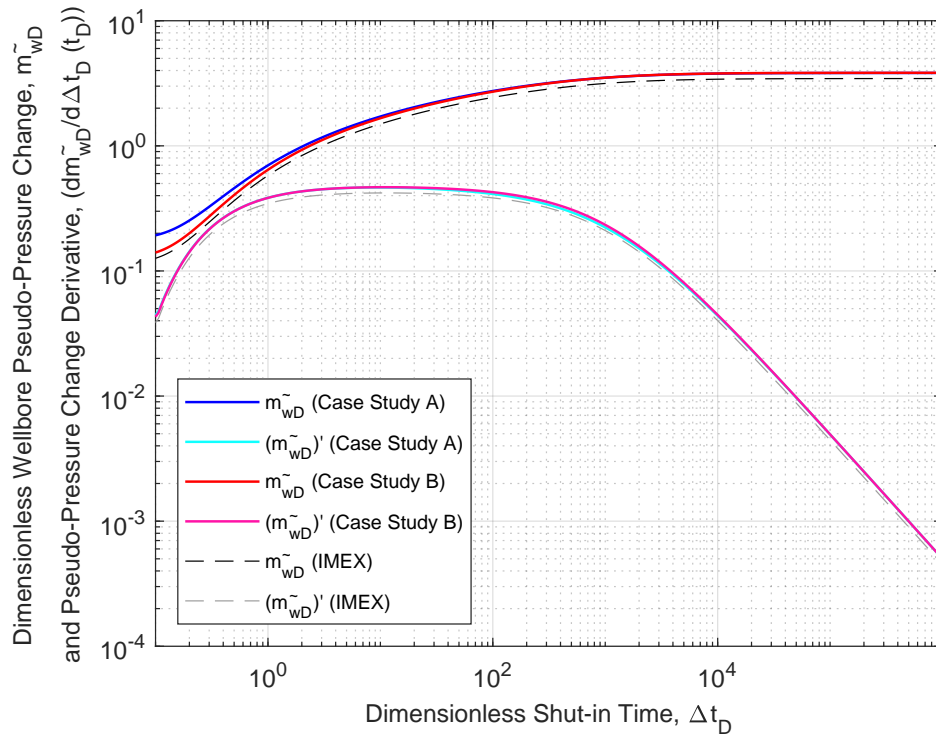


Figure 6.16: Log-log plot of the calibration of the pseudo-pressure change and its derivative against IMEX®.

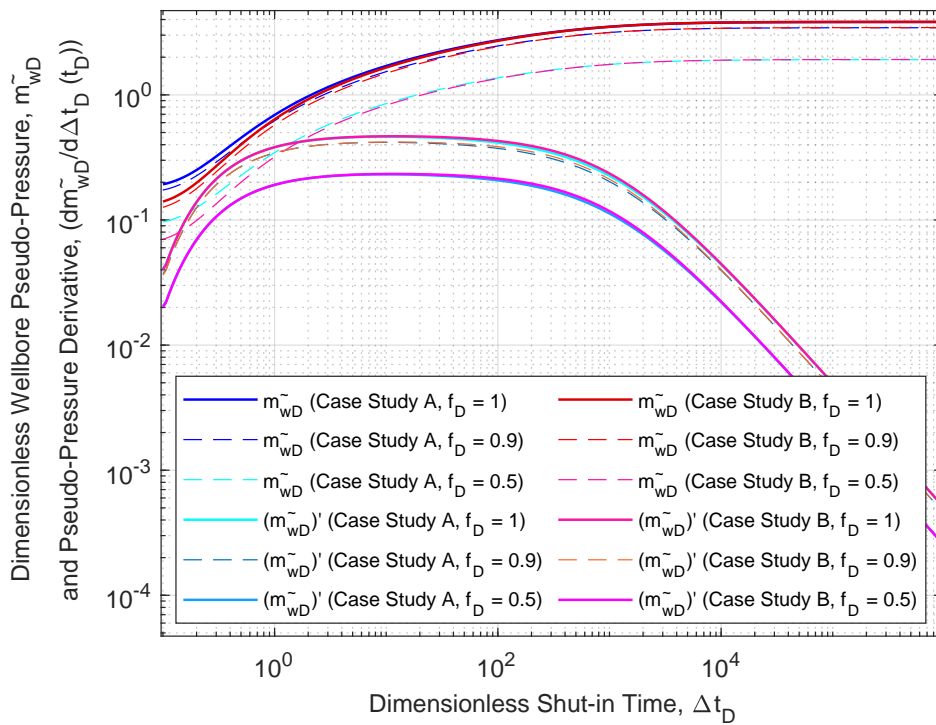


Figure 6.17: Log-log plot of the pseudo-pressure change and its derivative for several dimensionless oil sources.

Figure 6.18 presents the \tilde{m}_{wD} term and its derivative for several deviator factors in a Log-log plot. The increase of this factor also results in a pseudo-pressure change drops and, consequently, in the well-reservoir impairment caused by the permeability loss.

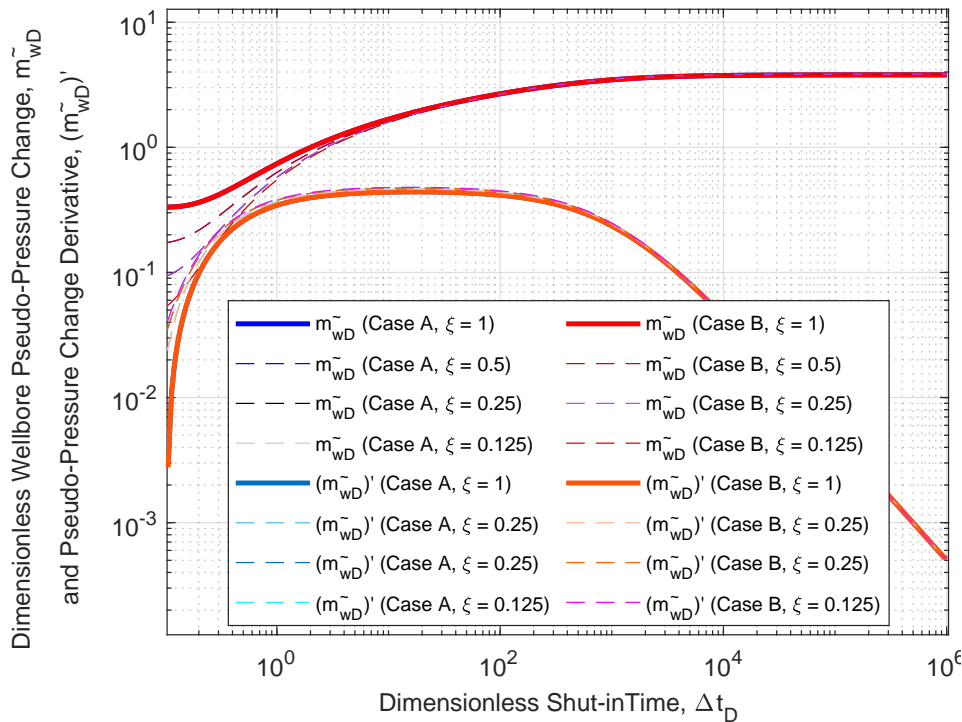


Figure 6.18: Log-log plot of the pseudo-pressure change and its derivative for several hydraulic deviator factors.

Figure 6.19 presents the \tilde{m}_{wD} term and its derivative for several dimensionless production's time in a log-log plot.

The plot shows that, the increase of the dimensionless production's time leads to the increase of the pseudo-pressure change. It means that, the difference between the pseudo-pressure in the end of the drawdown and the beginning of the build-up periods increases.

As the pseudo-pressure provides, instantaneously, the value of the reservoir permeability, an increasing of the pseudo-pressure change results in the increase of permeability variation. The pseudo-pressure change derivative remains constant and only deviates in the shut-in time axis.

Figure 6.20 shows the role of the hydraulic deviator factor in the dimensionless pseudo-pressure during the drawdown-build-up solution. A low deviation is noticed among the curves.

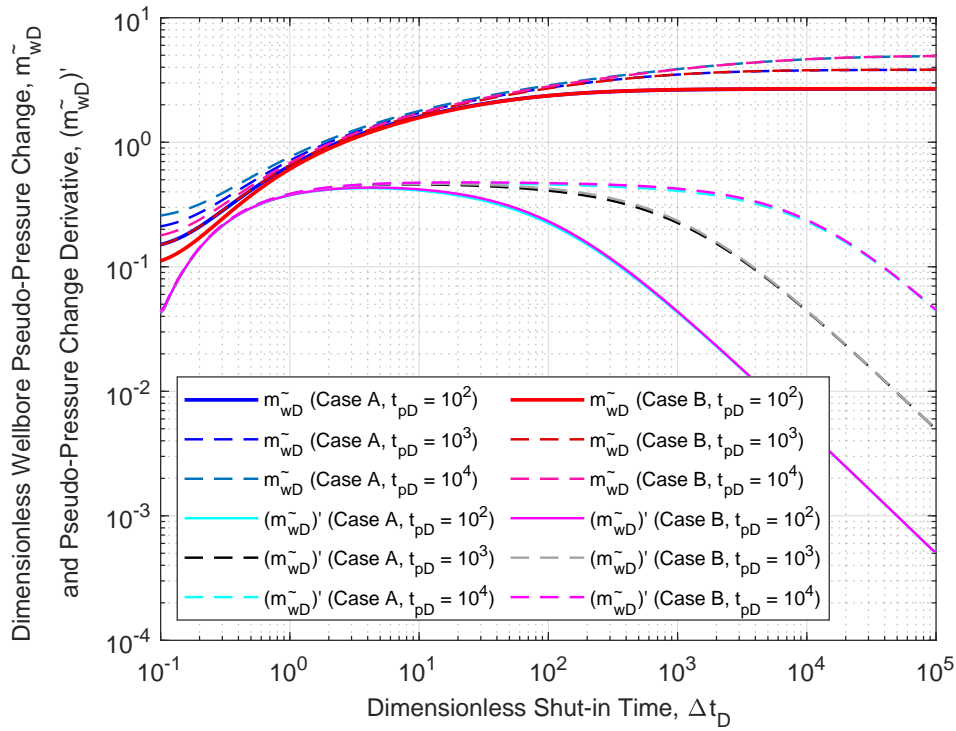


Figure 6.19: Log-log plot of the pseudo-pressure change and its derivative for several dimensionless production's time.

PUC-Rio - Certificação Digital N° 1912769/CA

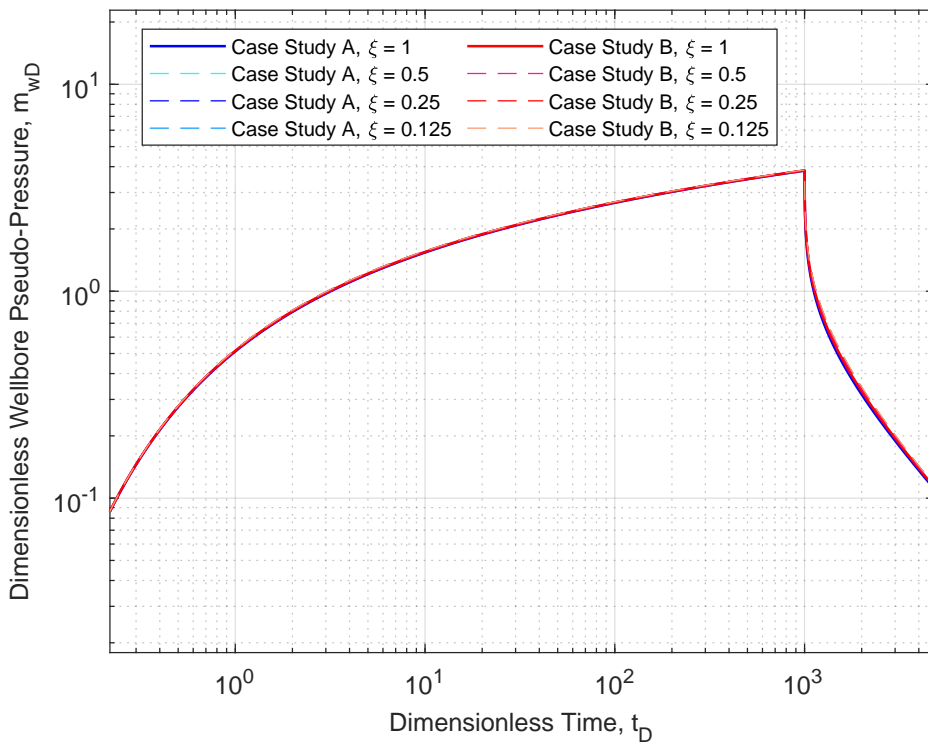


Figure 6.20: Log-log plot of the dimensionless pseudo-pressure for several hydraulic diffusivity deviator factors for drawdown and build-up periods.

The effect of the hydraulic diffusivity deviator factor variation in the general solution since the beginning of the drawdown until the end of the build-up period can be realized in the Figures 6.21 to 6.25.

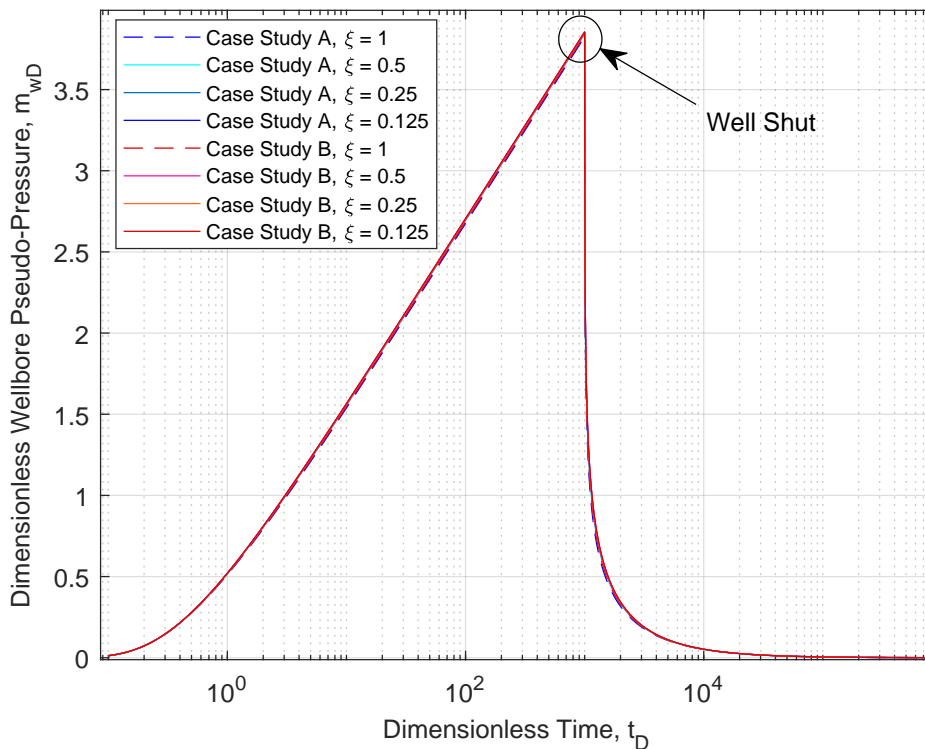


Figure 6.21: Semi-log plot of the dimensionless pseudo-pressure for several hydraulic diffusivity deviator factors for drawdown and build-up periods.

In the Figures 6.22 and 6.24, during the well-reservoir drawdown period (well-reservoir unloading), the slope of the pseudo-pressure is positive, therewith, the permeability is decreasing during this time. Furthermore, the deviator factor provides a smooth displacement and slope variation in the pseudo-pressure curve, therefore, its monitoring is important to avoid early-permeability loss and maintain the well-reservoir performance. In the Figure 6.25, the well is shut to the build-up test (well-reservoir reloading) in a dimensionless production's time $t_{pD} = 10^3$ and the pseudo-pressure slope is negative. Thereby, the rock grains tend to return to their original arrangement state, before the well-reservoir's production and the permeability is restored. Moreover, it is possible to notice that, as the dimensionless time increases, the effect of deviator factor decreases and it becomes insignificant in the pseudo-pressure response. This fact is caused by the time necessary to the reservoir grains rearrange themselves. Therewith, the model presented in this thesis allows to support the formation evaluation team to chose the appropriate dimensionless shut-in time Δt_D in order to minimize the permeability loss during the build-up period.

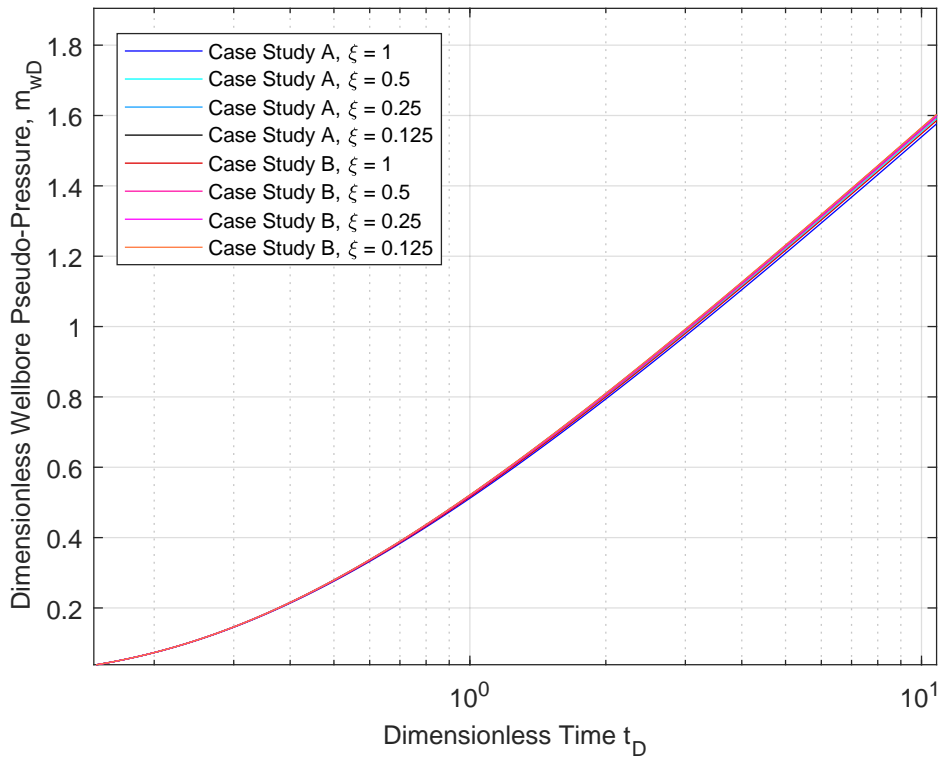


Figure 6.22: Semi-log plot of the dimensionless pseudo-pressure for several hydraulic diffusivity deviator factors for drawdown period.

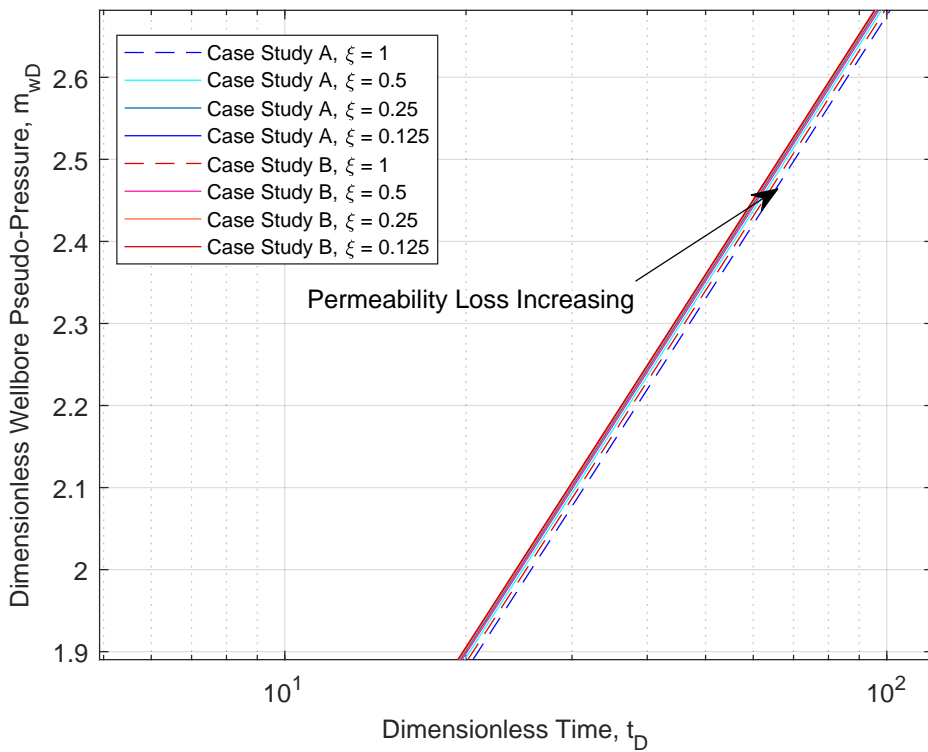


Figure 6.23: Semi-log plot of the amplification of the dimensionless pseudo-pressure for several hydraulic diffusivity deviator factors for drawdown period.

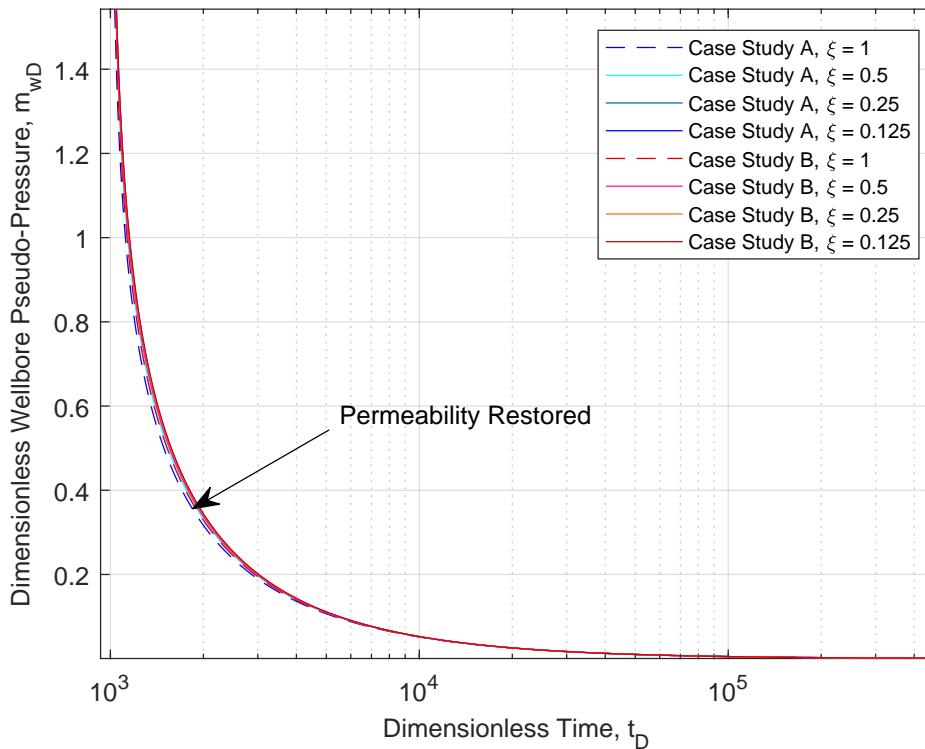


Figure 6.24: Semi-log plot of the amplification of the dimensionless pseudo-pressure for several hydraulic diffusivity deviator factors for build-up period.

The pseudo-pressure $m[p(t)]$ as a function of the time for the case studies A and B are presented in the Figure 6.26 and Figure 6.27.

These diagnostic plots illustrate the pseudo-pressure decline during the drawdown period ($t < t_p$), where t_p is the production's time. As the pseudo-pressure definition represents the permeability change with respect to the pore pressure, this behavior of $m[p(t)]$ means that, the permeability is declining over the drawdown period. For the build-up period ($t > t_p$), the restoration of the permeability is remarkable. As the effect of the rock-fluid hysteresis caused by the pore collapse is not considered in this work, the pressure and, consequently, the permeability returns to the initial value. The role of the oil flow rate is also shown in these plots. We notice that, the increase of the oil flow rate provides the change of the pseudo-pressure slope $m'[p(t)]$.

By the pseudo-pressure definition, its slope represents the instantaneous permeability value, therewith, the oil flow rate increase, results in the permeability variation increase. Therefore, this model provides a useful mathematical tool to support the well-reservoir performance management through the appropriate choice of the oil flow rate, in order to avoid economical impairments in the oil production's curve caused by uncontrolled permeability decline.

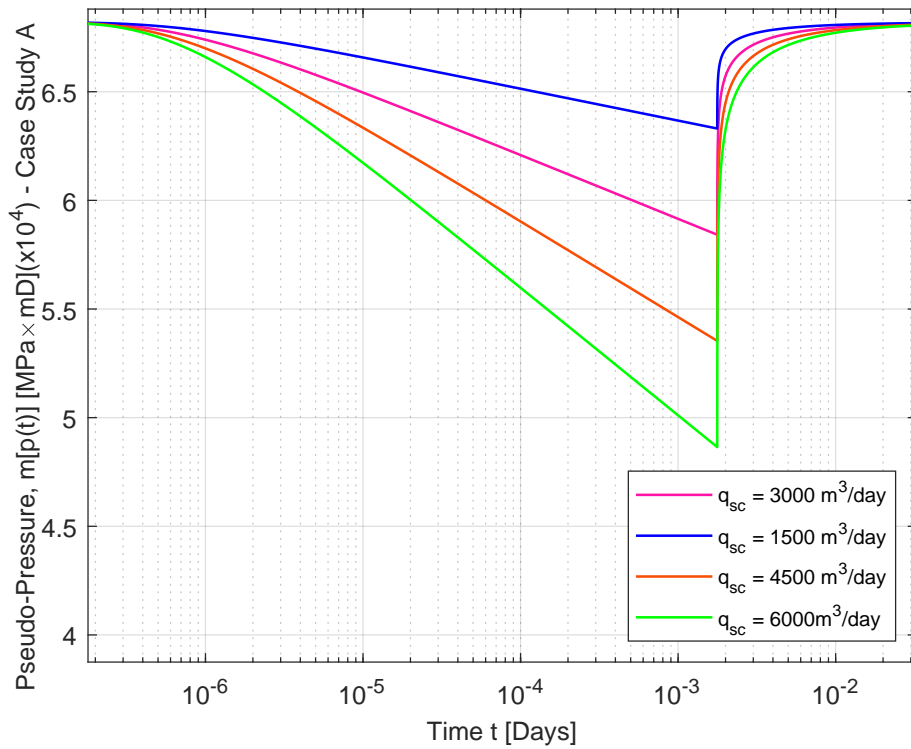


Figure 6.25: Semi-log plot of pseudo-pressure as a function of the time for several oil flow rates for the case study A.

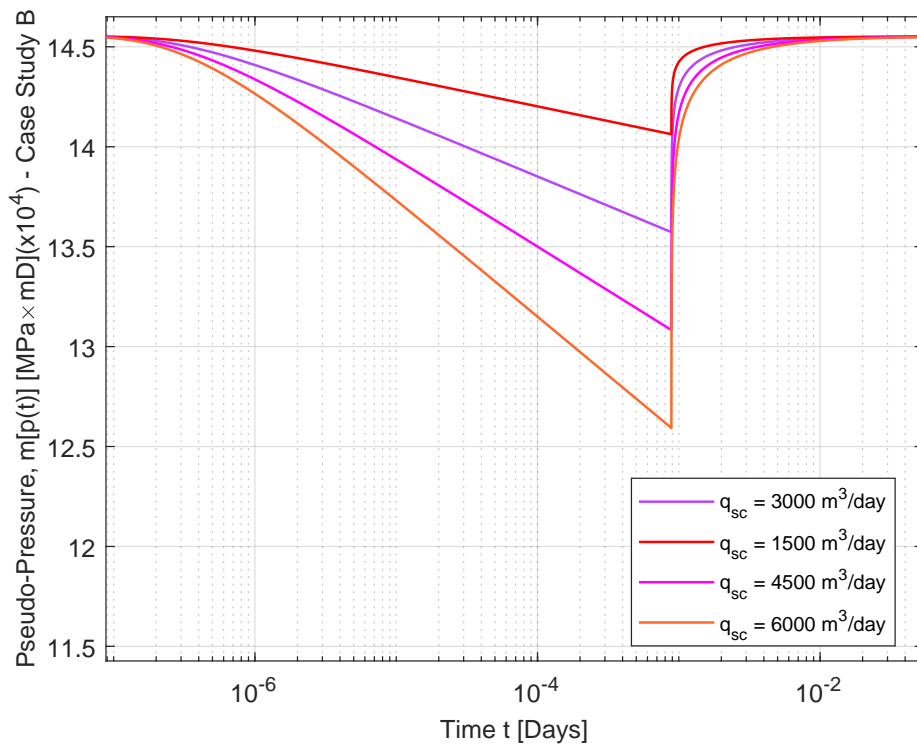


Figure 6.26: Semi-log plot of pseudo-pressure as a function of the time for several oil flow rates for the case study B.

An alternative manner to interpret the permeability response during the drawdown and build-up periods is using the pseudo-pressure variation $\Delta m[p(t)]$ definition.

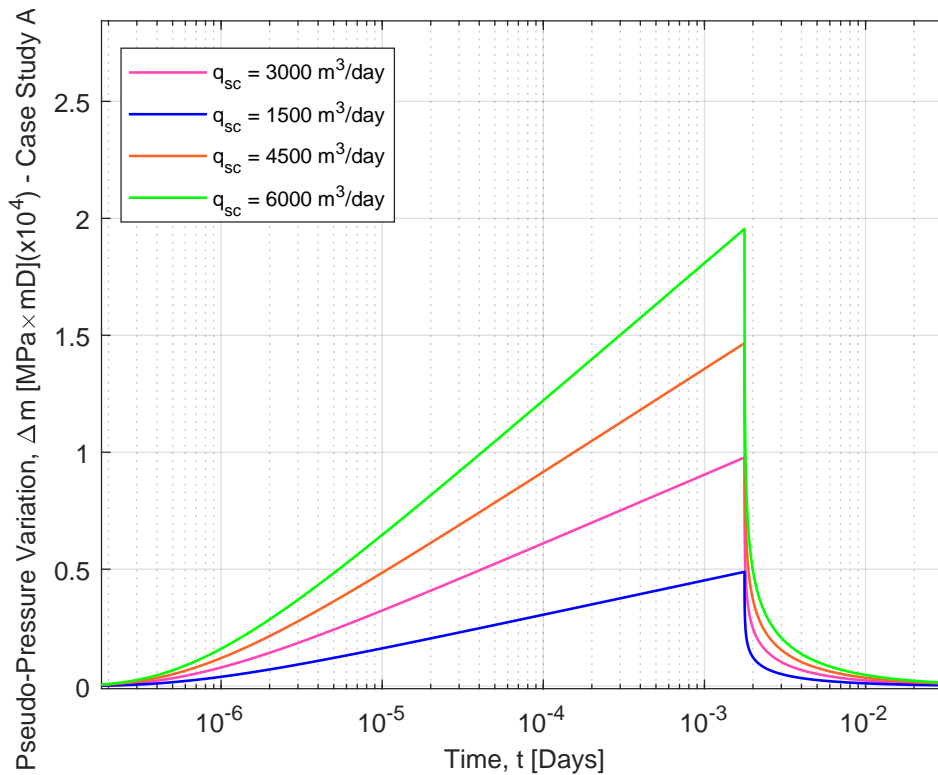


Figure 6.27: Semi-log plot of pseudo-pressure variation as a function of the time for several oil flow rates for the case study B.

In the Figures 6.27 and 6.28 it is possible to realize that $\Delta m[p(t)]$ increases in the drawdown and it decreases during the build-up period, *i.e.*, the pseudo-pressure $m[p(t)]$ is deviating with respect to the initial value $m[p(0)] = m(p_i)$ in the drawdown period. Therewith, the permeability is lowering with respect to its initial permeability $k[p(0)] = k(p_i)$.

Analogously, during the build-up period, the pseudo-pressure variation vanishes and, we conclude that, the permeability is restored to its initial value $k(p_i)$. As presented in the Figures 6.27 and 6.28, we can also notice the effect of the oil flow rates in the $\Delta m[p(t)]$ *semi-log plots*. As the oil flow rate increase, the slope $\Delta m'[p(t)]$ also increases, resulting in a permeability variation rise. As aforementioned, the model developed in this work provides a practical mathematical tool to support the well-reservoir management through a simple graphical interpretation in a Semi-log plot.

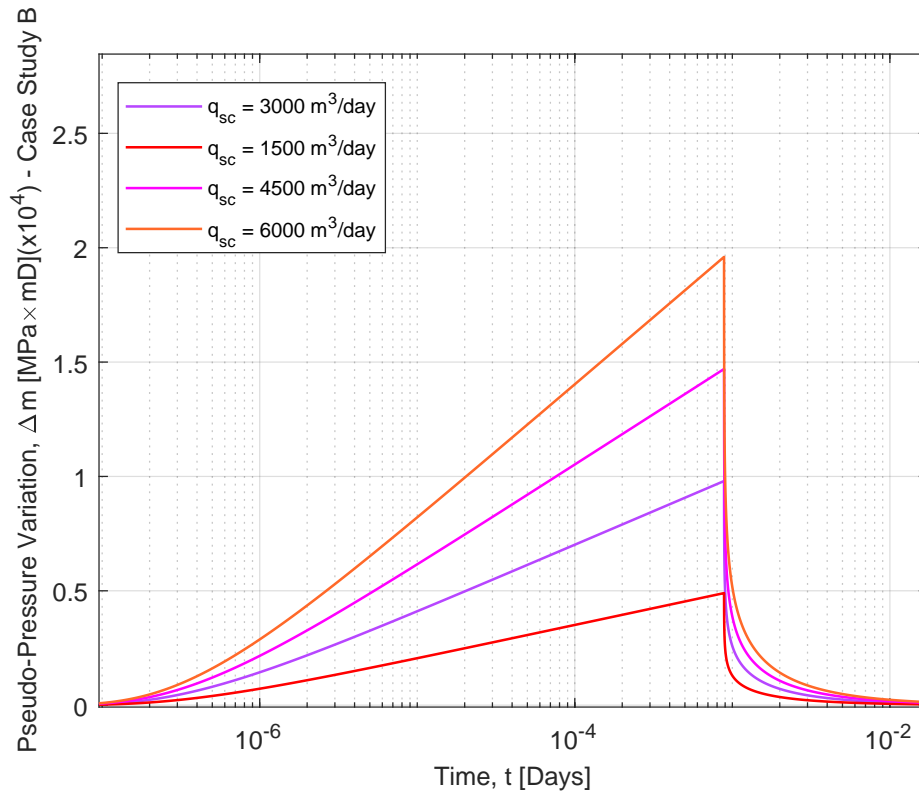


Figure 6.28: Semi-log plot of pseudo-pressure variation as a function of the time for several oil flow rates for the case study B.

6.2

Permeability-Hysteresis Identification During Oil Loading-Unloading Well-Reservoir Cycles

The uncontrolled formation mechanical damage occurred by the premature permeability loss may leads to significant impairment in an oilfield development. The results presented previously in this thesis have shown that, the permeability loss effect begins smooth and the deviation with respect to the linear solution, *i.e.*, constant permeability response, tends to become larger over the elapsed time. Therefore, the prediction of the permeability-hysteresis effect throughout the drawdown/build-up periods is extremely important to the well-reservoir performance management.

In this section, this phenomenon was researched in order to evaluate its effect in the dimensionless pseudo-pressure response during one drawdown/build-up cycle. Figures 6.29 and 6.30 present the permeability-hysteretic response as a function of the pressure for the case studies A and B, respectively.

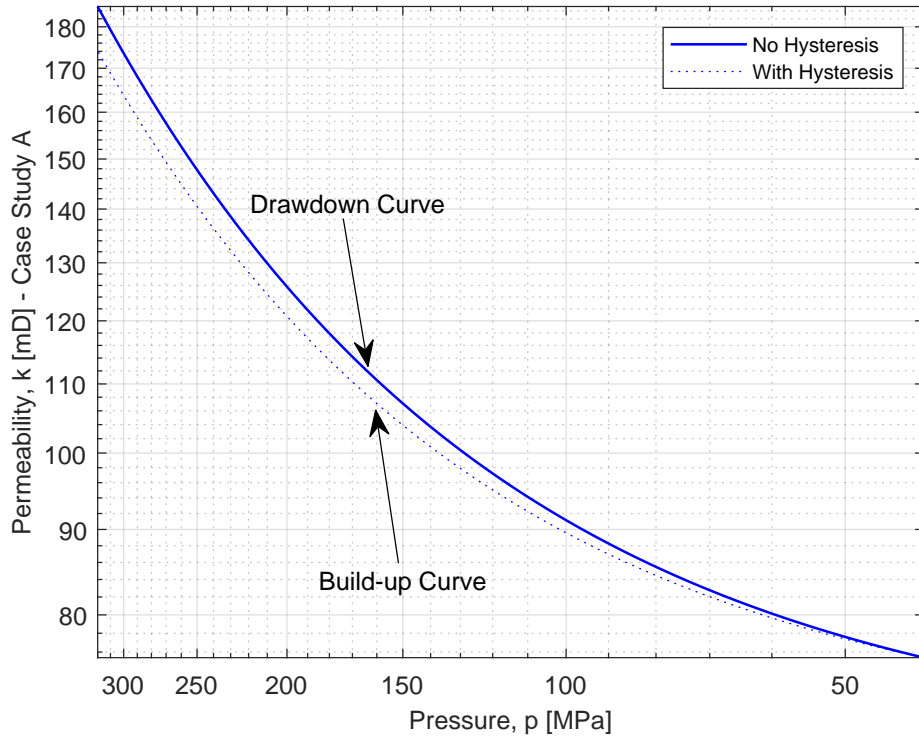


Figure 6.29: Log-log plot of the permeability-hysteresis response for the case study A.

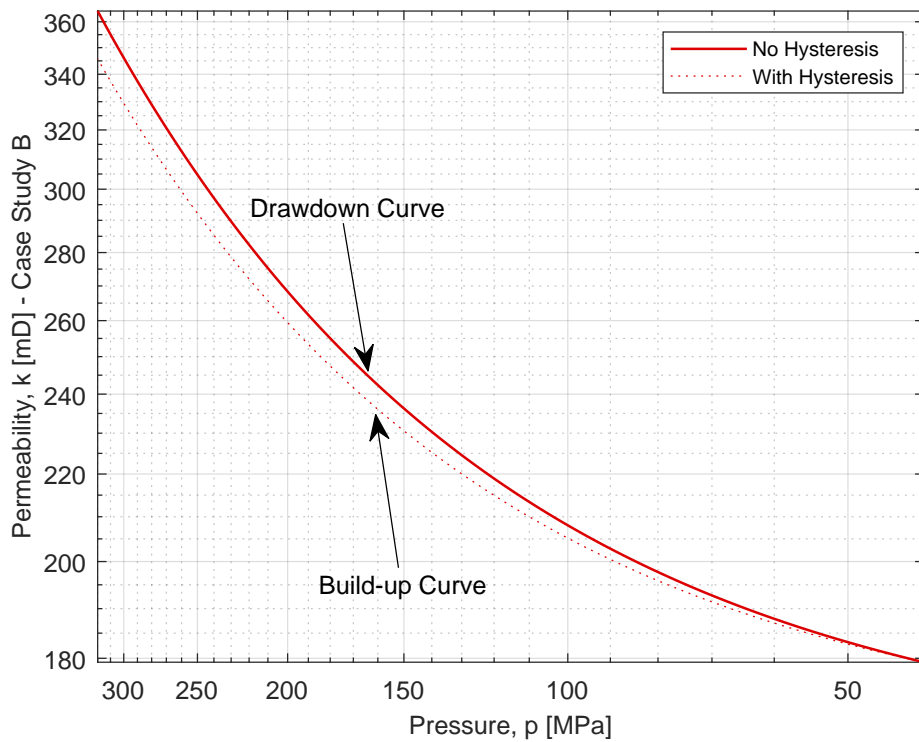


Figure 6.30: Log-log plot of the permeability-hysteresis response for the case study B.

A hysteresis factor $\mathcal{H} = k[p_{wD}(t_D - t_{pD})]/k[p_{wD}(t_D)]$ was coupled to Eq. 6-37 to consider the permeability partial restoration when the well is shut to the build-up test. Where $k[p_{wD}(t_D - t_{pD})]$ and $k[p_{wD}(t_D)]$ represent the permeability response during the build-up and the drawdown periods, respectively, [md]. The continuous lines of the Figures 6.29 and 6.30 represent the permeability loss during the drawdown period, whereas the dot lines in both plots are related to the partial restoration of the permeability when the well is shut to the build-up response. The model was implemented in a computational code in Matlab[®] and calibrated through IMEX[®] by the *CROCK TAB* command. A computational table with the pore pressure and permeability synthetic field data was built in both softwares to represent the physical phenomenon of the permeability loss. For this approach, none of the permeability-pressure sensitive functions provided close accuracy. Therefore, a cubic spline was used to fit the data and it presented high convergence with respect to IMEX[®]. Several sensitive runs were performed in the Matlab[®] in order to represent clearly the hysteretic effect in the both case studies presented in this work and a hysteresis factor $\mathcal{H} = 0.75$ was used in the aforementioned code and in the table of the IMEX[®]. Figures 6.31 and 6.32 present the influence of the dimensionless production's time in the hysteretic response for the dimensionless permeability and the deviator factor, respectively.

In the Figure 6.31, we notice that a permeability-hysteresis has different values as the dimensionless production's time changes. Consequently, occurs a hysteresis-difference $\Delta k_D(p) = k_D(t_{pD2}) - k_D(t_{pD1})$ between the dimensionless times t_{pD1} and t_{pD2} . For t_{pD2} , the hysteresis-difference is larger and we can conclude that, lower production's times are more adequate for the hysteresis control. In the Figure 6.32, the same effect is noticed in the hydraulic diffusivity deviator factor and the difference $\Delta \xi(p) = \xi(t_{pD2}) - \xi(t_{pD1})$ also occurs between the dimensionless times t_{pD1} and t_{pD2} . For larger dimensionless production's time, this factor difference also increases. Figure 6.33 presents the diagnostic plot of the dimensionless first-order term for the build-up period. The permeability-hysteresis effect is noticed as a smooth displacement among the curves. We also realize that, the hysteresis increases for large dimensionless shut-in time values. It occurs because when the well is shut, it is still under influence of the drawdown effect and the permeability restoration did not begin to occur. Figure 6.34 illustrates the effect of the dimensionless production's time in the first-order term hysteretic response.

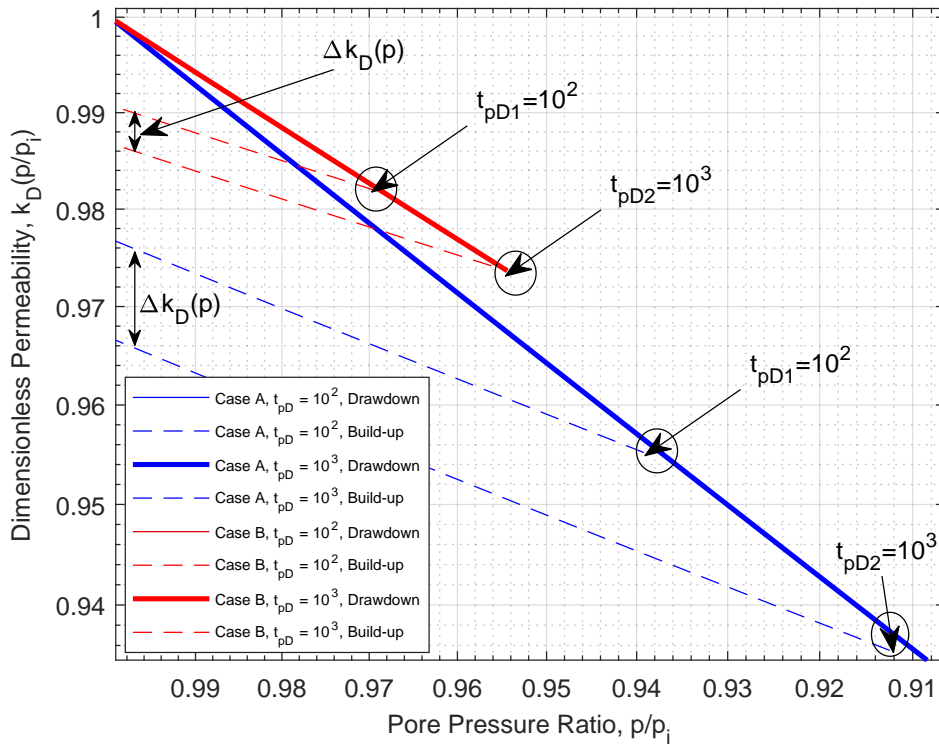


Figure 6.31: Log-log plot of the hysteresis variation with respect to different dimensionless production's times for the case studies A and B.

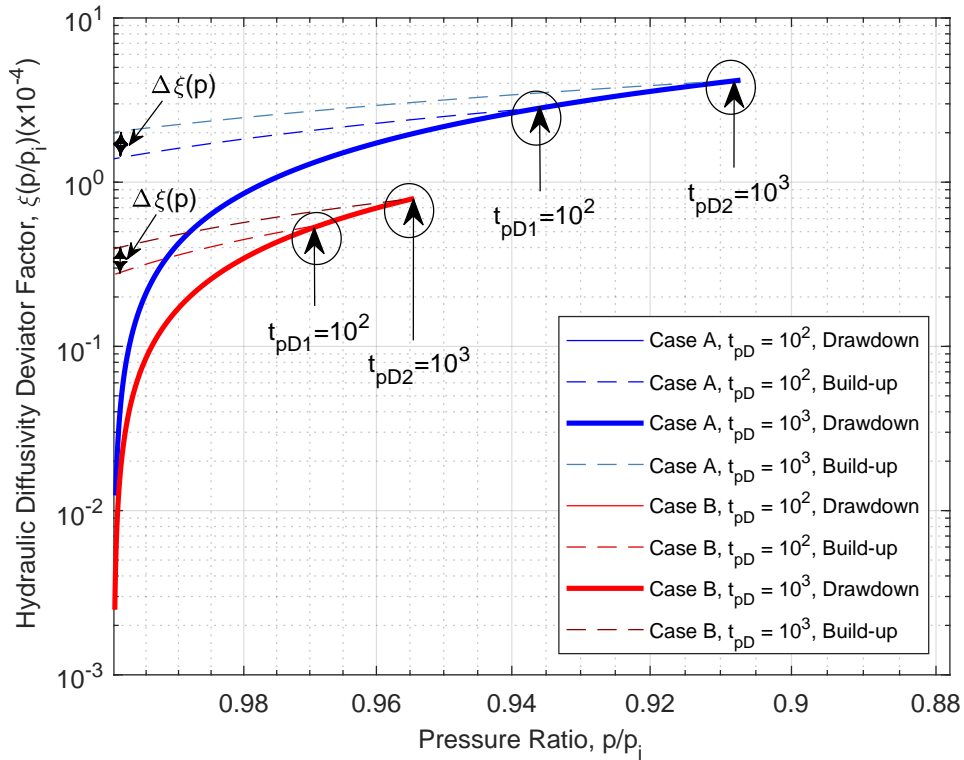


Figure 6.32: Log-log plot of the hydraulic diffusivity deviator factor variation with respect to different dimensionless production's times for the case studies A and B.

Comparing the Figures 6.33 and 6.34, we conclude that, the dimensionless production's time increases significantly the hysteresis in the first-order term.

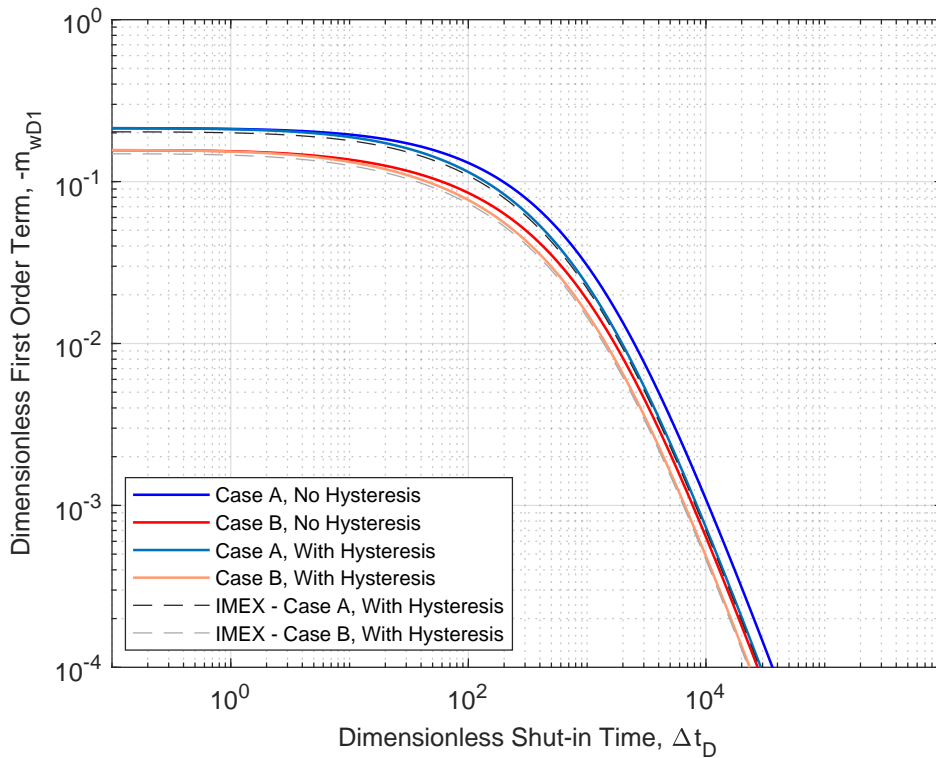


Figure 6.33: Log-log plot of the permeability-hysteresis response in the first-order term for $t_{pD} = 10^3$.

This hysteretic effect is larger in the case study A, because its permeability on initial pressure $k(p_i)$ is lower than the case study B. This response may leads to severe permeability loss and lower restoration during the build-up period. For this analysis, it was used the dimensionless production's time values of $t_{pD} = 10^3$ (Figure 6.33) and $t_{pD} = 10^4$ (Figure 6.34). The dimensionless first-order term response during the drawdown and build-up periods is presented in the Semi-log plot of the Figures 6.35 and 6.36. The influence of the dimensionless production's time was also analyzed and it was used the dimensionless production's time values of $t_{pD} = 10^3$ (Figure 6.35) and $t_{pD} = 10^4$ (Figure 6.36). The permeability-hysteresis is noticed when the well is shut for the build-up period and we can also realize the increase of the dimensionless first-order term's peak caused by the hysteresis presence. For larger production's time ($t_{pD} = 10^4$ in Figure 6.36), both, the peak and the deviation from non-hysteretic response increase significantly. It increases the nonlinearity of the general solution and, consequently, the formation damage caused by the permeability loss. The results were calibrated with IMEX[®] and they presented high accuracy.

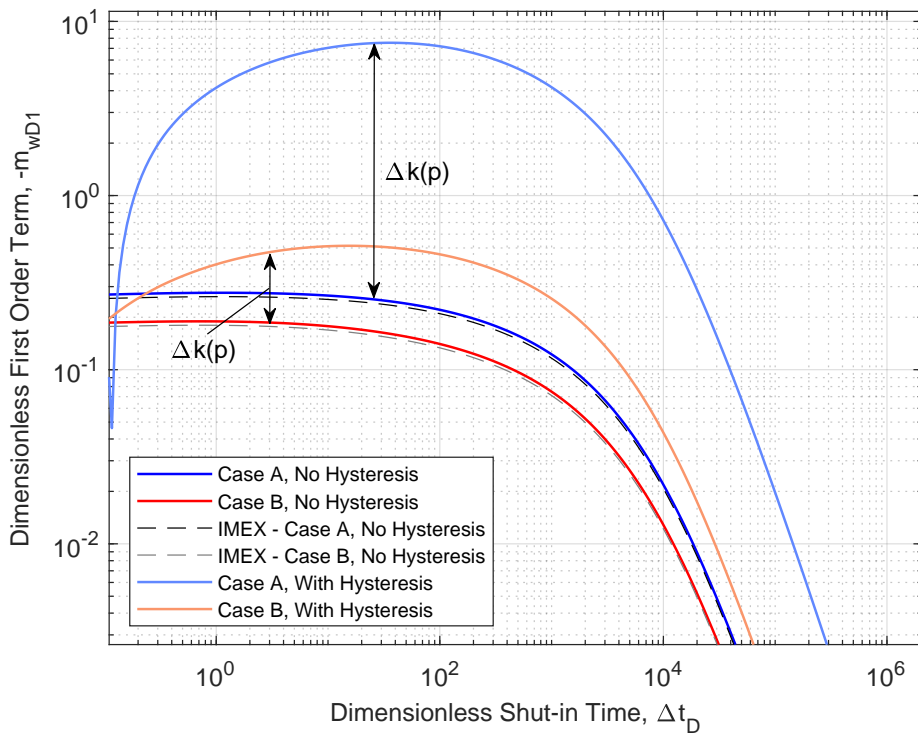


Figure 6.34: Log-log plot of the permeability-hysteresis response in the first-order term for $t_{pD} = 10^4$.

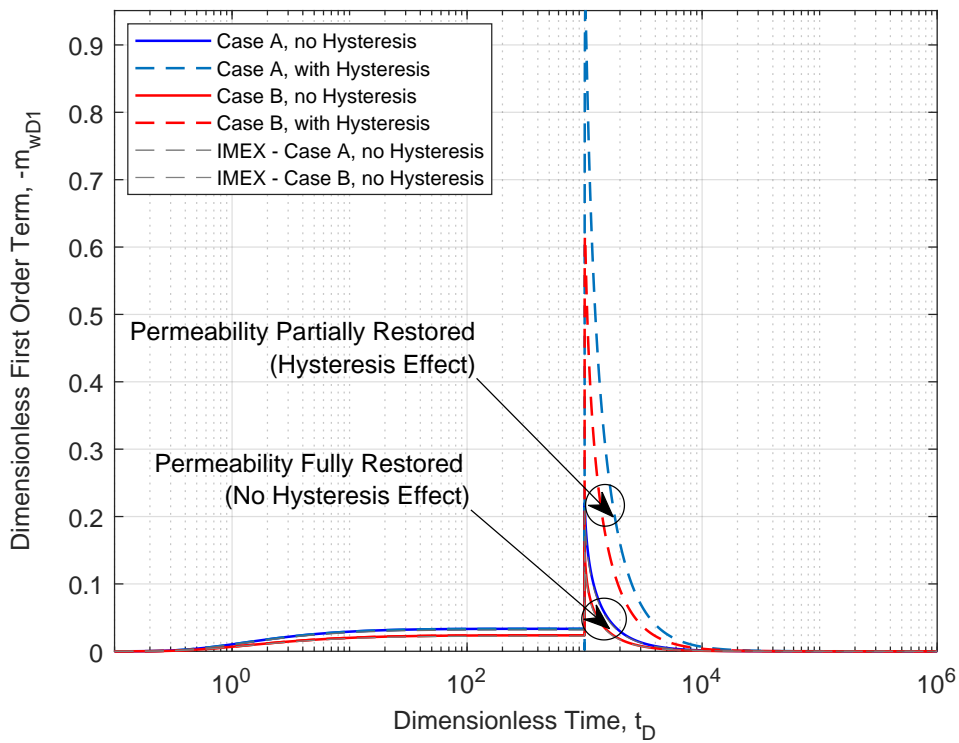


Figure 6.35: Semi-log plot of the permeability-hysteresis response in the first-order term for $t_{pD} = 10^3$.

Figure 6.37 shows the hydraulic diffusivity deviator factor on the dimensionless first-order term considering the permeability-hysteresis. The results show that, larger values of the deviator factor results in the increase of the hysteretic response. Thereby, as the nonlinearity get larger, the permeability restoration becomes lower caused by the hysteresis growth.

Figure 6.38 presents the Semi-log plot of the deviator factor on the dimensionless first-order term for the drawdown and build-up periods considering the permeability-hysteresis. We can notice the same effect presented in Figure 6.37.

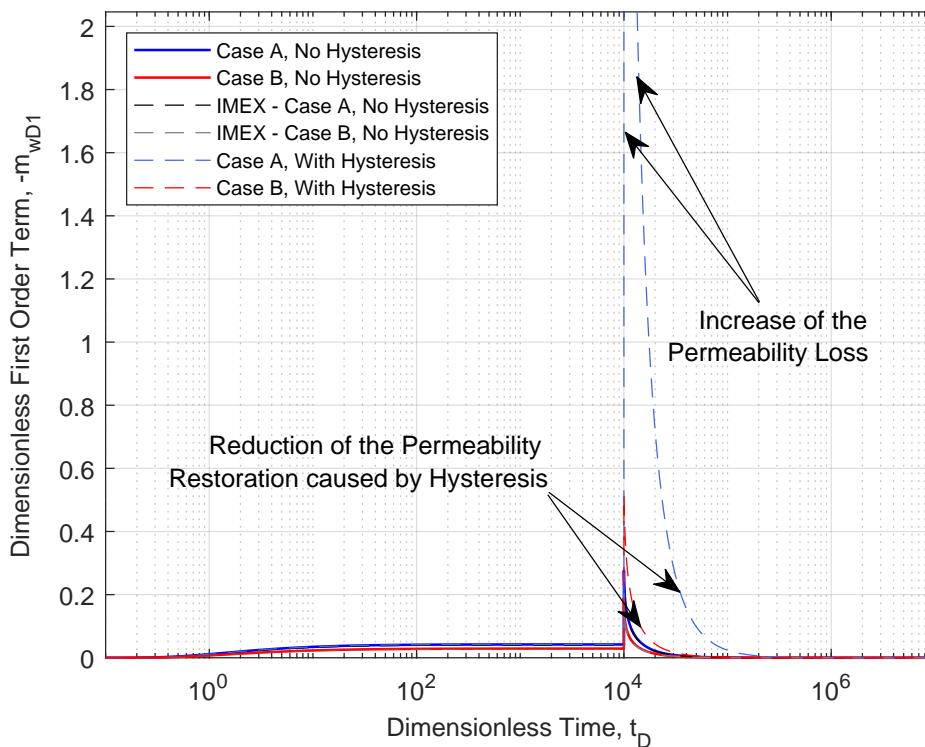


Figure 6.36: Semi-log plot of the permeability-hysteresis response in the first-order term for $t_{pD} = 10^4$.

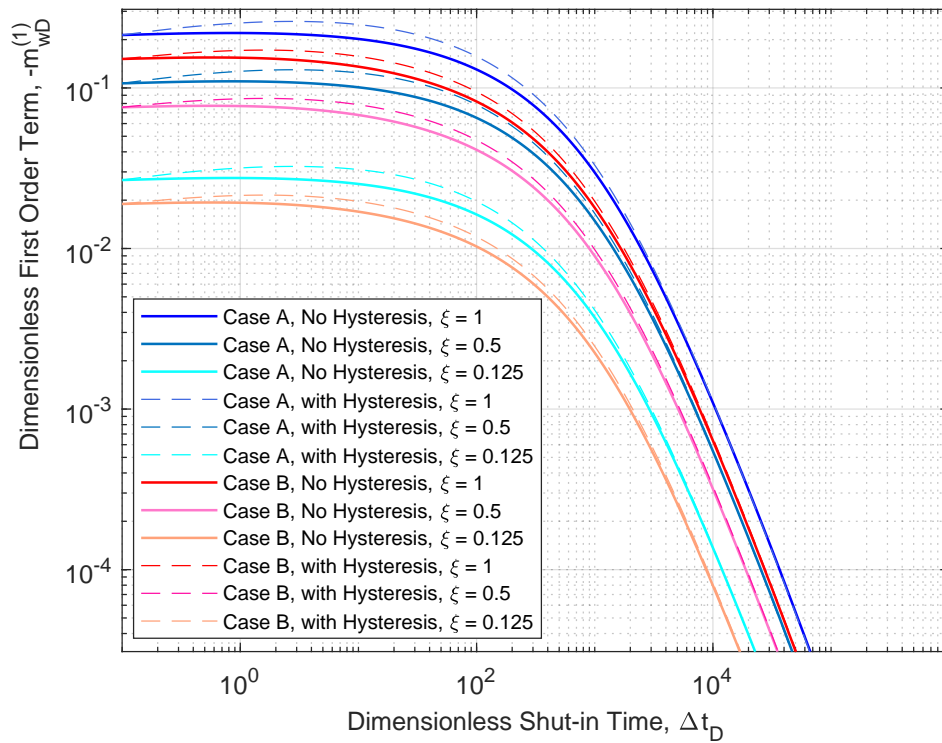


Figure 6.37: Log-log plot of the effect from the hydraulic diffusivity deviator factor on the first-order term with permeability-hysteresis.

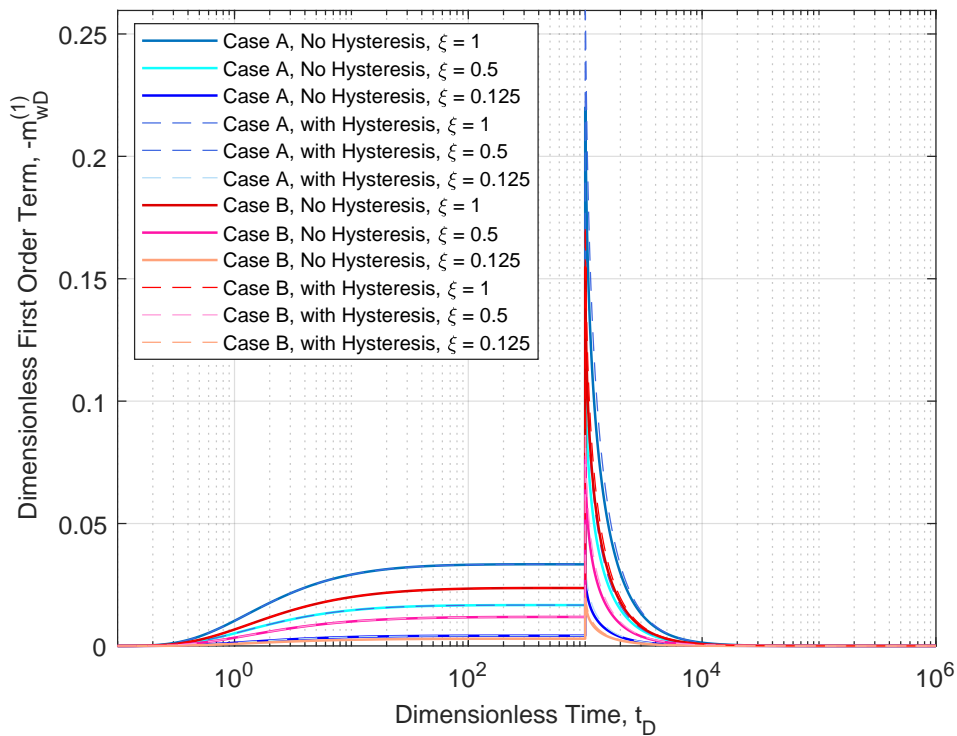


Figure 6.38: Semi-log plot of pseudo-pressure variation as a function of the time for several oil flow rates for the case study B.

Figures 6.39 and 6.40 present the hysteretic behavior of the dimensionless pseudo-pressure and the constant permeability change in the Horner plot.

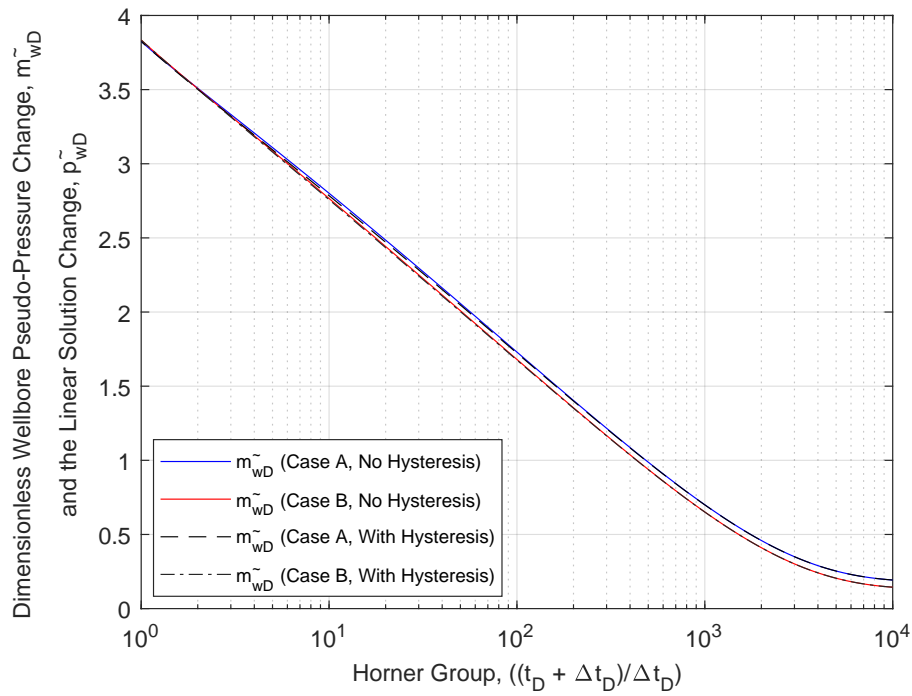


Figure 6.39: Semi-log plot of dimensionless pseudo-pressure change with hysteresis for the case studies A and B.

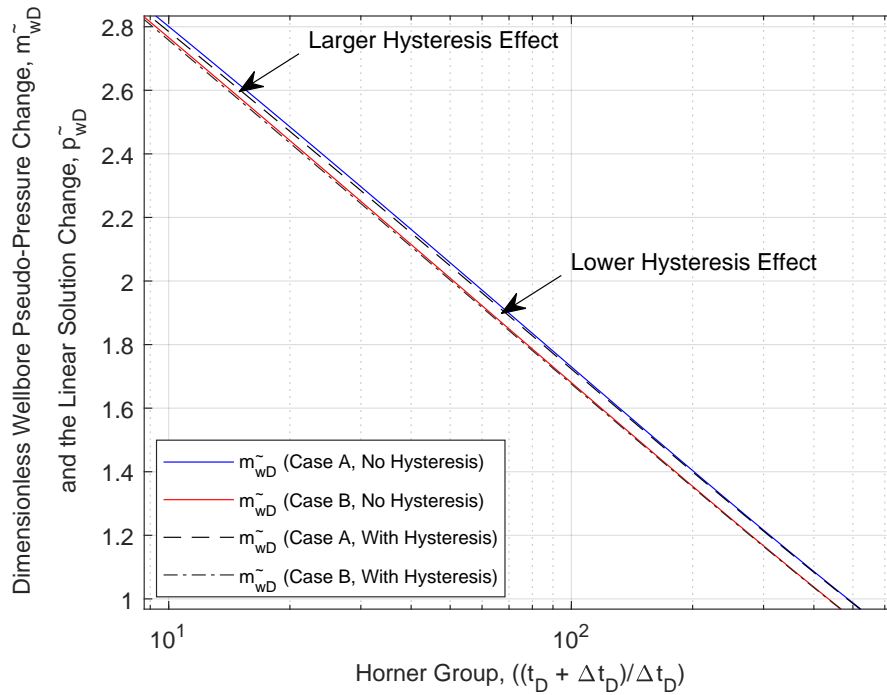


Figure 6.40: Semi-log plot of the amplification of the dimensionless pseudo-pressure change with hysteresis for the case studies A and B.

It is possible to notice, that the hysteresis effect is quite low in the Horner plot. The amplification of this response is shown in Figure 6.40 and can realize the smooth displacements with respect to the non-hysteretic curves, so that, when hysteresis is considered, the values of the pseudo-pressure change curves become lower. We also realize that, the hysteretic behavior is stronger in lower Horner group values.

7

Integro-Differential Solution for Permeability Loss Management with Geomechanical Coupling

This chapter develops a new analytical solution for the nonlinear hydraulic diffusivity equation (NHDE) with instantaneous point-source/sink effects in Biot's effective stress-sensitive oil reservoirs. The proposed model considers Biot's effective stress change in the permeability response, and a new deviation factor is derived from comparing the nonlinear effect concerning the constant permeability classical solution and a decoupled case available in the literature. The mathematical modeling derived in this chapter uses Biot's equation for coupling the set of pressure and permeability field data $(p, k(p))$ to the values of Biot's effective stress and permeability $(\sigma', k(\sigma'))$. Hence, $(p, k(p)) \mapsto (\sigma', k(\sigma'))$. The solution presented in this work allows representing in a simple and accurate manner the permeability response during the production's time and supports the well-reservoir performance management. The dimensionless Biot's effective stress-sensitive permeability is presented in Figure 7.1.

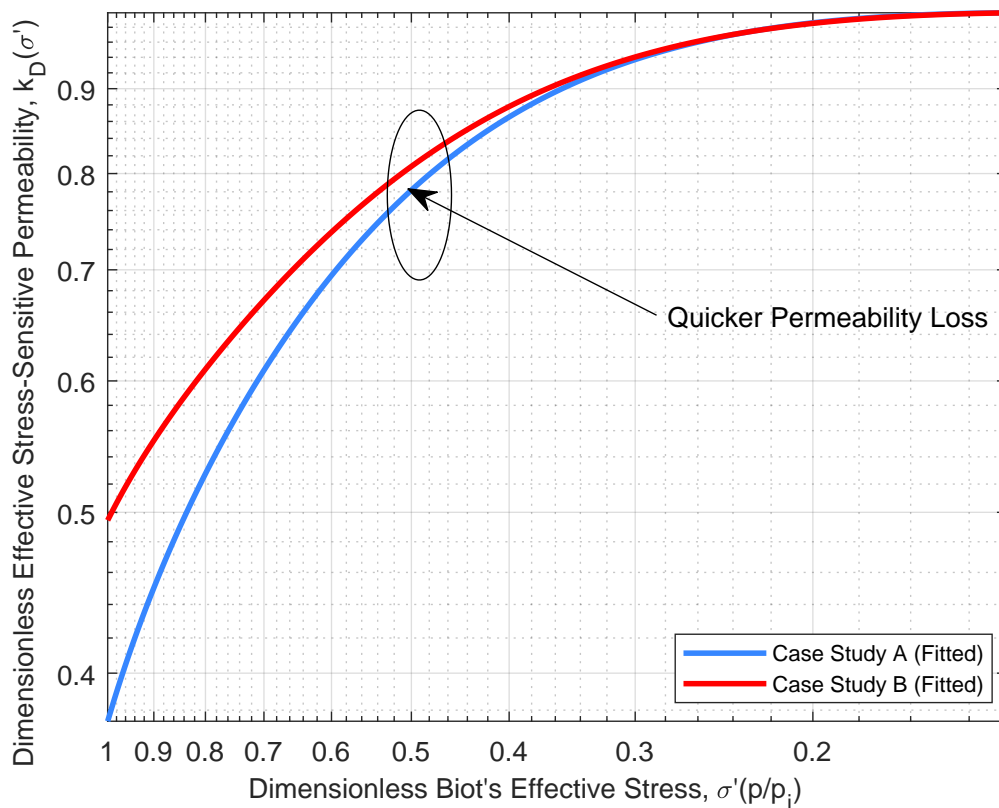


Figure 7.1: Log-log plot of the dimensionless permeability as a function of the dimensionless Biot's effective stress.

We can notice that, as the dimensionless effective stress raises, the dimensionless permeability drops. For values of dimensionless effective stress over 0.5, the dimensionless permeability drops significantly.

7.1

Theoretical Definitions

Let the oil flow through an infinite reservoirs in a permeability effective stress-sensitive reservoir in the cylindrical coordinates $\underline{r} = (r, 0, 0) \in \mathbb{R}^2$ and $t \in \mathbb{R}$. The NHDE in terms of pore pressure and source/sink effects is:

$$\frac{1}{r} \frac{\partial}{\partial r} \left[rk(p) \frac{\partial p}{\partial r} \right] - \phi \mu c_t \frac{\partial p}{\partial t} = -\tilde{q} \mu \quad (7-1)$$

The right-hand side of Eq. 7-1 represents the source/sink term. The variable p is the pressure field inside the reservoir pores, [MPa]; $k(\sigma')$ is the permeability-pressure-sensitive, [md]; ϕ is the porosity, [dimensionless]; μ is the dynamic viscosity, [Pa sec]; t is the time, [sec]; c_t the total compressibility, [1/MPa] and \tilde{q} is the oil flow rate per volume, [sec⁻¹]. Let us transform pore pressure field (p) into effective stress (σ') using Biot's equation of poro-elasticity (Biot, 1941):

$$\sigma'(p) = \sigma_{ob} - \alpha p \quad (7-2)$$

Where σ_{ob} is overburden stress, [MPa] and α is Biot's coefficient, [dimensionless]. The pore pressure as a function of effective stress is given by:

$$p = \frac{\sigma_{ob} - \sigma'}{\alpha} \quad (7-3)$$

Pore pressure gradient is:

$$\frac{\partial p}{\partial r} = -\frac{1}{\alpha} \frac{\partial \sigma'}{\partial r} \quad (7-4)$$

Pore pressure rate is:

$$\frac{\partial p}{\partial t} = -\frac{1}{\alpha} \frac{\partial \sigma'}{\partial t} \quad (7-5)$$

After using Biot's equation, pressure-sensitive permeability becomes effective stress-sensitive, *i.e.*, $k(p) \mapsto k(\sigma')$. Replacing Eqs. 7-4 and 7-5 into Eq. 7-1:

$$-\frac{1}{\alpha r} \frac{\partial}{\partial r} \left[rk(\sigma') \frac{\partial \sigma'}{\partial r} \right] + \frac{\phi \mu c_t}{\alpha} \frac{\partial \sigma'}{\partial t} = \tilde{q} \mu \quad (7-6)$$

Multiplying both sides of Eq. 7-6 by -1 , the effective stress-sensitive NHDE becomes:

$$\frac{1}{\alpha} \left\{ \frac{1}{r} \frac{\partial}{\partial r} \left[rk(\sigma') \frac{\partial \sigma'}{\partial r} \right] - \frac{\partial \sigma'}{\partial t} \right\} = -\tilde{q}\mu \quad (7-7)$$

Multiplying both sides of Eq. 7-7 by Biot's coefficient α :

$$\frac{1}{r} \frac{\partial}{\partial r} \left[rk(\sigma') \frac{\partial \sigma'}{\partial r} \right] - \frac{\partial \sigma'}{\partial t} = -\alpha \tilde{q}\mu \quad (7-8)$$

7.1.1

Biot's Effective Stress-Sensitive Pseudo-Pressure Function

Incorporating geomechanics to flow models become the mathematical formulation regarding well-test and reservoir engineering more realistic because geomechanical parameters, *e.g.*, in situ and overburden stress, as well as Biot's coefficient, play a fundamental role in pressure response. In order to evaluate the permeability loss caused by geomechanical effects, let us define Biot's stress-sensitive pseudo-pressure function $m(\sigma')$:

$$m(\sigma') = \int_{\sigma'(p_i)}^{\sigma'(p)} k(\hat{\sigma}') d\hat{\sigma}' \quad (7-9)$$

Where $\hat{\sigma}'$ is the dummy integration variable and $\sigma'(p_i) = \sigma'_i$ (initial effective stress, [MPa]).

Stress-sensitive pseudo-pressure gradient is:

$$\frac{\partial m(\sigma')}{\partial r} = \frac{\partial m(\sigma')}{\partial \sigma'} \frac{\partial \sigma'}{\partial r} \quad (7-10)$$

Stress-sensitive pseudo-pressure derivative in respect to effective stress is:

$$\frac{\partial m(\sigma')}{\partial \sigma'} = \frac{\partial}{\partial \sigma'} \left[\int_{\sigma'(p_i)}^{\sigma'(p)} k(\hat{\sigma}') d\hat{\sigma}' \right] \quad (7-11)$$

That results in

$$\frac{\partial m(\sigma')}{\partial \sigma'} = k(\sigma') \quad (7-12)$$

Replacing Eq. 7-12 into Eq. 7-10, the stress-sensitive pseudo-pressure gradient yields to:

$$\frac{\partial m(\sigma')}{\partial r} = k(\sigma') \frac{\partial \sigma'}{\partial r} \quad (7-13)$$

Regrouping Eq. 7-13:

$$\frac{\partial \sigma'}{\partial r} = \frac{1}{k(\sigma')} \frac{\partial m(\sigma')}{\partial r} \quad (7-14)$$

Stress-sensitive pseudo-pressure rate is:

$$\frac{\partial m(\sigma')}{\partial t} = k(\sigma') \frac{\partial \sigma'}{\partial t} \quad (7-15)$$

Rewriting Eq. 7-15 as a function of Biot's effective stress rate:

$$\frac{\partial \sigma'}{\partial t} = \frac{1}{k(\sigma')} \frac{\partial m(\sigma')}{\partial t} \quad (7-16)$$

Replacing Eqs. 7-13 and 7-16 into Eq. 7-8, Biot's stress-sensitive NHDE becomes:

$$\frac{1}{r} \frac{\partial}{\partial r} \left[\frac{\partial m(\sigma')}{\partial r} \right] - \frac{\phi \mu c_t}{k(\sigma')} \frac{\partial m(\sigma')}{\partial t} = -\alpha \tilde{q} \mu \quad (7-17)$$

This partial differential equation couples geomechanical effects, *e.g.*, overburden stress, Biot's coefficient, and effective stress into the hydraulic diffusivity equation for modeling of permeability loss during oil flow over the well-reservoir production curve.

7.1.2 Dimensionless Model

The dimensionless geomechanical-flow modeling of the effective permeability loss is based on the following relationships present in **Table 7.1**:

Table 7.1: Dimensionless parameters used in the model presented in this paper (Lee, Rollins & Spivey, 2003)

Dimensionless Parameter	Equation
Radial Component	$r_D = r/r_w$
Time	$t_D = k(\sigma'_i)t/\phi\mu c_t r_w^2$
Permeability	$k_D(\sigma') = k(\sigma')/k(\sigma'_i)$
Pseudo-Pressure	$m_D = 2\pi h/q\mu\Delta m(\sigma')$

Where h is the reservoir net pay, [m] and r_w is the wellbore radius, [m]. The Biot's stress-sensitive pseudo-pressure change is:

$$\Delta m(\sigma') = \int_{\sigma'_i}^{\sigma'_b} k(\hat{\sigma}') d\hat{\sigma}' - \int_{\sigma'_i}^{\sigma'^{(p)}} k(\hat{\sigma}') d\hat{\sigma}' \quad (7-18)$$

That results in:

$$\Delta m(\sigma') = \int_{\sigma'(p)}^{\sigma'_b} k(\hat{\sigma}') d\hat{\sigma}' \quad (7-19)$$

Where σ'_b and σ'_i represent Biot's effective stress under reference, and initial conditions, respectively, [MPa]. Hence, Eq. 7-17 also can be expressed in terms of stress-sensitive pseudo-pressure change as follows:

$$\frac{1}{r} \frac{\partial}{\partial r} \left[\frac{\partial \Delta m(\sigma')}{\partial r} \right] - \frac{\phi \mu c_t}{k(\sigma')} \frac{\partial \Delta m(\sigma')}{\partial t} = -\alpha \tilde{q} \mu \quad (7-20)$$

Based on the dimensionless variables defined in Table 7.1, it is possible to compute the dimensionless gradient:

$$\frac{\partial}{\partial r} = \frac{\partial}{\partial (r_w r_D)} = \frac{1}{r_w} \frac{\partial}{\partial r_D} \quad (7-21)$$

The rate operator is

$$\frac{\partial}{\partial t} = \frac{k(\sigma'_i)}{\phi \mu c_t r_w^2} \frac{\partial}{\partial t_D} \quad (7-22)$$

Since:

$$\Delta m(\sigma') = \frac{q \mu m_D}{2\pi h} \quad (7-23)$$

Replacing the Eqs. 7-21, 7-22 and 7-23 into the Eq. 7-20:

$$\frac{q}{2\pi r_w^2 h} \left[\frac{1}{r_D} \frac{\partial}{\partial r_D} \left(r_D \frac{\partial m_D}{\partial r_D} \right) - \frac{1}{k_D(\sigma')} \frac{\partial m_D}{\partial t_D} \right] = -\alpha \tilde{q} \quad (7-24)$$

Rewriting Eq. 7-24

$$\frac{1}{r_D} \frac{\partial}{\partial r_D} \left(r_D \frac{\partial m_D}{\partial r_D} \right) - \frac{1}{k_D(\sigma')} \frac{\partial m_D}{\partial t_D} = -\frac{2\pi \alpha \tilde{q} r_w^2 h}{q \mu} \quad (7-25)$$

Let the definition of oil flow rate per volume unit \tilde{q} be expressed in terms of the wellbore geometric parameters

$$\tilde{q} = \frac{q}{r_w^2 h} \quad (7-26)$$

The final form of the dimensionless stress-sensitive NHDE in terms of pseudo-pressure for modeling the geomechanical-flow coupling for estimating permeability loss during oil flow in an infinite oil reservoir is:

$$\frac{1}{r_D} \frac{\partial}{\partial r_D} \left(r_D \frac{\partial m_D}{\partial r_D} \right) - \frac{1}{k_D(\sigma')} \frac{\partial m_D}{\partial t_D} = -2\pi\alpha \quad (7-27)$$

The dimensionless initial condition (IC) is

$$m_D(r_D, t_D = 0) = 0 \quad (7-28)$$

And the the external boundary condition (EBC) is

$$\lim_{|r_D| \rightarrow \infty} m_D(r_D, t_D) = 0 \quad (7-29)$$

7.1.3 Geomechanical-Integro-Differential Solution

Using a first-order asymptotic series expansion, the NHDE becomes:

$$m_D = -\frac{\alpha}{2} \mathbf{Ei} \left(-\frac{1}{4t_D} \right) + m_D^{(1)} \quad (7-30)$$

Where $\mathbf{Ei}(-1/4t_D) = \mathbf{Ei} \left[-\frac{\phi\mu c_t r_w^2}{4k(\sigma'_i)t} \right]$ is the transcendental exponential integral function, expressed by (Abramowitz & Stegun, 1972):

$$\mathbf{Ei} \left[-\frac{\phi\mu c_t r_w^2}{4k(\sigma'_i)t} \right] = -\int_{-\frac{\phi\mu c_t r_w^2}{4k(\sigma'_i)t}}^{+\infty} \frac{e^{-u}}{u} du \quad (7-31)$$

The first-order corrective term is:

$$m_D^{(1)} = \int_0^\infty \int_0^{t_D} \left[\frac{1}{k_D(p_D)} - 1 \right] \frac{\partial p_D}{\partial t'_D} G_D(r_D, r'_D, t_D, t'_D) \mathbf{I}_0 \left[\frac{r'_D r_{D0}}{2(t'_D - t_{D0})} \right] dt'_D dr'_D \quad (7-32)$$

The dimensionless GF associated to the problem is (Carslaw & Jaeger, 1959):

$$G_D(r_D, r_{D0}, t_D, t_{D0}) = \frac{e^{-\frac{(r_D^2 + r_{D0}^2)}{4(t_D - t_{D0})}}}{4\pi(t_D - t_{D0})} \mathbf{I}_0 \left[\frac{r_D r_{D0}}{2(t_D - t_{D0})} \right] \quad (7-33)$$

Where \mathbf{I}_0 is the modified zeroth order and first kind Bessel function. Hence, the corrective term yields to:

$$m_D^{(1)} = \int_0^\infty \int_0^{t_D} \left[\frac{1}{k_D(p_D)} - 1 \right] \frac{\partial p_D}{\partial t'_D} \frac{e^{-\frac{(r'_D)^2 + r_{D0}^2}{4(t'_D - t_{D0})}}}{4\pi(t'_D - t_{D0})} \mathbf{I}_0 \left[\frac{r'_D r_{D0}}{2(t'_D - t_{D0})} \right] dt'_D dr'_D \quad (7-34)$$

Replacing Eq. 7-34 in Eq. 7-30 and, combining the first-order asymptotic series expansion to the developed integro-differential solution, the dimensionless general solution in an infinite radial domain in the wellbore ($r_D = 1$) is:

$$m_D = -\frac{\alpha}{2} \mathbf{Ei} \left(-\frac{1}{4t_D} \right) - \int_0^\infty \int_0^{t_D} \left[\frac{1}{k_D(p_D)} - 1 \right] \frac{\partial p_D}{\partial t'_D} \times \frac{e^{-\frac{(r'_D)^2 + r_{D0}^2}{4(t'_D - t_{D0})}}}{4\pi(t'_D - t_{D0})} \mathbf{I}_0 \left[\frac{r'_D r_{D0}}{2(t'_D - t_{D0})} \right] dt'_D dr'_D \quad (7-35)$$

Using a linear stress-sensitive permeability function, as suggested by [Fernandes \(2022\)](#), the dimensionless general solution yields to:

$$m_D = -\frac{\alpha}{2} \mathbf{Ei} \left(-\frac{1}{4t_D} \right) - \int_0^\infty \int_0^{t_D} \left[\frac{1}{-\frac{c_1 \alpha}{2} \mathbf{Ei} \left(-\frac{1}{4t'_D} \right) + c_2} - 1 \right] \frac{\partial p_D}{\partial t'_D} \times \frac{e^{-\frac{(r'_D)^2 + r_{D0}^2}{4(t'_D - t_{D0})}}}{4\pi(t'_D - t_{D0})} \mathbf{I}_0 \left[\frac{r'_D r_{D0}}{2(t'_D - t_{D0})} \right] dt'_D dr'_D \quad (7-36)$$

Eq. 7-36 is the dimensionless general solution composed by the linear solution (first term) and the nonlinear one (second term inside the double integral) to predict the permeability loss over the oil well-reservoir life-cycle. The constants c_1 and c_2 are obtained from the experimental points and fitting curve.

7.2 Model Calibration, Results and Discussions

This doctoral thesis presented a new method for providing permeability loss prediction during the oil production curve in Biot's effective stress-sensitive reservoirs. Some stress-sensitive parameters, model calibration, sensitivity analysis and a comparison between the developed solution and constant permeability case are addressed in this section.

7.2.1 Effective Stress-Sensitive Parameters

To evaluate the nonlinearities caused by permeability change as a function of the pressure, the effective stress-sensitive deviation factor, $\xi(\sigma')$ is presented in Figure 7.2. This plot reveals that, as Biot's effective stress raises, the deviation in respect to constant permeability case increases quickly. As aforementioned, to solve the NHDE, it was developed a new Biot's effective stress-sensitive pseudo-pressure, $m(\sigma')$. After applying the transformation $p \mapsto m(\sigma', k(\sigma'))$, the pseudo-pressure data were inserted into the code to verify the response of the solutions (Figure 7.3).

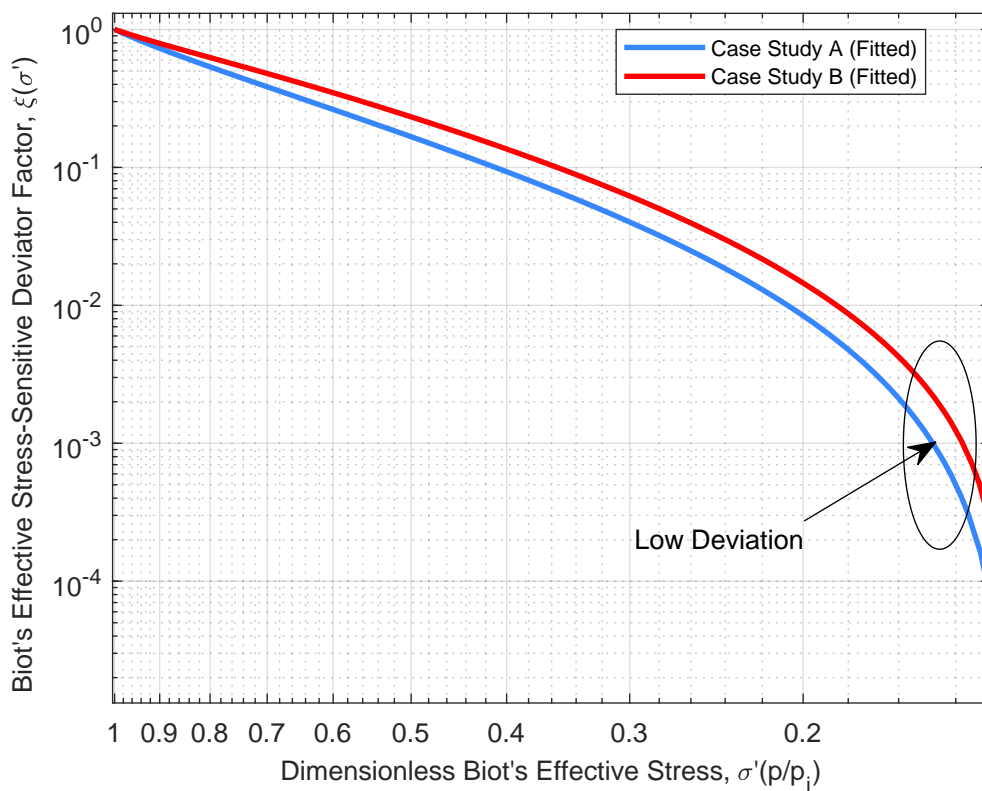


Figure 7.2: Log-log plot of Biot's effective stress-sensitive deviation factor versus dimensionless effective stress.

As the pseudo-pressure provides the information of the permeability change instantaneously as a function of the pressure, it is possible to notice that, as the pore pressure ratio decreases, the stress-sensitive pseudo-pressure ratio vanishes. This response is caused by the permeability dependence in the pseudo-pressure function. The model developed in this study allows the adequate well-reservoir management by formation evaluation and reservoir engineering team by the surveillance of pressure and effective stress response during drawdown period.

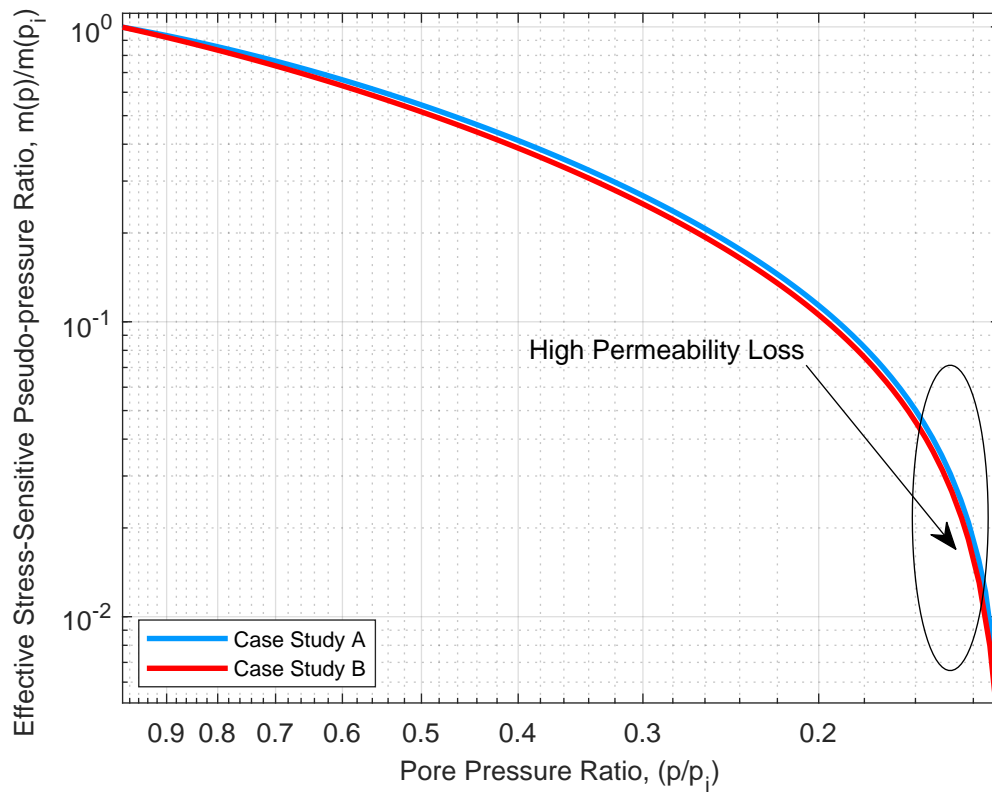


Figure 7.3: Log-log plot of the effective stress-sensitive pseudo-pressure ratio versus the pore pressure ratio.

7.2.2 Model Calibration

To check the model accuracy, the code developed for both case studies was compared to a porous media numerical simulator named IMEX[®]. The calibration methodology was performed by replacing the set of values of $(\sigma', k(\sigma'))$ from the experimental data for the case studies as an input information to IMEX[®]. The value of Biot's coefficient was kept in 0.9 (consolidated sandstones). This parameter has an important role in effective stress response, because it is responsible for the hydraulic damping of the overburden applied to the reservoir. The calibration of the dimensionless linear solution (exponential integral function for constant permeability) against IMEX[®] is shown in Figure 7.4 and we notice high convergence. To perform this calibration, it was used the command $ei(t_D)$ from Matlab[®] with time steps of 0.01 and, the computational code ran quite fast. Figure 7.5 shows the Log-log plot of the calibration of the dimensionless first-order term $m_D^{(1)}(t_D)$ and it has shown an excellent convergence, when compared to IMEX[®], even in the early-times.

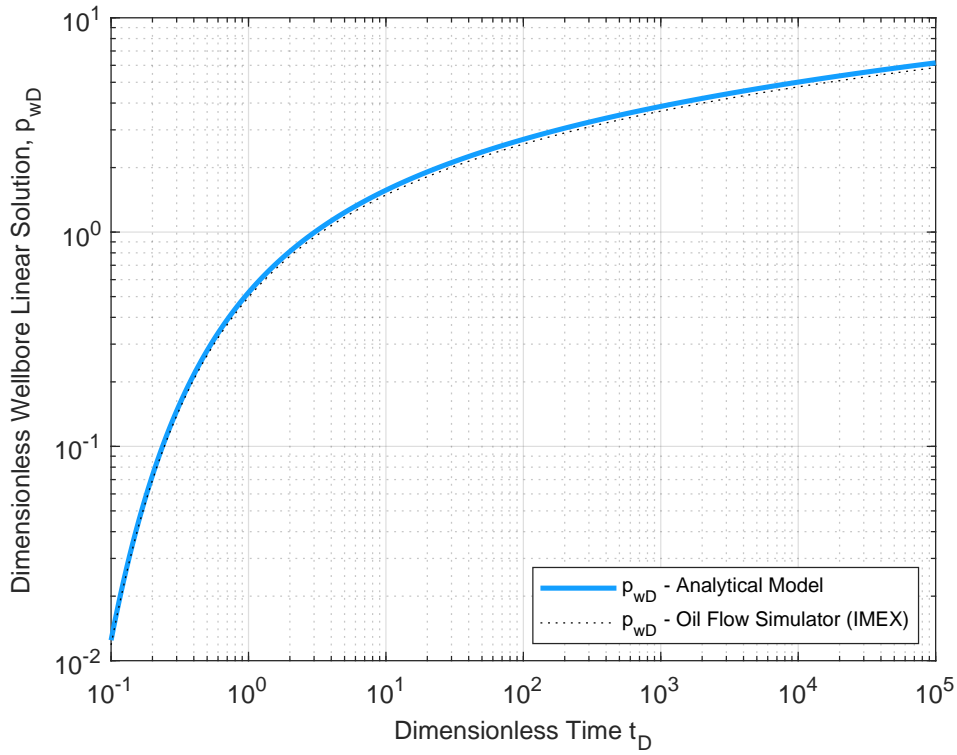


Figure 7.4: Log-log plot of the constant permeability solution calibrated by IMEX®.

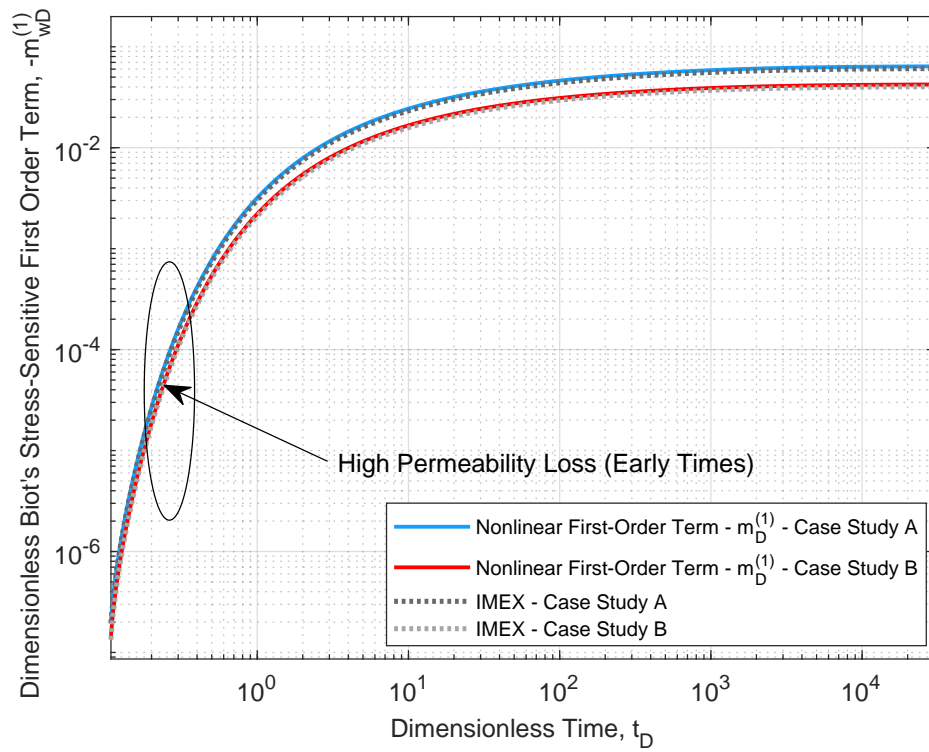


Figure 7.5: Log-log plot of Biot's effective stress-sensitive first-order term calibrated by IMEX®. This plot shows that, the nonlinearity that results in permeability loss is more severe during the early-times.

Therewith, as presented in previous work of [Peres, Serra & Reynolds \(1989\)](#) it is possible to conclude that the first-order asymptotic series expansion represents, accurately, the nonlinearity caused by the permeability change as a function of Biot's effective stress in the analytical model presented in this thesis. This plot also reveals the high accuracy of the model developed with respect to IMEX[®] (dot and dashed lines).

7.2.3 Sensitivity Analysis

In order evaluating which geomechanical and flow parameters have the most influence on permeability drop, a sensitivity analysis was carried out. Thereby, some changes in overburden stress, Biot's coefficient, source/sink term, and the stress-sensitive deviation factor were performed. The influence of overburden stress in the nonlinear stress-sensitive first-order term becomes clearer in in Figure 7.6.

PUC-Rio - Certificação Digital N° 1912769/CA

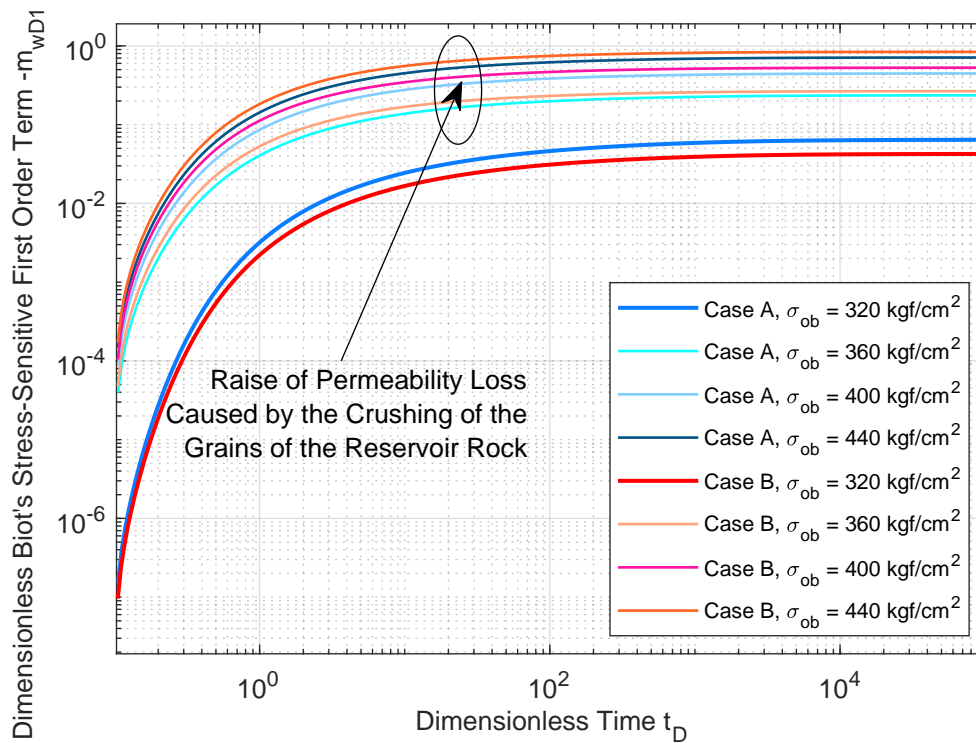


Figure 7.6: Log-log plot of the first-order term for several overburden stress.

Thus, the hydraulic damping caused by the second term of Eq. 7-36 reduced the nonlinearity of the corrective term. Biot's effective stress magnitude may increase or decrease permeability loss, and it depends on a balance between overburden stress σ_{ob} and the term αp . If overburden is high and this second term of Biot's equation is low or moderate, permeability

loss will increase. On the other hand, if overburden is low, *e.g.* shallow wells environments and αp term is high, thus effective stress declines and permeability response reaches higher values. As the nonlinearity of the NHDE is related to permeability loss, we can conclude that Biot's stress change results in a lowering or rise in permeability drop. The role of the nonlinearity responsible for permeability effective stress-sensitive decline is presented in Figure 7.7. This plot compares the linear solution, where permeability is considered a constant, and the proposed model that considers its change over the well-reservoir life-cycle. A clear deviation caused by the coupling of geomechanical-flow effects on permeability loss (blue and red lines) is noticed concerning the constant permeability solution (black line). For this simulation, Biot's coefficient was also fixed at the value $\alpha = 0.9$ (consolidated sandstones).

PUC-Rio - Certificação Digital N° 1912769/CA

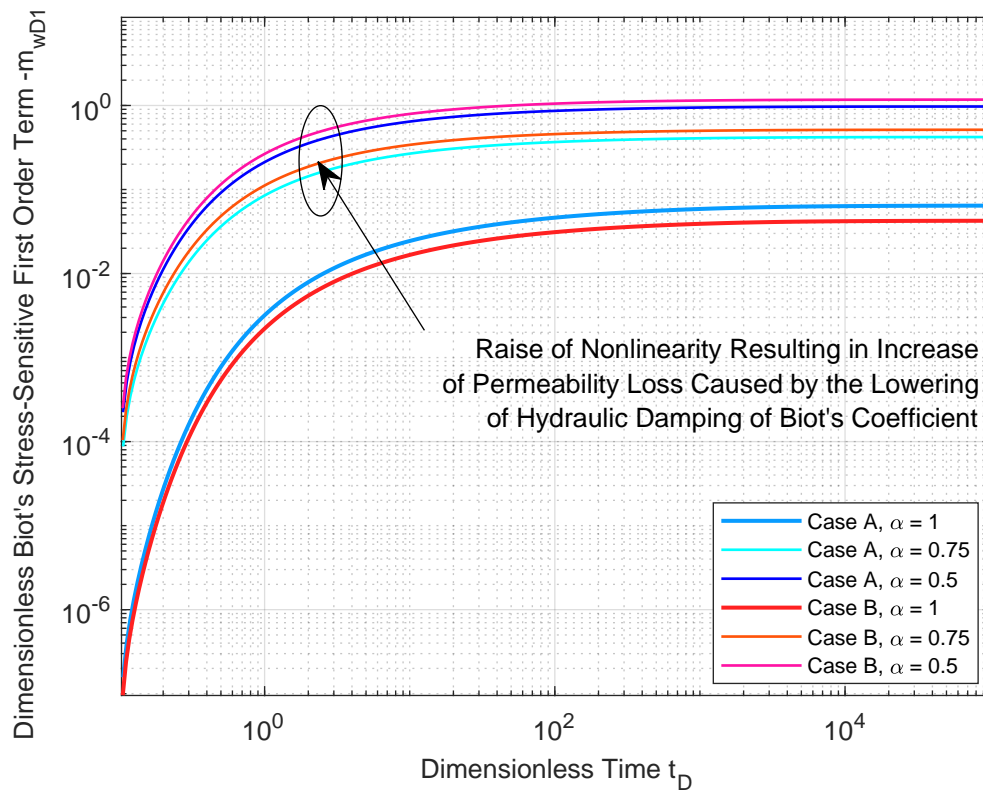


Figure 7.7: Log-log plot of influence of Biot's coefficient in the permeability loss raise.

The role of the dimensionless first-order oil source in the general effective stress-sensitive pseudo-pressure and first-order term is presented in Figure 7.8. Clearly, we can realize that, the increase of source term (dimensionless oil flow rate) results in permeability loss. Figure 7.9 presents the influence of the effective stress-sensitive deviation factor in the nonlinear term. The results show that, as this factor increases (green, navy blue, pink, clear blue and orange curves), the permeability change becomes larger.

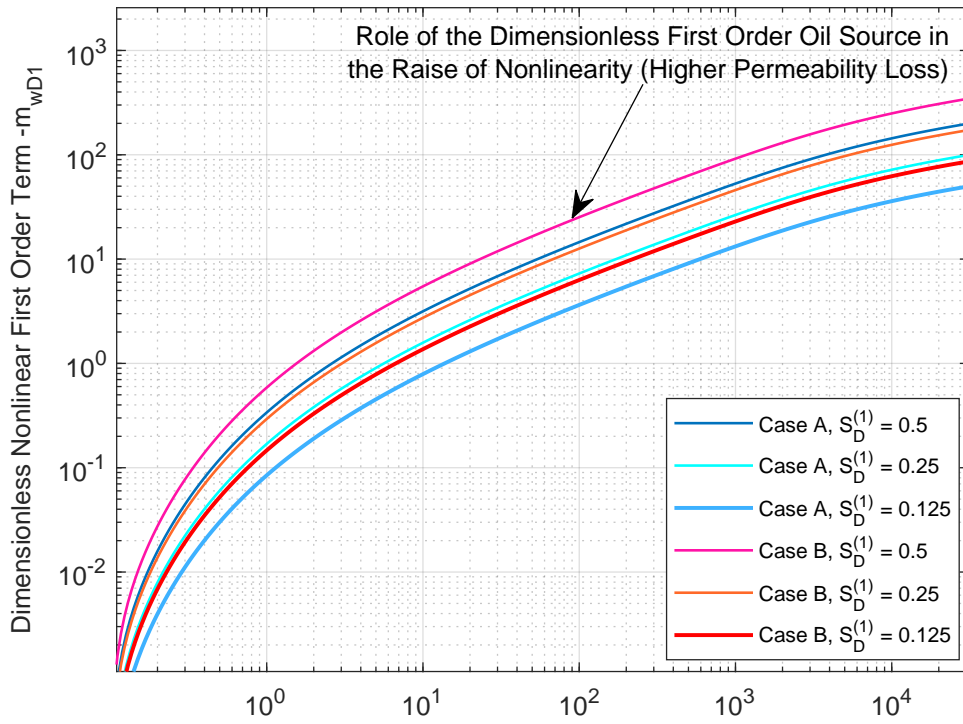


Figure 7.8: Log-log plot of influence of dimensionless first-order source in the permeability loss lowering (first-order term).

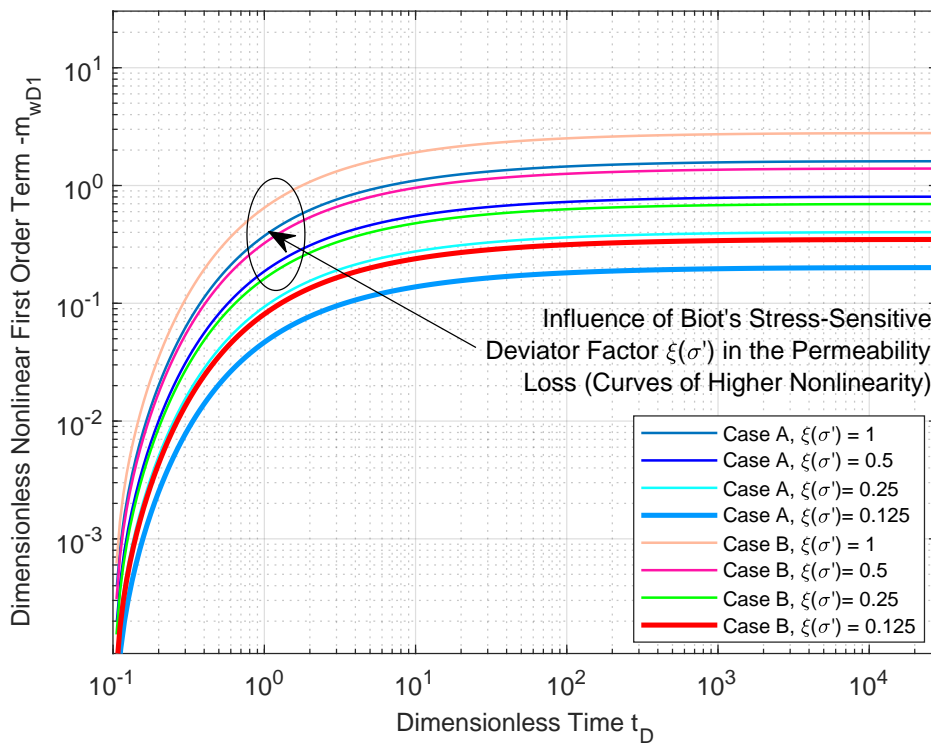


Figure 7.9: Log-log plot of influence of effective stress-sensitive deviator factor in the permeability loss lowering over the dimensionless elapsed time.

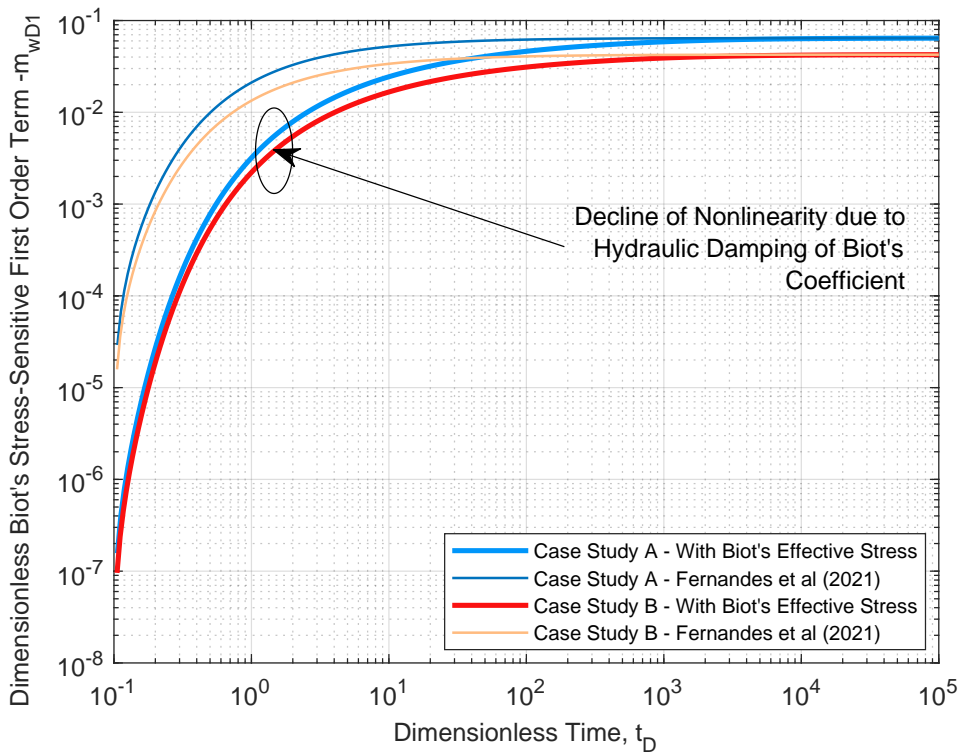


Figure 7.10: Log-log plot of the comparison between the model developed in this work with Biot's effective stress-sensitive effect and the solution presented by Fernandes et al. (2021a). For this simulation, Biot's coefficient was fixed at the value $\alpha = 0.9$ (consolidated sandstones).

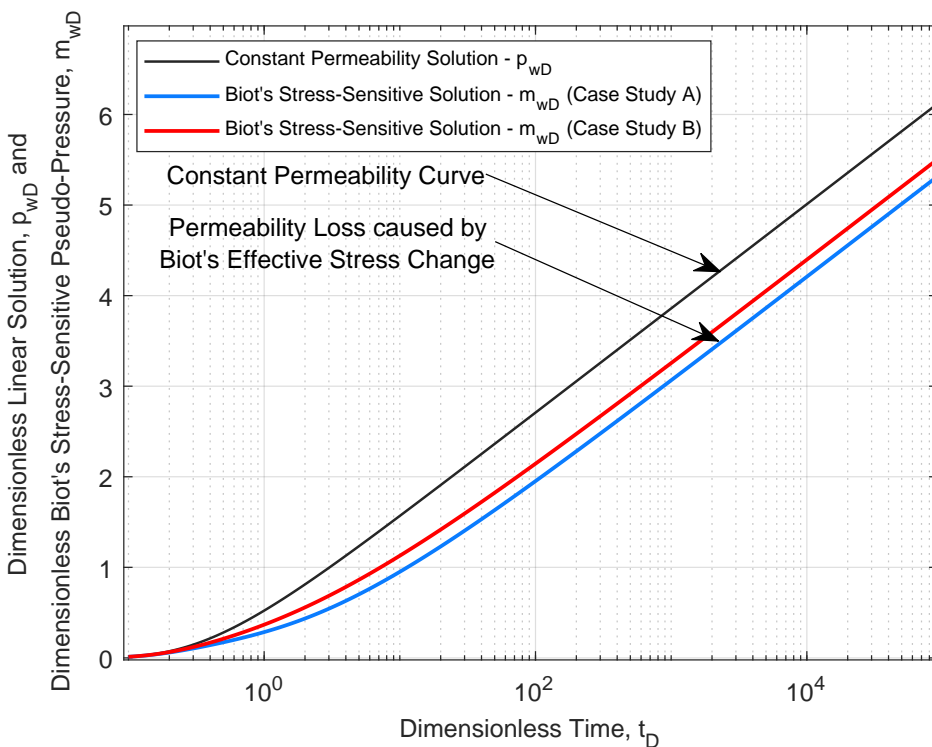


Figure 7.11: Semi-log plot of the comparison between constant permeability and Biot's effective stress-sensitive solution.

An important comparison between the model derived by [Fernandes et al. \(2021b\)](#) where the permeability did not have Biot's effective stress dependence and this work, where this effect is considered in the deviation factor, is presented in Figure 7.10. The effect of the effective stress in the first-order corrective term is clearly observed in this plot. For this simulation, it was used Biot's coefficient $\alpha = 0.9$, which represents a high value for this parameter. Thus, the hydraulic damping provided by the second term of Biot's equation reduced the nonlinearity of the corrective term. Biot's effective stress magnitude may increase or decrease permeability loss and it depends on a balance between overburden stress and the term αp of Biot's equation. If overburden is high and this second term of Biot's equation is low or moderate, permeability loss will increase. On the other hand, if overburden is low, *e.g.* shallow wells environments and αp term is high, thus effective stress declines and permeability response reaches higher values. As the nonlinearity of the NHDE is related to permeability loss, we can conclude that Biot's stress change results in a lowering or raise in permeability drop. The role of the nonlinearity responsible for permeability effective stress-sensitive decline is presented in Figure 7.11.

Conclusions and Future Works

This doctoral thesis extended the formulation developed by [Barreto Jr., Peres & Pires \(2010\)](#) and presented some integro-differential solutions for several nonlinear oil flow problems in different well-reservoir settings in permeability pressure-sensitive reservoirs. The solutions developed in this thesis allowed us to predict the instantaneous permeability loss and support the well-reservoir performance management through pressure monitoring and the appropriate choice of the oil flow rate. The results show that the developed solution is accurate compared to IMEX[®]. Therefore, the first-order perturbative asymptotic series expansion is sufficient to represent the nonlinear effect caused by the permeability changes in the reservoir. This model constitutes a reliable and valuable mathematical tool to calibrate new models related to formation evaluation and reservoir engineering, saving computational costs compared to the numerical simulators' acquisition costs. The model was also able to represent clearly the permeability change effect through a smooth deviation of the dimensionless pseudo-pressure $m_D(t_D)$ compared to the linear solution $p_D(t_D)$ in the Semi-log plot with respect to the dimensionless time. Therefore, it allows the evaluation of the effect of the permeability decline in the oil's production curve over the well-reservoir life-cycle and provides instantaneous information for the reservoir and formation evaluation team to improve reservoir management. The results showed that the dimensionless oil source, which considers the rock and fluid parameters, has a vital role in the hydraulic diffusivity deviator factor and, consequently, in the dimensionless pseudo-pressure solution. The results showed that the rise of the dimensionless source causes permeability change in the rock reservoir, which may lead to the early oil production's decline and impair the well-reservoir life-cycle.

The hysteretic response of the reservoir was simulated, and the results showed that this effect increases the nonlinearity and, thereby, the permeability loss. The fact that most functions involved in the analytical model are available in the Matlab[®] library results in an easy computational solution implementation, and it constitutes a significant advantage of the proposed solution for practical field operations.

A geomechanical coupling considering Biot's effective stress was developed to predict permeability stress-sensitive response. It was concluded that Biot's coefficient and overburden stress have an essential role in permeability loss and well-reservoir management.

8.1

Model Advantages

The advantages of the proposed model are:

The pseudo-pressure derivative, with respect to the pressure, provides the instantaneous permeability value at each point of the pseudo-pressure curve. This is key information to the well-reservoir management and predicts its economic life-cycle. The developed model also allows computing the instantaneous permeability value from quite a few experimental or field data.

As the first-order series expansion is sufficient to represent the permeability loss, the model runs quickly, and it presents a low computational cost compared to the acquisition costs of the commercial simulators in the petroleum industry. The solution is accurate, allowing the calibration of new numerical or analytical models that may arise in the scientific literature. Possibility to solve different nonlinear problems with source term because the GF for different well-reservoir settings and boundary conditions are widely available in the scientific transport phenomena literature.

Ease computational implementation because almost the functions involved in the model are available in the Matlab library. It allows the oil flow rate prediction through the permeabilities curves to avoid severe permeability drops over the well-reservoir life-cycle and minimize economic losses. The practical use for field applications for a wide set of well-reservoir settings problems because it uses the GF, few pressure and permeability field data, and the linear solution $p_D(t_D)$ (to compute its Bourdet derivative) to run the model. It allows noticing clearly the nonlinear effect caused by the permeability variation in a simple manner through a Semi-log plot

8.2

Model Limitations

The model limitations are:

The asymptotic series expansion must be truncated in the first-order term because the recursive algorithm demands the knowledge of the $k - 1$ order derivative in the whole reservoir domain, and it could not be provided for this method. The proposed solution also requires some pressure and permeability field data to input in the hydraulic diffusivity deviator factor in the computational code.

8.3

Model Extension

This work can be extended to:

1. Evaluate the permeability decline for pressure and permeability data from other types of rock reservoirs *e.g.* pre-salt carbonates and unconventional reservoirs.
2. Consider storage and skin effects.
3. Approach multi-layer flow.
4. Simulate different boundary conditions *e.g.* bounded reservoir and other types of well-reservoir settings *e.g.* horizontal wells, fractured wells, finite-acting-radial-flow, partial penetrating well, and limited entry.
5. Couple a non-isothermal oil flow in porous media.
6. Propose new pseudo-pressure functions based on porosity, viscosity, total compressibility.

ABRAMOWITZ, M.; STEGUN, I. A. Handbook of mathematical functions. new york: Dover publications. **Dover Publications**, 1972. 5.1.6, 5.1.6, 5.3.5, 5.4.3, 7.1.3, E, E

ADACHI, J.; SIEBRITS, E.; PEIRCE, A.; J., D. Computer simulation of hydraulic fractures. **International Journal of Rock Mechanics and Mining Sciences and Geomechanics Abstracts 2007**; **44:739–757**, 2007. 2.3

AGARWAL, R. G. A new method to account for producing time effects when drawdown type curves are used to analyze pressure build-up and other test data. **SPE 9289, presented at the 55th Annual Technical Conference and Exhibition, Dallas, Texas, Sept. 21-24, 1980**, 1980. 2.4, 6.1

AGARWAL, R. G.; AL-HUSSAINY; Ramey Jr., H. J. An investigation of wellbore storage and skin effect unsteady liquid flow: I. analytical treatment. **SPE 44 th Annual Fall Meeting, held in Denver, Colo., Sept.28 - Oct.1. American Institute of Mining, Metallurgical and Petroleum Engineers, Inc. SPE 2466**, v. 249, 1970. 2.4

AGARWAL, R. G.; GARDNER, D. C.; KLEINSTEIBER, S. W.; FUSSELL, D. D. Analyzing well production data using combined-type-curve and decline-curve analysis concepts. **Spe Reservoir Evaluation Engineering**, v. 2, p. 478–486, 1999. 2.4, 6.1

AGUILERA, R. Multiple-rate analysis for pressure-buildup tests in reservoirs with tectonic, regional, and contractional natural fractures. **SPE Formation Evaluation**, v. 2, p. 253–260, 1987. 2.4

AGUILERA, R. Well test analysis of naturally fractured reservoirs. **SPE Formation Evaluation**, v. 2, p. 239–252, 1987. 2.4

AHMED, T. Fundamentals of reservoir fluid flow. **Working Guide to Reservoir Rock Properties and Fluid Flow**, **117–246**, 2010. 1, 4.1, 4.1, 4.2

AKBAR, M. N.; SALAM, A.; AWAB, M.; PRAKOSO, S. Interrelationships of rock elastic properties to petrophysical pore structure and geometric details of sandstone. Day 2 Wed, October 30, 2019, 10 2019. 3.4.1

AL-HUSSAINY; Ramey Jr., H. J.; CRAWFORD, P. B. The flow of real gases through porous media. **Society of Petroleum Engineers. doi:10.2118/1243-A-PA**, 1966. 1, 2.2

ALFATAIERGE, A.; MISKIMINS, J. L.; DAVIS, T. L.; BENSON, R. D. 3D Hydraulic-Fracture Simulation Integrated With 4D Time-Lapse Multicomponent Seismic and Microseismic Interpretations, Wattenberg Field, Colorado. **SPE Production Operations**, v. 34, n. 01, p. 57–71, 09 2018. 1.3

- ALMISNED, O. A.; AL-QURAIISHI, A. A.; AL-AWAD, M. N. Effect of triaxial in situ stresses and heterogeneities on absolute permeability of laminated rocks. **Journal of Petroleum Exploration and Production Technology**, 2017. 1.3
- AMBASTHA, A. K.; Ramey Jr., H. J. Well-test analysis for a well in a finite, circular reservoir. **Journal of Canadian Petroleum Technology**, v. 32, 1993. 2.4
- AYAN, C.; LEE, W. The Effects of Multiphase Flow on the Interpretation of Pressure Buildup Tests. 1988. 2.4
- Barreto Jr., A. B.; PERES, A. M. M.; PIRES, A. P. General solution for gas flow in porous media, phd thesis, universidade estadual norte-fluminense (in portuguese). **Society of Petroleum Engineers**. doi:10.2118/173470-PA, 2010. 1.2, 1.4, 2.2, 2.5, 4.5, 4.5, 5.2.4, 5.2.6, 6.1.2, 8
- Barreto Jr., A. B.; PIRES, A. P.; PERES, A. M. M. A rigorous analytical solution for a vertical fractured well in gas reservoirs. **SPE Latin American and Caribbean Petroleum Engineering Conference held in Mexico City, Mexico, 16-18 April, 2012**. 1.2, 2.2, 2.5
- Barreto Jr., A. J.; PERES, A.; PIRES, A. A variable-rate solution to the nonlinear diffusivity gas equation by use of green's-function method. **SPE Journal (SPE 145468)**, 2012. 1.2
- BEAR, J. Dynamics of fluids in porous media. **Dover Classic of Science and Mathematics**, 1972. 1, 4.1, 4.1, 4.2, 4.2
- BECK, J. V.; COLE, K. D.; HAJI-SHEIKH, A.; LITKOUHI, B. Heat conduction using green's functions. **Philadelphia: Hemisphere Publishing Corporation**, 1992. 1.2, 1.2, 5.1.4, 5.2.5, 5.2.5, 5.3.5, 5.4.3, 6.1.2
- BEDRIKOVETSKY, P. G.; FURTADO, C. J. A.; SOUZA, A. L. Serra de; MUHAMMAD, A.; CHANG, G. Taking Advantage of Injectivity Decline for Sweep Enhancing during Waterflood with Horizontal Injectors. 05 2009. 2.1
- BENGTSON, C. A. Statistical curvature analysis techniques for structural interpretation of dipmeter data. **AAPG Bulletin**, p. 312–332, 1981. 5.2
- BIOT, M. A. General theory of three-dimensional consolidation. **Journal of Applied Physics** **12**, 155. <https://doi.org/10.1063/1.1712886>, v. 12, 1941. 2.1, 3.4, 7.1
- BIOT, M. A. Theory of propagation of elastic waves in a fluid-saturated porous solid. i. low-frequency range. **The Journal of the Acoustical Society of America** **28**, 168. <https://doi.org/10.1121/1.1908239>, v. 12, 1956. 2.1, 3, 3.4
- BJØRLYKKE, K. Fluid-flow processes and diagenesis in sedimentary basins. in: Parnell, j. (ed.), geofluids, origin, migration and evolution of fluids in sedimentary basins. **Geol. Soc. Lond. Spec Publ.**, **78**, 127-140, 1994. 1.2

- BLACKER, L. K. An Analysis of Rate-Sensitive Skin in Oil Wells. 09 1982. 2.4
- BLASINGAME, T.; LEE, W. Pressure-buildup test analysis- variable-rate case: A new approach. **SPE Formation Evaluation**, 1989. 2.4
- BOURDET, D. Well test analysis: The use of advanced interpretation models. **Elsevier Science, Amsterdam**, 2002. 5.2.6, 6.1, 6.1.2
- BOURDET, D.; AYOUB, J. A.; PIRARD, Y. M. Use of pressure derivative in well test interpretation. **Society of Petroleum Engineers**. doi:10.2118/12777-PA, 1989. 2.4, 5.2.6, 6.1, 6.1.2
- BOUTECA, M.; SARDA, J.; VINCKE, O. Constitutive law for permeability evolution of sandstones during depletion. **SPE International Symposium on Formation Damage Control**, v. 3, 2000. 2.1
- BRACE, W. F. Permeability from resistivity and pore shape. **Journal of Geophysical Research (1896-1977)**, ISN - 0148-0227. DOI: <https://doi.org/10.1029/JB082i023p03343>, 1977. 2.2
- BROWN, K.; SAWYER, W.; FRANTZ, J. Estimating Non-Darcy Flow Coefficient From Buildup-Test Data With Wellbore Storage. 08 2004. 2.4
- CARSLAW; JAEGER. Conduction of heat in solids. **New York: Oxford Science Publications**, 1959. 1.2, 1.2, 1.2, 5.1, 5.1.4, 5.2.4, 5.2.5, 5.2.5, 5.3.5, 5.4.3, 6.1.2, 7.1.3
- CEIA, M.; MISSAGIA, R.; FASOLO, R.; I.L., N. Relationship between porosity, permeability and pore compressibility. **International Congress of the Brazilian Geophysical Society held in Rio de Janeiro, Brazil**, 2019. 1.3
- CELIS, V.; SILVA, R.; RAMONES M.AND GUERRA, J.; PRAT, G. D. A new model for pressure transient analysis in stress sensitive naturally fractured reservoirs. **SPE Advanced Technology Series**, 2(01), p. 126–135, 1994. 2.1
- CHIN, L. Y.; RAGHAVAN, R.; THOMAS, L. K. Fully coupled geomechanics and fluid-flow analysis of wells with stress-dependent permeability. **Spe Journal**, v. 05, 03 2000. 2.3
- CHO, Y.; APAYDIN, O.; OZKAN, E. Pressure-dependent natural-fracture permeability in shale and its effect on shale-gas well production. **SPE Reservoir Evaluation Engineering**, p. 216–228, 2013. 5.3.2, 5.4.2
- CINCO-LEY, H. Transient pressure analysis for fractured wells. **Journal of petroleum technology**, 1981. 2.3
- CINCO-LEY, H.; SAMANIEGO, F. Effect of wellbore storage and damage on the transient pressure behavior of vertically fractured wells. **SPE annual fall technical conference and exhibition**, 1977. 2.3
- CINCO-LEY, H.; SAMANIEGO, F. Transient Pressure Analysis for Fractured wells. **SPE Formation Evaluation**, v. 1, 1981. 2.3

- CINCO-LEY, H.; SAMANIEGO, F. Pressure Transient Analysis for Naturally Fractured Reservoirs. 09 1982. 2.3, 2.4
- CIVAN, F. Effective-stress coefficients of porous rocks involving shocks and loading/unloading hysteresis. **SPE Journal**, 2020. 1.3
- CLARK, J. B. A hydraulic process for increasing the productivity of wells. **J Pet Technol 1 (1949)**, 1949. 2.3
- COBB, W.; SMITH, J. An investigation of pressure-buildup tests in bounded reservoirs. **Journal of Petroleum Technology**, v. 27, p. 991–996, 1975. 2.4
- COLE; BECK; HAJI-SHEIKH. Heat conduction using green's functions. **second edition. New York: CRC Press**, 2011. 1.2, 1.2, 5.1.4, 5.2.5, 5.2.5, 5.3.5, 5.4.3, 6.1.2
- CORREA, A. C. F.; NEWMAN, R. B.; NAVEIRA, V. P.; SOUZA, A. L. S. de; ARAUJO, T.; SILVA, A. A. C. da; SOARES, A. C.; HERWANGER, J. V.; MEURER, G. B. Integrated Modeling for 3D Geomechanics and Coupled Simulation of Fractured Carbonate Reservoir. 10 2013. 2.1
- CUNNINGHAM, R.; NELSON, R. A new method for determining a well's in-place hydrocarbons from a pressure buildup test. **Journal of Petroleum Technology**, 1967. 2.4
- DANESHY, A. Analysis of off-balance fracture extension and fall-off pressures. **Paper presented at the SPE International Symposium and Exhibition on Formation Damage Control, Lafayette, Louisiana, February 2004**, 2004. 2.3
- DANESHY, A. Pressure variations inside the hydraulic fracture and their impact on fracture propagation, conductivity, and screenout. **SPE Prod Oper 22**, p. 107–111, 2007. 2.3
- DANESHY, A.; BLÜMLING, P.; MARSCHALL, P.; PIET, Z. Interpretation of field experiments and observation of fracturing process. **Paper presented at the SPE International Symposium and Exhibition on Formation Damage Control, Lafayette, Louisiana, February 2004**, 2004. 2.3
- DARCY, H. Les fontaines publiques de la vile de dijon. paris: Dalmont. **Les fontaines Report**, 1856. 1, 1, 3.4.4, 4.1
- DAVIES, J.; DAVIES, D. Stress-dependent permeability: Characterization and modeling. **SPE Annual Technical Conference and Exhibition: Houston**, 1999. 2.1
- DENG, Q.; NIE, R.-s.; JIA, Y.-l.; WANG, X.-l.; CHEN, Y.-y.; XIONG, Y. A New Method of Pressure Buildup Analysis for a Well in a Multiwell Reservoir. Day 2 Tue, September 15, 2015, 09 2015. 2.4
- DUFFY, D. Green's functions with applications. **Chapman and Hall/CRC; 1st edition**, 2001. 1.2, 1.2, 1.2, 5.1.4, 5.2.5, 5.2.5, 5.3.5, 5.4.3, 6.1.2

ECONOMIDES, M. J.; NOLTES, K. G. Reservoir stimulation. **John Wiley Sons, Inc., 605 Third Avenue, New York**, 2000. 5.3

EHLIG-ECONOMIDES, C. A.; NDUONYI, M. A.; ABIAZIE, J. Test Design for Vertical Permeability Determination from a Conventional Pressure Buildup Test. 08 2006. 2.4

EHLIG-ECONOMIDES, C. A.; WELLS, K. L. Average Reservoir Pressure from a Horizontal Well Pressure Buildup Test. 11 2005. 2.4

ESCOBAR, F. H.; BONILLA, L. F.; HERNÁNDEZ, C. M. A practical calculation of the distance to a discontinuity in anisotropic systems from well test interpretation. **DYNA**, **85(207)**, p. 65–73, 2018. 1.3

EVERDINGEN, A. V.; HURST, W. The application of the laplace transformation to flow problems in reservoirs. **Journal of Petroleum Technology**, v. 10, p. 305–324, 1949. 2.1

EVERDINGEN, V. A. F.; HURST, W. The application of the laplace transformation to flow problems in reservoirs. **Society of Petroleum Engineers**. doi:10.2118/949305-G, 1949. 1

FERNANDES, F. Permeability decay evaluation for a nonlinear oil flow through porous media in a wellbore near a sealing fault through green's functions (gf's). **International Conference of Porous Media (Interpore) 13th annual meeting– 31 May – 4 June 2021**, 2021. 1.2, 1.3

FERNANDES, F. Pore pressure sensitivity-permeability decay evaluation for nonlinear oil flow in porous media through green's functions (gf's). **International Conference of Porous Media (Interpore) 13th annual meeting– 31 May – 4 June 2021**, 2021. 1.2, 1.3, 3, 3.3

FERNANDES, F.; JR., A. B.; BRAGA, A.; SOARES, A. Integro-differential solution for nonlinear oil flow through porous media near a sealing fault using green's functions. **American Association of Rock Mechanics, (ARMA) Conference held in Houston, Texas**, 2021. (document), 1.2, 1.3, 6.1.2, 7.10

FERNANDES, F.; JR., A. B.; BRAGA, A.; SOARES, A. Integro-differential solution for nonlinear radial oil flow through porous media using green's functions (gfs). **American Association of Rock Mechanics, (ARMA) Conference held in Houston, Texas no June, 20-23 of 2021.**, 2021. 1.3, 3, 7.2.3

FERNANDES, F. B. Perturbative-Integro-Differential Solution for the Non-linear Hydraulic Diffusivity Equation for Infinite-Acting-Oil Flow in a Permeability-Pressure-Sensitive Reservoir. v. 4, 02 2022. 1.2, 1.3, 4.3, 4.5, 4.5, 5.1.2, 5.1.5, 5.2.2, 5.2.6, 5.2.6, 6.1.2, 7.1.3

FERNANDES, F. B.; BRAGA, A. M. B.; SOUZA, A. L. S.; SOARES, A. C. Analytical Model to Effective Permeability Loss Prediction and Formation Mechanical Damage Control in Fractured Oil Wells. **Paper presented at**

the Offshore Technology Conference, Houston, Texas, USA, May 3-6 of 2022, 2022. 1.3

FERNANDES, F. B.; BRAGA, A. M. B.; SOUZA, A. L. S.; SOARES, A. C. Wellbore Solution for Formation Mechanical Damage Control During Oil Flow through Infinite Permeability- Pressure-Sensitive Reservoirs. **Paper presented at the 56th U.S. Rock Mechanics/Geomechanics Symposium, June 2022. American Rock Mechanics Association.**, 2022. 1.3

GEERTSMA, J. The effect of fluid pressure decline on volumetric changes of porous rocks. **Society of Petroleum Engineers, SPE-AIME**, 1957. 2.1

GEERTSMA, J. Problems of Rock Mechanics In Petroleum Production Engineering. 09 1966. 1, 3.4

GONZALEZ; A., M.; CINCO-LEY, H. Effect Of Pressure In A Well With A Vertical Fracture With Variable Conductivity And Skin Fracture. 08 2006. 2.1

GRAY, D.; FATT, I. The effect of stress on permeability of sandstone cores. **Society of Petroleum Engineers Journal**, v. 3, p. 95–100, 1963. 2.1

GRINGARTEN, A. C. Interpretation of Tests in Fissured and Multilayered Reservoirs With Double-Porosity Behavior: Theory and Practice. v. 36, 01 1984. 1.2, 1.2, 2.4, 5.1.4

GRINGARTEN, A. C. From Straight Lines to Deconvolution: The Evolution of the State of the Art in Well Test Analysis. v. 11, 2008. 1.2, 2.4, 5.1.4, 6.1

GRINGARTEN, A. C.; BOURDET, D. P.; LANDEL, P. A.; KNIAZEFF, V. J. A Comparison Between Different Skin and Wellbore Storage Type-Curves For Early-Time Transient Analysis. 09 1979. 1.2, 1.2, 2.4, 5.1.4

GRINGARTEN, A. C.; J., R. H. Unsteady-state pressure distributions created by a well with a single horizontal fracture, partial penetration, or restricted entry. **SPE Journal. SPE Paper 3819**, v. 14, p. 413–426, 1974. 1.2, 5.1.4

GRINGARTEN, A. C.; Ramey Jr., H.; RAGHAVAN, R. Applied Pressure Analysis for Fractured Wells. v. 27, 01 1975. 1.2, 1.2, 2.4, 5.1.4, 6.1

GRINGARTEN, A. C.; Ramey Jr., H. J. The use of source and green's functions in solving unsteady-flow problems in reservoirs. **SPE Journal. SPE Paper 3818**, v. 13, p. 285–296, 1973. 1.2, 2.2, 5.1.4

GRINGARTEN, A. C.; Ramey Jr., H. J. Unsteady-state pressure distributions created by a well with a single infinite-conductivity vertical fracture. **SPE Journal. SPE Paper 4051**, v. 14, p. 347–360, 1974. 1.2, 1.2, 2.4, 5.1.4

HOLT, R. Permeability reduction induced by a nonhydrostatic stress field. **SPE Formation Evaluation**, p. 444–448., 1990. 2.1

HORNER, D. Pressure build-up in wells. **Proc. Third World Pet. Congress, E.J. Brill, Leiden, 1951, II**, 1951. 2.4, 6.1, 6.1.2, 6.1.3

HOWARD, G. C.; FAST, C. R. Optimum fluid characteristics for fracture extension. **Paper presented at the Spring Meeting of the Midcontinent district, Division of Production, Tulsa, Okla, 1957.** 2.3

JIANG, L.; LIU, T.; YANG, D. Effect of stress-sensitive fracture conductivity on transient pressure behavior for a horizontal well with multistage fractures. **SPE Journal**, 2019. 1.3

JIANG, L.; LIU, T.; YANG, D. A semianalytical model for predicting transient pressure behavior of a hydraulically fractured horizontal well in a naturally fractured reservoir with non-darcy flow and stress-sensitive permeability effects. **SPE Journal**, v. 24, 2019. 1.3

JOHNSTON, J.; LEE, W. Interpreting Short-Term Buildup Tests From Low-Productivity Gas Wells Using Deconvolution. 01 1991. 2.4, 6.1.2

JONES, C.; SOMERVILLE, J.; SMART, B.; KIRSTETTER, O.; HAMILTON, S.; EDLMANN, K. Permeability prediction using stress sensitive petrophysical properties. **Petroleum Geoscience**, 2001. 2.1

JONES, L.; SEETHARAM, R. The Maximum-Rate Horner Method: An Improved Method of Analysis for Afterflow-Dominated Buildup Tests. 04 1990. 2.4

KALE, D.; MATTAR, L. Solution of a nonlinear gas flow equation by the perturbation technique. **JCPT, PETSOC**, p. 63–67, 1980. 3.1, 4.5, 4.5, 5.1.4, 5.2.4

KEANEY, G. M. J.; MEREDITH, P. G.; MURREL, S. A. F. Laboratory study of permeability evolution in a tight sandstone under non-hydrostatic stress conditions. **EUROCK 98**, v. 1, p. 329–335., 1998. 2.1

KELVIN, T. Mathematical and physical papers. **Cambridge University Press: London, UK**, 1882. 2.2

KIKANI, J.; Pedrosa Jr., O. Perturbation analysis of stress-sensitive reservoirs. **SPE Formation Evaluation** 6, p. 379–386, 1991. 2, 2.2, 4.5, 5.1.4, 5.2.4

KING, M. J.; WANG, Z.; DATTA-GUPTA, A. Asymptotic solutions of the diffusivity equation and their applications. **Society of Petroleum Engineers**. doi:10.2118/180149-MS, 2016. 1.3

KNIPE, R. J.; JONES, G.; FISHER, Q. J. Faulting, fault sealing and fluid flow in hydrocarbon reservoirs: an introduction. Geological Society of London, v. 147, n. 1, p. vii–xxi, 1998. 5.2

KUCHUK, F.; BIRYUKOV, D. Pressure Transient Tests and Flow Regimes in Fractured Reservoirs. **Paper presented at the SPE Annual Technical Conference and Exhibition, New Orleans, Louisiana, USA, September 2013**, 2013. 2.3

KUCHUK, F.; KABIR, S. Well test interpretation for reservoirs with a single linear no-flow barrier. **Journal of Petroleum Science and Engineering**, v. 1, n. 3, p. 195–221, 1988. ISSN 0920-4105. 5.2

KUCHUK, F.; MORTON, K.; BIRYUKOV, D. Pressure Transient Behavior of Horizontal Wells Intersecting Multiple Hydraulic and Natural Fractures in Conventional and Unconventional Unfractured and Naturally Fractured Reservoirs. **Paper presented at the SPE Annual Technical Conference and Exhibition, Houston, Texas, USA, September 2015, 2015.** 2.3

KUCHUK, F.; MORTON, K.; BIRYUKOV, D. Rate-Transient Analysis for Multistage Fractured Horizontal Wells in Conventional and Unconventional Homogeneous and Naturally Fractured Reservoirs. **Paper presented at the SPE Annual Technical Conference and Exhibition, Dubai, UAE, September 2016, 2016.** 2.3

LAMBE, T. W.; WHITMAN, R. V. Soil Mechanics. **John Wiley Sons, New York, USA, v. 116, 1979.** 1

LEE, W. J. Well testing. **New York: Society of Petroleum Engineers of AIME, 1982.** 6.1.2, 6.1.3

LEE, W. J.; ROLLINS, J. B.; SPIVEY, J. P. Pressure transient testing. **Richardson, Texas: Society of Petroleum Engineers Inc, 2003.** (document), 6.1.2, 6.1.2, 6.1.3, 7.1

LIAO, Y.; LEE, W. Equivalent Drawdown Time for Pressure Buildup Test Analysis for Hydraulically Fractured Wells. 06 1993. 2.4

LONARDELLI, J. N.; SILVA; FALCÃO F. O. L. S., M.; ABREU, C. Evaluation of oil production related effects through geomechanical modeling: A case study from marimbá field, campos basin, brazil. **Journal of Petroleum Science and Engineering (2017), doi: 10.1016/j.petrol.2017.08.029., 2017.** 1.3

Mc Latchie, A.; HEMSTOCK, R.; YOUNG, J. The effective compressibility of reservoir rock and its effects on permeability. **Society of Petroleum Engineers, SPE-AIME, 1958.** 2.1

MISKIMINS, J. L. Hydraulic fracturing: Fundamentals and advancements. **Monography Series, Society of Petroleum Engineers, SPE, 2019.** 1.3, 5.3

MISKIMINS, J. L.; ALOTAIBI, M. The Impacts of Proppant Sorting and Dune Shape on Slickwater Hydraulic Fracturing Conductivity. Day 2 Tue, November 19, 2019, 11 2019. 1.3

MUSKAT, M. Use of Data Oil the Build-up of Bottom-hole Pressures. **Transactions of the AIME, v. 123, n. 01, p. 44–48, 12 1937.** 2.4

NAYFEH, A. Introduction to perturbation techniques. v. 14, 1991. 1

NOLTE, K. G. Fluid flow considerations in hydraulic fracturing. **Paper presented at the SPE Eastern Regional Meeting, Charleston, West Virginia, 1988.** 2.3

- NOLTE, K. G.; SMITH, M. B. Interpretation of fracturing pressures. **Journal of Petroleum Technology**, v. 33, 1981. 2.3
- NUNES, M. J. d. S.; BEDRIKOVETSKY, P. G.; NEWBERY, B.; FURTADO, C. J. A.; SOUZA, A. L.; PAIVA, R. Formation Damage Zone Radius and its Applications to Well Stimulation. 05 2009. 2.1
- ONUR, M.; AYAN, C.; KUCHUK, F. J. Pressure-Pressure Deconvolution Analysis of Multi-Well Interference and Interval Pressure Transient Tests. 12 2009. 2.4, 6.1
- ONUR, M.; CINAR, M.; ILK, D.; VALKO, P. P.; BLASINGAME, T. A.; HEGEMAN, P. S. An investigation of recent deconvolution methods for well-test data analysis. **SPE Journal**, 2008. 2.4, 6.1
- ONUR, M.; HEGEMAN, P.; GOK, I.; KUCHUK, F. A Novel Analysis Procedure for Estimating Thickness-Independent Horizontal and Vertical Permeabilities From Pressure Data at an Observation Probe Acquired by Packer-Probe Wireline Formation Testers. v. 14, 2011. 2.4, 6.1
- OZISIKI, M. N. Heat conduction. **New York City: John Wiley Sons. Second edition**, 1993. 1.2, 1.2, 5.1.4, 5.2.5, 5.2.5, 5.3.5, 5.4.3, 6.1.2
- OZKAN, E.; BROWN, M.; RAGHAVAN, R.; KAZEMI, H. Comparison of fractured horizontal-well performance in conventional and unconventional reservoirs. **Paper presented at the SPE Western Regional Meeting, San Jose, California, March 2009**, 03 2009. 2.3
- OZKAN, E.; RAGHAVAN, R. New Solutions for Well-Test-Analysis Problems: Part 1—Analytical Considerations. 09 1991. 2.3
- Pedrosa Jr., O. Pressure transient response in stress-sensitive formations. **In: SPE Paper 15115 presented at SPE California Regional Meeting, Oakland, California, USA.**, 1986. 1, 2.2, 4.5, 5.1.4, 5.2.4
- PERES, A. M. M.; ONUR, M.; REYNOLDS, A. C. A New General Pressure Analysis Procedure for Slug Tests. 04 1989. 2.4, 6.1.2
- PERES, A. M. M.; SERRA, K. V.; REYNOLDS, A. C. Toward a unified theory of well testing for nonlinear-radial-flow problems with application to interference tests. **SPE formation evaluation**, Society of Petroleum Engineers, v. 5, n. 02, p. 151–160, 1989. 1, 1, 2.2, 3.1, 5.2.6, 7.2.2
- RAGHAVAN, R.; CHIN, L. Y. Productivity changes in reservoirs with stress-dependent permeability. **SPE Reservoir Evaluation Engineering**, 2004. 2.3
- RAGHAVAN, R. S.; C., C.; AGARWAL, B. An analysis of horizontal wells intercepted by multiple fractures. **SPE Journal - SPE-27652-PA**, March 1997. 2.3
- RAHIM, Z.; LEE, W. J. A New Technique for Analyzing Buildup Tests From Hydraulically Fractured Wells. 1989. 2.4

- RAMEY, H. J. J.; COBB WILLIAM, M. A general pressure buildup theory for a well in a closed drainage area. **SPE Annual Fall Meeting held in Houston, Oct. 4-7, 1970**, 1970. 2.4
- Ramey Jr., H. J. Short-time well test data interpretation in the presence of skin effect and wellbore storage. **Journal of Petroleum Technology**, v. 22, p. 97–104, 1970. 2.4
- Ramey Jr., H. J. Advances in practical well-test analysis (includes associated paper 26134). **Journal of Petroleum Technology**, v. 44, 1992. 2.4
- REID, M. G.; MELO, V. L.; LIMA, L. M.; SOUZA, A. L. Water Injection in Espadarte Module I Field. 05 2009. 2.1
- REN, J.; GUO, P. A general analytical method for transient flow rate with the stress-sensitive effect. **Journal of Hydrology. ISSN 0022-1694**. <https://doi.org/10.1016/j.jhydrol.2018.08.019>, v. 565, p. 262–275, 2018. 1.3, 3
- RISNES; RASMUS; BRATLI; K., R.; HORSRUD., P. Sand stresses around a wellbore." spe j. 22 (1982): 883–898. <https://doi.org/10.2118/9650-pa>. **Society of Petroleum Engineers**. doi:10.2118/949305-G, 1982. 2.1
- ROBINSON, J.; CHU, W.-C.; WOODS, M.; HUTCHISON, H. Pressure Buildup Testing as an Aid in Well Stimulation: Case History. 10 1991. 2.4
- RODRÍGUEZ, F.; CINCO-LEY, H.; SAMANIEGO, F. Evaluation of Fracture Asymmetry of Finite-Conductivity Fractured Wells. **SPE Prod Eng 7: 233–239**, 1992. 2.3
- SA, A. N.; SOARES, A. C. Coring samples and obtaining geomechanical properties for wellbore stability analysis in deepwater brazilian horizontal wells. **Latin American and Caribbean Petroleum Engineering Conference**, 1997. 2.1
- SAMANIEGO, V.; BRIGHAM, W. E.; MILLER, F. G. An investigation of transient flow of reservoir fluids considering pressure-dependent rock and fluid properties. **Society of Petroleum Engineers**. doi:10.2118/5593-PA, 1977. 2.2
- SCHROETER, T. von; GRINGARTEN, A. Deconvolution of Well-Test Data as a Nonlinear Total Least-Squares Problem. v. 9, 2004. 2.4
- SCHROETER, T. von; GRINGARTEN, A. C. Superposition principle and reciprocity for pressure transient analysis of data from interfering wells. **SPE Journal, SPE Paper 110465**, 2007. 1.2, 2.4
- SMITS, R.; WAAL, J. de; KOOTEN, J. van. Prediction of Abrupt Reservoir Compaction and Surface Subsidence Caused By Pore Collapse in Carbonates. **SPE Formation Evaluation**, v. 3, n. 02, p. 340–346, 06 1988. 1
- SOARES, A. Um estudo experimental para definição de colapso de poros em rochas carbonáticas. **Tese de mestrado: COPPE/UFRJ, Rio de Janeiro**, 2000. 1, 1.2, 1.4, 2.1, 2.5, 3.3, 3.4, 5.2.6

- SOARES, A.; FERREIRA, F.; Vargas Jr., E. n experimental study for mechanical formation damage. **SPE Reservoir Evaluation Engineering**, 2002. 1.2, 1.4, 2.1, 2.5, 5.2.6
- SOARES, A.; FERREIRA, F. H. An experimental study for mechanical formation damage. **Society of Petroleum Engineers**. doi:10.2118/73734-MS, 2002. 1, 1.2, 1.4, 2.1, 2.5, 3.3, 3.4, 5.2.6
- SOARES, A.; FREITAS, S.; VELLOSO, R. Q. Porous Media Elastic Parameters Analysis. **Paper presented at XVI Brazilian Congress on Mechanic Engineering, Uberlandia, Brazil**, 2001. 1, 1.2, 1.4, 2.1, 2.5, 3, 3.3, 3.4, 5.2.6
- SOUZA; Barreto Jr., A. B.; PERES, A. M. M. Analytical treatment of pressure-transient solutions for gas wells with wellbore storage and skin effects by the green's functions method. **Society of Petroleum Engineers**, 2016. 1.2, 1.3, 2.5, 5.1.4
- SOUZA; Barreto Jr., A. B.; PERES, A. M. M. Finite-wellbore-radius solution for gas wells by green's functions. **Society of Petroleum Engineers**, 2016. 1.3, 2.5
- SOUZA, A. L. S. Prediction of Thermal Induced Fracture during Waterflooding in a High Pressure High Temperature Field in Offshore Brazil. 10 2016. 2.1
- SOUZA, A. L. S.; FALCÃO, F. O. Research and Developments in Reservoir Geomechanics in Brazil: Perspectives and Challenges. Day 3 Thu, October 29, 2015, 10 2015. 2.1
- SOUZA, A. L. S.; FARIAS, M. L. Rocha de; CARVALHO, M. S. Numerical and Experimental Investigation of Produced Water Reinjection on Viscous Oil Recovery. 10 2013. 2.1
- TABATABAIE, S. H.; POOLADI-DARVISH, M.; MATTAR, L. Draw-down management leads to better productivity in reservoirs with pressure-dependent permeability - or does it? **Society of Petroleum Engineers.SPE Conference SPE/CSUR Unconventional Resources Conference, held in Calgary, Alberta, Canada, 20-22 October, 2015**. 1.3
- TABATABAIE, S. H.; POOLADI-DARVISH, M.; MATTAR, L.; TAVALLALI, M. Analytical modeling of linear flow in pressure-sensitive formations. **Society of Petroleum Engineers.SPE Reservoir Evaluation and Engineering**, 2016. 1.3
- TENG, B.; LI, H.; YU, H. A Novel Analytical Fracture-Permeability Model Dependent on Both Fracture Width and Proppant-Pack Properties. **SPE Journal**, v. 25, n. 06, p. 3031–3050, 2020. 5.3.3, 5.4.2
- TERZAGHI, V. K. Theoretical soil mechanics, ny, wiley. 1943. 2, 2.1
- TEUFEL, L.; RHETT, D.; FARRELL, H.; LORENZ, J. Control of fractured reservoir permeability by spatial and temporal variations in stress magnitude and orientation. **SPE Annual Technical Conference and Exhibition**, 1993. 2.1

- THEIS, C. V. The source of water derived from wells. **Civil Engineering Conference**, v. 10, p. 277–280, 1940. 2.2
- van Baaren, J. P. Quick-Look Permeability Estimates Using Sidewall Samples and Porosity Logs. **6th Annual European Logging Symposium, London, UK, 19-25**, 1979. 5.3.3
- VIRIEUX, J.; FLORES-LUNA, C.; GIBERT, D. Asymptotic theory for diffusive electromagnetic imaging. **Geophysics J. Int.**, 1994. 1
- WANG; XIANGYI. Transient pressure behavior of a fractured vertical well with a finite-conductivity fracture in triple media carbonate reservoir. journal of porous media. **JPorMedia.v20.i8.30.**, v. 20, p. 707–722, 2017. 1.3
- WANG, Z.; LI, C.; KING, M. Validation and extension of asymptotic solutions of diffusivity equation and their applications to synthetic cases. **Society of Petroleum Engineers. doi:10.2118/182716-MS**, 2017. 1.3
- WARPINSKI, N.; BRANAGAN, P.; WILMER, R. In situ stress measurements at u.s. doe's multiwell experiment site, mesaverde group, rifle, colorado. **JPT 37. SPE- 12142-PA**, v. 3, p. 527–536, 1985. 2.3
- WARPINSKI, N.; FNLEY, S.; VOLLENDORF, W.; O'BRIEN, M.; ESHOM, E. The interface test series: An in situ study of factors affecting the containment of hydraulic fractures. **Sandia National Laboratories Report No. SAND81 2408, Livermore, CA (February)**, 1982. 2.3
- WARPINSKI, N.; LORENZ, J.; BRANAGAN; MYAL, F.; GALL, B. Examination of a cored hydraulic fracture in a deep gas well. **SPE Production Facilities. SPE- 22876-PA**, v. 3, 1993. 2.3
- WARPINSKI, N.; NORTHROP, D.; SCHMIDT, R.; VOLLENDORF, W.; FINLEY, S. The formation interface fracturing experiment: An in situ investigation of hydraulic fracture behavior near a material property interface. **Sandia National Laboratories Report No. SAND81 0938, Livermore, CA (June)**, 1981. 2.3
- WARPINSKI, N.; SCHMIDT, R.; NORTHROP, D. In situ stresses: The predominant influence on hydraulic fracture containment. **JPT. 34 (3): 653–664. SPE- 8932-PA.**, 1982. 2.3
- WARPINSKI, N. R.; TYLER, L. D.; VOLLENDORF, W. C.; NORTHROP, D. A. Direct observation of a sand propped hydraulic fracture. **Sandia National Laboratories Report No. SAND81 0225. Livermore, CA (May)**, 1981. 2.3
- WEIJERMARS, R.; PHAM, T.; STEGENT, N.; DUSTERHOFT, R. Hydraulic Fracture Propagation Paths Modeled using Time-Stepped Linear Superposition Method (TLSM): Application to Fracture Treatment Stages with Interacting Hydraulic and Natural Fractures at the Wolfcamp Field Test Site (HFTS). All Days, 06 2020. 1.3

WILHELMI, B.; SOMERTON, W. Simultaneous measurement of pore and elastic properties of rocks under triaxial stress conditions. **Society of Petroleum Engineers, SPE-AIME**, 1967. 2.1

WU, Y.; PRUESS, K. Integral solutions for transient fluid flow through a porous medium with pressure-dependent permeability. **Int. J. Rock Mech. Min. Sci.**, v. 37, p. 51–61, 2000. 2.2

WU, Z.; CUI, C.; CHENG, X.; WANG, Z.; SUI, Y.; ZHAO, X. Pressure Analysis for Volume Fracturing Well in Tight Reservoirs Considering Dynamic Threshold Pressure Gradient and Stress Sensitivity. Day 2 Tue, November 19, 2019, 11 2019. 1.3

XU, Y.; LI, X.; LIU, Q.; TAN, X. Pressure performance of multi-stage fractured horizontal well considering stress sensitivity and dual permeability in fractured gas reservoirs. **Journal of Petroleum Science and Engineering**, v. 201, p. 108154, 2021. ISSN 0920-4105. Disponível em: <<https://www.sciencedirect.com/science/article/pii/S0920410520312080>>. 1.3

YALE, D.; CRAWFORD, B. Plasticity and permeability in carbonates: Dependence on stress path and porosity. **EUROCK 98**, v. 2, p. 485–494, 1998. 2.1

YAO, S.; ZENG, F.; LIU, H. A Semi-analytical Model for Hydraulically Fractured Wells With Stress-Sensitive Conductivities. 11 2013. 2.1

ZHANG, Y.; YANG, D. Evaluation of transient pressure responses of a hydraulically fractured horizontal well in a tight reservoir with an arbitrary shape by considering stress-sensitive effect. **Journal of Petroleum Science and Engineering**, v. 202, p. 108518, 2021. ISSN 0920-4105. Disponível em: <<https://www.sciencedirect.com/science/article/pii/S0920410521001777>>. 1.3

ZHANG, Z.; HE, S.; LIU, G.; GUO, X.; MO, S. Pressure buildup behavior of vertically fractured wells with stress-sensitive conductivity. **Journal of Petroleum Science and Engineering**, v. 122, p. 48–55, 2014. ISSN 0920-4105. Disponível em: <<https://www.sciencedirect.com/science/article/pii/S0920410514001235>>. 2.1

ZHU, H.; TANG, X.; LIU, Q.; LIU, S.; ZHANG, B.; JIANG, S.; MCLENNAN, J. D. Permeability stress-sensitivity in 4D flow-geomechanical coupling of Shouyang CBM reservoir, Qinshui Basin, China. v. 232, 2018. 1.3

ZHU, W.; WONG, T. Permeability reduction in a dilating rock: Network modeling of damage and tortuosity. **Geophysical Research Letters.**, v. 23, p. 3099–3102, 1996. 2.1

A

Transcendental Functions

Since some wellbore solutions approached in this work for NHDE were constituted by transcendental functions, this appendix deals with their definitions.

A.1 Modified Bessel's Functions

Modified Bessel's functions are the linearly independent solutions of the Bessel differential equation below:

$$r^2 \frac{d^2 \mathcal{U}}{dr^2} + r \frac{d\mathcal{U}}{dr} - (r^2 + \nu^2) \mathcal{U} = 0 \quad (\text{A.1.1})$$

The Bessel's differential equation above produces first and second kind Bessel's functions, respectively denoted by $\mathbf{I}_\nu(\dots)$ and $\mathbf{K}_\nu(\dots)$. Where ν is the order of the modified Bessel's function, $\nu \in \mathbb{Z}$.

A.1.1 Series Expansion of Modified Bessel's Functions

The first kind and ν order modified Bessel's function $\mathbf{I}_\nu(z)$ can be expressed by the series:

$$\mathbf{I}_\nu(z) = \sum_{n=0}^{+\infty} \frac{1}{n! \Gamma(n + \nu + 1)} \left(\frac{z}{2}\right)^{2n+\nu} \quad (\text{A.1.2})$$

The second kind and ν order modified Bessel's function $\mathbf{K}_\nu(z)$ can be expressed by the expression:

$$\mathbf{K}_\nu(z) = \frac{\pi \mathbf{I}_{-\nu}(z) - \mathbf{I}_\nu(z)}{2 \sin(\pi \nu)} \quad (\text{A.1.3})$$

A.2 Exponential Integral Function

$$\mathbf{Ei}(x) \stackrel{\text{def.}}{=} \int_{-x}^{+\infty} \frac{e^{-t}}{t} dt \stackrel{\text{def.}}{=} \int_{-\infty}^x \frac{e^{-t}}{t} dt, \quad (x > 0) \quad (\text{A.2.1})$$

A.2.1**Expansion of Exponential Integral Function in Taylor Series**

The expansion of the exponential integral function in Taylor series is:

$$\mathbf{Ei}(x) = \gamma + \ln(x) + \sum_{n=1}^{+\infty} \frac{x^n}{nn!} \quad (\text{A.2.2})$$

Where γ is the Euler's constant, given by series:

$$\gamma = \lim_{n \rightarrow +\infty} \left[1 + \frac{1}{2} + \frac{1}{3} + \frac{1}{4} + \dots + \frac{1}{n} - \ln(n) \right] \quad (\text{A.2.3})$$

The Euler's constant's value is: $\gamma = 0.5772156649\dots$

A.3**Error Function**

$$\mathbf{erf}(x) = \frac{2}{\sqrt{\pi}} \int_0^x e^{-t^2} dt \quad (\text{A.3.1})$$

A.3.1**Expansion of Error Function in Taylor Series**

$$\mathbf{erf}(x) = \frac{2}{\sqrt{\pi}} \left(x - \frac{x^3}{3} + \frac{x^5}{10} - \frac{x^7}{42} + \frac{x^9}{216} - \dots \right) \quad (\text{A.3.2})$$

A.4**Complementary Error Function**

$$\mathbf{erfc}(x) = 1 - \mathbf{erf}(x) \quad (\text{A.4.1})$$

A.4.1**Expansion of Complementary Error Function in Taylor Series**

$$\mathbf{erfc}(x) = 1 - \frac{2}{\sqrt{\pi}} \left(x - \frac{x^3}{3} + \frac{x^5}{10} - \frac{x^7}{42} + \frac{x^9}{216} - \dots \right) \quad (\text{A.4.2})$$

B Laplace Transforms and Inverses

Let $f(u, t)$ a function of exponential order and sectionally continuous, such that, $t \in \mathbb{R}$. The Laplace transform is the integral operator that takes the function $f(u, t)$ to a image function $\bar{f}(u, s)$, which $\bar{f}(u, s)$ is the function in Laplace domain and the new variable s is the Laplace variable, $s \in \mathbb{C}$.

The Laplace transform definition for for a two variables, but just the time variable t being transformed to the Laplace domain, is:

$$\mathcal{L}\{f(u, t)\} \stackrel{\text{def.}}{=} \int_0^{+\infty} e^{-ut} f(u, t) dt \stackrel{\text{def.}}{=} \bar{f}(u, s) \quad (\text{B.0.1})$$

The Laplace transform definition for a two variables function being transformed to the Laplace domain is:

$$\mathcal{L}\{f(u, t)\} \stackrel{\text{def.}}{=} \int_0^{+\infty} \int_0^{+\infty} e^{-\mathcal{U}u-st} f(u, t) du dt \stackrel{\text{def.}}{=} \bar{f}(\mathcal{U}, s) \quad (\text{B.0.2})$$

Where the function $\bar{f}(\mathcal{U}, s)$ is the function in Laplace domain and the new variables \mathcal{U} and s are the Laplace variables, $\mathcal{U}, s \in \mathbb{C}$.

B.1 Inversion Formula

The Laplace inverse operator \mathcal{L}^{-1} , takes a function in the Laplace domain $\bar{f}(\mathcal{U}, s)$ to the original function in time domain $f(u, t)$ through the formula below:

$$\mathcal{L}^{-1}\{\bar{f}(\mathcal{U}, s)\} \stackrel{\text{def.}}{=} \frac{1}{2\pi i} \int_{c-i\infty}^{c+i\infty} \int_{c-i\infty}^{c+i\infty} e^{-\mathcal{U}u-st} \bar{f}(\mathcal{U}, s) d\mathcal{U} ds \quad (\text{B.1.1})$$

Where the integration is done along the vertical line γ in the complex plane. Since the complex line integral above is difficulty to solve and the subject is widely developed in scientific literature, the inverse Laplace transform is computed through tables.

B.2**Table of Laplace Transform Properties**

Let the original functions $f(u, t), g(u, t)$ and the image functions $\bar{f}(u, s), \bar{g}(u, s)$, and let yet a and $b, \in \mathbb{R}$. Some properties of Laplace transform are listed in **Table B.2** below:

Table B.1: Laplace Transform Properties

Property	$\mathcal{L}\{f(u, t)\}$	$\bar{f}(u, s)$
Linearity	$\mathcal{L}\{af(u, t) + bg(u, t)\}$	$a\bar{f}(u, s) + b\bar{g}(u, s)$
Scale Change	$\mathcal{L}\{f(u, at)\}$	$\frac{1}{a}\bar{f}\left(u, \frac{s}{a}\right)$
Differentiation ¹	$\mathcal{L}\{f'(u, t)\}$	$s\bar{f}(u, s) - f(u, 0)$
Differentiation ²	$\mathcal{L}\{f''(u, t)\}$	$s^2\bar{f}(u, s) - sf(u, 0) - f'(u, 0)$
Integration	$\mathcal{L}\left\{\int_0^t f(u, t)dt\right\}$	$\frac{\bar{f}(u, s)}{s}$
Reciprocal	$\mathcal{L}\left\{\frac{f(u, t)}{t}\right\}$	$\int_s^{+\infty} \bar{f}(u, s)ds$
Convolution	$\mathcal{L}\{f(u, t) * g(u, t)\}$	$\bar{f}(u, s)\bar{g}(u, s)$
Translation	$\mathcal{L}\{f(u, t - a)g(u, t - a)\}$	$e^{-as}\bar{f}(u, s)$

C

Verification of Duhamel's Principle (Time's Superposition)

Let the dimensionless Euclidean plan $\mathbf{r}_D = (r_D, 0, 0) \in \mathbb{R}^2$ and $t_D \in \mathbb{R}$.
Let yet the dimensionless NHDE in terms of the permeability pseudo-pressure:

$$\frac{1}{r_D} \frac{\partial}{\partial r_D} \left(r_D \frac{\partial m_D}{\partial r_D} \right) = \mathcal{D} \frac{\partial m_D}{\partial t_D} \quad (\text{C.0.1})$$

Let yet the homogeneous initial condition:

$$m_D(r_D, t_D = 0) = 0 \quad (\text{C.0.2})$$

With the external boundary condition:

$$\lim_{r_D \rightarrow \infty} m_D(r_D, t_D) = 0 \quad (\text{C.0.3})$$

And the inner boundary condition:

$$\lim_{r_D \rightarrow 0} \left(r_D \frac{\partial m_D}{\partial r_D} \right) = -q_{wD}(t_D) \quad (\text{C.0.4})$$

Where the function $m_D(r_D, t_D)$ is the same function approached in the whole paper and it denotes the dimensionless general solution with transient oil flow rate. In this formulation, the oil source term is included in the inner boundary condition instead of in the NHDE. This approach is broadly used in the formation evaluation literature. In this appendix, we analyse whether the general solution $m_D(r_D, t_D)$ can be expressed in terms of a new function $m_{DC}(r_D, t_D)$ denominated dimensionless pseudo-pressure at constant oil flow rate.

The mathematical formulation becomes:

$$\frac{1}{r_D} \frac{\partial}{\partial r_D} \left(r_D \frac{\partial m_{DC}}{\partial r_D} \right) = \mathcal{D} \frac{\partial m_{DC}}{\partial t_D} \quad (\text{C.0.5})$$

Let yet the homogeneous initial condition:

$$m_{DC}(r_D, t_D = 0) = 0 \quad (\text{C.0.6})$$

With the external boundary condition:

$$\lim_{r_D \rightarrow \infty} m_{DC}(r_D, t_D) = 0 \quad (\text{C.0.7})$$

And the inner boundary condition:

$$\lim_{r_D \rightarrow 0} \left(r_D \frac{\partial m_{DC}}{\partial r_D} \right) = -1 \quad (\text{C.0.8})$$

Taking as an analogy the constant permeability solution through the Duhamel's principle, the dimensionless general solution $m_D(r_D, t_D)$ can be expressed as follows:

$$m_D(r_D, t_D) = \int_0^{t_D} q_{wD}(t'_D) \frac{\partial m_{DC}(r_D, t_D - t'_D)}{\partial t_D} dt'_D \quad (\text{C.0.9})$$

That can be transformed in:

$$m_D(r_D, t_D) = \frac{\partial}{\partial t_D} \int_0^{t_D} q_{wD}(t'_D) m_{DC}(r_D, t_D - t'_D) dt'_D \quad (\text{C.0.10})$$

The equivalence of the right-hand side of the Eq. C.9 and C.10, it is necessary to differentiate the integral of the right-hand side of the Eq. C.10 and use the initial condition in the constant permeability solution $m_{DC}(r_D, t_D)$. To verify whether the solution expressed by the Eq. C.9 satisfies the Eqs. C.1 to C.4, it is necessary to use:

$$\frac{m_D(r_D, t_D)}{\partial t_D} = \frac{\partial}{\partial t_D} \int_0^{t_D} q_{wD}(t'_D) \frac{\partial m_{DC}(r_D, t_D - t'_D)}{\partial t_D} dt'_D \quad (\text{C.0.11})$$

The partial derivative with respect to the dimensionless radial component r_D is:

$$\frac{m_D(r_D, t_D)}{\partial r_D} = \frac{\partial}{\partial r_D} \frac{\partial}{\partial t_D} \int_0^{t_D} q_{wD}(t'_D) m_{DC}(r_D, t_D - t'_D) dt'_D \quad (\text{C.0.12})$$

Assuming that:

$$\frac{\partial}{\partial r_D} \frac{\partial}{\partial t_D} = \frac{\partial}{\partial t_D} \frac{\partial}{\partial r_D} \quad (\text{C.0.13})$$

The Eq. C.12 yields to:

$$\frac{m_D(r_D, t_D)}{\partial r_D} = \frac{\partial}{\partial t_D} \int_0^{t_D} q_{wD}(t'_D) \frac{\partial m_{DC}(r_D, t_D - t'_D)}{\partial r_D} dt'_D \quad (\text{C.0.14})$$

Thereby, the left-hand side of the Eq. C.1 can be expanded and the Eq. C.14

can be applied to obtain:

$$\begin{aligned} \frac{1}{r_D} \frac{\partial}{\partial r_D} \left(r_D \frac{\partial m_D}{\partial r_D} \right) &= \frac{1}{r_D} \frac{\partial}{\partial t_D} \int_0^{t_D} q_{wD}(t'_D) \frac{\partial m_{DC}(r_D, t_D - t'_D)}{\partial r_D} dt'_D + \\ &+ \frac{\partial}{\partial t_D} \int_0^{t_D} q_{wD}(t'_D) \frac{\partial^2 m_{DC}(r_D, t_D - t'_D)}{\partial r_D^2} dt'_D \quad (\text{C.0.15}) \end{aligned}$$

From the Eqs. C.11, C.12, C.14 and C.15 it is necessary to analyze if the Duhamel's principle (Eq. C.9) satisfies the problems C.1 to C.4. We can verify that, when $t_D \rightarrow 0$, the Eq. C.1 vanishes and we obtain the Eq. C.2. Using the external boundary condition (Eq. C.3), we have:

$$\lim_{r_D \rightarrow \infty} m_D(r_D, t_D) = \lim_{r_D \rightarrow \infty} \frac{\partial}{\partial t_D} \int_0^{t_D} q_{wD}(t'_D) m_{DC}(r_D, t_D - t'_D) dt'_D \quad (\text{C.0.16})$$

Rewriting the Eq. C.16:

$$\lim_{r_D \rightarrow \infty} m_D(r_D, t_D) = \frac{\partial}{\partial t_D} \int_0^{t_D} q_{wD}(t'_D) \left[\lim_{r_D \rightarrow \infty} m_{DC}(r_D, t_D - t'_D) \right] dt'_D \quad (\text{C.0.17})$$

As the term inside the brackets is zero (Eq. C.7), the right-hand side of the Eq. C.17 is null and, therewith, external boundary condition (Eq. C.3) is also satisfied. Now, let us verify the inner boundary condition. Replacing the Eq. C.14 in the Eq. C.4:

$$\begin{aligned} \lim_{r_D \rightarrow 0} \left[r_D \frac{\partial}{\partial t_D} \int_0^{t_D} q_{wD}(t'_D) \frac{\partial m_{DC}(r_D, t_D - t'_D)}{\partial r_D} dt'_D \right] &= \\ &= \frac{\partial}{\partial t_D} \int_0^{t_D} q_{wD}(t'_D) \left[\lim_{r_D \rightarrow 0} \left[r_D \frac{\partial m_{DC}(r_D, t_D - t'_D)}{\partial r_D} \right] \right] dt'_D \quad (\text{C.0.18}) \end{aligned}$$

According to the Eq. C.8, the term inside the brackets of the right-hand side of the Eq. C.18 is -1. Thus:

$$\frac{\partial}{\partial t_D} \int_0^{t_D} q_{wD}(t'_D) \left[\lim_{r_D \rightarrow 0} \left[r_D \frac{\partial m_{DC}(r_D, t_D - t'_D)}{\partial r_D} \right] \right] dt'_D = - \frac{\partial}{\partial t_D} \int_0^{t_D} q_{wD}(t'_D) dt'_D \quad (\text{C.0.19})$$

The differentiation of the integral above yields to:

$$- \frac{\partial}{\partial t_D} \int_0^{t_D} q_{wD}(t'_D) dt'_D = -q_{wD}(t_D) \quad (\text{C.0.20})$$

Thereby, the Eq. C.20 is the right-hand side term of the Eq. C.4, so the inner

boundary condition is satisfied for the formulation of the pseudo-pressure at variable oil flow rate $m_D(r_D, t_D)$.

Finally, it is necessary to verify if the solution expressed by the Eq. C.10 (Duhamel's principle) satisfies the hydraulic diffusivity equation in terms of $m_D(r_D, t_D)$ (Eq. C.1). Replacing the Eq. C. 15 in the left-hand side of the Eq. C.1 and replacing the Eq. C. 11 in the right-hand side of C.1:

$$\begin{aligned} \frac{\partial}{\partial t_D} \int_0^{t_D} \left[q_{wD}(t'_D) \frac{1}{r_D} \frac{\partial m_{DC}(r_D, t_D - t'_D)}{\partial r_D} + q_{wD}(t'_D) \frac{\partial^2 m_{DC}(r_D, t_D - t'_D)}{\partial r_D^2} \right] dt'_D + \\ - \mathcal{D}(r_D, t_D) \frac{\partial}{\partial t_D} \int_0^{t_D} q_{wD}(t'_D) \frac{\partial m_{DC}(r_D, t_D - t'_D)}{\partial t_D} dt'_D = 0 \quad (\text{C.0.21}) \end{aligned}$$

Adding and subtracting the term

$$\frac{\partial}{\partial t_D} \int_0^{t_D} q_{wD}(t'_D) \mathcal{D}(r_D, t_D - t'_D) \frac{\partial m_{DC}(r_D, t_D - t'_D)}{\partial t_D} dt'_D \quad (\text{C.0.22})$$

in the Eq. C.21:

$$\begin{aligned} \frac{\partial}{\partial t_D} \int_0^{t_D} q_{wD}(t'_D) \left[\frac{1}{r_D} \frac{\partial m_{DC}(r_D, t_D - t'_D)}{\partial r_D} + \frac{\partial^2 m_{DC}(r_D, t_D - t'_D)}{\partial r_D^2} - \mathcal{D}(r_D, t_D - t'_D) \times \right. \\ \left. \times \frac{\partial m_{DC}(r_D, t_D - t'_D)}{\partial t_D} \right] dt'_D + \frac{\partial}{\partial t_D} \int_0^{t_D} q_{wD}(t'_D) \mathcal{D}(r_D, t_D - t'_D) \times \\ \times \frac{\partial m_{DC}(r_D, t_D - t'_D)}{\partial t_D} dt'_D - \mathcal{D}(r_D, t_D) \frac{\partial}{\partial t_D} \int_0^{t_D} q_{wD}(t'_D) \frac{\partial m_{DC}(r_D, t_D - t'_D)}{\partial t_D} dt'_D = 0 \quad (\text{C.0.23}) \end{aligned}$$

The term inside the brackets in the first integral of the Eq. C. 23 is the hydraulic diffusivity equation in terms of $m_{DC}(r_D, t_D)$, then:

$$\frac{1}{r_D} \frac{\partial m_{DC}(r_D, t_D - t'_D)}{\partial r_D} + \frac{\partial^2 m_{DC}(r_D, t_D - t'_D)}{\partial r_D^2} - \mathcal{D}(r_D, t_D - t'_D) \frac{\partial m_{DC}(r_D, t_D - t'_D)}{\partial t_D} = 0 \quad (\text{C.0.24})$$

Therewith, the first integral of the Eq. C. 23 is zero for all r_D and t_D . So, the Eq. C. 23 becomes:

$$\begin{aligned} \frac{\partial}{\partial t_D} \int_0^{t_D} q_{wD}(t'_D) \mathcal{D}(r_D, t_D - t'_D) \frac{\partial m_{DC}(r_D, t_D - t'_D)}{\partial t_D} dt'_D - \mathcal{D}(r_D, t_D) \times \\ \times \frac{\partial}{\partial t_D} \int_0^{t_D} q_{wD}(t'_D) \frac{\partial m_{DC}(r_D, t_D - t'_D)}{\partial t_D} dt'_D = 0 \quad (\text{C.0.25}) \end{aligned}$$

According to the Eq. C. 10, the second integral from Eq. C. 25 is $m_D(r_D, t_D)$, thus:

$$\frac{\partial}{\partial t_D} \int_0^{t_D} q_{wD}(t'_D) \mathcal{D}(r_D, t_D - t'_D) \frac{\partial m_{DC}(r_D, t_D - t'_D)}{\partial t_D} dt'_D - \mathcal{D}(r_D, t_D) \frac{\partial m_D(r_D, t_D)}{\partial t_D} = 0 \quad (\text{C.0.26})$$

The Eq. C. 26 shows that the solution expressed by the Eq. C.10 does not satisfy the hydraulic diffusivity equation for permeability pressure-sensitive (Eq. C.1). For the particular case of the inverse hydraulic diffusivity $\mathcal{D}(r_D, t_D)$ is constant, *i.e.*, the permeability does not change during the drawdown and build-up periods, so, the Eq. C. 26 yields to:

$$\frac{\partial}{\partial t_D} \int_0^{t_D} q_{wD}(t'_D) \frac{\partial m_{DC}(r_D, t_D - t'_D)}{\partial t_D} dt'_D - \frac{\partial m_D(r_D, t_D)}{\partial t_D} = 0 \quad (\text{C.0.27})$$

Replacing the Eq. C. 10 in the Eq. C. 26:

$$\frac{\partial m_D(r_D, t_D)}{\partial t_D} = \frac{\partial m_D(r_D, t_D)}{\partial t_D} \quad (\text{C.0.28})$$

Thereby, the Eq. C. 1 is satisfied for constant inverse hydraulic diffusivity. Let us verify the dimensionless constant oil flow rate case. In this paper, $q_{wD} = 1$, thus, according the Eq. C. 26:

$$\begin{aligned} \frac{\partial}{\partial t_D} \int_0^{t_D} \mathcal{D}(r_D, t_D - t'_D) \frac{\partial m_{DC}(r_D, t_D - t'_D)}{\partial t_D} dt'_D - \mathcal{D}(r_D, t_D) \times \\ \times \frac{\partial}{\partial t_D} \int_0^{t_D} \frac{\partial m_{DC}(r_D, t_D - t'_D)}{\partial t_D} dt'_D = 0 \quad (\text{C.0.29}) \end{aligned}$$

Let the following change variables:

$$\mathcal{U} = t - t'_D \quad (\text{C.0.30})$$

Thus:

$$d\mathcal{U} = -dt'_D \quad (\text{C.0.31})$$

Replacing the change variables above in the Eq. C. 29, the first term in the Eq. C. 29 is expressed as follows:

$$\frac{\partial}{\partial t_D} \int_0^{t_D} \mathcal{D}(r_D, t_D - t'_D) \frac{\partial m_{DC}(r_D, t_D - t'_D)}{\partial t_D} dt'_D = -\frac{\partial}{\partial t_D} \int_0^{t_D} \mathcal{D}(r_D, \mathcal{U}) \frac{\partial m_{DC}(r_D, \mathcal{U})}{\partial \mathcal{U}} d\mathcal{U} \quad (\text{C.0.32})$$

Applying the Leibniz's rule for differentiation of integrals, the Eq. C. 32 becomes:

$$\frac{\partial}{\partial t_D} \int_0^{t_D} \mathcal{D}(r_D, \mathcal{U}) \frac{\partial m_{DC}(r_D, \mathcal{U})}{\partial \mathcal{U}} d\mathcal{U} = \mathcal{D}(r_D, t_D) \frac{\partial m_{DC}(r_D, t_D)}{\partial t_D} \quad (\text{C.0.33})$$

According to the calculus fundamental theorem, the second term of the Eq. C. 29 can be expressed by:

$$\mathcal{D}(r_D, t_D) \frac{\partial}{\partial t_D} \int_0^{t_D} \frac{\partial m_{DC}(r_D, t_D)}{\partial \mathcal{U}} d\mathcal{U} = \mathcal{D}(r_D, t_D) \frac{\partial m_{DC}(r_D, t_D)}{\partial t_D} \quad (\text{C.0.34})$$

Finally, replacing the Eqs. C. 33 and C. 34 in the Eq. C. 29:

$$\mathcal{D}(r_D, t_D) \frac{\partial m_{DC}(r_D, t_D)}{\partial t_D} = \mathcal{D}(r_D, t_D) \frac{\partial m_{DC}(r_D, t_D)}{\partial t_D} \quad (\text{C.0.35})$$

The Eq. C. 35 shows that the Duhamel's principle satisfies the nonlinear hydraulic diffusivity equation for cases where the oil flow rate does not change in the time, which is the case presented in this paper.

D

Integro-Differential Solution Verification

Let the dimensionless Euclidean space $\mathbf{r}_D = (r_D, \theta_D, z_D) \in \mathbb{R}^3$ and $t_D \in \mathbb{R}$. Let us verify the NHDE integro-differential solution as follows:

$$\nabla^2 m_D(r_D, \theta_D, z_D, t_D) - \frac{\partial m_D(r_D, \theta_D, z_D, t_D)}{\partial t_D} = f_D(r_D, \theta_D, z_D, t_D) + \xi(m_D) \frac{\partial m_D(r_D, \theta_D, z_D, t_D)}{\partial t_D} \quad (\text{D.0.1})$$

The initial condition is:

$$m_D(r_D, \theta_D, z_D, t_D = 0) = 0 \quad (\text{D.0.2})$$

The external boundary condition is:

$$\lim_{|r_D, \theta_D, z_D| \rightarrow \infty} m_D(r_D, \theta_D, z_D, t_D) = 0 \quad (\text{D.0.3})$$

The integro-differential solution is:

$$m_D(r_D, \theta_D, z_D, t_D) = - \int_{-\infty}^{+\infty} \int_0^{2\pi} \int_0^\infty \int_0^{t_D} \left[f_D(r'_D, \theta'_D, z'_D, t'_D) + \xi(m_D) \frac{\partial m_D}{\partial t'_D} \right] \times \\ \times G_D(r_D, r'_D, \theta_D, \theta'_D, z_D, z'_D, t_D, t'_D) dt'_D dr'_D d\theta'_D dz'_D \quad (\text{D.0.4})$$

The dimensionless NHDE associated to the Green's problem is:

$$\nabla^2 G_D(r_D, r'_D, \theta_D, \theta'_D, z_D, z'_D, t_D, t'_D) - \frac{\partial G_D(r_D, r'_D, \theta_D, \theta'_D, z_D, z'_D, t_D, t'_D)}{\partial t_D} = \\ = -\delta(r_D - r'_D) \delta(\theta_D - \theta'_D) \delta(z_D - z'_D) \delta(t_D - t'_D) \quad (\text{D.0.5})$$

The associated initial condition is:

$$G_D(r_D, r'_D, \theta_D, \theta'_D, z_D, z'_D, t_D = 0, t'_D) = 0 \quad (\text{D.0.6})$$

And the external boundary condition is:

$$\lim_{|r_D, \theta_D, z_D| \rightarrow \infty} G_D(r_D, r'_D, \theta_D, \theta'_D, z_D, z'_D, t_D, t'_D) = 0 \quad (\text{D.0.7})$$

The dimensionless pseudo-pressure rate is:

$$\begin{aligned} \frac{\partial m_D}{\partial t_D} = & -\frac{\partial}{\partial t_D} \int_{-\infty}^{+\infty} \int_0^{2\pi} \int_0^\infty \int_0^{t_D} \left[f_D(r'_D, \theta'_D, z'_D, t'_D) + \xi(m_D) \frac{\partial m_D}{\partial t'_D} \right] \times \\ & \times G_D(r_D, r'_D, \theta_D, \theta'_D, z_D, z'_D, t_D, t'_D) dt'_D dr'_D d\theta'_D dz'_D \quad (D.0.8) \end{aligned}$$

Changing the integral notation:

$$\int_{-\infty}^{+\infty} \int_0^{2\pi} \int_0^\infty \int_0^{t_D} (\dots) dt'_D dr'_D d\theta'_D dz'_D \mapsto \int_{\mathbb{R}^3} \int_0^{t_D} (\dots) dt'_D dr'_D d\theta'_D dz'_D \quad (D.0.9)$$

Rewriting the Eq. D.8:

$$\begin{aligned} \frac{\partial m_D}{\partial t_D} = & -\int_{\mathbb{R}^3} \left[f_D(r'_D, \theta'_D, z'_D, t'_D = t_D) + \xi(m_D) \frac{\partial m_D}{\partial t'_D} \right] \times \\ & \times \frac{\partial}{\partial t_D} G_D(r_D, r'_D, \theta_D, \theta'_D, z_D, z'_D, t_D, t'_D = t_D) dr'_D d\theta'_D dz'_D + \\ & -\int_{\mathbb{R}^3} \int_0^{t_D} \left[f_D(r'_D, \theta'_D, z'_D, t'_D) + \xi(m_D) \frac{\partial m_D}{\partial t'_D} \right] \times \\ & \times \frac{\partial}{\partial t_D} G_D(r_D, r'_D, \theta_D, \theta'_D, z_D, z'_D, t_D, t'_D) dt'_D dr'_D d\theta'_D dz'_D \quad (D.0.10) \end{aligned}$$

According to the initial condition associated to the Green's problem:

$$G_D(r_D, r'_D, \theta_D, \theta'_D, z_D, z'_D, t_D, t_D) = 0 \quad (D.0.11)$$

Replacing the Eq. D.11 in the Eq. D.10:

$$\begin{aligned} \int_{\mathbb{R}^3} \left[f_D(r'_D, \theta'_D, z'_D, t'_D) + \xi(m_D) \frac{\partial m_D}{\partial t'_D} \right] \times \frac{\partial}{\partial t_D} \times \\ \times G_D(r_D, r'_D, \theta_D, \theta'_D, z_D, z'_D, t_D, t'_D) dr'_D d\theta'_D dz'_D = 0 \quad (D.0.12) \end{aligned}$$

Therefore, the dimensionless pseudo-pressure rate is constituted by only the second term of the Eq. D.10:

$$\begin{aligned} \frac{\partial m_D}{\partial t_D} = & -\int_{\mathbb{R}^3} \int_0^{t_D} \left[f_D(r'_D, \theta'_D, z'_D, t'_D) + \xi(m_D) \frac{\partial m_D}{\partial t'_D} \right] \times \\ & \times \frac{\partial}{\partial t_D} G_D(r_D, r'_D, \theta_D, \theta'_D, z_D, z'_D, t_D, t'_D) dt'_D dr'_D d\theta'_D dz'_D \quad (D.0.13) \end{aligned}$$

The dimensionless pseudo-pressure Laplacian is expressed as follows:

$$\begin{aligned} \nabla^2 m_D = & -\nabla^2 \int_{\mathbb{R}^3} \int_0^{t_D} \left[f_D(r'_D, \theta'_D, z'_D, t'_D) + \xi(m_D) \frac{\partial m_D}{\partial t'_D} \right] \times \\ & \times G_D(r_D, r'_D, \theta_D, \theta'_D, z_D, z'_D, t_D, t'_D) dt'_D dr'_D d\theta'_D dz'_D \end{aligned} \quad (\text{D.0.14})$$

Thus, the pseudo-pressure Laplacian yields to:

$$\begin{aligned} \nabla^2 m_D = & -\int_{\mathbb{R}^3} \int_0^{t_D} \left[f_D(r'_D, \theta'_D, z'_D, t'_D) + \xi(m_D) \frac{\partial m_D}{\partial t'_D} \right] \times \\ & \times \nabla^2 G_D(r_D, r'_D, \theta_D, \theta'_D, z_D, z'_D, t_D, t'_D) dt'_D dr'_D d\theta'_D dz'_D \end{aligned} \quad (\text{D.0.15})$$

Replacing Eq. D.13 and Eq. D.15 into the Eq. D.1:

$$\begin{aligned} & -\int_{\mathbb{R}^3} \int_0^{t_D} \left[f_D(r'_D, \theta'_D, z'_D, t'_D) + \xi(m_D) \frac{\partial m_D}{\partial t'_D} \right] \times \\ & \quad \times \nabla^2 G_D(r_D, r'_D, \theta_D, \theta'_D, z_D, z'_D, t_D, t'_D) dt'_D dr'_D d\theta'_D dz'_D + \\ & \quad + \int_{\mathbb{R}^3} \int_0^{t_D} \left[f_D(r'_D, \theta'_D, z'_D, t'_D) + \xi(m_D) \frac{\partial m_D}{\partial t'_D} \right] \times \\ & \quad \times \frac{\partial}{\partial t_D} G_D(r_D, r'_D, \theta_D, \theta'_D, z_D, z'_D, t_D, t'_D) dt'_D dr'_D d\theta'_D dz'_D = \\ & \quad = f_D(r_D, \theta_D, z_D, t_D) + \xi(m_D) \frac{\partial m_D}{\partial t_D} \end{aligned} \quad (\text{D.0.16})$$

Regrouping the terms of the Eq. D.16, we have:

$$\begin{aligned} & \int_{\mathbb{R}^3} \int_0^{t_D} \left[f_D(r'_D, \theta'_D, z'_D, t'_D) + \xi(m_D) \frac{\partial m_D}{\partial t'_D} \right] \left[-\nabla^2 G_D(r_D, r'_D, \theta_D, \theta'_D, z_D, z'_D, t_D, t'_D) + \right. \\ & \quad \left. + \frac{\partial}{\partial t_D} G_D(r_D, r'_D, \theta_D, \theta'_D, z_D, z'_D, t_D, t'_D) \right] dt'_D dr'_D d\theta'_D dz'_D = \\ & \quad = f_D(r_D, \theta_D, z_D, t_D) + \xi(m_D) \frac{\partial m_D}{\partial t_D} \end{aligned} \quad (\text{D.0.17})$$

Replacing the Eq. D.5 in the Eq. D.17:

$$\begin{aligned}
& - \int_{\mathbb{R}^3} \int_0^{t_D} \left[f_D(r'_D, \theta'_D, z'_D, t'_D) + \xi(m_D) \frac{\partial m_D}{\partial t'_D} \right] \times \\
& \quad \times \nabla^2 G_D(r_D, r'_D, \theta_D, \theta'_D, z_D, z'_D, t_D, t'_D) dt'_D dr'_D d\theta'_D dz'_D + \\
& \quad + \int_{\mathbb{R}^3} \int_0^{t_D} \left[f_D(r'_D, \theta'_D, z'_D, t'_D) + \xi(m_D) \frac{\partial m_D}{\partial t'_D} \right] \frac{\partial}{\partial t_D} \times \\
& \quad \times G_D(r_D, r'_D, \theta_D, \theta'_D, z_D, z'_D, t_D, t'_D) dt'_D dr'_D d\theta'_D dz'_D = \\
& \quad = \int_{\mathbb{R}^3} \int_0^{t_D} \left[f_D(r'_D, \theta'_D, z'_D, t'_D) + \xi(m_D) \frac{\partial m_D}{\partial t'_D} \right] \times \\
& \quad \times \delta(r_D - r'_D) \delta(\theta_D - \theta'_D) \delta(z_D - z'_D) \delta(t_D - t'_D) dt'_D dr'_D d\theta'_D dz'_D \quad (D.0.18)
\end{aligned}$$

Applying the sampling property of the Dirac's delta function:

$$\begin{aligned}
& \int_{\mathbb{R}^3} \int_0^{t_D} \left[f_D(r'_D, \theta'_D, z'_D, t'_D) + \xi(m_D) \frac{\partial m_D}{\partial t'_D} \right] \times \\
& \quad \times \delta(r_D - r'_D) \delta(\theta_D - \theta'_D) \delta(z_D - z'_D) \delta(t_D - t'_D) dt'_D dr'_D d\theta'_D dz'_D = \\
& \quad = f_D(r_D, \theta_D, z_D, t_D) + \xi(m_D) \frac{\partial m_D}{\partial t_D} \quad (D.0.19)
\end{aligned}$$

Finally, combining the Eq. D.19 to Eq. D.18, we proved that the proposed integro-differential solution satisfies the partial differential equation:

$$f_D(r_D, \theta_D, z_D, t_D) + \xi(m_D) \frac{\partial m_D}{\partial t_D} = f_D(r_D, \theta_D, z_D, t_D) + \xi(m_D) \frac{\partial m_D}{\partial t_D} \quad (D.0.20)$$

The next step, is to verify the initial and boundary condition, thus: The initial condition is:

$$m_D(r_D, \theta_D, z_D, t_D = 0) = 0 \quad (D.0.21)$$

Applying the integro-differential solution:

$$\begin{aligned}
m_D(r_D, \theta_D, z_D, 0) &= - \int_0^0 \int_{\mathbb{R}^3} \left[f_D(r'_D, \theta'_D, z'_D, t'_D) + \xi(m_D) \frac{\partial m_D}{\partial t'_D} \right] \times \\
& \quad \times G_D(r_D, r'_D, \theta_D, \theta'_D, z_D, z'_D, t_D, t'_D) dt'_D dr'_D d\theta'_D dz'_D \quad (D.0.22)
\end{aligned}$$

As the integral in the interval $\mathcal{I} = [a; b]$ when $a = b$ is zero, thus, the initial condition is satisfied. Let us verify the external boundary condition.

The external boundary condition is:

$$\lim_{|r_D, \theta_D, z_D| \rightarrow \infty} m_D(r_D, \theta_D, z_D, t_D) = 0 \quad (\text{D.0.23})$$

Thereby:

$$\begin{aligned} \lim_{|r_D, \theta_D, z_D| \rightarrow \infty} m_D(r_D, \theta_D, z_D, t_D) &= \\ &= - \lim_{|r_D, \theta_D, z_D| \rightarrow \infty} \int_{\mathbb{R}^3} \int_0^{t_D} \left[f_D(r'_D, \theta'_D, z'_D, t'_D) + \xi(m_D) \frac{\partial m_D}{\partial t'_D} \right] \times \\ &\quad \times G_D(r_D, r'_D, \theta_D, \theta'_D, z_D, z'_D, t_D, t'_D) dt'_D dr'_D d\theta'_D dz'_D \quad (\text{D.0.24}) \end{aligned}$$

Rewriting Eq. D.24:

$$\begin{aligned} \lim_{|r_D, \theta_D, z_D| \rightarrow \infty} m_D(r_D, \theta_D, z_D, t_D) &= - \int_{\mathbb{R}^3} \int_0^{t_D} \left[f_D(r'_D, \theta'_D, z'_D, t'_D) + \xi(m_D) \frac{\partial m_D}{\partial t'_D} \right] \times \\ &\quad \times \lim_{|r_D, \theta_D, z_D| \rightarrow \infty} G_D(r_D, r'_D, \theta_D, \theta'_D, z_D, z'_D, t_D, t'_D) dt'_D dr'_D d\theta'_D dz'_D \quad (\text{D.0.25}) \end{aligned}$$

According the GF external boundary condition:

$$\lim_{|r_D, \theta_D, z_D| \rightarrow \infty} G_D(r_D, r'_D, \theta_D, \theta'_D, z_D, z'_D, t_D, t'_D) = 0 \quad (\text{D.0.26})$$

Replacing Eq. D.26 in Eq. D.25:

$$\lim_{|r_D, \theta_D, z_D| \rightarrow \infty} m_D(r_D, r'_D, \theta_D, \theta'_D, t_D, t'_D) = 0 \quad (\text{D.0.27})$$

So, the external boundary condition is satisfied.

E

Dimensionless Wellbore Line-Source Solution Derivation

Dimensionless hydraulic diffusivity equation for radial flow in porous media is:

$$\frac{1}{r_D} \frac{\partial}{\partial r_D} \left(r_D \frac{\partial p_D}{\partial r_D} \right) = \frac{\partial p_D}{\partial t_D} \quad (\text{E.0.1})$$

Initial and boundary conditions are:

$$p_D(r_D, t_D = 0) = 0 \quad (\text{E.0.2})$$

$$\lim_{r_D \rightarrow \infty} p_D(r_D, t_D) = 0 \quad (\text{E.0.3})$$

Applying Laplace transform in equation (E-1):

$$\mathcal{L} \left\{ \frac{1}{r_D} \frac{\partial}{\partial r_D} \left(r_D \frac{\partial p_D}{\partial r_D} \right) \right\} = \mathcal{L} \left\{ \frac{\partial p_D}{\partial t_D} \right\} \quad (\text{E.0.4})$$

By Laplace transform definition:

$$\mathcal{L}\{p_D(r_D, t_D)\} \stackrel{\text{def.}}{=} \int_0^{+\infty} e^{-ut_D} p_D(r_D, t_D) dt_D \quad (\text{E.0.5})$$

Rewriting equation (E-5) in terms of Laplace variable:

$$\mathcal{L}\{p_D(r_D, t_D)\} = \bar{p}_D(r_D, u) \quad (\text{E.0.6})$$

Where: $\bar{p}_D(r_D, u)$ is the field pressure in Laplace domain and u is the Laplace variable. Equation (E-4) can be written as:

$$\int_0^{+\infty} e^{-ut_D} \left[\frac{1}{r_D} \frac{\partial}{\partial r_D} \left(r_D \frac{\partial p_D}{\partial r_D} \right) \right] dt_D = \int_0^{+\infty} e^{-ut_D} \left[\frac{\partial p_D}{\partial t_D} \right] dt_D \quad (\text{E.0.7})$$

After Laplace transform application in equation (E-1), we have:

$$\frac{1}{r_D} \frac{d}{dr_D} \left(r_D \frac{d\bar{p}_D(r_D, u)}{dr_D} \right) = u\bar{p}_D(r_D, u) - p_D(0) \quad (\text{E.0.8})$$

Since $p_D(0) = 0$, equation (E-8) becomes:

$$\frac{1}{r_D} \frac{d}{dr_D} \left(r_D \frac{d\bar{p}_D(r_D, u)}{dr_D} \right) - u\bar{p}_D(r_D, u) = 0 \quad (\text{E.0.9})$$

Expanding the left-hand side of equation (E-9):

$$\frac{d^2\bar{p}_D(r_D, u)}{dr_D^2} + \frac{1}{r_D} \frac{d\bar{p}_D(r_D, u)}{dr_D} - u\bar{p}_D(r_D, u) = 0 \quad (\text{E.0.10})$$

Dividing both sides by u :

$$\frac{d^2\bar{p}_D(r_D, u)}{d(r_D\sqrt{u})^2} + \frac{1}{r_D\sqrt{u}} \frac{d\bar{p}_D(r_D, u)}{d(r_D\sqrt{u})} - \bar{p}_D(r_D, u) = 0 \quad (\text{E.0.11})$$

According to (Abramowitz & Stegun, 1972), the general solution in Laplace domain is:

$$\bar{p}_D(r_D, u) = A\mathbf{I}_0(r_D\sqrt{u}) + B\mathbf{K}_0(r_D\sqrt{u}) \quad (\text{E.0.12})$$

Where: A and B are functions in Laplace domain, \mathbf{I}_0 and \mathbf{K}_0 are the zero order modified Bessel functions of first and second kind, respectively. Applying initial and boundary conditions, it can be seen that $A = 0$ and $B = 1/u$. Thus, equation (E-12) becomes:

$$\bar{p}_D(r_D, u) = \frac{1}{u}\mathbf{K}_0(r_D\sqrt{u}) \quad (\text{E.0.13})$$

Applying Laplace inverse transform in equation (E-13):

$$\mathcal{L}^{-1}\left\{\bar{p}_D(r_D, u)\right\} = \mathcal{L}^{-1}\left\{\frac{1}{u}\mathbf{K}_0(r_D\sqrt{u})\right\} \quad (\text{E.0.14})$$

According to (Abramowitz & Stegun, 1972) and after algebraic transformations, this inverse is:

$$p_D(r_D, t_D) = -\frac{1}{2}\mathbf{Ei}\left(-\frac{r_D^2}{4t_D}\right) \quad (\text{E.0.15})$$

The equation (E-15) is well-known in petroleum engineering literature and denominated as the line-source solution. This is the solution for the constant permeability oil flow in porous media.